

# Synthesis of novel vanillin derivatives: study of their antioxidant and potential neuroprotective properties.

SCIPIONI, M.

2019

The author of this thesis retains the right to be identified as such on any occasion in which content from this thesis is referenced or re-used. The licence under which this thesis is distributed applies to the text and any original images only – re-use of any third-party content must still be cleared with the original copyright holder.

*SYNTHESIS OF NOVEL VANILLIN  
DERIVATIVES: STUDY OF THEIR  
ANTIOXIDANT AND POTENTIAL  
NEUROPROTECTIVE PROPERTIES*

MATTEO SCIPIONI

School of Pharmacy and Life Science  
(PALS) **Robert Gordon University**

**PhD**

**2019**

*SYNTHESIS OF NOVEL VANILLIN  
DERIVATIVES: STUDY OF THEIR  
ANTIOXIDANT AND POTENTIAL  
NEUROPROTECTIVE PROPERTIES*

**MATTEO SCIPIONI**

A thesis submitted in partial fulfillment of the requirements of the Robert Gordon University for the degree of Doctor of Philosophy

This research programme was carried out in collaboration with the University of the Highlands and Islands

September 2019



*"The Lord gave us the atoms, and it's up to us to make 'em dance."*

*H. J. Simpson*

## **DECLARATION**

I declare that the work presented in this thesis is my own, except where otherwise acknowledged, and has not been submitted in any form for another degree or qualification at any other academic institution. Information derived from the published or unpublished work of others has been acknowledged in the text and a list of references is given.

Matteo Scipioni

## ABSTRACT

Vanillin (4-hydroxy-3-methoxybenzaldehyde) is a natural occurring phenolic compound and it is the main component of the bean and pod of vanilla orchids. It is widely used as flavouring agent in food and drinks and as preservative in the cosmetic and pharmaceutical industry. In the past decades, several studies had reported the antioxidant and protective effects of vanillin in several oxidative stress models, both *in vitro* and *in vivo*.

The aim of the project was to synthesise novel vanillin derivatives with enhanced antioxidant properties and to study their potential neuroprotective activities in *in vitro* oxidative stress models. To achieve this aim, novel vanillin derivatives were synthesised through reductive amination reaction, by reacting vanillin with a selection of amines, and all the derivatives were characterized using  $^1\text{H}$  and  $^{13}\text{C}$  NMR and Mass spectrometry.

Vanillin derivatives were tested in several antioxidant assays with different mechanisms of action in order to identify the functionalities that contributed to the antioxidant properties of this novel class of compounds. A structure-activity relationship (SAR) was therefore determined. The tetramer **4c** turned out to be the most efficient antioxidant in all the assays. The latter compound consists of four vanillin moieties together with a molecular structure that facilitates electrons delocalisation for enhanced antioxidant activity. A selection of vanillin derivatives, based on their chemical structures and antioxidant properties, was therefore tested as potential multi-target-directed ligands (MTDLs) for the treatment of Alzheimer's disease (AD), a multifactorial neurodegenerative disease. For this reason, the vanillin derivatives were tested for their ability to inhibit both acetylcholinesterase (AChE) enzyme and the self-mediated  $\text{A}\beta_{(1-42)}$  aggregation. The monomer **1f** displayed the best inhibitory activities toward both of the latter targets, with  $\text{IC}_{50}$  values at  $\mu\text{M}$  concentrations. *In silico* studies were performed to identify the molecular elements involved in the AChE inhibitory activities and to predict the ability of selected compounds to cross the blood-brain-barrier (BBB), which is of critical importance when targeting neurodegenerative diseases. Monomer **1f** was predicted cross the BBB.

A selection of vanillin derivatives, based on their antioxidant and AChE and amyloid inhibitory activities was then tested in oxidative stress models, by applying hydrogen peroxide or a mixture of rotenone/oligomycin A as stressors, in neuroblastoma SH-SY5Y cell line. Vanillin derivatives showed cellular protective effects, by increasing cell viability and reducing reactive oxygen species (ROS) production but they were unable to protect the cells' DNA from oxidative damage. Again, compound **4c** displayed the most efficient protective effects at micromolar concentrations.

Finally, in order to study the mechanism behind the protective effects of **4c** in SH-SY5Y cell line, its ability to activate the Nuclear factor (erythroid-derived 2)-like 2 (Nrf2) pathway, which is known to be a predominant mediator of cellular antioxidant response, was studied. Since no Nrf2 was observed in the nucleus confirms an alternative mechanism for the antioxidant activity of **4c**. Overall, compounds **1f** and **4c** showed promise for their further development, as potential for the treatment of AD.

**Keywords:** Vanillin, free radicals, antioxidants, oxidative stress, Nrf2, Alzheimer's disease, multi-target-directed ligands, acetylcholinesterase, beta-amyloid, molecular modelling, SH-SY5Y, neurodegeneration.



## ACKNOWLEDGEMENTS

First and foremost, I would like to thank my main supervisor, Prof. Paul Kong Thoo Lin. He has been an amazing supervisor during these past 3 years (and spare change) and it has been a pleasure to work with such an amazing scientist and person. I have loved every minute spent together talking about science and about our lives, and I will treasure it always. My PhD has been an exciting and tough journey, and Paul has always supported me and helped me.

I would also like to thank the other members of my supervisory team: Dr. Graeme Kay, for his invaluable feedback on the areas of my project that concerned Chemistry, and Prof. Ian Megson, for letting me tap into his extensive expertise in Biology (not really my field) and Statistics (DEFINITELY not my field).

I would like to thank Prof. Susan Duthie, Dr. Elena Lendoiro, and Dr. Katia Tortora for their help with the DNA comet assay, and Dr. Marie Goua for her help with flow cytometry.

I would like to thank Dr. Gemma Barron for her precious and unrelenting help with the western blot; I am surprised she did not try to hide from me at some point!

A special mention goes to Prof. Galli and Dr. Desiree Bartolini for their studies regarding Nrf2 activation; it has been a great pleasure for me to meet them in Lisbon and spend some time together.

I would like to thank Dr. Franzi Pohl for her help as I started to make my first steps in the lab; she turned out to be a great colleague and friend, always ready to help me out.

I would like to thank Prof. Andrey Shiryaev (*Samara Technical University, Russia*) for his feedback regarding the molecular modelling studies. It has been a pleasure for me to personally meet him during his stay in my sunny Italy.

I would like to thank Andrea McMillan from the graduate school for her administrative support; she has helped from the moment I first popped my head inside RGU.

I would like to thank the rest of my colleagues and friends, including Josh, Calum, Mhairi, Hazel, Cameron, PJ, Quirin, Benedicta, Priscila, Tesnime, Chrys, Moomin, Zoi, Kostas, Lenn, Ahmed, Amir, Krystof. Their help made the difference in being able to survive the long, dark Aberdeen winters.

Special thanks go to my Italian friends in Aberdeen: Guido, Giuseppe, and Fabio. They always made me feel like I was at home.

I would like to thank my family: my parents Giovanni and Marilena, my sister Amanda (who also made the picture for the comet assay scoring), my niece Diletta and my little nephew Leonardo, who has entered my life just a few months ago but who has already conquered my heart. Being separated from them for three years has been tough, but I have always felt their love, even from 2000 kilometers away. I could write hundreds more words about my feelings toward them, but they already know everything and I don't need to add a single word.

Finally, I would like to thank my girlfriend Serena. She has been supporting me since before I moved to Scotland, even though she knew that the distance would have been the biggest challenge yet in our relationship. We fought many times during this long period that we spent apart from each other, even if we tried to see each other at all conceivable occasions. In the end, we buried the hatchet and decided to move on; together. I don't know what the future has in store for me; what I do know is that she will be a part of it.

## RESEARCH OUTPUT

### Poster conference presentation

- 4th Royal Society of Chemistry Early Career Symposium 2016, 23<sup>rd</sup>-24<sup>th</sup> June, Glasgow, Scotland, United Kingdom. "The synthesis and biological activity of novel anti-oxidant based on natural products".
- Medicinal Chemistry Residential School 2017, 11<sup>th</sup>-16<sup>th</sup> June, Loughborough, England, United Kingdom. "The synthesis and biological activity of novel anti-oxidant based on natural products".
- 19<sup>th</sup> Biennial Meeting of Society for Free Radical Research International (SFRRI) 2018, 4<sup>th</sup>-7<sup>th</sup> June, Lisbon, Portugal. "Novel Vanillin Derivatives: an insight into their antioxidant properties". Published abstract:
  - Scipioni M. *et al.* 2018. "Novel Vanillin Derivatives: An Insight into Their Antioxidant Properties." *Free Radical Biology and Medicine* 120: S51–52.  
<https://doi.org/10.1016/j.freeradbiomed.2018.04.170>.

### Published Papers

- Scipioni, M. *et al.* (2018) 'Novel vanillin derivatives: Synthesis, anti-oxidant, DNA and cellular protection properties', *European Journal of Medicinal Chemistry*. Elsevier Masson SAS, 143, pp. 745–754. doi: 10.1016/j.ejmech.2017.11.072.
- Scipioni, M. *et al.* (2019) 'Synthesis of novel vanillin derivatives: novel multi-targeted scaffold ligands against Alzheimer's disease', *MedChemComm*, 10, pp. 764-777. doi: 10.1039/C9MD00048H).



Research paper

## Novel vanillin derivatives: Synthesis, anti-oxidant, DNA and cellular protection properties



Matteo Scipioni<sup>a</sup>, Graeme Kay<sup>a</sup>, Ian Megson<sup>b</sup>, Paul Kong Thoo Lin<sup>a,\*</sup>

<sup>a</sup> School of Pharmacy and Life Sciences, Robert Gordon University, Aberdeen, UK

<sup>b</sup> Department of Diabetes and Cardiovascular Science, UHI, Inverness, UK

### ARTICLE INFO

**Article history:**  
 Received 13 September 2017  
 Received in revised form  
 20 November 2017  
 Accepted 25 November 2017  
 Available online 2 December 2017

**Keywords:**  
 Vanillin derivatives  
 Synthetic antioxidants  
 Antioxidant assays  
 Oxidative stress  
 DNA and cell protection

### ABSTRACT

Antioxidants have been the subject of intense research interest mainly due to their beneficial properties associated with human health and wellbeing. Phenolic molecules, such as naturally occurring Resveratrol and Vanillin, are well known for their anti-oxidant properties, providing a starting point for the development of new antioxidants. Here we report, for the first time, the synthesis of a number of new vanillin through the reductive amination reaction between vanillin and a selection of amines. All the compounds synthesised, exhibited strong antioxidant properties in DPPH, FRAP and ORAC assays, with compounds **1b** and **2c** being the most active. The latter also demonstrated the ability to protect plasmid DNA from oxidative damage in the presence of the radical initiator AAPH. At cellular level, neuroblastoma SH-SY5Y cells were protected from oxidative damage (H<sub>2</sub>O<sub>2</sub>, 400 μM) with both **1b** and **2c**. The presence of a tertiary amino group, along with the number of vanillin moieties in the molecule contribute for the antioxidant activity. Furthermore, the delocalization of the electron pair of the nitrogen and the presence of an electron donating substituent to enhance the antioxidant properties of this new class of compounds. In our opinion, vanillin derivatives **1b** and **2c** described in this work can provide a viable platform for the development of antioxidant based therapeutics.

© 2017 Elsevier Masson SAS. All rights reserved.

MedChemComm



RESEARCH ARTICLE

View Article Online  
 View Journal | View Issue



Cite this: *Med. Chem. Commun.*,  
 2019, 10, 764

## Synthesis of novel vanillin derivatives: novel multi-targeted scaffold ligands against Alzheimer's disease†

Matteo Scipioni,<sup>a</sup> Graeme Kay,<sup>a</sup> Ian L. Megson<sup>b</sup> and Paul Kong Thoo Lin<sup>a,\*</sup>

Alzheimer's disease (AD) is the most common cause of dementia worldwide, normally affecting people aged over 65. Due to the multifactorial nature of this disease, a "multi-target-directed ligands" (MTDLs) approach for the treatment of this illness has generated intense research interest in the past few years. Vanillin is a natural antioxidant and it provides a good starting point for the synthesis of new compounds with enhanced antioxidant properties, together with many biological activities, including β-amyloid peptide aggregating and acetylcholinesterase inhibiting properties. Here we report novel vanillin derivatives, bearing a tacrine or a naphthalimido moiety. All compounds exhibited improved antioxidant properties using DPPH assay, with IC<sub>50</sub> as low as 19.5 μM, FRAP and ORAC assays, with activities up to 1.54 and 6.4 Trolox equivalents, respectively. In addition, all compounds synthesised showed inhibitory activity toward acetylcholinesterase enzyme at μmolar concentrations using the Ellman assay. Computational docking studies of selected compounds showed interactions with both the catalytic anionic site and the peripheral anionic site of the enzyme. Furthermore, these compounds inhibited Aβ<sub>1–42</sub> amyloid aggregation using the fluorometric ThT assay, with compound **4** showing comparable inhibitory activity to the positive control, curcumin. At cellular level compound **4** (1 μM) showed significant protective effects in neuroblastoma SH-SY5Y cell line when treated with hydrogen peroxide (400 μM). In our opinion, vanillin derivatives could provide a viable platform for future development of multi-targeted ligands against AD.

Received 28th January 2019,  
 Accepted 5th April 2019

DOI: 10.1039/c9md00048h

[rsc.li/medchemcomm](http://rsc.li/medchemcomm)

## CONTENTS

Thesis Layout .....	1
<b>Chapter 1: Introduction</b> .....	<b>2</b>
1.1 Oxidative Stress .....	3
1.1.1 The Theory of Oxidative Stress .....	3
1.1.2 Sources and formation of Oxygen and Nitrogen Reactive Species .....	3
1.1.3 The Role of Oxidative Stress in Diseases .....	8
1.1.3.1 Oxidative Stress in Inflammation and Cancer .....	8
1.1.3.2 Oxidative Stress and Neurodegenerative Diseases .....	11
1.1.3.3 Oxidative Stress and Cardiovascular Diseases .....	14
1.2 Antioxidants .....	16
1.2.1 Definition of Antioxidants .....	16
1.2.2 Mechanism of Action of Antioxidants .....	17
1.2.2.1 Free Radical Scavengers .....	17
1.2.2.2 Metal Chelation .....	18
1.2.2.3 Antioxidant Responsive Element (ARE)-mediated Pathway .....	18
1.2.3 Classification of Antioxidants .....	20
1.2.3.1 Natural Antioxidants .....	22
1.2.3.1.1 Endogenous Antioxidants .....	22
1.2.3.1.2 Exogenous Antioxidants .....	24
1.2.3.1.2.1 Vitamins .....	24
1.2.3.1.2.2 Phenolic Compounds .....	26
1.2.3.2 Synthetic Antioxidants .....	31
1.2.3.2.1 Multitarget-based Synthetic Antioxidants .....	35
1.2.3.2.1.1 Synthetic Antioxidants in AD .....	35
1.2.3.2.1.2 Synthetic Antioxidants in PD .....	39
1.2.3.2.1.3 Synthetic Antioxidants in Inflammation .....	43
1.3 Aims of Project .....	45
<b>Chapter 2: Synthesis of Novel Vanillin Derivatives</b> .....	<b>47</b>
2.1 Vanillin Derivatives .....	48
2.1.1 Overview on Vanillin Derivatives .....	48
2.2 Chemical Synthesis of Vanillin Derivatives .....	55
2.2.1 Rationale Behind the Synthesis of Novel Vanillin Derivatives .....	55
2.2.2 Nomenclature .....	57
2.3 Materials and Methods .....	58

2.3.1 Materials .....	58
2.3.2 Techniques for the Identification and Characterization of intermediates and new Vanillin Derivatives.....	58
2.3.3 Instrumentation .....	60
2.4 Methods .....	60
2.4.1 Synthesis of Intermediates .....	60
2.4.2 General Method for the Synthesis of Monomers .....	62
2.4.3 General Method for the synthesis of Dimers .....	66
2.4.4 General Method for the Synthesis of Tetramers .....	70
2.5 Results and Discussion .....	74
2.5.1 Synthesis of the Intermediates .....	74
2.5.2 Synthesis of the Monomers .....	77
2.5.3 Synthesis of the Dimers .....	79
2.5.4 Synthesis of the Tetramers .....	83
2.6 Conclusions .....	86
<b>Chapter 3: Antioxidant Properties of Vanillin Derivatives .....</b>	<b>89</b>
3.1 Introduction .....	90
3.1.1 Assays for the Evaluation of Antioxidant Activity .....	91
3.1.1.2 2,2-diphenyl-1-picrylhydrazyl (DPPH) Assay .....	91
3.1.1.3 Ferric Reducing/Antioxidant Power (FRAP) Assay .....	92
3.1.1.4 2,2-azino-bis(3-ethylbenz- thiazoline-6-sulfonic acid) (ABTS) Assay .....	93
3.1.1.5 Total Phenol Assay (Folin-Ciocalteu reagent) .....	94
3.1.1.6 Oxygen Radical Absorbance Capacity (ORAC) Assay .....	95
3.1.1.7 Thiobarbituric Acid Reactive Substances (TBARS) Assay .....	97
3.1.1.8 DNA Damage Protection Assay .....	98
3.2 Materials and Methods.....	100
3.2.1 Materials .....	100
3.2.2 Instrumentation .....	100
3.3 Methods .....	100
3.3.1 DPPH Assay .....	100
3.3.2 FRAP Assay .....	102
3.3.3 ORAC Assay .....	103
3.3.4 DNA Damage Protection Assay .....	104
3.4 Results and Discussion .....	106
3.4.1 DPPH Assay .....	106
3.4.2 FRAP Assay .....	114
3.4.3 ORAC Assay .....	118

3.4.4 DNA Damage Protection Assay.....	121
3.4.5 Structure Activity Relationship (SAR) .....	124
3.5 Conclusions.....	126
<b>Chapter 4: Protective Effects of Vanillin Derivatives in neuroblastoma SH-SY5Y Cell Line .....</b>	<b>128</b>
4.1. Introduction.....	129
4.1.1 The Use of SH-SY5Y Cell Line in Neurodegenerative Disease Research .....	129
4.1.2 Oxidative Stress Models in SH-SY5Y Cells.....	131
4.1.2 Neuroprotective Effects of Natural and Synthetic Antioxidants .....	135
4.1.3 Aims and Objectives .....	139
4.1.4 Introduction to the Analytical Techniques used in this chapter .....	140
4.1.4.1 Cell Viability Measurement-MTT assay .....	140
4.1.4.2 ROS determination using 2',7'-dichlorodihydrofluorescein diacetate (H <sub>2</sub> DCFDA) dye .....	141
4.1.4.3 DNA Damage Evaluation using the COMET assay .....	143
4.1.4.4 Western Blotting for the Detection of Nuclear Nrf2 protein .....	145
4.2 Materials and Methods .....	148
4.2.1 Materials.....	148
4.2.2 Instrumentation.....	148
4.3 Methods.....	149
4.3.1 Cell Culturing .....	149
4.3.2 Cellular Toxicity of Selected Vanillin Derivatives.....	149
4.3.3 Protective Effects of Selected Vanillin Derivatives in presence of H <sub>2</sub> O <sub>2</sub> or Rotenone/Oligomycin A Cocktail stressor .....	150
4.3.4 Protective Effects of Vanillin Derivatives from ROS Induced by H <sub>2</sub> O <sub>2</sub> .....	151
4.3.5 DNA Damage Determination by Comet Assay .....	152
4.3.6 Evaluation of Nrf2 Pathway Activation.....	154
4.3.7 Statistical Analysis .....	156
4.4 Results and Discussion.....	157
4.4.1 Cellular Toxicity of Selected Vanillin Derivatives.....	157
4.4.2 Protective Effects of Vanillin Derivatives from H <sub>2</sub> O <sub>2</sub> -Induced Toxicity.....	160
4.4.3 Protective Effects of Vanillin Derivatives from Rotenone/Oligomycin A Cocktail-Induced Toxicity.....	166
4.4.4 Protective Effects of Vanillin Derivatives from ROS Induced by H <sub>2</sub> O <sub>2</sub> .....	169
4.4.5 DNA Comet Assay .....	172
4.4.6 Evaluation of Nrf2 Pathway Activation.....	174
4.5 Conclusions.....	179

<b>Chapter 5: Vanillin Derivatives as Multi-Targeted-Directed Ligands for Alzheimer’s Disease</b> .....	182
5.1. Introduction .....	183
5.1.1 An Overview on Neurodegeneration .....	183
5.1.2 Alzheimer’s Disease as a Multifactorial Disorder .....	183
5.1.3 Current Therapies for AD .....	188
5.1.4 AD Drug Development .....	189
5.1.5 The Multi-Target-Directed Ligands Approach to AD.....	190
5.1.5.1 AChE, a “Gorge-ous Enzyme” .....	191
5.1.5.2 Assays for the Determination of AChE Activity.....	193
5.1.5.3 Measurement of Amyloid Aggregation.....	195
5.1.5.4 Measurement of Drug Blood-brain Barrier (BBB) Permeation .....	196
5.1.6 Aims and Objectives.....	197
5.2 Materials and Methods.....	198
5.2.1 Materials .....	198
5.2.2 Instrumentation .....	198
5.3 Methods .....	198
5.3.1 AChE Inhibition Assay.....	198
5.3.2 Molecular Modelling.....	199
5.3.3 A $\beta_{(1-42)}$ Aggregation Inhibition Assay.....	200
5.3.4 Prediction of BBB Permeation .....	200
5.4 Results and Discussion .....	201
5.4.1 AChE Inhibition Assay.....	201
5.4.2 Molecular Modelling.....	206
5.4.3 A $\beta_{(1-42)}$ Aggregation Inhibition Assay .....	212
5.4.4 Prediction of BBB Permeation .....	215
5.5 Conclusions .....	218
<b>Chapter 6: Conclusion and Future Work</b> .....	220
Future Work .....	226
<b>References</b> .....	230
<b>Appendix</b> .....	279
Spectral Data.....	279

## LIST OF TABLES

Table 3.1. Antioxidant properties of vanillin derivatives using the DPPH assay. ....	108
Table 3.2. Antioxidant properties of vanillin derivatives using the FRAP assay. ....	116
Table 3.3. Antioxidant properties of vanillin derivatives in ORAC assay. ....	120
Table 3.4. Protective effects of vanillin derivatives against AAPH-mediated DNA damage. ....	123
Table 5.1. AChE inhibitory activity of selected vanillin derivatives. ....	204
Table 5.2. BBB permeation prediction for selected vanillin derivatives. ....	216

## LIST OF FIGURES

Figure 1.1 ROS generation in mitochondria, adapted from Tang <i>et al.</i> (2014). .....	4
Figure 1.2. Free radical mechanism of the conversion of AA into prostaglandin GG2, adapted from Marnett <i>et al.</i> (1999).....	6
Figure 1.3. Cells and mediators of the inflammatory response (Newton and Dixit, 2012). .....	9
Figure 1.4. Hierarchal oxidative stress model, adapted from Gloire, Legrand-Poels, and Piette (2006) with copyright agreement © 2006 Elsevier Inc. ....	11
Figure 1.5. Chemical structures of L-DOPA (left) and Selegiline (right). ....	12
Figure 1.6. Chemical structure of resveratrol. ....	13
Figure 1.7. Chemical structure of curcumin.....	14
Figure 1.8. Cholesterol transport in human body, adapted from Shinkai (2012).....	15
Figure 1.9. Chemical structure of 3-methyl-1-phenyl-2-pyrazolin-5-one (Edaravone) and its keto-enol tautomerization. ....	16
Figure 1.10. Chemical structures of sulphorapane (top left), dimethyl fumarate (top right), paraquat (bottom left) and 4-HNE (bottom right). ....	19
Figure 1.11. Proposed Nrf2-ARE signaling pathway, adapted from Cabrera <i>et al.</i> (2015). .....	19
Figure 1.12. Natural and synthetic antioxidants and their chemical structures.....	21
Figure 1.13. Chemical structure of L-Glutathione.....	22
Figure 1.14. Chemical structures of ( <i>R</i> )-DHHA (left) and ( <i>R</i> )-lipoic acid (right). ....	23
Figure 1.15. Chemical structures of functional vitamin A molecules, adapted from Tanumihardjo (2011). ....	24
Figure 1.16. <i>L</i> -ascorbic acid (vitamin C). ....	25
Figure 1.17. Synergistic effects of Vitamin C and E against lipid peroxidation, adapted from Marian Valko <i>et al.</i> (2004) with copyright agreement © 2006 Springer Nature...	26
Figure 1.18. Chemical structures of Flavonoids. ....	27
Figure 1.19. Benzoic acid derivatives (left) and Cinnamic acid derivatives (right) chemical structures. The substituents in the aromatic rings (R) are often hydrogen, hydroxy and methoxy groups. ....	28
Figure 1.20. Chemical structure of vanillin. ....	29
Figure 1.21. Mechanism of rotenone toxicity, adapted from Xu, Shang, and Jiang (2016) with copyright agreement © 2016 Royal Society of Chemistry. ....	30
Figure 1.22. BHA (left) and BHT (right) chemical structures.....	31
Figure 1.23. Propyl gallate chemical structure .....	32
Figure 1.24. Chemical structure of Trolox.....	32
Figure 1.25. Trolox-lipoic acid hybrid reported by Koufaki <i>et al.</i> (2001). ....	33

Figure 1.26. Chemical structures of 4-vinylphenol (4-VP), 4-vinylguaiacol (4-VG), 4-vinylsyringol (4-VS), 4-vinylcatechol (4-VC) and their corresponding hydroxycinnamic acids reported by Terpinc <i>et al.</i> (2011) .....	34
Figure 1.27. Most active gallic acid derivatives reported by (Khaledi <i>et al.</i> , 2011); compound 3e (X = Cl) and compound 3f (X = Br). .....	35
Figure 1.28. Synthetic resveratrol analogue reported by Li, Wang, and Kong (2014). ...	36
Figure 1.29. Resveratrol-pyridoxine hybrid reported by Yang <i>et al.</i> (2017).....	36
Figure 1.30. Tacrine-melatonin hybrid described by Benchekroun <i>et al.</i> (2016).....	37
Figure 1.31. General structures of tacrine-ferulic acid-NO donors reported by Chen <i>et al.</i> (2012).....	37
Figure 1.32. Chemical structure of ( <i>E</i> )-5,6-dihydroxy-2-(4-(methyl(propyl)amino)benzylidene)-2,3-dihydro-1H-inden-1-one reported by Huang <i>et al.</i> (2012).....	38
Figure 1.33. Chemical structure of ( <i>E</i> )- <i>N</i> -(4-((benzyl(methyl)amino)methyl)phenyl)-3-(3,4-dihydroxyphenyl)acrylamide described by Wang <i>et al.</i> (2017). .....	38
Figure 1.34. Dimethylaminomethyl substituted curcumin derivative reported by Fang <i>et al.</i> (2014).....	39
Figure 1.35. Synthetic triterpenoids TP-224 (X = -Me), TP-319 (X = -Et) and TP-500 (X = -CH <sub>2</sub> -CF <sub>3</sub> ) described by Kaidery <i>et al.</i> (2013). .....	40
Figure 1.36. Methyl (( <i>S</i> )-2-acetamido-3-(3,4-dihydroxyphenyl)propanoyl)-L-methioninate, reported by Pinnen <i>et al.</i> (2009). .....	41
Figure 1.37. CNB-001 chemical structure.....	41
Figure 1.38. <i>N</i> -(2-aminophenyl)-4-hydroxy-1-methyl-2-oxo-1,2-dihydroquinoline-3-carboxamide described by Detsi <i>et al.</i> (2007).....	43
Figure 1.39. 4-methyl-2-(10H-phenothiazin-2-yl)morpholin-2-ol reported by Matralis and Kourounakis (2014). .....	44
Figure 1.40. ( <i>E</i> )-2-(2-(5-(benzo[d][1,3]dioxol-5-yl)-1-(4-sulfamoylphenyl)-1H-pyrazole-3-carbonyl)hydrazineylidene)propanoic acid reported by El Razik <i>et al.</i> (2017).....	45
Figure 2.1. Synthetic approach for the synthesis of vanillin derivatives reported by Harini <i>et al.</i> (2012), adapted with copyright agreement © 2012 Elsevier Ltd. ....	48
Figure 2.2. Synthetic strategy for the synthesis of vanillin derivatives reported by Rangaswamy <i>et al.</i> (2012), adapted with copyright agreement © 2012 Elsevier Ltd.....	49
Figure 2.3. Synthetic approach for the synthesis of vanillin derivatives reported by Dangar, Borkhataria, and Shah (2014). .....	50
Figure 2.4. Synthetic process for the synthesis of ethylvanillin. ....	51
Figure 2.5. Synthetic strategy for the dendrimer reported by Lee <i>et al.</i> (2009), with copyright agreement © 2009 Elsevier Ltd.....	52
Figure 2.6. Synthetic strategy for the synthesis of dendrimer adapted from Lee <i>et al.</i> (2015), with copyright agreement © 2015 Elsevier Ltd. ....	53
Figure 2.7. Synthetic strategy for the synthesis of the vanillin derivatives reported by Chigurupati <i>et al.</i> (2018). Reproduced with copyright agreement © 2017, Springer Science Business Media, LLC. ....	54

Figure 2.8. General structures of the proposed vanillin derivatives. ....	55
Figure 2.9. Thin Layer Chromatography plate. ....	59
Figure 2.10. <sup>1</sup> H NMR spectrum of Intermediate 1 ( <b>I-1</b> ). ....	75
Figure 2.11. <sup>13</sup> C NMR spectrum of intermediate 1 ( <b>I-1</b> ). ....	76
Figure 2.12. LRMS spectrum of intermediate 1 ( <b>I-1</b> ). ....	77
Figure 2.13. <sup>1</sup> H NMR spectrum of <b>1d</b> . ....	78
Figure 2.14. <sup>13</sup> C NMR spectrum of <b>1d</b> . ....	79
Figure 2.15. HRMS spectrum of compound <b>1d</b> . ....	79
Figure 2.16. Reaction pathway of reductive amination, described by (Baxter and Reitz, 2002). ....	80
Figure 2.17. <sup>1</sup> H NMR spectrum of dimer <b>2b</b> . ....	81
Figure 2.18. <sup>13</sup> C NMR spectrum of dimer <b>2b</b> . ....	82
Figure 2.19. HRMS of dimer <b>2b</b> . ....	83
Figure 2.20. <sup>1</sup> H NMR spectrum of tetramer <b>4c</b> . ....	84
Figure 2.21. <sup>13</sup> C NMR spectrum of tetramer <b>4c</b> . ....	84
Figure 2.22. HRMS spectrum of tetramer <b>2c</b> . ....	85
Figure 2.23. Chemical structures of related vanillin derivatives bearing different hydroxy and methoxy groups. ....	86
Figure 2.24. Chemical structures of compounds <b>4c</b> (left) and <b>4b</b> (right). ....	87
Figure 3.1. Electronic delocalisation of the lone electron in DPPH molecule. ....	91
Figure 3.2. Mechanism of DPPH assay. ....	92
Figure 3.3. Mechanism of FRAP assay, adapted from Pérez-Cruz <i>et al.</i> (2018). ....	93
Figure 3.4. Formation of ABTS radical cation from ABTS with potassium persulfate, adapted from Moon and Shibamoto (2009) with Copyright agreement © 2009, American Chemical Society. ....	94
Figure 3.5. Mechanism of peroxy radical generation mediated by AAPH, adapted from Nimse and Pal (2015) Published by The Royal Society of Chemistry. ....	95
Figure 3.6. Example of NET area under the curve for ORAC assay. The latter can be measured calculating the area between the sample curve(s) and the blank. ....	96
Figure 3.7. Proposed fluorescein oxidation pathway in the presence of AAPH, adapted from Ou, Hampsch-Woodill, and Prior (2001) with Copyright agreement © 2001, American Chemical Society. ....	97
Figure 3.8. Formation of the MDA-TBA adduct, adapted from Janero (1990) with Copyright agreement © 1990 Published by Elsevier In. ....	98
Figure 3.9. DNA fragments separation using gel electrophoresis. Supercoiled DNA moves faster compared to the circular and linear fragments. ....	99
Figure 3.10. 96-well plate settings for DPPH assay. Two compounds can be tested at the same time. DPPH control is represented in purple, the first antioxidant is represented in blue and the second antioxidant is represented in red (different shades represent different concentrations tested). ....	101

Figure 3.11. 96-well plate settings for FRAP assay. Two compounds can be tested at once. Different concentrations of Trolox are represented in blue colour. The first antioxidant is represented in yellow and the second antioxidant is represented in red (different shades represent different concentrations tested).....	102
Figure 3.12. 96-well plate settings for ORAC assay. Fluorescein control is represented in purple colour and AAPH control is represented in grey colour. Different concentrations of Trolox are represented in blue colour whereas different concentrations of the antioxidant are represented in red (different shades represent different concentrations tested).....	103
Figure 3.13. 96-well plate for DPPH assay. Two compounds were tested per experiment. The wells in the red circle represent the DPPH control. The wells in the green and yellow circles represent two different compounds at different concentrations. The compound in the green circle showed higher activity in the assay due to the loss of colouration whereas the compound in the yellow circle did not show any activity in the assay.....	106
Figure 3.14. Example of DPPH assay results for derivative <b>1d</b> . The concentrations of compound were plotted in a graph along with the amount of unscavenged DPPH expressed as percentage. The linear portion of the curve was isolated and the IC <sub>50</sub> was calculated using the equation of the line. ....	107
Figure 3.15. Chemical structures of dimer <b>2g</b> and tetramer <b>4e</b> .....	109
Figure 3.16. Chemical structures of imines <b>1a</b> and <b>1b</b> .....	109
Figure 3.17. Chemical structure of compounds <b>1a</b> , <b>1c</b> and <b>2f</b> .....	110
Figure 3.18. Chemical structures of vanillin derivatives <b>1d</b> and <b>2f</b> and syringaldehyde derivatives <b>1e</b> and <b>2i</b> .....	111
Figure 3.19. Chemical structures of derivatives <b>2a-2e</b> .....	111
Figure 3.20. Chemical structures of derivatives <b>4a</b> , <b>4c</b> , <b>4d</b> and <b>4f</b> .....	112
Figure 3.21. Chemical structures of compounds <b>4b</b> and <b>4c</b> . The strong antioxidant properties of <b>4c</b> could be explained by the critical role of electronic delocalisation in the antioxidant activity.....	113
Figure 3.22. Chemical structures of Tacrine and monomer <b>1f</b> .....	113
Figure 3.23. 96-well plate for FRAP assay. Two compounds were tested at once. The wells within the red perimeter represent the Trolox control, with the highest concentrations on top. The wells within the green and yellow perimeters represent two different compounds at different concentrations. The compound in the green perimeter showed no activity in the assay, whereas the compound in the yellow perimeter was found to be active due the increase in blue colouration. ....	114
Figure 3.24. Example of results for derivative <b>1f</b> from the FRAP assay . The concentrations of Trolox and compound were plotted graphically, along with their corresponding absorbances. The slope of the line obtained were then compared to give the results, expressed in Trolox Equivalents (TE).....	115
Figure 3.25. Example of results for derivative <b>1f</b> using the ORAC assay. The areas under the curve (AUC) obtained were plotted against the corresponding concentrations of Trolox and antioxidant. The net AUCs were obtained by subtracting the curve from the blank. The linear portion of the calibration curve obtained for the antioxidant was	119

Figure 3.26. Example of DNA protection assay's results for tetramer <b>4c</b> . The intensity of each band was measured using Image J software and the amount of supercoiled DNA (%) was calculated by comparison with the DNA control. The linear portion of the curve was isolated and the IC <sub>50</sub> was determined using the equation of the line.....	122
Figure 3.27. Tetramer reported by (Lee <i>et al.</i> , 2009). .....	124
Figure 3.28. SAR for this class of vanillin derivatives. The number of vanillin moieties (blue), the phenolic and methoxy functionalities of the vanillin core (yellow and green, respectively), the nitrogen nucleophilicity (red) and electronic delocalisation (purple) are the key features for the antioxidant activity. ....	124
Figure 4.1. Undifferentiated SH-SY5Y cells (20x magnification, picture size adjusted to fit page). .....	130
Figure 4.2. Mechanism of decomposition of tBHP by Fe <sup>2+</sup> adapted from (Hix and Augusto, 1999), with copyright agreement © 1999 Elsevier Science Ireland Ltd. ....	132
Figure 4.3. Chemical structure of the macrolide oligomycin A.....	133
Figure 4.4. Mechanisms of rotenone and oligomycin A cocktail toxicity. ....	133
Figure 4.5. Chemical structures of dopamine and its related 6-OHDA.....	134
Figure 4.6. Chemical structure of salidroside. ....	136
Figure 4.7. Chemical structure of the pineal hormone melatonin. ....	137
Figure 4.8. Chemical structure of the synthetic lipoic acid derivative lipocrine, reported by (Rosini <i>et al.</i> , 2005).....	139
Figure 4.9. Summary of the experimental work described in this chapter. ....	140
Figure 4.10. MTT conversion in metabolic active cells. ....	141
Figure 4.11. Mechanism of fluorescence enhancement of the H <sub>2</sub> DCFDA induced by ROS, adapted from Eruslanov and Kusmartsev (2010), with copyright agreement © 2010, Humana Press, a part of Springer Science Business Media, LLC.....	142
Figure 4.12. Schematic of a flow cytometer. ....	143
Figure 4.13. Principle of protein detection through Western Blotting.....	146
Figure 4.14. Reaction mechanism of luminol-based chemiluminescence, adapted from Alegria-Schaffer, Lodge, and Vattem (2009).....	146
Figure 4.15. 96-well plate settings for MTT assay. Media control is coloured in purple whereas the hydrogen peroxide or the rotenone/oligomycin mixture controls are rendered in pink. The different shades of blue represent different concentrations of the vanillin derivative tested ( <b>1f</b> , <b>2b</b> or <b>4c</b> ). ....	151
Figure 4.16. DNA Comet scoring criteria.....	153
Figure 4.17. MTT cell viability assay using compound <b>2b</b> (25 - 1000 µM, for 24 hrs). One-way ANOVA analysis was used for the comparison between the media control and each condition. ***p ≤ 0.001, ns = not significant, n=3. ....	158
Figure 4.18. The <i>p</i> -phenylene diamine moiety (in red) in both compounds <b>1f</b> and <b>4c</b> . In addition, the tacrine moiety of compound <b>1f</b> is highlighted in blue. ....	158
Figure 4.19. MTT cell viability assay using compound <b>4c</b> (0.1 - 50 µM, for 24 hrs). One-way ANOVA analysis was used for the comparison between the media control and each condition. ***p ≤ 0.001, ns = not significant, n=3. ....	159

Figure 4.20. MTT cell viability assay using compound <b>1f</b> (3.125 - 100 $\mu$ M, for 24 hrs). One-way ANOVA analysis was used for the comparison between the media control and each condition. *** $p \leq 0.001$ , ns = not significant, n=3. ....	159
Figure 4.21. Tacrine-dihydrobenzofuran hybrid reported by Zha et al. (2016) .....	160
Figure 4.22. Protective effects of vanillin in hydrogen peroxide (400 $\mu$ M)-stressed cells. One-way ANOVA analysis was used for the comparison between the peroxide control and each condition. ns = not significant, n=3. ....	161
Figure 4.23. Protective effects of <b>1f</b> in hydrogen peroxide (400 $\mu$ M)-stressed cells. One-way ANOVA analysis was used for the comparison between the peroxide control and each condition. *** $p \leq 0.001$ , * $p \leq 0.05$ , ns = not significant, n=3. ....	162
Figure 4.24. Neuroprotective agent against hydrogen peroxide-induced oxidative insult reported by Benchekroun <i>et al</i> (2016). The tacrine moiety is highlighted in red. ....	162
Figure 4.25. Protective effects of <b>2b</b> in hydrogen peroxide (400 $\mu$ M)-stressed cells. One-way ANOVA analysis was used for the comparison between the peroxide control and each condition. *** $p \leq 0.001$ , ** $p \leq 0.01$ , ns = not significant, n=3. ....	163
Figure 4.26. Protective effects of <b>4c</b> in hydrogen peroxide (400 $\mu$ M)-stressed cells. One-way ANOVA analysis was used for the comparison between the peroxide control and each condition. *** $p \leq 0.001$ , ** $p \leq 0.01$ , * $p \leq 0.05$ , ns = not significant, n=3. ....	164
Figure 4.27. Morphology of untreated (a), hydrogen peroxide-stressed (400 $\mu$ M) (b) or pre-treated with <b>4c</b> (10 $\mu$ M) (c) cells during MTT assay (20x magnification, picture size adjusted to fit page). ....	165
Figure 4.28. An example of MTT assay for the evaluation of the protective effects of compound <b>4c</b> in the hydrogen peroxide oxidative stress model. The wells circled in green correspond to the media control, whereas the wells circled in red correspond to the hydrogen peroxide control. Decreasing concentrations of compound 4c (from left to right) are circled in orange. ....	166
Figure 4.29. Protective effects of vanillin in rotenone/oligomycin (3 and 1 $\mu$ M, respectively)-stressed cells. One-way ANOVA analysis was used for the rotenone/oligomycin A control and each condition. *** $p \leq 0.001$ , ns = not significant, n=3. ....	167
Figure 4.30. Protective effects of <b>1f</b> and <b>2b</b> in rotenone/oligomycin (3 and 1 $\mu$ M, respectively)-stressed cells. One-way ANOVA analysis was used for the rotenone/oligomycin A control and each condition. *** $p \leq 0.001$ , ns = not significant, n=3. ....	168
Figure 4.31. Protective effects of <b>4c</b> in rotenone/oligomycin (3 and 1 $\mu$ M, respectively)-stressed cells. One-way ANOVA analysis was used for the rotenone/oligomycin A control and each condition. *** $p \leq 0.001$ , ns = not significant, n=3. ....	169
Figure 4.32. Raw data obtained from flow cytometry, showing the number of cells (events) and their associated fluorescence intensity on a logarithmic scale (FL1 LOG). ....	170
Figure 4.33. Protective effects of dimer <b>2b</b> against ROS production induced by hydrogen peroxide (1 mM, 30 mins). Statistically significant difference determined using One-Way ANOVA. *** $p \leq 0.001$ , ns = not significant n = 3. ....	171

Figure 4.34. Protective effects of tetramer <b>4c</b> against ROS production induced by hydrogen peroxide (1 mM, 30 mins). Statistically significant difference determined using One-Way ANOVA. *** $p \leq 0.001$ , ns = not significant $n = 3$ .....	171
Figure 4.35. Chemical structure of glycoside loganin. ....	172
Figure 4.36. Comet classes (0-4) obtained in the comet assay. Leica DMRB microscope (100x) with Leica DFC 300FX camera (0.63x).....	173
Figure 4.37. Cellular DNA protection from H <sub>2</sub> O <sub>2</sub> -induced (300 $\mu$ M) DNA strand breaks after pre-treatment with <b>2b</b> (200 $\mu$ M) or <b>4c</b> (10 $\mu$ M) for 24 hours. Statistically significant difference using One-Way ANOVA compared with peroxide control. *** $p \leq 0.001$ , ns = not significant, $n = 3$ . ....	173
Figure 4.38. Western Blot for cytoplasmic (green) and nuclear (red) extracts after different time exposure of the cells to tetramer <b>4c</b> . ....	175
Figure 4.39. A) Representative western blot analysis performed by Prof. Galli and co-workers at the University of Perugia showing Nrf2 expression in SH-SY5Y cells after treatment with compound <b>4c</b> (10 $\mu$ M). B) Densitometry for the WB analysis. Data represent the means $\pm$ SD of 3 experiments (* $p < 0.05$ , compared with the control group).....	177
Figure 4.40. Examples of known Nrf2 activator.....	178
Figure 5.1. APP cleavage in the non-amyloidogenic and amyloidogenic pathways, altered from (Munoz and Feldman, 2000; Bachurin, Bovina and Ustyugov, 2017; Cheignon <i>et al.</i> , 2018). ....	185
Figure 5.2. Chemical structure of acetylcholine .....	187
Figure 5.3. Chemical structures of current AChE inhibitors for AD treatment (donepezil, galantamine and rivastigmine) and the discontinued tacrine. ....	189
Figure 5.4. Chemical structure of memantine. ....	189
Figure 5.5. Active site of TcAChE (pdb:1EVE) (Kryger, Silman and Sussman, 1999). The residues are rendered accordingly to their positions. Esteratic site: purple, CAS: yellow, Acyl Pocket: grey, Oxyanion Hole: green and PAS: orange.....	192
Figure 5.6. Mechanism of acetylcholine hydrolysis catalysed by AChE, altered from (Houghton, Ren and Howes, 2006; Colovic <i>et al.</i> , 2013) .....	193
Figure 5.7. Mechanism of Ellman assay for the determination of AChE inhibition, altered from (Worek, Eyer and Thiermann, 2012; Badawy and El-Aswad, 2014). ....	194
Figure 5.8. Chemical structure of Thioflavin T. ....	195
Figure 5.9. 96-well plate settings for Ellman assay. Two compounds can be tested at the same time. The control is represented in yellow, the first AChE inhibitor is represented in blue and the second AChE inhibitor is represented in orange (different shades represent different concentrations tested). ....	199
Figure 5.10. Vanillin derivatives tested in the Ellman assay. ....	201
Figure 5.11. 96-well plate for Ellman assay. Two compounds were tested at once. The wells in the red circle represent the control. The wells in the blue and green circles represent two different compounds at different concentrations. The loss in yellow colouration compared to the control is proportional to the AChE inhibitory activity. ....	202

Figure 5.12. Example of Ellman assay's results for derivative <b>1f</b> . The concentrations of compound were plotted in a graph along with the amount of active AChE expressed as percentage. The linear portion of the curve was isolated and the IC <sub>50</sub> was calculated using the equation of the line. ....	203
Figure 5.13. Derivatives reported by Gao <i>et al.</i> (2016). The naphthalimido moiety is rendered in red.....	205
Figure 5.14. Multialkoxybenzene derivatives reported by Luo <i>et al.</i> (2011).....	205
Figure 5.15. Superimposition of original (yellow) and redocked (red) ligands in their corresponding crystal structures and relative RMSD.....	207
Figure 5.16. Superimposed structures of compound <b>1d</b> (left) and <b>1f</b> (right) with the original ligand (yellow) in 2CMF AChE structure.....	208
Figure 5.17. Predicted binding model of <b>1d</b> in the CAS of 2CMF AChE structure.....	208
Figure 5.18. Predicted binding model of <b>1f</b> in the CAS of 2CMF AChE structure.....	209
Figure 5.19. Predicted binding model of <b>1d</b> in the PAS of 2CMF AChE structure.....	210
Figure 5.20. Predicted binding model of <b>1f</b> in the PAS of 2CMF AChE structure.....	211
Figure 5.21. Predicted binding models for compounds <b>1d</b> and <b>1f</b> within the active site of TcAChE.....	211
Figure 5.22. Self-mediated amyloid aggregation inhibitory effects of vanillin derivatives. All the compounds were tested at concentration of 10 μM. Values are expressed as the percentage of the control and represented as mean ± SD of three independent experiments in each group. ***p < 0.001, *p < 0.05, ns = no significantly different compared to the control. ....	213
Figure 5.23. Vanillin derivatives tested in the amyloid aggregation inhibition assay. The aromatic moieties are coloured in black whereas the linker is rendered in red. Phenolic moieties are circled in blue. ....	214
Figure 5.24. Prediction of BBB permeation for tacrine obtained through the online predictor <a href="http://www.cbligand.org/BBB">www.cbligand.org/BBB</a> .....	215
Figure 6.1. Summary of the properties of most promising vanillin derivatives, monomer <b>1f</b> and tetramer <b>4c</b> .....	226
Figure 6.2. Possible mechanisms behind the protective effects of compound <b>4c</b> in SH-SY5Y cell line. Adapted from (Mattson and Camandola, 2001; Palanki, 2002; Ye <i>et al.</i> , 2014; Lan <i>et al.</i> , 2017) .....	227
Figure 6.3. Synthetic strategy for novel vanillin-tacrine hybrids.....	228
Figure A1. <sup>1</sup> H NMR spectrum of intermediate <b>I-1</b> . ....	280
Figure A2. <sup>13</sup> C NMR spectrum of intermediate <b>I-1</b> . ....	281
Figure A3. LRMS spectrum of intermediate <b>I-1</b> . ....	282
Figure A4. <sup>1</sup> H NMR spectrum of intermediate <b>I-2</b> . ....	283
Figure A5. <sup>13</sup> C NMR spectrum of intermediate <b>I-2</b> . ....	284
Figure A6. LRMS spectrum of intermediate <b>I-2</b> . ....	285
Figure A7. <sup>1</sup> H NMR spectrum of intermediate <b>I-3</b> . ....	286
Figure A8. <sup>13</sup> C NMR spectrum of intermediate <b>I-3</b> . ....	287

Figure A9. LRMS spectrum of intermediate <b>1-3</b> .....	288
Figure A10. <sup>1</sup> H NMR spectrum of compound <b>1a</b> .....	289
Figure A11. <sup>13</sup> C NMR spectrum of compound <b>1a</b> .....	290
Figure A12. HRMS spectrum of compound <b>1a</b> .....	291
Figure A13. <sup>1</sup> H NMR spectrum of compound <b>1b</b> .....	292
Figure A14. <sup>13</sup> C NMR spectrum of compound <b>1b</b> .....	293
Figure A15. HRMS spectrum of compound <b>1b</b> .....	294
Figure A16. <sup>1</sup> H NMR spectrum of compound <b>1c</b> .....	295
Figure A17. <sup>13</sup> C NMR spectrum of compound <b>1c</b> .....	296
Figure A18. HRMS spectrum of compound <b>1c</b> .....	297
Figure A19. <sup>1</sup> H NMR spectrum of compound <b>1d</b> .....	298
Figure A20. <sup>13</sup> C NMR spectrum of compound <b>1d</b> .....	299
Figure A21. HRMS spectrum of compound <b>1d</b> .....	300
Figure A22. <sup>1</sup> H NMR spectrum of compound <b>1e</b> .....	301
Figure A23. <sup>13</sup> C NMR spectrum of compound <b>1e</b> .....	302
Figure A24. HRMS spectrum of compound <b>1e</b> .....	303
Figure A25. <sup>1</sup> H NMR spectrum of compound <b>1f</b> .....	304
Figure A26. <sup>13</sup> C NMR spectrum of compound <b>1f</b> .....	305
Figure A27. HRMS spectrum of compound <b>1f</b> .....	306
Figure A28. <sup>1</sup> H NMR spectrum of compound <b>2a</b> .....	307
Figure A29. <sup>13</sup> C NMR spectrum of compound <b>2a</b> .....	308
Figure A30. HRMS spectrum of compound <b>2a</b> .....	309
Figure A31. <sup>1</sup> H NMR spectrum of compound <b>2b</b> .....	310
Figure A32. <sup>13</sup> C NMR spectrum of compound <b>2b</b> .....	311
Figure A33. HRMS spectrum of compound <b>2b</b> .....	312
Figure A34. <sup>1</sup> H NMR spectrum of compound <b>2c</b> .....	313
Figure A35. <sup>13</sup> C NMR spectrum of compound <b>2c</b> .....	314
Figure A36. HRMS spectrum of compound <b>2c</b> .....	315
Figure A37. <sup>1</sup> H NMR spectrum of compound <b>2d</b> .....	316
Figure A38. <sup>13</sup> C NMR spectrum of compound <b>2d</b> .....	317
Figure A39. HRMS spectrum of compound <b>2d</b> .....	318
Figure A40. <sup>1</sup> H NMR spectrum of compound <b>2e</b> .....	319
Figure A41. <sup>13</sup> C NMR spectrum of compound <b>2e</b> .....	320
Figure A42. HRMS spectrum of compound <b>2e</b> .....	321
Figure A43. <sup>1</sup> H NMR spectrum of compound <b>2f</b> .....	322
Figure A44. <sup>13</sup> C NMR spectrum of compound <b>2f</b> .....	323
Figure A45. HRMS spectrum of compound <b>2f</b> .....	324

Figure A46. $^1\text{H}$ NMR spectrum of compound <b>2g</b> .	325
Figure A47. $^{13}\text{C}$ NMR spectrum of compound <b>2g</b> .	326
Figure A48. HRMS spectrum of compound <b>2g</b> .	327
Figure A49. $^1\text{H}$ NMR spectrum of compound <b>2h</b> .	328
Figure A50. $^{13}\text{C}$ NMR spectrum of compound <b>2h</b> .	329
Figure A51. HRMS spectrum of compound <b>2h</b> .	330
Figure A52. $^1\text{H}$ NMR spectrum of compound <b>2i</b> .	331
Figure A53. $^{13}\text{C}$ NMR spectrum of compound <b>2i</b> .	332
Figure A54. HRMS spectrum of compound <b>2i</b> .	333
Figure A55. $^1\text{H}$ NMR spectrum of compound <b>4a</b> .	334
Figure A56. $^{13}\text{C}$ NMR spectrum of compound <b>4a</b> .	335
Figure A57. HRMS spectrum of compound <b>4a</b> .	336
Figure A58. $^1\text{H}$ NMR spectrum of compound <b>4b</b> .	337
Figure A59. $^{13}\text{C}$ NMR spectrum of compound <b>4b</b> .	338
Figure A60. HRMS spectrum of compound <b>4b</b> .	339
Figure A61. $^1\text{H}$ NMR spectrum of compound <b>4c</b> .	340
Figure A62. $^{13}\text{C}$ NMR spectrum of compound <b>4c</b> .	341
Figure A63. HRMS spectrum of compound <b>4c</b> .	342
Figure A64. $^1\text{H}$ NMR spectrum of compound <b>4d</b> .	343
Figure A65. $^{13}\text{C}$ NMR spectrum of compound <b>4d</b> .	344
Figure A66. HRMS spectrum of compound <b>4d</b> .	345
Figure A67. $^1\text{H}$ NMR spectrum of compound <b>4e</b> .	346
Figure A68. $^{13}\text{C}$ NMR spectrum of compound <b>4e</b> .	347
Figure A69. HRMS spectrum of compound <b>4e</b> .	348
Figure A70. $^1\text{H}$ NMR spectrum of compound <b>4f</b> .	349
Figure A71. $^{13}\text{C}$ NMR spectrum of compound <b>4f</b> .	350
Figure A71. HRMS spectrum of compound <b>4f</b> .	351



## LIST OF ABBREVIATIONS AND ACRONYMS

4-HNE	4-hydroxynonenal
6-OHDA	6-hydroxydopamine
AA	Arachidonic acid
AAPH	2,2'-azobis(2-amidinopropane)
ABS	Absorbance
ABTS	2,2-azino-bis(3-ethylbenz-thiazoline-6-sulfonic acid)
ACh	Acetylcholine
AChE	Acetylcholinesterase
AD	Alzheimer's disease
ADME	Absorption, distribution, metabolism and excretion
ADP	Adenosine diphosphate
ATCC	American type culture collection
ALS	Amyotrophic lateral sclerosis
AMP	Adenosine monophosphate
AP-1	Activator protein 1
APP	Amyloid precursor protein
APS	Ammonium persulfate
ARE	Antioxidant responsive element
ATP	Adenosine triphosphate
AUC	Area under the curve
A $\beta$	Amyloid beta
BACE	$\beta$ -Secretase
BBB	Blood brain barrier
BChE	Butyrylcholinesterase
BHA	Butylated hydroxyanisole
BHT	Butylated hydroxytoluene
BSA	Bovine serum albumin
CAMs	Cell adhesion molecules
CAS	Catalytic anionic site
CBA	Cyclohexyl bisphenol A
CER	Cytoplasmic extraction reagent
CNS	Central nervous system

COXs	Cyclooxygenases
DA	Dopamine
DAPI	4',6-diamidino-2-phenylindole
DAT	Dopamine transporter
DCF	Dichlorofluorescein
DCFDA	2',7'-dichlorodihydrofluorescein diacetate
DCFH	2',7'-dichlorodihydrofluorescein
DCM	Dichloromethane
DGLA	Dihomo-gamma-linoleic Acid
DHLA	Dihydrolipoic acid
DMF	<i>N,N</i> -dimethylformamide
DMNQ	2,3-dimethoxy-1,4-naphtoquinone
DMSO	Dimethyl sulfoxide
DMTs	Disease-modifying therapies
DNA	Deoxyribonucleic acid
DPPH	2,2-diphenyl-1-picrylhydrazyl
DTNB	5,5'-dithiobis-(2-nitrobenzoic acid)
EDTA	Ethylenediaminetetraacetic acid
Enos	Endothelial nitric oxide synthase
EPA	Eicosapentaenoic acid
EPSRC	Engineering and physical sciences research council
ERKs	Extracellular signal-regulated kinases
ET	Electron transfer
FBS	Fetal serum bovine
FCR	Folin-Ciocalteu reagent
FRAP	Ferric reducing/antioxidant power
FSC	Forward scatter
GCLc	Glutamate-cysteine ligase catalytic subunit
GCLM	Glutamate-cysteine ligase regulatory subunit
GPx	Glutathione peroxidase
GSH	Glutathione
GSR	Glutathione-disulfide reductase
GSSG	Glutathione disulfide
GST	Glutathione S-transferase
H <sub>2</sub> DCFDA	2',7'-dichlorodihydrofluorescein diacetate
HAT	Hydrogen atom transfer

HDL	High-density lipoprotein
HO-1	Haem-oxygenase-1
HRMS	High resolution mass spectrometry
HRP	Horseradish peroxidase
IC <sub>50</sub>	Half maximal inhibitory concentration 50
IL	Interleukin
Inos	Inducible nitric oxide synthase
JNKs	c-Jun N-terminal kinases
KEAP	Kelch-like ECH-associated protein
LA	Lipoic acid
LC <sub>50</sub>	Lethal concentration 50
LDH	Lactate dehydrogenase
LDL	Low-density lipoproteins
LogP	Partition coefficient
LOXs	Lipoxygenases
LPS	Lipopolysaccharide
LRMS	Low resolution mass spectrometry
MAOs	Monoaminoxidases
MAPK	Mitogen-activated protein kinases
MC65	Human neuroblastoma cell line
MCI	Mild cognitive impairment
MDA	Malondialdehyde
MPP	1-methyl-4-phenylpyridinium
MPTP	1-methyl-4-phenyl-1,2,3,6-tetrahydropyridine
MS	Mass spectrometry
MTDLs	Multi-target-directed ligands
MTT	(3-(4,5-dimethylthiazol-2-yl)-2,5-diphenyltetrazolium bromide)
NAC	<i>N</i> -acetyl cysteine
NADPH	Nicotinamide adenine dinucleotide phosphate
NEAA	Non-essential amino acids
NER	Nuclear extraction reagent
NFTs	Neurofibrillary tangles
NF $\kappa$ B	Nuclear factor kappa-light-chain-enhancer
NMDA	<i>N</i> -methyl- <i>D</i> -aspartate
NMR	Nuclear magnetic resonance
xxx	

NOS	Nitric oxide synthase
NQO1	NAD(P)H dehydrogenase (quinone1)
NRF2	Nuclear factor E2-related factor 2
NSAIDs	Nonsteroidal anti-inflammatory drugs
ORAC	Oxygen radical absorbance capacity
PAMPA	Parallel artificial membrane permeation assay
PAS	Peripheral anionic site
PBS	Phosphate buffered saline
PC-12	Rat cell line
PD	Parkinson's disease
PG	Propyl gallate
PHF	Paired helical filaments
PKB	Protein kinase B
PUFA	Polyunsaturated fatty acids
PVDF	Polyvinylidene fluoride
RA	Retinoic acid
RMSD	Root-mean-square deviation
RNS	Reactive nitrogen species
ROS	Reactive oxygen species
RT	Room temperature
SAR	Structure-activity relationship
SDS	Sodium dodecylsulfate
SFRRI	Society for Free Radical Research International
SH-SY5Y	Human neuroblastoma cell line
SK-N-SH	Human neuroblastoma cell line
SOD	Superoxide dismutase
SQS	Squalene synthase
SSC	Side scatter
TBA	Thiobarbituric acid
tBHP	<i>Tert</i> -butyl hydroperoxide
tBHQ	<i>Tert</i> -butyl hydroquinone
TBST	Tris-buffered-saline + polysorbate 20
TE	Trolox Equivalents
TEA	Triethylamine
TAE	Tris-Acetic acid-EDTA
TEAC	Trolox equivalent antioxidant capacity

TEMED	Tetramethylethylenediamine
TH	Tyrosine hydroxylase
THF	Tetrahydrofuran
ThT	Thioflavin T
TLC	Thin layer chromatography
TNF	Tumor necrosis factor
TPA	12-O-tetradecanoyl-phorbol-13 acetate
TPTZ	2,4,6-Tri(2-pyridyl)-s-triazine
UV	Ultraviolet
VLDL	Very low-density lipoproteins
VMAT2	Vesicular monoamine transporter 2





# Thesis Layout

This thesis has been arranged in 6 chapters.

Each chapter has its own specific introduction, material and methods, results, discussion and conclusion sections.

Chapter 1 provides a general introduction on the background to the work

Chapter 2 discuss the chemical synthesis and characterization of novel vanillin derivatives.

In chapter 3, the antioxidant properties of this new class of compounds were studied using a number of *in vitro* assays including the 2,2-diphenyl-1-picrylhydrazyl (DPPH), ferric reducing/antioxidant power (FRAP), oxygen radical absorbance capacity (ORAC) and DNA protection assays.

Chapter 4 entails the cellular studies of a selection of the novel compounds using neuroblastoma SH-SY5Y cell line. Furthermore the cellular protective effects of those compounds against hydrogen peroxide and a mixture of the mitochondrial inhibitors (rotenone and oligomycin A) are discussed.

Chapter 5 introduces the concept of multi-targeted therapy for Alzheimer's disease, with particular attention to the antioxidant properties, the inhibitory activity towards acetylcholinesterase enzyme and the amyloid  $A\beta_{(1-42)}$  self-induced aggregation. The blood-brain-barrier permeability using *in silico* studies is also discussed.

Chapter 6 summarizes all the findings from this study and includes conclusions and future work sections.

# Chapter 1: Introduction

# 1.1 Oxidative Stress

## 1.1.1 *The Theory of Oxidative Stress*

Over the past few decades it has been proposed that oxidative stress is linked to the imbalance between reactive oxygen and nitrogen species (ROS and RNS) production and antioxidant defences, leading to oxidative damage to lipids, proteins and genetic material that contributes to the development of a range of different pathophysiological conditions (Sies, 1991, 2015). For a number of years, there has been strong evidence that linked oxidative stress to many different chronic conditions including neurodegenerative diseases (Alzheimer, Parkinson, Huntington), cardiovascular pathologies (atherosclerosis, heart failure), cancer and inflammation (Madamanchi, Vendrov and Runge, 2005; Lin and Beal, 2006; Reuter *et al.*, 2010).

## 1.1.2 *Sources and formation of Oxygen and Nitrogen Reactive Species*

ROS include both free radical and non-free radical oxygenated molecules. They are normally produced in aerobic processes such as respiration, immune system activation and physical activity or after exposure to toxins and/or pollutants such as alcohol, cigarette smoke, ionizing and UV radiations, pesticides and ozone. In contrast, at low concentrations, ROS are involved in different and important physiological processes, e.g. as signalling molecule in cell proliferation and apoptosis (Poljsak, Šuput and Milisav, 2013b).

The most important endogenous source of ROS is the mitochondrial electron transport chain that leads to the production of heat and chemical energy in the form of adenosine 5-triphosphate (ATP) after the oxidation of carbon and hydrogen-containing biomolecules (Gutteridge, 1994).

A detailed scheme of ROS production and regulation in mitochondria is illustrated in figure 1.1.

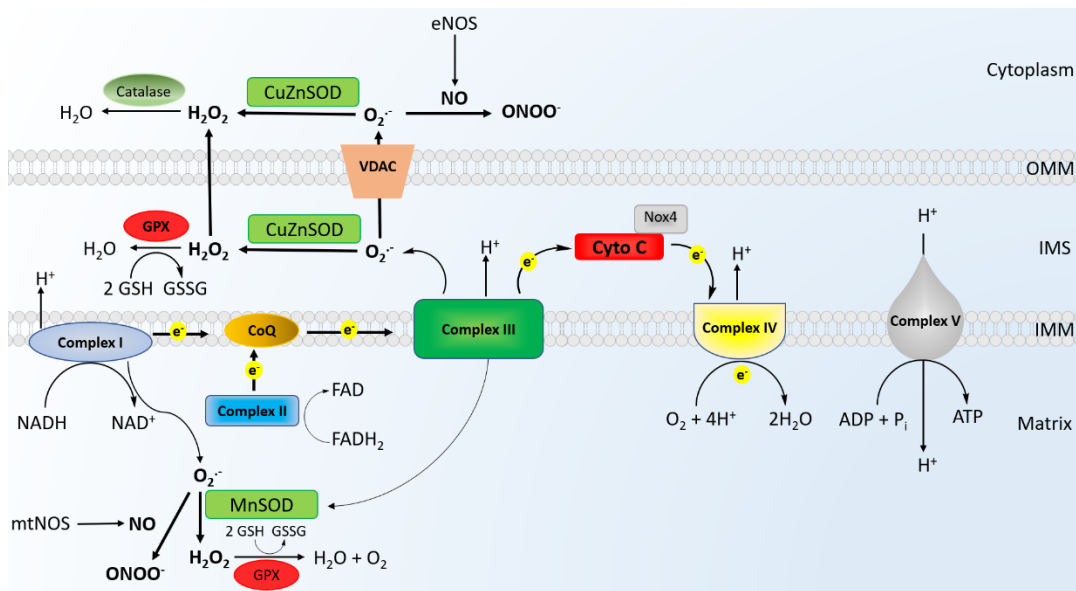
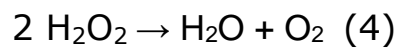
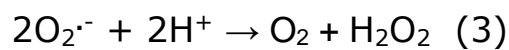
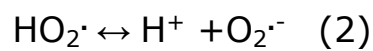
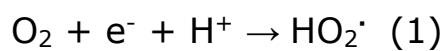


Figure 1.1 ROS generation in mitochondria, adapted from Tang *et al.* (2014), Copyright © 2014 Tang, Luo, Chen and Liu.

Mitochondria are the cell's metabolic site involved in ATP production, as well as in the regulation of apoptosis (Kroemer, Galluzzi and Brenner, 2007; Zhou *et al.*, 2011). The respiratory chain generates the proton gradient over the mitochondrial inner membrane that drives ATP generation by ATP synthase (complex V).

During this process, molecular oxygen is reduced stepwise into a series of intermediate and highly reactive species as shown by the following equations (Gutteridge, 1994):



Although molecular oxygen ( $\text{O}_2$ ) is not a free radical, it is however considered as a highly reactive oxygen species in which the spin restriction of oxygen (two unpaired electrons with parallel spins) is removed, which

enhances its oxidative power (Gutteridge, 1994). In equation (1), molecular oxygen is reduced into hydroperoxyl ( $\text{HO}_2\cdot$ ) radical which is in equilibrium, in aqueous solution, with the superoxide radical anion ( $\text{O}_2\cdot^-$ ) (2). The latter can be converted into hydrogen peroxide ( $\text{H}_2\text{O}_2$ ), a non-radical ROS, by enzymes belonging to the superoxide dismutase family (3) (Jomova *et al.*, 2010). Finally, hydrogen peroxide can be depleted by catalase (4) (Alfonso-Prieto *et al.*, 2009) or glutathione peroxidase (5) (Day, 2009).

Along with the electron transport chain, it is well established that enzymes such oxidases can produce high levels of ROS during normal physiological processes (Cadenas and Davies, 2000; Zangar, Davydov and Verma, 2004; Valko *et al.*, 2007).

The oxidase enzymes family includes:

- Cytochrome P450s: insert an oxygen atom into an aliphatic chain during the process of metabolism.
- Monoamine oxidase: removes the amino group from monoamines during the deamination process.
- NADPH oxidases: produce superoxide anion in response to pathogens, such as bacteria and fungi.
- Xanthine oxidase: promotes the oxidation of hypoxanthine to xanthine and can further catalyse the oxidation of xanthine to uric acid during the catabolism of purines.

ROS production is also linked with eicosanoid synthesis, a physiological process that converts free fatty acids into corresponding oxygenated derivatives during inflammation and immune response. Eicosanoids are produced from three different fatty acids, arachidonic acid (AA), eicosapentaenoic acid (EPA) and dihomo-gamma-linoleic acid (DGLA) through three different enzymes: cyclooxygenases (COXs), which produce prostanoids from AA, lipoxygenases (LOXs), which produce leukotrienes from AA and epoxygenases, involved in epoxyeicosatrienoic acids synthesis (Wang and DuBois, 2010). This family of compounds are involved in many physiological processes; for example, the prostanoids (prostaglandins, thromboxanes and prostacyclins) mediate symptoms of inflammation, such

as vascular permeability and fever, whereas leukotrienes stimulate immune responses (Rothwell, 1992; Dennis and Norris, 2015).

It has been shown that COX enzymes oxidize AA through a free radical mechanism that leads to the generation of prostaglandin after the formation of a lipid peroxy radical (see figure 1.2). (Marnett *et al.*, 1999); however, AA can be reduced, *via* non-enzymatic peroxidation into isoprostanes and other lipid peroxidation end-products, all are highly reactive and harmful to the cellular membranes (Ayala, Muñoz and Argüelles, 2014)

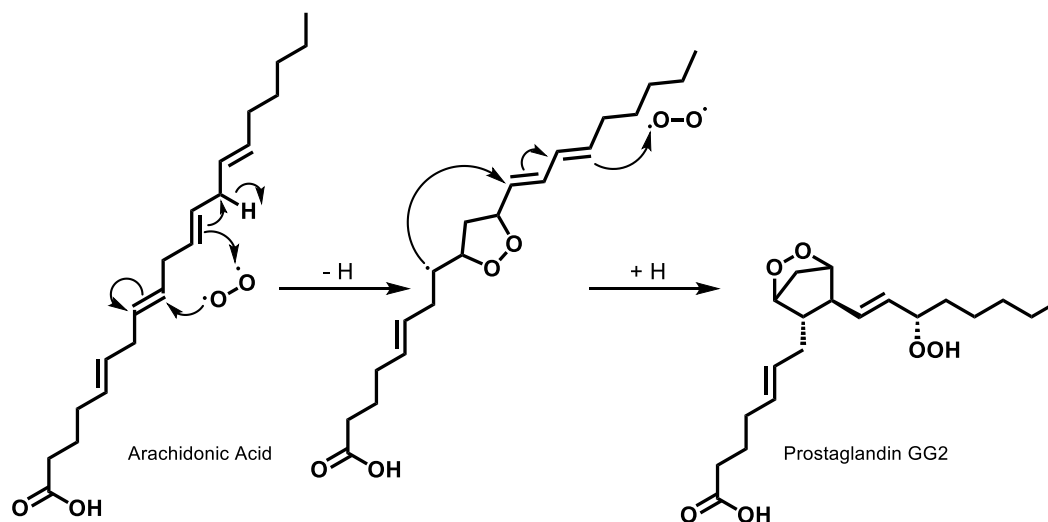
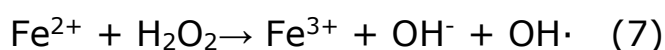


Figure 1.2. Free radical mechanism of the conversion of AA into prostaglandin GG2, adapted from Marnett *et al.* (1999), Copyright © AMERICAN SOC FOR BIOCHEMISTRY & MOLECULAR BIOLOGY .

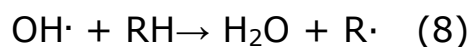
Furthermore, metal-catalysed processes are linked with ROS production. Almost one-third of all proteins contain transition metal ions such iron and copper: two of the most active and abundant redox-actives metals in the human body. It has been shown that divalent metal ions can reduce molecular oxygen to superoxide radicals (equation 6):



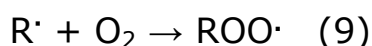
Furthermore, these ions can react with hydrogen peroxide, leading to the formation of the hydroxyl radical (Jomova, Baros and Valko, 2012) known as the Fenton reaction (equation 7). The latter plays a critical role in the oxidative stress process, since hydroxyl radical is the most reactive free radical.



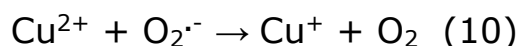
Due to its extreme reactivity, the hydroxyl radical has a short life-span and can react with alkyl chains of different molecules, removing the terminal hydrogen atom (equation 8) (Pignatello, Oliveros and MacKay, 2006):



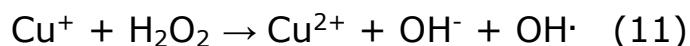
Finally, the alkyl radical easily reacts with molecular oxygen, leading to the formation of peroxy radical (equation 9):



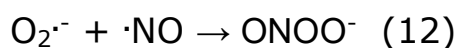
At the same time, copper ions can be involved in oxidation and reduction reactions; for example, cupric ions can be reduced into cuprous ions by superoxide radical ions (equation 10) (Gutteridge and Wilkins, 1983):



Cuprous ions can then lead to the generation of hydroxyl radicals *via* the Fenton reaction (equation 11).

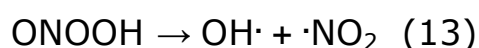


Along with ROS, reactive nitrogen species (RNS) play a critical role in oxidative stress. Nitric oxide ( $\cdot\text{NO}$ , commonly referred to as "NO") and nitrogen dioxide ( $\cdot\text{NO}_2$ ) contain unpaired electrons and are therefore considered to be free radicals. NO is biosynthesized by enzymes belonging to the nitric oxide synthase (NOS) family from L-arginine, oxygen and NADPH or by reduction of inorganic nitrate. This reactive nitrogen species exerts the role of signaling molecule, being involved in vasodilation, platelet aggregation and neurotransmission (Radomski, Palmer and Moncada, 1990; Moncada and Higgs, 1991). NO can react with superoxide radical anion leading to the generation of the highly reactive RNS peroxynitrite, a powerful oxidant against many biological molecules (equation 12) (Beckman and Crow, 1993)



The protonation of the latter can occur, yielding a strong oxidizing agent (ONOOH) that is able to oxidize proteins and to cause DNA damage, in addition to the nitration of aromatic amino acids such as tyrosine (Sawa, Akaike and Maeda, 2000).

Furthermore, it can decompose to yield hydroxyl radicals (equation 13) (Gutteridge, 1994):



### *1.1.3 The Role of Oxidative Stress in Diseases*

#### *1.1.3.1 Oxidative Stress in Inflammation and Cancer*

Over 5000 years ago, the traditional Ayurvedic medical system reported that continuous irritation over long period can lead to cancer (Reuter *et al.*, 2010).

However, the relationship between inflammation and cancer was only confirmed two centuries ago, when Rudolph Virchow noted leukocytes, cells of the immune system, in neoplastic tissue. He suggested that the infiltration of white blood cells in tumour tissue reflects the origin of cancer at sites of chronic inflammation (Balkwill and Mantovani, 2001). Today, although most of the molecular and cellular mechanism for the link between inflammation and cancer are still unresolved, the relationship has been generally accepted.

Inflammation is the biological response to tissue injury and a detailed scheme is reported in figure 1.3.

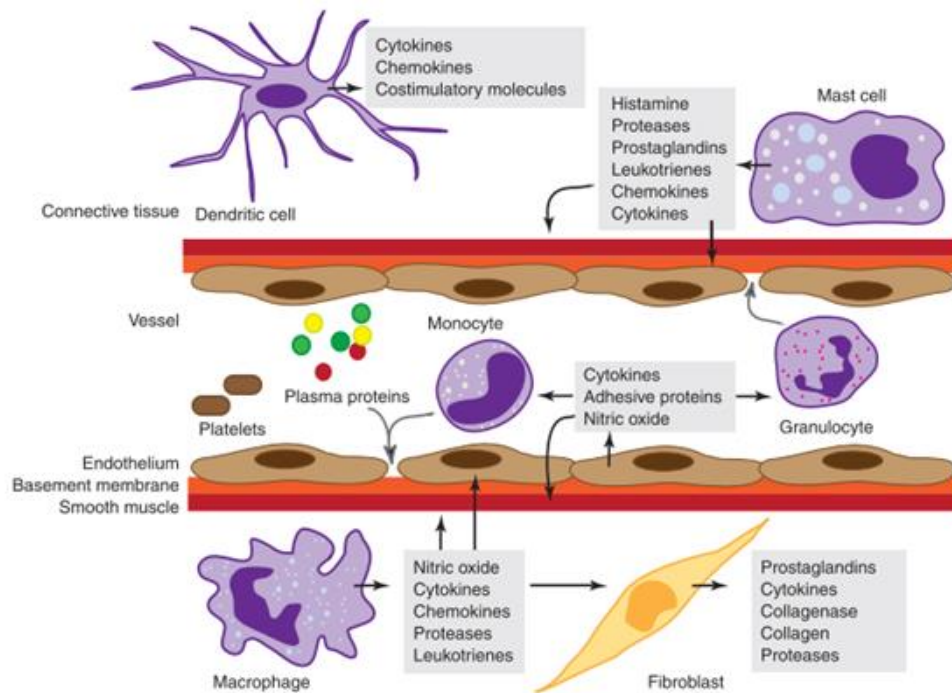


Figure 1.3. Cells and mediators of the inflammatory response Newton and Dixit (2012), with copyright agreement © 2012 Cold Spring Harbor Laboratory Press.

The inflammatory process is mediated by a complex network of chemical signals, including cytokines (Interleukin-2, known as IL2, Interferon- $\gamma$ , IL-10, tumour necrosis factor alpha; TNF- $\alpha$ ), eicosanoids, cell adhesion molecules (CAMs) and chemokines, that cause the migration of the immune system cells (leukocytes) to the site of damage, the immobilization of neutrophils on the surface of vascular endothelium and the progression of inflammatory process (Balkwill and Mantovani, 2001; Coussens and Werb, 2002; Newton and Dixit, 2012).

There are two stages of inflammation: acute and chronic. The first one reflects the controlled inflammation (innate immunity) mediated by the immune system. This first stage of inflammation usually lasts for a short time and it is aimed to remove the causes of the inflammation. However, if the process lasts for a longer period, chronic inflammation sets in (Reuter *et al.*, 2010).

Free radicals may initiate or amplify inflammation, upregulating several genes involved in the inflammatory response (Conner and Grisham, 1996). Although the molecular pathway is not completely understood, it has been demonstrated that the activation of certain transcription factors, such as NF $\kappa$ B, can upregulate the production of different cytokines, including IL-2

and TNF- $\alpha$ , contributing to the chronic nature of inflammation. Several antioxidants such as vitamin E,  $\alpha$ -lipoic acid ((*R*)-5-(1,2-Dithiolan-3-yl)pentanoic acid) and *N*-acetylcysteine, all free radical scavengers, showed inhibition of NF $\kappa$ B, confirming its activation through a free radical mechanism (Conner and Grisham, 1996).

Chronic inflammation is associated with several carcinogenesis stages, such as cellular transformation, promotion, proliferation, invasion, angiogenesis and metastasis (Mantovani, 2005). It is also well established that oxidative stress is strictly linked with cancer during the three stages of initiation, promotion and progression (Klaunig *et al.*, 1998). It has been shown that high ROS concentrations can lead to DNA strand breaks, point mutations and abnormal DNA cross-linking, thus leading to neoplastic transformation (Hussain, Hofseth and Harris, 2003). However, the harmful actions of ROS are not only based on their ability to react with DNA.

In fact, it has been reported recently that these reactive molecules can mediate the cellular signal transduction pathways involved in tumour cell survival. These effects can be observed in mitogen-activated protein kinase (MAPK)/AP-1 and NF $\kappa$ B pathways, both of which are involved in tumour cell proliferation. MAPK represents a wide family of proteins involved in gene expression through phosphorylation of different transcription factors (Pearson *et al.*, 2001). Among these pathways, the MAPK/ERF pathway is that which is most commonly linked with the cell proliferation control which is overexpressed in response to changes in the cellular redox balance, along with JNK and p38 subfamilies. (Xia *et al.*, 1995; McCain, 2013). In addition, it has been shown that carcinogens and tumour promoters, such as asbestos, ionizing radiation and benzo[a]pyrene are able to activate NF $\kappa$ B through free radical pathway (Mohan and Meltz, 1994; Janssen *et al.*, 1995).

It is well established that its activation is linked with an increase in cell proliferation and angiogenesis, both crucial for cancer cell survival, due to the high energy requirements for cell division. However, the mechanism for activation of NF $\kappa$ B by ROS and RNS is not completely understood. In fact it has been demonstrated that mild oxidative stress can lead to an increase in

NFκB activation, while extensive oxidative stress can inhibit the latter and induce mitochondrial permeability transition pore. This leads to the disruption of the electron transfer, resulting in apoptosis or necrosis (Gloire, Legrand-Poels and Piette, 2006). This pathway is described in figure 1.4.

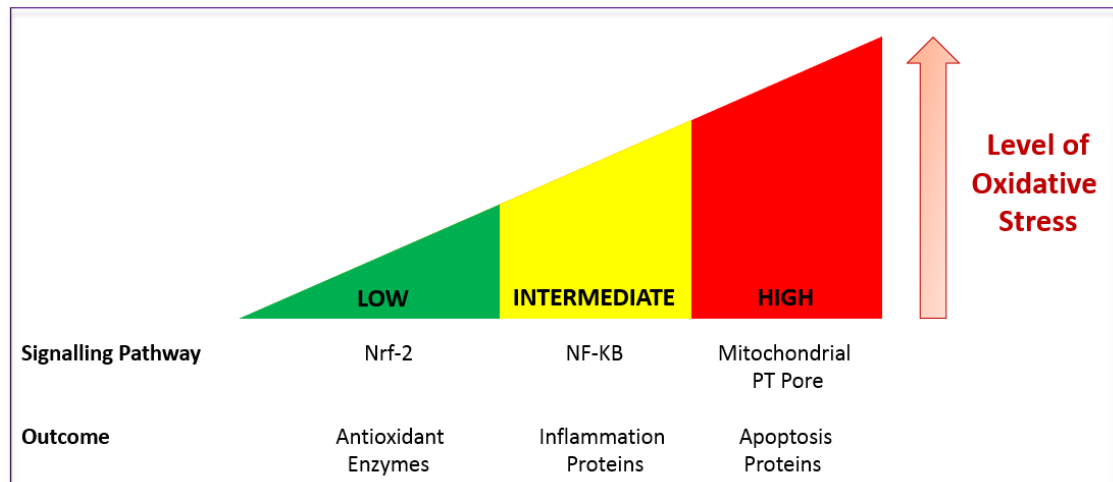


Figure 1.4. Hierarchical oxidative stress model, adapted from Gloire, Legrand-Poels, and Piette (2006), with copyright agreement © 2006 Elsevier Inc.

### 1.1.3.2 Oxidative Stress and Neurodegenerative Diseases

Neurodegenerative diseases are characterized by a slow progressive loss of neurons (Lin and Beal, 2006); although their aetiology has not been fully understood and can follow different pathways, oxidative stress has been suggested as one of the potential common contributing factors (Gandhi and Abramov, 2012). It is well established that the latter induces cellular damage which are both key factors in the development of neurodegenerative disorders.

Parkinson's disease (PD) is a neurodegenerative disorder characterized by loss of dopaminergic (DA) neurons in the substantia nigra pars compacta (SNc), with the consequential depletion of dopamine levels in the nigrostriatal dopaminergic pathway in the brain (Blesa *et al.*, 2015). Although the aetiology of PD has not been completely elucidated, oxidative stress has been considered as one of the causes behind this neurodegenerative illness.

In PD, the concentration of polyunsaturated free fatty acids in the substantia nigra is lowered, with consequential enrichment in 4-hydroxynonenal and malondialdehyde, both of which are hallmarks of lipid peroxidation (Dexter *et al.*, 1989). Furthermore, in the past few decades, several studies have suggested a possible link between the reduced activity of complex I of the respiratory chain in SNc, with the consequential generation of ROS, and PD.

In fact, several complex I inhibitors (see figure 1.21, page 30), such as 1-methyl-4-phenyl-1,2,3,6-tetrahydropyridine (MPTP) and rotenone ((2*R*,6*aS*,12*aS*)-8,9-dimethoxy-2-(prop-1-en-2-yl)-1,2,12,12*a*-tetrahydrochromeno[3,4-*b*]furo[2,3-*h*]chromen-6(6*aH*)-one)), exert cytotoxic effects on dopaminergic neurons (Langston *et al.*, 1983; Li *et al.*, 2003), resulting in clinical PD phenotype. For these reasons, several studies on antioxidant therapy have been conducted to confirm the radical cause of PD, but the results have been conflicting: for example, treatment of 800 patients with early stage of PD with vitamin E, a liposoluble antioxidant, at 2000 IU/d had no impact in delaying the need of L-DOPA (see figure 5), a common PD treatment, after a follow-up of 14 months. In contrast, treatment with 10 mg of selegiline ((*R*)-*N*-methyl-*N*-(1-phenylpropan-2-yl)prop-2-yn-1-amine) (see figure 1.5) per day delayed the need of the L-DOPA by 9 months (Delanty and Dichter, 2000).

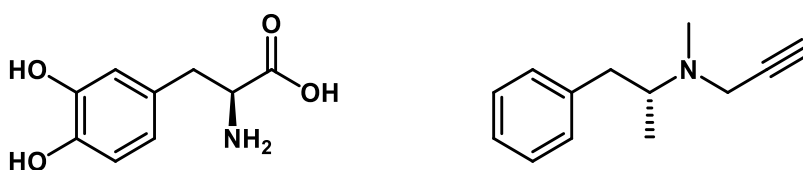


Figure 1.5. Chemical structures of L-DOPA (left) and Selegiline (right).

Although selegiline has shown to be able to protect against MPTP (*N*-methyl-4-phenyl-1,2,3,6-tetrahydropyridine) toxicity by scavenging the highly toxic cation MPP<sup>+</sup> (1-methyl-4-phenyl-pyridinium), it is a well-known selective inhibitor of monoamine oxidase B (MAO-B), thus increasing dopamine levels in the brain. For this reason, the beneficial effects of the latter could not be associated to the antioxidant activity of selegiline (Mytilineou and Cohen, 1985; Olanow *et al.*, 1995).

Alzheimer's disease (AD) is an age-related neurodegenerative disorder characterized by neuronal loss, reduced cholinergic transmission, extracellular amyloid beta-peptide (A $\beta$ )-rich senile plaques and oxidative stress (Mufson *et al.*, 2009; Butterfield, Swomley and Sultana, 2013). Oxidative stress has been shown to play a fundamental role during the early stage of the disease. For example several studies have shown an increase of ROS and RNS mediated injuries in AD brain along with increased levels of oxidized biomolecules (proteins, nucleic acids and lipids) and altered regulation of antioxidant enzymes (Mecocci and Polidori, 2012; Rosini *et al.*, 2013).

Several studies have been conducted to evaluate the potential therapeutic effects of antioxidants on the onset and delay of AD. Similar to the PD studies, the antioxidant therapy for AD produced contrasting results: a study conducted on 341 patients with moderate to severe AD showed that a daily intake of vitamin E of 2000 UI/d for 2 years showed a slower progression of the disease whereas no significant improvements were obtained in 769 patient with mild cognitive impairment (MCI) (Sano *et al.*, 1997; Mecocci and Polidori, 2012).

In addition, other natural antioxidants failed to improve AD patients' symptoms; for example resveratrol ((*E*)-5-(4-hydroxystyryl)benzene-1,3-diol) (see figure 1.6), a stilbene compound, has shown no short term positive effects on cognitive performance in AD patients in a double blind, placebo controlled study (Bass *et al.*, 2007; Kennedy *et al.*, 2010).

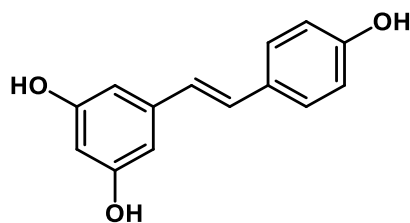


Figure 1.6. Chemical structure of resveratrol.

Curcumin ((1*E*,6*E*)-1,7-Bis(4-hydroxy-3-methoxyphenyl)-1,6-heptadiene-3,5-dione) (see figure 1.7), a strong antioxidant and a known  $\beta$ -amyloid aggregation inhibitor naturally found in turmeric, has shown no significant

improvement in cognitive performance on a study involving 34 AD patients (Mecocci and Polidori, 2012).

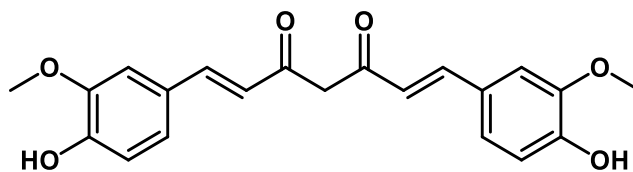


Figure 1.7. Chemical structure of curcumin.

However, a supplementation of lipoic acid, the coenzyme of mitochondrial pyruvate dehydrogenase and  $\alpha$ -ketoglutarate dehydrogenase, reduced memory loss and stabilized cognitive function in a 48 months study involving 43 patients (Hager *et al.*, 2007).

### 1.1.3.3 Oxidative Stress and Cardiovascular Diseases

Oxidative stress plays a fundamental role in different cardiovascular pathologies that include atherosclerosis, heart failure and stroke. It has been recently shown that the oxidation of the low density lipoproteins (LDL) in the arterial walls is linked with the thickening of the latter (Madamanchi, Vendrov and Runge, 2005), the principal hallmark of atherosclerosis. Lipoproteins are biomolecular structures containing both lipids and proteins; these particles effectively emulsify fatty molecules, facilitating their transport in the aqueous environment of the blood.

These biomolecules are classified, depending on their density, into very low-density lipoproteins (VLDL), low-density lipoproteins (LDL) and high-density lipoproteins (HDL). HDL are involved in the transport of cholesterol and other fatty molecules from tissues and artery vessels to the liver whereas VLDL and LDL carry their fatty contents to the artery vessels and, after oxidation, they can invade endothelium and contribute to the atherosclerosis process (Shinkai, 2012) as illustrated in figure 1.8.

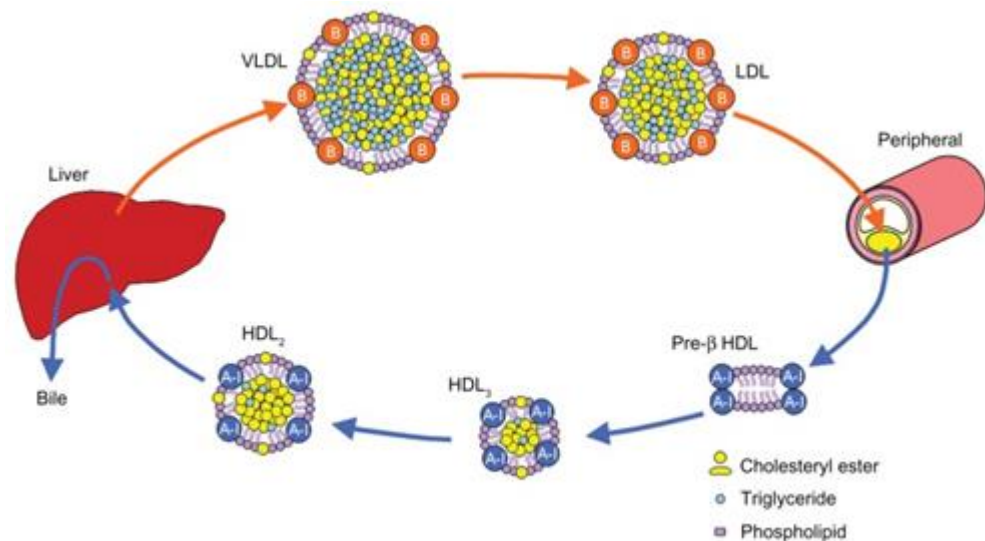


Figure 1.8. Cholesterol transport in human body, adapted from Shinkai (2012) with copyright agreement © 2012 DOVE MEDICAL PRESS LTD.

In addition, free radicals, such as superoxide, can inactivate the signaling molecule NO (see equation 12, page 8), involved in the blood vessel muscle tone regulation, leading to impairment of vasorelaxation, a condition linked with heart failure (Ogita and Liao, 2004). Furthermore, a meta-analysis of 23 randomized controlled trials published between 2001 and 2013 showed that perioperative supplementations with vitamin C (L-ascorbic acid), *N*-acetyl cysteine (NAC) and poly-unsaturated fatty acids (PUFA) prevented atrial fibrillation after cardiac surgery (Ali-Hassan-Sayegh *et al.*, 2014). However, a study conducted on 14641 men showed no significant effects of a daily multivitamin intake on major cardiovascular events after 14 years of treatment (Sesso *et al.*, 2013). In addition, another study involving 161808 women treated with multivitamins showed, after 8 and 7.9 years of median follow-up, little or no influence on the risk of cardiovascular diseases.

Furthermore, oxidative stress plays a fundamental role in brain ischaemic injury, enhancing peroxidation of unsaturated fatty acids of cell membranes leading to neuronal death and oedema (Yoshida *et al.*, 2006). Recent studies demonstrated the beneficial effects of edaravone (3-methyl-1-phenyl-2-pyrazolin-5-one), a potent free radical scavenger, in brain ischaemia/reperfusion, attenuating vascular and cellular damage. Although edaravone does not bear phenolic functionality, it undergoes keto-enol tautomerization (see figure 1.9) and generates the aromatic hydroxyl group

which exhibits free radical scavenging activities (Watanabe, Tahara and Todo, 2008).

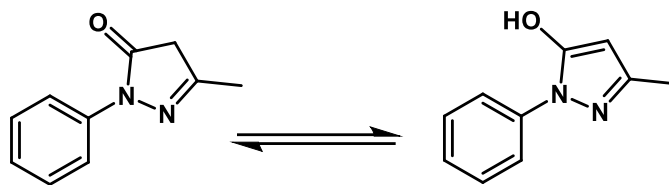


Figure 1.9. Chemical structure of 3-methyl-1-phenyl-2-pyrazolin-5-one (Edaravone) and its keto-enol tautomerization.

The protective effects of edaravone in brain ischaemia/reperfusion injury are not based only on its antioxidant properties since the compound had shown to increase the expression of NO through activation of endothelial NO synthase (eNOS), ameliorating the blood flow and thus reducing post-ischaemic reperfusion-induced tissue damage. Edaravone is commercially available in Japan (since 2015) and USA (since 2017) for patients recovering from stroke and for treatment of amyotrophic lateral sclerosis (ALS) (Rothstein, 2017).

## 1.2 Antioxidants

### 1.2.1 Definition of Antioxidants

Different definitions of antioxidants have been described over the years; Halliwell defined antioxidant as “any substance that, when present at low concentrations compared with that of an oxidizable substrate, significantly delays or inhibits oxidation of that substrate” (Halliwell and Gutteridge, 1995). Lately, after the increasing knowledge on oxidative stress and its role in several diseases, he described antioxidants as “any substance that delays, prevents or removes oxidative damage to a target molecule” (Halliwell, 2007). In addition, to be considered as an antioxidant, a molecule should be able to generate a new stable radical (through intramolecular hydrogen bonding) after scavenging a free radical (Halliwell, 1990). Being more stable, the new free radical will be less reactive towards biological structures such as DNA, lipids and proteins.

## 1.2.2 Mechanism of Action of Antioxidants

### 1.2.2.1 Free Radical Scavengers

The classical mechanism of action from an antioxidant can be shown by equation 14:



Where AH is the antioxidant and R· is the free radical. This equation explains the ability of antioxidants to inhibit (or delay) many damaging processes induced by free radicals on biological structures, such as lipids, proteins or DNA and to generate a new stable free radical (A·) that is less reactive compared with the original one (R·) (López-Alarcón and Denicola, 2013). However, the ability of the antioxidant to react with the free radical is of critical importance and it can be described by equation 15:

$$r = k_1 [\text{AH}] [\text{R}]_{ss} \quad (15)$$

where  $r$  is the reactivity,  $k_1$  is the kinetic rate constant (the higher this value is, the stronger is the antioxidant),  $[\text{AH}]$  is the concentration of the antioxidant and  $[\text{R}]$  is the concentration of the free radical at the steady state.

In addition, the ability of the antioxidant to reach the biological site where the free radicals are exerting their damaging activity is another crucial limiting factor. For example, an antioxidant that can prevent lipid peroxidation should possess relevant chemico-physical properties in order to reach the cell membranes and reacts with free radicals (Niki, 1987).

Another important aspect is the stability of the secondary free radicals A· formed after the reaction with the reactive intermediates. It is well known that some secondary free radicals could damage DNA, proteins and other biological targets (Kagan and Tyurina, 1998). Furthermore, secondary free radicals can react with oxygen, yielding peroxy and superoxide free radicals, as shown by equations (16) and (17):



#### 1.2.2.2 Metal Chelation

As described previously (equations 7 and 11),  $Fe^{2+}$  and  $Cu^+$  are involved in the generation of free radicals through the Fenton reaction (see equations 7 and 11) (Gutteridge and Wilkins, 1983; Jomova, Baros and Valko, 2012). In particular, ferrous ion ( $Fe^{2+}$ ) is the most powerful pro-oxidant among the metal ions whereas ferric ion ( $Fe^{3+}$ ) can produce free radicals from peroxides at a rate 10-fold less than  $Fe^{2+}$  (Gülçin, 2006).

Most polyphenol compounds are effective metal chelators; in particular, acidic polyphenols such as gallol (benzene-1,2,3-triol) and catechol (1,2-dihydroxybenzene), are easily deprotonated, and can form stable complexes with both ferrous and ferric ions (Perron and Brumaghim, 2009). Once complexed, these metals cannot exert their toxic effects on biological macromolecules through the Fenton reaction. At the same time, phenolic compounds such naringenin and catechin can form complexes with both cuprous and cupric ions in stoichiometries 1:1 or 1:2 (Fernandez *et al.*, 2002).

#### 1.2.2.3 Antioxidant Responsive Element (ARE)-mediated Pathway

The first observations of inducible anti-oxidation were made in 1978 by Benson *et al.* when they noticed that phenolic antioxidants, such as the synthetic butylated hydroxyanisole (BHA) (2-*tert*-Butyl-4-methoxyphenol and 3-*tert*-butyl-4-methoxyphenol), protected animals from benzo[a]pyrene-induced tumour formation, inhibiting mutagenic metabolites of the latter and inducing the expression of two different drug-metabolizing enzymes, glutathione S-transferases (GSTs) and NAD(P)H dehydrogenase (quinone1) (NQO1) (Benson *et al.*, 1978).

In recent years, the list of the inducers of these enzymes has increased and it includes a wide range of natural and synthetic compounds such as sulphorapane (1-Isothiocyano-4-methylsulfinylbutane) and triterpenoids,

therapeutics such as dimethyl fumarate, poisons such as paraquat (*N,N'*-dimethyl-4,4'-bipyridinium dichloride) and arsenic and even endogenous molecules such as prostaglandin J<sub>2</sub>, hydrogen peroxide and 4-hydroxynonenal (4-HNE) (see figure 1.10) (Nguyen, Nioi and Pickett, 2009; Ma, 2014).

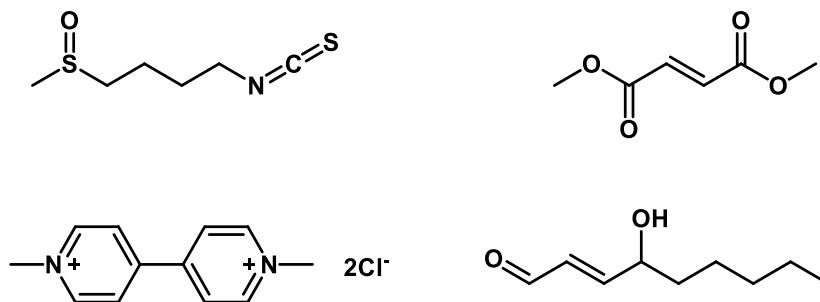


Figure 1.10. Chemical structures of sulphorapane (top left), dimethyl fumarate (top right), paraquat (bottom left) and 4-HNE (bottom right).

The induction of the cytoprotective enzymes is regulated at transcriptional level, mediated by a *cis*-acting element termed antioxidant responsive element (ARE) (Friling *et al.*, 1990) (see figure 1.11).

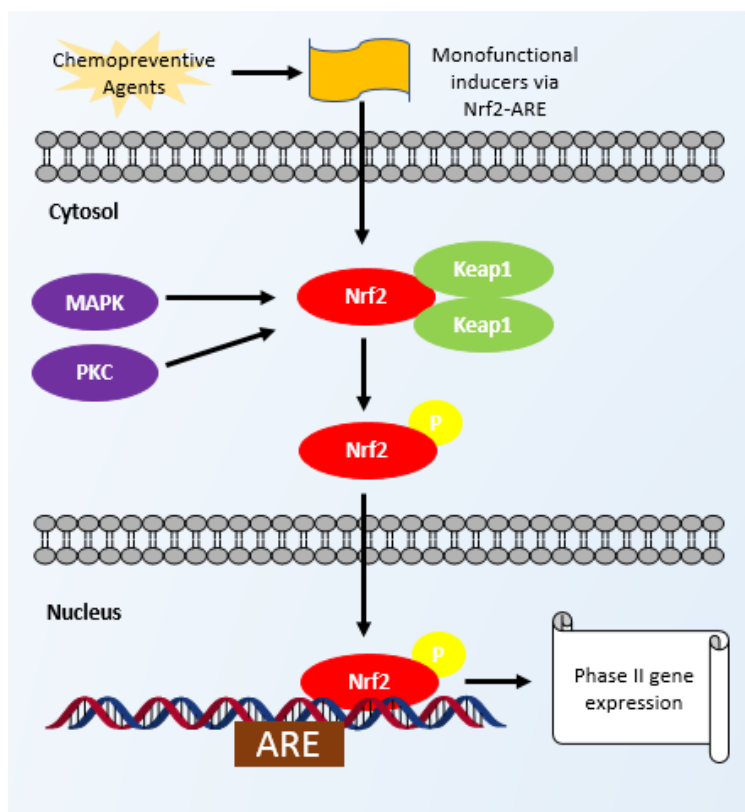


Figure 1.11. Proposed Nrf2-ARE signaling pathway, adapted from Cabrera *et al.* (2015), with permission from Future Science OA.

The main mediator of the ARE activation is the nuclear factor E2-related factor 2 (Nrf2), which is regulated by the actin-associated Keap1 protein. Nrf2 is an unstable protein with a half-life of about 15 minutes. Due to its short lifespan, the activation of this factor is associated with its accumulation in the cell (Nguyen, Nioi and Pickett, 2009; Ma, 2014). Under normal conditions, Nrf2 is bound to Keap1 and compartmentalized in the cytoplasm, where it is degraded after ubiquitination. However, under oxidative conditions, the cysteine residues in Keap1, involved in the bond with Nrf2, can be oxidized, leading to the translocation of the latter into the nucleus, where it can induce the transcription of antioxidant genes. This mechanism is supported by the fact that the inducers of ARE pathway are electrophiles, suggesting an inducer-cysteine thiol interaction as the early stage for Nrf2 activation (Itoh *et al.*, 1999; Kobayashi *et al.*, 2004; Nguyen, Nioi and Pickett, 2009; Ma, 2014).

### 1.2.3 *Classification of Antioxidants*

Antioxidants can be classified, according to their source, in natural or synthetic antioxidants (Carocho and Ferreira, 2013). Although the interest in new synthetic antioxidants has dramatically increased in the past decades, due to the potential beneficial properties of the latter to human health and wellbeing, the natural antioxidant family is still the most popular and with high level of diversity. A detailed scheme of this classification is shown in figure 1.12.

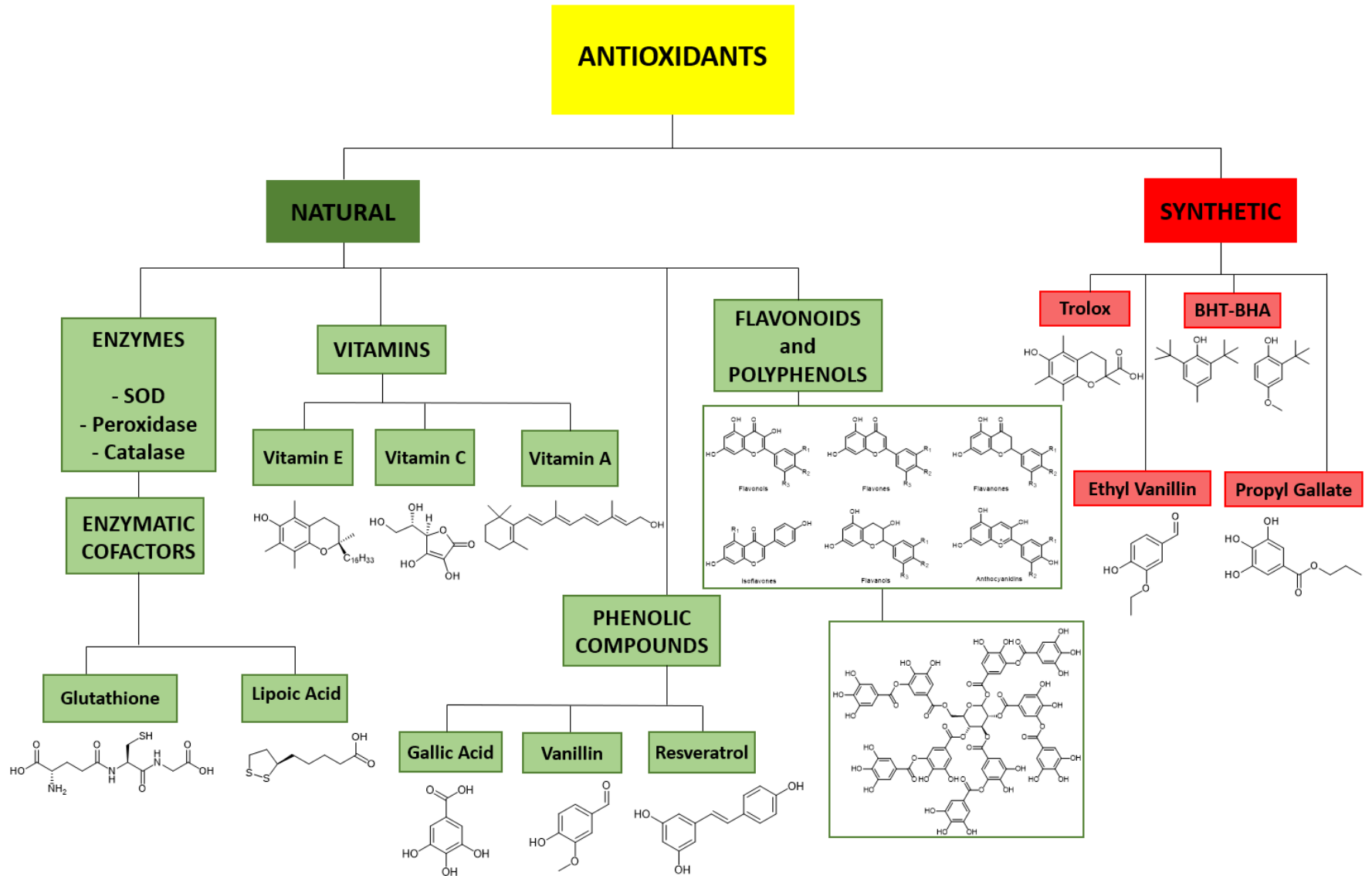


Figure 1.12. Natural and synthetic antioxidants and their chemical structures.

### 1.2.3.1 Natural Antioxidants

#### 1.2.3.1.1 Endogenous Antioxidants

Endogenous antioxidants represent the first line of defense against oxidative stress and these include antioxidant enzymes and their cofactors. The main antioxidant enzymes are: superoxide dismutase (SOD), glutathione peroxidases and catalase. SOD converts the superoxide anion radical into hydrogen peroxide. There are three isoforms of the SOD enzyme known as (I) the cytosolic, which uses zinc or copper as cofactors, (II) mitochondrial, which uses manganese as cofactor, and (III) extracellular, which is less involved in oxidative stress, since it is expressed through a cytokine-mediated pathway. The antioxidant effects of SOD are exerted by successive oxidative and reductive cycles of the transition metal ions at its active site (Landis and Tower, 2005; Rahman, 2007).

Glutathione peroxidases catalyse the reduction of hydrogen peroxide into water and organic hydroperoxides into the respective alcohols. This enzyme bears a selenol moiety (R-Se-OH) in its active site which can be oxidized by hydrogen peroxide into seleninic acid (R-SeO<sub>2</sub>H) (Bhabak and Govindasamy, 2010). The latter is then reduced to its initial status by two molecules of the antioxidant glutathione (GSH). Reduced glutathione is an endogenous tripeptide (figure 1.13) which protects the cells against free radicals acting either as hydrogen donors or electron donors due to its thiol moiety (Carocho and Ferreira, 2013).

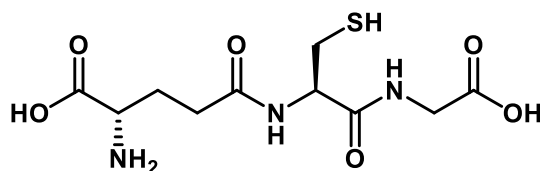
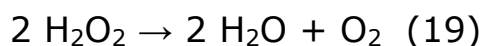


Figure 1.13. Chemical structure of L-Glutathione.

It is synthesized from precursor amino acids and its concentration in the human body ranges from 2 up to 7 mM in the liver (Kaplowitz, 1981). When it reacts with hydrogen peroxide, the reduced tripeptide is oxidized into its disulphide form (GS-SG) (Bhabak and Govindasamy, 2010), as depicted in equation (18).



Catalase is an antioxidant enzyme expressed in the peroxisome of cells and it is involved in the conversion of hydrogen peroxide into water and molecular oxygen (equation 19).



This enzyme is selective toward hydrogen peroxide, since it is not able to deplete other peroxides (Pisoschi and Pop, 2015). Interestingly, catalase has one of the highest turnover rates for all enzymes since one molecule of the latter can convert almost 6 million molecules of hydrogen peroxide into water and oxygen each minute (Rahman, 2007).

(*R*)-lipoic acid and its reduced form (*R*)-dihydrolipoic acid (DHHLA) (figure 1.14) are endogenous antioxidants able to react with reactive oxygen species such as superoxide radicals, hydroxyl radicals, hypochlorous acid, peroxy radicals, and singlet oxygen.

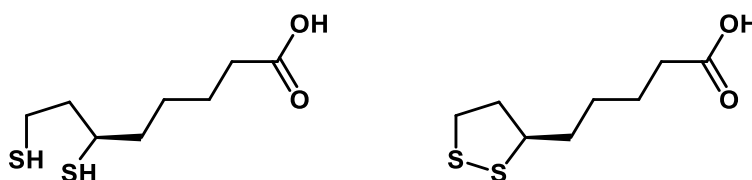


Figure 1.14. Chemical structures of (*R*)-DHHLA (left) and (*R*)-lipoic acid (right).

These molecules exert protective effects on cellular membranes, interacting with vitamin C and glutathione, promoting the recycling of vitamin E (Packer, Witt and Tritschler, 1995; Kagan and Tyurina, 1998). Several studies have demonstrated the beneficial effects of DHHLA administration in rats and guinea pigs; DHHLA treated animals showed reduced symptoms of vitamin E and C deficiency and reduced lipid peroxidation in the brain and liver after treatment with the stressor azobis (2,4-dimethylvaleronitrile) (Packer, Witt and Tritschler, 1995).

### 1.2.3.1.2 Exogenous Antioxidants

Exogenous antioxidants are molecules that cannot be biosynthesized by cells and are obtained through the diet. These molecules can be found in fruits and vegetables and their intake is commonly linked with health and wellbeing since the latter work synergistically with endogenous antioxidant to maintain the physiological redox homeostasis (Bouayed and Bohn, 2010). However, it has been showed that the ingestion of high amount of exogenous antioxidants (for example through supplements) may result in pro-oxidant effects or in the so called "antioxidant stress" (Poljsak and Milisav, 2012).

#### 1.2.3.1.2.1 Vitamins

Vitamins are organic and essential compounds that an organism is not able to produce in sufficient amounts and thus must be obtained through the diet. Among these wide family of molecules, three vitamins that have strong antioxidant properties are vitamin A, C and E. Vitamin A includes several antioxidant compounds such as its active form retinoic acid and derivatives, for example retinal, retinol and provitamin A carotenoids (Fragoso *et al.*, 2012). Retinol and retinyl esters such as palmitate are dietary sources which are metabolized into the active form retinoic acid (see figure 1.15).

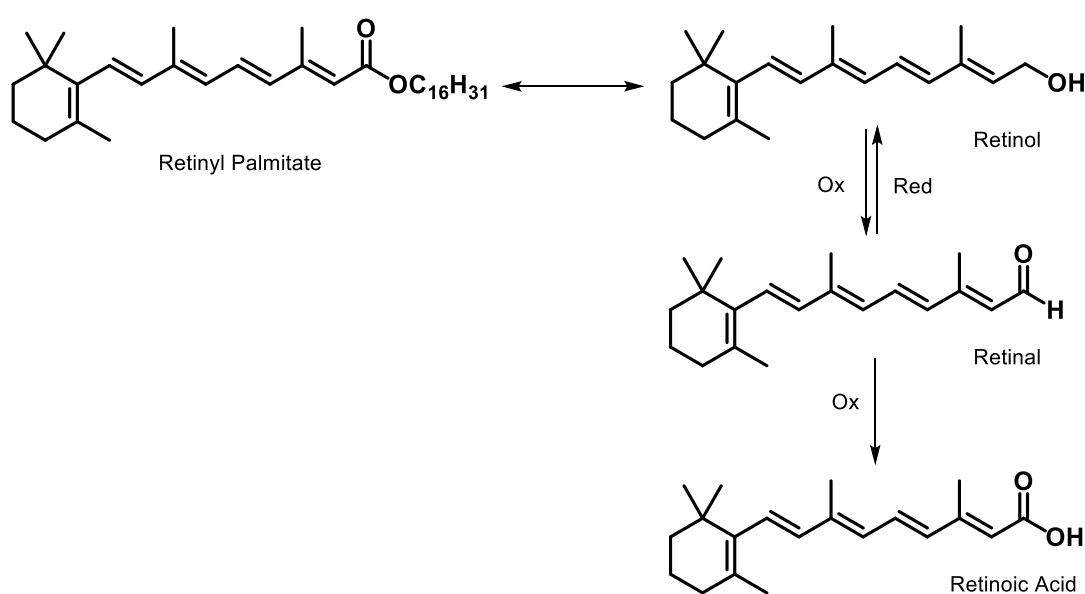


Figure 1.15. Chemical structures of functional vitamin A molecules, adapted from Tanumihardjo (2011).

In addition to their role in vision, growth and other cellular functions, these fat soluble molecules exert strong antioxidant activities due to their conjugated double bonds, which stabilize unpaired electrons (Rahman, 2007). Recent studies have shown that high consumption of carotenoids (precursors of vitamin A) in diet is linked with lower risk of age-related diseases; however, these molecules can act as pro-oxidant at high concentrations or in the presence of high oxygen pressure (Stahl and Sies, 2003).

Vitamin C (figure 1.16) is the *L*-enantiomer of ascorbic acid and is one of the most ubiquitous, water-soluble antioxidants. It has several roles in cells: it is involved in maintaining tissue integrity, in neuroprotection, in iron absorption and collagen biosynthesis (Pisoschi and Pop, 2015). Vitamin C can scavenge hydroxyl and superoxide radicals, along with NRS, and it can even protect lipids from peroxidation in combination with vitamin E. Moreover, although vitamin C is water soluble, it can regenerate the tocopherol free radical at the lipid-aqueous interface (Kojo, 2004; Du, Cullen and Buettner, 2012; Sung *et al.*, 2013).

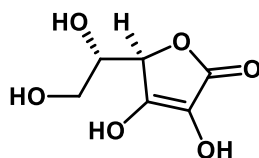


Figure 1.16. *L*-ascorbic acid (vitamin C).

Vitamin E exists in eight isoforms ( $\alpha$ ,  $\beta$ ,  $\gamma$ ,  $\delta$  tocopherols and tocotrienols) with the  $\alpha$ -tocopherol being the most active and abundant. It is a liposoluble antioxidant and, for this reason, its main role is the protection of lipids from peroxidation, in combination with ascorbic acid. Its synergistic effect with vitamin C is shown in figure 1.17.

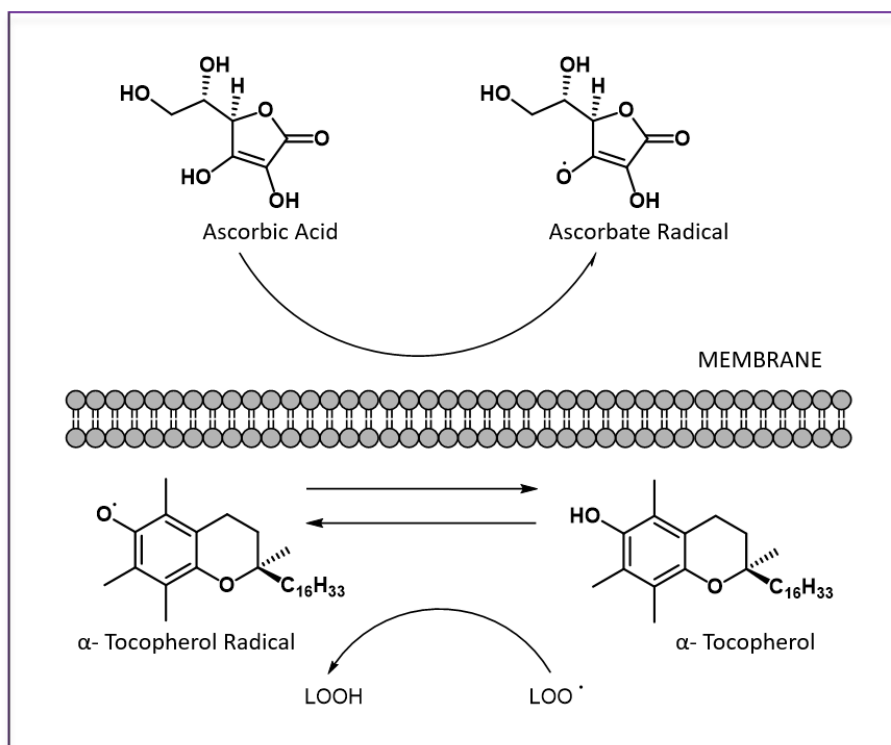


Figure 1.17. Synergistic effects of Vitamin C and E against lipid peroxidation, adapted from Marian Valko *et al.* (2004) with copyright agreement © 2006 Springer Nature.

### 1.2.3.1.2.2 Phenolic Compounds

Phenolic compounds are characterized by one or more aromatic rings to which is linked at least one hydroxyl group. This wide family of antioxidants can be further divided into flavonoids and non-flavonoid compounds. Flavonoids are the most common phenolic compounds that are introduced through the diet; their chemical structure consists of two aromatic carbon rings, benzopyran (A and C rings) and benzene (B ring) (Figure 1.18).

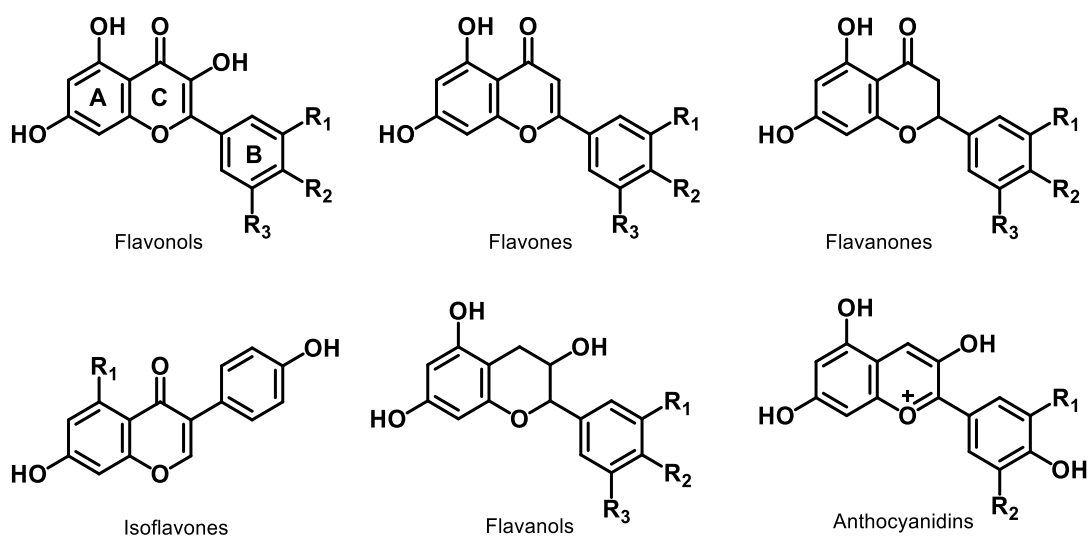


Figure 1.18. Chemical structures of Flavonoids.

Depending on the degree of oxidation of the C-ring, the substitution at the 3-position and the hydroxylation in the ring, flavonoids can be classified in six groups: flavonols (for example kaempferol and quercetin), flavones (luteolin and apigenin), isoflavones (genistein), flavanones (naringenin), flavanols (catechin) and anthocyanidins (cyanidin) (Manach *et al.*, 2004; Spencer, 2008).

These molecules can be found in a wide variety of vegetables and fruits that include broccoli, leeks, onions, parsley, berries, tea and citrus fruits. Flavonoids have shown strong antioxidant activity *in vitro* while several studies have demonstrated the ability of flavonoids to act as both free radical scavengers and to activate Nrf2 pathway *in vitro* (Hollman and Katan, 1997; Gao *et al.*, 1999; Johnson, Maher and Hanneken, 2009; Zhai *et al.*, 2013). However, these phenolic compounds showed reduced activity *in vivo*, due to their poor absorption, high metabolism and rapid excretion (Manach *et al.*, 2004; Spencer, 2008; Goszcz *et al.*, 2015).

Stilbenes are a small family of plant secondary metabolites biosynthesized *via* the phenylpropanoid pathway; their antimicrobial and antifungal activities along with their pathogen-mediated induction suggest their importance in plant defense (Chong, Poutaraud and Hugueney, 2009). Resveratrol (see figure 1.6, page 13) is probably the most studied member of the phenolic family of compounds. Resveratrol is relatively abundant in grape skins and red wine and it showed interesting biological properties. In

fact, along with its ability to scavenge ROS to form a stable free radical due to the conjugation between the two aromatic rings *via* a double bond, it can act as metal chelating agent, NO synthase inducer, Nrf2 pathway inducer and COX-2 inhibitor (Harikumar and Aggarwal, 2008; Chong, Poutaraud and Huguene, 2009; Nakata, Takahashi and Inoue, 2012; Pisoschi and Pop, 2015). Several other studies have shown resveratrol to have interesting properties *in vivo*, reducing oxidation of LDL, inhibiting angiogenesis, reducing chronic inflammation and decreasing brain lipid peroxidation, due its ability to cross the blood-brain barrier (Baur and Sinclair, 2006).

Phenolic acids are compounds containing a benzoic or cinnamic acid moiety and at least one hydroxyl group (figure 1.19). The latter are commonly found in the human diet and their daily intake is estimated to be 200 mg (Heleno *et al.*, 2015). Among the benzoic acid derivatives, gallic acid is one of the most studied, since it is often used as standard for different antioxidant assays; it can be found in its free acid form or esterified with glucose (to form hydrolysable tannins known as gallotannins), flavanols (to form epigallocatechin) or other phenolic structures.

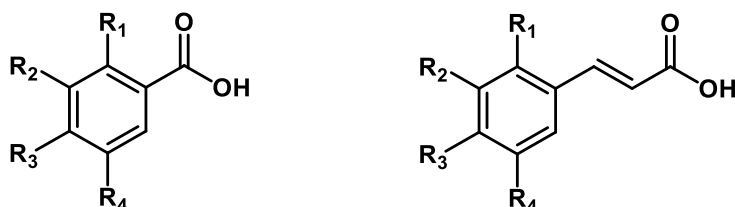


Figure 1.19. Benzoic acid derivatives (left) and Cinnamic acid derivatives (right) chemical structures. The substituents in the aromatic rings (R) are often hydrogen, hydroxy and methoxy groups.

Among the cinnamic acid derivatives, caffeic acid ((*E*)-3-(3,4-dihydroxyphenyl)acrylic acid) is the most abundant, often esterified with quinic acid as in chlorogenic acid ((1*S*,3*R*,4*R*,5*R*)-3-(((*E*)-3-(3,4-dihydroxyphenyl)acryloyl)oxy)-1,4,5-trihydroxycyclohexane-1-carboxylic acid), the major phenolic compound in coffee (Dai and Mumper, 2010). Recently ferulic acid, a cinnamic acid derivative, showed to block rotenone-induced dopaminergic neurodegeneration in a mice PD model in a 4 weeks study. During this study, ferulic acid showed to reduce inflammatory mediators such as cyclooxygenase and iNOS and to restore antioxidant enzymes and the glutathione levels (Ojha *et al.*, 2015).

It is interesting to note that, whereas small phenolic acids such as gallic acid can act as pro-oxidants under conditions that favour their autoxidation (high pH and high concentrations of transition metal ions), high molecular weight phenolics such as gallotannins have little or no prooxidant activity (Hagerman *et al.*, 1998).

Vanillin (4-hydroxy-3-methoxybenzaldehyde, figure 1.20) is a phenolic compound and is the main component of the bean and pod of tropical vanilla orchids (*v. planifolia*, *v. tahitensis* and *v. pompona*).

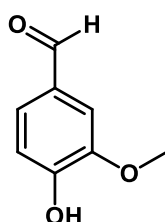


Figure 1.20. Chemical structure of vanillin.

Vanillin is widely used as flavouring agent in food industry and preservative in food, cosmetics and drugs industry with an estimated annual consumption in the world of more than 2000 tons (Kamat, Ghosh and Devasagayam, 2000). In addition to the flavouring properties, vanillin has shown promising biological activities in several studies; this included antimicrobial activities against a wide spectrum of bacteria (Fitzgerald *et al.*, 2004), as well as antimutagenic (King *et al.*, 2007) and anticarcinogenic properties (Kapoor, 2013). Moreover, it has been reported recently that vanillin can decrease angiogenesis *in vivo* and inhibit cancer cell migration and metastasis (Lirdprapamongkol *et al.*, 2009). Interestingly, vanillin showed protective effects against oxidative stress in both *in vitro* and *in vivo* studies. In fact, this phenolic compound also exhibited protection of SH-SY5Y neuroblastoma cells in rotenone-induced oxidative stress. Rotenone is a lipophilic pesticide that can easily cross cell membranes, inhibiting mitochondrial complex I activity, leading to an increase in ROS and oxidative stress (Dhanalakshmi *et al.*, 2015) (see figure 21). This property makes rotenone a valid compound to model PD phenotype (Betarbet *et al.*, 2000); its mechanism of toxicity is shown in figure 1.21.

In a study by Dhanalakshmi et al., vanillin was shown to protect SH-SY5Y cells at concentration as low as 100 nM, when stressed with rotenone (100 nM), by increasing the cell viability by 25% compared to the control.

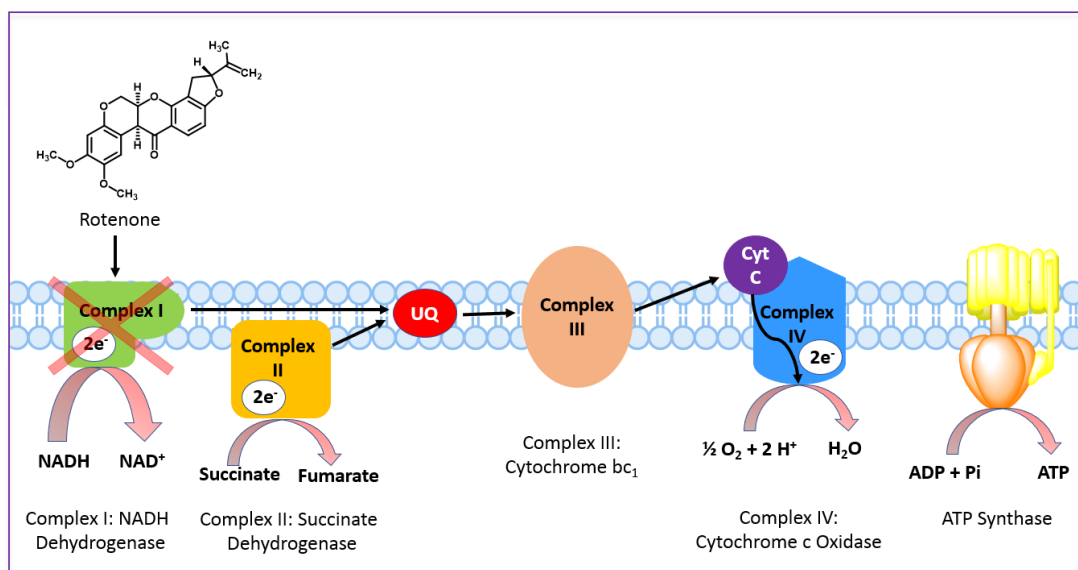


Figure 1.21. Mechanism of rotenone toxicity, adapted from Xu, Shang, and Jiang (2016) with copyright agreement © 2016 Royal Society of Chemistry.

In addition, two different *in vivo* experiments from Makni *et al.* showed the protective effects of vanillin in rats. Using carbon tetrachloride (CCl<sub>4</sub>) as an oxidative stress inducer, the authors measured the protective effects of vanillin in brain and liver, showing lower levels of lipid peroxidation, reduced pro-inflammatory cytokines release, increase in antioxidant enzymes expression and in glutathione levels (Makni *et al.*, 2011, 2012). Furthermore, vanillin protected hepatic mitochondria against oxidative damage in rats induced by photosensitization at concentrations normally found in food preparations (2.5 mM), reducing lipid peroxidation and preventing protein oxidation (Kamat, Ghosh and Devasagayam, 2000).

The free radical scavenging activities of vanillin are well established: it is a powerful peroxynitrite inhibitor and a scavenger of hydroxyl and superoxide radicals (Kamat, Ghosh and Devasagayam, 2000; Kumar, Priyadarsini and Sainis, 2004). However, this natural compound showed weak or no activity in scavenging synthetic free radicals such as 2,2-diphenyl-1-picrylhydrazyl (DPPH) and galvinoxyl radicals; the latter is a well-established *in vitro* assay to determine free radical scavenging activity of antioxidants. It is worth noting that latter assay, involving the use of a synthetic radical, is less

relevant to biological system (Brand-Williams, Cuvelier and Berset, 1995; Tai *et al.*, 2011).

In contrast, vanillin is able to scavenge the peroxy free radical generated in the oxygen radical absorbance capacity (ORAC) assay, which mimics the lipid peroxy radicals occurring in the lipid peroxidation process *in vivo*. For this reason, the latter assay is more relevant to biological system (Isa *et al.*, 2012). In this assay, vanillin exhibited more effective antioxidant properties when compared to ascorbic acid and the synthetic vitamin E-related antioxidant, Trolox (Tai *et al.*, 2011).

### 1.2.3.2 Synthetic Antioxidants

Antioxidant research has focused on the search for new compounds with improved antioxidant properties due to their important role in human health and wellbeing. However, the main use of synthetic antioxidants nowadays is in food preservation and cosmetics, in particular for the prevention of fatty acid oxidation (Carocho and Ferreira, 2013). Today, almost all processed foods have synthetic antioxidants incorporated in them in order to increase their shelf-life. For example, BHA and butylated hydroxytoluene (BHT) (2,6-Di-*tert*-butyl-4-methylphenol) (figure 1.22) are widely used in the cosmetic and food industries.

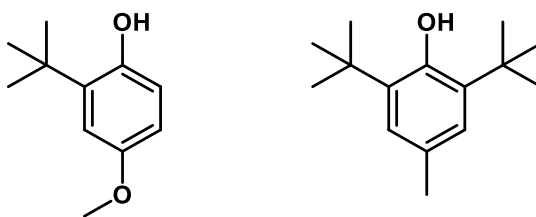


Figure 1.22. BHA (left) and BHT (right) chemical structures.

Several studies have shown contrasting results on the potential for food preservatives in chemoprevention and carcinogenesis (Hocman, 1988). For example, propyl gallate (PG) is a synthetic gallic acid derivative (figure 1.23) commonly used as food preservative, obtained by its condensation with propanol; its antioxidant properties have been exploited using different stable free radicals. It has been showed that PG has free radical scavenging activity against ABTS and DPPH comparable to vitamin C (Soares, Andrezza and Salvador, 2003).

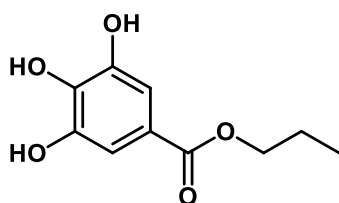


Figure 1.23. Propyl gallate chemical structure

Other modifications of natural antioxidants' chemical structures to improve their antioxidant activity have been made. For example, Trolox (6-hydroxy-2,5,7,8-tetramethylchroman-2-carboxylic acid, figure 1.24) is one of the most common synthetic antioxidants used in research laboratories since it is widely used as standard in many antioxidant activity assays (often expressed as Trolox Equivalent, TE).

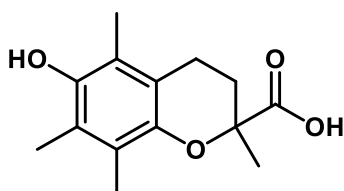


Figure 1.24. Chemical structure of Trolox.

Trolox was developed by Scott *et al.* in the early 1970s at Hoffman-La Roche research laboratories during the search for new antioxidants that are able to prevent the oxidation of animal fats and vegetable oils. Chemically, it is a derivative of  $\alpha$ -tocopherol in which the isoprenoid chain, which is not involved in the antioxidant activity, has been replaced by a carboxylic group; this substitution makes the derivative water-soluble (Scott *et al.*, 1974).

Several attempts were made to improve the antioxidant activity of Trolox and to target specific biological structures. In 1998, Moulin *et al.* described a series of *N*-(aza)arylcarboxamides derivatives of Trolox with strong anti-inflammatory activity in rats, using the carrageenin-induced paw oedema test. Those compounds were orally administered at 0.4 and 0.1 mmol/kg, with the most active showing a 97.1% of oedema inhibition, and turning out to be more active than common anti-inflammatory drug such as indomethacin (Moulin *et al.*, 1998). In 2001, Koufaki *et al.* reported a series of strong lipid peroxidation inhibitors in rat liver microsomal membranes induced by ferrous ions and ascorbate bearing both Trolox and lipoic acid

moieties, linked together by different chemical spacers (Koufaki *et al.*, 2001). That study was based on a previous finding by Coombes *et al.* where the synergistic effect of tocopherol and  $\alpha$ -lipoic acid in the reduction of lipid peroxidation during *in vivo* ischaemia-reperfusion in young adult rats was shown (Coombes *et al.*, 2000). The most active compound, *N*-(4-(4-(5-(1,2-dithiolan-3-yl)pentanamido)phenoxy)phenyl)-6-hydroxy-2,5,7,8-tetramethylchromane-2-carboxamide (figure 1.25), reported by Koufaki *et al.*, inhibited lipid peroxidation at nanomolar concentrations and totally suppressed arrhythmias induced by reoxygenation during reperfusion in an *in vitro* model (Koufaki *et al.*, 2001).

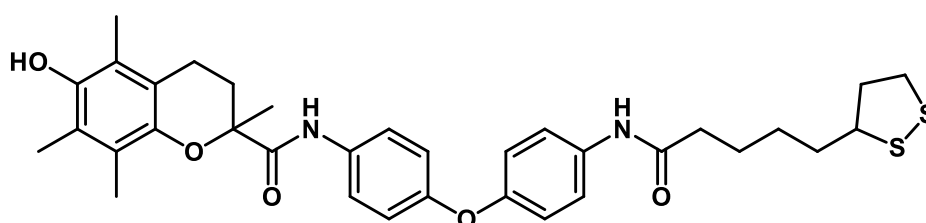


Figure 1.25. Trolox-lipoic acid hybrid reported by Koufaki *et al.* (2001).

Interest around the resveratrol moiety (see figure 1.6, page 13) and its apparently powerful antioxidant properties, both *in vitro* and *in vivo*, had led to a substantial volume of work published during the past 20 years.

It is well established that the scavenging activity of phenolic compounds against DPPH free radical is due to their hydrogen-donating ability. Wang *et al.* tested different stilbene derivatives using the DPPH assay and they showed that increasing the number of phenolic moieties resulted in an increase of antioxidant activity. In particular, the pentahydroxy stilbene derivatives turned out to be more active than tetrahydroxy and trihydroxy stilbene derivatives (Wang, Jin and Ho, 1999). In another example, Lee *et al.* confirmed the vital role for antioxidant activity of phenolic group in the stilbene chemical moiety by replacing them with a methoxy group, that resulted in the complete loss of the free radical scavenging activity (Lee *et al.*, 2004).

The role of the hydroxycinnamic acid moiety in antioxidant property has been studied by Gaspar *et al.* and Terpinic *et al.* for a number of years. Gaspar *et al.* reported a series of 5-bromo derivatives of caffeic acid, ferulic acid and their corresponding ethyl esters. These derivatives showed

enhanced partition coefficients (logP) compared with the respective starting compounds, a fundamental requirement for what concern absorption, distribution, metabolism and excretion (ADME), however no significant difference was observed for their antioxidant activities in both DPPH and ABTS assays (Gaspar *et al.*, 2009).

Subsequently, 4-vinyl derivatives of hydroxycinnamic acids have been described by Terpinc *et al.* These novel compounds 4-vinylphenol, 4-vinylguaiacol, 4-vinylsyringol and 4-vinylcatechol were prepared from the corresponding acids and their antioxidant activities were tested (see figure 1.26).

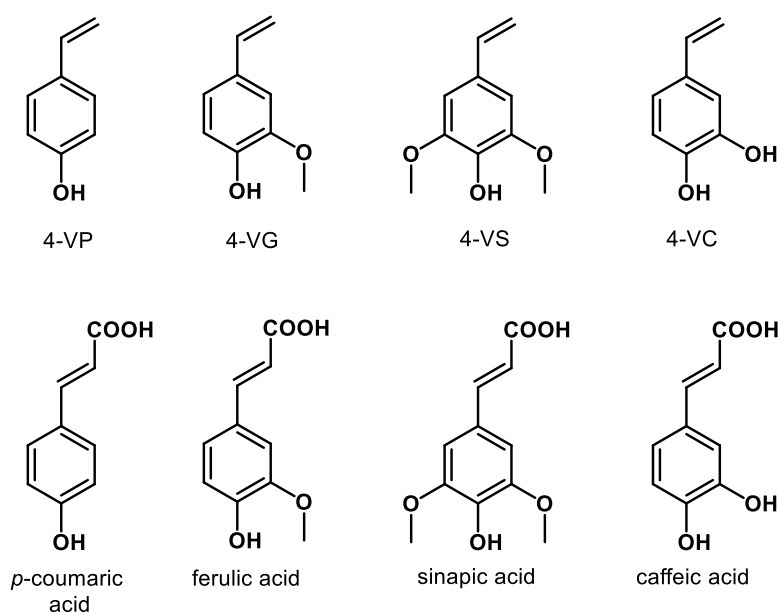


Figure 1.26. Chemical structures of 4-vinylphenol (4-VP), 4-vinylguaiacol (4-VG), 4-vinylsyringol (4-VS), 4-vinylcatechol (4-VC) and their corresponding hydroxycinnamic acids reported by Terpinc *et al.* (2011)

Interestingly, those derivatives showed weaker antioxidant activities compared with the starting compounds in DPPH and superoxide anion scavenging assays, both using polar media. However they showed better performances in the  $\beta$ -carotene bleaching test, which was performed in an emulsion system, indicating the enhanced activity of the latter due to the improved lipophilicity (Terpinc *et al.*, 2011).

Gallic acid derivatives were described by Khaledi *et al.* in 2011 and they were hydrazone derivatives (figure 1.27) containing an indole moiety. All the 8 derivatives reported were more active in the DPPH assay compared

with ascorbic acid and  $\alpha$ -Tocopherol, whereas only two showed similar anti-lipid peroxidation effects to these natural antioxidants (Khaledi *et al.*, 2011).

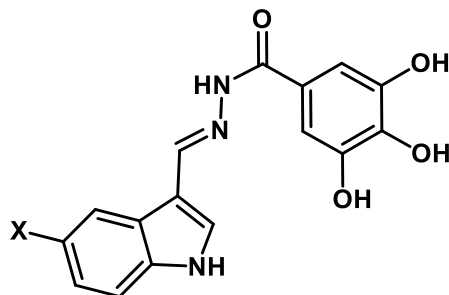


Figure 1.27. Most active gallic acid derivatives reported by (Khaledi *et al.*, 2011); compound 3e (X = Cl) and compound 3f (X = Br).

#### 1.2.3.2.1 Multitarget-based Synthetic Antioxidants

Drugs hitting a single biological target could be inadequate for the treatment of diseases which involve multiple factors, such as neurodegenerative diseases, cancer, cardiovascular diseases and diabetes. Recently, the idea of multi-target-directed ligands (MTDLs), able to hit multiple target thought to be responsible for the diseases has rapidly gain the attention of researchers (Cavalli *et al.*, 2008). A wide number of synthetic antioxidants have been recently described for their possible use in the treatment of pathologies for which oxidative stress is not the only hallmark.

##### 1.2.3.2.1.1 Synthetic Antioxidants in AD

It is well established that Alzheimer's disease (AD) is characterized by neuronal loss, depletion of cholinergic transmission, extracellular amyloid beta-peptide (A $\beta$ )-rich senile plaques and oxidative stress (Mufson *et al.*, 2009; Butterfield, Swomley and Sultana, 2013). For this reason, recent research has focused on the synthesis of new antioxidants able to reduce oxidative stress as well as prevent amyloid aggregation and improve cholinergic transmission by inhibiting acetylcholinesterase enzyme (Leon, Garcia and Marco-Contelles, 2013; Benchekroun *et al.*, 2016). Recently, Li, Wang and Kong reported the synthesis of several imine resveratrol derivatives with strong antioxidant properties (almost 8 times more active than resveratrol using the DPPH assay) and furthermore they were able to

inhibit the amyloid  $A\beta_{(1-42)}$  self-induced aggregation. In addition, these derivatives showed improved protective effects on hydrogen peroxide-stressed SH-SY5Y cells when compared with resveratrol (Li, Wang and Kong, 2014). The most active compound of the series, (*E*)-4-(((2-hydroxyphenyl)imino)methyl)benzene-1,2-diol, is reported in figure 1.28.

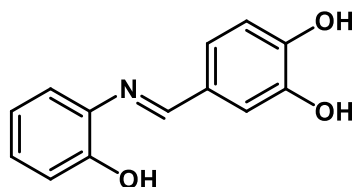


Figure 1.28. Synthetic resveratrol analogue reported by Li, Wang, and Kong (2014).

In another example, Yang *et al.* reported several resveratrol-pyridoxine hybrids bearing antioxidant and anticholinesterase properties. These compounds prevented the oxidation of the fluorescent probe fluorescein in the ORAC assay, showing better free radical scavenging properties compared with the synthetic antioxidant Trolox, and good inhibitory activity towards cholinesterase enzyme, with an  $IC_{50}$  as low as  $1.56 \mu M$  ((*E*)-2-((diethylamino)methyl)-5-(2-(2,2,8-trimethyl-4H-[1,3]dioxino[4,5-c]pyridin-5-yl)vinyl)phenol, see figure 1.29) (Yang *et al.*, 2017).

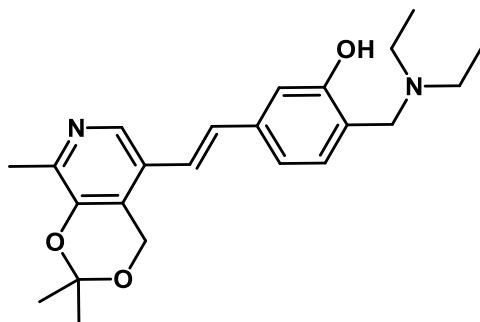


Figure 1.29. Resveratrol-pyridoxine hybrid reported by Yang *et al.* (2017).

Recently, several molecules obtained by the combination of tacrine (1,2,3,4-tetrahydroacridin-9-amine), a well-known cholinesterase inhibitor, with several antioxidant moieties, have been reported. Benchekroun *et al.* showed tacrine derivatives with a melatonin moiety, have shown to activate the Nrf2/ARE pathway, together with a lipoic acid or ferulic acid moiety, both of which exhibit antioxidant properties. In particular, compound ((*E*)-3-(4-hydroxy-3-methoxyphenyl)-*N*-(7-((7-methoxy-1,2,3,4-

tetrahydroacridin-9-yl)amino)heptyl)-*N*-(2-((2-(5-methoxyindolin-3-yl)ethyl)amino)-2-oxoethyl)acrylamide, figure 1.30) turned out to be the most active of the series, with strong cholinesterase affinity ( $IC_{50}$  of 1.29  $\mu$ M), strong antioxidant properties in the ORAC assay (9.11 Trolox Equivalents) and an ability to activate the Nrf2/ARE pathway in AREc32 cells at concentration as low as 3  $\mu$ M (Benchekroun *et al.*, 2016).

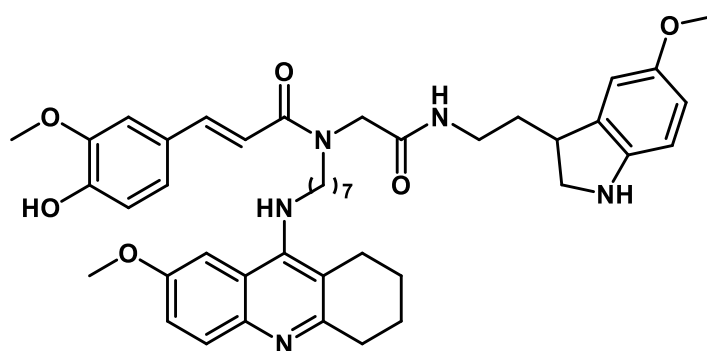


Figure 1.30. Tacrine-melatonin hybrid described by Benchekroun *et al.* (2016).

Previously, Rodríguez-Franzo *et al.* reported tacrine-melatonin hybrids with higher cholinesterase activities, with  $IC_{50}$  value of 0.5 nM, but with reduced antioxidant properties (4 Trolox Equivalents, compared to the 9.11 TE of the hybrids reported by Benchekroun *et al.*) (Rodríguez-Franco *et al.*, 2006).

In 2012, Chen *et al.* described a series of tacrine-ferulic acid-NO donors with cholinesterase activities at nanomolar levels. These compounds were able to improve cognition activities in mice when treated with scopolamine. The ability of these compounds to release NO was important because increasing evidences showed the beneficial effects of increasing blood supply in cerebral circulation in AD treatment. It is worth noting that all the derivatives (general structures reported in figure 1.31) showed weak or no antioxidant activities, due to the substitution of the phenolic group in the ferulic acid moiety (Chen *et al.*, 2012, 2013).

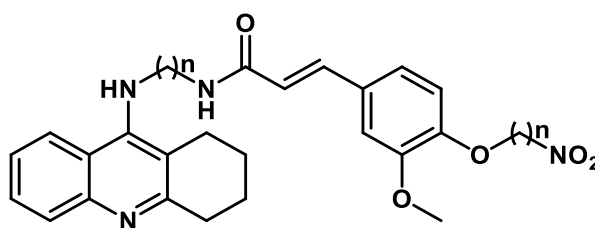


Figure 1.31. General structures of tacrine-ferulic acid-NO donors reported by Chen *et al.* (2012).

In the same year, Huang *et al.* reported a series of benzylideneindanone derivatives with significant antioxidant activities (ranging from 2.60 up to 9.37 TE using the ORAC assay) and able to prevent self-mediated A $\beta_{(1-42)}$  amyloid peptide aggregation (up to 80.1%, compared with the positive control, curcumin, 52.1%). In addition, the compound (*E*)-5,6-dihydroxy-2-(4-(methyl(propyl)amino)benzylidene)-2,3-dihydro-1H-inden-1-one (figure 1.32) exhibited chelating properties toward Cu<sup>2+</sup> ion, which is involved in oxidative stress through the Fenton reaction and in Cu(II)-induced A $\beta$  aggregation (Huang *et al.*, 2012).

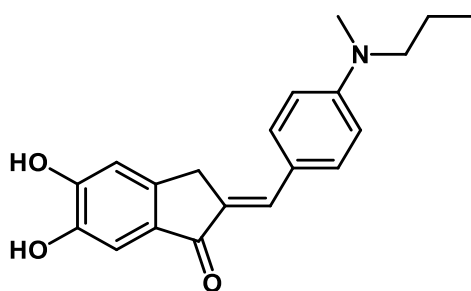


Figure 1.32. Chemical structure of (*E*)-5,6-dihydroxy-2-(4-(methyl(propyl)amino)benzylidene)-2,3-dihydro-1H-inden-1-one reported by Huang *et al.* (2012).

More recently, Wang *et al.* described new cinnamamide-dibenzylamine hybrids with modest antioxidant properties (ranging from 0.26 up to 4.24 TE in ORAC assay) and anti-cholinesterase activity (with IC<sub>50</sub> ranging from 1.05 to 6.63  $\mu$ M). Furthermore, these compounds showed interesting abilities in preventing the self-mediated A $\beta_{(1-42)}$  amyloid peptide aggregation (up to 56.8%, compared with the positive control curcumin 42.5%) and in chelating metal ions, with derivative (*E*)-*N*-(4-((benzyl(methyl)amino)methyl)phenyl)-3-(3,4-dihydroxyphenyl)acrylamide (figure 1.33) was able to chelate Cu<sup>2+</sup>, Zn<sup>2+</sup> and Fe<sup>3+</sup> but not Fe<sup>2+</sup>.

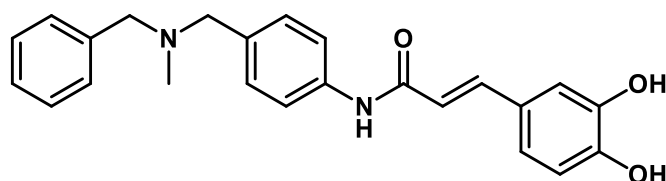


Figure 1.33. Chemical structure of (*E*)-*N*-(4-((benzyl(methyl)amino)methyl)phenyl)-3-(3,4-dihydroxyphenyl)acrylamide described by Wang *et al.* (2017).

The latter compound was then tested in a learning and memory impairment model in rats. Beneficial effects were detected at concentration of 10 mg/kg

in a scopolamine-induced memory deficit involving the step-down passive avoidance test, showing comparable effects to donepezil (5 mg/kg) (Wang *et al.*, 2017).

Due to the ability of curcumin to inhibit amyloid aggregation, several synthetic derivatives have been synthesized in an attempt to improve its antioxidant activities and solubility. In 2014, Fang *et al.* reported several dimethylaminomethyl substituted curcumin derivatives with improved antioxidant activities toward DPPH and galvinoxyl radicals; in particular, derivative (1*E*,4*Z*,6*E*)-1,7-bis(3-((dimethylamino)methyl)-4-hydroxyphenyl)-5-hydroxyhepta-1,4,6-trien-3-one (figure 1.34) showed an IC<sub>50</sub> of 1.6 μM in DPPH assay and 4.9 μM in galvinoxyl, compared with curcumin (26.5 and >100 μM, respectively).

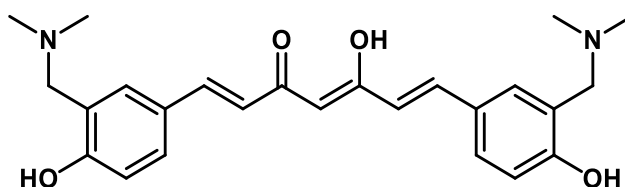


Figure 1.34. Dimethylaminomethyl substituted curcumin derivative reported by Fang *et al.* (2014)

Moreover, the latter showed similar activity compared with curcumin in the inhibition of the self-aggregation of Aβ<sub>(1-42)</sub> amyloid at concentrations of 50 and 100 μM, whereas both compounds were not active at concentrations of 5 μM. Of note, the hydrochloride salt of the curcumin derivative (figure 1.34) showed a solubility of 16.7 mg/ml, far higher than that of curcumin (<0.1mg/ml), making it amenable for possible clinical application (Fang *et al.*, 2014).

#### 1.2.3.2.1.2 Synthetic Antioxidants in PD

Parkinson's disease (PD) is a neurodegenerative disease associated with the loss of dopaminergic neurons in the substantia nigra pars compacta (SNc), with the consequential depletion of dopamine levels in the nigrostriatal dopaminergic pathway in the brain. Although the molecular pathway is not completely understood, mitochondrial dysfunction, protein misfolding,

protein phosphorylation and oxidative stress play a major role in development of the disease (Cavalli *et al.*, 2008; Blesa *et al.*, 2015).

Kaidery *et al.* described new synthetic triterpenoids (TP-224, TP-319 and TP-500) (see figure 1.35) that were able to activate the Nrf2/ARE pathway in 1-methyl-4-phenyl-1,2,3,6-tetrahydropyridine (MPTP) mouse model of PD.

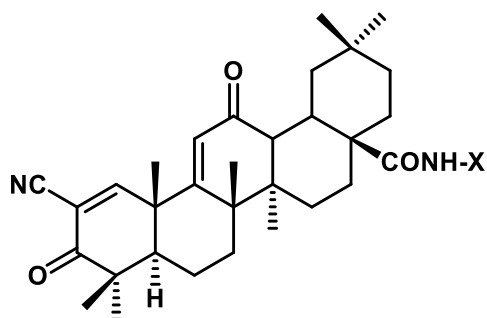


Figure 1.35. Synthetic triterpenoids TP-224 (X = -Me), TP-319 (X = -Et) and TP-500 (X = -CH<sub>2</sub>-CF<sub>3</sub>) described by Kaidery *et al.* (2013).

Mice were treated with the synthetic triterpenoids (4  $\mu$ mol) twice a day for 12 weeks and the levels of ARE-controlled gene expression, such as glutamate-cysteine ligase regulatory subunit (GCLM), glutamate-cysteine ligase catalytic subunit (GCLc), haem-oxygenase-1 (HO-1), NAD(P)H dehydrogenase quinone 1 (NQO1) and glutathione-disulfide reductase (GSR) were measured in the liver and striatum. The expression of all these genes was significantly increased (between 5 to 25-fold times) in the liver, but only NQO1 and HO-1 were upregulated in the striatum.

These synthetic triterpenoids were then tested in the MPTP model of PD, where mice were treated with 10 mg MPTP/kg three times a day every 2 hours, causing 50% dopamine loss in the SNc compared with the saline control. The synthetic triterpenoids were found to reduce cell death while increasing the levels of dopamine up to 37% compared with the MPTP control. In addition, the inflammatory marker, 3-nitrotyrosine, in SNc was completely depleted in this area of the brain from the triterpenoid-treated mice. Finally, to confirm the Nrf2-dependent pathway in the neuroprotection identified, these triterpenoids were tested in Nrf2 KO mice, where they did not show significant protection against MPTP toxicity (Kaidery *et al.*, 2013).

In 2009, Pinnen *et al.* reported a series of L-Dopa derivatives with antioxidant properties to avoid the pro-oxidative effects of the L-Dopa treatment for PD. These compounds were found to release L-Dopa and dopamine in the plasma after enzymatic hydrolysis and had a higher antioxidant activity compared with *N*-acetylcysteine. In addition, one of the synthetic compounds (methyl ((*S*)-2-acetamido-3-(3,4-dihydroxyphenyl)propanoyl)-*L*-methioninate, see figure 1.36) increased the level of dopamine in the rat's striatum, after intracerebroventricular injection, compared with the L-Dopa-treated group, showing a longer half-life in the brain (Pinnen *et al.*, 2009).

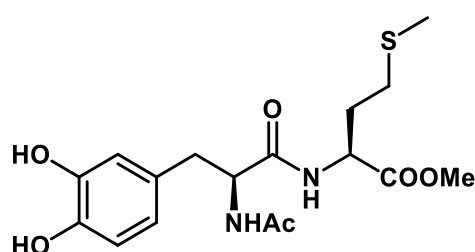


Figure 1.36. Methyl ((*S*)-2-acetamido-3-(3,4-dihydroxyphenyl)propanoyl)-*L*-methioninate, reported by Pinnen *et al.* (2009).

In 2008, Liu *et al.* described a synthetic hybrid of cyclohexyl bisphenol A (CBA) and curcumin known as CNB-001 (figure 1.37). Previously, CBA had shown to protect cells from  $A\beta_{(1-42)}$  and glutamate toxicity as well as from the loss of trophic factor support, whereas curcumin was protective in a transgenic animal model for AD.

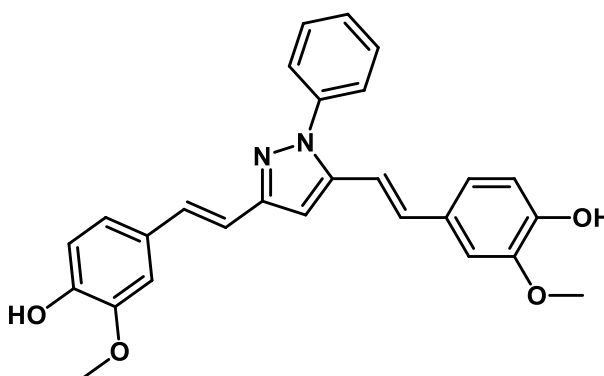


Figure 1.37. CNB-001 chemical structure.

In that study, the hybrid showed lower antioxidant activity compared with curcumin, but similar activity to that of CBA. However, CNB-001 showed

neurotrophic factor-like activities several fold better than CBA in rat cortical neurons. It is worth noting that these neurotrophic factors play a predominant role in the maintenance of cell survival following CNS injury. In addition, the synthetic hybrid inhibited amyloid-induced cell death in MC65 cell line with an IC<sub>50</sub> of 300 nM, compared with CBA (>10 µM) and curcumin (inactive) (Liu *et al.*, 2008). These findings prompted a great deal of interest on CNB-001. Jayaraj *et al.* reported a protective effect of this curcumin derivative in a SK-N-SH cellular model of PD. The cells were pretreated with CNB-001 for 2 hours, with concentrations ranging from 0.5 up to 4 µM before the exposure to rotenone (100 nM). The results showed that CNB-001 protected the cells at all the tested concentrations, with higher protection at 2 µM concentration. In addition, CNB-001 showed a reduction of ROS formation after treatment with rotenone (100 nm), using 2',7'-dichlorodihydrofluorescein diacetate (H<sub>2</sub>DCFDA) as a fluorescent probe for ROS detection. Furthermore, pretreatment with the drug significantly attenuated the expression of pro-apoptotic proteins and increased the expression of the anti-apoptotic protein Bcl-2, implicating a dual mechanism of protection against rotenone toxicity that included both antioxidant and anti-apoptotic pathways (Jayaraj *et al.*, 2013).

A year later, another work by Jayaraj *et al.* reported the protective effect of CNB-001 in a different PD model, using MPTP in adult mice. In this work, the authors observed an increase in dopamine levels in the mice pretreated with concentrations of drug ranging from 6-48 mg/kg, with its maximum between 24 and 48 mg/kg. Mice pretreated with 24 mg/kg of CNB-001 showed attenuation of Parkinsonian impairments, reduced lipid peroxidation, activation of antioxidant response and reduced dopaminergic neuron loss compared with the MPTP control. In particular, the drug increased the levels of reduced glutathione, GPx activity and the expression of tyrosine hydroxylase (TH), dopamine transporter (DAT) and vesicular monoamine transporter 2 (VMAT2), compared with the MPTP control (Jayaraj *et al.*, 2014).

More recently, CNB-001 was found to suppress lipopolysaccharide (LPS)-induced NO production and the expression of the inducible NO synthase (iNOS) in primary cultured rat microglia more effectively than curcumin. In

addition, CNB-001 suppressed the LPS-induced nuclear translocation of NF $\kappa$ B and p38 MAPK phosphorylation, both involved in the inflammatory response (Akaishi and Abe, 2018).

#### 1.2.3.2.1.3 Synthetic Antioxidants in Inflammation

Several works have reported that antioxidants also exert anti-inflammatory properties. For example, the quinolinone moiety has attracted the interest of several research groups due to its antioxidant and anti-inflammatory properties and, in 2007, Detsi *et al.* reported a series of quinolinone-3-aminoamides and their adducts with  $\alpha$ -lipoic acid. Almost all these derivatives demonstrated interesting scavenging activity toward DPPH and hydroxyl free radicals, as well as the ability to inhibit 5-lipoxygenase (5-LOX), a well-known pro-inflammatory enzyme involved in the conversion of arachidonic acid into eicosanoids, in an *in vitro* assay. Furthermore these compounds reduced carrageenin-induced rat paw oedema *in vivo*, with *N*-(2-aminophenyl)-4-hydroxy-1-methyl-2-oxo-1,2-dihydroquinoline-3-carboxamide (see figure 1.38) the most active, with an activity almost two times fold compared to the reference drug, indomethacin (Detsi *et al.*, 2007).

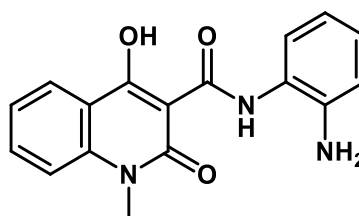


Figure 1.38. *N*-(2-aminophenyl)-4-hydroxy-1-methyl-2-oxo-1,2-dihydroquinoline-3-carboxamide described by Detsi *et al.* (2007)

In 2014, Matralis and Kourounakis described several phenothiazine derivatives with strong antioxidant and anti-inflammatory properties. Their work was based on the finding that phenothiazine moiety is able to inhibit lipid peroxidation and to exert cytoprotective effects due to their antioxidant properties (Yu *et al.*, 1992). Compounds synthesized by Matralis and Kourounakis were able to inhibit lipid peroxidation at concentrations as low as 0.33  $\mu$ M, together with the complete inhibition of cyclooxygenase-2 (COX-2) at concentration of 20  $\mu$ M *in vitro*. The latter enzyme is involved in

pro-inflammatory prostaglandin biosynthesis and is the target of several nonsteroidal anti-inflammatory drugs (NSAIDs). In addition, these phenothiazine derivatives turned out to be excellent inhibitors of squalene synthase (SQS) - a key enzyme in the biosynthesis of cholesterol - in an *in vitro* model. The derivative, 4-methyl-2-(10H-phenothiazin-2-yl)morpholin-2-ol (see figure 1.39), exhibited anti-hyperlipidaemic properties in an experimentally-induced hyperlipidaemic rat model (reducing total cholesterol by 70%, LDL by 80% and triglyceride by 94%) and in mice fed a high-fat diet (reducing the total cholesterol by 53% and the LDL by 76%) (Matralis and Kourounakis, 2014).

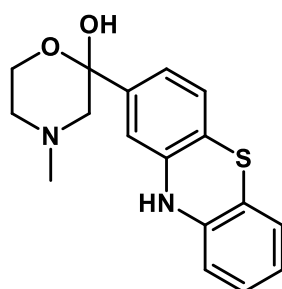


Figure 1.39. 4-methyl-2-(10H-phenothiazin-2-yl)morpholin-2-ol reported by Matralis and Kourounakis (2014).

More recently, Abd El Razik *et al.* reported a series of benzodioxole-pyrazole hybrids with strong anti-inflammatory properties, both *in vitro* and *in vivo*, and antioxidant activity comparable with ascorbic acid. The chemical structures of these derivatives were based on Celecoxib and Lonazolac, two pyrazoles currently used as analgesic and anti-inflammatory agents. Interestingly, the compounds synthesized by Abd El Razik *et al.* turned out to be potent COX-2 and 5-LOX inhibitors *in vitro*, with  $IC_{50}$  ranging from 0.33-3.56  $\mu$ M and 3.11-9.94  $\mu$ M, respectively. These activities are comparable with the NSAIDs currently on the market such as celecoxib and meclufenamate. Furthermore, two of these derivatives decreased TNF- $\alpha$  expression in LPS-stimulated cells by 85.19 and 97.71%, with activities comparable to hydrocortisone (94.74%). In terms of antioxidant potential, the ability of several benzodioxole-pyrazole hybrids compounds to scavenge the DPPH free radical and to inhibit the lipid peroxidation was comparable to that of ascorbic acid. Finally, *in vivo* studies confirmed the anti-inflammatory and analgesic properties of these derivatives; in the rat paw oedema test, the compounds showed reduced volume of oedema by up to

55.5% compared to the control, whereas, after intra-peritoneal injection of acetic acid, rats pretreated with the compounds showed less writhing compared to the controls, confirming the analgesic effects of these benzodioxole-pyrazole hybrids, with (*E*)-2-(2-(5-(benzo[d][1,3]dioxol-5-yl)-1-(4-sulfamoylphenyl)-1H-pyrazole-3-carbonyl)hydrazineylidene)propanoic acid (see figure 1.40) the most active (El Razik *et al.*, 2017).

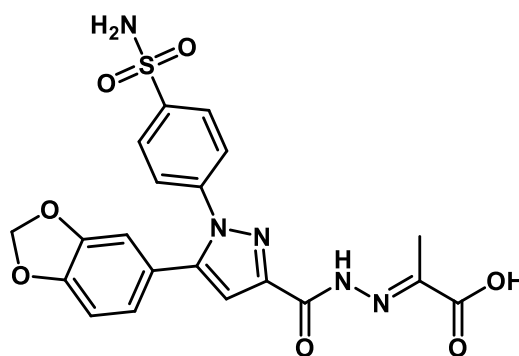


Figure 1.40. (*E*)-2-(2-(5-(benzo[d][1,3]dioxol-5-yl)-1-(4-sulfamoylphenyl)-1H-pyrazole-3-carbonyl)hydrazineylidene)propanoic acid reported by El Razik *et al.* (2017)

Due to the central role that oxidative stress plays in neurodegenerative diseases, cancer, cardiovascular diseases and inflammation, the synthesis of novel synthetic antioxidants, with improved antioxidant activities, that could hit different biological target is a promising strategy for the treatment or prevention of these illness.

### 1.3 Aims of Project

The aim of the project was to synthesize novel vanillin derivatives and determine their antioxidant activities, their cytoprotective effects on neuroblastoma SH-SY5Y cell line and the mechanism that may contribute to their protective effects.

Several derivatives were synthesized to predict a structure-activity relationship (SAR) for this class of compounds in different antioxidant assays, which exploited different antioxidant mechanisms.

Furthermore, selected compounds were tested in the SH-SY5Y neuroblastoma cell line and their abilities to protect the cells from oxidative insult were evaluated.

In addition, the abilities of the selected compounds to suppress ROS and to protect the DNA in SH-SY5Y cells after the treatment of the cells with hydrogen peroxide were investigated.

Moreover, the ability of the selected compounds to trigger the Nrf2 antioxidant pathway was investigated through western blot.

The use of selected compounds in the multi-target-directed strategy for AD therapy was assessed by evaluating their inhibitory activities toward the acetylcholinesterase enzyme and the amyloid  $A\beta_{(1-42)}$  self-induced aggregation. Modeling studies were performed to better understand the molecular elements contributing to the AChE inhibitory activity of latter compounds.

Finally, simulations on the ability of selected compounds to cross the blood-brain-barrier (BBB) were run.

# **Chapter 2: Synthesis of Novel Vanillin Derivatives**

## 2.1 Vanillin Derivatives

### 2.1.1 Overview on Vanillin Derivatives

In the past decade, several vanillin derivatives with different biological activities have been reported, indicating the versatility of this moiety. In particular, a substantial amount of work has been carried out regarding the antifungal and antimicrobial activity of vanillin derivatives.

In 2012 Harini *et al.* described a novel vanillin derived from piperidin-4-one oxime esters that possessed antimicrobial properties and modest antioxidant activities. Their synthetic approach (figure 2.1) was first based on a Mannich condensation reaction between vanillin, acetone and ammonium acetate followed by *N*-alkylation using iodomethane to yield the corresponding 2,6-bis(4-hydroxy-3-methoxyphenyl)-1-methylpiperidin-4-one. The latter was then converted into the corresponding oxime using hydroxylamine hydrochloride and finally esterified with different benzoyl chlorides to yield the final products.

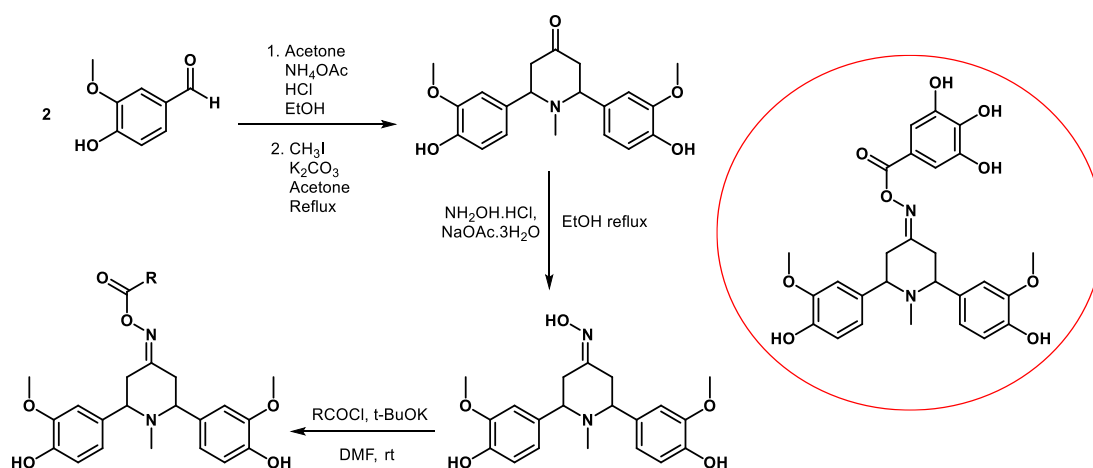


Figure 2.1. Synthetic approach for the synthesis of vanillin derivatives reported by Harini *et al.* (2012), adapted with copyright agreement © 2012 Elsevier Ltd.

The derivatives reported in this work showed inhibitory activity towards *E. Coli*, *S. Aureus* and *P. Aeruginosa* comparable with streptomycin, a common antibiotic. Of note, 2,6-bis(4-hydroxy-3-methoxyphenyl)-1-methylpiperidin-4-one O-(3,4,5-trihydroxybenzoyl) oxime (circled in red) showed similar antioxidant activity to BHA in DPPH, ABTS and lipid peroxidation assays.

The antioxidant activity of this derivative was found to be due to the presence of two vanillin moieties and a gallic acid moiety in its chemical structure (Harini *et al.*, 2012).

In the same year, Rangaswami *et al.* described a series of antimicrobial benzofuran based 1,3,5-substituted pyrazole bearing the vanillin moiety in its structure to boost their antioxidant properties. The synthetic pathway, depicted in figure 2.2, involved a five-step reaction strategy; the starting material (2-acetyl benzofuran) was prepared by cyclocondensation between salicylic aldehyde and chloroacetone in DCM in the presence of 1,8-diaza bicyclo[5.4.0]undec-7-ene (DBU) and molecular sieves.

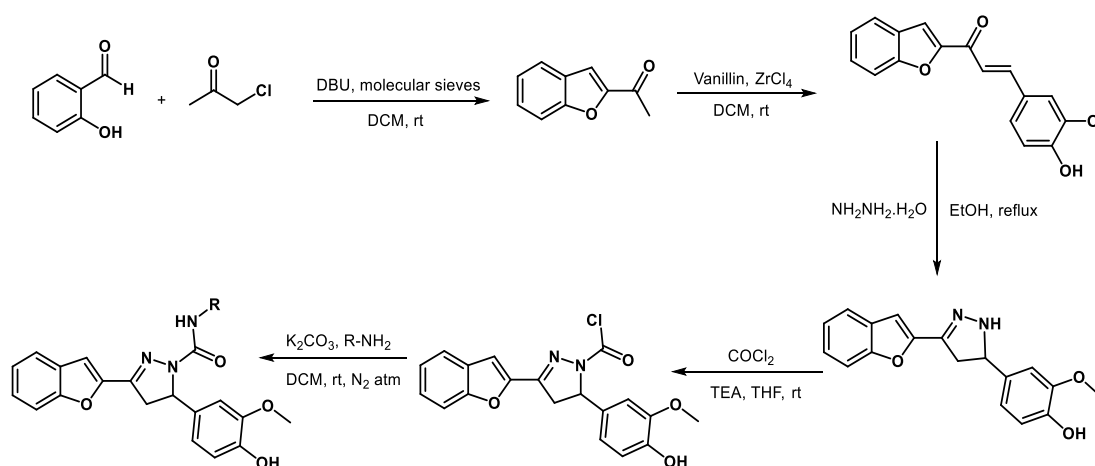


Figure 2.2. Synthetic strategy for the synthesis of vanillin derivatives reported by Rangaswamy *et al.* (2012), adapted with copyright agreement © 2012 Elsevier Ltd.

The latter was then reacted with vanillin to afford benzofuran chalcone (E)-1-(benzofuran-2-yl)-3-(4-hydroxy-3-methoxyphenyl)prop-2-en-1-one through Claisen-Schmidt condensation, which was subsequently reacted with hydrazine hydrate to yield 4-(3-(benzofuran-2-yl)-4,5-dihydro-1H-pyrazol-5-yl)-2-methoxyphenol. The latter was treated with phosgene in the presence of triethylamine to afford 3-(benzofuran-2-yl)-5-(4-hydroxy-3-methoxyphenyl)-4,5-dihydro-1H-pyrazole-1-carbonyl chloride which was finally reacted with different substituted anilines to yield the desired products.

All the compounds were tested for their antioxidant properties through the DPPH and microsomal LPO assays; it is interesting to note that the derivative which bears an extra vanillin moiety in the chemical structure (R = vanillin) showed antioxidant activities in both DPPH and lipid peroxidation

assays, comparable to BHA. On the other hand, almost all the derivatives showed modest antimicrobial and antifungal properties when compared with therapeutic agents, streptomycin and fluconazole (Rangaswamy *et al.*, 2012).

In addition, Dangar, Borkhataria and Shah (2014) reported in the same year Schiff's base vanillin derivatives, and corresponding reduced products, with modest antimicrobial and antifungal activities. The synthetic approach of the work is described in figure 2.3. Schiff's bases are characterized by the  $-CH=N$  group, obtained by reacting an aldehyde (or ketone) with an amine with the loss of water. The resulting imine was reduced to yield the corresponding secondary amine.

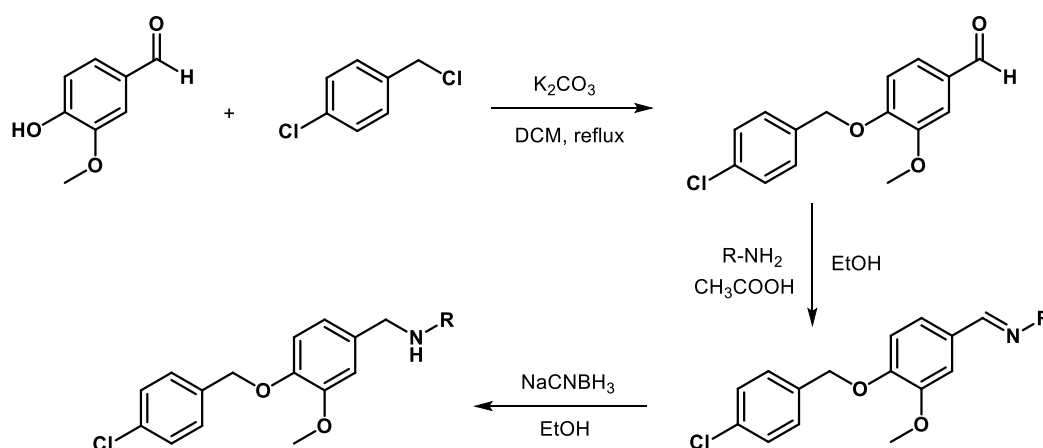


Figure 2.3. Synthetic approach for the synthesis of vanillin derivatives reported by Dangar, Borkhataria, and Shah (2014).

These compounds reported by this group showed modest antimicrobial activity when compared with amoxicillin and ampicillin (two common antibiotics) against *E. Coli* and *S. Aureus* and antifungal activity comparable to griseofulvin (a common antifungal agent) (Dangar, Borkhataria and Shah, 2014).

In addition to the antimicrobial vanillin-based agents, several other antioxidants vanillin derivatives have been reported in the literature.

The synthetic derivative, ethylvanillin (3-ethoxy-4-hydroxybenzaldehyde), is extensively used in the chocolate industry due to its intense flavouring capacity ( $\sim 3$  fold compared to vanillin). It is synthetically produced following the same procedure as for the synthesis of vanillin, but using

guethol (2-ethoxyphenol) instead guaiacol (2-methoxyphenol) as the starting compound (Fahlbusch *et al.*, 2012), as depicted in figure 2.4.

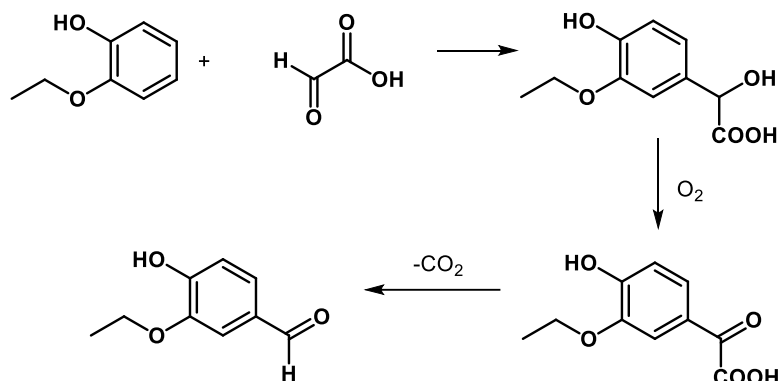


Figure 2.4. Synthetic process for the synthesis of ethylvanillin.

The antioxidant activity of ethylvanillin is comparable to vanillin in both ORAC and ABTS scavenging assays, where it turned out to possess stronger antioxidant activity compared to Trolox, but was completely inactive in the DPPH assay (Tai, Sawano and Yazama, 2011).

In the last decade, Lee *et al.* published several works on vanillin-based dendrimers. In 2009, the group reported three novel dendrimers which possessed strong free radical scavenging properties toward DPPH, with IC<sub>50</sub> ranging from 3.7 to 6.0  $\mu$ M compared with the standard Trolox (27.6  $\mu$ M). In addition, these compounds showed protection against LDL and fatty acids oxidation and an ability to reduce plasmid DNA damage after the incubation of pBR322 DNA plasmid with 2,2'-Azobis(2-amidinopropane) (AAPH) at 10 mM concentration. In particular, dendrimer 4,4',4'',4'''-(((1,4-phenylenebis(methylene)))bis(azanetriyl))tetrakis(methylene))tetrakis(2,6-dimethoxyphenol) completely protected the DNA at concentration of 11  $\mu$ M with only partial protection at 3  $\mu$ M.

The dendrimer was generally prepared in a one-step reaction by mixing syringaldehyde and 4-aminomethylbenzylamine in 1,2-dichloroethane in the presence of sodium triacetoxyborohydride as reducing agent, as described in figure 2.5.

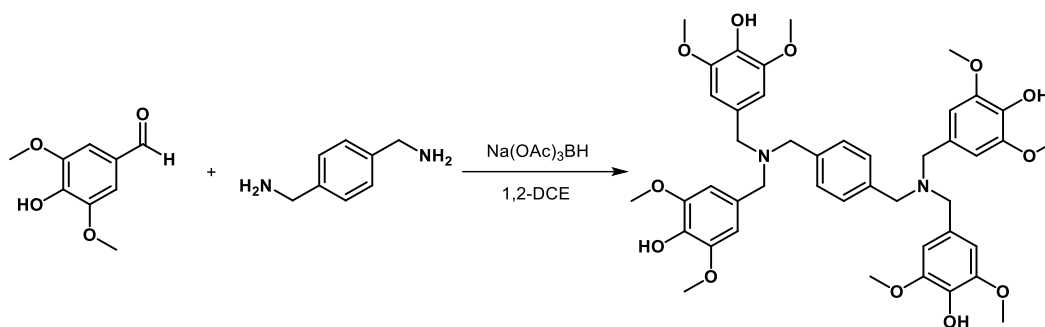


Figure 2.5. Synthetic strategy for the dendrimer reported by Lee *et al.* (2009), with copyright agreement © 2009 Elsevier Ltd.

In 2015, new dendrimers bearing electron donating groups were reported by the same group. Interestingly, they found that the free radical scavenging activities in DPPH assay of these dendrimers were proportional to the number of methoxy group in the aromatic ring. Indeed, syringaldehyde derivatives, bearing two methoxy moieties (see figure 2.6) were better scavenger than vanillin derivatives (with only one methoxy moiety) and 4-hydroxybenzaldehyde derivatives (with no methoxy group) showed no activity in the assay.

In the DNA protection assay, the dendrimers followed the same trend with the syringaldehyde derivative being the most active, followed by the vanillin derivatives and the 4-hydroxybenzaldehyde derivatives (Lee *et al.*, 2015).

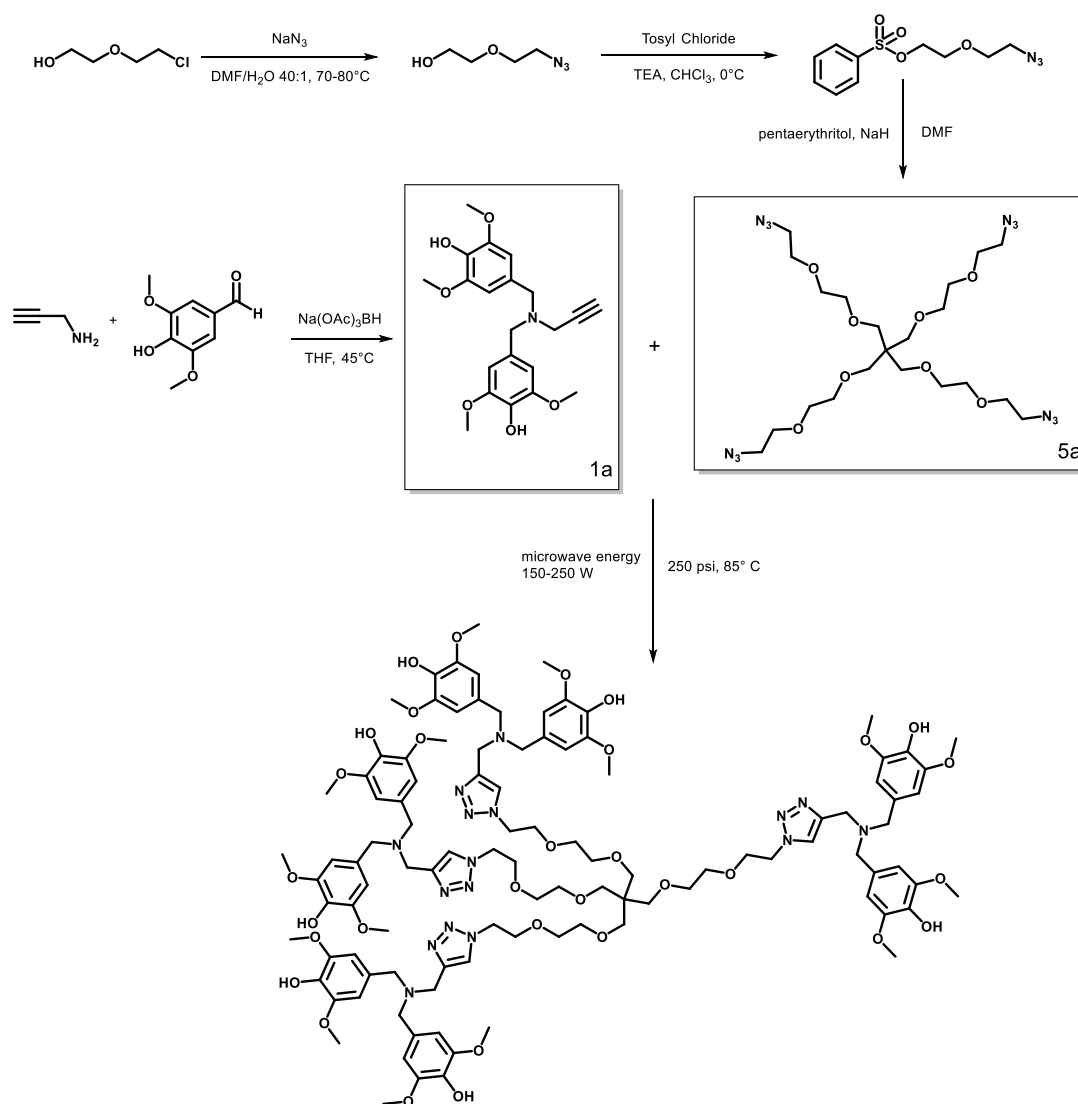


Figure 2.6. Synthetic strategy for the synthesis of dendrimer adapted from Lee *et al.* (2015), with copyright agreement © 2015 Elsevier Ltd.

To obtain the final product, the two building blocks 1a and 5a, represented in the squares of figure 2.6, were synthesized.

4,4'-((prop-2-yn-1-ylazanediy)bis(methylene))bis(2,6-dimethoxyphenol) (1a) was obtained through reductive amination between propargylamine and syringaldehyde in THF using sodium triacetoxyborohydride as reducing agent.

1,15-diazido-8,8-bis((2-(2-azidoethoxy)ethoxy)methyl)-3,6,10,13-tetraoxapentadecane (5a) was prepared through a three-step reaction; sodium azide was reacted with 2-(2-chloroethoxy)ethanol in DMF/ $\text{H}_2\text{O}$  40:1 to yield 2-(2-azidoethoxy)ethan-1-ol which was treated with triethylamine (TEA) and tosyl chloride in chloroform to afford 2-(2-azidoethoxy)ethyl benzenesulfonate.

The latter was reacted with pentaerythritol in anhydrous DMF in the presence of sodium hydride to yield 5a. Finally, microwave energy-assisted reaction between the two building blocks (1a and 5a) afforded the desired compound.

Very recently, work from Chigurupati *et al.* reported several vanillin and cinnamaldehyde derivatives bearing an imine group. These compounds turned out to be good free radical scavengers in DPPH and ABTS assays, with activities comparable to ascorbic acid. The general synthetic approach for the synthesis of the vanillin derivatives reported in this work is reported in figure 2.7.

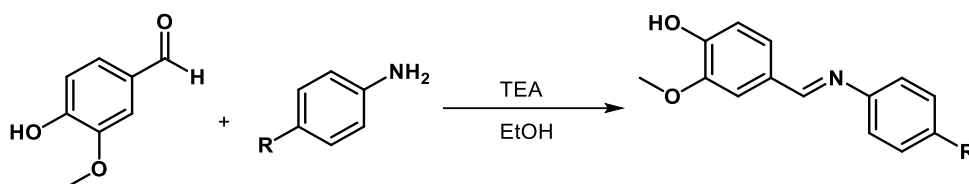


Figure 2.7. Synthetic strategy for the synthesis of the vanillin derivatives reported by Chigurupati *et al.* (2018). Reproduced with copyright agreement © 2017, Springer Science Business Media, LLC.

The most active compound (*E*)-4-((4-hydroxy-3-methoxybenzylidene)amino)benzoic acid (R=-COOH) yielded an IC<sub>50</sub> value of 14.07 and 15.06  $\mu$ M in DPPH and ABTS assays, respectively, compared to ascorbic acid (15.73 and 16.79, respectively) (Chigurupati *et al.*, 2018).

Due to the potential role of novel synthetic antioxidants in health and wellbeing, and the small amount of work on synthetic vanillin derivatives, the aim of the experimental work presented in this chapter was to design, synthesize and characterize a series of new vanillin derivatives with the potential for enhanced activity, particularly in the neurodegenerative disease setting.

## 2.2 Chemical Synthesis of Vanillin Derivatives

### 2.2.1 Rationale Behind the Synthesis of Novel Vanillin Derivatives

Several vanillin derivatives with different structural features were synthesized to allow a SAR study as regard to their antioxidant and neuroprotective properties.

All the compounds prepared are represented by the general structures shown in figure 2.8:

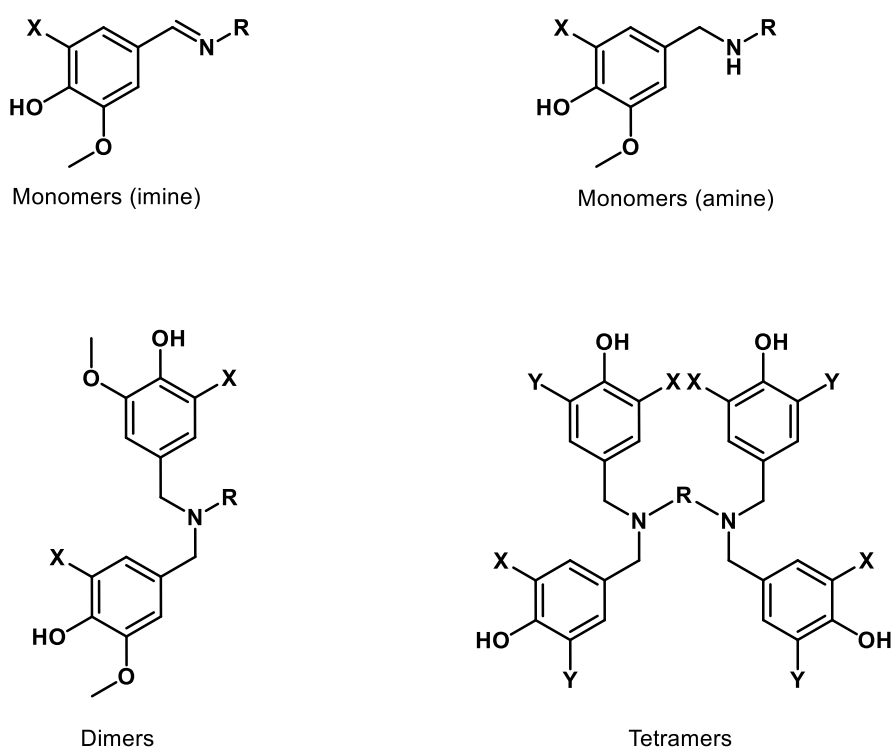


Figure 2.8. General structures of the proposed vanillin derivatives.

The vanillin derivatives presented in this work can be classified into four groups:

- (i) Monomers (imine): characterized by only one vanillin moiety in their chemical structure along with an imine group (-CH=N-).
- (ii) Monomers (amine): characterized by only one vanillin moiety in their chemical structure along with a secondary amino group (-CH<sub>2</sub>-NH-).

- (iii) Dimers: characterized by two vanillin moieties in their chemical structure.
- (iv) Tetramers: characterized by four vanillin moieties in their chemical structure.

Different substituents (R) linked to the nitrogen atom(s) and other modifications were exploited to determine their impact on antioxidant activity (see schemes 1, 2, 3 and 4 in the results and discussion section).

For example:

- (i) A selection of alkanolamines ( $\text{HO-CH}_{2(n)}\text{-NH}_2$ ) and alkylamines ( $\text{R-NH}_2$ ) were employed to generate different vanillin derivatives
- (ii) The role of an extra methoxy substituent in the vanillin ring ( $\text{X} = \text{-OCH}_3$ , syringaldehyde derivatives) in the antioxidant activities was also evaluated.
- (iii) Several modifications in the vanillin rings of the tetramers were made to study the impact of hydroxy and methoxy groups in the vanillin ring.
- (iv) The impact of the electronic conjugation between the two nitrogen atoms in the tetramers was studied by using an aromatic ring system, which is able to delocalise nitrogen's lone pair of electrons, and a cyclohexane ring, which is not able to delocalise nitrogen's electrons, as linkers between the latter.
- (v) The impact of the protonation of nitrogen atoms on the antioxidant activities was also investigated.
- (vi) Finally, several monomers bearing a tacrine or a naphthalimido moiety were prepared for the evaluation of their cholinesterase inhibitory activities along with their antioxidant activities (this will be discussed in chapter 5).

Tacrine is a well-known acetylcholinesterase enzyme inhibitor, a common target in the Alzheimer's Disease therapy (Colovic *et al.*, 2013).

On the other hand, the lack of studies on the naphthalimido moiety as a potential scaffold for the synthesis of novel cholinesterase inhibitors prompted further investigation with this moiety (Gao *et al.*, 2016).

### *2.2.2 Nomenclature*

The nomenclature used in this thesis is based on the number of vanillin moieties in each structure to facilitate the discussion of this work. Therefore, all the monomers are labelled as compound **1** followed by a letter, all the dimers as **2** and all the tetramers as **4** followed by a letter. The intermediates prepared for the final synthesis of the compounds are labelled with **I** followed by a number.

## 2.3 Materials and Methods

### 2.3.1 Materials

All reagents were purchased from Sigma Aldrich unless otherwise stated and were used without any further purification.

Chloroform-d	Cambridge Isotopes Laboratories Inc
Dichloromethane	Fisher Scientific
Diethyl Ether	Acros Organics
Dimethyl Sulfoxide	Fisher Scientific
DMSO-d6	Cambridge Isotopes Laboratories Inc
Potassium Iodide	Fisher Scientific
Silica 60 F <sub>254</sub> Gel	Merck
Silica 70-230 Mesh	Alfa Aesar
Sodium Sulfate Anhydrous	Fisher Scientific
Zinc Chloride	Fisher Scientific

### 2.3.2 Techniques for the Identification and Characterization of intermediates and new Vanillin Derivatives

Techniques employed for the characterization of the products were thin layer chromatography (TLC), nuclear magnetic resonance (NMR) and mass spectrometry (MS).

#### *Thin Layer Chromatography (TLC)*

TLC is a separation technique used for the identification of several components within a solution (Meyers and Meyers, 2008). TLC was used to monitor the reactions and to determine the purity of the compounds. A small drop of reaction mixture was dispensed on a silica gel aluminium plate (stationary phase) using a capillary glass. Once dry, the silica gel plate was placed in the vertical position in a TLC development tank containing a

mixture of dichloromethane (DCM) and methanol (mobile phase). Due to capillary action, the mobile phase travels up the plate and the components, which show different affinities for both mobile and stationary phases, travel at different rates causing the separation. The spots can be then visualised under UV-light ( $\lambda=243$  nm, see figure 2.9).

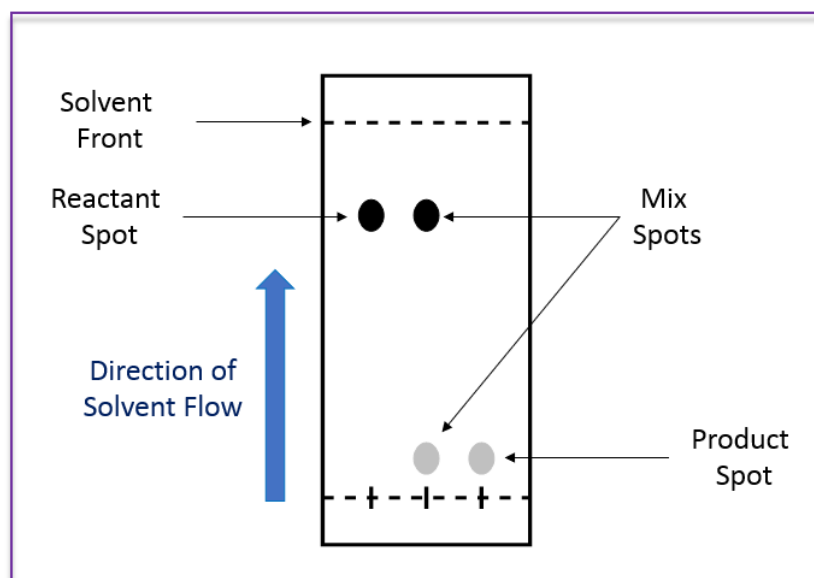


Figure 2.9. Thin Layer Chromatography plate.

### *Nuclear Magnetic Resonance (NMR)*

Nuclear Magnetic Resonance (NMR) spectroscopy is a common tool used for the confirmation of a proposed chemical structure. It relies upon the magnetic properties of atomic nuclei (nuclear spin); in particular, proton ( $^1\text{H}$ ) and carbon ( $^{13}\text{C}$ ) nuclei are useful for the characterization of novel compounds. In fact,  $^1\text{H}$  NMR and  $^{13}\text{C}$  NMR detect protons and carbon nuclei, respectively, in relation to their environment (Morris, 1986). For their structural confirmation, the compounds were dissolved in a convenient deuterated solvent, such as chloroform-d ( $\text{CDCl}_3$ ) or dimethyl sulfoxide-D6 ( $\text{DMSO-d}_6$ ) and transferred into an NMR tube before the introduction into the instrument (Bruker 400 Ultrashield). The experimental conditions were set using Bruker Topspin 1.3 software and the sample was analysed. An NMR spectrum was obtained and was then interpreted for the structural confirmation.

## *Mass Spectrometry (MS)*

Mass Spectrometry (MS) was employed for the structural characterization of the compounds. It is based on the ionization of molecules and the separation of charged fragments according to their mass-to-charge ratio ( $m/z$ ) using an electric and/or magnetic field. Molecules were injected into MS instrument and ionized through electrospray ionisation (ESI); the ions were then accelerated, amplified and detected (Siuzdak, 1996), generating a mass spectrum.

### *2.3.3 Instrumentation*

Thin Layer Chromatography (TLC) was performed on silica gel 60 F<sub>254</sub> Aluminium plates (2 cm x 5 cm) (Merck, Germany) using chloroform:methanol (95:5 or 90:10) mixture as mobile phase. Spots were visualised using UV-light (254 nm).

Nuclear Magnetic Resonance (NMR) spectroscopy was performed on a Bruker 400 Ultrashield spectrometer operating at 400.1 MHz for proton (<sup>1</sup>H) and, 100.6 MHz for carbon-13 (<sup>13</sup>C) NMR.

High Resolution Mass Spectrometry (HRMS) analysis was performed on the final compounds at the Engineering and Physical Sciences Research Council's (EPSRC) National Mass Spectrometry Service Centre at Swansea University, Swansea, UK.

Low Resolution Mass Spectrometry analysis was undertaken on the intermediates at Robert Gordon University using an Agilent Technologies 1200 series.

## *2.4 Methods*

### *2.4.1 Synthesis of Intermediates*

Amines **I-1** and **I-3** used for the synthesis of vanillin derivatives were not commercially available and were synthesized.

Amine **I-1** was prepared through a one-step reaction by reacting naphthalic anhydride and 1,3 diaminopropane in ethanol under reflux.

Amine **I-3** was prepared through a two-step reaction; the precursor 9-chloro-1,2,3,4-tetrahydroacridine (**I-2**) was obtained by treating a mixture of anthranilic acid and cyclohexanone with POCl<sub>3</sub>. The latter was then reacted with *p*-phenylenediamine in the presence of a catalytic amount of KI in 1-pentanol under reflux.

All NMR data are reported in the appendix (pages 279-351).

#### *Synthesis of 2-(3-aminopropyl)-1H-benzo[de]isoquinoline-1,3(2H)-dione - I-1*

Naphthalic anhydride (2.8 g, 10 mmol) was dissolved in ethanol (100 ml), followed by the addition of 1,3 diaminopropane (1.48 g, 20 mmol). The resulting solution was stirred for 1 hour under reflux. After cooling, the precipitate obtained, was filtered off and discarded, whereas the filtrate was evaporated to dryness using a rotary evaporator. The resulting solid was washed several times with diethyl ether through a Buchner funnel and dried to yield the product **I-1** as a pale-yellow solid (yield: 56%) (Noro *et al.*, 2015).

<sup>1</sup>HNMR(CDCl<sub>3</sub>): (solvent peak δ:7.27), 8.63-8.61 (dd, 2H, napht-H, J= 6.4 Hz, 0.8 Hz), 8.25-8.22 (dd, 2H, napht-H, J= 6.4, 0.8 Hz), 7.80-7.76 (t, 2H, napht-H, J= 7.6 Hz), 4.32-4.29 (t, 2H, N-CH<sub>2</sub>-CH<sub>2</sub>, J= 6.8 Hz), 2.80-2.77 (t, 2H, CH<sub>2</sub>-NH<sub>2</sub>, J= 6.4 Hz), 1.95-1.89 (m, 2H, CH<sub>2</sub>-CH<sub>2</sub>-CH<sub>2</sub>, J= 6.8 Hz), 1.52 (b, 2H, NH<sub>2</sub>). <sup>13</sup>CNMR(CDCl<sub>3</sub>): (solvent peak δ: 77.4-76.8) 164.4 (C=O), 134.0-122.65 (napht-C), 39.48 (N-CH<sub>2</sub>-CH<sub>2</sub>), 37.77 (CH<sub>2</sub>-CH<sub>2</sub>-NH<sub>2</sub>), 32.19 (CH<sub>2</sub>-CH<sub>2</sub>-CH<sub>2</sub>). LRMS calcd for C<sub>15</sub>H<sub>15</sub>N<sub>2</sub>O<sub>2</sub> [M+H]<sup>+</sup>, 255.1, *m/z* found 255.0.

#### *Synthesis of 9-chloro-1,2,3,4-tetrahydroacridine - I-2*

Intermediate **I-2** was prepared following the procedure reported in literature (Szymański, Zurek and Mikiciuk-Olasik, 2006). To a mixture of anthranilic acid (1.85 g, 1.3 mmol) and cyclohexanone (2.6 ml, 2.6 mmol) in an ice bath, was added POCl<sub>3</sub> (15 ml, 0.16 mol). The mixture was heated under reflux and stirred for 24 hours, then cooled down and concentrated under reduced pressure. The residue was diluted with ethyl acetate (50 ml), neutralized with saturated Na<sub>2</sub>CO<sub>3</sub> (30 ml) and washed 3 times with brine (30 ml). The organic layer was dried and the product was recrystallized from acetone (yield: 67%).

$^1\text{H NMR}$ ( $\text{CDCl}_3$ ): (solvent peak  $\delta$ :7.20), 8.11-8.08 (dd, 2H, Ar-H,  $J$ = 7.6, 0.8 Hz), 7.91-7.89 (d, 2H, Ar-H,  $J$ = 8.4 Hz), 7.62-7.57 (m, 2H, Ar-H,  $J$ = 5.6, 1.2 Hz), 7.49-7.45 (m, 2H, Ar-H,  $J$ = 5.2, 1.2 Hz), 3.07-3.04 (t, 2H, Ar-CH<sub>2</sub>-CH<sub>2</sub>,  $J$ = 6.4 Hz), 2.97- 2.94 (t, 2H, Ar-CH<sub>2</sub>-CH<sub>2</sub>,  $J$ = 6.4 Hz), 1.92- 1.84 (m, 4H, CH<sub>2</sub>-CH<sub>2</sub>-CH<sub>2</sub>-CH<sub>2</sub>,  $J$ = 6.4 Hz).  $^{13}\text{C NMR}$ ( $\text{CDCl}_3$ ): (solvent peak  $\delta$ : 77.8-76.7) 159.6 (Ar-C=N), 146.8 (Ar-C-N), 141.5 (C-Cl), 129.3-123.7 (Ar-C), 34.3 (Ar-CH<sub>2</sub>-CH<sub>2</sub>), 27.6 (Ar-CH<sub>2</sub>-CH<sub>2</sub>), 22.7 (CH<sub>2</sub>-CH<sub>2</sub>-CH<sub>2</sub>), 22.7 (CH<sub>2</sub>-CH<sub>2</sub>-CH<sub>2</sub>). LRMS calcd for C<sub>13</sub>H<sub>13</sub>ClN [M+H]<sup>+</sup> 218.7,  $m/z$  found 218.1.

### *Synthesis of N1-(1,2,3,4-tetrahydroacridin-9-yl)benzene-1,4-diamin - I-3*

9-chloro-1,2,3,4-tetrahydroacridine (107 mg, 0.5 mmol) and KI (80 mg) were dissolved in 1-pentanol (5 ml) and heated under reflux for 5 minutes. Then *p*-phenylenediamine (135 mg, 1.25 mmol) was added and the mixture was stirred under reflux for 24 hours. The solution was concentrated under pressure and the solid obtained was dissolved in 50 ml of DCM and extracted 3 times with a saturated solution of Na<sub>2</sub>CO<sub>3</sub> (50 ml). The organic layer was dried with anhydrous Na<sub>2</sub>SO<sub>4</sub>, filtered and evaporated through a rotary evaporator and the crude was purified by column chromatography (DCM/MeOH 99:1) to afford a brown solid (yield 39%).

$^1\text{H NMR}$ ( $\text{CDCl}_3$ ): (solvent peak  $\delta$ :7.30), 8.04-8.02 (d, 1H, Ar-H,  $J$ = 8 Hz), 7.76-7.73 (d, 1H, Ar-H,  $J$ = 8.4 Hz), 7.61-7.57 (t, 1H, Ar-H,  $J$ = 7.6 Hz), 7.30-7.27 (t, 1H, Ar-H,  $J$ = 8 Hz), 6.75-6.72 (t, 1H, Ar-H,  $J$ = 4 Hz), 6.65-6.61 (t, 1H, Ar-H,  $J$ = 8.8 Hz), 5.95 (s, 1H, Ar-NH-Ar), 3.59 (b, 2H, Ar-NH<sub>2</sub>), 3.20-3.17 (t, 2H, Ar-CH<sub>2</sub>-CH<sub>2</sub>,  $J$ = 6.4 Hz), 2.72-2.69 (t, 2H, Ar-CH<sub>2</sub>-CH<sub>2</sub>,  $J$ = 6.4 Hz), 1.99-1.95 (m, 2H, -CH<sub>2</sub>-CH<sub>2</sub>-,  $J$ = 5.6 Hz), 1.95-1.89 (m, 2H, -CH<sub>2</sub>-CH<sub>2</sub>-,  $J$ = 5.6 Hz).  $^{13}\text{C NMR}$ ( $\text{CDCl}_3$ ): solvent peak  $\delta$ : 77.4-76.7) 141.7 (Ar-C=N), 135.9-116.1 (Ar-C), 25.2 (Ar-CH<sub>2</sub>-CH<sub>2</sub>), 24.9 (Ar-CH<sub>2</sub>-CH<sub>2</sub>), 22.8 (Ar-CH<sub>2</sub>-CH<sub>2</sub>), 22.7 (Ar-CH<sub>2</sub>-CH<sub>2</sub>). LRMS calcd for C<sub>19</sub>H<sub>20</sub>N<sub>3</sub> [M+H]<sup>+</sup> 290.2,  $m/z$  found 290.2.

#### *2.3.4.2 General Method for the Synthesis of Monomers*

The vanillin monomers (imine) were obtained through condensation reaction between vanillin and the corresponding amine using methanol or 2-propanol as solvents. The imines were then reduced using sodium borohydride

(NaBH<sub>4</sub>) in methanol or 2-propanol to afford the corresponding vanillin monomers (amine).

#### *Synthesis of 4-((benzylimino)methyl)-2-methoxyphenol – 1a*

Vanillin (1g, 6.6 mmol) was reacted with benzylamine (1.07 g, 10 mmol) in methanol (10 ml) overnight at room temperature. Once the reaction was completed, the solvent was evaporated and the obtained solid was dissolved in chloroform followed by extraction with saturated NaHCO<sub>3</sub> solution. The organic phase was collected, dried with anhydrous sodium sulphate and evaporated to dryness to afford **1a** in 63% yield.

<sup>1</sup>HNMR(CDCl<sub>3</sub>): (solvent peak δ:7.38), 8.33 (s, 1H, Ar-CH=N), 7.54-7.53 (d, 1H, Ar-H, J= 2 Hz), 7.40-7.37 (dd, 4H, Ar-H, J= 3.2, 2.4 Hz), 7.33-7.31 (m, 1H, Ar-H, J= 2.4 Hz), 7.18-7.16 (dd, 1H, Ar-H, J= 6.4, 1.6 Hz), 6.97-6.95 (d, 1H, Ar-H, J= 8 Hz), 4.85 (s, 2H, Ar-CH<sub>2</sub>-N), 3.93 (s, 3H, -OCH<sub>3</sub>).  
<sup>13</sup>CNMR(CDCl<sub>3</sub>): (solvent peak δ: 77.4-76.7), 161.8 (Ar-CH=N), 148.4 (Ar-C-OH), 147.0 (Ar-C-OCH<sub>3</sub>), 139.5-108.3 (Ar-C), 64.9 (Ar-CH<sub>2</sub>-N), 56.1 (-OCH<sub>3</sub>). HRMS calcd for C<sub>15</sub>H<sub>16</sub>NO<sub>2</sub> [M+H]<sup>+</sup> 242.1176, m/z found 242.1170.

#### *Synthesis of 2-(3-((4-hydroxy-3-methoxybenzylidene)amino)propyl)-1H-benzo[de]isoquinoline-1,3(2H)-dione – 1b*

Vanillin (0.5 g, 3.3 mmol) was dissolved in methanol (10 ml), then 2-(3-aminopropyl)-1H-benzo[de]isoquinoline-1,3(2H)-dione (**I-1**) (0.83 g, 3.3 mmol) was added. The reaction was stirred overnight at room temperature. The resulting solution, was concentrated through a rotary evaporator and the solid obtained, was dissolved in 25 ml of DCM and extracted 3 times with saturated NaHCO<sub>3</sub> (20ml). The organic layer was collected and dried with anhydrous sodium sulphate and concentrated through rotary evaporator to afford an orange solid (yield: 73%).

<sup>1</sup>HNMR(CDCl<sub>3</sub>): (solvent peak δ:7.30), 8.61-8.59 (dd, 2H, naphth-H, J= 2 Hz, 1.2 Hz), 8.22-8.20 (dd, 2H, naphth-H, J= 7.6, 0.8 Hz), 8.22 (s, 1H, Ar-CH=N), 7.77-7.74 (dd, 2H, naphth-H, J= 7.6, 0.8 Hz), 7.25-7.25 (d, 1H, Ar-H, J= 1.6 Hz), 7.01-6.99 (dd, 1H, Ar-H, J= 6.4, 1.6 Hz), 6.87-6.85 (d, 1H, Ar-H, J= 8 Hz), 4.39-4.36 (t, 2H, N-CH<sub>2</sub>-CH<sub>2</sub>, J= 7.2 Hz), 3.81 (s, 3H, -OCH<sub>3</sub>), 3.79-3.77 (t, 2H, CH<sub>2</sub>-N=CH, J= 7.2 Hz), 2.26-2.23 (t, 2H, CH<sub>2</sub>-

CH<sub>2</sub>-CH<sub>2</sub>, J= 7.2 Hz). <sup>13</sup>CNMR(CDCl<sub>3</sub>): (solvent peak δ: 77.4-76.7) 164.3 (C=N), 161.0 (C=O), 148.0 (Ar-C-OH), 146.7 (Ar-C-OCH<sub>3</sub>), 133.8-107.8 (naph-C and Ar-C), 59.47 (-OCH<sub>3</sub>), 55.87 (CH=N-CH<sub>2</sub>), 38.95 (N-CH<sub>2</sub>-CH<sub>2</sub>), 29.17 (CH<sub>2</sub>-CH<sub>2</sub>-CH<sub>2</sub>). HRMS calcd for C<sub>23</sub>H<sub>21</sub>N<sub>2</sub>O<sub>4</sub> [M+H]<sup>+</sup> 389.1497, m/z found 389.1497.

#### Synthesis of 4-((benzylamino)methyl)-2-methoxyphenol – **1c**

Compound **1a** (0.7 g, 3 mmol) and sodium borohydride (0.11 g, 3 mmol) in methanol (10 ml) were stirred for 2 hours. The reaction was monitored by TLC until completion. The evaporation of the solvent yielded a solid which was washed thoroughly with deionized water and dried under *vacuo* to afford **1c** in 68% yield as a pale-yellow solid.

<sup>1</sup>HNMR((CD<sub>3</sub>)<sub>2</sub>SO): (solvent peak δ:2.42-2.40), (H<sub>2</sub>O, 3.25), 7.33-6.62 (m, 5H, Ar-H), 6.84-6.84 (d, 1H, Ar-H, J= 1.2 Hz), 6.63-6.62 (d, 2H, Ar-H, J= 2.8 Hz), 3.86 (s, 2H, Ar-CH<sub>2</sub>-N), 3.65 (s, 3H, -OCH<sub>3</sub>), 3.55 (s, 2H, Ar-CH<sub>2</sub>-N). <sup>13</sup>CNMR((CD<sub>3</sub>)<sub>2</sub>SO): (solvent peak δ: 40.6-39.4), 147.9 (Ar-C-OH), 145.9 (Ar-C-OCH<sub>3</sub>), 129.0-112.9 (Ar-C), 56.0 (CH<sub>2</sub>-NH-CH<sub>2</sub>), 52.2 (-OCH<sub>3</sub>). HRMS calcd for C<sub>15</sub>H<sub>18</sub>NO<sub>2</sub> [M+H]<sup>+</sup> 244.1332, m/z found 244.1333.

#### Synthesis of 2-(3-((4-hydroxy-3-methoxybenzyl)amino)propyl)-1H-benzo[de]isoquinoline-1,3(2H)-dione – **1d**

2-(3-((4-hydroxy-3-methoxybenzylidene)amino)propyl)-1H-benzo[de]isoquinoline-1,3(2H)-dione (**1b**) (0.4g, 1 mmol) was dissolved in methanol (10 ml), then NaBH<sub>4</sub> (0.057 g, 1.5 mmol) was added. The reaction was stirred for 2 hour at RT and monitored by TLC. At completion, the solution was reduced to dryness using a rotary evaporator. The solid obtained was dissolved in DCM (25 ml) and extracted 3 times with NaHCO<sub>3</sub> (20 ml). The organic layer was collected, dried with anhydrous sodium sulphate and concentrated through rotary evaporator to afford a pale-yellow solid (yield: 86%).

<sup>1</sup>HNMR(CDCl<sub>3</sub>): (solvent peak δ:7.31), 8.65-8.63 (dd, 2H, naph-H, J= 6.4, 1.2 Hz), 8.27-8.25 (dd, 2H, naph-H, J= 7.2, 1.2 Hz), 7.82-7.78 (dd, 2H, naph-H, J= 7.6, 0.4 Hz), 6.93-6.92 (dd, 1H, Ar-H, J= 1.6 Hz), 6.85-6.82 (dd, 2H, Ar-H, J= 3.2 Hz), 4.34-4.31 (t, 2H, N-CH<sub>2</sub>-CH<sub>2</sub>, J= 7.2 Hz), 3.91

(s, 3H, -OCH<sub>3</sub>), 3.76 (s, 2H, Ar-CH<sub>2</sub>-N), 2.78-2.74 (t, 2H, CH<sub>2</sub>-CH<sub>2</sub>-N, J= 6.4 Hz), 2.05-2.01 (t, 2H, CH<sub>2</sub>-CH<sub>2</sub>-CH<sub>2</sub>, J= 6.4 Hz). <sup>13</sup>CNMR(CDCl<sub>3</sub>): (solvent peak δ: 77.4-76.7) 164.3 (C=O), 146.6 (Ar-C-OH), 144.6 (Ar-C-OCH<sub>3</sub>), 134.0-110.9 (naphth-C and Ar-C), 55.9 (-OCH<sub>3</sub>), 53.8 (naphth-N-CH<sub>2</sub>), 46.4 (Ar-CH<sub>2</sub>-NH), 38.3 (CH<sub>2</sub>-CH<sub>2</sub>-NH), 28.3(CH<sub>2</sub>-CH<sub>2</sub>-NH). HRMS calcd for C<sub>23</sub>H<sub>23</sub>N<sub>2</sub>O<sub>4</sub> [M+H]<sup>+</sup> 391.1652, m/z found 391.1651.

*Synthesis of 2-(3-((4-hydroxy-3,5-dimethoxybenzyl)amino)propyl)-1H-benzo[de]isoquinoline-1,3(2H)dione - 1e*

Syringaldehyde (0.29 g, 1.57 mmol) was mixed with methanol (8 mL) followed by the addition of 2-(3-aminopropyl)-1H-benzo[de]isoquinoline-1,3(2H)dione (0.40g, 1.57 mmol). The solution was refluxed for 2 hours and left stirring overnight at RT to form a red solution. The solvent was evaporated under pressure to yield a red solid which was re-suspended in 2-propanol followed by the addition of NaBH<sub>4</sub> (3.0 mmol). The solution was refluxed for 48 hours. At the completion of the reaction, the solvent was removed under *vacuo* to afford a solid. The latter was collected by filtration, washed thoroughly with water and methanol to yield the final product (38%).

<sup>1</sup>HNMR(CDCl<sub>3</sub>): (solvent peak δ:7.20), 8.53-8.51 (dd, 2H, naphth-H, J= 6.4, 0.8 Hz), 8.16-8.13 (dd, 2H, naphth-H, J= 6.4, 0.8 Hz), (dd, 2H, naphth-H, J= 7.6, 0.4 Hz), 6.50 (s, 2H, Ar-H), 4.23-4.20 (t, 2H, N-CH<sub>2</sub>-CH<sub>2</sub>, J= 7.2 Hz), 3.80 (s, 6H, -OCH<sub>3</sub>), 3.64 (s, 2H, Ar-CH<sub>2</sub>-N), 2.68-2.64 (t, 2H, CH<sub>2</sub>-CH<sub>2</sub>-N, J= 6.8 Hz), 1.95-1.91 (t, 2H, CH<sub>2</sub>-CH<sub>2</sub>-CH<sub>2</sub>, J= 6.8 Hz). <sup>13</sup>CNMR(CDCl<sub>3</sub>): (solvent peak δ: 77.4-76.7) 164.3 (C=O), 147.1 (Ar-C-OH), 134.0-133.6 (Ar-C-OCH<sub>3</sub>), 131.6-104.9 (naphth-C and Ar-C), 56.2 (-OCH<sub>3</sub>), 54.2 (naphth-N-CH<sub>2</sub>), 46.5 (Ar-CH<sub>2</sub>-NH), 38.3 (CH<sub>2</sub>-CH<sub>2</sub>-NH), 28.3(CH<sub>2</sub>-CH<sub>2</sub>-NH). HRMS calcd for C<sub>23</sub>H<sub>25</sub>N<sub>2</sub>O<sub>5</sub> [M+H]<sup>+</sup> 421.1758, m/z found 421.1756.

*Synthesis of 2-methoxy-4-(((4-((1,2,3,4-tetrahydroacridin-9-yl)amino)phenylamino)methyl)phenol - 1f*

N1-(1,2,3,4-tetrahydroacridin-9-yl)benzene-1,4-diamin (**I-3**) (50 mg, 0.17 mmol) was dissolved in 2-propanol (10 ml), followed by vanillin (20 mg, 0.13 mmol). The reaction was stirred under reflux and monitored by TLC.

When the vanillin spot had disappeared, the solution was cooled down and NaBH<sub>4</sub> (25mg, 0.7 mmol) was added. The solvent was removed under *vacuo* and the solid obtained, was purified by column chromatography (DCM/MeOH 99:1) to afford an orange solid (yield 46%).

<sup>1</sup>HNMR(CDCl<sub>3</sub>): (solvent peak δ:7.19), 8.05-7.65 (m, 2H, Ar-H), 7.63-7.47 (m, 2H, Ar-H, J= 8.4, 1.6 Hz), 7.19-7.16 (dd, 2H, Ar-H, J= 7.2, 0.8 Hz), 6.83-6.78 (m, 2H, Ar-H), 6.73-6.70 (d, 1H, Ar-H, J= 8.8 Hz), 6.52-6.50 (t, 2H, Ar-H, J= 6.8 Hz), 4.14 (s, 2H, Ar-CH<sub>2</sub>-N), 3.81 (s, 3H, -OCH<sub>3</sub>), 3.13-3.11 (t, 2H, Ar-CH<sub>2</sub>-CH<sub>2</sub>, J= 6.4 Hz), 2.95-2.93 (d, 2H, Ar-CH<sub>2</sub>-CH<sub>2</sub>, J= 7.2 Hz), 2.60-2.56 (t, 2H, -CH<sub>2</sub>-CH<sub>2</sub>-, J= 6.4 Hz), 1.86-1.80 (m, 2H, -CH<sub>2</sub>-CH<sub>2</sub>-, J= 5.2 Hz). <sup>13</sup>CNMR(CDCl<sub>3</sub>): (solvent peak δ: 77.4-76.7), 146.8 (Ar-C=N), 145.0-110.3 (Ar-C), 56.0 (-OCH<sub>3</sub>), 48.8 (Ar-CH<sub>2</sub>-NH), 45.82 (Ar-CH<sub>2</sub>-CH<sub>2</sub>-CH<sub>2</sub>), 25.0 (Ar-CH<sub>2</sub>-CH<sub>2</sub>-CH<sub>2</sub>), 22.7 (CH<sub>2</sub>-CH<sub>2</sub>-CH<sub>2</sub>), 22.3 (CH<sub>2</sub>-CH<sub>2</sub>-CH<sub>2</sub>). HRMS calcd for C<sub>27</sub>H<sub>28</sub>N<sub>3</sub>O<sub>2</sub> [M+H]<sup>+</sup> 426.2176, *m/z* found 426.2172.

#### 2.3.4.3 General Method for the synthesis of Dimers

The dimers were prepared through reductive amination reaction, by reacting vanillin or syringaldehyde with an excess of corresponding amine, to enhance purification by DCM: saturated NaHCO<sub>3</sub> extraction, in methanol in the presence of sodium cyanoborohydride and zinc chloride as reducing agents.

#### Synthesis of 4,4'-(((2-hydroxyethyl)azanediyl)bis(methylene))bis(2-methoxyphenol)- **2a**

Vanillin (1g, 6.6 mmol) and 2-amino-1-ethanol (0.30 ml, 5 mmol) in presence of NaCNBH<sub>3</sub> (1.2 equiv.) and ZnCl<sub>2</sub> (1.2 equiv.) were stirred in methanol for 24 hours. The solvent was removed through a rotary evaporator and the residue was dissolved in warm chloroform and extracted with saturated NaHCO<sub>3</sub>. The organic layer was dried to afford **2a** as a thick orange oil (12% yield).

<sup>1</sup>HNMR(CDCl<sub>3</sub>): (solvent peak δ:7.21), 6.76-6.74 (d, 2H, Ar-H, J= 7.6 Hz), 6.70-6.67 (dd, 4H, Ar-H, J= 8, 1.6 Hz), 3.75 (s, 6H, -OCH<sub>3</sub>), 3.51-3.50 (t, 2H, CH<sub>2</sub>-CH<sub>2</sub>-OH, J= 5.6 Hz), 3.45 (s, 4H, Ar-CH<sub>2</sub>-N), 2.59-2.56 (t, 2H, N-CH<sub>2</sub>-CH<sub>2</sub>, J= 5.6 Hz). <sup>13</sup>CNMR(CDCl<sub>3</sub>): (solvent peak δ: 77.4-76.8), 146.8

(Ar-C-OH), 145.2 (Ar-C-OCH<sub>3</sub>), 133.8-111.2 (Ar-C), 58.5 (N-CH<sub>2</sub>-Ar), 57.9 (CH<sub>2</sub>-CH<sub>2</sub>-OH), 56.0 (N-CH<sub>2</sub>-CH<sub>2</sub>), 54.6 (-OCH<sub>3</sub>). HRMS calcd for C<sub>18</sub>H<sub>24</sub>NO<sub>5</sub> [M+H]<sup>+</sup> 334.1649, *m/z* found 334.1648.

*Synthesis of 4,4'-(((3-hydroxypropyl)azanediyl)bis(methylene))bis(2-methoxyphenol)- 2b*

Vanillin (1 g, 6.6 mmol) and 3-amino-1-propanol (0.326 ml, 5 mmol) were stirred overnight in presence of NaCNBH<sub>3</sub> (1.2 equiv.) and ZnCl<sub>2</sub> (1.2 equiv.) in methanol. The solvent was removed through a rotary evaporator and the residue was purified through column chromatography (elution with increasing volumes of DCM/MeOH) to afford **2b** (70% yield) as a thick orange oil.

<sup>1</sup>HNMR(CDCl<sub>3</sub>): (solvent peak δ:7.21), 6.82-6.80 (dd, 4H, Ar-H, J= 8 Hz), 6.74-6.72 (dd, 2H, Ar-H, J= 5.6, 1.6 Hz), 3.83 (s, 6H, -OCH<sub>3</sub>), 3.65-3.62 (t, 2H, CH<sub>2</sub>-CH<sub>2</sub>-OH, J= 5.2 Hz), 3.45 (s, 4H, Ar-CH<sub>2</sub>-N), 2.62-2.59 (t, 2H, N-CH<sub>2</sub>-CH<sub>2</sub>, J= 5.6 Hz), 1.74-1.71 (t, 2H, CH<sub>2</sub>-CH<sub>2</sub>-CH<sub>2</sub>, J= 5.2 Hz). <sup>13</sup>CNMR(CDCl<sub>3</sub>): (solvent peak δ: 77.6-74.8), 147.0 (Ar-C-OH), 145.7 (Ar-C-OCH<sub>3</sub>), 129.8-110.7 (Ar-C), 64.3 (Ar-CH<sub>2</sub>-N), 58.4 (CH<sub>2</sub>-CH<sub>2</sub>-OH), 55.9 (N-CH<sub>2</sub>-CH<sub>2</sub>), 53.3 (-OCH<sub>3</sub>), 27.4 (CH<sub>2</sub>-CH<sub>2</sub>-CH<sub>2</sub>). HRMS calcd for C<sub>19</sub>H<sub>26</sub>NO<sub>5</sub> [M+H]<sup>+</sup> 348.1805, *m/z* found 348.1801.

*Synthesis of 4,4'-(((4-hydroxybutyl)azanediyl)bis(methylene))bis(2-methoxyphenol)- 2c*

Vanillin (1 g, 6.6 mmol) and 4-amino-1-butanol (0.461 ml, 5 mmol) were stirred overnight in presence of NaCNBH<sub>3</sub> (1.2 equiv.) and ZnCl<sub>2</sub> (1.2 equiv.) in methanol. The solvent was removed through rotary evaporator and the residue was dissolved in warm chloroform and extracted with saturated NaHCO<sub>3</sub>. The organic layer was dried to afford **2c** as a thick orange oil (14% yield).

<sup>1</sup>HNMR(CDCl<sub>3</sub>): (solvent peak δ:7.21), 6.81-6.76 (t, 4H, Ar-H, J= 8 Hz), 6.72-6.70 (m, 2H, Ar-H, J= 2 Hz), 3.80 (s, 6H, -OCH<sub>3</sub>), 3.65 (s, 4H, Ar-CH<sub>2</sub>-N), 3.52-3.49 (t, 2H CH<sub>2</sub>-CH<sub>2</sub>-OH, J= 5.6 Hz), 2.65-2.63 (t, 2H, N-CH<sub>2</sub>-CH<sub>2</sub>, J= 5.6 Hz), 2.39-2.37 (d, 2H, CH<sub>2</sub>-CH<sub>2</sub>-CH<sub>2</sub>, J= 6 Hz), 1.61-1.60 (t, 2H, CH<sub>2</sub>-CH<sub>2</sub>-CH<sub>2</sub>, J= 2.4 Hz). <sup>13</sup>CNMR(DMSO): (solvent peak δ: 40.6-39.3),

147.8 (Ar-C-OH), 145.7 (Ar-C-OCH<sub>3</sub>), 130.9-112.8 (Ar-C), 60.5 (Ar-CH<sub>2</sub>-N), 56.1 (-OCH<sub>3</sub>), 46.8 (CH<sub>2</sub>-CH<sub>2</sub>-OH), 29.9 (N-CH<sub>2</sub>-CH<sub>2</sub>-CH<sub>2</sub>), 23.3 (CH<sub>2</sub>-CH<sub>2</sub>-CH<sub>2</sub>-OH). HRMS calcd for C<sub>20</sub>H<sub>28</sub>NO<sub>5</sub> [M+H]<sup>+</sup>. 362.1962, *m/z* found 362.1962.

*Synthesis of 4,4'-(((5-hydroxypentyl)azanediyl)bis(methylene))bis(2-methoxyphenol)- 2d*

Vanillin (1 g, 6.6 mmol) and 5-amino-1-pentanol (0.326 ml, 5 mmol) were stirred overnight in presence of NaCNBH<sub>3</sub> (1.2 equiv.) and ZnCl<sub>2</sub> (1.2 equiv.) in methanol. The solvent was removed through a rotary evaporator and the residue was purified through column chromatography (DCM/MeOH) to afford **2d** as thick orange oil (82% yield).

<sup>1</sup>HNMR((CD<sub>3</sub>)<sub>2</sub>SO): (solvent peak δ:2.52-2.50), (H<sub>2</sub>O 3.38), 7.21-7.21 (d, 2H, Ar-H, J= 1.6 Hz), 6.90-6.88 (m, 2H, Ar-H, J= 2Hz), 6.81-6.79 (d, 2H, Ar-H, J= 2 Hz), 3.99 (s, 4H, Ar-CH<sub>2</sub>-N), 3.75 (s, 6H, -OCH<sub>3</sub>), 2.83-2.80 (t, 2H, CH<sub>2</sub>-CH<sub>2</sub>-OH, J= 6.4 Hz), 2.52-2.50 (t, 2H, N-CH<sub>2</sub>-CH<sub>2</sub>, J= 6.4 Hz), 1.65-1.62 (t, 2H, CH<sub>2</sub>-CH<sub>2</sub>-CH<sub>2</sub>, J= 6.4 Hz), 1.43-1.40 (t, 2H, CH<sub>2</sub>-CH<sub>2</sub>-CH<sub>2</sub>, J= 6.4 Hz), 1.38-1.34 (t, 2H, CH<sub>2</sub>-CH<sub>2</sub>-CH<sub>2</sub>, J= 6.4 Hz). <sup>13</sup>CNMR(D<sub>2</sub>O): 147.7 (Ar-C-OH), 146.7 (Ar-C-OCH<sub>3</sub>), 124.2-113.8 (Ar-C), 61.2 (Ar-CH<sub>2</sub>-N), 57.2 (N-CH<sub>2</sub>-CH<sub>2</sub>), 55.9 (-OCH<sub>3</sub>), 50.7 (CH<sub>2</sub>-CH<sub>2</sub>-OH), 46.5, 30.6, 25.2, 22.2 (alkyl-C). HRMS calcd for C<sub>21</sub>H<sub>23</sub>O<sub>5</sub> [M+H]<sup>+</sup> 376.2118, *m/z* found 376.2108.

*Synthesis of 4,4'-((butylazanediyl)bis(methylene))bis(2-methoxyphenol)- 2e*

Vanillin (1 g, 6.6 mmol) and *n*-butylamine (0.5 ml, 5 mmol) were stirred in presence of NaCNBH<sub>3</sub> (1.2 equiv.) and ZnCl<sub>2</sub> (1.2 equiv.) in methanol. The solvent was removed through a rotary evaporator and the residue was dissolved in warm chloroform and extracted with saturated NaHCO<sub>3</sub>. The organic layer was dried to afford **2e** as a thick orange oil (23% yield).

<sup>1</sup>HNMR(CDCl<sub>3</sub>): (solvent peak δ:7.20), 6.77-6.76 (d, Ar-H, 2H, J= 1.6 Hz), 6.67-6.63 (m, 4H, Ar-H, J= 8 Hz), 3.73 (s, 4H, Ar-CH<sub>2</sub>-N), 3.64 (s, 6H, -OCH<sub>3</sub>), 2.59-2.55 (t, 2H, N-CH<sub>2</sub>-CH<sub>2</sub>, J= 7.6 Hz), 1.46-1.40 (m, 2H, CH<sub>2</sub>-CH<sub>2</sub>-CH<sub>2</sub>, J= 5.6, 2.4 Hz), 1.26-1.20 (m, 5H, CH<sub>2</sub>-CH<sub>2</sub>-CH<sub>3</sub>). <sup>13</sup>CNMR(CDCl<sub>3</sub>):

(solvent peak  $\delta$ : 77.8-76.7), 146.6 (Ar-C-OH), 144.6 (Ar-C-OCH<sub>3</sub>), 132.4-110.8 (Ar-C), 55.8 (Ar-CH<sub>2</sub>-N), 49.2 (-OCH<sub>3</sub>), 32.2-20.5 (alkyl-C). HRMS calcd for C<sub>20</sub>H<sub>27</sub>NO<sub>4</sub> [M+H]<sup>+</sup> 346.2013, *m/z* found 346.2013.

*Synthesis of 4,4'-((benzylazanediy)bis(methylene))bis(2-methoxyphenol)-**2f***

Vanillin (1.5 g, 10mmol) and benzylamine (0.55 ml, 5 mmol) in presence of NaCNBH<sub>3</sub> (1.2 equiv.) and ZnCl<sub>2</sub> (1.2 equiv.) in methanol gave a precipitate which after filtration, washing with deionized water and methanol, afforded **2f** as a white solid (90% yield).

<sup>1</sup>HNMR((CD<sub>3</sub>)<sub>2</sub>SO): (solvent peak  $\delta$ :2.42-2.40), (H<sub>2</sub>O, 3.26), 7.30-6.59 (m, Ar-H, 11H), 3.67 (s, 6H, -OCH<sub>3</sub>), 3.56 (s, 2H, Ar-CH<sub>2</sub>-N), 3.47 (s, 4H, Ar-CH<sub>2</sub>-N), <sup>13</sup>CNMR((CD<sub>3</sub>)<sub>2</sub>SO): (solvent peak  $\delta$ : 40.6-39.3), 141.3 (Ar-C-OH), 141.1 (Ar-C-OCH<sub>3</sub>), 128.9-115.5 (Ar-C), 55.9 (Ar-CH<sub>2</sub>-N), 52.5 (Ar-CH<sub>2</sub>-N), 45.6 (-OCH<sub>3</sub>). HRMS calcd for C<sub>23</sub>H<sub>26</sub>NO<sub>4</sub> [M+H]<sup>+</sup> 380.1856, *m/z* found 380.1849.

*Synthesis of N<sup>1</sup>,N<sup>1</sup>-bis(4-hydroxy-3-methoxybenzyl)propane-1,3-diaminium chloride- **2g***

Vanillin (1 g, 6.6 mmol) and 1,3-diaminopropane (0.84 ml, 10 mmol) in presence of NaCNBH<sub>3</sub> (1.2 equiv.) and ZnCl<sub>2</sub> (1.2 equiv.) in methanol afforded a precipitate which was filtered and washed with deionized water and methanol. Suspension of the precipitate in methanol (5 mL) followed by the addition of concentrated hydrochloric acid, gave a solid. The solvent was removed using a rotary evaporator and the resulting solid washed with diethyl ether and dried under *vacuo* to yield **2g** as a white solid (67% yield).

<sup>1</sup>HNMR((CD<sub>3</sub>)<sub>2</sub>SO): (solvent peak  $\delta$ :2.51) (H<sub>2</sub>O, 3.64), 7.12 (s, 2H, Ar-H), 7.12-6.90 (d, 2H, Ar-H, J= 8 Hz), 6.81-6.79 (d, 2H, Ar-H, J= 8 Hz), 4.00 (s, 4H, Ar-CH<sub>2</sub>-N), 3.78 (s, 6H, -OCH<sub>3</sub>), 2.97-2.94 (t, 2H, N-CH<sub>2</sub>-CH<sub>2</sub>, J= 3.6 Hz), 2.89-2.85 (t, 2H, CH<sub>2</sub>-CH<sub>2</sub>-NH<sub>3</sub><sup>+</sup>, J= 3.6 Hz), 1.93 (s, CH<sub>2</sub>-CH<sub>2</sub>-CH<sub>2</sub>, 2H). <sup>13</sup>CNMR(D<sub>2</sub>O): 147.6 (Ar-C-OCH<sub>3</sub>), 123.3-113.8 (Ar-C), 55.9 (Ar-CH<sub>2</sub>-N), 51.0 (-OCH<sub>3</sub>), 43.6, 36.5, 23.7 (alkyl-C). HRMS calcd for C<sub>19</sub>H<sub>26</sub>ClN<sub>2</sub>O<sub>4</sub> 347.1965 [M-H<sub>2</sub>Cl]<sup>+</sup>, *m/z* found 347.1965.

*Synthesis of 4,4'-(((3-hydroxypropyl)azanediyl)bis(methylene))bis(2,6-dimethoxyphenol)- 2h*

Syringaldehyde (0.5 g, 2.7 mmol) and 3-amino-1-propanol (0.2 ml, 1.7 mmol) were stirred overnight in presence of NaCNBH<sub>3</sub> (1.2 equiv.) and ZnCl<sub>2</sub> (1.2 equiv.) in methanol. The solvent was removed through a rotary evaporator and the residue was purified through column chromatography (DCM/MeOH) to afford **2h** as a thick colourless oil (65% yield).

<sup>1</sup>HNMR(MeOD): (solvent peak δ:3.34), 6.81 (s, 4H, Ar-H), 4.17 (s, 4H, Ar-CH<sub>2</sub>-N), 3.84 (s, 12H, -OCH<sub>3</sub>), 3.75-3.72 (t, 2H, CH<sub>2</sub>-CH<sub>2</sub>-OH, J= 5.6 Hz), 3.24-3.21 (t, 2H, N-CH<sub>2</sub>-CH<sub>2</sub>, J= 5.6 Hz), 1.97 (t, 2H, CH<sub>2</sub>-CH<sub>2</sub>-CH<sub>2</sub>, J= 6.4 Hz), <sup>13</sup>CNMR(MeOD) (solvent peak δ: 48.2), 149.0 (Ar-C-OH), 148.0 (Ar-C-OCH<sub>3</sub>), 144.9-106.8 (Ar-C), 59.4 (Ar-CH<sub>2</sub>-N), 55.7 (CH<sub>2</sub>-CH<sub>2</sub>-OH), 51.6 (-OCH<sub>3</sub>), 45.6-28.2 (alkyl-C). HRMS calcd for C<sub>21</sub>H<sub>30</sub>NO<sub>7</sub> [M+H]<sup>+</sup> 408.2017, m/z found 408.2012.

*Synthesis of 4,4'-((benzylazanediyl)bis(methylene))bis(2,6-dimethoxyphenol)- 2i*

Syringaldehyde (1 g, 5.4 mmol) and benzylamine (0.2 ml, 1.8 mmol) in presence of NaCNBH<sub>3</sub> (1.2 equiv.) and ZnCl<sub>2</sub> (1.2 equiv.) in methanol, gave a precipitate which was filtered and washed with deionized water and methanol and dried to afford **2i** (46% yield).

<sup>1</sup>HNMR((CD<sub>3</sub>)<sub>2</sub>SO): (solvent peak δ:2.40), (H<sub>2</sub>O, 3.25), 7.28-7.12 (m, 5H, Ar-H), 6.49 (s, 4H, Ar-H), 3.64 (s, 12H, -OCH<sub>3</sub>), 3.56 (s, 4H, Ar-CH<sub>2</sub>-N), 3.46 (s, 2H, Ar-CH<sub>2</sub>-N). <sup>13</sup>CNMR((CD<sub>3</sub>)<sub>2</sub>SO): (solvent peak δ: 40.6-39.3), 140.3 (Ar-C-OH), 128.7-127.0 (Ar-C), 56.3 (Ar-CH<sub>2</sub>-N), 45.4 (-OCH<sub>3</sub>). HRMS calcd for C<sub>25</sub>H<sub>30</sub>NO<sub>6</sub> [M+H]<sup>+</sup> 440.2058, m/z found 440.2058.

#### 2.3.4.4 General Method for the Synthesis of Tetramers

The synthesis of the tetramers was achieved following the same method used for the preparation of the dimers; however, an excess of aldehydes was used since all the products, except compound **4f**, precipitated from the methanol solution, enabling the purification of the final products by simple filtration.

*Synthesis of N<sup>1</sup>,N<sup>1</sup>,N<sup>4</sup>,N<sup>4</sup>-tetrakis(3-methoxybenzyl)benzene-1,4-diamine – 4a*

m-Anisaldehyde (0.82 g, 6 mmol) and *p*-phenylenediamine (0.1 g, 1 mmol) in presence of NaCNBH<sub>3</sub> (1.2 equiv.) and ZnCl<sub>2</sub> (1.2 equiv.) in methanol afforded a precipitate which upon filtration, washed with deionized water and methanol and drying gave **4a** (54% yield).

<sup>1</sup>HNMR(CDCl<sub>3</sub>): (solvent peak δ: 6.81), 7.38-7.34 (t, 4H, Ar-H, J= 8 Hz), 7.02-6.97 (t, 8H, Ar-H, J= 8 Hz), 6.93-6.90 (dd, 4H, Ar-H, J= 6, 2 Hz), 6.81 (s, 4H, Ar-H), 4.62 (s, 8H, Ar-CH<sub>2</sub>-N), 3.87 (s, 12H, -OCH<sub>3</sub>). <sup>13</sup>CNMR(CDCl<sub>3</sub>): (solvent peak δ: 77.6-77.0), 160.0 (Ar-C-OCH<sub>3</sub>), 141.9-112.2 (Ar-C), 55.5 (Ar-CH<sub>2</sub>-N), 55.2 (-OCH<sub>3</sub>). HRMS calcd for C<sub>38</sub>H<sub>41</sub>N<sub>2</sub>O<sub>4</sub> [M+H]<sup>+</sup> 589.3061, *m/z* found 589.3047.

*Synthesis of 4,4',4'',4'''-((((1*r*,4*r*)-cyclohexane-1,4-diyl)bis(azanetriyl))tetrakis(methylene))tetrakis(2-methoxyphenol) – 4b*

Vanillin (1.82 g, 12 mmol) and trans-1,4-diaminocyclohexane (0.2 g, 2 mmol) in presence of NaCNBH<sub>3</sub> (1.2 equiv.) and ZnCl<sub>2</sub> (1.2 equiv.) in methanol afforded a precipitate which after filtration and washing with methanol gave a solid. The latter was dissolved in water, filtered and extracted with chloroform. The water phase was freeze dried, using an EF4 Edwards Modulyo freeze dryer, to yield **4b** (18% yield).

<sup>1</sup>HNMR((CD<sub>3</sub>)<sub>2</sub>SO): (solvent peak δ: 2.40), (H<sub>2</sub>O, 3.26), 7.10 (s, 4H, Ar-H), 6.80-6.77 (dd, 4H, Ar-H, J= 6.4, 1.6 Hz), 6.69-6.67 (d, 4H, Ar-H, J= 7.2), 3.88 (s, 8H, Ar-CH<sub>2</sub>-N), 3.68 (s, 12H, -OCH<sub>3</sub>), 2.79 (s, 2H, N-CH-(CH<sub>2</sub>)<sub>2</sub>), 2.10-2.09 (d, 4H, CH-CH<sub>2</sub>-CH<sub>2</sub>, J= 6 Hz), 1.33-1.30 (d, 4H, CH-CH<sub>2</sub>-CH<sub>2</sub>, J= 8.8 Hz). <sup>13</sup>CNMR((CD<sub>3</sub>)<sub>2</sub>SO): (solvent peak δ: 39.9-39.0), 148.0 (Ar-C-OH), 147.4 (Ar-C-OCH<sub>3</sub>), 123.0-114.4 (Ar-C), 56.2 (Ar-CH<sub>2</sub>-N), 55.0 (-OCH<sub>3</sub>), 48.2 (N-CH(CH<sub>2</sub>)<sub>2</sub>), 27.3 (N-CH(CH<sub>2</sub>)<sub>2</sub>). HRMS calcd for C<sub>38</sub>H<sub>47</sub>N<sub>2</sub>O<sub>8</sub> [M+H]<sup>+</sup> 659.3327, *m/z* found 659.3327.

*Synthesis of 4,4',4'',4'''-((1,4-phenylenebis(azanetriyl))tetrakis(methylene))tetrakis(2-methoxyphenol) – 4c*

Vanillin (1 g, 6.6 mmol) and *p*-phenylenediamine (0.1 g, 1 mmol) in presence of NaCNBH<sub>3</sub> (1.2 equiv.) and ZnCl<sub>2</sub> (1.2 equiv.) in methanol afforded a precipitate which was filtered and washed with deionized water and methanol. The solid was then dissolved in chloroform and extracted with saturated NaHCO<sub>3</sub>. The organic phase was dried and evaporated to dryness to give **4c** (74% yield).

<sup>1</sup>HNMR(CDCl<sub>3</sub>): (solvent peak δ: 7.30), 6.88-6.86 (d, 4H, Ar-H, J= 8 Hz), 6.79-6.76 (m, 12H, Ar-H, J= 2 Hz), 4.39 (s, 8H, Ar-CH<sub>2</sub>-N), 3.83 (s, 12H, -OCH<sub>3</sub>). <sup>13</sup>CNMR(CDCl<sub>3</sub>): (solvent peak δ: 77.4-76.7), 164.5 (Ar-C-OH), 144.4 (Ar-C-OCH<sub>3</sub>), 142.3-109.9 (Ar-C), 55.9 (Ar-CH<sub>2</sub>-N), 55.1 (-OCH<sub>3</sub>). HRMS calcd for C<sub>38</sub>H<sub>41</sub>N<sub>2</sub>O<sub>8</sub> [M+H]<sup>+</sup> 653.2857, *m/z* found 653.2851.

*Synthesis of N<sup>1</sup>,N<sup>1</sup>,N<sup>4</sup>,N<sup>4</sup>-tetrabenzylbenzene-1,4-diamine – 4d*

Benzaldehyde (1.27 g, 12 mmol) and *p*-phenylenediamine (0.2 g, 2 mmol) in presence of NaCNBH<sub>3</sub> (1.2 equiv.) and ZnCl<sub>2</sub> (1.2 equiv.) in methanol afforded a precipitate which was filtered and washed with deionized water and methanol. The solid was then dissolved in chloroform and extracted with saturated NaHCO<sub>3</sub>. The organic phase was dried and evaporated to dryness to afford **4d** (80% yield).

<sup>1</sup>HNMR(CDCl<sub>3</sub>): (solvent peak δ: 7.25), 7.40-7.25 (m, 20H, Ar-H), 6.68 (s, 4H, Ar-H linker), 4.55 (s, 8H, Ar-CH<sub>2</sub>-N). <sup>13</sup>CNMR(CDCl<sub>3</sub>): (solvent peak δ: 77.4-76.7), 141.7-114.77 (Ar-C), 55.1 (Ar-CH<sub>2</sub>-N). HRMS calcd for C<sub>34</sub>H<sub>32</sub>N<sub>2</sub> [M]<sup>+</sup> 468.2560, *m/z* found 468.2550.

*Synthesis of N<sup>1</sup>,N<sup>1</sup>,N<sup>3</sup>,N<sup>3</sup>-tetrakis(4-hydroxy-3-methoxybenzyl)propane-1,3-diaminium chloride – 4e*

Vanillin (1.8 g, 12 mmol) and 1,3 diaminopropane (0.17 ml, 2 mmol) in presence of NaCNBH<sub>3</sub> (1.2 equiv.) and ZnCl<sub>2</sub> (1.2 equiv.) in methanol afforded a precipitate. The latter was washed with deionized water and methanol. The resulting solid was suspended in methanol (5 mL), followed by the addition concentrated hydrochloric acid. All the solvent was removed

by rotary evaporator and the solid obtained, was washed with diethyl ether to yield the pure **4e** (38% yield).

$^1\text{HNMR}((\text{CD}_3)_2\text{SO}+\text{D}_2\text{O})$ : (solvent peak  $\delta$ :2.51), ( $\text{H}_2\text{O}$ , 4.03), 7.06-7.05 (d, 4H, Ar-H,  $J= 1.6$  Hz), 6.86-6.86 (d, 4H, Ar-H,  $J= 2$  Hz), 6.80-6.78 (d, 4H, Ar-H,  $J= 8$  Hz), 3.99 (s, 8H, Ar-CH<sub>2</sub>-N), 3.76 (s, 12H, -OCH<sub>3</sub>), 2.96 (s, 4H, N-CH<sub>2</sub>-CH<sub>2</sub>), 2.51-2.51 (t, 2H, CH<sub>2</sub>-CH<sub>2</sub>-CH<sub>2</sub>,  $J= 1.6$  Hz).  $^{13}\text{CNMR}((\text{CD}_3)_2\text{SO})$ : (solvent peak  $\delta$ : 39.8-38.6), 149.0 (Ar-C-OH), 147.9 (Ar-C-OCH<sub>3</sub>), 147.3-114.2 (Ar-C), 56.1 (Ar-CH<sub>2</sub>-N), 50.7 (N-CH<sub>2</sub>-CH<sub>2</sub>), 43.8 (-OCH<sub>3</sub>), 22.5 N-CH<sub>2</sub>-CH<sub>2</sub>). HRMS calcd for C<sub>35</sub>H<sub>44</sub>ClN<sub>2</sub>O<sub>8</sub> [M-H<sub>2</sub>Cl]<sup>+</sup> 619.3014,  $m/z$  found 619.3002 [M-H<sub>2</sub>Cl]<sup>+</sup>.

*Synthesis of 4,4',4'',4'''-((1,4-phenylenebis(azanetriyl))tetrakis(methylene)) tetraphenol – **4f***

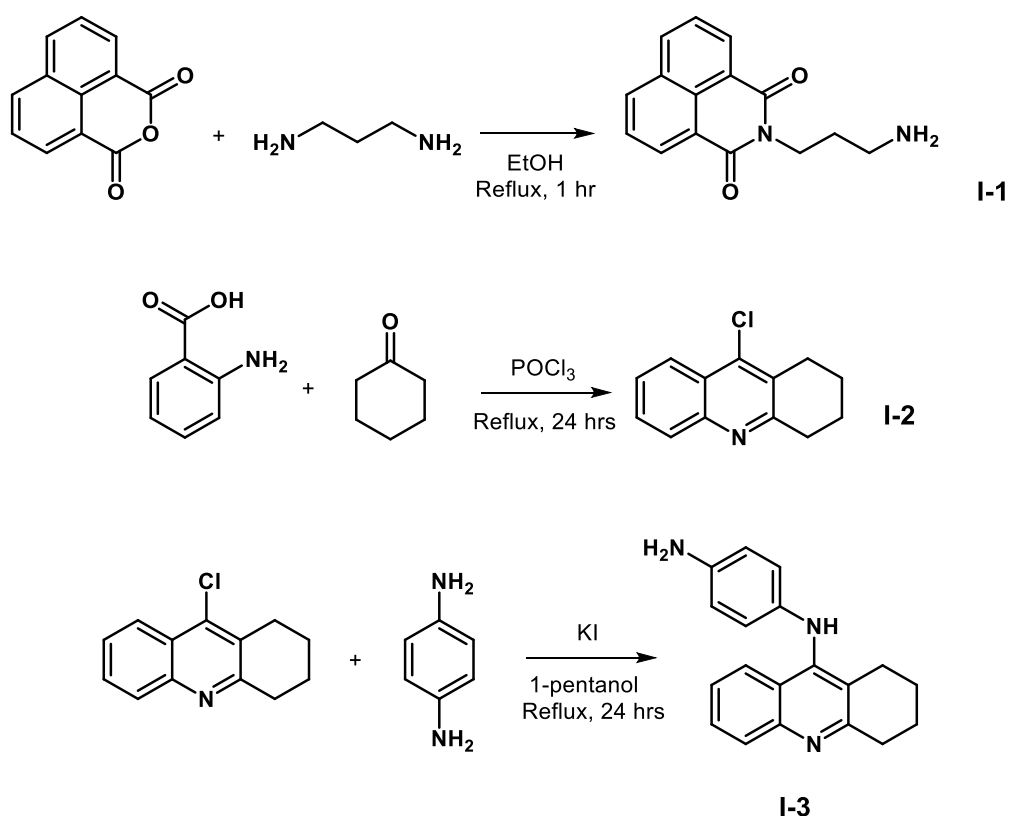
The reaction between 4 hydroxybenzaldehyde (1.5 g, 12 mmol) and *p*-phenylenediamine (0.2 g, 2 mmol) in methanol was evaporated to dryness. The resulting solid was washed thoroughly with water, chloroform and after drying, gave **4f** (66% yield).

$^1\text{HNMR}((\text{CD}_3)_2\text{SO})$ : (solvent peak  $\delta$ :2.52-2.50), ( $\text{H}_2\text{O}$ , 3.37), 9.23 (s, 4H, Ar-OH), 7.02-7.00 (d, 8H, Ar-H,  $J= 8$  Hz), 6.68-6.55 (d, 8H, Ar-H,  $J= 8$  Hz), 6.55 (s, 4H, Ar-H), 4.27 (s, 8H, Ar-CH<sub>2</sub>-N).  $^{13}\text{CNMR}((\text{CD}_3)_2\text{SO})$ : (solvent peak  $\delta$ : 40.6-39.3), 156.5 (Ar-C-OH), 141.3-128.7 (Ar-C), 115.5 (Ar-C linker), 54.8 (Ar-CH<sub>2</sub>-N). HRMS calcd for C<sub>34</sub>H<sub>33</sub>N<sub>2</sub>O<sub>4</sub> [M+H]<sup>+</sup> 533.2435,  $m/z$  found 533.2427.

## 2.5 Results and Discussion

### 2.5.1 Synthesis of the Intermediates

The synthetic strategy for the synthesis of the intermediates **I-1** - **I-3** is shown in scheme 1.



Scheme 1. Synthetic strategy for the synthesis of non-commercially available amines used for the synthesis of vanillin derivatives.

Intermediate **I-1** was prepared in a one-step reaction by reacting 1,8 naphthalic anhydride and 1,3 diaminopropane in ethanol under reflux. After the removal of the precipitate by filtration, the solution was dried and the solid obtained was washed with diethyl ether to afford the pure compound in 56% yield. Intermediate **I-2** is commercially available but was instead prepared by following the method reported by (Szymański, Zurek and Mikiciuk-Olasik, 2006). Anthranilic acid and cyclohexanone were reacted in  $\text{POCl}_3$  under reflux for 24 hours.

The solution was then dried and the product recrystallized from acetone to afford the pure compound in 67% yield. Intermediate **I-3** was prepared by

reacting **I-2** with a catalytic amount of potassium iodide (KI) and an excess of *p*-phenylenediamine in 1-pentanol under reflux for 24 hours. The final product was obtained after purification through column chromatography (DCM:MeOH 95:5) in 39% yield. The compounds were characterized through  $^1\text{H}$  and  $^{13}\text{C}$  NMR and finally through LRMS. As an example, the NMR and mass spectra of **I-1** are shown in figures 2.10-2.12.

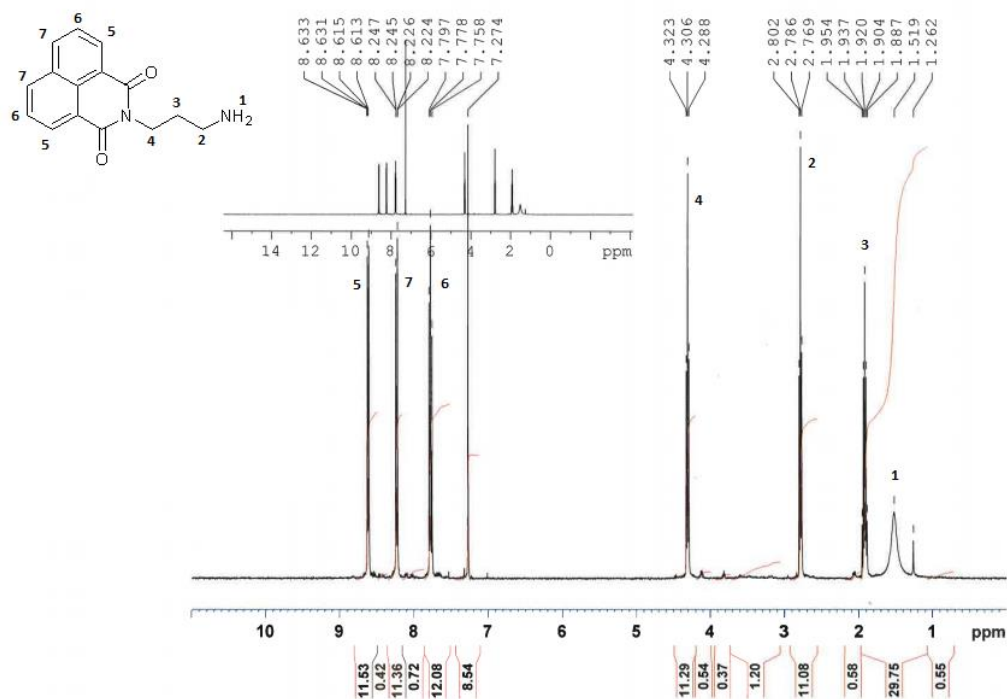


Figure 2.10.  $^1\text{H}$  NMR spectrum of Intermediate 1 (**I-1**).

Three different signals, integrating for two protons each, are present between 8.63 and 7.78, due to the de-shielding effect of the aromatic moieties in the naphthalimido structure (peaks 5, 6 and 7). The three methylene groups (2, 3 and 4) are observed between 4.31 and 1.92 ppm, each integrating for two protons.

The signal at 4.31 ppm refers to the methylene linked to the nitrogen of the naphthalimide moiety (4); the de-shielding is due to the electronegativity of the nitrogen atom and the presence of the two carbonyl groups, both electron-withdrawing. The signal at 2.79 ppm represents the methylene (2) attached to the terminal amino moiety ( $-\text{NH}_2$ ); whereas, the multiplet centred at 1.92 ppm is due to the remaining methylene group (3). The broad signal at 1.52 ppm integrating for two protons, is assigned to the

terminal -NH<sub>2</sub> group (1). The broad shape of the peak is due to hydrogen-bonding.

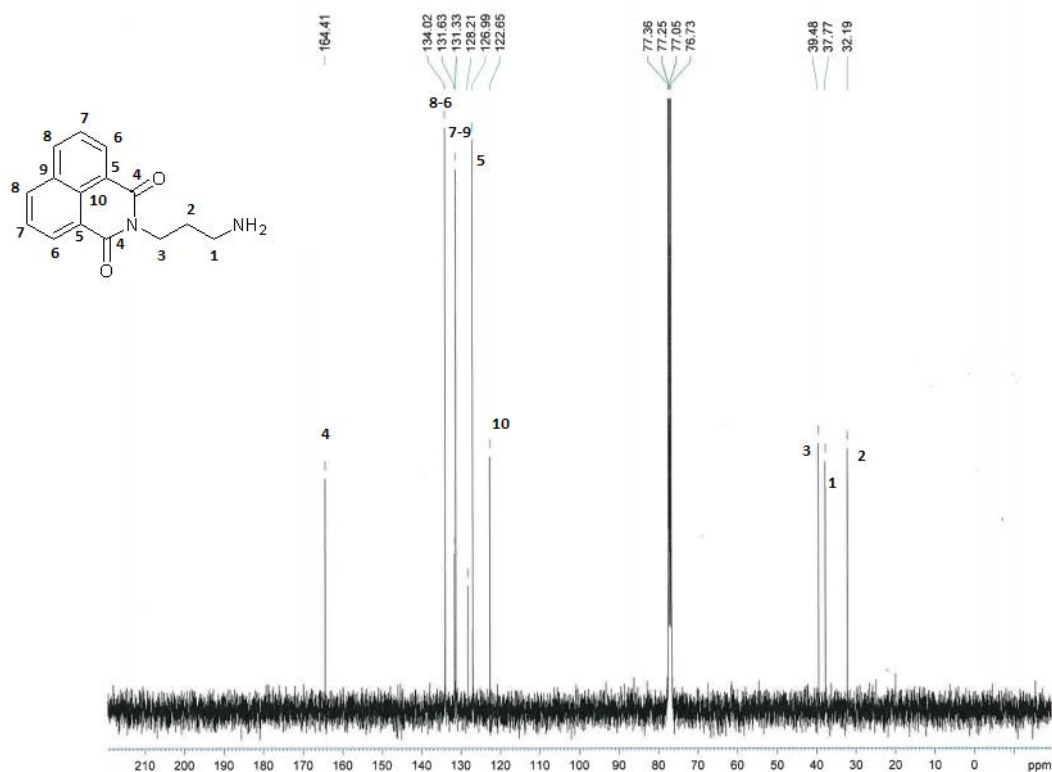


Figure 2.11. <sup>13</sup>C NMR spectrum of intermediate 1 (I-1).

In the <sup>13</sup>C NMR spectrum, the solvent signals (CDCl<sub>3</sub>) are observed at 77.1 ppm. The one at 164.4 ppm refers to the two carbons (4) linked with the oxygen (carbonyl groups); the electronegativity of the oxygen atom and the double bond cause the high de-shielding and the consequential shift of the peak to downfield in the spectrum. The six singals between 134.0 and 122.7 ppm are due to the remaining 6 different carbons in the naphthalimide moiety (5 to 10); although a total of twelve carbon atoms are present in the naphthalimide structure, only seven signals are observed due to the symmetry of the molecule, creating chemical equivalence.

The three singnals between 39.5 and 32.2 ppm refer to the three aliphatic carbons (1, 2 and 3). Finally, the LMRS confirmed the molecular weight of the compound (figure 2.12).

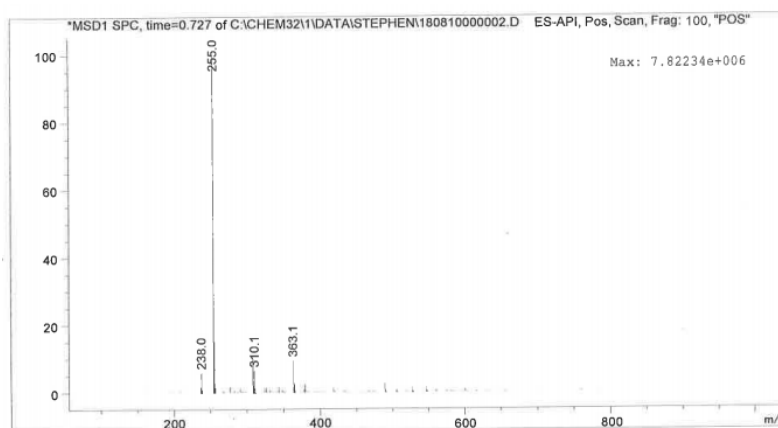
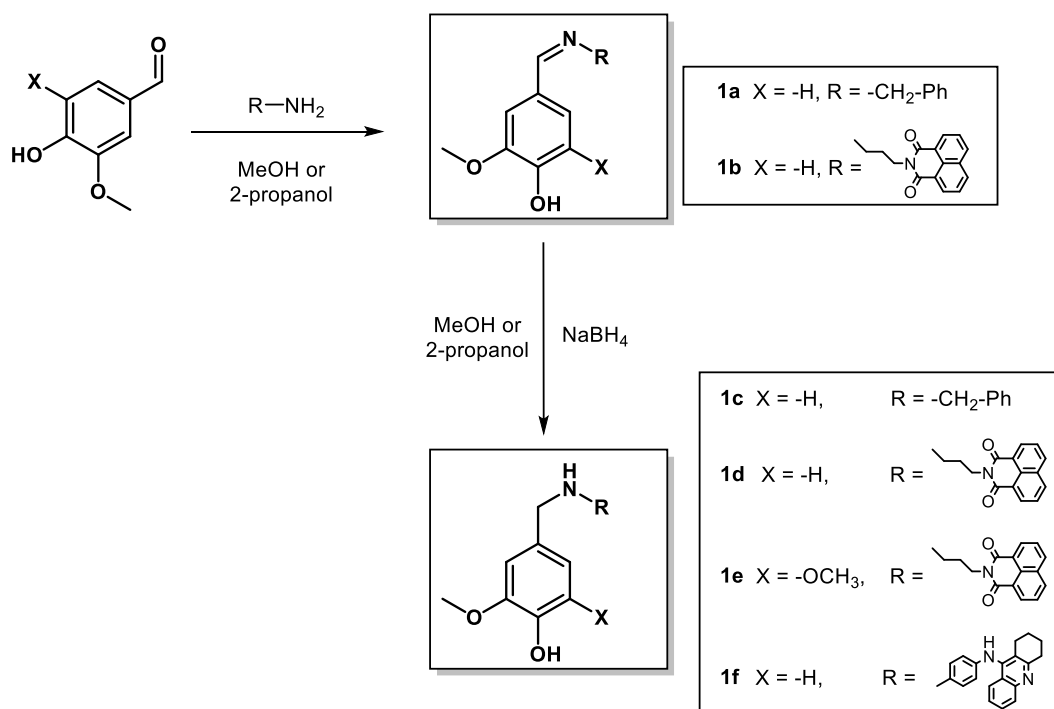


Figure 2.12. LRMS spectrum of intermediate 1 (**I-1**).

### 2.5.2 Synthesis of the Monomers

The synthetic strategy for the synthesis of the vanillin monomers (**1a-1f**) is shown in scheme 2.



Scheme 2. Synthetic strategy for the synthesis of monomers and their nomenclature.

The imines (**1a** and **1b**) were prepared by reacting vanillin or syringaldehyde with equimolar amounts of the corresponding amines in methanol with yields ranging from 63-70 %. The imines were then reduced with an excess of sodium borohydride (NaBH<sub>4</sub>) in methanol to give the corresponding secondary amines with yields ranging from 68-86%.

Compounds **1e** and **1f** were prepared without the isolation of the corresponding imine; vanillin or syringaldehyde were reacted with a slight excess of the corresponding amine. Once the vanillin or syringaldehyde was completely consumed (monitored by TLC), a slight excess of NaBH<sub>4</sub> was added. Once the reaction was complete, the solution was dried and the products were purified through DCM/saturated NaHCO<sub>3</sub> or column chromatography to afford the pure compounds with yields ranging from 38-67 %. These compounds were fully characterized via <sup>1</sup>H, <sup>13</sup>C NMR and HRMS spectroscopy. As an example, the NMR and mass spectra of **1d** are discussed in the following pages (Figure 2.13-2.15).

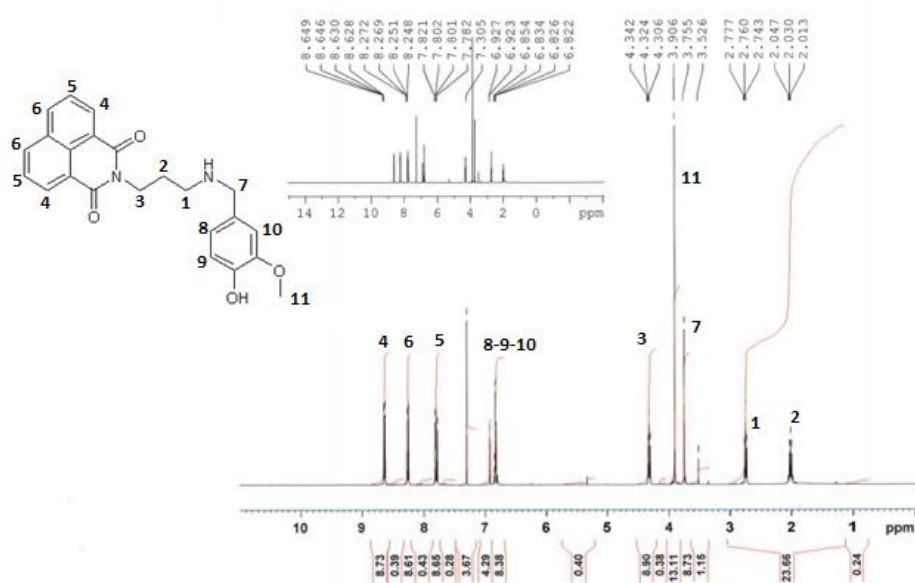


Figure 2.13. <sup>1</sup>H NMR spectrum of **1d**.

From figure 2.13, the six aromatic protons of the naphthalimido moiety are found between 8.65 and 7.78 ppm (4, 5 and 6). The three aromatic protons in the vanillin moiety (8, 9 and 10) are situated between 6.93 and 6.82 ppm. The three protons of the methoxy group (11) in the vanillin moiety appear as a singlet at 3.91 ppm, whereas the two protons of the methylene group (7) between the nitrogen and the vanillin moiety are located at 3.76 ppm. The remaining six protons of the three methylene groups (1, 2 and 3) appear at 4.32, 2.76 and 2.03 ppm, respectively.

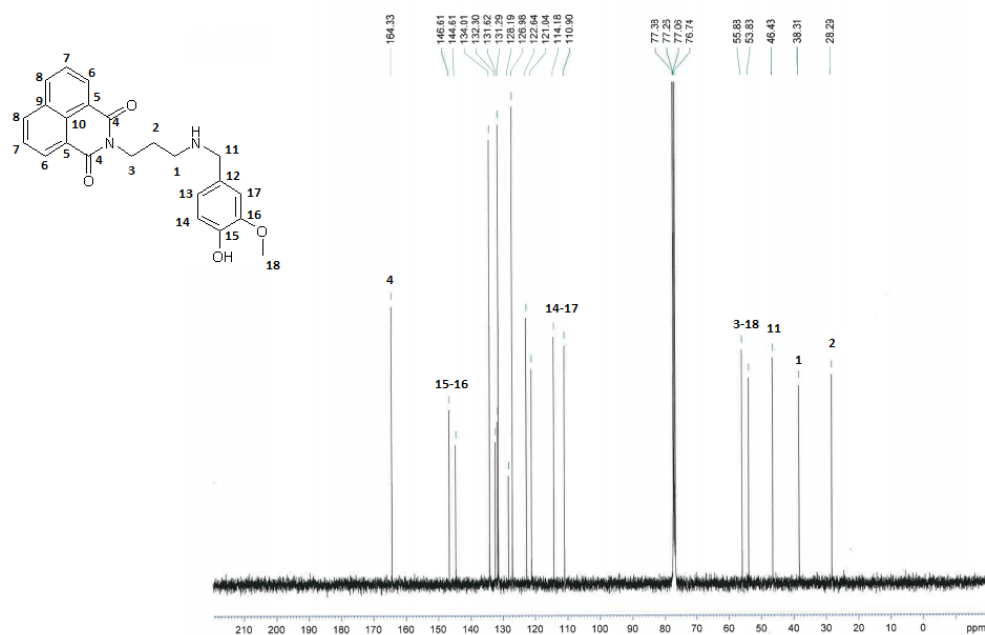


Figure 2.14.  $^{13}\text{C}$  NMR spectrum of **1d**.

For the  $^{13}\text{C}$  NMR spectrum, solvent peaks ( $\text{CDCl}_3$ ) are located between 77.4 and 76.7 ppm. The thirteen different aromatic carbons (4 to 17) are located between 164.3 and 110.9 ppm. The carbon of the methoxy group (18) and the carbons of the four methylene groups (1, 2, 3 and 11) are located between 55.8 and 28.3 ppm. Finally, the HRMS confirmed the molecular weight of compound **1d**; the spectra is shown in figure 2.15.

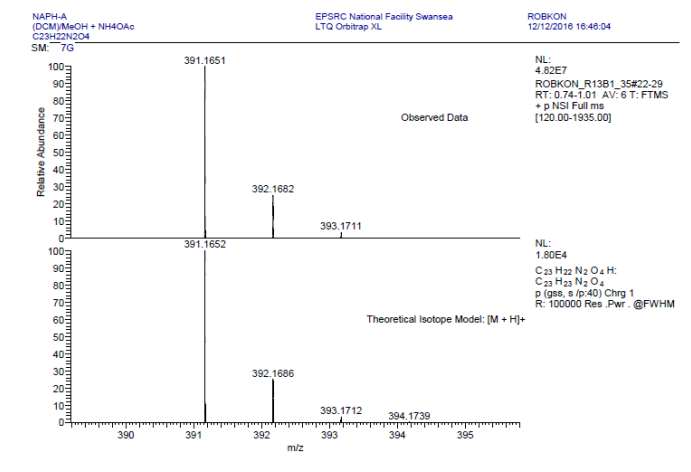


Figure 2.15. HRMS spectrum of compound **1d**.

### 2.5.3 Synthesis of the Dimers

The dimers were synthesized *via* a one-step reductive amination reaction, which involved the condensation of an aldehyde (or ketone) and an amine,

followed by reduction of the imine group. Sodium cyanoborohydride (NaCNBH<sub>3</sub>) was used as the reducing agent, along with zinc chloride, due to its selectivity toward the imine group and its inability to reduce the aldehyde group of vanillin (Borch, Bernstein and Durst, 1971; Baxter and Reitz, 2002). The solvent used in all the reaction was methanol. The reaction pathway of reductive amination is reported in figure 2.16.

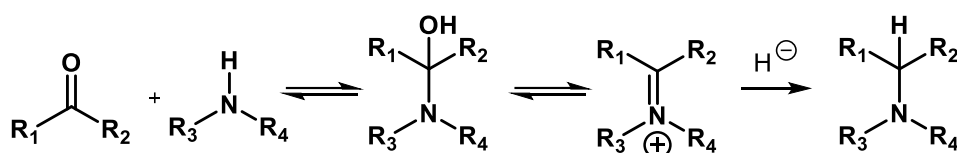
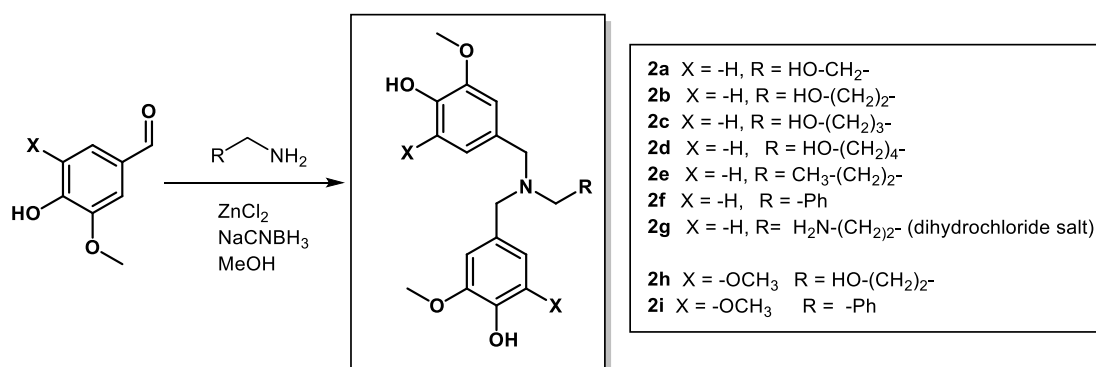


Figure 2.16. Reaction pathway of reductive amination, described by (Baxter and Reitz, 2002).

An excess of amine and reducing agents was used in each reaction to enhance the purification of the final product by simple extraction using chloroform/saturated NaHCO<sub>3</sub>, in order to avoid the presence of vanillin in the chloroform phase. The strategy for the synthesis of the vanillin dimers (**2a-2i**) is shown in scheme 3.



Scheme 3. Synthetic strategy for the synthesis of dimers and their nomenclature.

Vanillin or syringaldehyde were reacted with an excess of the corresponding amine in the presence of an excess of ZnCl<sub>2</sub> and NaCNBH<sub>3</sub> in methanol for 24 hours. The solution was dried through rotary evaporator and the residue was purified through extraction (3x DCM/NaHCO<sub>3</sub>) or through column chromatography (DCM:MeOH 95:5) (see method section). Compounds **2f**, **2g** and **2i** precipitated out of the solution and were filtered off, then washed with deionized water and methanol. In addition, due to insolubility of **2g** in most common solvents, the latter compound was suspended in methanol and concentrated hydrochloric acid was added to afford the dihydrochloride

salt. The yields (12 to 23%) were generally poor for the compounds purified through DCM/saturated NaHCO<sub>3</sub> extraction (for example **2a**, **2c** and **2e**) compared to the compounds purified through column chromatography. This was due to their apparent slight solubility of the latter in the aqueous phase during extraction.

In contrast, purification through column chromatography (compounds **2b**, **2d** and **2h**) afforded higher yields, ranging from 46 to 82%. Compounds isolated by filtration (**2f**, **2g** and **2i**) were obtained in yields ranging from 46 to 90%. The compounds were characterized through <sup>1</sup>H, <sup>13</sup>C NMR and HRMS. As an example of a dimer where the NMR and mass spectra of **2b** are shown (figures 2.17-2.18) and discussed in the following pages.

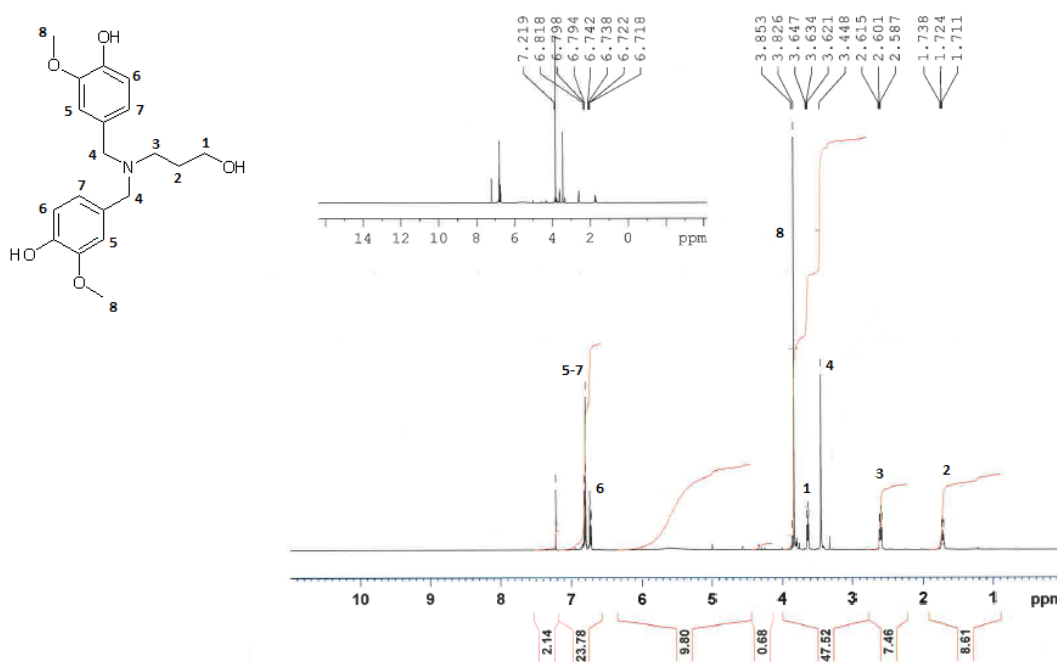


Figure 2.17. <sup>1</sup>H NMR spectrum of dimer **2b**.

In the <sup>1</sup>H NMR spectrum of **2b**, the six aromatic protons (5, 6 and 7) are found between 6.82 and 6.72 ppm. The hydrogens from the two methoxy groups (8) occur as singlet at 3.83 ppm, due to the de-shielding caused by the oxygens linked to the aromatic moieties. The integration of those protons, accounted for a total of 6 atoms, confirms that two vanillin moieties are present in the molecule (dimer). The two methylene groups (4) between the tertiary nitrogen and the vanillin moiety are shown at 3.45 ppm, integrating for four protons. Due to the de-shielding effect caused by the terminal hydroxy group, the protons of the methylene group (1) linked

to it are represented at 3.63 ppm. The protons in the methylene group linked to the nitrogen (3) occur at 2.60 ppm, due to the lower de-shielding activity of the latter compared to the oxygen. Finally, the protons of the remaining methylene (2) experience the lower de-shielding force, occurring at 1.72 ppm.

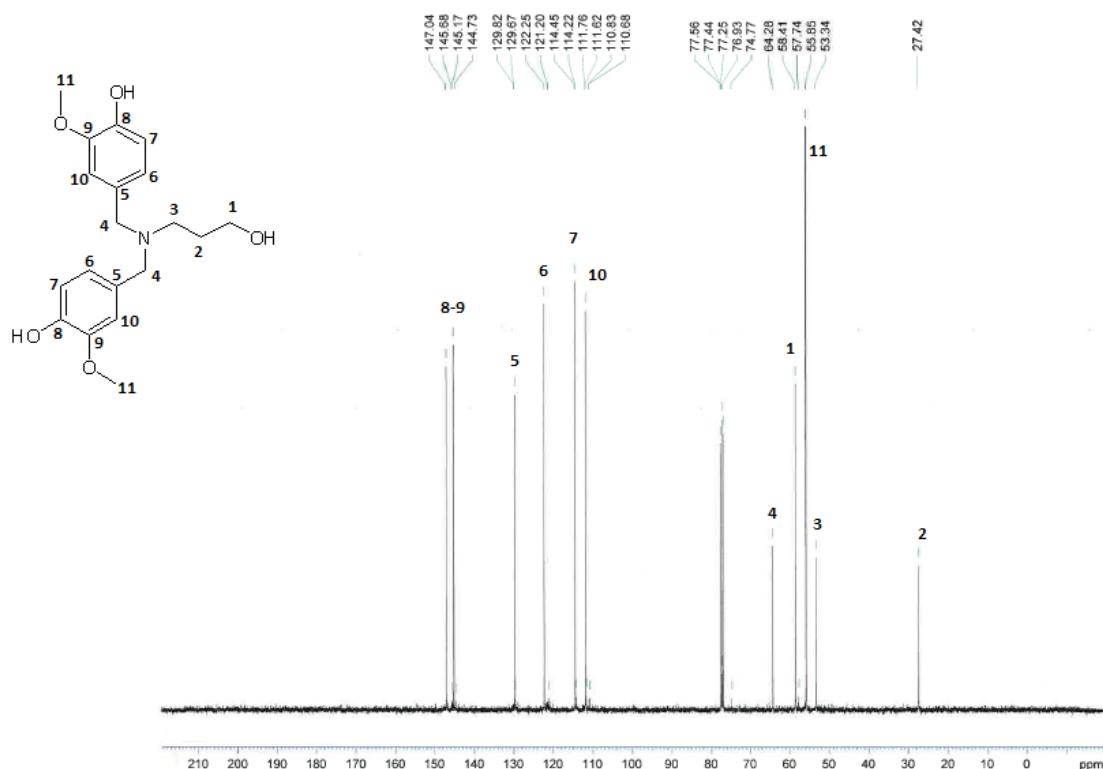


Figure 2.18.  $^{13}\text{C}$  NMR spectrum of dimer **2b**.

In the  $^{13}\text{C}$  NMR spectrum of **2b**, the six aromatic carbons (5 to 10) lie between 147.0 and 110.8 ppm whereas the methylene carbons between the nitrogen and the aromatic ring (4) occur at 64.30ppm. The three aliphatic carbons (1, 2 and 3) are located at 27.40, 53.34 and 58.40ppm, respectively whereas the two carbons of the methoxy groups (1) occur at 55.9 ppm. Finally, the HRMS confirmed the molecular weight of compound **2b** (figure 2.19).

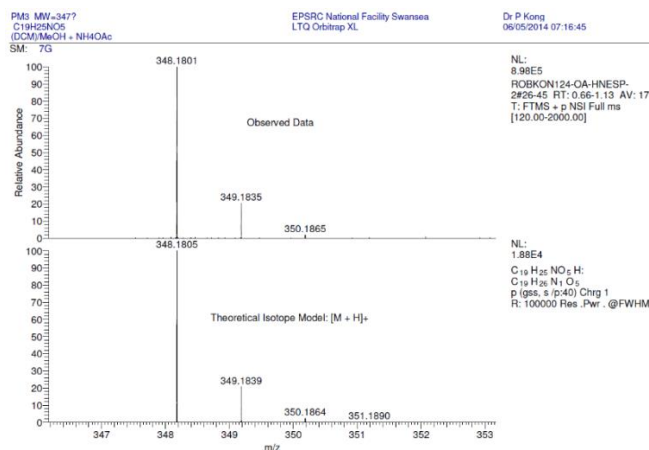
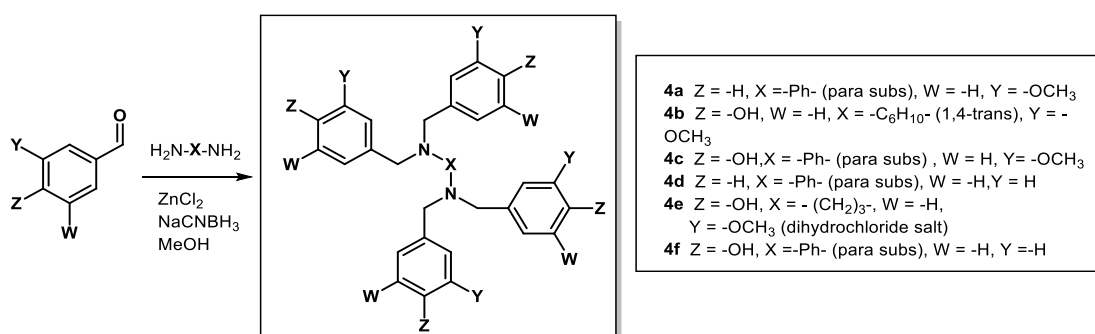


Figure 2.19. HRMS of dimer **2b**.

### 2.5.4 Synthesis of the Tetramers

The synthetic strategy for the synthesis of the vanillin tetramers (**4a-4f**) is depicted in scheme 4.



Scheme 4. Synthetic strategy for the synthesis of tetramers and their nomenclature.

An excess of vanillin, syringaldehyde, benzaldehyde or 4-hydroxy benzaldehyde was reacted with the corresponding amine in the presence of an excess of ZnCl<sub>2</sub> and NaCNBH<sub>3</sub> in methanol for 24 hours. The precipitates obtained were then filtered off, washed thoroughly with fresh solvent, affording the pure compounds in yields ranging from 18-80%. In addition, due to the insolubility of **4e** in most common solvents, **4e** was suspended in methanol and concentrated hydrochloric acid was added to afford the dihydrochloride salt in 38% yield. Compound **4f** was obtained, after the removal of the methanol and after thorough washing of the residue with water and chloroform (66% yield). The compounds were characterized through <sup>1</sup>H, <sup>13</sup>C NMR and LRM spectroscopy. As an example, the NMR and mass spectra of compound **4c** are discussed in the following pages.

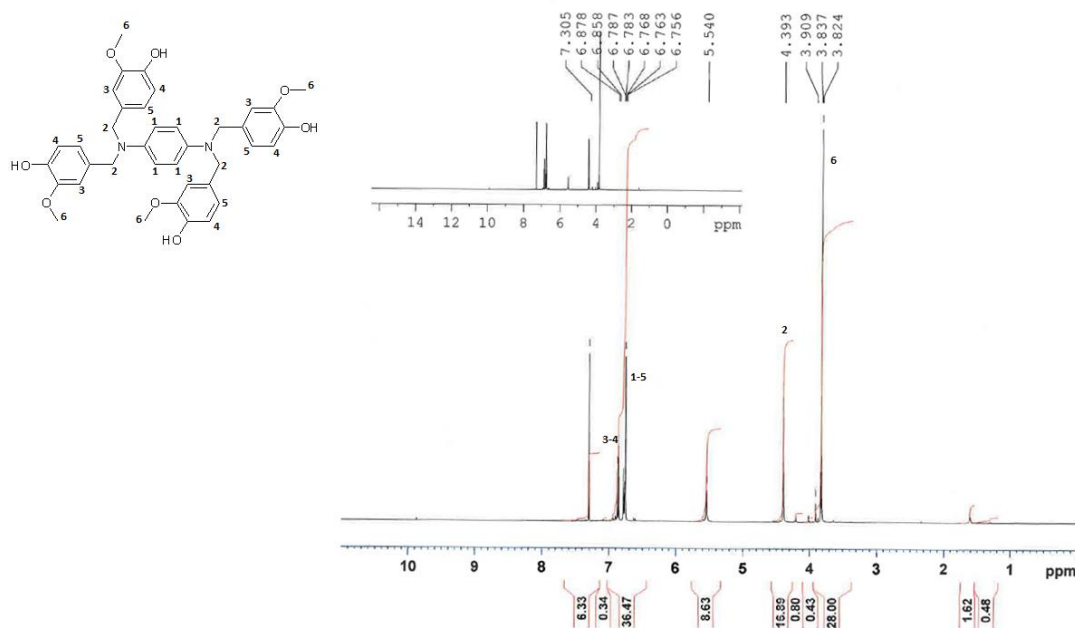


Figure 2.20.  $^1\text{H}$  NMR spectrum of tetramer **4c**.

In the  $^1\text{H}$  NMR spectrum of **4c**, the sixteen aromatic protons (at carbons 1, 3, 4 and 5) occur between 6.88 and 6.76 ppm. The eight protons in the four methylene moieties (2) are found at 4.39 ppm whereas the twelve protons from the four methoxy groups (6) are centred at 3.84 ppm.

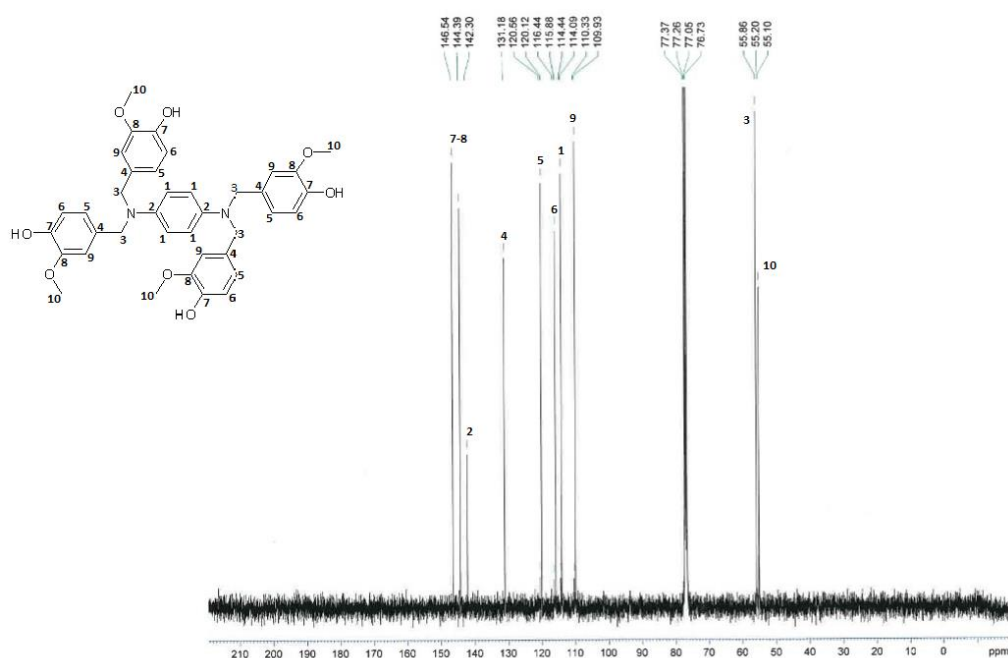


Figure 2.21.  $^{13}\text{C}$  NMR spectrum of tetramer **4c**.

In the  $^{13}\text{C}$  NMR spectrum of **4c** (figure 2.21), the eight different aromatic carbons (1, 2 and 4 to 9) are located between 146.5 and 109.9 ppm. The four carbons in the methylene groups (3) are located at 55.9 ppm whereas the carbons of the methoxy groups (10) are situated at 55.2 ppm. Finally, the HRMS confirmed the molecular weight of compound **4c** (figure 2.22).

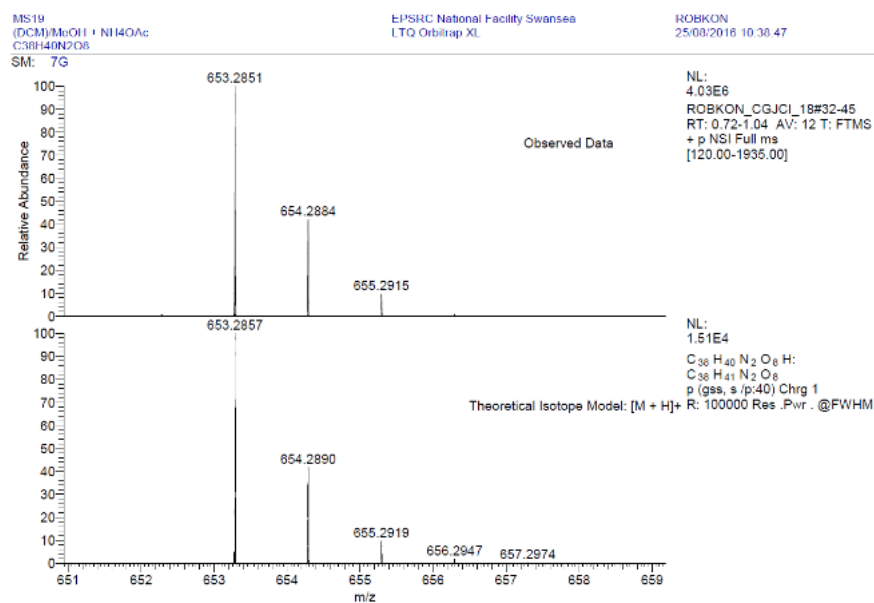


Figure 2.22. HRMS spectrum of tetramer **2c**.

## 2.6 Conclusions

Twenty-one novel vanillin derivatives were successfully designed, synthesized and characterized. Six derivatives consist of only one vanillin moiety (monomers), nine derivatives have two vanillin moieties (dimers) and six derivatives with four vanillin moieties (tetramers) (see schemes 1, 2, 3 and 4 in section 2.4).

The rationale for the synthesis of these derivatives was to evaluate:

- (v) The impact of the number of vanillin moieties may have on their antioxidant activities; this was carried out by comparing the antioxidant activities of dimers, tetramers and monomers (see schemes 1, 2, 3 and 4 in the previous pages).
- (vi) The impact of methoxy and hydroxy groups in the vanillin moieties on the antioxidant activities; this can be exploited by comparing derivatives **4a**, **4c**, **4d** and **4f** or compounds **2b** and **2h**, **2f** and **2i** or **1d** and **1e** (see figure 2.23).

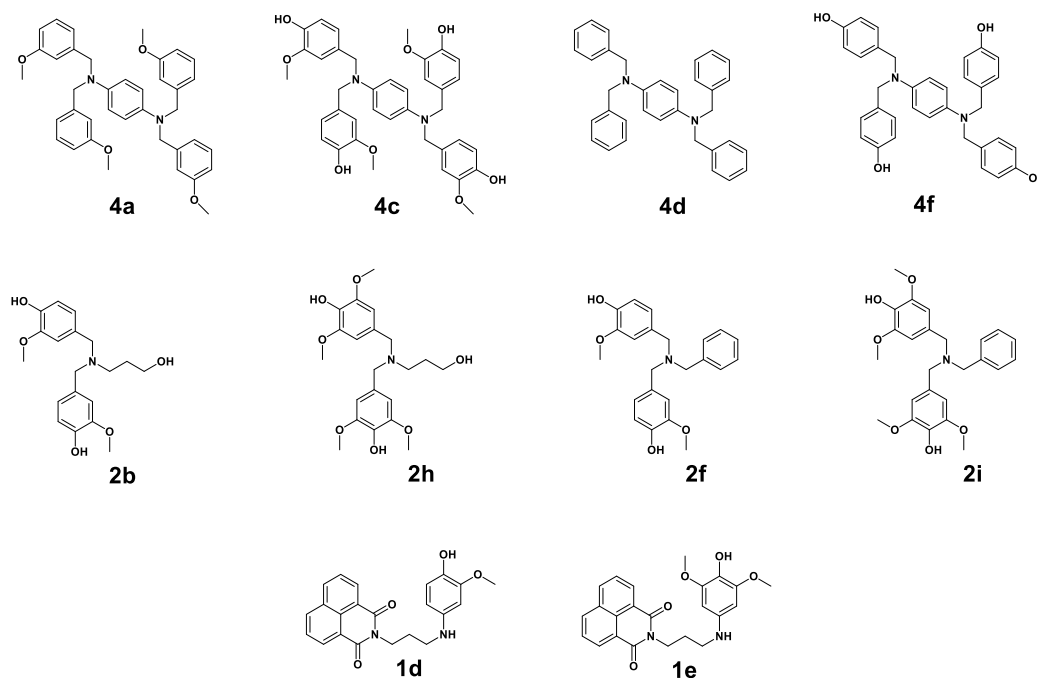


Figure 2.23. Chemical structures of related vanillin derivatives bearing different hydroxy and methoxy groups.

- (vii) The presence of nitrogen atom(s) on the antioxidant activity; the derivatives prepared were imines (compounds **1a** and **1b**), secondary (**1c**, **1d**, **1e** and **1f**) or tertiary amines (the rest of the compounds). In addition, the nitrogen atoms were also protonated as two hydrochloric salts were prepared to evaluate their antioxidant properties (compound **2g** and **4e**) (see schemes 1, 2, 3 and 4 in the previous pages).
- (viii) The role of alkyl chains linked to the nitrogen atom and their impact on the antioxidant activity; compounds **2a**, **2b**, **2c** and **2d** differ just for the length of the alkyl chain. In addition, the impact on antioxidant activity of heteroatoms on the alkyl chain has been evaluated by replacing the methyl group of compound **2e** with a hydroxy group in compound **2b** (see scheme 3).
- (ix) The impact of electronic conjugation on the antioxidant properties; for example, the electrons of nitrogen atoms in compound **4c** can be delocalised throughout the linker (the aromatic moiety) whereas this is not possible for compound **4b** which bears a cyclohexane moiety between its nitrogen atoms (see figure 2.24).

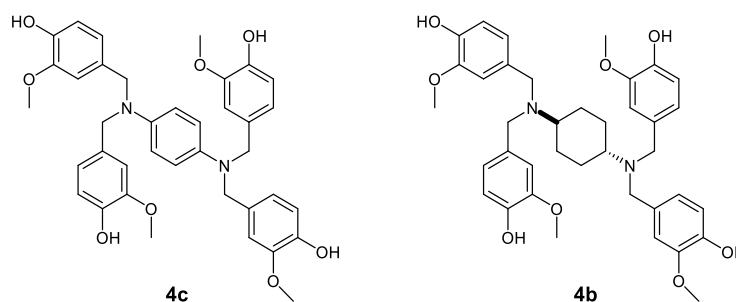


Figure 2.24. Chemical structures of compounds **4c** (left) and **4b** (right).

- (x) The impact of naphthalimide and tacrine moieties (in compounds **1c**, **1d**, **1e** and **1f**) on antioxidant properties, cholinesterase activity and  $A\beta_{(1-42)}$  and amyloid aggregation, which will be discussed in chapter 5.

The synthetic route for the preparation of the monomers involved a multi-step strategy, with the isolation of the Schiff base (imine), obtained by condensation of vanillin or syringaldehyde with the corresponding amine, and followed by the reduction using sodium borohydride. The yields for this class of derivatives ranged from 38 to 86%.

The dimers were obtained through reductive amination, by reacting vanillin or syringaldehyde with an excess of the corresponding amine in the presence of zinc chloride and sodium cyanoborohydride with yields ranging from 12 to 90%.

The tetramers were obtained through reductive amination, by reacting an excess of vanillin, syringaldehyde, benzaldehyde or 4-hydroxy benzaldehyde with the corresponding amine in the presence of zinc chloride and sodium cyanoborohydride with yields ranging from 18 to 80%.

The successful synthetic strategies adopted for the novel vanillin derivatives has led to the following evaluation of their antioxidant properties (Chapter 3), protective effects toward SH-SY5Y neuroblastoma cell line (Chapter 4) and their potential use in a multitargeted-based Alzheimer's Disease therapy (Chapter 5).

# **Chapter 3: Antioxidant Properties of Vanillin Derivatives**

### 3.1 Introduction

As described in chapter 1, numerous studies have linked oxidative stress to the pathogenesis of many major age-related diseases such as cancer, cardiovascular and neurodegenerative diseases (Firuzi *et al.*, 2011; Poljsak, Šuput and Milisav, 2013a). Many studies have reported the possible use of natural and synthetic antioxidants for the prevention or treatment of such diseases. For example, vitamin E, vitamin C and  $\beta$ -carotene was widely employed as antioxidant in both animal and human trials for coronary diseases and cancer, although the results are far from conclusive (Creagan *et al.*, 1979; van Poppel and van den Berg, 1997; Gilgun-Sherki *et al.*, 2002; Tinkel, Hassanain and Khouri, 2012; Hu *et al.*, 2015).

At the same time, polyphenols have shown protective effects in both *in vitro* and *in vivo* neurodegenerative disease models, acting as modulator of different biological pathways, such as the signalling cascades and anti-apoptotic processes; however the beneficial effects are not only conferred by antioxidant activity (Ramassamy, 2006; Ajami *et al.*, 2017).

In addition, a wide number of synthetic compounds, often based on natural antioxidants, have been reported. For example, synthetic derivatives of gallic acid have been recently reported, showing neuroprotective effects in Parkinson's Disease model, at a cellular level (Lu *et al.*, 2006). More recently, melatonin-cinnamate hybrids showed neuroprotective effects in Alzheimer's Disease model at cellular level (Buendia *et al.*, 2015). In the same year, a curcumin-melatonin hybrid known as Z-CM-I-1 was reported to show protective effects against oxidative stress, decreased accumulation of A $\beta$  amyloid in the cortex regions of the brain and reduction in inflammatory response in a transgenic *in vivo* APP/PS1 AD mouse model (Gerenu *et al.*, 2015).

Although the antioxidant therapy produced contrasting results in the past years, natural and synthetic antioxidants represent an interesting and promising approach for the treatment of neurodegenerative diseases. Thus, the decision of the adequate assays for the determination of the antioxidant

activity of a target molecule is of critical importance (Moon and Shibamoto, 2009).

### 3.1.1 Assays for the Evaluation of Antioxidant Activity

The scientific literature reports a wide number of *in vitro* antioxidant assays, based on different molecular mechanism, for the determination of the antioxidant activity of pure compounds and natural extracts.

The employment of different antioxidant assays leads to a major understanding regarding the capabilities of latter extracts or compounds.

The most common assays employed are reported in the following pages.

#### 3.1.1.2 2,2-diphenyl-1-picrylhydrazyl (DPPH) Assay

DPPH assay was developed in 1958 by Blois with the aim to determine the antioxidant activity using a stable free radical (Blois, 1958). It involves the use of 2,2-diphenyl-1-picrylhydrazyl (DPPH), a synthetic free radical with an absorption maximum at 517 nm which decreases with reduction by an antioxidant (Dudonné *et al.*, 2009). The stability of this free radical lies on the delocalisation of the spare electron over the molecule as a whole (see figure 3.1) (Kedare and Singh, 2011).

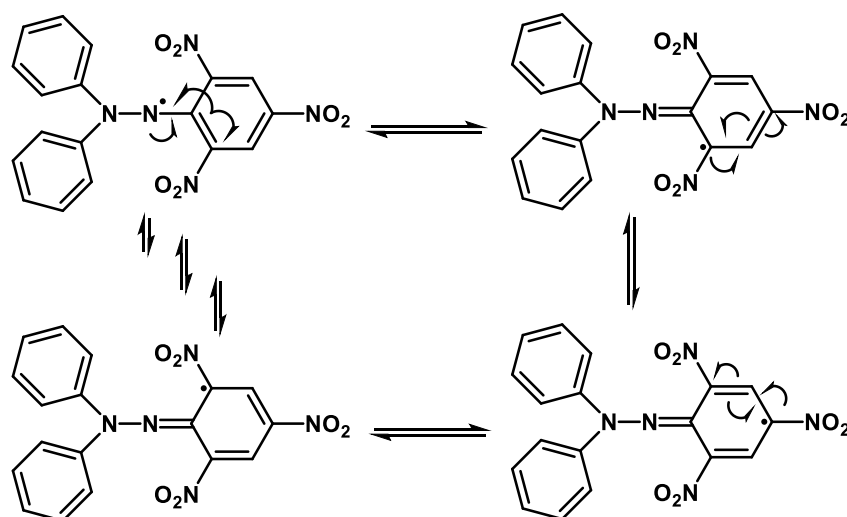


Figure 3.1. Electronic delocalisation of the lone electron in DPPH molecule.

The assay is based on both hydrogen atom transfer (HAT) and electron transfer (ET) from an antioxidant to the DPPH free radical, depending on the

nature of the solvent and the redox potentials of the species involved. In fact, the HAT mechanism is predominant in non-polar solvents whereas ET mechanism becomes predominant in polar solvents where hydrogen bonds can be formed with the antioxidant molecules such as methanol or ethanol (Foti, Daquino and Geraci, 2004; Villaño *et al.*, 2007).

The reduction of DPPH free radical is linked with the loss in absorbance at 517 nm which can be measured with a uv/vis spectrophotometer (Blois, 1958). The mechanism of the assay is described in figure 3.2.

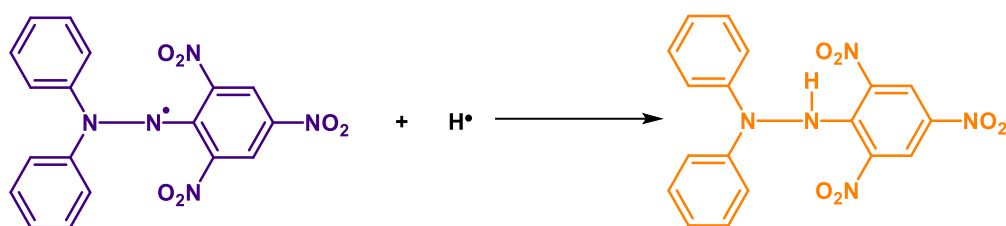


Figure 3.2. Mechanism of DPPH assay.

The results from the DPPH assay are expressed as  $IC_{50}$ , which is defined as the concentration of sample able to scavenge 50% of the free radical and can be determined by plotting the absorbance obtained at each concentration (Villaño *et al.*, 2007).

The  $IC_{50}$  can then be determined using the equation of the linear portion of the curve line. This assay is convenient in its application and it is one of the most popular antioxidant assay; however, its application is limited as a non-physiological free radical is employed (Floegel *et al.*, 2011).

### 3.1.1.3 Ferric Reducing/Antioxidant Power (FRAP) Assay

The FRAP assay was developed by Benzie and Strain in 1996 at the Hong Kong Polytechnic University with the original name of "ferric reducing ability of plasma", since it was used for the measurement of the antioxidant activity of plasma (Benzie and Strain, 1996). Subsequently, the assay was applied to other substrates such as wine and tea and was then renamed as the "ferric reducing/antioxidant power" assay (Pulido, Bravo and Saura-Calixto, 2000).

FRAP is based on the reduction of ferric ions ( $Fe^{3+}$ ) to ferrous ions ( $Fe^{2+}$ ) through electron transfer pathway at low pH with the subsequent formation

of a blue-coloured ferrous-tryptiridyltriazine complex. The molecular mechanism of the assay is described in figure 3.3.

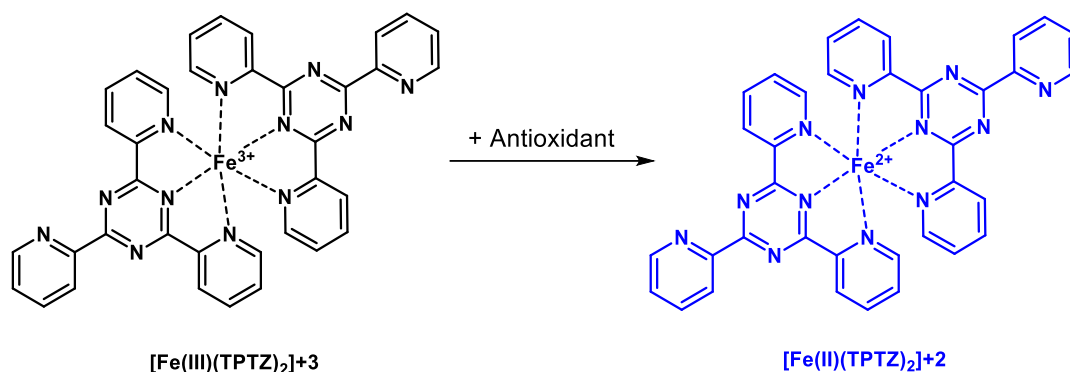


Figure 3.3. Mechanism of FRAP assay, adapted from Pérez-Cruz *et al.* (2018).

The results can be obtained by plotting the absorbance at 593 nm at each concentration of the sample tested and comparing the curve obtained with the calibration curve obtained for antioxidants such as ascorbic acid or Trolox (Benzie and Strain, 1996; Pulido, Bravo and Saura-Calixto, 2000). Strictly, this is a measure of the reducing power of a compound, as opposed to its ability to scavenge ROS, but there is obviously a close link between the two. Nevertheless, associating the ability to reduce iron ions to antioxidant capacity is an extrapolation, and should be approached with caution.

#### 3.1.1.4 2,2-azino-bis(3-ethylbenz- thiazoline-6-sulfonic acid) (ABTS) Assay

The 2,2-azino-bis(3-ethylbenz- thiazoline-6-sulfonic acid) (ABTS) assay has been widely used for the evaluation of food and beverage components due to its applicability in both aqueous and lipid phases (MacDonald-Wicks, Wood and Garg, 2006). ABTS assay was firstly developed by Miller *et al.* in 1993 and it involved the activation of metmyoglobin by hydrogen peroxide in the presence of ABTS (Miller *et al.*, 1993). In the modern version of the assay, the ABTS is oxidised to the blue-green ABTS radical cation using potassium persulfate (see figure 3.4).

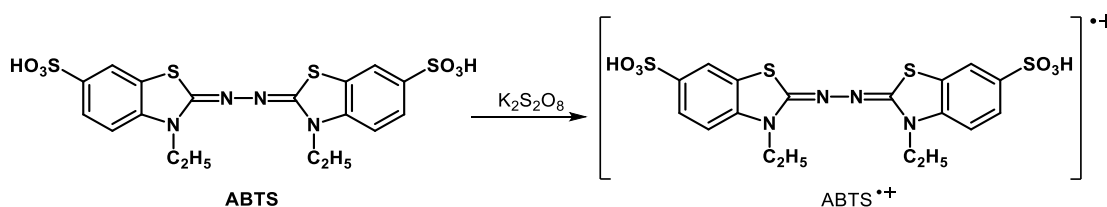


Figure 3.4. Formation of ABTS radical cation from ABTS with potassium persulfate, adapted from Moon and Shibamoto (2009) with Copyright agreement © 2009, American Chemical Society.

The addition of the antioxidant causes the decolorization of the ABTS which can be measured at 734 nm.

The absorbance of the reaction mixture of ABTS and the antioxidant is compared to the mixture of ABTS and Trolox, and the results are expressed as Trolox equivalent antioxidant capacity (TEAC) (Moon and Shibamoto, 2009).

Again, this assay measures the ability of a compound to scavenge a stable radical that is substantially less reactive than oxygen-centred radicals in biology. Extrapolating the results to an *in vivo* situation should be approached with caution.

### 3.1.1.5 Total Phenol Assay (Folin-Ciocalteu reagent)

This assay was originally introduced as “Folin-Ciocalteu assay” for protein analysis, exploiting the phenolic moiety of the amino acid tyrosine (Folin and Ciocalteu, 1927). Subsequently, Singleton, Orthofer and Lamuela-Raventós adapted the assay for the measure of phenols in wine, leading to the actual name, total-phenol assay (Singleton, Orthofer and Lamuela-Raventós, 1999; MacDonald-Wicks, Wood and Garg, 2006).

It is based on the electron transfer from phenolic molecules to phosphomolybdic and phosphotungstic acid complexes, the Folin-Ciocalteu reagent (FCR), which are coloured in blue and can be spectroscopically measured at 760 nm.

Although the exact chemical nature of the final product from this assay is still unknown, it is believed that the intense blue colouration is given by the formation of the  $(\text{PMoW}_{11}\text{O}_{40})^{4-}$  complex (Ainsworth and Gillespie, 2007).

It is worth noting that, due to the non-selective chemistry behind this assay, the FCR is not specific for phenolic molecules and it can be reduced by many non-phenolic compounds such as vitamin C, aromatic amines,

sulphites and sugars (when present in high concentrations) (Huang, Boxin and Prior, 2005; Ainsworth and Gillespie, 2007).

### 3.1.1.6 Oxygen Radical Absorbance Capacity (ORAC) Assay

The ORAC assay was developed for the first time by Cao, Alessio and Cutler in 1993 at the National Institute on Ageing in Baltimore and at the Department of Physical Education of Miami University (Cao, Alessio and Cutler, 1993).

It was based on a previous method developed in Glazer's laboratories at the University of California where phycoerythrin fluorescence emission was used to measure the rate of free radical-mediated damage induced by 2,2'-azobis(2-amidinopropane) (AAPH) after thermal decomposition (DeLange and Glazer, 1989). AAPH undergoes thermal decomposition in solution, generating two amidinopropane radicals, which can react with oxygen to yield peroxy radicals, as depicted in figure 3.5 (Nimse and Pal, 2015).

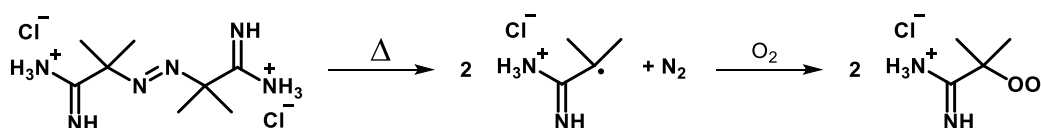


Figure 3.5. Mechanism of peroxy radical generation mediated by AAPH, adapted from Nimse and Pal (2015) Published by The Royal Society of Chemistry.

The use of the peroxy free radical, which is commonly found in the body, makes this assay more applicable to biological systems (Isa *et al.*, 2012). However, the DeLange and Glazer's method was not able to quantify the results obtained and was limited to the screening of the free radical scavenging capacity of the sample.

Cao, Alessio and Cutler's method introduced the ORAC values, which refer to the net protection area under the quenching curve of the fluorescent probe in the presence of the antioxidant (see figure 3.6)

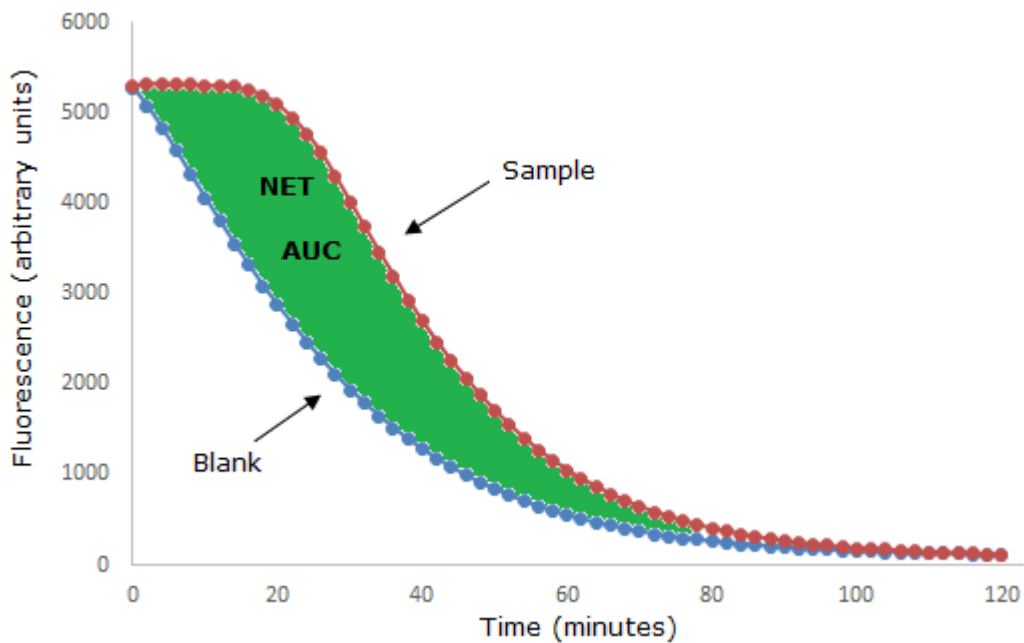


Figure 3.6. Example of NET area under the curve for ORAC assay. The latter can be measured calculating the area between the sample curve(s) and the blank.

The ORAC values are obtained by comparison with the synthetic antioxidant standard Trolox (Cao, Alessio and Cutler, 1993).

At present, fluorescein is the most employed fluorescent probe since it is photostable and does not show photo bleaching property after exposure to excitation light for certain time, which was the limitation with phycoerythrin (Ou, Hampsch-Woodill and Prior, 2001; Alarcón *et al.*, 2008). The fluorescein oxidative pathway follows the HAT mechanism, as depicted in figure 3.7.

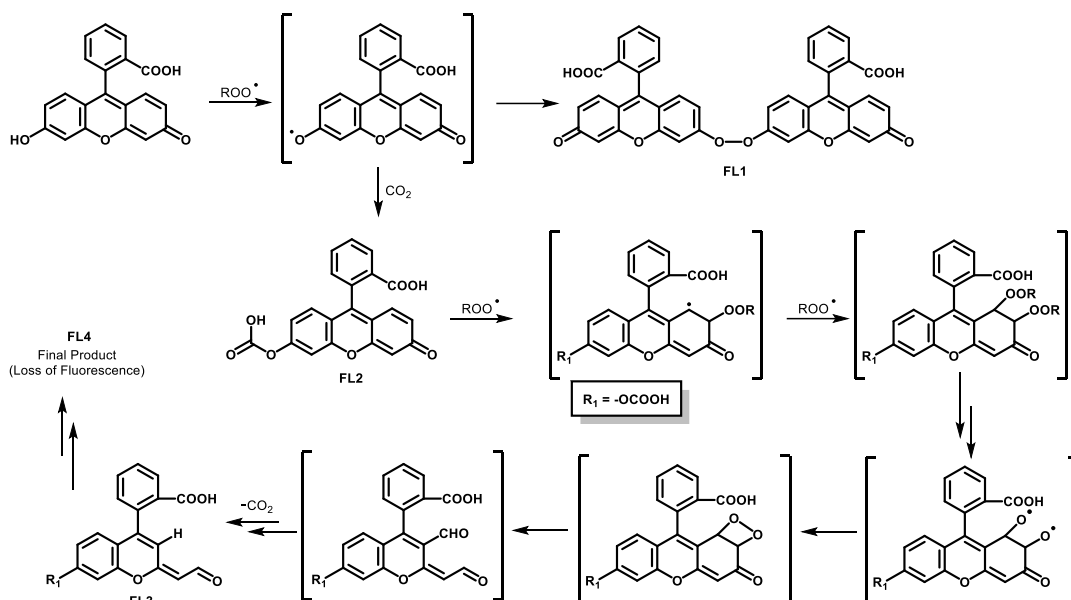


Figure 3.7. Proposed fluorescein oxidation pathway in the presence of AAPH, adapted from Ou, Hampsch-Woodill, and Prior (2001) with Copyright agreement © 2001, American Chemical Society.

The first step of this process involves the abstraction of the hydrogen of the phenolic moiety in the fluorescein molecule by the peroxy radical generated by AAPH, generating a stable phenoxyl radical that can undergo dimerization (FL1).

However, the same phenoxyl radical can react with carbon dioxide in the buffer to yield 2-(6-(carboxyoxy)-3-oxo-3H-xanthen-9-yl)benzoic acid (FL2). The latter can react with two peroxy radicals to afford the endoperoxide intermediate which can decompose into FL3. The oxidative process can further continue to generate an unknown FL4, with  $m/z$  221.3, which does not show fluorescent emission at 495/515 nm (Ou, Hampsch-Woodill and Prior, 2001).

### 3.1.1.7 Thiobarbituric Acid Reactive Substances (TBARS) Assay

The thiobarbituric acid test has been employed to measure the lipid peroxidation in chemicals, food and biological matrices (Janero, 1990). The assay is based on the reactivity of malondialdehyde (MDA), a common end product of oxidative lipid degradation, toward thiobarbituric acid (TBA) following a 1:2 stoichiometry, leading to the formation of a red chromophore with an absorption maximum at 532 nm (Hodges *et al.*, 1999). The reaction between malondialdehyde and TBA is depicted in figure 3.8.

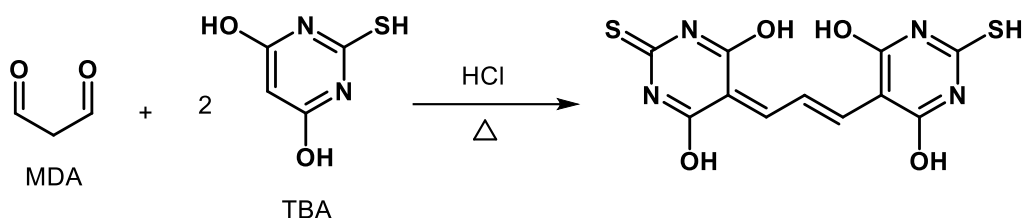


Figure 3.8. Formation of the MDA-TBA adduct, adapted from Janero (1990) with Copyright agreement © 1990 Published by Elsevier In.

It consists in an acid-catalysed nucleophilic addition involving the C-5 of TBA toward one of the carbonyl group of MDA, followed by dehydration and subsequent reaction of the 1:1 adduct with another molecule of TBA.

Linoleic acid (LA) is the common substrate employed for the generation of MDA in *in vitro* assays due its availability at high purity; however, due to the variety of conditions reported in a wide number of works, the assay has been criticised for its lack of robustness (Buenger *et al.*, 2006; Ghani *et al.*, 2017).

### 3.1.1.8 DNA Damage Protection Assay

Agarose gel electrophoresis is an efficient technique for the analysis of DNA structure; in fact, the electrophoretic migration rate of the latter moving through an agarose gel matrix is dependent on conformation, molecular size and net charge (Johnson and Grossman, 1977).

In the past, different studies reported the ability of several compounds to induce DNA damage through the production of oxygen radicals. For example, benzene and its metabolites such as hydroquinone and 1,2,4-benzenetriol can undergo autoxidation and to generate superoxide (Lewis, Stewart and Adams, 1988). At the same time, AAPH is known to cause oxidative damage to pBR332 plasmid DNA, resulting in the DNA strand breaks of the supercoiled form into both the open circular and linear forms (Wei *et al.*, 2006).

In untreated pBR332 plasmid DNA, the supercoiled form is predominant, representing the intact form (Zhang and Omaye, 2001). The conversion of the plasmid supercoiled form to the open-circular and linear forms can be used as an index of DNA damage (Jeong *et al.*, 2009). In fact, the circular

form is indicative of single-strand breakage whereas the linear form is indicative of double-strand breakage.

An example of electrophoretic DNA gel separation is shown in figure 3.9.

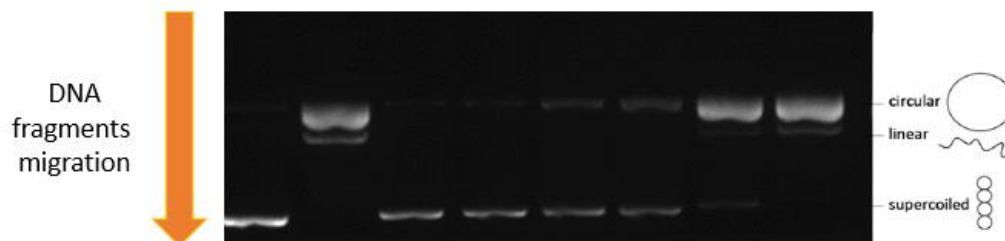


Figure 3.9. DNA fragments separation using gel electrophoresis. Supercoiled DNA moves faster compared to the circular and linear fragments.

The difference between the treatments in this assay can be determined by comparing the intensities of the three bands (Zhang and Omaye, 2001).

The aim of the work reported in this chapter was to evaluate the antioxidant activities of all the novel vanillin derivatives synthesised and to discuss their mechanism of action with respect to the SAR of this new class of compounds.

To achieve these aims, several antioxidant assays, based on different mechanisms of action, were performed. These include the DPPH, FRAP, ORAC and DNA damage protection assays. Furthermore, our data will be compared and contrasted with other relevant published work.

## 3.2 Materials and Methods

### 3.2.1 Materials

All reagents were purchased from Sigma Aldrich, unless otherwise stated, without any further purification.

2,4,6-Tri(2-pyridyl)-s-triazine (TPTZ)	Fluka
Agarose	FisherScientific
DNA Plasmid pbr332	ThermoFisher Scientific
GelRed® Nucleic Acid Gel Stain	Biotium
Phosphate Buffered Saline (PBS) Tablets	Oxoid

### 3.2.2 Instrumentation

Absorbances for DPPH and FRAP assays were measured using a Bio-Rad iMark microplate reader.

Fluorescence for ORAC assay was measured using a BioTek Synergy HT microplate reader.

The gels prepared for DNA protection assay were electrophoresed using Life Technologies Horizon 58 gel tank and Thermo EC 105 power pack and analysed with a Peqlab Fusion FX7 system (Fusion 15.11 software) for chemiluminescence and fluorescence and pictures were taken through high resolution camera system.

## 3.3 Methods

### 3.3.1 DPPH Assay

The ability of novel compounds to scavenge DPPH free radicals was determined on a 96-well plate platform by following Payet, Sing and Smadja's procedure with minor modifications (Payet, Sing and Smadja, 2005). A DPPH solution (0.1 mM) was prepared in methanol. A dilution

series of antioxidant was made in methanol using Eppendorf® tubes, then 50 µl of each solution was pipetted in the corresponding well of a 96-well plate. 50 µl of methanol was transferred in the control wells. Finally, 100 µl of DPPH solution was added to each well and the plate was wrapped with aluminium foil and kept in the dark for 30 minutes. The absorbance was measured at 517 nm.

An example of the 96-well plate settings is reported in figure 3.10.

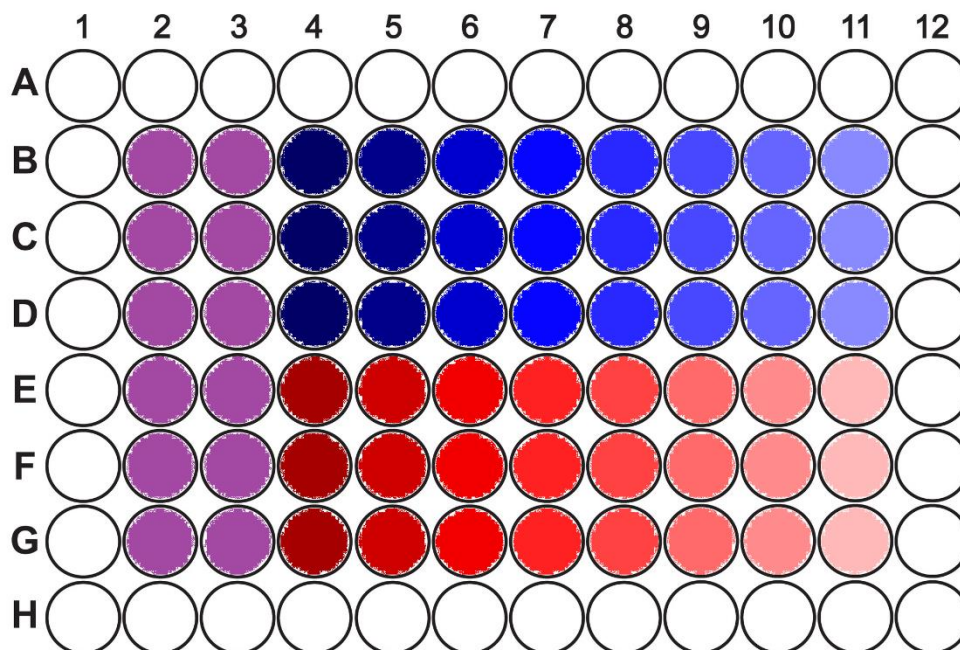


Figure 3.10. 96-well plate settings for DPPH assay. Two compounds can be tested at the same time. DPPH control is represented in purple, the first antioxidant is represented in blue and the second antioxidant is represented in red (different shades represent different concentrations tested).

The results were obtained after plotting the graph of concentration of compound (µM) in the x-axis against %ABS in the y-axis (calculated as shown in the formula below):

$$\% ABS = \frac{ABS_{sample}}{ABS_{neg.control}} * 100$$

The linear portion of the curve was isolated and 50% absorbance was determined using the equation of the line obtained.

### 3.3.2 FRAP Assay

The ability of novel compounds to reduce  $\text{Fe}^{3+}$  into  $\text{Fe}^{2+}$  was determined on a 96-well plate platform, following the method of Firuzi *et al.* with minor modifications (Firuzi *et al.*, 2005). A dilution series of antioxidants and Trolox in methanol was made in Eppendorf® tubes. A TPTZ solution (10 mM) was prepared in 40 mM HCl whereas a  $\text{FeCl}_3$  solution (20 mM) was prepared in deionized water. A 300 mM acetate buffer was prepared and the pH was adjusted to 3.6. The FRAP reagent was prepared by mixing 2.5 ml of TPTZ solution with 2.5 ml of  $\text{FeCl}_3$  solution and 25 ml of acetate buffer. 10  $\mu\text{l}$  of Trolox or antioxidant solution was pipetted in a 96-well plate, followed by 190  $\mu\text{l}$  of FRAP reagent in each well. An example of the 96-well plate settings is reported in figure 3.11.

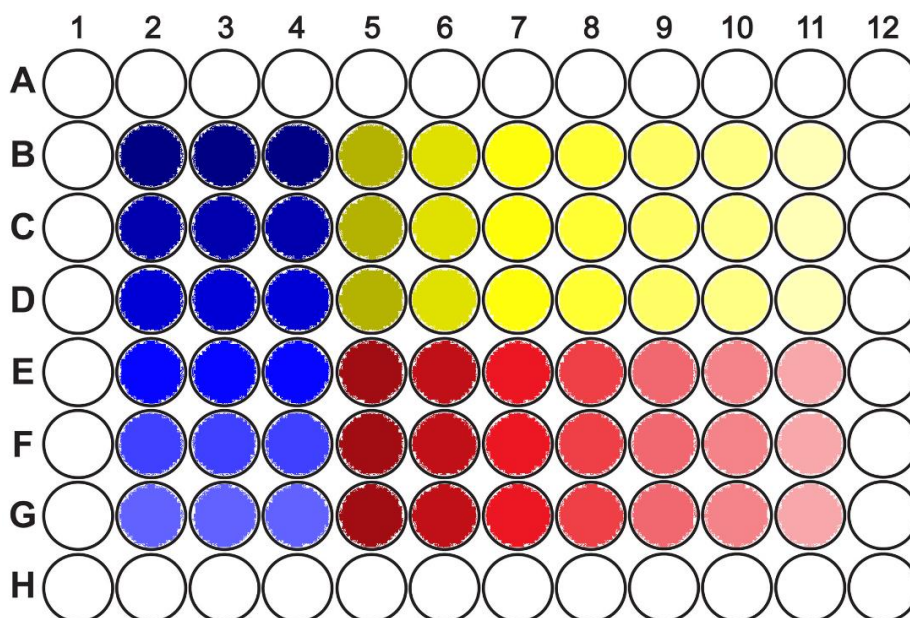


Figure 3.11. 96-well plate settings for FRAP assay. Two compounds can be tested at once. Different concentrations of Trolox are represented in blue colour. The first antioxidant is represented in yellow and the second antioxidant is represented in red (different shades represent different concentrations tested).

The plate was wrapped in aluminium foil and stored in the dark for 30 minutes after which the absorbance was measured at 593 nm. The calibration curves for both standard Trolox and antioxidant were obtained after plotting the graph of concentration of compound ( $\mu\text{M}$ ) in the x-axis against ABS in the y-axis. The results, expressed as Trolox Equivalent (TE), were obtained by comparison of the slope of the calibration curve obtained for the Trolox with the compound in analysis.

### 3.3.3 ORAC Assay

The ability of the vanillin derivatives to prevent oxidative degradation of the fluorescent probe fluorescein was determined using the ORAC assay following the protocols described by Huang *et al.* and Roy *et al.* with minor modifications using a black-walled 96-well plate (Huang *et al.*, 2002; Roy *et al.*, 2010). A phosphate buffer solution (75 mM) was prepared and the pH was adjusted to 7.4. Stock AAPH (0.15 M) and sodium fluorescein solutions (4 mM) were prepared in phosphate buffer. The sodium fluorescein stock solution was further diluted to a working concentration of 25 nM. A series dilution of Trolox and antioxidants was made in phosphate buffer in Eppendorf® tubes then 25 µl of Trolox standard or antioxidant solutions was pipetted in the corresponding well in the 96-well plate whereas 25 µl of phosphate buffer was added in the fluorescein and AAPH controls. 150 µl of fluorescein solution (25 nM) was pipetted in each well and the plate was incubated at 37°C for 30 minutes. Then, 25 µl of AAPH solution was pipetted in each well except for the fluorescein control in which 25 µl of phosphate buffer was added.

An example of the 96-well plate settings is shown in figure 3.12.

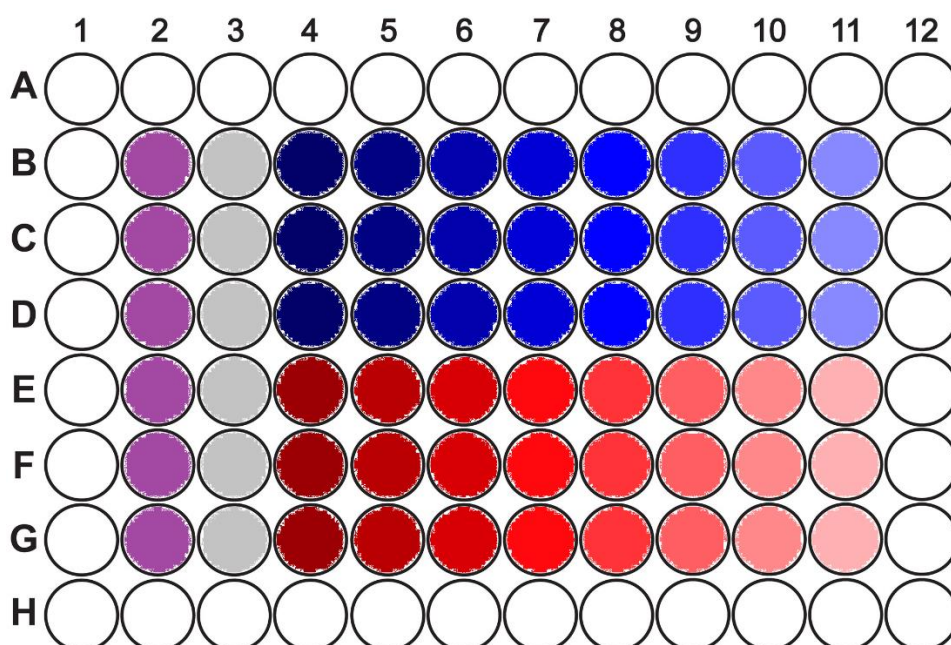


Figure 3.12. 96-well plate settings for ORAC assay. Fluorescein control is represented in purple colour and AAPH control is represented in grey colour. Different concentrations of Trolox are represented in blue colour whereas different concentrations of the antioxidant are represented in red (different shades represent different concentrations tested).

The fluorescence was measured every 2 minutes over a period of 2 hours at 37°C (485/20 nm excitation, 525/20 nm emission). The area under the curve at each concentration was calculated applying the following formula:

$$AUC = 0.5 + \frac{f_{2min}}{f_{0min}} + \frac{f_{4min}}{f_{0min}} + \frac{f_{6min}}{f_{0min}} + \dots + \frac{f_{118min}}{f_{0min}} + 0.5 \left( \frac{f_{120min}}{f_{0min}} \right)$$

$$net\ AUC = AUC_{sample} - AUC_{neg\ control}$$

where AUC = area under the curve,  $f_{xmin}$  = fluorescence measurement at the respective minute.

The area under the curve obtained for each concentration of antioxidants and standards were plotted in a graph against the corresponding concentrations and the linear portion was isolated. The final results were obtained by comparison of the slope of the calibration curve of the selected compounds with the standard Trolox.

### 3.3.4 DNA Damage Protection Assay

The ability of the novel compounds to prevent oxidative stress-mediated strand breakage in supercoiled DNA plasmid was measured following the methods previously described by Lee *et al.* and Pohl *et al.* with minor modifications (Lee *et al.*, 2002; Pohl *et al.*, 2018). Phosphate buffered saline (PBS) buffer was prepared from tablets according to the instructions reported by the manufacturer. A dilution series of Trolox and antioxidants was prepared in phosphate buffer in Eppendorf® tubes. A 10 mM AAPH solution was prepared in phosphate buffer. A Tris-Acetic acid-EDTA (TAE) buffer (50x), consisting of 40 mM tris acetate and 1mM EDTA, was prepared and the pH was adjusted to 8.5. The buffer was diluted 50 times with deionized water before use (TAE 1x). The loading dye was obtained by dissolving 5 mg of bromophenol blue in 1 ml of water/glycerol (50:50). The samples were prepared in Eppendorf® tubes by mixing 6 µl of phosphate buffer with 8 µl of antioxidant solution at different concentrations, 8 µl of AAPH solution and 1 µl of DNA plasmid solution (0.5 µg/µl). DNA control was prepared by mixing 1 µl of DNA plasmid solution with 22 µl of phosphate buffer whereas AAPH control was prepared by mixing 1 µl of DNA plasmid with 8 µl of AAPH and 14 µl of phosphate buffer.

The Eppendorf® tubes were incubated in the dark for 1 hour at 37 °C then 2 µl of loading dye were added in each tube. Finally, 10 µl of each sample was loaded in a 0.7 % agarose gel prepared in 50 ml of TAE (1x) along with 5 µl of GelRed® Nucleic Acid Gel Stain. The gel underwent electrophoresis for 70 minutes at 80 V before visualization and image capture under UV-light. The results were obtained after calculation of the intensity of the bands in the gel using Image J software and the application of the following formula:

$$\text{Inhibition of DNA strand breakage} = \frac{\text{band intensity of DNA+STRESSOR+COMPOUND}}{\text{band intensity of DNA without stressor}} * 100$$

## 3.4 Results and Discussion

### 3.4.1 DPPH Assay

DPPH is a synthetic nitrogen free radical with a maximum absorption at 517 nm. Its reduction mediated by antioxidants was measured spectrophotometrically (Payet, Sing and Smadja, 2005).

An example of the plate is reported in figure 3.13.

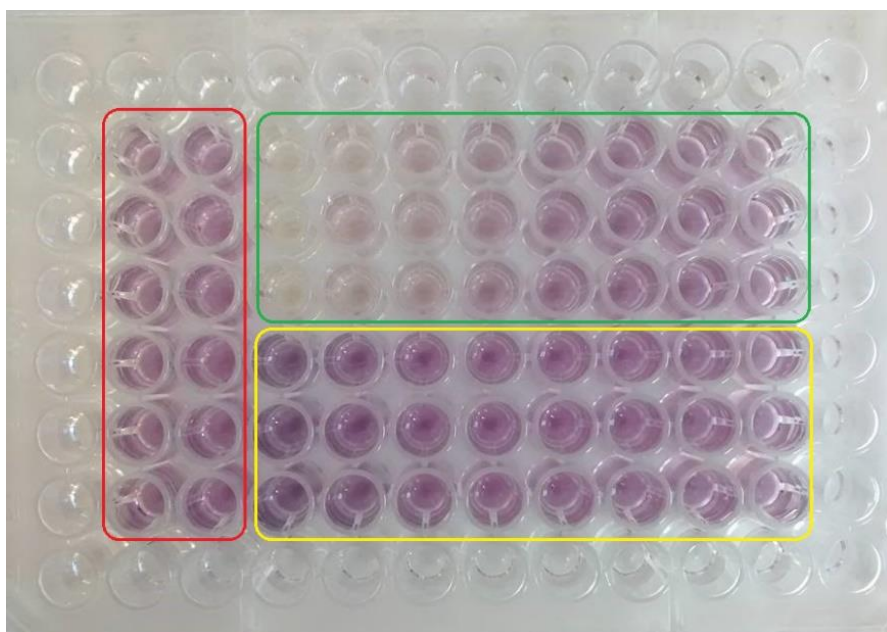


Figure 3.13. 96-well plate for DPPH assay. Two compounds were tested per experiment. The wells in the red circle represent the DPPH control. The wells in the green and yellow circles represent two different compounds at different concentrations. The compound in the green circle showed higher activity in the assay due to the loss of colouration whereas the compound in the yellow circle did not show any activity in the assay.

All the novel vanillin derivatives were tested, along with vanillin, syringaldehyde, Trolox and tacrine, in the DPPH assay. The results, expressed as concentration in  $\mu\text{M}$ , are reported as their  $\text{IC}_{50}$  values which are defined as the concentration of compound able to scavenge the 50% of the DPPH free radical. The  $\text{IC}_{50}$  was determined by plotting a graph with concentrations (in  $\mu\text{M}$ ) on the x-axis and their corresponding % absorbance values on the y-axis to obtain a curve. The linear portion of the curve was considered for the determination of the  $\text{IC}_{50}$  values using the equation of the line as shown in figure 3.14.

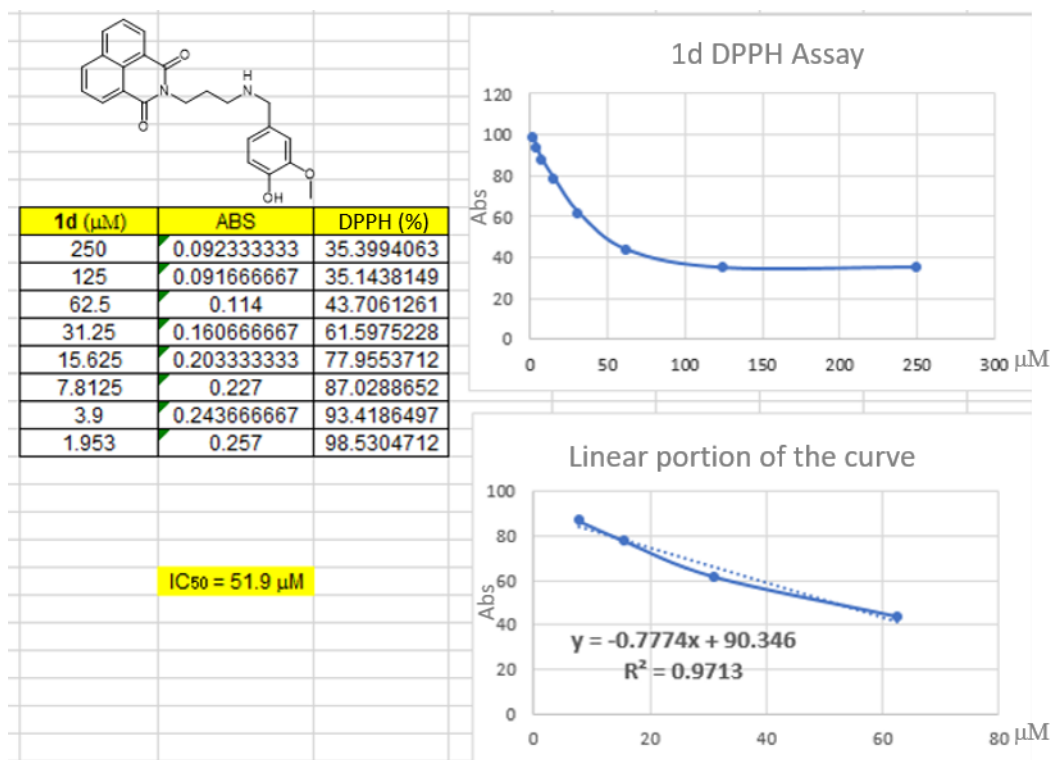


Figure 3.14. Example of DPPH assay results for derivative **1d**. The concentrations of compound were plotted in a graph along with the amount of unscavenged DPPH expressed as percentage. The linear portion of the curve was isolated and the IC<sub>50</sub> was calculated using the equation of the line.

The DPPH results of all the compounds tested, are shown in table 3.1.

Table 3.1. Antioxidant properties of vanillin derivatives using the DPPH assay.

Compound	DPPH (IC <sub>50</sub> μM)
<b>1a</b>	248.5 ± 24.50
<b>1b</b>	>250
<b>1c</b>	107 ± 1
<b>1d</b>	50.7 ± 0.8
<b>1e</b>	19.5 ± 0.3
<b>1f</b>	20.5 ± 0.3
<b>2a</b>	12.8 ± 0.11
<b>2b</b>	13.7 ± 0.15
<b>2c</b>	21 ± 0.4
<b>2d</b>	24 ± 2
<b>2e</b>	21.9 ± 1.7
<b>2f</b>	29.7 ± 1.3
<b>2g</b>	INACTIVE <sup>a</sup>
<b>2h</b>	12.3 ± 1.2
<b>2i</b>	15.4 ± 1
<b>4a</b>	>250
<b>4b</b>	137.5 ± 5.5
<b>4c</b>	5.8 ± 0.1
<b>4d</b>	>250
<b>4e</b>	INACTIVE <sup>a</sup>
<b>4f</b>	98 ± 5.51
<b>Vanillin</b>	4050 ± 25 <sup>b</sup>
<b>Syringaldehyde</b>	1150 ± 22 <sup>b</sup>
<b>Trolox</b>	24.4 ± 0.9
<b>Tacrine</b>	INACTIVE <sup>a</sup>

Results from each experiment are expressed as mean ± SD of three independent experiments.

<sup>a</sup> compounds were tested up to 250 μM.

<sup>b</sup> compounds were tested up to 10 mM.

For chemical structures of all the compounds, refer to schemes 2,3 and 4 of the second chapter.

The standard Trolox showed an IC<sub>50</sub> of 24.4 μM, which is in close agreement to previously reported results (27.6 μM), confirming the reliability of this assay (Lee *et al.*, 2009).

All the derivatives showed increased activities compared to the parent compounds, vanillin and syringaldehyde, except for **2g** and **4e** (see figure 3.15)

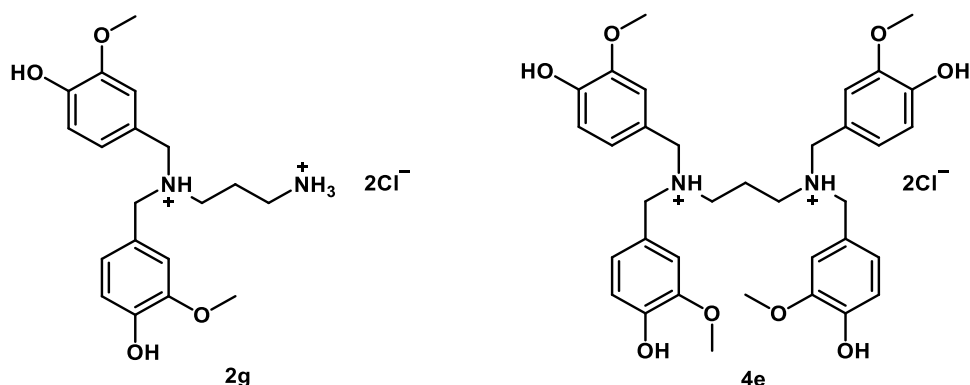


Figure 3.15. Chemical structures of dimer **2g** and tetramer **4e**.

It is interesting to note that both **2g** and **4e** are the hydrochloride salts with protonated nitrogen atoms, thus are unable to donate their lone electron pairs. The latter is a feature that contributes to antioxidant activity in this assay. Indeed, the antioxidant activity in this assay was strictly linked to the availability of the electrons on the nitrogen(s) atoms together with the presence of vanillin moieties in the chemical structure. However, imines **1a** and **1b**, bearing only one vanillin moiety, showed weak antioxidant activities (with  $IC_{50}$  248.5 and  $>250 \mu\text{M}$ , respectively) in this assay. It is worth noting that the electrons of the nitrogen are less available compared to the corresponding amines due to the  $sp^2$  hybridization of the nitrogen with consequent low electron density (see figure 3.16).

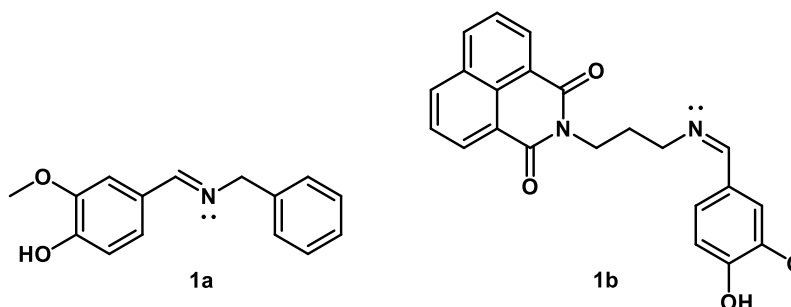


Figure 3.16. Chemical structures of imines **1a** and **1b**.

This can be further confirmed when comparing **1a** ( $IC_{50}$  248.5  $\mu\text{M}$ ) with **1c** ( $IC_{50}$  107  $\mu\text{M}$ ) and **2f** ( $IC_{50}$  29.7  $\mu\text{M}$ ) (see figure 3.17).

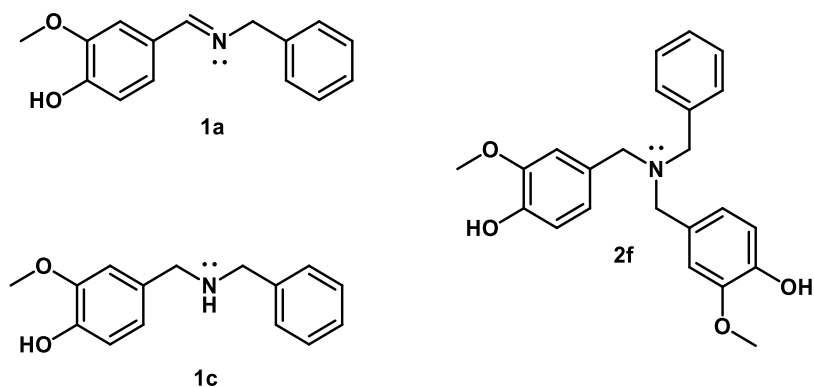


Figure 3.17. Chemical structure of compounds **1a**, **1c** and **2f**.

Compound **1c** is the secondary amine obtained after the reduction of the imine group of compound **1a**; the lone pair of electrons on the nitrogen atom are more accessible due to the  $sp^3$  hybridization of the nitrogen with consequent higher electron density and increased nucleophilicity. At the same time, compound **2f** is the tertiary amine obtained by the addition of compound **1a** with an extra vanillin moiety; the increased nucleophilicity of the nitrogen due to the inductive effect of the extra substituent, along with the extra vanillin moiety, can explain its increased antioxidant activity.

Syringaldehyde derivatives turned out to be more active than the corresponding vanillin derivatives, following the same pattern of behaviour of their parent compounds (vanillin itself is almost four times less active than syringaldehyde in the DPPH assay (4050 and 1150  $\mu\text{M}$ , respectively)). Accordingly, the syringaldehyde derivatives **1e** and **2i** (with  $\text{IC}_{50}$  19.5 and 15.4  $\mu\text{M}$ , respectively) showed a two-fold increase in activity compared to the corresponding vanillin derivatives **1d** and **2f** (with  $\text{IC}_{50}$  50.7 and 29.7  $\mu\text{M}$ , respectively), highlighting the importance of the extra methoxy group in the syringaldehyde for enhanced antioxidant activity. The chemical structures of the latter compounds are shown in figure 3.18.

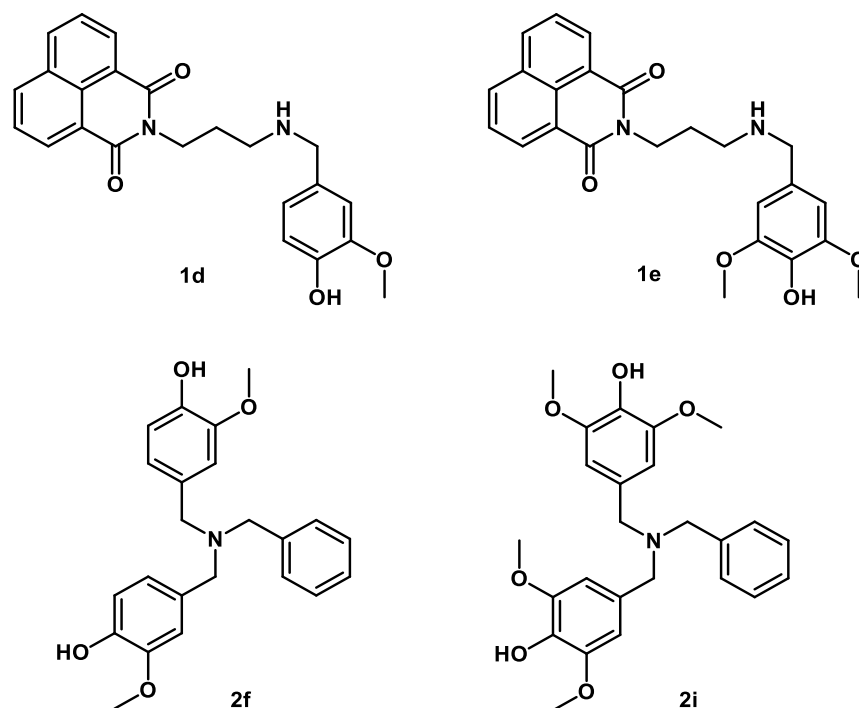


Figure 3.18. Chemical structures of vanillin derivatives **1d** and **2f** and syringaldehyde derivatives **1e** and **2i**.

Dimers **2a**, **2b**, **2c**, **2d** and **2e** (see figure 3.19) showed similar activities, with  $IC_{50}$  ranging from 12.8 to 21.9  $\mu$ M, confirming that the nature of the alkyl chain linked to the nitrogen has little impact on the antioxidant activity, while shorter alkyl chains enhance the antioxidant power.

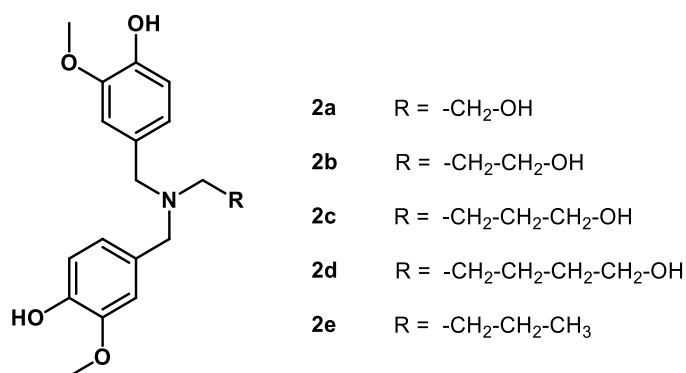


Figure 3.19. Chemical structures of derivatives **2a-2e**.

In addition, the removal of the terminal -OH functional group in the alkyl chain of compound **2c** ( $IC_{50}$  21  $\mu$ M) had no impact on the antioxidant activity (compound **2e**,  $IC_{50}$  21.9  $\mu$ M). This could be explained by the fact that an hydroxy group has no free radical scavenging effects if the oxygen is not able to delocalise the negative charge (as in phenolic moieties).

The tetramer **4c** turned out to be the most active compound in this assay, with an  $IC_{50}$  of 5.8  $\mu$ M, showing similar activity to the vanillin and syringaldehyde dendrimers reported by Lee *et al.* with  $IC_{50}$  ranging from 3.7-9  $\mu$ M (Lee *et al.*, 2009). Tetramer **4c** bears four vanillin moieties and two nitrogen atoms, linked by an aromatic ring. Several substitutions were made to explore the role of the different functional groups on antioxidant activity. The hydroxy and methoxy groups of the vanillin moieties were removed in order to establish their effect on their antioxidant activity (see figure 3.20). The removal of the hydroxy group (compound **4a**) or both the moieties (compound **4d**) caused a dramatic decreased in the activity ( $IC_{50}$  >250  $\mu$ M), whereas the removal of the methoxy groups (compound **4f**) caused only a minor loss in activity ( $IC_{50}$  98  $\mu$ M).

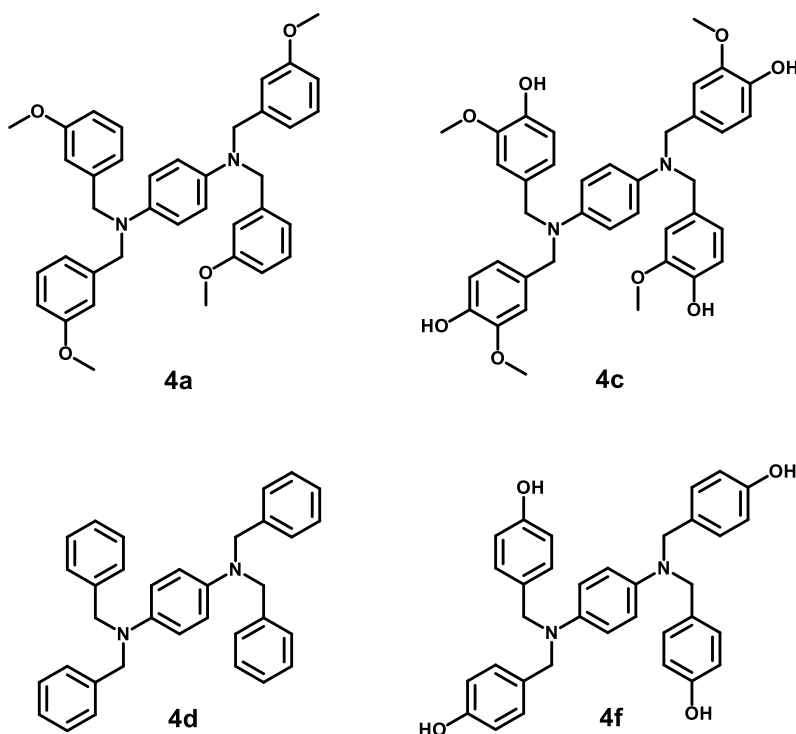


Figure 3.20. Chemical structures of derivatives **4a**, **4c**, **4d** and **4f**.

This result could be explained by the ability of the hydroxy groups to donate electrons in the HAT antioxidant mechanism; the absence of the methoxy group (an electron donor substituent) in compound **4f** makes the oxygen in the hydroxy group less prone to donate the hydrogen atom thus reducing the antioxidant activity of the latter compared to **4c**.

Interestingly, the substitution of the aromatic linker in compound **4c** with a cyclohexane moiety (compound **4b**) (see figure 3.21) resulted in a dramatic loss of activity in DPPH assay with the IC<sub>50</sub> falling down to 137.5 μM.

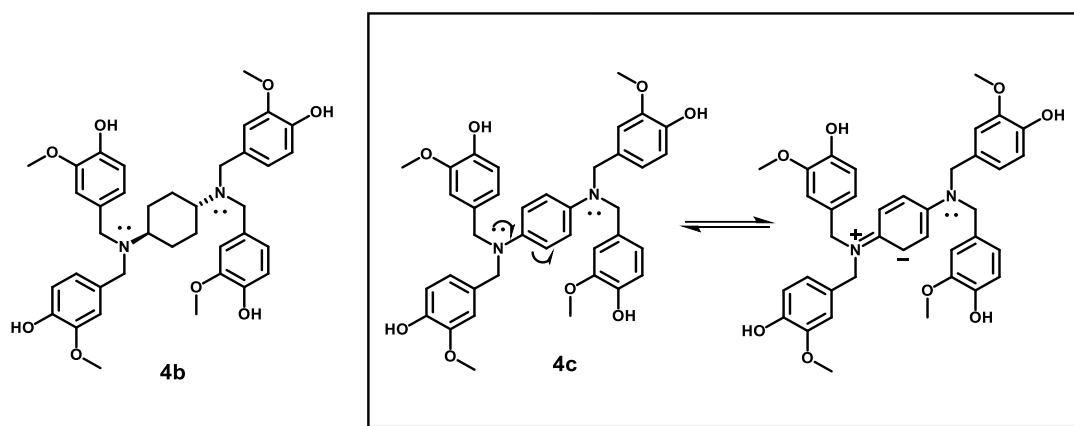


Figure 3.21. Chemical structures of compounds **4b** and **4c**. The strong antioxidant properties of **4c** could be explained by the critical role of electronic delocalisation in the antioxidant activity.

This phenomenon could be explained by the crucial role of the aromatic linker in the antioxidant activity of compound **4c**, suggesting the importance of the delocalisation of the nitrogen's electrons for the antioxidant activity and the possible electron transfer mechanism.

The importance of electronic delocalisation can also be appreciated by comparing the activity of compound **1f**, depicted in figure 3.22, with the rest of the monomers; although bearing only one vanillin moiety, it showed an IC<sub>50</sub> of 20.5 μM, and was therefore the most active vanillin monomer of the series, achieving a similar activity to the syringaldehyde monomer **1e** (IC<sub>50</sub> 19.5 μM).

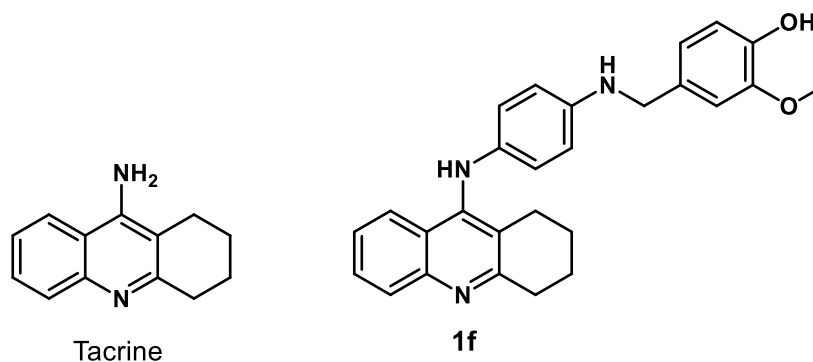


Figure 3.22. Chemical structures of Tacrine and monomer **1f**.

It is worth noting that this is the first time the electronic delocalisation of the nitrogen lone pair has been linked to antioxidant activity.

Finally, tacrine alone turned out to be completely inactive, suggesting that the vanillin moiety, the secondary amino groups and the aromatic linker are the only groups contributing to the antioxidant activity of **1f**.

### 3.4.2 FRAP Assay

The reducing capacity of the novel vanillin derivatives toward ferric ion, along with controls vanillin, syringaldehyde and tacrine, was determined using FRAP assay. The reduction of ferric ion leads to the formation of the ferrous-tripyridyltriazine complex exhibiting a maximum absorption at 593 nm.

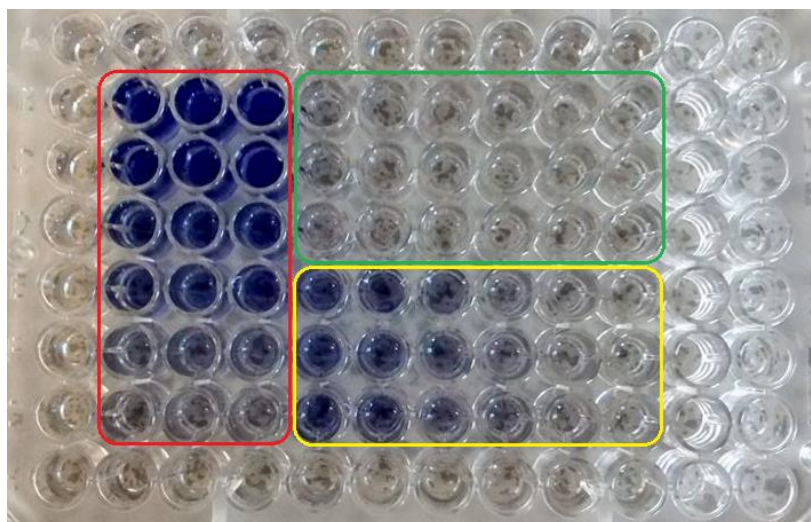


Figure 3.23. 96-well plate for FRAP assay. Two compounds were tested at once. The wells within the red perimeter represent the Trolox control, with the highest concentrations on top. The wells within the green and yellow perimeters represent two different compounds at different concentrations. The compound in the green perimeter showed no activity in the assay, whereas the compound in the yellow perimeter was found to be active due the increase in blue colouration.

Trolox was used as standard reference and the results are expressed as Trolox Equivalent (TE). The concentrations of antioxidant and Trolox were plotted with their correspond absorbances, then the results were obtained by the comparison of the slope of both curves. An example is depicted in figure 3.24.

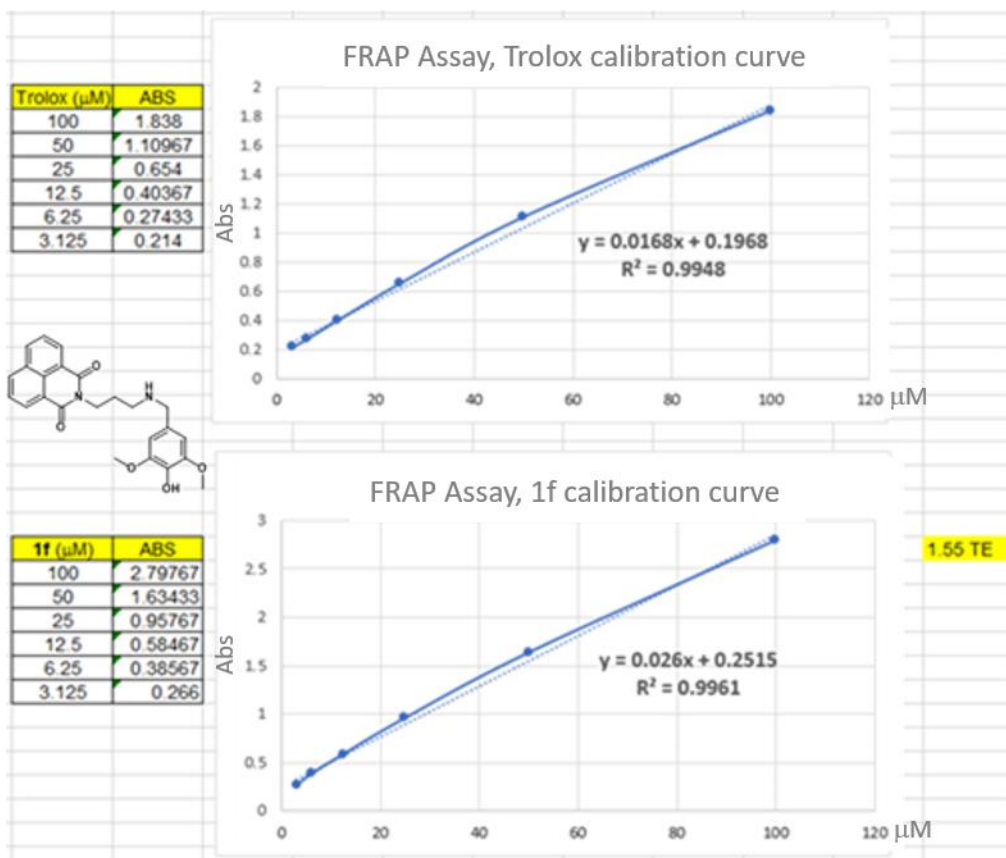


Figure 3.24. Example of results for derivative **1f** from the FRAP assay . The concentrations of Trolox and compound were plotted graphically, along with their corresponding absorbances. The slope of the line obtained were then compared to give the results, expressed in Trolox Equivalents (TE)

The results are shown in table 3.2.

Table 3.2. Antioxidant properties of vanillin derivatives using the FRAP assay.

Compound	FRAP (TE)
<b>1a</b>	0.06 ± 0.003
<b>1b</b>	0.07 ± 0.002
<b>1c</b>	0.16 ± 0.08
<b>1d</b>	0.26 ± 0.04
<b>1e</b>	1.45 ± 0.02
<b>1f</b>	1.54 ± 0.15
<b>2a</b>	0.62 ± 0.05
<b>2b</b>	0.68 ± 0.02
<b>2c</b>	0.62 ± 0.03
<b>2d</b>	0.63 ± 0.03
<b>2e</b>	0.6 ± 0.01
<b>2f</b>	0.55 ± 0.05
<b>2g</b>	0.28 ± 0.02
<b>2h</b>	1.14 ± 0.04
<b>2i</b>	1.11 ± 0.03
<b>4a</b>	2.54 ± 0.56
<b>4b</b>	0.56 ± 0.05
<b>4c</b>	5.29 ± 0.62
<b>4d</b>	2.81 ± 0.45
<b>4e</b>	0.74 ± 0.13
<b>4f</b>	2.78 ± 0.03
<b>Vanillin</b>	0.11 ± 0.07
<b>Syringaldehyde</b>	0.93 ± 0.03
<b>Trolox</b>	1
<b>Tacrine</b>	INACTIVE <sup>a</sup>

Results from each experiment are expressed as mean ± SD of three independent experiments.

<sup>a</sup> compounds were tested up to 250 µM.

All vanillin derivatives showed better activities than the respective parent compounds, except for imines **1a** and **1b** (see figure 3.16), which were ~15x less active than the standard Trolox (0.06 and 0.07 TE, respectively). However, syringaldehyde derivatives showed better activities than the

corresponding vanillin derivatives, following the same pattern of their precursors, with syringaldehyde to be nine times more active than vanillin (0.93 and 0.11 TE, respectively). In fact, the syringaldehyde derivatives **1e**, **2h** and **2i** (1.45, 1.14 and 1.11 TE, respectively) showed better activities in the FRAP assay compared to their corresponding vanillin derivatives **1d**, **2b** and **2f** (0.26, 0.68 and 0.55 TE, respectively) (see figure 3.18 in the previous section). This could be explained by the electron donating mesomeric effect (+M) of the extra methoxy group in the syringaldehyde moiety, causing an increase in the electronic density in the phenolic moiety, thus resulting in a greater electron transfer activity.

All the vanillin dimers **2a-2e** showed similar activities ranging from 0.55-0.68 TE, showing weaker antioxidant activities compared to the standard Trolox; thus highlighting the lack of impact from the different alkyl chains present in these compounds (see figure 3.19).

Both the hydrochloride salts, the dimer **2g** and the tetramer **4e** (see figure 3.15), showed modest activities (0.28 and 0.74 TE, respectively) with the dimer three times less active than the tetramer, neither as active as Trolox. All the tetramers showed strong antioxidant power in this assay (2.54 - 5.29 TE), except for the above cited hydrochloric salt **4e** and **4b** (0.74 and 0.56 TE, respectively), which bear a cyclohexane moiety as the linker between the two nitrogen atoms (see figures 3.20 and 3.21).

It is interesting to note that all the tetramers bearing an aromatic ring as the linker between the two nitrogen atoms (as in **4a**, **4c**, **4d** and **4f** (2.54, 5.29, 2.81 and 2.78 TE, respectively) (see figure 3.20)) showed improved activities in this assay compared to Trolox, highlighting the predominant role of the electronic conjugation in the antioxidant activity for this assay (figure 3.21).

The removal of the hydroxy group, the methoxy group, or both, in the vanillin moieties of the tetramers caused a loss of activity, as is clearly shown by comparing **4a**, **4f** and **4d** with **4c** (2.54, 2.78, 2.81 and 5.29 TE, respectively).

The role of electron delocalisation in the FRAP assay is also evident in the strong activity of the vanillin monomer **1f** (1.54 TE) (see figure 3.22), which

showed similar activities to the syringaldehyde monomer **1e** (1.45 TE) and higher activities compared to the other vanillin monomers **1c** and **1d** (0.16 and 0.26 TE, respectively), which are not able to delocalise the electrons associated with the nitrogen atom.

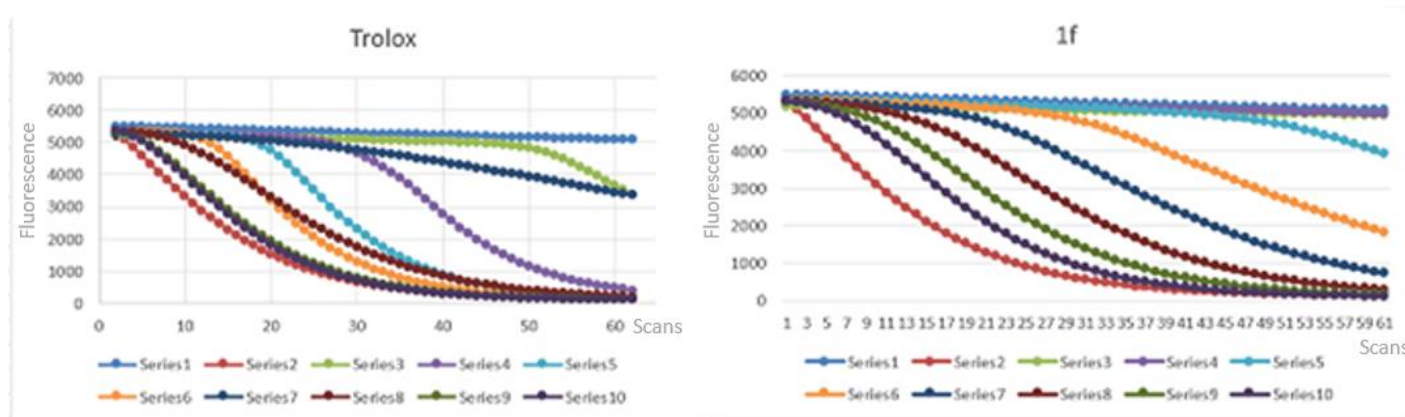
It is worth noting that tacrine is completely inactive in this assay.

### 3.4.3 ORAC Assay

The ability of a selection of compounds to prevent AAPH-mediated oxidative degradation of the fluorescent probe, fluorescein, was tested, along with vanillin and syringaldehyde, using the ORAC assay (Huang *et al.*, 2002; Roy *et al.*, 2010). The selection of compounds was based on the different nitrogen nucleophilicity and number of vanillin moieties in their chemical structures.

Trolox was used as standard reference and the results, shown in table 3.3, are expressed as Trolox Equivalent (TE).

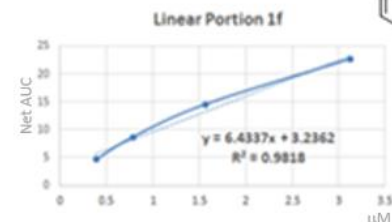
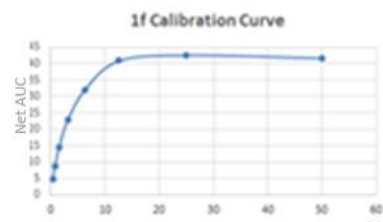
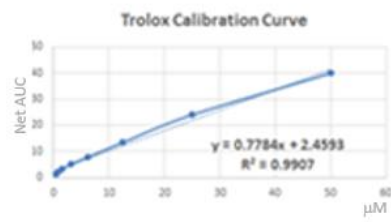
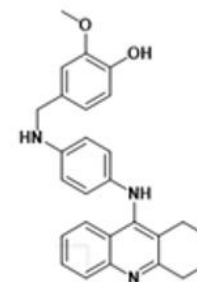
The areas under the curve (AUC) for each concentration of standard and antioxidant were calculated. Then the area under the curve of the blank was subtracted from each AUC to obtain the net AUC. The standard curve for both Trolox and antioxidant were obtained by plotting the Net AUC at different concentrations of both against their concentrations. The ORAC values were finally calculated by comparison of the slopes of the antioxidant and Trolox standard curves. An example is shown in figure 3.24.



Fluorescence control	Trolox μM																
50	25	12.5	6.25	3.125	1.56	0.78	0.39	0.195	0.0975	0.04875							
55.26822282	11.33730437	51.28145	35.38347	24.80296	19.27413	47.36379	20.69064	13.56046	12.56002	39.94414	24.04617	13.46535	7.93683	5.121543	3.236145	2.213158	1.242717

Fluorescence control	1f μM																
50	25	12.5	6.25	3.125	1.56	0.78	0.39	0.195	0.0975	0.04875							
55.26822282	11.33730437	53.13925	54.049	52.28565	43.33386	34.07149	25.89231	20.00347	15.99582	41.80196	42.7117	40.94835	31.99656	22.73418	14.555	8.666169	4.658612



8.26 TE

Figure 3.25. Example of results for derivative **1f** using the ORAC assay. The areas under the curve (AUC) obtained were plotted against the corresponding concentrations of Trolox and antioxidant. The net AUCs were obtained by subtracting the curve from the blank. The linear portion of the calibration curve obtained for the antioxidant was isolated and its slope was compared with the Trolox calibration curve to obtain the results, expressed as Trolox Equivalents (TE).

Table 3.3. Antioxidant properties of vanillin derivatives in ORAC assay.

Compound	ORAC (TE)
<b>1a</b>	1.9 ± 0.9
<b>1b</b>	2.1 ± 0.5
<b>1c</b>	3.2 ± 1.2
<b>1d</b>	3.9 ± 1.3
<b>1e</b>	2.0 ± 0.5
<b>1f</b>	6.4 ± 1.6
<b>2b</b>	6.0 ± 0.6
<b>2f</b>	5.3 ± 1.5
<b>2g</b>	4.1 ± 0.8
<b>4a</b>	INSOLUBLE
<b>4c</b>	20.4 ± 1.3
<b>4e</b>	7.5 ± 1.3
<b>Vanillin</b>	2.2 ± 0.3
<b>Syringaldehyde</b>	1.5 ± 0.1
<b>Tacrine</b>	<0.01 <sup>a</sup>

Results from each experiment are expressed as mean ± SD of three independent experiments.

<sup>a</sup> reported by (Rodríguez-Franco *et al.*, 2006).

All the derivatives showed better activities than the corresponding starting compounds vanillin or syringaldehyde. In accordance with previous studies, vanillin had shown higher antioxidant activities (2.2 TE) than standard Trolox in this assay (Tai, Sawano and Yazama, 2011). Contrary to the results obtained in the previous assays, vanillin turned out to be more active compared to its methoxy derivative syringaldehyde (2.2 and 1.5 TE, respectively).

At the same time, the vanillin derivative, **1d**, was found to be more active than its corresponding syringaldehyde derivative, **1e** (3.9 and 2.0 TE, respectively) (see figure 3.18) following the same pattern of their precursors.

The vanillin dimer, **2f**, showed higher antioxidant activity when compared to its corresponding reduced (**1c**) and imine (**1a**) monomers (5.3, 3.2 and 1.9 TE, respectively) confirming the role of the number of vanillin moieties and hence contribution to antioxidant property in this assay (see figure 3.17).

As in the previous assays, the nucleophilicity of the nitrogen generated significant impact on the antioxidant activity in this assay, since the imines **1a** and **1b** (1.9 and 2.1 TE, respectively) showed weaker activities compared to their corresponding reduced amine **1c** and **1d** (3.2 and 3.9 TE, respectively) (figure 3.16-3.18). However, both hydrochloride salts **2g** and **4e** (figure 3.15) showed strong antioxidant properties (4.1 and 7.5 TE, respectively), although the nitrogen atoms are not nucleophilic, since they are involved in the saline bond. This could be explained by the fact that the assay is performed at pH 7.4, thus free amines can be formed from the original hydrochloric salts.

Electronic delocalization played a major role in the antioxidant activity in this assay, with tetramer **4c** to be the most active compound (20.4 TE) and monomer **1f** (6.4 TE) with similar activity compared to the dimers **2b** and **2f** (6.0 and 5.3 TE, respectively) (see figures 3.18, 3.19, 3.21 and 3.22).

Interestingly the new tacrine-vanillin hybrid **1f** showed higher ORAC values compared to a series of tacrine-melatonin hybrids reported by Rodríguez-Franco *et al.* whose activities ranged from 1.7-4.0 TE (Rodríguez-Franco *et al.*, 2006). It is worth noting that tacrine has previously been found to be virtually inactive in this assay, being almost one hundred times less active than Trolox (Rodríguez-Franco *et al.*, 2006).

#### 3.4.4 DNA Damage Protection Assay

The ability of a selection of vanillin derivatives, vanillin and syringaldehyde to prevent oxidative stress-mediated strand breakage in supercoiled DNA plasmid was determined using the DNA damage protection assay (Lee *et al.*, 2002; Pohl *et al.*, 2018).

The selection of compounds was based on the presence of different nitrogen nucleophilicity and the number of vanillin moieties in their chemical structures.

In this assay the results are expressed as their IC<sub>50</sub> values, which are defined by the concentration (μM) of compound that is able to protect 50% of supercoiled DNA from its conversion to open circular or linear DNA mediated by AAPH.

The determination of the IC<sub>50</sub> was made by measuring the band intensities of the supercoiled DNA in the gel at each concentration of compound used

and compared the intensities obtained with the DNA control. The linear part of the curve was used in the equation of the line to obtain the IC<sub>50</sub> of each compound.

An example is reported in figure 3.25 for compound **4c**.

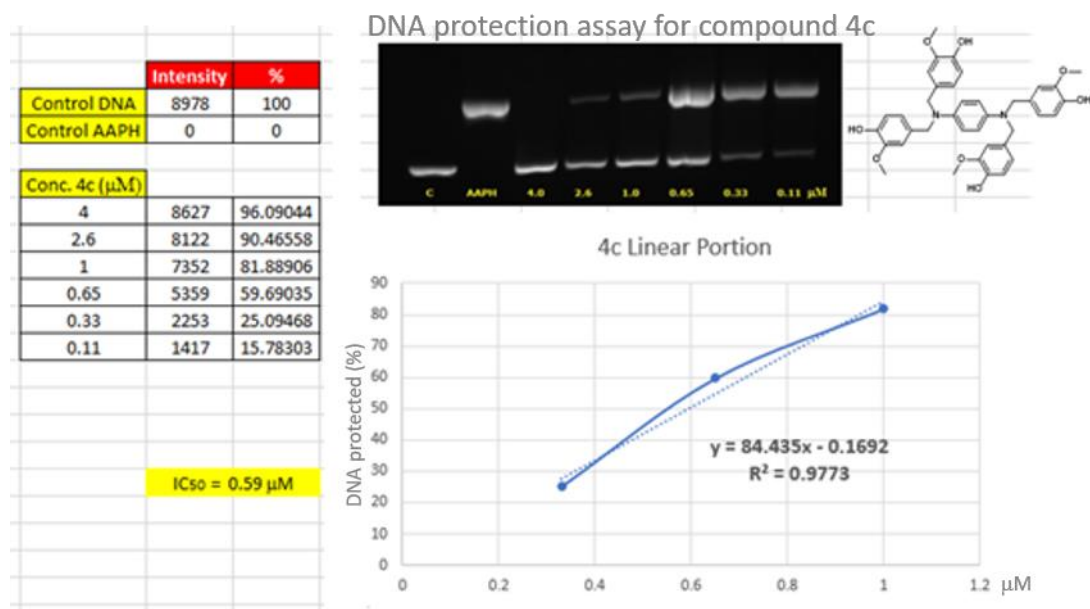


Figure 3.26. Example of DNA protection assay's results for tetramer **4c**. The intensity of each band was measured using Image J software and the amount of supercoiled DNA (%) was calculated by comparison with the DNA control. The linear portion of the curve was isolated and the IC<sub>50</sub> was determined using the equation of the line.

The results are reported in table 3.4.

Table 3.4. Protective effects of vanillin derivatives against AAPH-mediated DNA damage.

Compound	DNA Protection (IC <sub>50</sub> μM)
<b>1a</b>	3.8 ± 1.2
<b>1c</b>	4.1 ± 1.9
<b>2b</b>	3.6 ± 0.9
<b>2f</b>	3.8 ± 1.4
<b>2g</b>	61.5 ± 5.2
<b>4a</b>	13.6 ± 1.2
<b>4c</b>	0.6 ± 0.1
<b>4e</b>	13.9 ± 4.2
<b>Vanillin</b>	5.6 ± 0.6
<b>Syringaldehyde</b>	9.5 ± 0.3

Results from each experiment are expressed as mean ± SD of three independent experiments.

Similar to the ORAC assay, vanillin exhibited a better activity compared to its methoxy derivative syringaldehyde, being almost two times more active (5.6 and 9.5 μM, respectively).

Dimer **2f** showed similar activity to the corresponding imine (**1a**) and reduced (**1c**) monomers (3.8, 3.8 and 4.1 μM, respectively) (see figure 3.17), showing a lack of impact from the nucleophilicity of the nitrogen on the activity in this assay. However, protonation of the nitrogen caused a dramatic loss of activity, as shown in the hydrochloride salts of dimer **2g** and tetramer **4e** (61.5 and 13.9 μM, respectively), the chemical structures of which are shown in figure 3.15.

Tetramer **4c** was the most active compound, with an IC<sub>50</sub> of 0.6 μM, being almost ten times more active than the starting compound vanillin demonstrating the role of electronic delocalisation in the DNA protective activity.

It is interesting to note that a structurally related tetramer reported by Lee *et al.*, lacks the ability to delocalise the electrons in the aromatic linker (see figure 3.26), showing only detectable DNA protection at concentrations above 45 μM, highlighting the role of the electronic delocalisation (see figure 3.21) in the activity (Lee *et al.*, 2009).

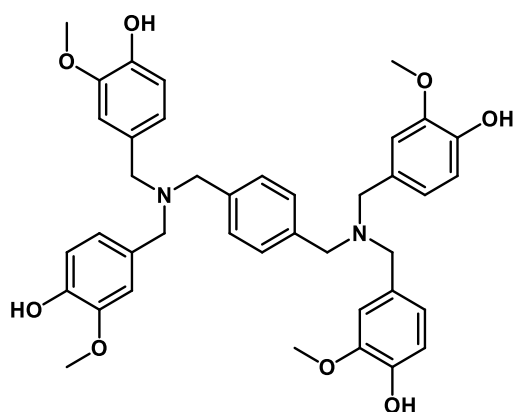


Figure 3.27. Tetramer reported by (Lee *et al.*, 2009).

In addition, compound **4c** showed 15% DNA protection at concentrations as low as 0.11  $\mu\text{M}$  whereas vanillin showed no protection at concentration of 2.2  $\mu\text{M}$ . Finally, the removal of the hydroxyl groups from the vanillin moieties of tetramer **4c** (see figure 3.20) caused a dramatic loss of activity (tetramer **4a**,  $\text{IC}_{50}$  13.6  $\mu\text{M}$ ), highlighting the important role of the hydroxyl group in DNA protection activity.

### 3.4.5 Structure Activity Relationship (SAR)

In this chapter, novel vanillin derivatives were tested in different antioxidant assays to determine a structure activity relationship (SAR) for this class of compounds.

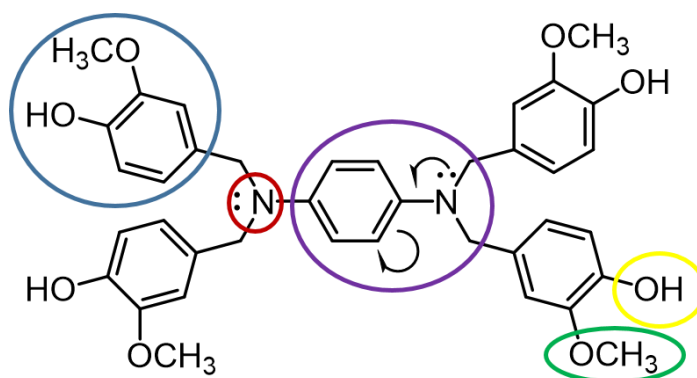


Figure 3.28. SAR for this class of vanillin derivatives. The number of vanillin moieties (blue), the phenolic and methoxy functionalities of the vanillin core (yellow and green, respectively), the nitrogen nucleophilicity (red) and electronic delocalisation (purple) are the key features for the antioxidant activity.

Syringaldehyde derivatives (**1e**, **2h** and **2i**) showed better activities compared to their corresponding vanillin derivatives (**1d**, **2b** and **2g**) in both DPPH and FRAP assays.

However, in the ORAC assay, a more relevant method to biological systems since it is based on peroxy free radicals and is performed at physiological pH, vanillin derivative **1d** showed higher scavenging activities compared to its corresponding syringaldehyde derivative **1e**.

At the same time, vanillin showed better activities in the same assay compared to syringaldehyde.

In addition, the number of vanillin moieties is strictly linked to the activities in DPPH, FRAP and ORAC assays, where tetramers exhibited better results when compared to the respective dimers and the monomers.

However, the number of vanillin moieties in the derivatives had lower impact in the activity on DNA protection assay, where the monomer **1c** showed similar activities compared to its related dimer **2f**. The removal of one of the substituents in the vanillin moiety, for example the hydroxy or methoxy group, caused a dramatic fall in all the antioxidant assays, suggesting the major role of the hydroxy group in the scavenging activity and the auxiliary contribution of the methoxy group as an electron donor group.

For the first time, the nucleophilicity of the nitrogen in all the derivatives, has been linked with antioxidant activity; in fact, secondary amines (**1c** and **1d**) showed better activities in DPPH, FRAP and ORAC compared to their corresponding imines (**1a** and **1b**), while tertiary amines (**2f**) showed better activities compared to the secondary amines (**1c**). Furthermore, the presence of electronic delocalisation of electrons associated with the nitrogen caused a dramatic increase in the antioxidant activities in all the assays. For example, both tetramer **4c** and monomer **1f** showed enhanced antioxidant activities in all the assays. In addition, tetramers **4a**, **4d** and **4f**, although devoid of the methoxy and hydroxy functionalities of their vanillin moieties, achieved strong antioxidant properties in the FRAP assay, suggesting the predominant role of the electronic delocalisation in the electron transfer antioxidant mechanism of the assay.

## 3.5 Conclusions

Novel vanillin derivatives were tested in a number antioxidant assays based on different mechanisms of action:

- (i) DPPH assay was performed to investigate the ability of the novel compounds to scavenge the synthetic 2,2-diphenyl-1-picrylhydrazyl free radical.
- (ii) FRAP assay was employed to measure the electron transfer capacity of the vanillin derivatives acting as reducing agent toward  $\text{Fe}^{3+}$  ion.
- (iii) ORAC assay was applied to determine the hydrogen transfer ability of the vanillin derivatives in the scavenging of the peroxy free radical generated by AAPH at physiological pH.
- (iv) DNA damage protection assay was employed to determine the protective effects of those novel compounds against oxidative stress-mediated DNA strand breakage in supercoiled DNA plasmid.

In all the assays, most of the novel derivatives showed improved antioxidant activities when compared to the starting compound, vanillin.

Based on the results obtained in the different assays discussed in this chapter, a SAR can be presented: the key features responsible for the antioxidant activity in this class of novel compounds are: the number of the vanillin moieties in the chemical structures, the presence of hydroxy and methoxy functionalities in the vanillin core structure, the nucleophilicity of the nitrogen atom(s) and the electronic delocalisation of the nitrogen(s) lone pair(s).

Therefore, compound **4c** has all the above key features, and was found to be the most active compound in this series, showing 700-times fold increased activity in DPPH assay, a 50-times fold increase in FRAP assay and almost 10-times fold increase in ORAC and DNA damage protection assays, when compared to vanillin.

Based on the results obtained in the different assays, a monomer (**1f**), a dimer (**2b**) and a tetramer (**4c**) were chosen for further testing of their ability to protect against oxidative stress in a cellular model. This will be discussed in chapter 4.

# **Chapter 4: Protective Effects of Vanillin Derivatives in neuroblastoma SH-SY5Y Cell Line**

## 4.1. Introduction

### 4.1.1 *The Use of SH-SY5Y Cell Line in Neurodegenerative Disease Research*

The choice of the right cell line for undertaking research on neurodegenerative diseases is of critical importance. The molecular and biological basis behind neurodegeneration, with particular attention to Alzheimer's disease (AD), will be described in chapter 5. A literature review on this topic highlighted that research work in neurosciences use both primary neurons and secondary cell lines derived from neuronal cancers. The use of primary cultures is desirable because of their non-cancerous origins, hence they are more likely to show similar properties to neuronal cells *in vivo*. However, primary cell cultures are not immortal, thus the number of cells available for the experiments is limited (Gordon, Amini and White, 2013). To deal with this issue, the use of secondary cell lines, which are derived from tumours and are immortalized, is a valid option for obtaining an unlimited number of cells for experiments.

Neuroblastoma SH-SY5Y cell line used in this work, deposited to the American Type Culture Collection (ATCC) in 1970, is a human catecholaminergic neuroblastoma derived from SK-N-SH, which resembles immature sympathetic neuroblasts in culture (Lopes *et al.*, 2010; Kovalevich and Langford, 2013). Despite its cancerous origin and the related genetic aberrations, this cell line preserves most genes and pathways that are usually dysregulated in Parkinson's Disease (PD) (Xicoy, Wieringa and Martens, 2017), thus making this cell line a good model for this particular neurodegenerative disease. However, the use of SH-SY5Y is not restricted to PD-related research; in fact, several works reported its use in other neurodegenerative disease models, including Alzheimer's Disease, amyotrophic lateral sclerosis (ALS) and neurotoxicity studies (Agholme *et al.*, 2010; Ma *et al.*, 2015; Shipley, Mangold and Szpara, 2016; Xicoy, Wieringa and Martens, 2017).

When undifferentiated (see figure 4.1), SH-SY5Y cells rapidly proliferate, growing in clumps and show low dopamine- $\beta$ -hydroxylase activity which converts dopamine into noradrenaline.

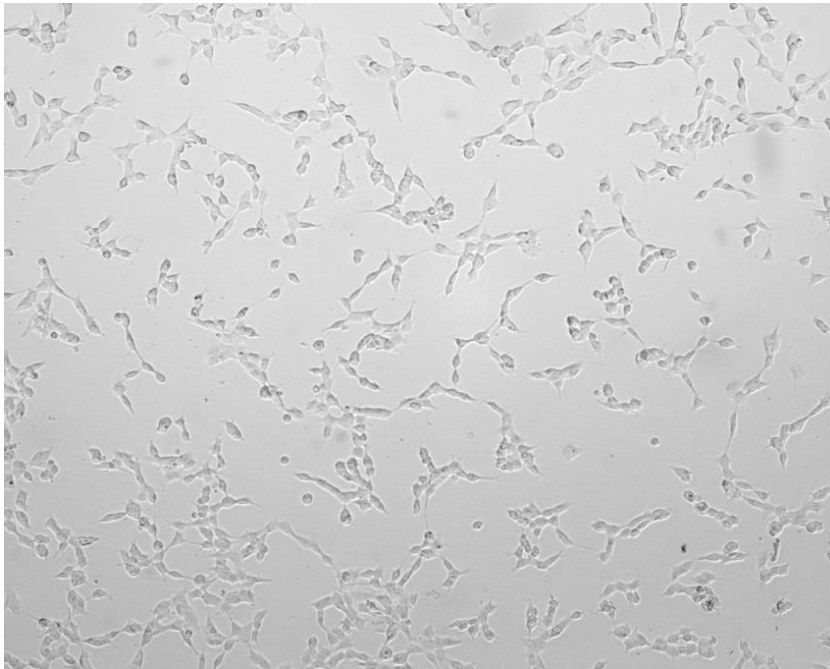


Figure 4.1. Undifferentiated SH-SY5Y cells (20x magnification, picture size adjusted to fit page).

Furthermore, in the undifferentiated state, the cells are linked to low levels of acetylcholinesterase/butyrylcholinesterase and tyrosine hydroxylase activities. The latter enzyme is involved in the conversion of tyrosine into L-dopa, the precursor of dopamine (Xicoy, Wieringa and Martens, 2017).

Once differentiated, SH-SY5Y cells experience a decrease in proliferation, due to cell population growth inhibition, and show markers of mature neurons including neuron specific enolase, synaptophysin and a stellate shape abundant in neurites (Lopes *et al.*, 2010; Kovalevich and Langford, 2013; Teppola *et al.*, 2016). The cells can undergo differentiation once treated with retinoic acid (RA), phorbol esters, such as 12-O-tetradecanoylphorbol-13 acetate (TPA), dibutyryl cyclic AMP, or cholesterol (Teppola *et al.*, 2016).

Differentiated cells showed increased resistance to oxidative stress in recent works, displaying higher tolerance to treatment with 6-hydroxydopamine (6-OHDA), 1-methyl-4-phenylpyridinium (MPP) (Cheung *et al.*, 2009) and 2,3-dimethoxy-1,4-naphthoquinone (DMNQ) (Schneider *et al.*, 2011)

compared to undifferentiated cells. In addition, differentiation with retinoic acid promotes the up-regulation of survival signalling pathways such as Akt and ERK1/2, and increases the neuroprotection of differentiated cells in response to 6-OHDA insult (Cheung *et al.*, 2009).

For the evaluation of the neuroprotective effects of the novel vanillin derivatives, undifferentiated SH-SY5Y cells were chosen due to the easy maintenance, the relative weak resistance to oxidative stress and the amount of works reported in the scientific literature, facilitating the comparison of the results with the latter.

#### *4.1.2 Oxidative Stress Models in SH-SY5Y Cells*

Considering the link between oxidative stress and neurodegenerative diseases, the development of oxidative stress models is of critical importance for the evaluation of protective effects of drugs in neurodegenerative research. In the literature, several oxidative stress models, based on the use of pesticides, metals and other chemicals, have been exploited and optimized in neuroblastoma cell lines. These will be further discussed below.

Hydrogen peroxide is enzymatically produced in the mitochondria from superoxide free radical and can be converted into hydroxyl free radical through Fenton reactions (see equations 3 and 7 in the first chapter, pages 4-6). The homeostatic concentration of hydrogen peroxide ranges from 1 – 700 nM and it is hypothesized that at concentration above 1  $\mu$ M, this can induce oxidative stress (Gülden *et al.*, 2010). Whittemore *et al.* reported nuclear changes in cultured cortical neurons cells, for example chromatin condensation and fragmentation characteristics of apoptosis after treatment with hydrogen peroxide (30  $\mu$ M) (Whittemore *et al.*, 1995). More recently, hydrogen peroxide toxicity has been studied in other neuronal cell lines, such as SH-SY5Y and PC-12, with results showing great variability (Othman and Yabe, 2015). In particular, SH-SY5Y cells showed different responses with respect to hydrogen peroxide toxicity; for example, Ruffels and co-workers reported a LC<sub>50</sub> higher than 750  $\mu$ M (Ruffels, Griffin and Dickenson, 2004) whereas Suematsu and co-workers obtained an LC<sub>50</sub> lower than 100

$\mu\text{M}$  (Suematsu, Hosoda and Fujimori, 2011). The toxicity of hydrogen peroxide is believed to lie in its capacity to cause lipid peroxidation, DNA oxidative damage and protein oxidation along with its ability to increase ERK 1/2, JNK and PKB phosphorylation (Ruffels, Griffin and Dickenson, 2004; Othman and Yabe, 2015).

*Tert*-butyl hydroperoxide (*t*BHP) is a membrane-permeable oxidant compound which can generate *tert*-butoxyl free radicals in an iron-dependent pathway similar to the Fenton reaction (see figure 4.2), leading to lipid peroxidation, depletion of glutathione levels, oxidation of thiols in the proteins and reduced cell viability (Zhao *et al.*, 2005), all the hallmarks of oxidative stress.

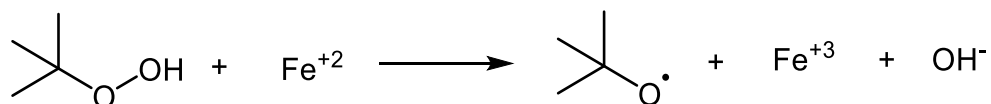


Figure 4.2. Mechanism of decomposition of *t*BHP by  $\text{Fe}^{2+}$  adapted from (Hix and Augusto, 1999), with copyright agreement © 1999 Elsevier Science Ireland Ltd.

The pesticide rotenone is another well-established oxidative stress model in SH-SY5Y cell line (see figure 1.21, page 30, chapter 1), which is able to evoke PD symptoms, causing the degeneration of the substantia nigra neurons with the induction of cytoplasmic inclusions similar to Lewy bodies *in vivo*, both are hallmarks of PD (Betarbet *et al.*, 2000). Rotenone is a well-known complex I inhibitor of respiratory chain in the mitochondria (see figure 1.21, page 30 of the first chapter) which forms ROS and consequently leads to cell death (Dhanalakshmi *et al.*, 2015). The treatment of SH-SY5Y cells with rotenone (250 nM) has been reported to cause cellular apoptosis due to the presence of nuclear fragmentation and chromatin condensation. However, at higher pesticide concentrations, both apoptotic and non-apoptotic morphological changes were observed. Similarly to the hydrogen peroxide model, rotenone toxicity is linked with activation of JNK and p38 pathways although being not associated to ERK 1/2 activation (Newhouse *et al.*, 2004).

Rotenone is also used in a more complex oxidative stress model, in association with the macrolide antibiotic oligomycin A (see figure 4.3).

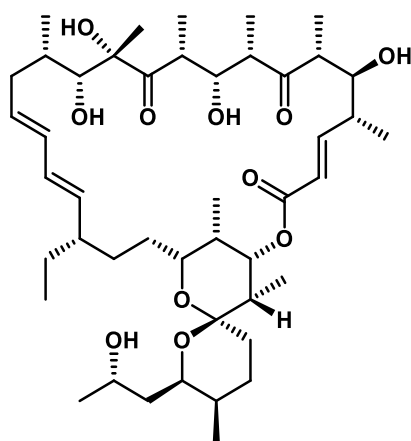


Figure 4.3. Chemical structure of the macrolide oligomycin A.

Its mechanism of action is based on the inhibition of the subunit Fo (which derives its name from being the binding fraction of the oligomycin A) in the complex V of the respiratory chain, which is critical for the oxidative phosphorylation of ADP to ATP (Lardy, Connelly and Johnson, 1964; McCarty, 1992; Kim, Moon and Hwang, 1999) (see figure 4.4).

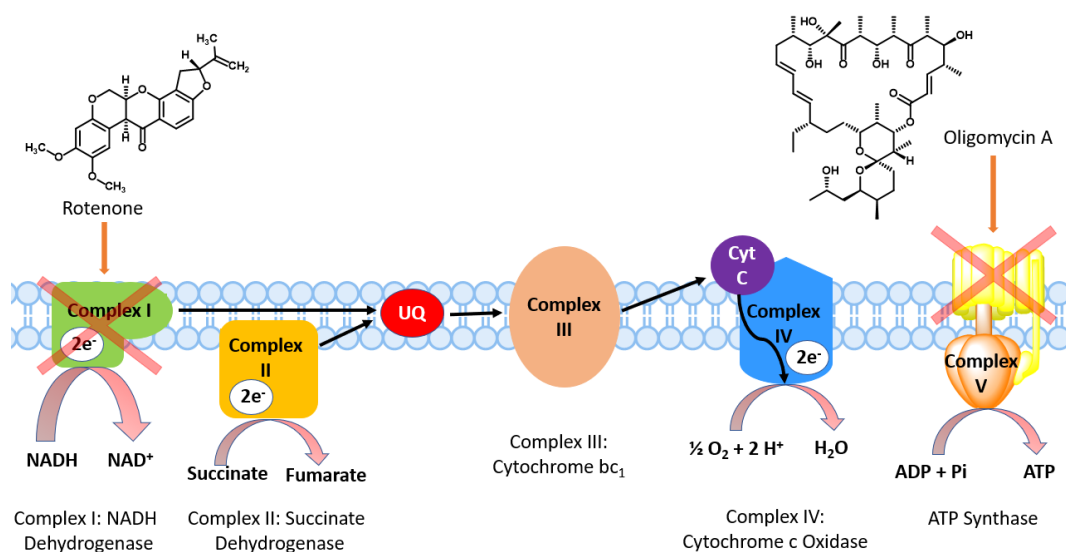


Figure 4.4. Mechanisms of rotenone and oligomycin A cocktail toxicity, adapted from (Kim, Moon and Hwang, 1999; Xu, Shang and Jiang, 2016).

Thus, the combination of rotenone and oligomycin A leads to a dual mitochondrial disruption; that is the cells are not able to synthesize ATP, and ROS are generated beyond the capacity of the cell to buffer them, leading to cell death (Canas *et al.*, 2007).

6-OHDA (figure 4.5) is a dopamine chemical-related neurotoxin which is used in PD models, due to its selective toxicity against dopaminergic neurons (Rodriguez-Pallares *et al.*, 2007).

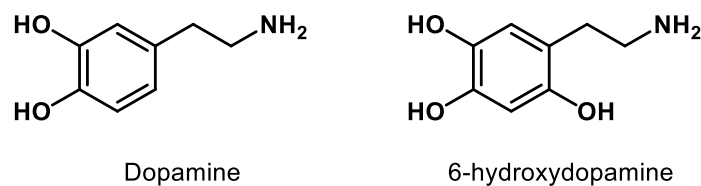


Figure 4.5. Chemical structures of dopamine and its related 6-OHDA.

Although the exact mechanism of 6-OHDA-induced toxicity is not completely elucidated, it has however been shown that it uses the same catecholamine transport system as DA and accumulates in the cytosol of dopaminergic neurons. Then, it is rapidly oxidized by molecular oxygen to form  $H_2O_2$  and the corresponding *p*-quinone, increasing the amount of ROS leading to subsequent cell death (Soto-Otero *et al.*, 2000; Rodriguez-Pallares *et al.*, 2007).

Amyloid peptides  $A\beta_{(1-40)}$  and  $A\beta_{(1-42)}$  have been recently evaluated for their use in oxidative stress models. These proteins, derived from the 110-130 kDa amyloid precursor protein (APP), represent the major constituents of senile plaques, a common hallmark for AD. Recently, it has been shown that amyloid-associated free radical generation is linked to the aggregational state of the peptides (Monji *et al.*, 2001; Butterfield, Swomley and Sultana, 2013). Although the mechanism is not completely understood, it has been hypothesized that increased  $\beta$ -sheet conformation that occurs during protein aggregation causes homolytic bond scission and radical production through mechanically activated thermal decomposition. The free radicals produced in this process can further react with oxygen to yield peroxy free radicals (Monji *et al.*, 2001).

Finally, transition and heavy metals are known to induce oxidative stress through Fenton reaction-like pathways. For example, iron has been reported to induce oxidative stress in SH-SY5Y at a concentration of 200  $\mu M$ , increasing the levels of lactate dehydrogenase (LDH) and oxidized

glutathione and depleting the levels of glutathione peroxidase (GPx) (Bermejo-Bescós, Piñero-Estrada and Villar del Fresno, 2008).

Copper is an essential element that represent the prosthetic group of several enzymes and is involved in the transfer of electrons in key reactions of metabolism. However, when copper is not bound to proteins, it can cause oxidative modifications to proteins, DNA and lipids by leading to the formation of ROS (Halliwell and Gutteridge, 1990). In 2005, a study revealed the ability of copper sulphate (150  $\mu$ M) to induce ROS in SH-SY5Y after 30 minutes exposure. In addition, the cells accumulated this metal in the mitochondria, where it caused the depletion of complex I and the  $\alpha$ -subunit of complex V (both reported in neurodegenerative diseases) after 24 hours exposure with copper sulphate (150  $\mu$ M) (Arciello, Rotilio and Rossi, 2005).

Cobalt is another essential element since it is the metal cofactor of vitamin B<sub>12</sub> and several enzymes, including dehydrogenases, dehydratases and transferases (Kubrak *et al.*, 2011). However, high concentrations of the latter can be toxic for humans, animals and plants. Its toxicity is reliant on the ability of cobalt to trigger the production of ROS in a Fenton-like pathway, leading to oxidative damage to lipids, DNA and proteins (Valko, Morris and Cronin, 2005). Recently, cobalt toxicity has been evaluated in SH-SY5Y cells and the LC<sub>50</sub> was found to be  $\sim$ 50  $\mu$ M (Fedorova *et al.*, 2016).

#### 4.1.2 Neuroprotective Effects of Natural and Synthetic Antioxidants

The strong link between oxidative stress and neurodegenerative diseases (Smith *et al.*, 2000; Jenner, 2003; Rosini *et al.*, 2013; Blesa *et al.*, 2015) has led to the proposal for the use of antioxidants for the prevention or treatment of PD and AD. For several years, a large number of natural and synthetic antioxidants have been reported to protect SH-SY5Y cell line in different models of oxidative stress.

For example, naturally occurring curcumin (see figure 1.7, page 14 of the first chapter), the principal curcuminoid in turmeric, showed protective effects on SH-SY5Y cells in two different models, involving A $\beta$  aggregation (Thapa, Jett and Chi, 2016) and 6-hydroxydopamine (6-OHDA)-induced toxicity (Jaisin *et al.*, 2011). In these studies, curcumin showed protective

effects on SH-SY5Y cells by increasing the cell viability by almost 35% at concentrations as low as 5  $\mu\text{M}$ , compared to the amyloid control, modifying the amyloid aggregation pathway and protecting cell membranes against amyloid-induced membrane disruption (Thapa, Jett and Chi, 2016). In addition, curcumin (20  $\mu\text{M}$ ) protected the same cell line against 6-OHDA (25  $\mu\text{M}$ ), almost completely preventing its toxicity; even concentrations as low as 5  $\mu\text{M}$  showed significant protection. Furthermore, in the same study, curcumin significantly reduced the 6-OHDA-induced ROS generation in SH-SY5Y cells at concentrations as low as 5  $\mu\text{M}$  and reduced the phosphorylation of p53, which plays a critical role in cellular apoptosis by translocating to the nucleus and increasing the expression of pro-apoptotic genes (Jaisin *et al.*, 2011).

Resveratrol (see figure 1.6, page 13, chapter 1), a natural polyphenol present in red wine, showed protective effects toward SH-SY5Y cells in both amyloid A $\beta$  (10  $\mu\text{M}$ ) and H<sub>2</sub>O<sub>2</sub> (50  $\mu\text{M}$ ) oxidative stress models at concentrations of 15  $\mu\text{M}$ . In addition, resveratrol completely restored the levels of the antioxidant glutathione (GSH, see figure 1.13, page 22, chapter 1) after treatment with the amyloid A $\beta$  stressor, but was unable to restore the level of GSH in the hydrogen peroxide model, suggesting different mechanisms of action for the cellular protective effects (Savaskan *et al.*, 2003).

Salidroside ((2*R*,3*S*,4*S*,5*R*,6*R*)-2-(hydroxymethyl)-6-(4-hydroxyphenethoxy)tetrahydro-2H-pyran-3,4,5-triol) (figure 4.6), a phenylpropanoid glycoside isolated from *Rhodiola rosea*, showed significant protection against hydrogen peroxide (150  $\mu\text{M}$ )-induced oxidative insult in SH-SY5Y cells, reducing the H<sub>2</sub>O<sub>2</sub>-induced cytotoxicity by almost 20% at concentrations ranging from 10-100  $\mu\text{M}$ , showing similar activity to vitamin E (50  $\mu\text{M}$ ) (Zhang *et al.*, 2007).

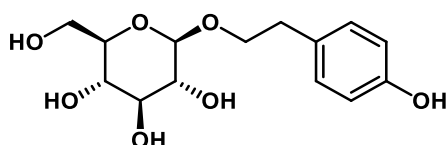


Figure 4.6. Chemical structure of salidroside.

The protective effects of salidroside in this oxidative stress model included the induction of several antioxidant enzymes such, as haeme-oxygenase 1, the upregulation of anti-apoptotic genes, such as Bcl-2, and the downregulation of the pro-apoptotic gene, Bax (Zhang *et al.*, 2007).

In another study, salidroside showed protective effects in a different oxidative stress model based on  $\beta$ -amyloid-induced cytotoxicity. Pre-treatment (50 and 100  $\mu$ M) with the glycoside increased cell viability by almost 30% compared to the positive control amyloid (25  $\mu$ M). In addition, salidroside reduced the amount of intracellular ROS generated when treated with  $\beta$ -amyloid protein compared to the positive control, and inhibited the amyloid-induced phosphorylation of JNK and p38 MAP kinase (Zhang *et al.*, 2010).

As reported in chapter 1, Dhanalakshmi *et al.* recently reported the protective effect of vanillin (see figure 1.20, page 29, chapter 1) toward SH-SY5Y cells in a PD model employing the pesticide rotenone (Dhanalakshmi *et al.*, 2015). In that study, the cells that were treated with vanillin, showed a concentration-dependent increase in viability after treatment with rotenone (100 nM) compared to the control, with maximum protection at 100 nM. In addition, vanillin (100 nM) showed a decrease in ROS production by almost one third compared to the rotenone control, with decreased expression of pro-apoptotic proteins such as p38, p-JNK and p-ERK (Dhanalakshmi *et al.*, 2015).

Olivieri *et al.* reported the protective effects of the endogenous antioxidant, melatonin (figure 4.7) an indoleamine hormone produced by the pineal gland against oxidative stress induced by cobalt in SH-SY5Y cells (Olivieri *et al.*, 2001).

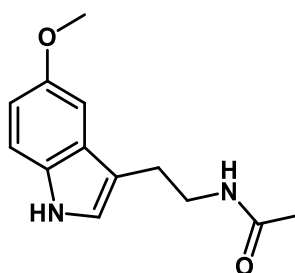


Figure 4.7. Chemical structure of the pineal hormone melatonin.

Pre-treatment with melatonin (1  $\mu\text{M}$ ) for 12 hours significantly increased the cell viability and GSH levels compared to the cobalt control (330  $\mu\text{M}$ ). In addition, treatment with cobalt was linked with increased  $\text{A}\beta$  release from SH-SY5Y, which was significantly reduced after treatment with melatonin (1  $\mu\text{M}$ ) (Olivieri *et al.*, 2001).

A series of synthetic derivatives of melatonin has been recently reported by Benchekroun *et al.* to protect SH-SY5Y cells in a rotenone/oligomycin A model of oxidative stress (Benchekroun *et al.*, 2016). These derivatives were obtained by the fusion of melatonin with a ferulic acid and a tacrine moiety (see figure 1.30, page 37, chapter 1). They showed an increase in cell viability up to 60% when the cells were pre-treated with these compounds at concentrations of 1 or 3  $\mu\text{M}$ , before incubating with a stressor cocktail (rotenone/oligomycin; 30 and 10  $\mu\text{M}$ , respectively) for 24 hours (Benchekroun *et al.*, 2016). In addition, the authors reported the protective effects of these compounds in other oxidative stress models, such as  $\text{H}_2\text{O}_2$  (300  $\mu\text{M}$ ) and the amyloid proteins  $\text{A}\beta_{(1-40)}$  and  $\text{A}\beta_{(1-42)}$  (30  $\mu\text{M}$ ), with increases in cell viability ranging from 5-85 % compared to the corresponding control. Finally, the compounds turned out to be strong antioxidants, with ORAC values up to 9 Trolox Equivalents, as well as exhibiting Nrf2 activation effects. Taken together, this could explain the highly protective properties of those derivatives in the cellular models (Benchekroun *et al.*, 2016).

Synthetic derivatives of naturally occurring lipoic acid (see figure 1.14, page 23, chapter 1), have been reported by Rosini *et al.* to exert neuroprotective effects in SH-SY5Y cellular models of oxidative stress. In particular, lipocrine (figure 4.8) showed, along with its strong anti-cholinesterase activity (at nanomolar concentrations), a decrease by almost 50% of ROS detected in SH-SY5Y cells (at concentrations ranging from 0.1-50  $\mu\text{M}$ ), after exposure to stressor tert-butyl hydroperoxide, when compared to the control (Rosini *et al.*, 2005).

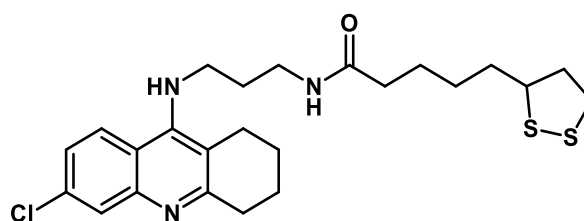


Figure 4.8. Chemical structure of the synthetic lipoic acid derivative lipocrine, reported by (Rosini *et al.*, 2005).

#### 4.1.3 Aims and Objectives

The critical role of oxidative stress in neurodegenerative diseases has led to the search for novel molecules that provide antioxidant protection and assist prevention or treatment of such diseases.

The aim of the experiments described in this chapter was to evaluate the protective effects of selected novel vanillin derivatives using two different oxidative stress models: hydrogen peroxide and a mixture of rotenone/oligomycin A.

In order to achieve the above aim, the following objectives were completed:

- Assessment of cytotoxic effects of selected vanillin derivatives in SH-SY5Y cell line.
- Evaluation of protective effects of selected vanillin derivatives from hydrogen peroxide and rotenone/oligomycin A induced toxicity in the same cell line.
- Determination of the ability of selected vanillin derivatives to prevent hydrogen-peroxide induced ROS formation in SH-SY5Y cells.
- Evaluation of protective effects of selected vanillin derivatives from hydrogen peroxide-induced DNA damage.
- Determination of the ability of selected vanillin derivative to trigger Nrf2 pathway.

For clarity, a summary of the work described in this chapter is described in Figure 4.9.

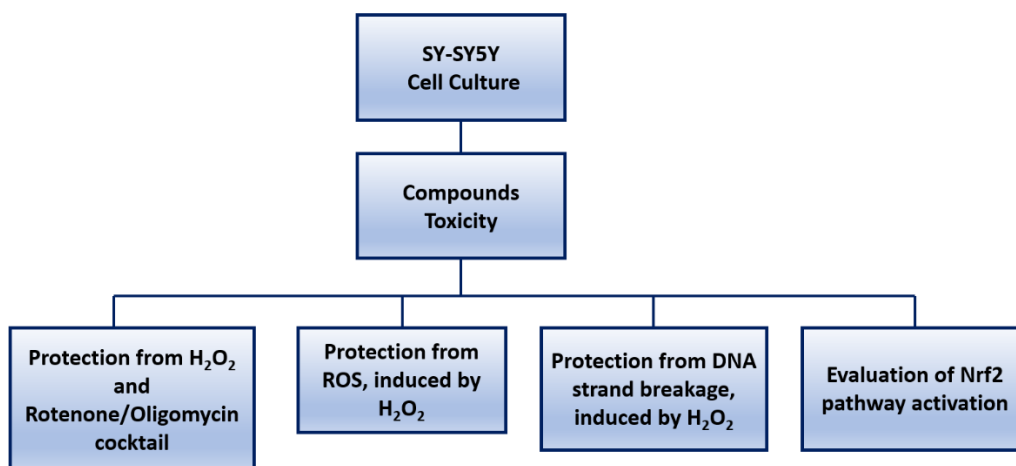


Figure 4.9. Summary of the experimental work described in this chapter.

#### 4.1.4 Introduction to the Analytical Techniques used in this chapter

##### 4.1.4.1 Cell Viability Measurement-MTT assay

(3-(4,5-dimethylthiazol-2-yl)-2,5-diphenyltetrazolium bromide) (MTT) assay was employed for the measurement of the cell viability in the cytotoxicity experiments and in the protection studies against hydrogen peroxide and the rotenone/oligomycin A cocktail. The latter assay is a colorimetric method that measures their metabolic activity, which is often extrapolated to indicate cell viability. It was first introduced by Pearse in 1957 for the evaluation of dehydrogenase activity (Pearse, 1957) and it is currently widely used for the assessment of cell viability along with other techniques such as resazurin assay (Borra *et al.*, 2009), or the trypan blue exclusion assay (Tennant, 1964). The MTT assay relies on the ability of viable and metabolically active cells to reduce this salt into its insoluble formazan form; the latter is characterized by the purple crystal structure, which can be dissolved with an appropriate organic solvent (for example, DMSO). The absorbance of the resulting solution can be measured with a spectrophotometer ( $\lambda=560$  nm). The mechanism of MTT assay is depicted in figure 4.10.

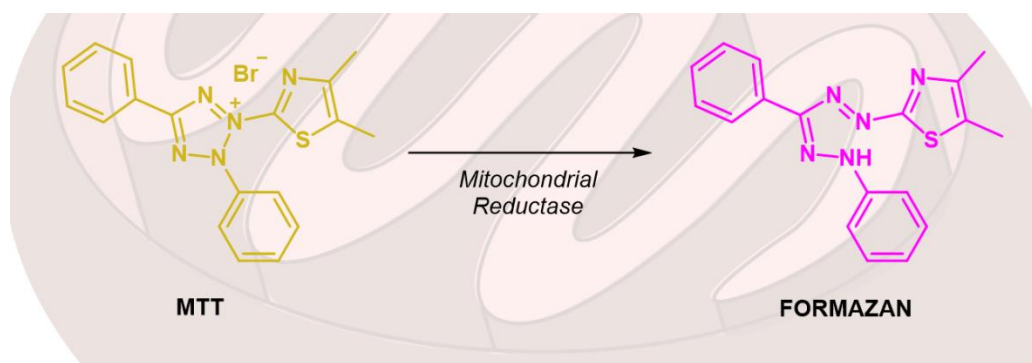


Figure 4.10. MTT conversion in metabolic active cells.

#### 4.1.4.2 ROS determination using 2',7'-dichlorodihydrofluorescein diacetate (H<sub>2</sub>DCFDA) dye

For the measurement of ROS, different techniques, such as chemiluminescence of luminol, lucigenin, cytochrome C reduction, xylanol and 2',7'-dichlorodihydrofluorescein diacetate (H<sub>2</sub>DCFDA) can be employed (Dahlgren and Karlsson, 1999; Eruslanov and Kusmartsev, 2010). H<sub>2</sub>DCFDA is one of the most widely used dye used for ROS measurement since it is easy to use, sensitive to changes in the redox state of the cells and inexpensive. For these reasons, this dye was employed for the evaluation of the alleviating properties of vanillin derivatives against the ROS production induced by hydrogen peroxide. H<sub>2</sub>DCFDA is resistant to oxidation, since the phenolic moieties are protected by the acetate groups but, once taken up by the cells, it is deacetylated by intracellular esterases and converted into 2',7'-dichlorodihydrofluorescein (DCFH) as depicted in figure 4.11.

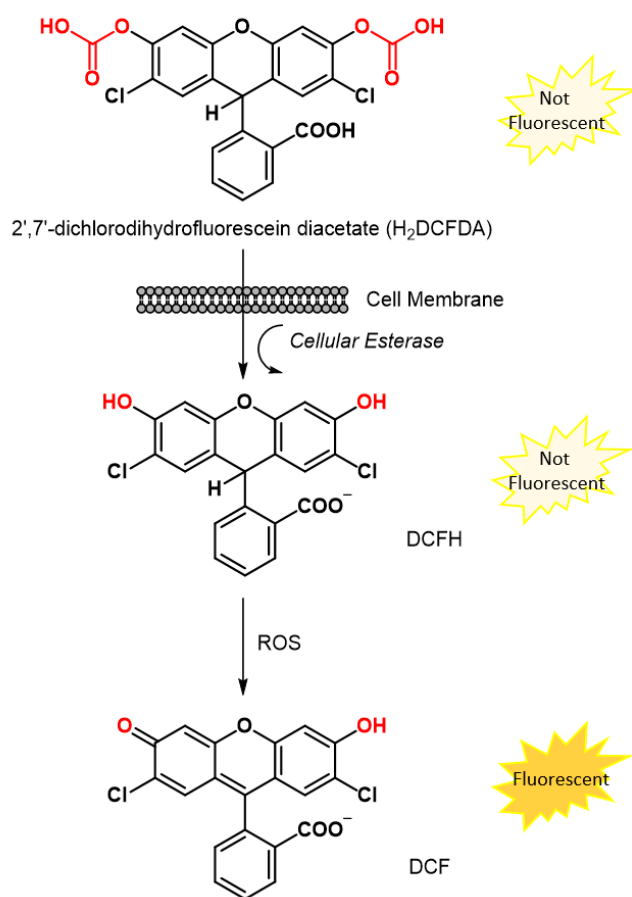


Figure 4.11. Mechanism of fluorescence enhancement of the H<sub>2</sub>DCFDA induced by ROS, adapted from Eruslanov and Kusmartsev (2010), with copyright agreement © 2010, Humana Press, a part of Springer Science Business Media, LLC.

The loss of the acetate groups makes the DCFH more hydrophilic and unable to cross the cell membranes again, and for this reason the dye is retained within the cells. Finally, the dye can be then be oxidized by ROS, yielding the fluorescent dichlorofluorescein (DCF). The resulting fluorescence can be measured, with appropriate excitation sources and emission filters (ex: 490/20, em: 525/20) (Wojtala *et al.*, 2014), with multi-well plate reader, fluorescence microscope, fluorimeter or flow cytometer.

Although the use of a multi-well plate reader offers the advantage of measuring the fluorescence *in situ*, avoiding the use of trypsin to detach the cells, it is only able to measure the total fluorescence, without discriminating between extracellular and intracellular fluorescence. For this reason, flow cytometry was employed to detect the fluorescence within the cells. In addition, this technique can produce quantitative data on the

number of cells emitting fluorescence instead providing the arbitrary fluorescence units. On the other hand, cells must be in suspension, requiring the use of trypsin, which is known to induce oxidative stress, and controlled conditions are needed (Eruslanov and Kusmartsev, 2010).

A schematic representation of flow cytometry is depicted in figure 4.12.

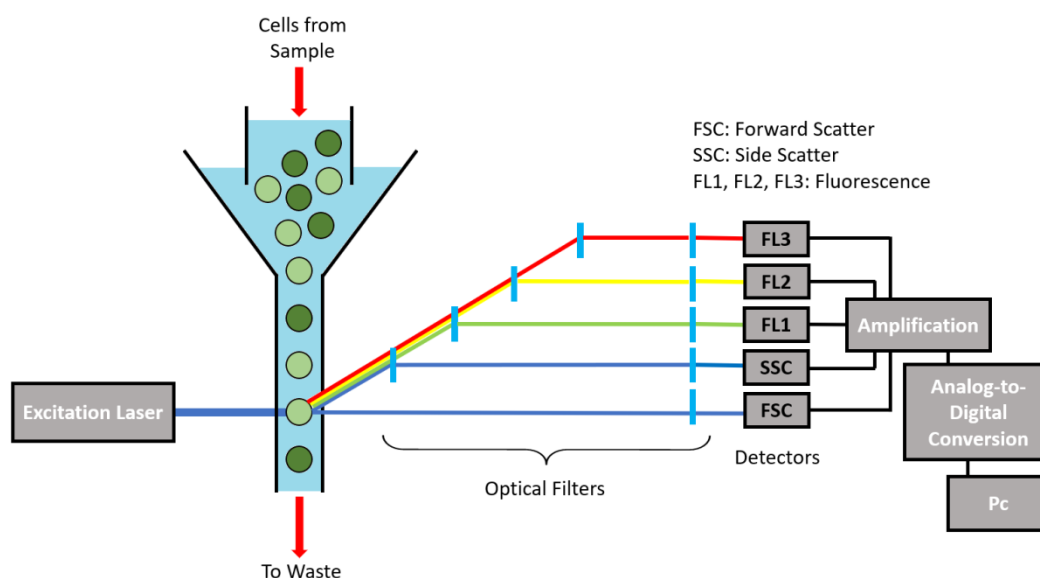


Figure 4.12. Schematic of a flow cytometer.

Cells are loaded into the instrument and are aligned in single file; where they pass through the excitation laser, also known as the interrogation point. Detectors can collect data regarding the forward scatter (FSC), the side scatter (SSC) and fluorescent emissions. Scattered light can be used to measure volume (FSC) and morphological complexity (SSC) of the cells, whereas the fluorescence emission is proportional to the amount of fluorescent probe within a cell. Hence, the ROS amounts of different samples can be compared depending on the counts of fluorescent cells.

#### 4.1.4.3 DNA Damage Evaluation using the COMET assay

For the evaluation of protective effects of vanillin derivatives against oxidative stress-induced DNA damage, the comet assay was employed. The latter, also known as single cell gel electrophoresis, was firstly introduced by Ostling and Johanson in 1984 for the detection of DNA damage in mammalian cells after exposure to radiation (Ostling and Johanson, 1984). In the past decades, the DNA comet assay has been employed in a wide

number of human clinical studies, with several variants of the assay having been optimized. The alkaline comet assay was employed in this study. The latter is useful to detect double and single DNA strand breaks and it is based on the use of high pH solution (>13) after cell lysis to unwind the supercoiled DNA. If strand breaks are present, the DNA supercoils, which are negatively charged, will relax and migrate toward the anode during the electrophoretic process, forming a shape similar to a comet, hence the name of the assay (Pu, Wang and Klaunig, 2015).

For the evaluation of the protective effects of selected vanillin derivatives against oxidative stress-induced DNA damage, the cells were pre-treated with selected compounds before the addition of hydrogen peroxide (300  $\mu$ M). Cells were then harvested with trypsin, centrifuged and suspended in low melting point agarose gel on top of frosted microscope slides. The latter were suspended in lysis buffer containing high salt and detergent to remove membranes, cytoplasm and nucleoplasm, leaving only the nucleoid, consisting of the nuclear matrix composed of RNA, proteins and DNA. For the survival of the supercoiled DNA, the inability of the latter to freely rotate is of critical importance and the presence of agarose gel, which embeds the cells causes DNA immobilization (Collins, 2004). After lysis, the alkali treatment caused the unwinding of the double DNA strand and the DNA is ready for electrophoresis. DNA containing strand breaks loses its supercoiling and become free to extend toward the anode leading to the typical "comet" shape. On the other hand, undamaged DNA lacks free ends and its large size prevents the migration toward the cathode leading to the absence of the "comet" shape. For DNA visualization, a fluorescent dye such as 4',6-diamidino-2-phenylindole (DAPI) is needed along with a fluorescence microscope. DAPI is a DNA intercalating agent which binds to adenine-thymine rich regions of double stranded DNA. The comets are finally scored according to their shape with arbitrary numbers ranging from 0 (no DNA damage, circular comets) to 4 (maximum damage, small head and big tail). The scoring criteria is reported in figure 4.14 in the methods section.

#### 4.1.4.4 Western Blotting for the Detection of Nuclear Nrf2 protein

As described in chapter 1, (pages 18-20), the nuclear factor E2-related factor 2 (Nrf2) is the main mediator of ARE activation. Under physiological conditions, Nrf2 is bound to actin-associated keap1 protein and compartmentalized in the cytoplasm. Under oxidative conditions, Nrf2 translocates into the nucleus, inducing the transcription of antioxidant genes (Itoh *et al.*, 1999; Kobayashi *et al.*, 2004; Nguyen, Nioi and Pickett, 2009; Ma, 2014).

In order to evaluate the ability of the selected compound to activate the Nrf2 antioxidant pathway, Western Blot analysis was employed. The latter is a technique developed by Towbin, Staehelint and Gordon in 1977, aimed to separate and transfer ribosomal proteins from gel containing urea (Towbin, Staehelint and Gordon, 1979). Two years later, Burnette introduced the name "western blotting", playing with the name of two previously reported techniques, southern and northern blotting, for the separation of DNA and RNA, respectively (Burnette, 1981).

This technique is based on the separation of the proteins according to their molecular weight in a sample (for example a cell lysate), through electrophoresis and consequent transfer of the latter into a polyvinylidene fluoride (PVDF) or nitrocellulose membrane. The membrane is then blocked with 5% milk or bovine serum albumin (BSA) for a usual period of one hour, and then incubated with an appropriate dilution of primary antibody (specific for the protein of interest) overnight at 4°C (Kaur and Bachhawat, 2009; Mahmood and Yang, 2015). The membrane is washed with TBST, which is composed of Tris-buffered-saline + polysorbate 20 (known as Tween 20) and incubated with an optimized dilution of the secondary antibody for one hour at room temperature. After washing the membrane with TBST, protein detection is carried out employing different techniques using chemiluminescent reagents, organic dyes, fluorescent labels, silver staining, colloidal particles or autoradiography (Kurien and Scofield, 2006).

For this study, the cells were incubated with the selected vanillin derivative for different periods, then harvested, washed with PBS and centrifuged.

Cells were lysed and the nuclear extract was collected. The protein content for each lysate was quantified through Bradford assay and 20 µg of protein from each sample was loaded for the electrophoresis run. The proteins were then transferred into a PVDF membrane and the procedure above was followed. For the detection of the protein of interest, a mouse primary antibody for Nrf2 was employed and an anti-mouse secondary antibody was added after a careful washing procedure (figure 4.13).

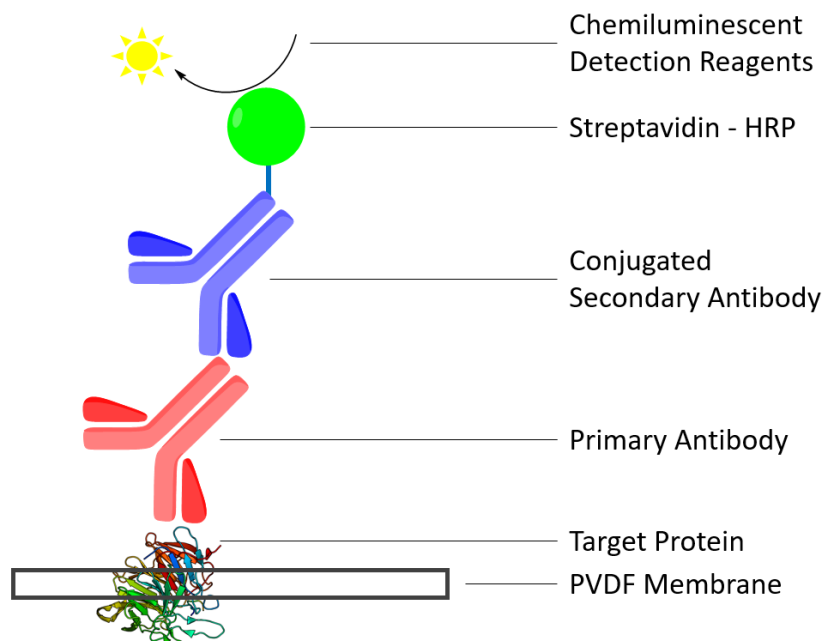


Figure 4.13. Principle of protein detection through Western Blotting.

The secondary antibody is conjugated with Horseradish peroxidase (HRP), a haeme-containing enzyme found in the horseradish plant that utilises hydrogen peroxide to oxidise organic and inorganic compounds (Veitch, 2004). This enzyme catalyses the oxidation of luminol induced by hydrogen peroxide (the components of the chemiluminescent detection kit) as depicted in figure 4.14.

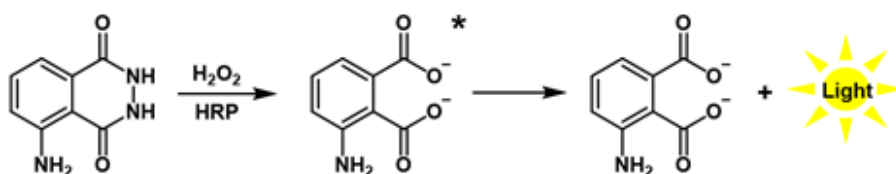


Figure 4.14. Reaction mechanism of luminol-based chemiluminescence, adapted from Alegria-Schaffer, Lodge, and Vattem (2009).

The HRP-catalysed reaction of luminol yields the excited state of the oxidized product, which decays to the ground state emitting light at 425 nm. The chemiluminescent signal is finally acquired using dark room with a development technique.

## 4.2 Materials and Methods

### 4.2.1 Materials

All reagents were purchased from Sigma Aldrich, unless otherwise stated, without any further purification.

30% Acrylamide/Bis solution 19:1	Bio-Rad
Agarose gel (high melting point)	Fisher Scientific
Antibody Nrf2 A-10	Santa Cruz
Bradford Protein Assay	Bio-Rad
Developer and Fixer (RP X-OMAT LO)	Kodak, carestream
DMEM (1x) high glucose, pyruvate	Fisher Scientific
FBS	Fisher Scientific
Goat Anti-Mouse IgG H&L (HRP)	Abcam
H <sub>2</sub> DCFDA	Invitrogen
HALT™ Protease Inhibitor Cocktail (100x)	Fisher Scientific
Milk powder	Asda
MTT	Acros Organics
NE-PER Nuclear and Cytoplasmic Extraction Reagents	Fisher Scientific
Phosphate Buffered Saline (PBS) Tablets	Oxoid
Precision Plus Protein Dual Colours Standards	Bio-Rad
Sheath Buffer (flow cytometry)	Beckman Coulter Inc
SuperSignal™ West Pico PLUS Chemiluminescent Substrate	Fisher Scientific
Tris Base	Fisher Scientific
Triton X-100	Acros Organics

### 4.2.2 Instrumentation

A Leica DMIL microscope was used for cell culture.

Absorbances for MTT assay were measured using a Bio-Rad iMark microplate reader.

Flow cytometry analysis was carried out using Coulter Epics XL-MCL flow cytometer.

DNA comet assay was performed using Anachem 3003 electrophoretic tank and a Leica DMRB fluorescence microscope was used for the comet scoring.

## 4.3 Methods

### 4.3.1 Cell Culturing

SH-SY5Y cells were maintained as previously reported with minor modifications (Smith *et al.*, 2005). DMEM media supplemented with 10% FBS, 1% non-essential amino acids (NEAA) and 1% penicillin (100 U/ml), streptomycin (100 µg/ml) was employed. Cell plates and flask were maintained in a 5 % CO<sub>2</sub> humidified incubator at 37°C. Cells were passaged, once 80% confluence levels were reached, by discarding the old media, washing with PBS and trypsinizing for 5 minutes. Trypsin was deactivated with fresh media and the cells were centrifuged for 5 minutes at 1500 rpm, 414 g. The supernatant was then discarded and the cells were suspended in fresh media. Finally, the cells were counted using a haemocytometer and seeded in plates or flasks for further experiments.

### 4.3.2 Cellular Toxicity of Selected Vanillin Derivatives

For the evaluation of cytotoxicity, the selected vanillin derivatives were tested at different concentrations and the MTT assay was employed for the evaluation of cell viability. The assay was carried out according to Barron *et al.* with minor changes (Barron *et al.*, 2010). Briefly, 7000 cells (100 µl) were seeded in a 96-well plate and allowed to attach for 24 hours. Then, 50 µl containing different concentrations of drug was added in the corresponding wells, whereas 50 µl of media was added to the control wells. The plate was incubated for 24 hours. On the following day, cell morphology at each condition was observed under a light microscope before culture media was removed from each well and 100 µl of sterile-filtered (0.22 µm) MTT solution (1 mg/ml) was added. After 4 hours of incubation, the MTT solution was pipetted off from each well and 100 µl of DMSO was added in each well. The plate was wrapped in foil and gently shaken for 20 minutes, then the absorbance was measured at 560 nm. Three independent experiments were performed for each compound tested.

### *4.3.3 Protective Effects of Selected Vanillin Derivatives in presence of H<sub>2</sub>O<sub>2</sub> or Rotenone/Oligomycin A Cocktail stressor*

The same vanillin derivatives tested for their toxicity with SH-SY5Y cells were studied, along with vanillin, for their protective effects against H<sub>2</sub>O<sub>2</sub> (400 μM) and rotenone/oligomycin A cocktail (3 and 1 μM, respectively) toxicity. The use of these specific concentrations of stressor is linked to their toxicity on the SH-SY5Y cell line and represent approximately the LC<sub>50</sub> (data not shown). The experiments were run using a 96-well platform; briefly, 7000 cells (100 μl) were seeded in each well and allowed to attach for 24 hours. 50 μl containing different concentrations of drug was added in the corresponding wells, whereas 50 μl of media was added to the control wells. The plate was incubated for 24 hours. Then, 50 μl of H<sub>2</sub>O<sub>2</sub> (1.6 mM, to yield a 400 μM final concentration in the well) or 50 μl of rotenone/oligomycin (12 and 4 μM, to yield a final concentration of 3 and 1 μM in the well, respectively) were added in the corresponding wells. After 24 hours (for hydrogen peroxide) or 48 hours (for the rotenone/oligomycin mixture) incubation, the culture media was removed from each well and the cell viability was measured through MTT assay, following the procedure mentioned above. Three independent experiments were performed for each compound tested. The 96-well plate set-up is shown in figure 4.15.

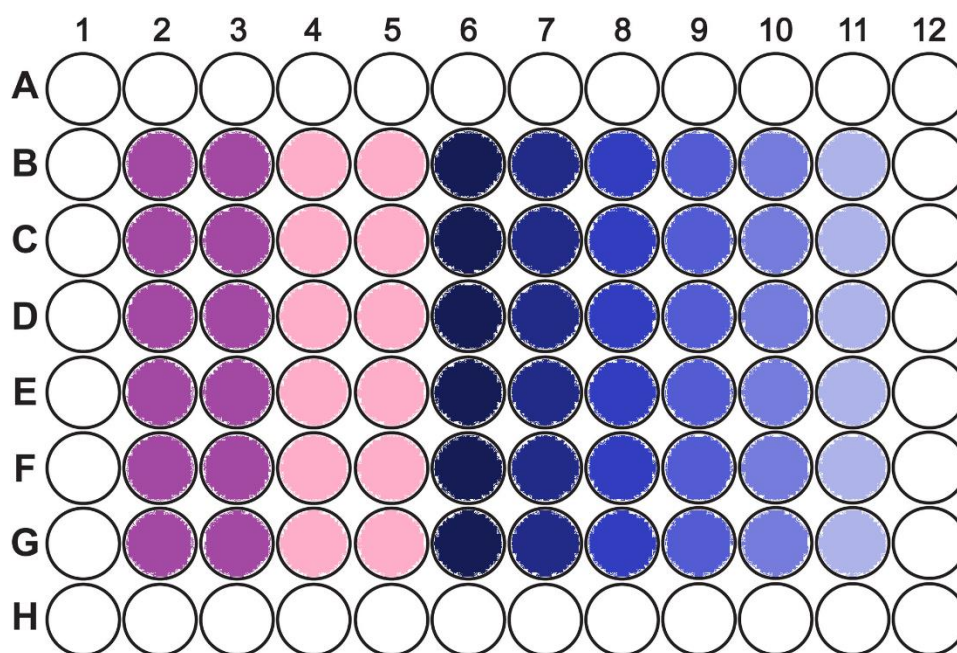


Figure 4.15. 96-well plate settings for MTT assay. Media control is coloured in purple whereas the hydrogen peroxide or the rotenone/oligomycin mixture controls are rendered in pink. The different shades of blue represent different concentrations of the vanillin derivative tested (**1f**, **2b** or **4c**).

#### 4.3.4 Protective Effects of Vanillin Derivatives from ROS Induced by $H_2O_2$

The ability of the selected vanillin derivatives to alleviate the ROS production induced by hydrogen peroxide was evaluated. For the detection of ROS in SH-SY5Y cells, 2,7'-dichlorodihydrofluorescein diacetate ( $H_2DCFDA$ ) was employed. Cells were cultured in T25 culture flasks (1 million in 3 ml of media) in duplicate and allowed to attach for 24 hours. Then, cells were treated with compound **2b** (1ml, 800  $\mu M$ , for a final concentration of 200  $\mu M$ ) or compound **4c** (1 ml, 40  $\mu M$ , for a final concentration of 10  $\mu M$ ) for an additional 24 hours, whereas the controls were treated with media. After 24 hours,  $H_2O_2$  (1ml, 5 mM, for a final concentration of 1 mM) was added and the cells were incubated for 30 minutes. The media was then removed and 5 ml of  $H_2DCFDA$  (1.2  $\mu M$ ) in fresh media was added. The cells were incubated for 4 hours, washed twice with PBS, trypsinized and collected using PBS. The cells were then centrifuged (5 mins, 1500 rpm, 414 g), the supernatant discarded and resuspended in 1 ml of PBS for flow-cytometry analysis. Three independent experiments were performed.

#### 4.3.5 DNA Damage Determination by Comet Assay

Comet assay was performed in a 12-well plate platform following the method reported by Duthie *et al.* with minor modifications (Duthie *et al.*, 2009). Cells ( $10^5$  in 800  $\mu\text{l}$  of media) were seeded in each well and allowed to attach for 24 hours. Then, 200  $\mu\text{l}$  of compound **2b** (1 mM, for a final concentration of 200  $\mu\text{M}$ ) or 200  $\mu\text{l}$  of compound **4c** (50  $\mu\text{M}$ , for a final concentration of 10  $\mu\text{M}$ ) was added to the corresponding wells, whereas 200  $\mu\text{l}$  of fresh media was added to the control wells. After 24 hours incubation,  $\text{H}_2\text{O}_2$  (1 ml, 600  $\mu\text{M}$ , for a final concentration of 300  $\mu\text{M}$ ) was added to the corresponding wells and the plate was incubated for 30 minutes. The concentration of hydrogen peroxide employed in this experiment was based on previous studies reported by Dr. Pohl in her PhD thesis "The potential application of rapeseed pomace extracts in the prevention and treatment of neurodegenerative diseases" (Pohl, 2019) which reported a significant amount of damage without detrimental DNA damage or cell death. Cells were then washed with PBS and harvested using trypsin (100  $\mu\text{l}$ ); the latter was inactivated with 900  $\mu\text{l}$  of fresh media and the cells were transferred into Eppendorf® tubes. Cells were counted using a haemocytometer, centrifuged for 5 minutes (4°C, 2000 rpm, 370 g) and the supernatant carefully removed using a pipette. The pellets obtained were kept on ice. The bottom gel (1% w/v standard melting point agarose) was prepared and kept at 40°C to avoid solidification, in a water bath, then 80  $\mu\text{l}$  of the latter was pipetted on frosted microscopy slides (Richardson Supply Ltd) and covered with 18x18 mm coverslips (Fisher Scientific). The gels were left to solidify at 4°C for 10 minutes. A 1% (w/v) low melting point agarose gel was prepared and a certain amount, depending on the number of cells counted for each condition, was pipetted into the Eppendorf® tube containing the cell pellet to achieve a concentration of around  $3 \times 10^4$  cells in 85  $\mu\text{l}$  of gel. The coverslips were removed from the top of the previous gel and a second layer of gel, containing the desired number of cells, was added on top. New coverslips (18x18 mm) were added and the gel were left to solidify for 10 minutes. The coverslips were then removed and the microscopy slides were soaked in lysis buffer (2.5 M NaCl, 0.1 M EDTA, 10 mM Tris and 4% Triton X-100, pH 10) for one hour at 4 °C. At that point, the slides were placed in the electrophoresis tank, containing the

electrophoresis buffer (0.3 M NaOH, 1 mM EDTA, pH 13), for the alkaline treatment (40 minutes at 4 °C). Finally, the electrophoresis was run at 25 V for additional 40 minutes at 4°C. After the electrophoresis, the slides were washed three times with neutralising buffer (0.4 M Tris, pH 7.5) and the gels were covered using 22x22 mm microscope coverslips (Fisher Scientific) and stored in the fridge. For the scoring, coverslips were removed and 20 µl of DAPI staining solution (1 µg/ml in distilled water) was added to the gels. Comets were scored manually according to Heuser *et al.* (Heuser *et al.*, 2007) using a Leica DMRB fluorescence microscope (excitation 340-380 nm, emission 425 nm). 100 comets were scored (with scores ranging from 0 to 4 for each comet, depending on the intensity of DNA damage, see figure 4.16) and the values were summed to obtain arbitrary numbers between 0-400 for each scored gel.

 <p style="text-align: right;">0</p>	<ul style="list-style-type: none"> <li>- Big circular comet head with sharp contour</li> <li>- No tail</li> </ul>
 <p style="text-align: right;">1</p>	<ul style="list-style-type: none"> <li>- Big circular comet head with sharp contour</li> <li>- Sparkle tail, same length as the head</li> </ul>
 <p style="text-align: right;">2</p>	<ul style="list-style-type: none"> <li>- Big circular comet head with sharp contour</li> <li>- Significant tail</li> </ul>
 <p style="text-align: right;">3</p>	<ul style="list-style-type: none"> <li>- Fainter head with loss of sharp contour</li> <li>- Tail merge with the head</li> </ul>
 <p style="text-align: right;">4</p>	<ul style="list-style-type: none"> <li>- Small head with decreased brightness</li> <li>- Tail's diameter is bigger than the head</li> </ul>

Figure 4.16. DNA Comet scoring criteria.

For each experimental condition three gels were scored, and their mean value calculated. Statistical analysis was done on three independent experiments.

#### *4.3.6 Evaluation of Nrf2 Pathway Activation*

Nrf2 activation studies were performed in T25 flasks. Cells ( $1.5 \times 10^6$ ) were seeded in a total volume of 2.997 ml and allowed to attach for 24 hours. The next day, compound **4c** was added (3  $\mu$ l, 10 mM in pure DMSO, to yield a final compound concentration of 10  $\mu$ M) whereas 3  $\mu$ l of DMSO was added in the control flask. The cells were incubated for different periods (3, 6 and 24 hours), then washed with PBS, trypsinized, centrifuged, washed twice with PBS and suspended in PBS in pre-cooled Eppendorf® tubes. Cells were centrifuged at 1500 rpm, 414 g, for 5 minutes and the supernatant was discarded. Nuclear extraction was performed following the instructions reported on the kit employed for the experiment (NE-PER nuclear and cytoplasmic extraction reagents, Fisher Scientific). Briefly, the cell pellets were suspended in ice-cold Cytoplasmic Extraction Reagent I (CER I) (200  $\mu$ l) containing 2  $\mu$ l of protease inhibitor cocktail, vortexed for 15 seconds and incubated on ice for 10 minutes. Then, 11  $\mu$ l of Cytoplasmic Extraction Reagent II (CER II) was added and the Eppendorf® tubes were vortexed for 5 seconds before the incubation on ice for 1 minute. The tubes were vortexed again for 5 seconds and centrifuged at 16000 g for 5 minutes at 4°C. the supernatants (cytoplasmic extracts) were collected and stored at -80°C and the insoluble pellets obtained were suspended in 100  $\mu$ l of ice-cold Nuclear Extraction Reagent (NER) containing 1  $\mu$ l of protease inhibitor cocktail. The tubes were vortexed for 15 seconds and incubated on ice for 40 minutes, vortexing for 15 seconds every 10 minutes. The tubes were finally centrifuged at 16000 g for 10 minutes at 4°C and the supernatant (nuclear extract) was transferred into a pre-chilled microtube and stored at -80°C until further use.

The protein content of each sample was determined using the Bradford assay; the latter is a quick and common method for the quantification of proteins based on the absorption shift of the Coomassie Brilliant Blue G-250 dye, from 465 to 595 nm, once bound to protein (Bradford, 1976). Briefly,

BSA standards ranging from 0.2 to 2 mg/ml were prepared in PBS. 5  $\mu$ l of each sample or standard was pipetted along with 250  $\mu$ l of Bradford reagent in the corresponding well of a 96-well plate and incubated for 5 minutes. The absorbances were measured at 595 nm and the protein content of each sample was measured by comparison with the standard curve obtained for the BSA.

Once the protein content of each sample had been determined, the volume corresponding to 20  $\mu$ g of protein from each sample was loaded in the corresponding well of a 13% polyacrylamide gel along with the protein ladder control (Precision plus protein dual Color standards, Bio-Rad).

The latter was prepared in two steps; firstly, the separating gel was prepared by mixing 2.4 ml of deionized water with 3.47 ml of acrylamide/bis solution, 2ml of Tris solution (1.5 M, pH 8.8), 80  $\mu$ l of sodium dodecyl sulfate (SDS) solution (10% w/v), 80  $\mu$ l of ammonium persulfate (APS) solution (10% w/v) and 8  $\mu$ l of tetramethylethylenediamine (TEMED). The solution obtained was pipetted (4 ml) between two glass plates (casting frames) on the casting stands previously set up. Propan-2-ol (400  $\mu$ l) was added on top of the gel to remove air bubbles and the gel was left to solidify for 30 minutes. The stacking gel was then prepared, by mixing 2.6 ml of deionized water with 1 ml of acrylamide/bis solution, 1.25 ml of Tris solution (0.5 M, pH 6.8), 50  $\mu$ l of SDS solution (10% w/v), 50  $\mu$ l of APS solution (10% w/v) and 5  $\mu$ l of TEMED. The solution obtained (2 ml) was added on top of the separating gel after the removal of the propan-2-ol lying above the latter. The well-forming comb was inserted and the gel was allowed to solidify for 20 minutes. The glass plates were taken out the casting frames, placed in the cell buffer dam and covered with running buffer (25 mM Tris-HCl, 200 mM glycine, 0.1% w/v SDS) in the electrophoresis tank. The electrophoresis was run for 1.5 hours at 120 V and the gel was separated from the glass plates. A PVDF membrane was activated by soaking it in methanol and was placed on top of the gel, then both were placed between two filter papers. A sponge was placed at the top and the bottom of the equipment and placed in the specific cassette for the protein transfer. The cassette was positioned in the electrophoresis tank and covered with transfer buffer (20% methanol, 80% of the previous

running buffer) before the electrophoretic process (100 V for 1 hour). The presence of the colored protein ladder in the PVDF membrane confirmed the successful transfer of the proteins from the gel. The membrane was blocked with milk (5% w/v) for 1 hour before the addition of the Nrf2 antibody (1:5000 dilution, 4  $\mu$ l of antibody in 20 ml of 5% milk). The membrane was incubated overnight at 4°C. The next day, the membrane was washed with TBST solution (3x15 ml) and incubated with the HRP-conjugated secondary antibody (1:10000 dilution, 2  $\mu$ l of secondary antibody in 20 ml of 5% milk) for 1 hour at room temperature. After washing with TBST solution (3x15 ml), the membrane was placed over cling film and 2 ml of the chemiluminescent reagent (SuperSignal™ West Pico PLUS Chemiluminescent Substrate, Fisher Scientific) was pipetted on top. The membrane was incubated for 5 minutes in the dark and the excess reagent was removed. The membrane was placed in a film cassette, transferred into a dark room and placed close to an x-ray film. The cassette was sealed and soaked in the developer solution for 2 minutes, washed with water for 1 minute, soaked again in the fixer solution and washed again with water for a minute (RP X-OMAT LO Kodak, Carestream). Finally, the cassette was opened and the x-ray film was left to dry.

#### *4.3.7 Statistical Analysis*

Statistical analysis was carried out using GraphPad Prism 6. The statistical methods used for each experiment are described in the results section. At least 3 replicates were performed for each experiment and the results are shown as mean  $\pm$  standard deviation.

## 4.4 Results and Discussion

### 4.4.1 Cellular Toxicity of Selected Vanillin Derivatives

The monomer **1f**, the dimer **2b** and the tetramer **4c** were selected for the evaluation of their protective effects towards SH-SY5Y in different models of oxidative stress. This selection was based on their antioxidant properties (described in chapter 3) and their cholinesterase and amyloid inhibitory properties, which will be described and discussed in chapter 5. However, to achieve this objective, a preliminary screening regarding their toxicity towards the same cell line needed to be assessed in order to determine their safe working concentrations.

MTT assay was employed to measure cell viability; the latter is a widely employed assay based on the conversion of the water soluble MTT into its reduced insoluble reduced form (formazan) which can be dissolved in DMSO to yield a deep purple colouration with a maximum absorbance at 560 nm. The LC<sub>50</sub>, corresponding to the concentration needed to kill the 50% of the cells, was determined using the following formula:

$$\% \text{ of viable cells} = \frac{ABS(\text{treatment})}{ABS(\text{control})} * 100$$

Three independent experiments were performed for each compound tested. MTT performed on the three vanillin derivatives (**1f**, **2b** and **4c**) showed low toxicity for the dimer **2b** and modest toxicity for both monomer **1f** and tetramer **4c**.

Compound **2b** was tested at concentrations ranging between 25 and 1000 µM and showed the lowest toxicity toward SH-SY5Y cell line with LC<sub>50</sub> value higher than 1 mM and significant toxic effects only observed at concentrations of 800 µM or above (see figure 4.17).

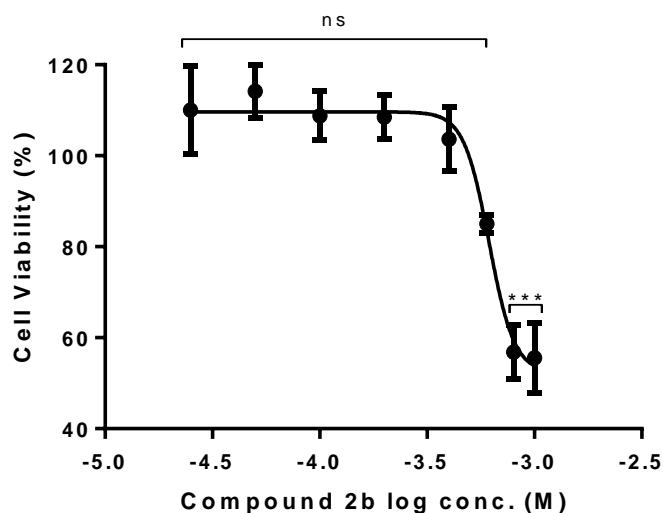


Figure 4.17. MTT cell viability assay using compound **2b** (25 - 1000  $\mu$ M, for 24 hrs). One-way ANOVA analysis was used for the comparison between the media control and each condition. \*\*\* $p \leq 0.001$ , ns = not significant,  $n=3$ .

Monomer **1f** and tetramer **4c** (figure 4.18) were tested at lower concentrations compared to **2b**. The presence of the *p*-phenylene diamine moiety in both the compounds and the tacrine structure in compound **1f** appear to contribute to the toxic effect in SH-SY5Y cells.

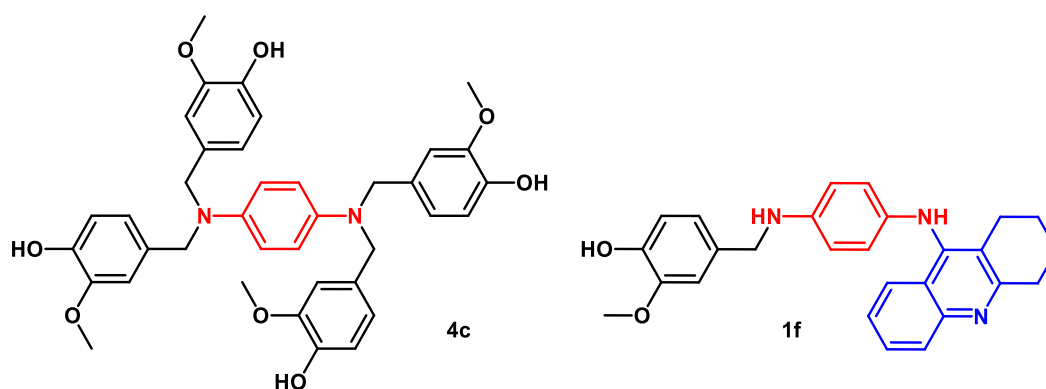


Figure 4.18. The *p*-phenylene diamine moiety (in red) in both compounds **1f** and **4c**. In addition, the tacrine moiety of compound **1f** is highlighted in blue.

For those reasons, **4c** and **1f** were tested at concentrations up to 50 and 100  $\mu$ M, respectively. Tetramer **4c** did not show significant toxic effects at concentration of 25  $\mu$ M, displaying a  $LC_{50}$  of  $45.1 \pm 3.5 \mu$ M (figure 4.19).

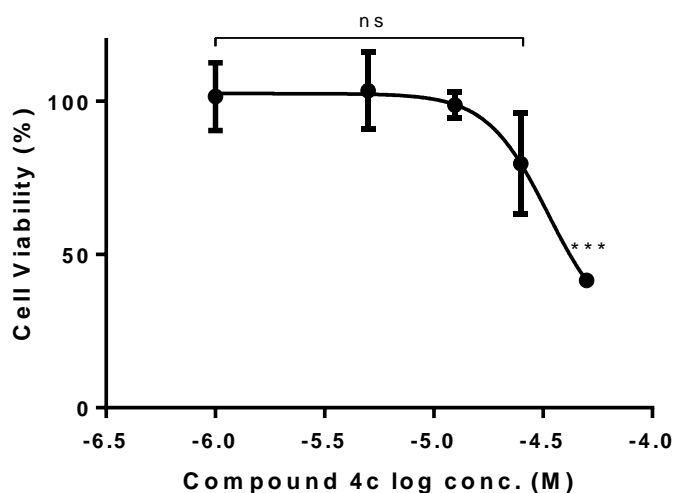


Figure 4.19. MTT cell viability assay using compound **4c** (0.1 - 50  $\mu$ M, for 24 hrs). One-way ANOVA analysis was used for the comparison between the media control and each condition. \*\*\* $p \leq 0.001$ , ns = not significant, n=3.

On the other hand, monomer **1f** showed increased toxicity, displaying significant cytotoxic effects at concentration as low as 25  $\mu$ M and a  $LC_{50}$  of  $43.7 \pm 1.9 \mu$ M (figure 4.20).

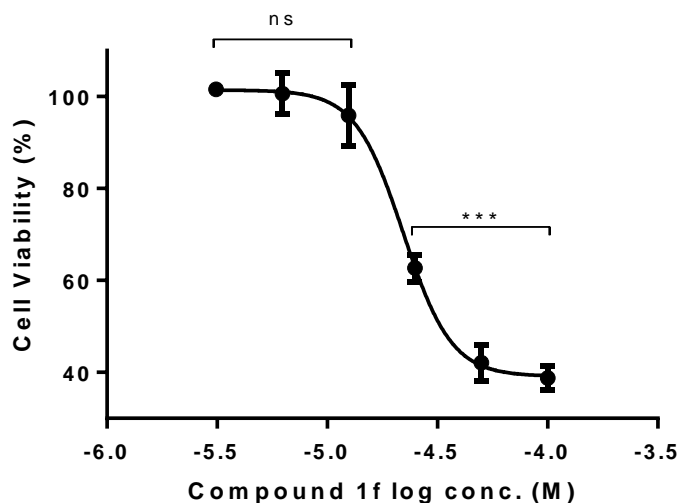


Figure 4.20. MTT cell viability assay using compound **1f** (3.125 - 100  $\mu$ M, for 24 hrs). One-way ANOVA analysis was used for the comparison between the media control and each condition. \*\*\* $p \leq 0.001$ , ns = not significant, n=3.

The higher toxicity showed by monomer **1f** compared to its related tetramer **4c** could be explained by the presence of the tacrine moiety, which contributes to the extra toxic effect of the monomer, since the vanillin moiety had a little impact on the toxicity as dimer **2b** showed very low effects on SH-SY5Y.

Similar toxicities were recently reported by Zha *et al.*, who tested tacrine and one of its dihydrobenzofuran derivative (figure 4.21) in SH-SY5Y cell line showing no toxicity at concentrations up to 10  $\mu\text{M}$  but significant toxic effects at concentration of 30  $\mu\text{M}$  (Zha *et al.*, 2016).

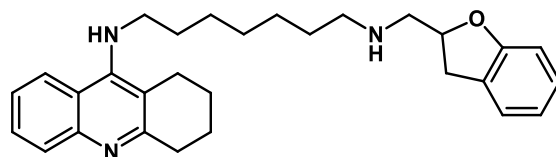


Figure 4.21. Tacrine-dihydrobenzofuran hybrid reported by Zha *et al.* (2016)

#### 4.4.2 Protective Effects of Vanillin Derivatives from $\text{H}_2\text{O}_2$ -Induced Toxicity

Once the relative toxicity of the three selected vanillin derivatives was established, they were then evaluated, along with vanillin, for their protective effects in a hydrogen peroxide oxidative stress model. The concentrations used for the three vanillin derivatives (**1f**, **2b** and **4c**) were 5, 200 and 10  $\mu\text{M}$ , respectively. Oxidative stress was induced by incubating SH-SY5Y cells with hydrogen peroxide (400  $\mu\text{M}$ ) for 24 hours. At this  $\text{H}_2\text{O}_2$  concentration  $\sim 50\%$  of cells death was observed. Cells were pre-treated with vanillin or the selected vanillin derivatives for 24 hours before the addition of the stressor.

Vanillin (0.1-800  $\mu\text{M}$ ) itself did not show any increase in cell viability when compared to  $\text{H}_2\text{O}_2$  control at concentrations up to 800  $\mu\text{M}$ ; thus confirming no protective effects toward the cells at any of the concentrations tested (see figure 4.22).

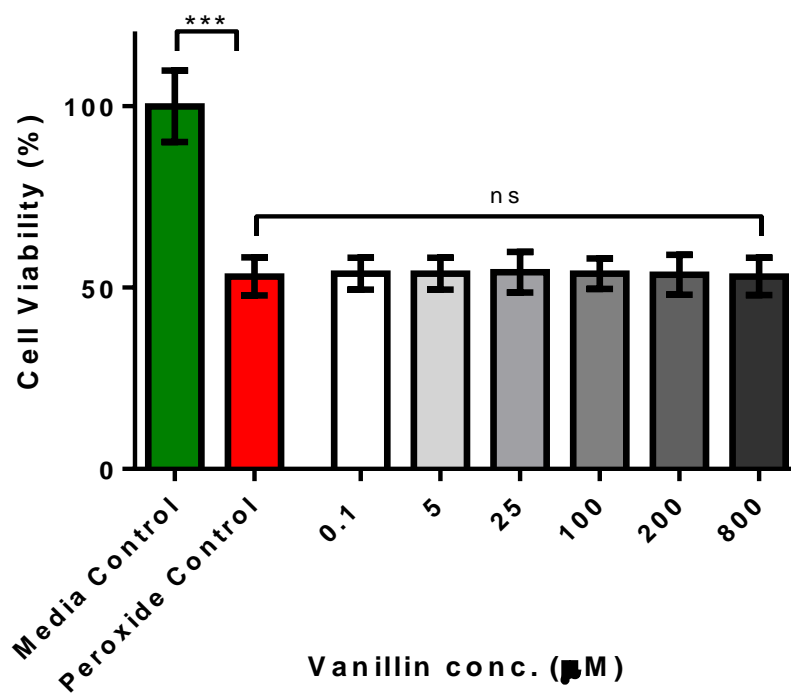


Figure 4.22. Protective effects of vanillin in hydrogen peroxide (400 µM)-stressed cells. One-way ANOVA analysis was used for the comparison between the peroxide control and each condition. ns = not significant, n=3.

On the other hand, all of the vanillin derivatives (**1f**, **2b** and **4c**) tested in this assay exhibited cellular protection against the oxidative insult induced by hydrogen peroxide in a concentration-dependent manner. Monomer **1f** showed significant cellular protection at concentrations as low as 1 µM (with an increase of 15% of cell viability) and a maximum at 5 µM, by increasing the cell viability by 30% (figure 4.23).

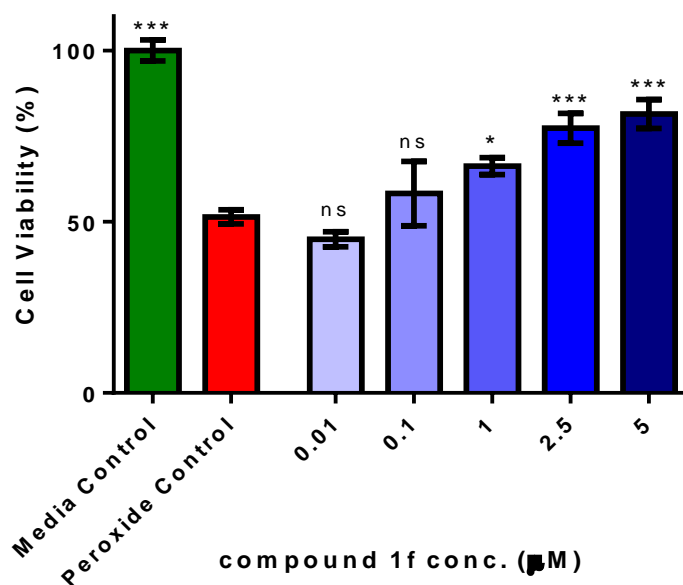


Figure 4.23. Protective effects of **1f** in hydrogen peroxide (400  $\mu\text{M}$ )-stressed cells. One-way ANOVA analysis was used for the comparison between the peroxide control and each condition. \*\*\* $p \leq 0.001$ , \* $p \leq 0.05$ , ns = not significant,  $n=3$ .

Similar protective effects were recently reported by Benchekroun and co-workers who described ferulic and lipoic acid-tacrine hybrids bearing a melatonin moiety (see figure 4.24) able to protect SH-SY5Y cells against hydrogen peroxide-induced oxidative damage at concentration as low as 1  $\mu\text{M}$  (Benchekroun *et al.*, 2016).

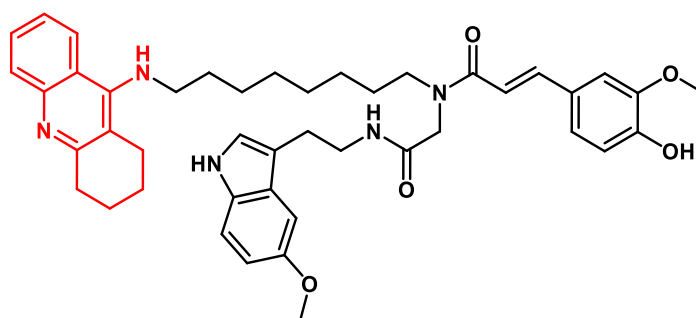


Figure 4.24. Neuroprotective agent against hydrogen peroxide-induced oxidative insult reported by Benchekroun *et al.* (2016). The tacrine moiety is highlighted in red.

Dimer **2b** displayed the weakest protective properties among the three vanillin derivatives, showing significant protection at concentrations as low as 5  $\mu\text{M}$  (with an increase in cell viability of only 6%) and an increase of cell viability by almost 20% at concentration of 200  $\mu\text{M}$  (see figure 4.25).

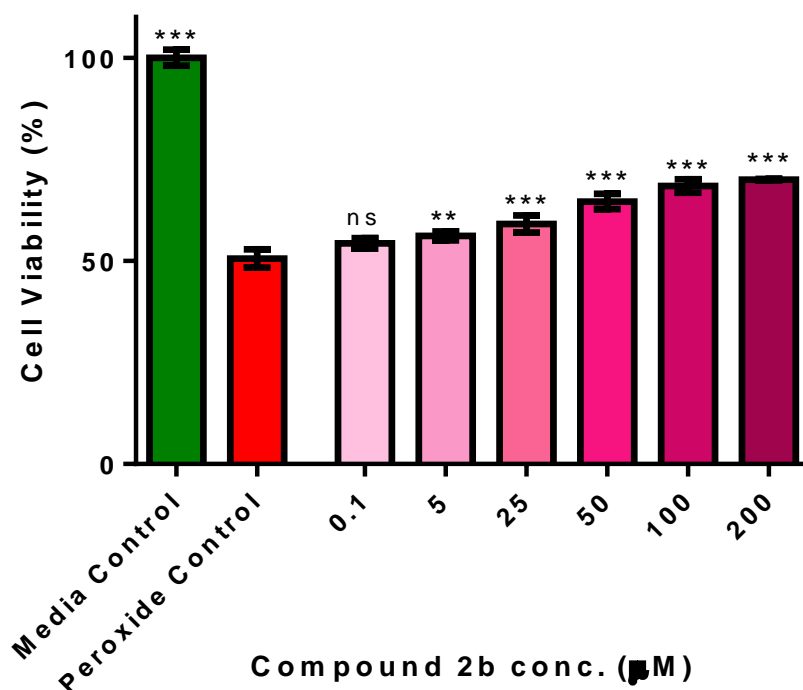


Figure 4.25. Protective effects of **2b** in hydrogen peroxide (400µM)-stressed cells. One-way ANOVA analysis was used for the comparison between the peroxide control and each condition. \*\*\* $p \leq 0.001$ , \*\* $p \leq 0.01$ , ns = not significant, n=3.

Finally, tetramer **4c** turned out to be the most efficient protective agent in this assay, displaying significant cellular protection at concentrations as low as 0.1 µM, increasing the cell viability by almost 10% and a maximum at 10 µM, with an increase of cell viability of almost 30% (see figures 4.26).

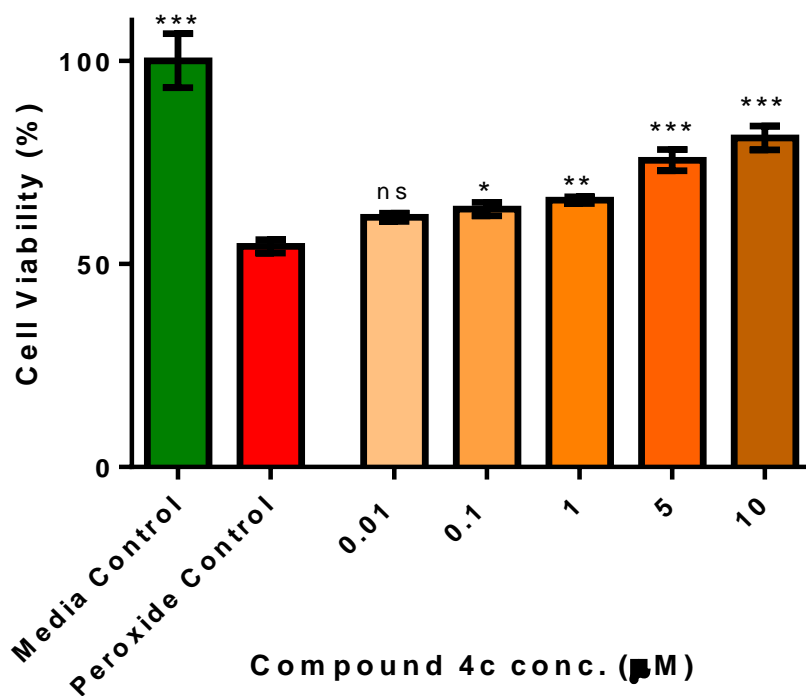


Figure 4.26. Protective effects of **4c** in hydrogen peroxide (400µM)-stressed cells. One-way ANOVA analysis was used for the comparison between the peroxide control and each condition. \*\*\* $p \leq 0.001$ , \*\* $p \leq 0.01$ , \* $p \leq 0.05$ , ns = not significant,  $n=3$ .

The protective effects of the latter can be appreciated as shown in Figure 4.27, showing the cells morphology of the different groups (media control, peroxide control and after **4c** pre-treatment) and the 96-well plate after one of the MTT assay (figure 4.28) performed on the vanillin derivative **4c**.

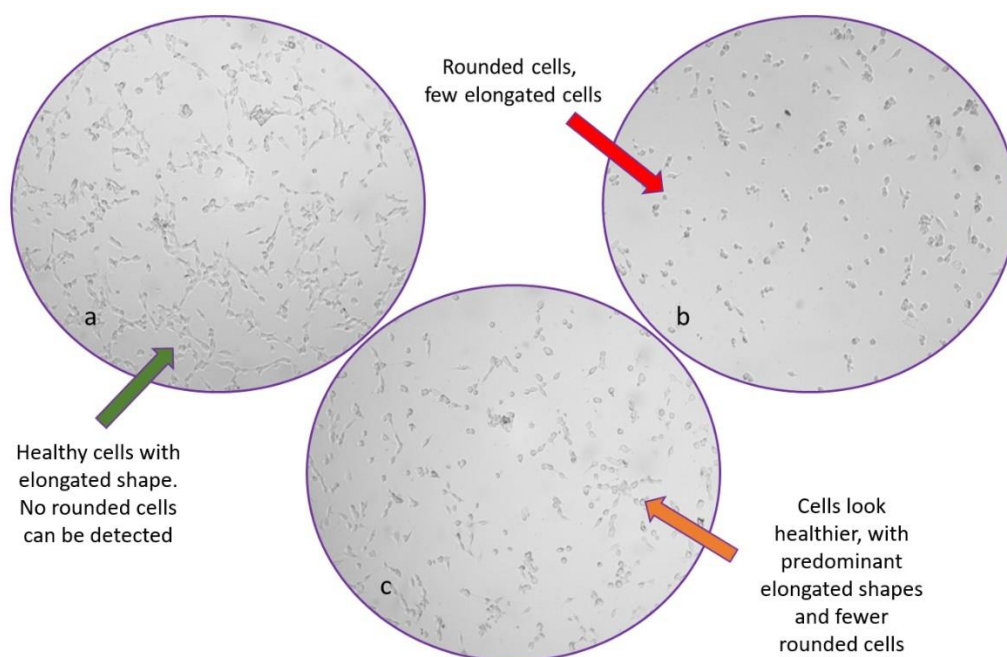


Figure 4.27. Morphology of untreated (a), hydrogen peroxide-stressed (400  $\mu\text{M}$ ) (b) or pre-treated with **4c** (10  $\mu\text{M}$ ) (c) cells during MTT assay (20x magnification, picture size adjusted to fit page).

Untreated cells showed the characteristic elongated shape of healthy SH-SY5Y cells. Once stressed with hydrogen peroxide (400  $\mu\text{M}$ ) for 24 hours, the morphology of the cells changed to rounded conformation with the loss of their original elongated shape. Pre-treatment with compound **4c** (10  $\mu\text{M}$ ) partially prevented the oxidative damage induced by hydrogen peroxide; the cells looked healthier maintaining their original shape while showing only fewer rounded shape cells when compared to the peroxide control.

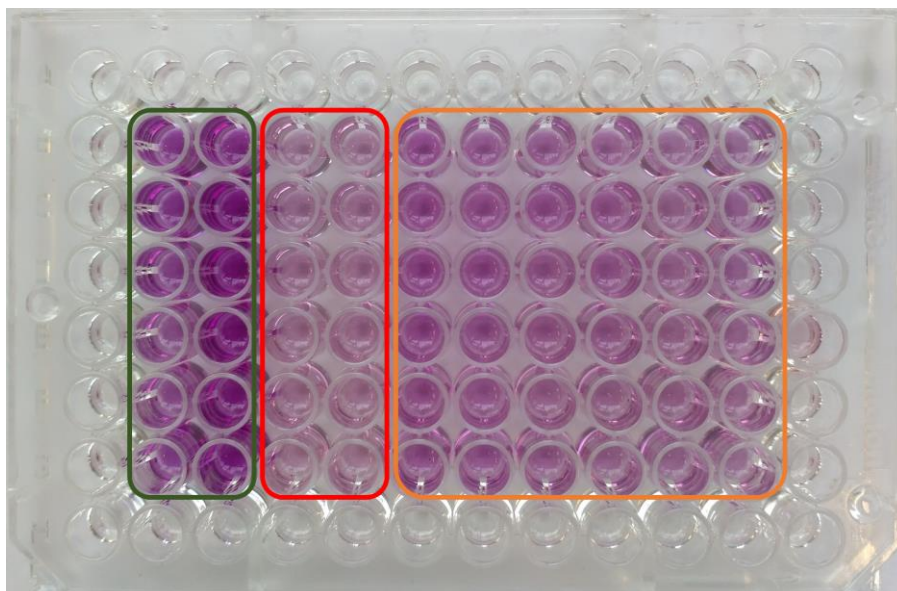


Figure 4.28. An example of MTT assay for the evaluation of the protective effects of compound **4c** in the hydrogen peroxide oxidative stress model. The wells circled in green correspond to the media control, whereas the wells circled in red correspond to the hydrogen peroxide control. Decreasing concentrations of compound **4c** (from left to right) are circled in orange.

The loss of colouration in the wells circled in red (hydrogen peroxide control) compared to the strong purple colour in the wells circled in green (media control) suggests the decrease in cell viability in the peroxide control. In contrast, the increased in purple colouration in the wells circled in orange (**4c** pre-treatment) compared to the stressor control highlights the increased cell viability compared to the latter.

It is interesting to note that monomer **1f** and tetramer **4c** showed similar protective effects, although these compounds displayed different antioxidant properties (see chapter 3). In addition, the dimer **2b** showed modest protection toward SH-SY5Y cells even at higher concentrations (up to 200  $\mu\text{M}$ ), suggesting the minor role of the vanillin moieties on the protective effects (vanillin itself showed no protective effects at concentrations up to 800  $\mu\text{M}$ ). It is worth to note that, working with cellular models; different defensive mechanisms could also be triggered.

#### *4.4.3 Protective Effects of Vanillin Derivatives from Rotenone/Oligomycin A Cocktail-Induced Toxicity*

The same vanillin derivatives as above were tested, along with vanillin, for their protective effects in a rotenone/oligomycin A cocktail (3 and 1  $\mu\text{M}$ ,

respectively) oxidative stress model. The cells were pre-treated with vanillin or the selected vanillin derivative for 24 hours before the addition of the stressor cocktail and then incubated for additional 48 hours. Again, vanillin did not show significant protective effects at any concentration tested (see figure 4.29).

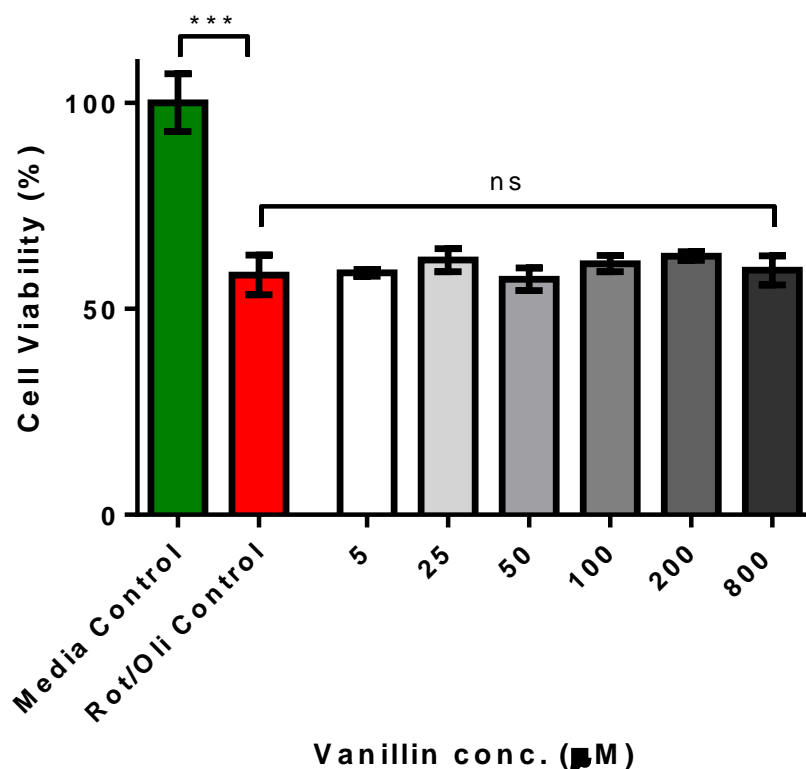


Figure 4.29. Protective effects of vanillin in rotenone/oligomycin (3 and 1 µM, respectively)-stressed cells. One-way ANOVA analysis was used for the rotenone/oligomycin A control and each condition. \*\*\* $p \leq 0.001$ , ns = not significant,  $n=3$ .

It is worth noting that vanillin was previously reported to protect SH-SY5Y cells from oxidative damage induced by rotenone (Dhanalakshmi *et al.*, 2015); the presence of oligomycin A, which is an inhibitor of the complex V the respiratory chain, could nullify the protective effects of this natural product.

Both monomer **1f** and dimer **2b** did not show significant protection at the concentrations tested, as depicted in figure 4.30.

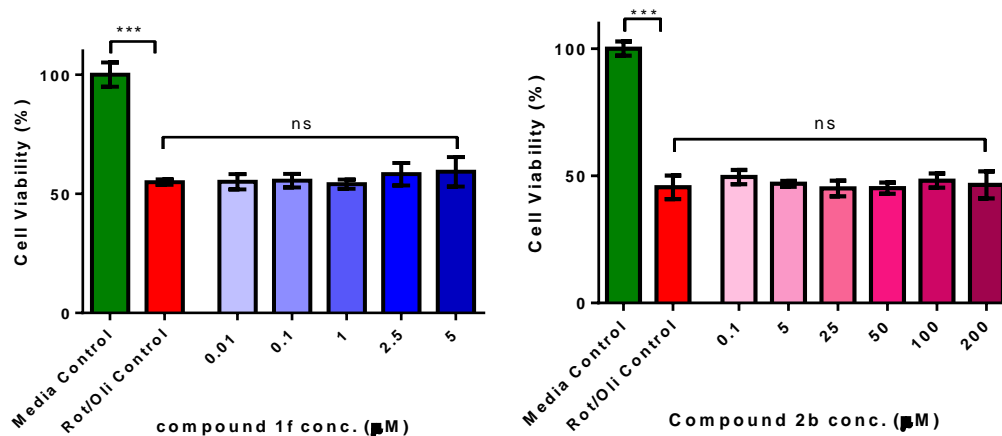


Figure 4.30. Protective effects of **1f** and **2b** in rotenone/oligomycin (3 and 1  $\mu\text{M}$ , respectively)-stressed cells. One-way ANOVA analysis was used for the rotenone/oligomycin A control and each condition. \*\*\* $p \leq 0.001$ , ns = not significant,  $n=3$ .

An interesting work from Benchekroun *et al.* reported ferulic and lipoic acid-tacrine hybrids bearing a melatonin moiety with protective effects toward the same cell line against rotenone/oligomycin A induced oxidative damage. In particular, the most active compound (see figure 4.24) showed neuroprotection at concentrations as low as 1  $\mu\text{M}$  (Benchekroun *et al.*, 2016).

However, tetramer **4c** showed significant protective effects at concentrations of 5 and 10  $\mu\text{M}$ , increasing the cell viability by almost 20 and 25%, respectively. No significant protection was observed at lower concentrations (see figure 4.31).

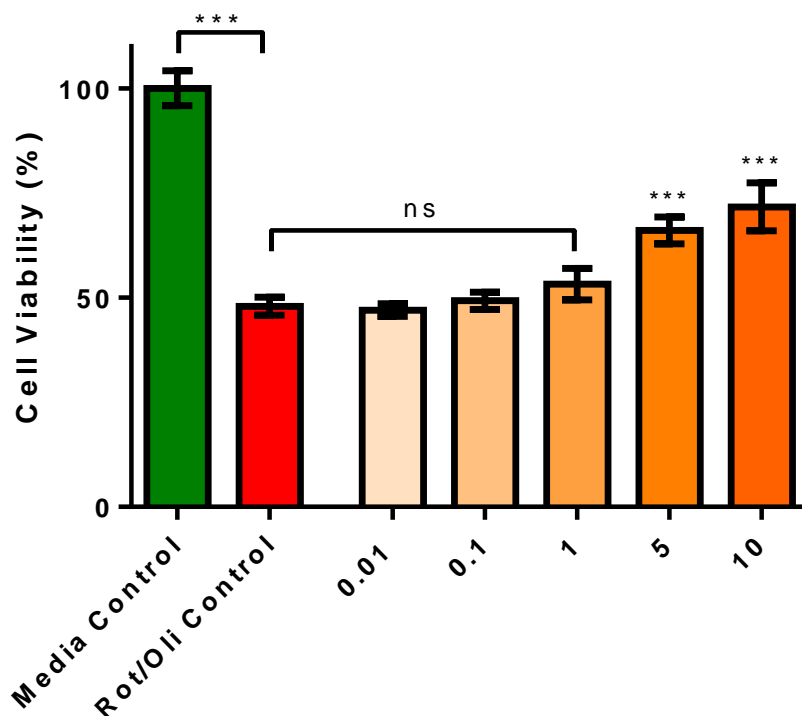


Figure 4.31. Protective effects of **4c** in rotenone/oligomycin (3 and 1  $\mu$ M, respectively)-stressed cells. One-way ANOVA analysis was used for the rotenone/oligomycin A control and each condition. \*\*\* $p \leq 0.001$ , ns = not significant, n=3.

The lack of protection displayed by compounds **1f** and **2b** and the modest activity of tetramer **4c** could rely on the fact that the rotenone/oligomycin A cocktail toxicity is manifested in the mitochondria, thus the tested compounds might not be able to reach this site of action.

#### 4.4.4 Protective Effects of Vanillin Derivatives from ROS Induced by $H_2O_2$

Following the protection studies against oxidative insult by hydrogen peroxide or rotenone/oligomycin, the ability of selected vanillin derivatives to alleviate the production of ROS after treatment with  $H_2O_2$  (1 mM, 30 minutes) in SH-SY5Y cells was evaluated. At that concentration of hydrogen peroxide significantly increased the levels of ROS while maintaining non-significant levels of cytotoxicity.  $H_2DCFDA$  was employed to detect the ROS generated within the cells and the fluorescence was measured by flow cytometry. An example of the data obtained in this experiment is depicted in figure 4.32.

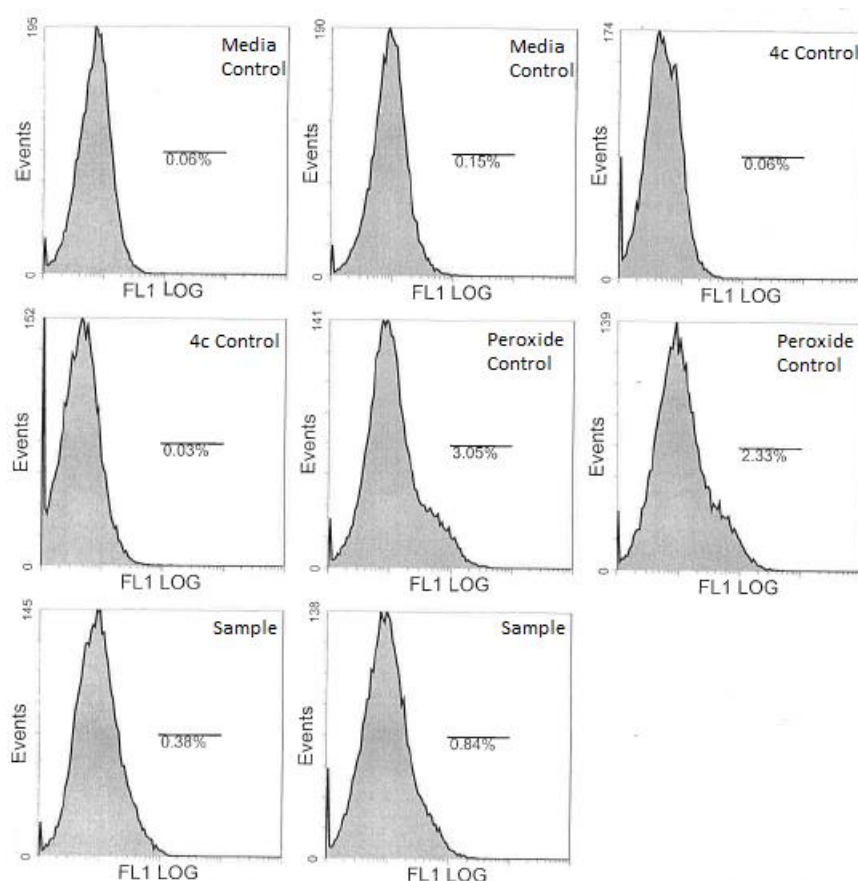


Figure 4.32. Raw data obtained from flow cytometry, showing the number of cells (events) and their associated fluorescence intensity on a logarithmic scale (FL1 LOG).

Due to instrumental issues at the time those experiments were carried out, only dimer **2b** and tetramer **4c** were tested in this assay. The concentrations used for each compound were the highest used in the cellular protection studies against hydrogen peroxide and rotenone/oligomycin A cocktail i.e. 200 and 10  $\mu\text{M}$  respectively. The relative fluorescence of each group (media control, compound control and sample) was compared with fluorescence from the peroxide control group, which was set as 100% of relative fluorescence.

Both compounds tested, did not show significant increase in ROS production compared to the media control, suggesting their inability to act as pro-oxidant at the concentrations tested (see figures 4.33 and 4.34).

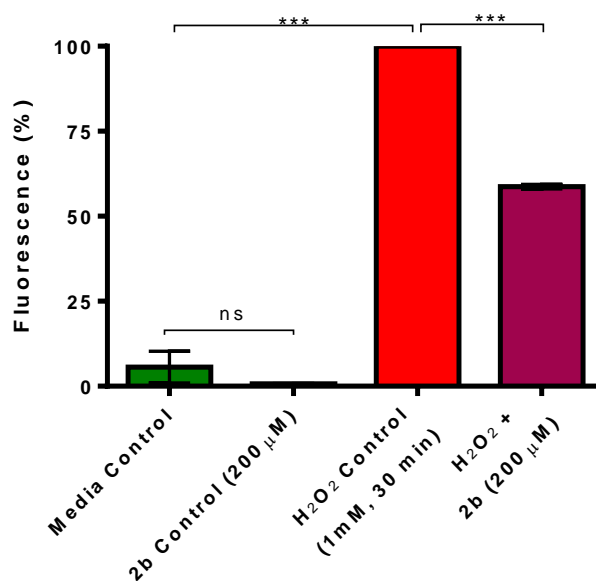


Figure 4.33. Protective effects of dimer **2b** against ROS production induced by hydrogen peroxide (1 mM, 30 mins). Statistically significant difference determined using One-way ANOVA. \*\*\* $p \leq 0.001$ , ns = not significant  $n = 3$ .

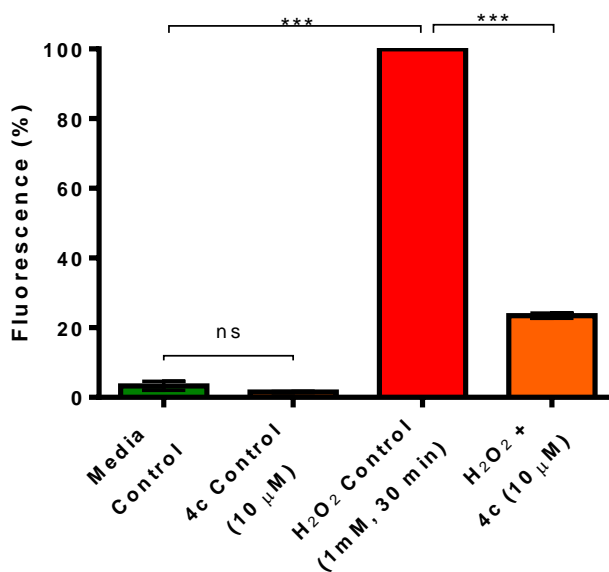


Figure 4.34. Protective effects of tetramer **4c** against ROS production induced by hydrogen peroxide (1 mM, 30 mins). Statistically significant difference determined using One-way ANOVA. \*\*\* $p \leq 0.001$ , ns = not significant  $n = 3$ .

As expected, dimer **2b** showed a modest ability to reduce the amount of ROS after hydrogen peroxide treatment with a decrease of fluorescence by 40% (see figure 4.34). In fact, the latter showed the weakest activity regarding the protective effects against hydrogen peroxide-induced insult. In contrast, tetramer **4c** remarkably reduced ROS formation by 76%,

confirming its strong protective properties in SH-SY5Y cells against oxidative insult induced by hydrogen peroxide (see figure 4.35).

Similar results were described by Kwon and co-workers when they studied the protective effects of loganin methyl ((1*S*,4*aS*,6*S*,7*R*,7*aS*)-6-hydroxy-7-methyl-1-(((2*S*,3*R*,4*S*,5*S*,6*R*)-3,4,5-trihydroxy-6-(hydroxymethyl)tetrahydro-2*H*-pyran-2-yl)oxy)-1,4*a*,5,6,7,7*a*-hexahydrocyclopenta[*c*]pyran-4-carboxylate) (figure 4.35), an iridoid glycoside found in *Flos Ionicerae*, *Fruit cornus* and *Strychnos nux vomica*, which turned out to alleviate ROS formation by 63% compared to the control at concentrations of 12.5  $\mu$ M (Kwon *et al.*, 2011).

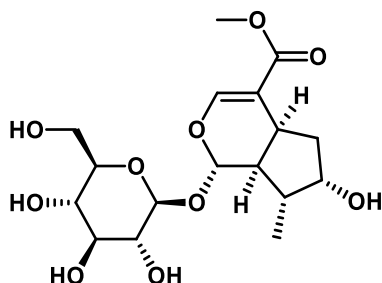


Figure 4.35. Chemical structure of glycoside loganin.

#### 4.4.5 DNA Comet Assay

The protective effects of selected vanillin derivatives toward pBR332 DNA plasmid against oxidative damage were described in the previous chapter. In particular, compounds **2b** and **4c** showed remarkable protective effects, with  $IC_{50}$  of 3.6 and 0.6  $\mu$ M, respectively (see table 3.4, page 123, chapter 3). To evaluate the ability of the latter to protect the nuclear DNA in SH-SY5Y cells against hydrogen peroxide-induced oxidative damage, the comet assay was employed.

The cells were incubated for 24 hours with the two vanillin derivatives at the same concentrations as before (200  $\mu$ M for **2b** and 10  $\mu$ M for **4c**) before the addition of hydrogen peroxide (300  $\mu$ M) for 30 minutes.

The scoring was performed according to Collins (Collins, 2004) on 100 comets in each of the three gels for each group (media control, compound

control, peroxide control and peroxide + compound group). An example of the comet classes obtained in the experiments is figure 4.36.

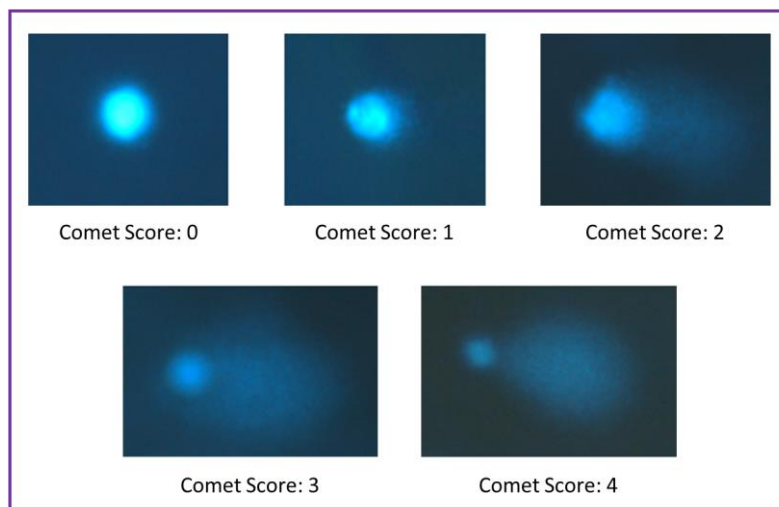


Figure 4.36. Comet classes (0-4) obtained in the comet assay. Leica DMRB microscope (100x) with Leica DFC 300FX camera (0.63x).

Both compounds tested did not show to have any impact on the DNA of SH-SY5Y cells as measured by the comet assay, since the arbitrary scores for media control, **2b** control and **4c** control were 11.4, 11.7 and 11.8 respectively (figure 4.37).

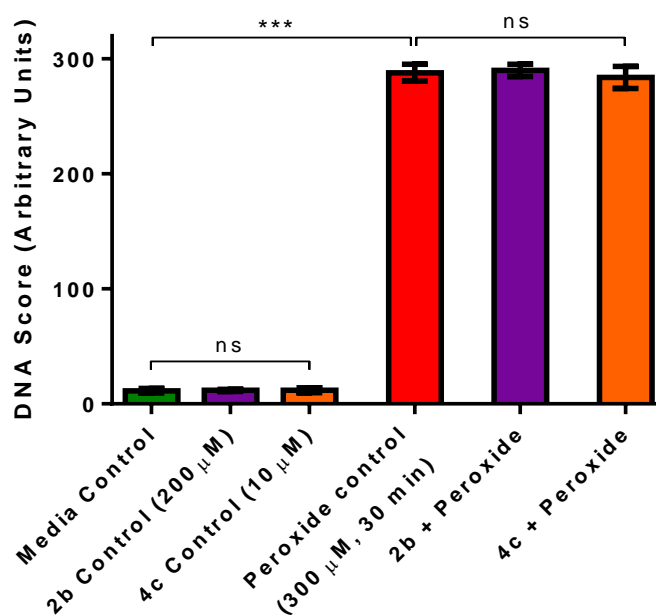


Figure 4.37. Cellular DNA protection from  $\text{H}_2\text{O}_2$ -induced (300  $\mu\text{M}$ ) DNA strand breaks after pre-treatment with **2b** (200  $\mu\text{M}$ ) or **4c** (10  $\mu\text{M}$ ) for 24 hours. Statistically significant difference using One-way ANOVA compared with peroxide control. \*\*\* $p \leq 0.001$ , ns = not significant,  $n = 3$ .

Treatment of cells with hydrogen peroxide (300  $\mu$ M for 30 minutes) caused a dramatic increase in DNA strand breaks, leading to an average arbitrary score of 287.9. Pre-treatment with dimer **2b** (200  $\mu$ M) or tetramer **4c** (10  $\mu$ M) did not cause a significant decrease in comet scoring (290.0 and 283.8 arbitrary units, respectively), highlighting the inability of the latter to protect nuclear DNA from the hydrogen peroxide-induced oxidative strand breakage.

The results obtained in the comet assay contrasts with the results obtained from the protection studies against hydrogen peroxide toxicity and the protective effects from ROS as described above, where both compounds showed significant protective effects. However, it is worth noting that the conditions employed to induce DNA damage did not show signs of cytotoxicity, when the cells were observed under the microscope after peroxide treatment. The lack of positive effects against DNA damage in this assay could depend on the fact that the DNA is located in the nucleus of the cells and the vanillin derivatives were unable to reach the relevant site of action. This could be further explained by the fact that both compounds showed remarkable protective effects on pBR332 plasmid DNA in a cell free system (table 3.4, page 123, chapter 3,).

#### *4.4.6 Evaluation of Nrf2 Pathway Activation*

Although vanillin derivatives showed strong antioxidant properties (see chapter 3), acting as free radical scavenger as well as reducing agents, their protective effects in cellular models could rely on more complex mechanisms. When working with antioxidants, the evaluation of the activation of the antioxidant responsive element (ARE) pathway (see pages 18-20, chapter 1) is a good starting point for studying the mechanism of the protective effects of synthetic and natural products. In order to explain the remarkable protective effects against oxidative stress in SH-SY5Y cellular model, the ability of tetramer **4c** to induce nuclear translocation of Nrf2 was evaluated using western blotting. The latter is a widely employed technique for the separation of proteins, based on their molecular weight, which consists of different steps (electrophoretic run, protein transfer into

membrane and protein detection with appropriate antibodies) (Kaur and Bachhawat, 2009; Mahmood and Yang, 2015).

Due to its relatively short half-life (approximately 20 minutes), the determination of nuclear Nrf2 is challenging and several attempts with different incubation times were made. The cells were incubated with the usual concentration of compound **4c** (10  $\mu$ M), which turned out to evoke the best protective effects against oxidative stress shown above.

The incubation times varied from 3 to 24 hours and the cells were collected, washed and the nuclear extraction was performed. 20  $\mu$ g of protein (quantified by Bradford assay) from each sample were loaded for the electrophoresis, then transferred into a PDVF membrane for the detection with the Nrf2 antibody (A-10, Santa Cruz Biotechnology).

The autoradiograph (figure 4.38) showed strong bands in the nuclear extracts (circled in red) at approximately 60 kDa, with minor intensity in the media control (0 hours) and increasing intensities moving from 3 to 6 and 24 hours incubation.

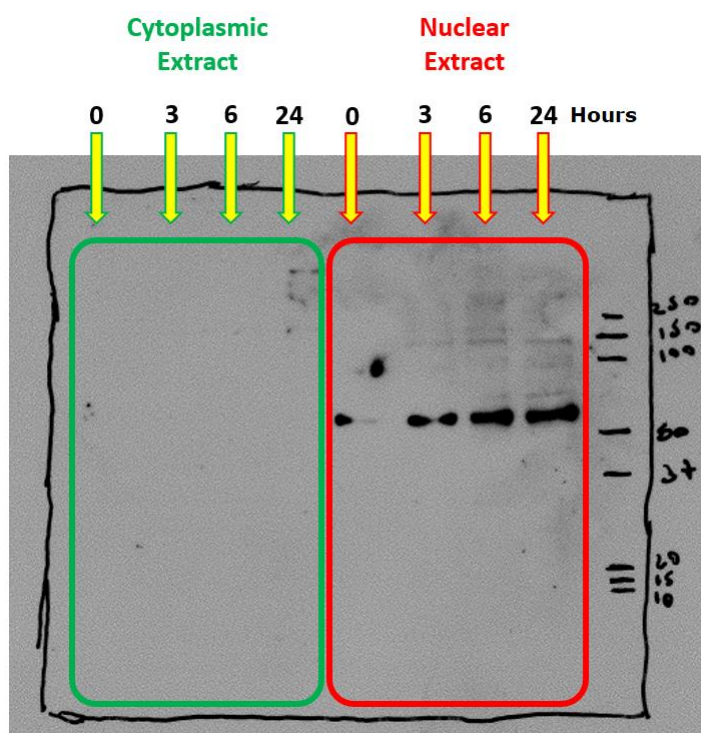


Figure 4.38. Western Blot for cytoplasmic (green) and nuclear (red) extracts after different time exposure of the cells to tetramer **4c**.

This may be related to the fact that longer exposure (*from 3 to 24 hours*) to **4c** increases the translocation of Nrf2 into the nucleus. However, no Nrf2 was detected in the cytoplasmic extracts (circled in green), which should show an inverted scenario in the case of pathway activation. In fact, a maximum amount of target protein should be detected in the media control and decreasing concentrations in the other cytoplasmic samples, due to the translocation into the nucleus. This could be due to ineffective inhibition of proteases during the extract preparation or the application of incorrect extraction process. In addition, although the molecular weight detected by the antibody (~60 kDa) has been reported as the molecular weight of the Nrf2 protein, this could be a misconception. In fact, Lau *et al.* reported the correct molecular weight for Nrf2 to be 95-110 kDa, claiming that antibody detecting molecular weight of approximately 60 kDa could not be specific for this protein and the manufacturing companies could even discard specific antibody detecting the correct molecular weight (Lau *et al.*, 2013).

Compound **4c** was then sent to Prof. Francesco Galli at university of Perugia, which I met at the 19<sup>TH</sup> SFRRRI conference in Lisbon (June 2018). Professor Galli and his co-worker Dr. Desiree Bartolini published several works on Nrf2 and its role in the antioxidant response to oxidative stress. In addition, they worked with the same cell line (SH-SY5Y) in the past.

The immunoblot performed by the Italian researchers involved protein quantification using BCA protein assay kit (Pierce, Thermo Scientific.) followed by denaturation of the proteins, electrophoresis thorough 10% SDS-PAGE and transfer into nitrocellulose membrane. The membrane was blocked in phosphate-buffered saline (PBS) containing 5% non-fat milk for 1 h at room temperature. It was subsequently incubated with anti-Nrf2 antibody (dilution 1:1,000; Cell Signaling) at 4°C overnight, followed by washing and treatment with HRP-labeled secondary antibody (1:2000; Cell Signaling) for 2 h at room temperature. The blots were incubated with ECL reagent for 5 min, and the signals were then detected with a chemiluminescence detection system (Bio-Rad). After stripping, the membrane was re-probed with human anti- $\alpha$ -Tubulin (1:1000; Cell Signaling) or Histone H3 (1:2000; Cell Signaling) antibodies as a control for equal protein loading and protein integrity.

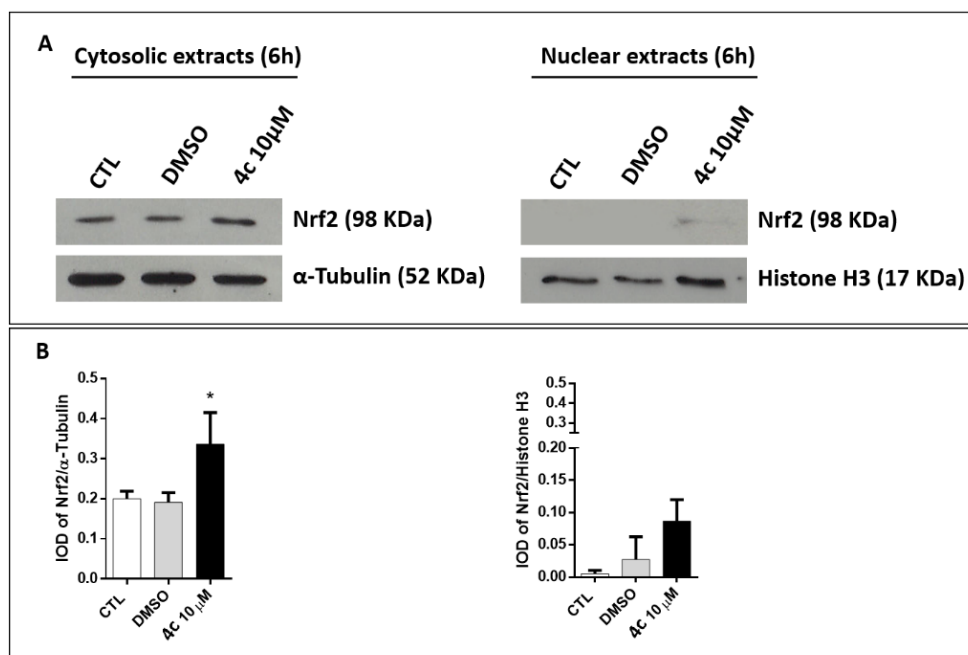


Figure 4.39. A) Representative western blot analysis performed by Prof. Galli and co-workers at the University of Perugia showing Nrf2 expression in SH-SY5Y cells after treatment with compound **4c** (10  $\mu$ M). B) Densitometry for the WB analysis. Data represent the means  $\pm$  SD of 3 experiments (\* $p$ <0.05, compared with the control group).

The results obtained by the colleagues in Perugia showed a significant increase in the cytosolic Nrf2 expression after treatment of the cells with compound **4c** (10  $\mu$ M) for 6 hours (see figure 4.39 A). However, no significant increase of the latter protein was detected in the nucleus, highlighting the inability of the vanillin derivative to induce Nrf2 nuclear translocation (see figure 4.39 B).

Bryan *et al.* recently reported the major classes of Nrf2 inducers. Among them, molecules bearing oxidizable diphenols, such as *tert*-Butylhydroquinone (*t*BHQ) or resveratrol, Michael reaction acceptors, such as curcumin, thiocarbamates, isothiocyanates, such as sulforaphane, dithiolethiones, hydroperoxides, heavy metals and arsenic turned out to be potent Nrf2 activators (see figure 4.40) (Bryan *et al.*, 2013).

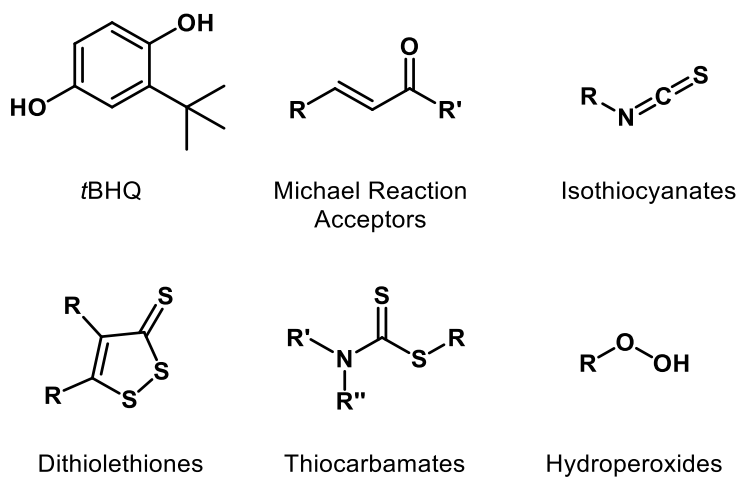


Figure 4.40. Examples of known Nrf2 activator.

It is evident that tetramer **4c** does not bear any resemblance of the latter structures; this could explain the inability of this vanillin derivative to activate Nrf2 pathway.

## 4.5 Conclusions

A selection of vanillin derivatives, based on their antioxidant properties (described in chapter 3) and their cholinesterase and amyloid aggregation inhibitory properties (which will be described in the next chapter), were tested for their neuroprotective effects in two different oxidative stress models, i.e. hydrogen peroxide or a mixture of rotenone/oligomycin A as stressors.

Before testing the selected compounds (**1f**, **2b** and **4c**) for their protective effects in these oxidative stress models, preliminary tests for the determination of cytotoxic effects towards SH-SY5Y cells were performed. Dimer **2b** turned out to be the least toxic vanillin derivative, with a  $LC_{50}$  above 1 mM. On the other hand, both **1f** and **4c** showed much higher toxicity, with  $LC_{50}$ s of 43.7 and 45.1  $\mu$ M, respectively. Although the latter compounds showed similar  $LC_{50}$ s, monomer **1f** displayed significant cytotoxic effects at concentrations of 25  $\mu$ M, decreasing the cell viability by almost 40% compared to the control, whereas tetramer **4c** turned out to be safe at that concentration. Hence, the decision to work with lower maximum concentration of **1f** compared to **4c**. All the compounds tested showed concentration-dependent protective effects against hydrogen peroxide (400  $\mu$ M) toxicity in SH-SY5Y cells, with the highest protection detected at the highest concentrations tested (5  $\mu$ M for **1f**, 200  $\mu$ M for **2b** and 10  $\mu$ M for **4c**). In addition, the latter showed significant protection at concentration of 1, 5 and 0.1  $\mu$ M, respectively. It is worth noting that vanillin did not show protective effects in this experiment at concentration as high as 800  $\mu$ M. However, only tetramer **4c** displayed protective effects on SH-SY5Y cells from rotenone/oligomycin cocktail-induced toxicity, increasing the cell viability at concentration as low as 5  $\mu$ M. Monomer **1f**, dimer **2b** and vanillin did not show significant protective effects at any concentration tested. Furthermore, both the vanillin derivatives tested (**2b** and **4c**) showed a reduction in ROS within the cells, compared to the control, after treatment with hydrogen peroxide (1 mM for 30 minutes). As expected, tetramer **4c** displayed the best alleviating properties in this assay, reducing the ROS by 76% compared to the control, whereas the dimer **2b** exerted more modest activity, decreasing the ROS production by 40%. Unfortunately, due to

instrumental issues, it was not possible to test the monomer **1f** for its protective effects against hydrogen peroxide-induced ROS formation.

On the other hand, no positive effects against hydrogen peroxide-induced DNA damage were determined in the comet assay, where both the vanillin derivatives tested (**2b** and **4c**) did not show significant reduction of DNA strand breaks compared to the peroxide control. It is worth noting that the compounds showed no increase in DNA damage compared to the media control, displaying no toxicity toward the nuclear DNA within the cells.

Finally, in order to explain the interesting protective effects of tetramer **4c** in the two oxidative stress models, the latter was tested for its ability to trigger the Nrf2 nuclear translocation, inducing the expression of critical antioxidant enzymes. The results obtained through western blotting experiment were contrasting. A time-dependent exposure increase of nuclear Nrf2 (with a maximum concentration after 24 hours of pre-treatment with the compound) compared to the untreated control was detected; however, the molecular weight of the protein detected by the antibody (approximately 60 kDa) was not associated with the correct molecular weight of the biological relevant protein (95-110 kDa), showing non-specific binding properties of the antibody employed for the western blotting.

The studies performed by Prof. Galli and co-workers at University of Perugia showed a significant increase of Nrf2 expression in the cytosol following exposure of the cells with compound **4c** (10  $\mu$ M). However, no nuclear translocation was detected at this time point.

These results highlight the inability of compound **4c** to trigger the Nrf2 pathway.

At this stage, no conclusions can be drawn regarding the mechanism of the cellular benefits of compound **4c**. The increased expression of Nrf2 in the cytosol could be counterbalanced by an increased expression of Keap1, which is involved in Nrf2 ubiquitination and degradation, thus avoiding the nuclear translocation of the latter protein (Tonelli, Chio and Tuveson, 2017).

Further studies are needed in order to establish the molecular pathways behind the protective effects of these vanillin derivatives.

The interesting neuroprotective effects of selected compounds in the cellular model described in this chapter can represent a valid starting point for their potential use in the treatment of neurodegenerative diseases such as Parkinson's and Alzheimer's Diseases, where oxidative stress and neuronal death is one of the hallmarks.

The potential application of vanillin derivatives in AD will be described in chapter 5.

# **Chapter 5: Vanillin Derivatives as Multi-Target-Directed Ligands for Alzheimer's Disease**

## 5.1. Introduction

### 5.1.1 An Overview on Neurodegeneration

As described in the previous chapters, oxidative stress is strongly linked with cellular damage, due to the ability of ROS and RNS to react with biological structures such as lipids, proteins and DNA (Sies, 1991, 2015).

Neuronal cells are very susceptible to oxidative damage due to low levels of enzymatic and non-enzymatic antioxidants (superoxide dismutase, catalase, glutathione), high metabolic activity and high levels of lipids susceptible to oxidation such as polyunsaturated fatty acids (Ahmed *et al.*, 2015).

Oxidative stress in neurons can lead to the gradual and progressive loss of neuronal cells which is known as neurodegenerative process (Brown, Lockwood and Sonawane, 2005).

In addition, specific regions in the nervous system have been reported to be vulnerable to oxidative damage; for example, the dopaminergic neurons of the *substantia nigra* are involved in the neurodegeneration that underpins Parkinson's disease, whereas the neurodegeneration of cholinergic neurons in the basal forebrain is involved in Alzheimer's disease (Ahmed *et al.*, 2015).

For the purpose of this chapter, only the neurodegenerative process involved in AD will be further discussed.

### 5.1.2 Alzheimer's Disease as a Multifactorial Disorder

AD is the most common cause of dementia among the elderly people and it is characterized by progressive neurodegenerative alterations with consequent reductions in cognitive and functional abilities, including aphasia (language disturbance), agnosia (failure in people recognition), apraxia (movement impairment) and executive functions (e.g. planning and organization) (Brown, Lockwood and Sonawane, 2005; Mecocci and Polidori, 2012).

The symptoms of AD vary among individuals. It usually starts with a gradual worsening ability to remember new information and it proceeds with memory loss, confusion with space and time, communication issues and changes in mood. With disease advancement, cognitive and functional abilities tend to decline, causing an inability to move and to recognize family members (Alzheimer's Association, 2015).

In the UK, the number of people suffering for dementia was estimated to be slightly more than 800000 in 2013, of whom almost 775000 were aged 65 years or over. In addition, due to increased life expectancy, this number is predicted to be over 2 million in 2051, with 62% of the incidence predicted to be AD related, followed by vascular dementia (17%) and mixed dementia (10%) (Prince *et al.*, 2014).

AD was first diagnosed by Alois Alzheimer in 1907, when he noted the occurrence of neuritic plaques and neurofibrillary tangles (NFTs) in the cerebral cortex during the autopsy of a 56-year old woman with dementia (Carreiras *et al.*, 2013). Subsequently, Perry *et al.* reported the depletion of the neurotransmitter acetylcholine, which is involved in cognition and attention, in the brain of AD patients (Perry *et al.*, 1978).

The main hallmark of AD is the abnormal aggregation of harmful proteins, with the A $\beta$  ( $\beta$ -amyloid) peptide and tau protein the most common, leading to amyloid plaques and NFTs, respectively, which are toxic to the neuronal cells (Hurtado-Puerto, Russo and Fregni, 2018; Iaccarino *et al.*, 2018).

The main constituent of the amyloid plaques is the  $\beta$ -amyloid peptide (A $\beta$ ); However, they may contain other proteins (e.g. acetyl and butyryl cholinesterases, superoxide dismutases) and metal ions such as copper and zinc (Lovell *et al.*, 1998; Atwood *et al.*, 2002). The latter peptide is a 38-43 amino acid residues, with the code sequence Asp-Ala-Glu-Phe-Arg-His-Asp-Ser-Gly-Tyr-Glu-Val-His-His-Gln-Lys-Leu-Val-Phe-Phe-Ala-Glu-Asp-Val-Gly-Ser-Asn-Lys-Gly-Ala-Ile-Ile-Gly-Leu-Met-Val-Gly-Gly-Val-Val-Ile-Ala-Thr. It is generated through enzymatic cleavage by  $\beta$ - and  $\gamma$ - secretase of the amyloid precursor protein (APP), a type-1 trans-membrane protein widely expressed in the central nervous system (Cheignon *et al.*, 2018). The

physiological role of APP is not fully understood, but it is linked to beneficial effects on neurons, including promotion of neurite outgrowth, synaptogenesis and cell adhesion while also protecting the cells against oxygen-glucose deprivation and excitotoxicity through inhibition of calcium currents (Chow *et al.*, 2010). The metabolism of APP can follow two different pathways, known as amyloidogenic and non-amyloidogenic pathways (see figure 5.1).

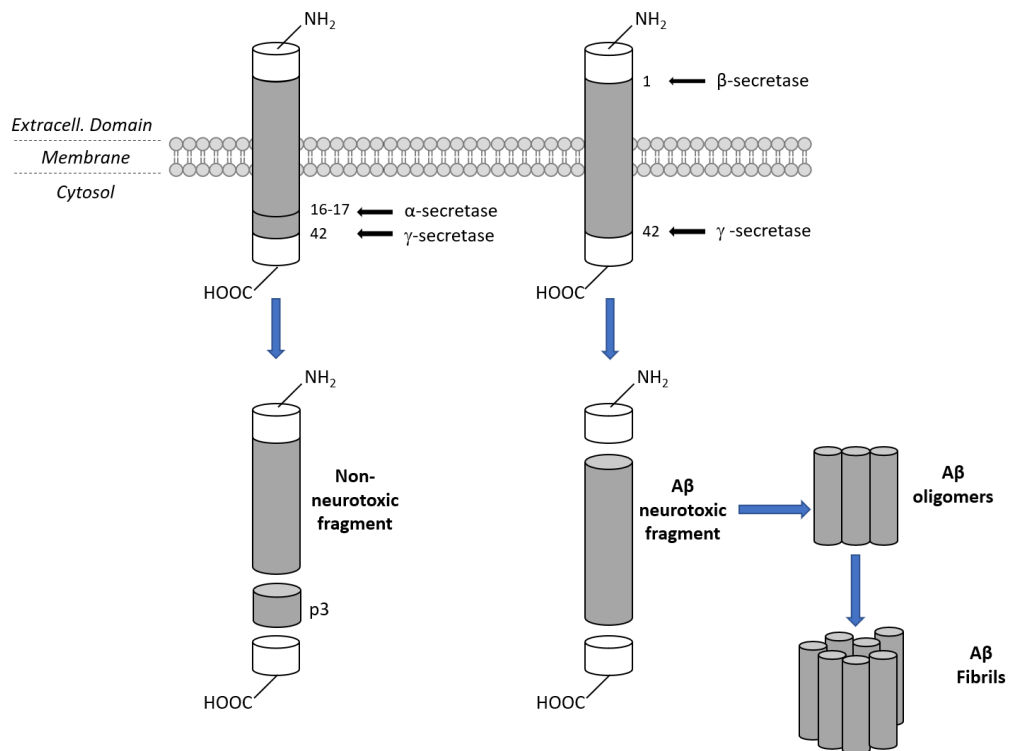


Figure 5.1. APP cleavage in the non-amyloidogenic and amyloidogenic pathways, altered from (Munoz and Feldman, 2000; Bachurin, Bovina and Ustyugov, 2017; Cheignon *et al.*, 2018).

In the normal non-amyloidogenic pathway, APP is cleaved by  $\alpha$ -secretase followed by  $\gamma$ -secretase, yielding the non-toxic truncated (p3) peptide. In the amyloidogenic pathway, APP is cleaved by  $\beta$ -secretase followed by  $\gamma$ -secretase, yielding the full length amyloid peptides, mainly  $A\beta_{(1-40)}$  and  $A\beta_{(1-42)}$  (Nalivaeva and Turner, 2013). It is worth noting that these two amyloid fragments exert different toxicities: the  $A\beta_{(1-42)}$  form promotes greater fibrillar formation compared to  $A\beta_{(1-40)}$ , due to the presence of two extra hydrophobic amino acids (isoleucine and valine), hence showing higher toxicity (Butterfield, Swomley and Sultana, 2013). The fibrillar formation is the result of an aggregation process which involves the sequential aggregation of the monomers into oligomers followed by mature fibrils

formation (Verma, Vats and Taneja, 2015). Very recently, it has been proposed that although amyloid plaques are strictly related to AD, the oligomers are the main contributor to the neurotoxicity (Verma, Vats and Taneja, 2015). He *et al.* demonstrated that oligomeric amyloid infused into the left ventricles of rat brains displayed significant impairment of learning and memory functions whereas no significant effects were observed after fibrils infusion (He *et al.*, 2012). The toxicity of oligomers relies on their ability to insert themselves in the bilayer of the membrane in neuronal cells and the generation of ROS leads to lipid peroxidation (Butterfield, Swomley and Sultana, 2013).

The aggregation of tau protein in NFTs is another hallmark of AD. Tau protein belongs to the family of microtubule-associated proteins (MAP) family, with MAP1 (A and B) and MAP2 the most common, and is mostly expressed in neuronal cells where it is involved in the assembly and stabilization of microtubules (Buée *et al.*, 2000; Iqbal *et al.*, 2005).

The binding of tau protein to microtubules is modulated by phosphorylation. For optimal activity, tau contains 2-3 mol of phosphate/mol of protein; once hyperphosphorylated, it loses its affinity for microtubules, leading to the loss of structural integrity in the neurons with consequent impairment of normal cellular trafficking and possible neuron death (Iqbal *et al.*, 2005; Tramutola *et al.*, 2017).

A couple of decades ago, Bramblett *et al.* located the residue, SER-396, as the possible site on tau protein where abnormal phosphorylation occurred, hence contributing to the loss of affinity for microtubules (Bramblett *et al.*, 1993).

In addition, hyperphosphorylated tau protein tends to aggregate as paired helical filaments (PHF), leading to the NFTs (Iqbal *et al.*, 2005); however, the exact mechanism of aggregation is still under investigation. Tau hyperphosphorylation and the subsequent NFT formation can induce neurodegeneration in the absence of other brain amyloids, for example in other tauopathies such as Pick's disease and Guadeloupean Parkinsonism. This led to the hypothesis that tau plays a role in the final, shared pathway leading to neuronal death or dysfunction, which can be triggered by other events (Skovronsky, Lee and Trojanowski, 2006; Williams, 2006).

Along with abnormal protein aggregation, oxidative stress, disturbed metal homeostasis and cholinergic neurons depletion are the main hallmarks of AD.

As described before, oxidative stress is strictly linked with amyloid oligomers, which are able to generate ROS in the membrane of neuronal cells (Uttara *et al.*, 2009; Butterfield, Swomley and Sultana, 2013). It is worth noting that neuronal cells are very susceptible to oxidative stress due to low levels of enzymatic and non-enzymatic antioxidants (Ahmed *et al.*, 2015).

Homeostasis of zinc, copper and iron are significantly altered in the AD brain tissue; for example, abnormal levels of the latter metals have been found in subcortical regions such as the hippocampus, amygdala, and olfactory bulb, as well as the neocortex (Cuajungco *et al.*, 2006). In addition, these redox-active metals are known to contribute to the misfolding and aggregation of amyloid proteins and are found in high concentrations in amyloid plaques of AD patients (Picciano and Vaden, 2013).

Moreover, the link between transition metals and oxidative stress, through Fenton reaction, has been widely discussed in the first chapter (see equations 7 and 11, pages 6-7, chapter 1).

The depletion of cholinergic neurons in the basal forebrain is one of the earliest hallmarks of AD observed in post-mortem brains although cholinergic transmission was unaffected in other brain regions such as the ganglia, cerebellum and thalamus (Parent *et al.*, 2013). Cholinergic neurons use the neurotransmitter, acetylcholine (ACh) (see figure 5.2), and contain the acetyltransferase enzyme which, along with acetylcholine transporter, is found in the presynaptic component of the cholinergic pathway (Mesulam, 2004).

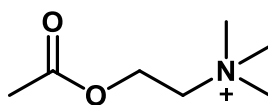


Figure 5.2. Chemical structure of acetylcholine

The postsynaptic components in the cholinergic pathway consist in nicotinic and muscarinic receptors, which are able to bind acetylcholine molecules. Nicotinic channels are a family of ligand-gated ion channels (Gotti and Clementi, 2004), whereas muscarinic receptors are G-protein coupled receptors involved in the second messenger cascade (Caulfield, 1993). The interaction of acetylcholine with the latter receptors is strongly involved in memory and learning processes as well as muscle activation (Caulfield, 1993; Gotti and Clementi, 2004; Hasselmo, 2006). The termination of the synaptic action of ACh is achieved through its catalytic hydrolysis by cholinesterases enzymes, such as acetylcholinesterase (AChE) and butyrylcholinesterase (BChE). The evident depletion of cholinergic neurons in AD is thus strongly linked with memory loss and cognitive and behavioural impairment (Mesulam, 2004).

### *5.1.3 Current Therapies for AD*

At present, no cures are available for AD; however, several symptomatic treatments are available for AD patients.

The application of cholinesterase inhibitors aims to increase the availability of acetylcholine in the basal forebrain by inhibiting the hydrolysis of the latter neurotransmitter mediated by acetylcholinesterase. Three AChE inhibitors are currently used in AD therapy: galantamine ((4a*S*,6*R*,8a*S*)-3-methoxy-11-methyl-4a,5,9,10,11,12-hexahydro-6H-benzo[2,3]benzofuro[4,3-*cd*]azepin-6-ol), rivastigmine ((*S*)-3-(1-(dimethylamino)ethyl)phenyl ethyl(methyl)carbamate) and donepezil (2-((1-benzylpiperidin-4-yl)methyl)-5,6-dimethoxy-2,3-dihydro-1H-inden-1-one) (see figure 5.3) (Yiannopoulou and Papageorgiou, 2013). For the purpose of this thesis, it is also worth mentioning tacrine, the first AChE inhibitor approved for AD treatment and later discontinued due to liver toxicity (Crismon, 1994; Watkins *et al.*, 1994; Mehta, Adem and Sabbagh, 2012).

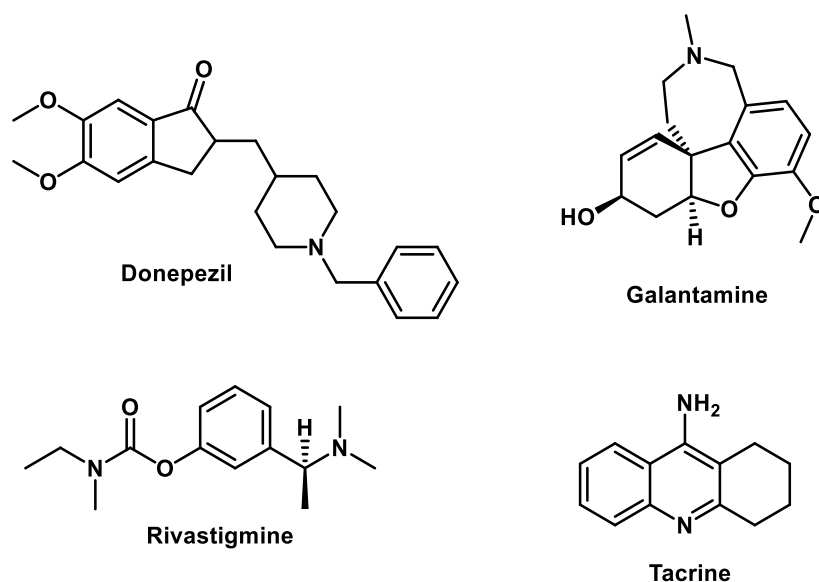


Figure 5.3. Chemical structures of current AChE inhibitors for AD treatment (donepezil, galantamine and rivastigmine) and the discontinued tacrine.

The only drug currently used for AD therapy not belonging to AChE inhibitors is memantine (3,5-dimethyladamantan-1-amine) (see figure 5.4), which is a *N*-methyl-*D*-aspartate (NMDA) receptor antagonist (Witt, Macdonald and Kirkpatrick, 2004).

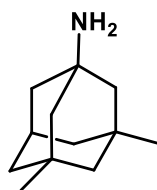


Figure 5.4. Chemical structure of memantine.

NMDA receptors are neuronal ligand-gated ion channels that bind to glutamate, the main excitatory neurotransmitter in the central nervous system, and allow the entrance of calcium ions. NMDA receptors are involved in learning and memory, but their overactivation due to increased glutamate release leads to excessive calcium entry, activating neuronal death, a phenomenon known as 'excitotoxicity' (Rothman and Olney, 1987; Witt, Macdonald and Kirkpatrick, 2004).

#### 5.1.4 AD Drug Development

Therapies for AD are urgently needed due to the large increase in individuals suffering from this illness. To date, 112 agents are in clinical

trials with 23 agents in 25 trials in phase I, 63 agents in 75 trials in phase II and 26 agents in 35 trials in phase III (Cummings *et al.*, 2018). Among the agents in phase III trials, 17 are disease-modifying therapies (DMTs) that should prevent or delay the onset or slow the progression of AD; one is a cognitive enhancer and 8 are targeting behavioural symptoms. Interestingly, among the 17 DMTs, 14 address amyloid targets (mainly in the form of immunotherapies), whereas only one is targeted at tau-related, neuroprotection or metabolic mechanisms (Cummings *et al.*, 2018). The cognitive enhancer is a cholinesterase inhibitor (octohydroaminoacridine succinate, known as NCT03283059), whereas the 8 agents addressing behavioural symptoms target agitation, sleep disorders and apathy (Cummings *et al.*, 2018).

#### 5.1.5 The Multi-Target-Directed Ligands Approach to AD

Due to the multiple factors involved in the physiopathology of AD, the drug development based on a “one target-one molecule” point of view is no longer preferred (Cavalli *et al.*, 2008). Recently, therefore, a multi-targeted approach, aimed at different steps of the neurotoxic cascade, has attracted much research attention on neurodegenerative diseases, such as AD (Singh *et al.*, 2016). In chapter 1 (pages 35-39), examples of multi-target-directed ligands (MTDLs) for AD treatment have been described.

The main targets of the multi-targeted-directed AD therapy are: cholinesterases (acetyl and butyryl), monoaminoxidases (in particular, MAO-B),  $\beta$ -Secretase (BACE), amyloid aggregation, metal chelation (in particular,  $Zn^{2+}$  and  $Cu^{2+}$ ), calcium channels. In addition, due the role of oxidative stress in AD, the presence of antioxidant moieties such as melatonin and lipoic acid in the MTDLs have been favoured (Cavalli *et al.*, 2008; Bajda *et al.*, 2011; Singh *et al.*, 2016; Sameem *et al.*, 2017).

For the purpose of this thesis, the antioxidant properties, the cholinesterase enzymes and amyloid aggregation process are the targets investigated for the potential use of selected vanillin derivatives in the multi-targeted-directed approach to AD.

The antioxidant properties of the vanillin derivatives have been described in chapter 3.

The amyloid aggregation pathway and cholinesterase enzyme have been described earlier in this chapter. However, the structural features of the AChE need to be described here in order to appreciate the evaluation of the molecular modelling results.

#### 5.1.5.1 AChE, a "Gorge-ous Enzyme"

As previously described, the cholinesterases are primarily responsible of the hydrolysis of the neurotransmitter acetylcholine into choline and acetic acid (Mesulam, 2004).

Vertebrates possess two cholinesterases: acetylcholinesterase and butyrylcholinesterase (also known as pseudocholinesterase). These enzymes are distinguished on their substrate specificity; AChE degrades the acetylcholine faster than other enzymes and it shows low affinity for the synthetic butyrylcholine, whereas BChE is able to hydrolyse both the choline esters (Massoulié *et al.*, 1993). In addition, AChE is mainly expressed in the nervous system and in muscles whereas BChE is mostly located in the liver and in the plasma (Massoulié *et al.*, 1993). In healthy brains, acetylcholinesterase predominates with BChE playing a minor role in regulating AChE levels (Greig, Lahiri and Sambamurti, 2002). However, it has been shown that during progression of AD, the activity of AChE remains unchanged or slightly decreases, whereas the activity of BChE significantly increases. Thus both the enzymes represent legitimate therapeutic targets in AD therapy (Greig, Lahiri and Sambamurti, 2002; Panek *et al.*, 2017).

AChE molecule has an ellipsoidal shape with dimensions approximately 45 Å x 60 Å x 65 Å; the monomer contains 12 stranded central mixed β sheet surrounded by 14 α helices (Colovic *et al.*, 2013).

The active site (see figure 5.5) lies at the bottom of a 20 Å deep gorge and it is characterized by the presence of the esteratic site, composed by the three residues SER-200, GLU-327 and HIS-440, involved in the hydrolysis of acetylcholine, and a catalytic anionic site (CAS), characterized by the presence of TRP-84, TYR-130, PHE-330 and PHE-331. TRP-84 plays a

fundamental role, binding with the acetylcholine molecule through a cation- $\pi$  interaction with its positive quaternary nitrogen (Xu *et al.*, 2008; Dvir *et al.*, 2010; Bajda *et al.*, 2013).

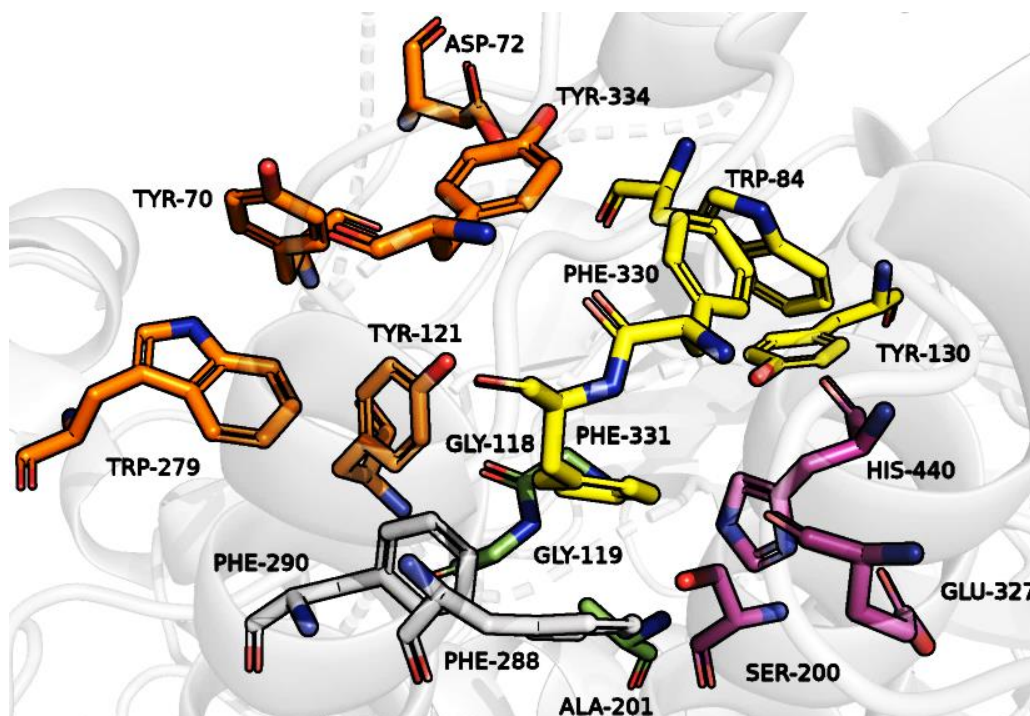


Figure 5.5. Active site of *TcAChE* (pdb:1EVE) (Kryger, Silman and Sussman, 1999). The residues are rendered accordingly to their positions. Esteratic site: purple, CAS: yellow, Acyl Pocket: grey, Oxyanion Hole: green and PAS: orange.

The peripheral anionic site (PAS) lies at the top of the gorge, approximately 20 Å above the active site. The PAS is involved in the sequestration of acetylcholine at the first step of the catalytic pathway through cation- $\pi$  interaction with TRP-279. It is composed of other residues such as TYR-70, ASP-72, TYR-121 and TYR-334 (Johnson and Moore, 2006). In addition, the peripheral anionic site is strongly involved in the selectivity of cholinesterase inhibitors. In fact, the selectivity of AChE inhibitors such as donepezil is due to their ability to bind TRP-279 in the PAS since the latter site is not present in BChE; on the other hand, inhibitors such as tacrine and eptastigmine, which bind the esteratic site and CAS are not selective for AChE (M., 1999).

PHE-288 and PHE-290 comprise the acyl pocket, preventing the access of hindered molecule into the active site whereas the oxyanion hole, composed by GLY-118, GLY-119 and ALA-201 is involved in the stabilization of the

transition complex during the enzymatic reaction (Bajda *et al.*, 2013; Colovic *et al.*, 2013) (see figure 5.6).

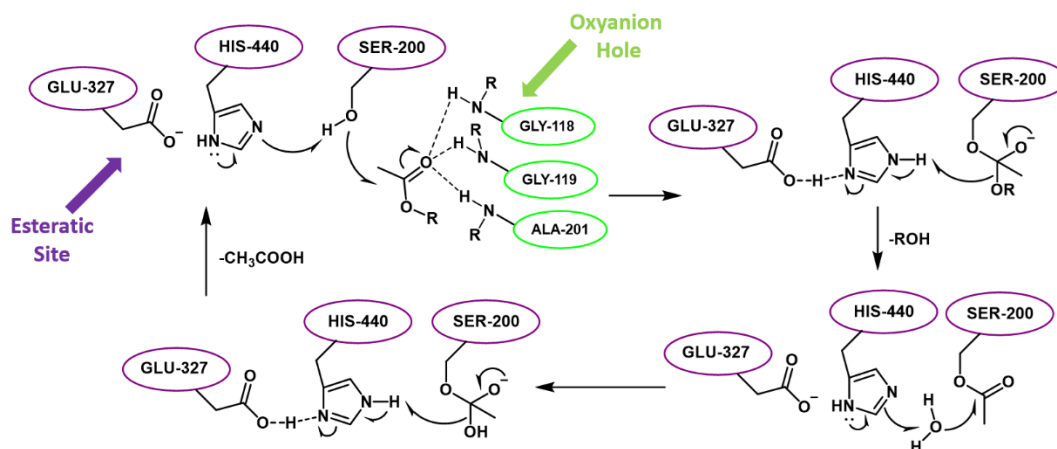


Figure 5.6. Mechanism of acetylcholine hydrolysis catalysed by AChE, altered from (Houghton, Ren and Howes, 2006; Colovic *et al.*, 2013).

The 3D structure of AChE is highly conserved, although the sequence can vary among species (Wiesner *et al.*, 2007; Colovic *et al.*, 2013).

#### 5.1.5.2 Assays for the Determination of AChE Activity

The inhibitory activity toward AChE is the main feature of many multi-target-directed ligands for AD treatment (Rosini *et al.*, 2008; Bolognesi *et al.*, 2010; Chen *et al.*, 2014; Liu *et al.*, 2015; Mohamed and Rao, 2017; Sameem *et al.*, 2017; Yang *et al.*, 2017) and several technologies and assays are available for the determination of AChE activity.

The Ellman assay is one of the most employed *in vitro* assays for this purpose. It was developed by George L. Ellman and co-workers in the early 1960s and it is based on the AChE-catalysed hydrolysis of acetylthiocholine into thiocholine, which can be oxidized by 5,5'-dithiobis-(2-nitrobenzoic acid) (DTNB) to yield the yellow 5-thio-2-nitrobenzoate. The latter has a maximum absorption at 412 nm and can be measured spectrophotometrically (Ellman *et al.*, 1961; Worek, Eyer and Thiermann, 2012). A schematic of the mechanism is depicted in figure 5.7.

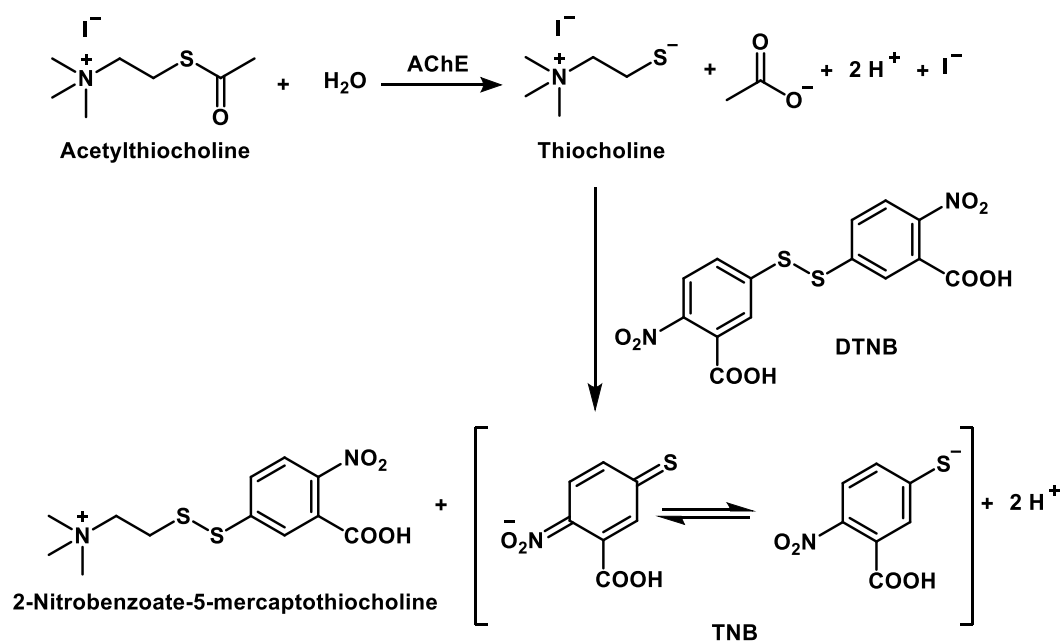


Figure 5.7. Mechanism of Ellman assay for the determination of AChE inhibition, altered from (Worek, Eyer and Thiermann, 2012; Badawy and El-Aswad, 2014).

In addition to the Ellman assay, fluorescent methods involving different probes have been developed.

The Amplex<sup>®</sup> Red Acetylcholine/Acetylcholinesterase assay kit is a fluorescent method for the evaluation of AChE inhibition based on the use of 10-acetyl-3,7-dihydroxyphenoxazine. In this assay, the choline obtained through the AChE-catalysed hydrolysis of acetylcholine chloride is oxidised into a betaine with the generation of hydrogen peroxide as a by-product. The latter can be quantified by its reaction with 10-acetyl-3,7-dihydroxyphenoxazine (1:1 stoichiometry) in the presence of a horseradish peroxidase to yield the fluorescent resorufin ( $\lambda_{\text{Ex}}$ : 571 nm,  $\lambda_{\text{Em}}$ : 585 nm) (Molecular Probes Invitrogen detection technologies, 2004).

Recently, continuous fluorometric assays for AChE activity and its inhibition involving the use of different polymers as fluorescent probes have been developed (Feng *et al.*, 2007; Wang *et al.*, 2009). The main advantage in using these organic compounds is the amplified fluorescence signal obtained due to the excitation energy transfer of the conjugated polymer compared to the small molecules usually employed in the bioassays (Feng *et al.*, 2007). However, no kits employing this technology are commercially available.

### 5.1.5.3 Measurement of Amyloid Aggregation

A very common feature of MTDLs for AD therapy is the inhibitory activity toward amyloid protein aggregation, which drives many of the toxic effects exerted in the neurons (Luo *et al.*, 2011; Chao *et al.*, 2012; Li *et al.*, 2014; Zha *et al.*, 2016; Panek *et al.*, 2018).

A wide variety of techniques are currently available for the evaluation of protein aggregation in the biotechnology industry, such as field flow fractionation, analytical ultracentrifugation, size-exclusion chromatography and dynamic light scattering (Pease *et al.*, 2008).

A simple method for this purpose involves the use of the amyloid indicator thioflavin T (4-(3,6-dimethyl-1,3-benzothiazol-3-ium-2-yl)-*N,N*-dimethylaniline chloride) (ThT). The latter (see figure 5.8) is a benzothiazole dye that is able to bind  $\beta$ -sheet rich proteins generating a fluorescence signal ( $\lambda$  Ex: 450 nm,  $\lambda$  Em: 482 nm) (Wolfe *et al.*, 2010).

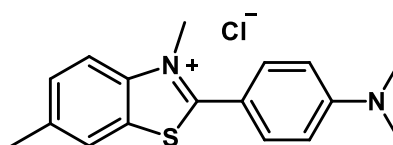


Figure 5.8. Chemical structure of Thioflavin T.

Despite its predominant use in AD research, the molecular mechanism of the ThT binding to aggregated amyloid protein is not fully understood.

Modelling studies led to the hypothesis of stacking interactions between the aniline moiety of thioflavin T and the peptide bone and CH- $\pi$  interaction between the GLY residue in the model peptide and the benzothiazole moiety; the decreased torsional relaxation upon binding is linked to the enhanced fluorescence properties (Rodriguez-Rodriguez *et al.*, 2010).

In addition, the crystal structure of amyloid-like protein in complex with the latter benzothiazole, showed that the intercalation of ThT between  $\beta$ -sheets orthogonal to the  $\beta$ -strands, with aromatic interactions to stabilize the electronic distribution of fluorophore. Thus,  $\beta$ -sheet conformations prevent

the preferred excited state configuration of ThT, hence increasing the quantum yield (Wolfe *et al.*, 2010; Wang *et al.*, 2012).

#### 5.1.5.4 Measurement of Drug Blood-brain Barrier (BBB) Permeation

The failure of many drugs targeting neurodegenerative diseases is often linked with their inability to cross the blood-brain barrier (BBB) (Pardridge, 2003). The BBB relates to the microvasculature of the central nervous system (CNS) composed of continuous non-fenestrated vessels that allows tight regulation of the movement of ions, molecules and cells. This selective regulation is mediated by the endothelial cells in the CNS held together by tight junctions, which limit the flux of solutes in the brain (Daneman and Prat, 2015).

Almost 100% of large molecules drugs (>500 Da) and 98% of small molecules (<500 Da) do not cross the BBB. In addition, although small molecules can cross the BBB, only a low percentage can penetrate in pharmacologically relevant concentrations. Molecules that cross the BBB are typically lipid soluble with a threshold mass of 400-500 Da and show the ability to establish a low number of hydrogen bonds with water (Pardridge, 2003). However, several transporters or endocytosis mechanisms are used by hydrophilic compounds such as amino acids, monocarboxylic acids, organic cations, sugars and peptides to penetrate the BBB. Drugs such as L-dopa for PD treatment and the opioid, fentanyl, have been reported to employ these transporters to cross the BBB (Tamai and Tsuji, 2000).

Recent research has focused on the development of novel CNS drug delivery technologies, such as polymeric nanoparticles, BBB selective disruption techniques (ultrasound, microbubbles, electromagnetic waves), cell mediated delivery and viral vectors (Spencer and Verma, 2007; Pandey, Sharma and Gupta, 2016).

When undertaking neurodegenerative research, several *in vitro* methods and computational models are available for the prediction of drug BBB permeation such as *logP/logD*, immobilized artificial membrane, polar surface area, membrane permeability across cell culture systems and

parallel artificial membrane permeation assay (PAMPA) (Kansy, Senner and Gubernator, 1998; Di *et al.*, 2003).

For the purpose of this thesis, an online BBB predictor was employed (<https://www.cbligand.org/BBB/>). The predictor belongs to the domain-specific chemogenomic knowledgebase *AlzPlatform* (Liu *et al.*, 2014). The latter is a cloud computing server implemented with computational algorithms for the studies regarding target identification and pharmacology of novel small molecules in AD therapy. The platform is comprehensive of 928 genes and 320 proteins related to AD, 194 approved or under clinical trial drugs for AD therapy and more than 400000 chemicals (Liu *et al.*, 2014).

#### *5.1.6 Aims and Objectives*

The aim of the experimental work described in this chapter was to evaluate the potential use of selected vanillin derivatives in the Multi-targeted approach for AD treatment.

To achieve the above aim, the following objectives were completed:

- Determination of inhibitory activity toward AChE of selected vanillin derivatives using the Ellman assay.
- Molecular modelling studies for the interpretation of the experimental results obtained in the Ellman Assay.
- Determination of inhibitory activity toward amyloid aggregation of selected vanillin derivatives through ThT assay.
- Prediction of BBB permeation using the BBB online predictor server (<https://www.cbligand.org/BBB/>).

## 5.2 Materials and Methods

### 5.2.1 Materials

All reagents were purchased from Sigma Aldrich, unless otherwise stated, and were used without any further purification.

$\beta$ -amyloid peptide (1-42)	Calbiochem
PBS	Oxoid
Thioflavin T	Acros Organics

### 5.2.2 Instrumentation

Absorbances for Ellman assay were measured using a Bio-Rad iMark microplate reader.

Fluorescence for ThT assay was measured using a Perkin Elmer LS55 fluorescence spectrophotometer.

Molecular modelling studies were performed using an ASUS F550L series laptop.

## 5.3 Methods

### 5.3.1 AChE Inhibition Assay

The inhibitory properties of selected vanillin derivatives toward AChE was determined using the Ellman method, with minor changes (Ellman *et al.*, 1961). An *Electrophorus electricus* AChE stock solution (22 U/ml) was prepared in 20 mM Tris HCl (pH 7.5) and was diluted 1:100 before use. A 5,5'-dithiobis-(2-nitrobenzoic acid) solution (3 mM) was prepared in phosphate/hepes buffer (50 and 90 mM, respectively, pH 7.5). A 15 mM acetylthiocholine iodide solution was prepared in deionized water. A series dilution of vanillin derivatives was made in methanol in Eppendorf® tubes and 25  $\mu$ l of each solution was pipetted in the corresponding well in a 96-well plate; 25  $\mu$ l of methanol was pipetted in the control wells. DTNB solution (125  $\mu$ l) was pipetted in each well along with diluted solution of AChE (25  $\mu$ l). The 96-multi wells plate was incubated at 37°C for 10 minutes before the addition of 25  $\mu$ l of acetylthiocholine iodide solution in

each well. The plate was incubated for an additional 10 minutes before absorbance measurement (415 nm) using a Bio-Rad iMark microplate reader. An example of the 96-well plate settings is shown in figure 5.9.

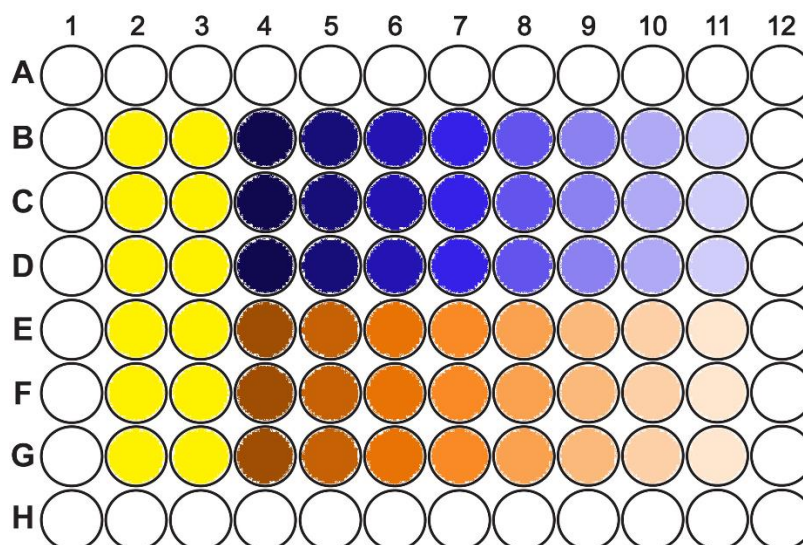


Figure 5.9. 96-well plate settings for Ellman assay. Two compounds can be tested at the same time. The control is represented in yellow, the first AChE inhibitor is represented in blue and the second AChE inhibitor is represented in orange (different shades represent different concentrations tested).

### 5.3.2 Molecular Modelling

For the docking procedure, three different pdb structures (2CMF, 1ACJ and 1EVE) were downloaded from the Protein Data Base (<http://www.rcsb.org>) (Harel *et al.*, 1993; Kryger, Silman and Sussman, 1999; Rydberg *et al.*, 2006). The original ligands were removed, along with water molecules, from the crystal structures by editing the file with notepad app for Windows. The structure obtained was loaded into Autodock Vina 1.1.2 (Trott and Olson, 2010) and optimized. Ligand optimization was performed using Chemdraw 16.0 (Cambridgesoft, Waltham, MA) and Chem3D Ultra 16 version (Cambridgesoft, Waltham, MA) using its MM2 force field energy minimization tool. Molecular binding studies were performed using Autodock Vina 1.1.2 on an ASUS F550L series laptop and PyMOL (the PyMOL Molecular Graphics System, Version 2.0.7 Schrödinger, LLC) was employed for the results visualization.

### 5.3.3 $A\beta_{(1-42)}$ Aggregation Inhibition Assay

The inhibitory properties of selected vanillin derivatives toward the self-mediated aggregation of  $A\beta_{(1-42)}$  peptide was determined using ThT fluorescence assay, following the method described by Luo and co-workers with minor modifications (Luo *et al.*, 2011). A 500  $\mu\text{M}$  stock solution of amyloid  $A\beta_{(1-42)}$  peptide was prepared by dissolving 0.25 mg of the latter in 110  $\mu\text{l}$  of DMSO. The stock solution was aliquoted in Eppendorf® tubes and stored at  $-20^{\circ}\text{C}$  until further use. Stock solutions of curcumin or selected vanillin derivatives (500  $\mu\text{M}$ ) were prepared in the same solvent. 2  $\mu\text{l}$  of amyloid solution was pipetted in 96  $\mu\text{l}$  of 10 mM phosphate/ 10 mM NaCl buffer (pH 8) along with 2  $\mu\text{l}$  of inhibitor stock solution or 2  $\mu\text{l}$  of DMSO (for the control). The final concentrations of both the amyloid peptide and inhibitors were 10  $\mu\text{M}$ . The solutions were then incubated for 24 hours at  $37^{\circ}\text{C}$ . After incubation, 300  $\mu\text{l}$  of 50 mM glycine/ NaOH buffer (pH 8.5) containing 5  $\mu\text{M}$  of ThT were added to all the samples. Each solution was finally transferred into a cuvette and the fluorescence was measured using a Perkin Elmer LS55 luminescence spectrometer (excitation 446 nm, emission 490 nm).

### 5.3.4 Prediction of BBB Permeation

The BBB permeation properties of selected vanillin derivatives were analysed by applying the BBB online predictor server (<https://www.cbligand.org/BBB/>).

The molecules in the analysis were drawn in the website ([www.cbligand.org/BBB/predictor.php](http://www.cbligand.org/BBB/predictor.php)) and the SVM (support vector machine) algorithm was selected along with the MAACS fingerprint in order to obtain the SVM\_MACCSFP BBB Scores (the threshold for BBB permeation was 0.02).

## 5.4 Results and Discussion

### 5.4.1 AChE Inhibition Assay

A selection of vanillin derivatives was made based on their chemical structures (preferring compounds bearing lipophilic moieties, since they are more likely to cross the BBB) and the antioxidant and cellular protective properties described in chapters 3 and 4. The AChE inhibitory properties of selected vanillin derivatives **1a**, **1b**, **1c**, **1d**, **1e**, **1f**, **2b**, **2f**, **4c** were determined through Ellman assay.

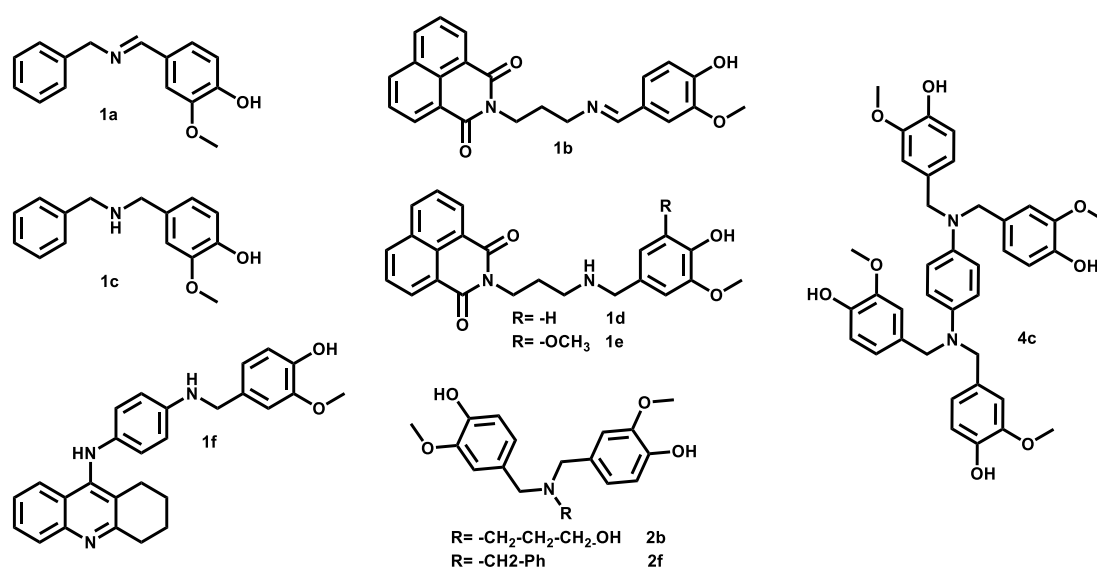


Figure 5.10. Vanillin derivatives tested in the Ellman assay.

The latter assay is based in the cholinesterase-catalysed conversion of acetylthiocholine into thiocholine, which can react with the Ellman reagent yielding a bright yellow colouration with a maximum absorbance at  $\lambda=415$  nm. An example of the 96-well plate is reported in figure 5.11.

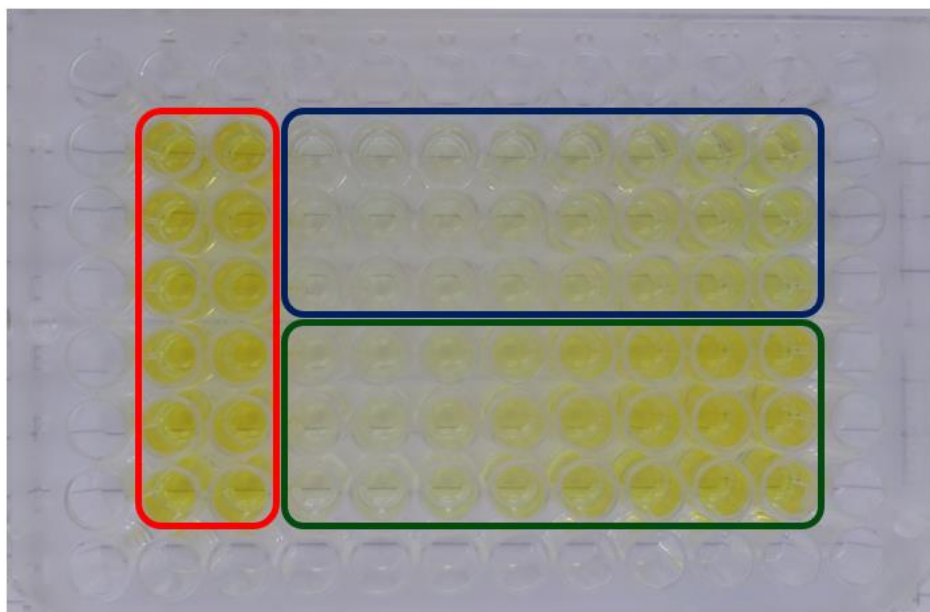


Figure 5.11. 96-well plate for Ellman assay. Two compounds were tested at once. The wells in the red circle represent the control. The wells in the blue and green circles represent two different compounds at different concentrations. The loss in yellow colouration compared to the control is proportional to the AChE inhibitory activity.

The results, expressed as concentration in  $\mu\text{M}$ , are reported as their  $\text{IC}_{50}$  values which are defined as the concentration of compound able to inhibit the 50% of AChE enzyme.

The  $\text{IC}_{50}$  was determined by plotting in a graph with concentrations (in  $\mu\text{M}$ ) on the x-axis and their corresponding % absorbance values on the y-axis to obtain a curve. The linear portion of the curve was considered for the determination of the  $\text{IC}_{50}$  values using the equation of the line as shown in Figure 5.12.

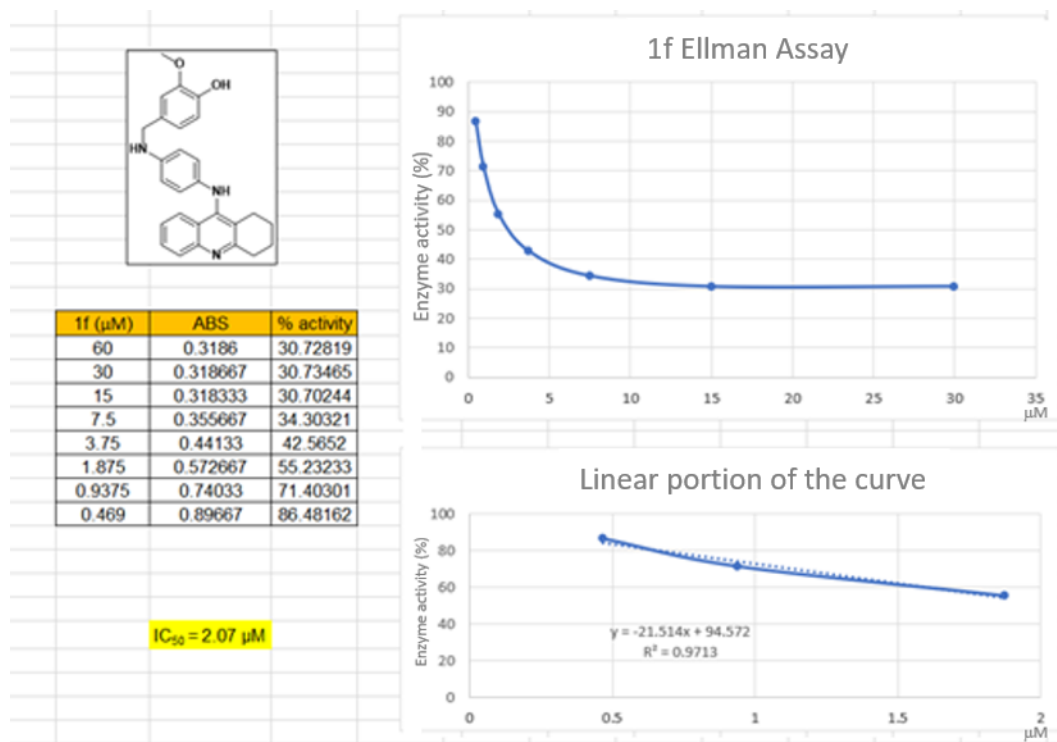


Figure 5.12. Example of Ellman assay's results for derivative **1f**. The concentrations of compound were plotted in a graph along with the amount of active AChE expressed as percentage. The linear portion of the curve was isolated and the IC<sub>50</sub> was calculated using the equation of the line.

The results are reported in table 5.1.

Table 5.1. AChE inhibitory activity of selected vanillin derivatives.

Compound	IC <sub>50</sub> (μM)
1a	> 250
1b	128.3 ± 6.1
1c	> 250
1d	10.1 ± 1.2
1e	24.3 ± 1.4
1f	2.1 ± 0.1
2b	> 250
2f	> 250
4c	26.9 ± 1.3 % <sup>a</sup>
Vanillin	INACTIVE <sup>b</sup>
Tacrine	0.9 ± 0.1

Results from each experiment are expressed as mean ± SD of three independent experiments.

<sup>a</sup> Compound was tested up to 15.5 μM due to solubility issues.

<sup>b</sup> Compounds were tested up to 250 μM.

Vanillin was inactive at concentrations up to 250 μM. On the other hand, all the tested vanillin derivatives showed moderate activity (IC<sub>50</sub> ranging from 2.1 – 128.3 μM) in this assay except for compounds **1a**, **1c**, **2b** and **2f** which showed no IC<sub>50</sub> up to 250 μM concentrations. Due to solubility issues, tetramer **2c** was tested at maximum concentration of 15.5 μM, at which it showed a 26.9% of acetylcholinesterase inhibition. Although a hydrochloride salt could have been prepared in order to increase its aqueous solubility, this would have caused a fall in antioxidant activity, since the nucleophilicity of the nitrogen atoms in the structure has been shown to be critical importance for the latter property (see conclusion section in chapter 3, pages 86-88). Compounds bearing a naphthalimido moiety showed different inhibitory activities towards acetylcholinesterase enzyme. Recently, a series of ranitidine derivatives have been reported for their AChE inhibitory activities, and the most active compounds (see figure 5.13) bore naphthalimido moieties (Gao *et al.*, 2016).

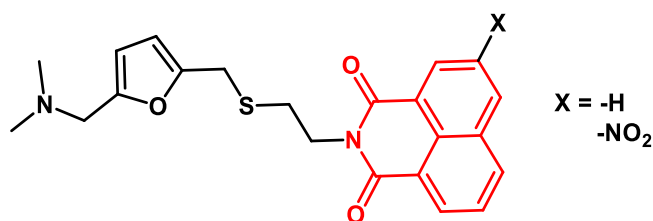


Figure 5.13. Derivatives reported by Gao *et al.* (2016). The naphthalimido moiety is rendered in red.

The imine **1b** displayed the weakest activity among all the compounds tested, with an  $IC_{50}$  of 128.3  $\mu\text{M}$  whereas its reduced derivative **1d** showed a 13-fold increase in activity, with an  $IC_{50}$  of 10.1  $\mu\text{M}$ . This may be due to the limited flexibility of imine bond in compound **1b** which could impede the correct fitting in the narrow gorge of acetylcholinesterase. In contrast, monomer **1d** could fit due to the absence of the rigid imine bond, facilitating the interactions with the amino acids in the gorge. It is interesting to note that monomer **1e**, bears an extra methoxy group turned out to be 2 times less active than **1d** (24.3  $\mu\text{M}$ ). This reduction in activity may be due to steric hindrance exhibited by the extra methoxy group at the entrance of the gorge. Finally, the tacrine-vanillin derivative **1f** showed the highest inhibitory activity, with an  $IC_{50}$  of 2.1  $\mu\text{M}$ ; however, tacrine itself turned out to be 2 times more active than **1f**, with an  $IC_{50}$  of 0.9  $\mu\text{M}$ . Luo *et al.* described novel tacrine-multialkoxybenzene derivatives characterized by the presence of long alkyl chains as linker between the two moieties. The latter displayed enhanced AChE inhibitory activities compared to tacrine (Luo *et al.*, 2011). In particular, the two most active compounds (reported in figure 5.14) turned out to be 20+ times more active than tacrine.

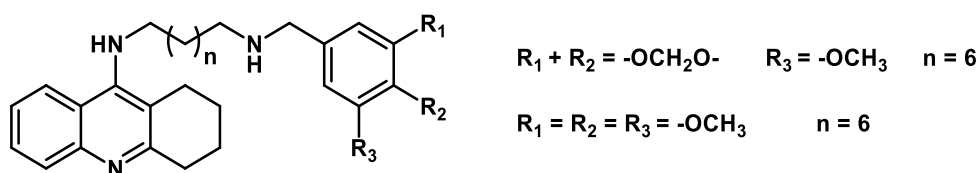


Figure 5.14. Multialkoxybenzene derivatives reported by Luo *et al.* (2011).

The small reduction in activity displayed by monomer **1f** could be associated with the presence of the rigid linker (the aromatic ring). However, this fall in AChE affinity is counterbalanced by the improved antioxidant activity of **1f** conferred by the presence of the aromatic ring.

### 5.4.2 Molecular Modelling

In order to identify and appreciate the molecular elements that contribute to the AChE inhibitory activities of these vanillin derivatives, molecular binding studies were performed on the most active compounds (**1d** and **1f**, see figure 5.10).

However, before starting the binding studies, the validation of molecular modelling protocol needed to be assessed. To do so, the original ligands from three different AChE crystal structures (2CMF, 1ACJ and 1EVE) were re-docked and their positions were compared with the original structures.

The choice of these three crystal structures was based on the good resolution of the latter and the chemical similarities of the vanillin derivatives with the original ligands in the structures.

The resolutions of 2CMF and 1 EVE structures, which bear a bis-tacrine derivative and donepezil as ligands, respectively, were 2.5 Å whereas the resolution of 1ACJ structure, which bear tacrine as ligand, was 2.8 Å. To compare the position of re-docked ligands with their corresponding original positions, the root-mean-squared distance (RMSD) value was measured using the following formula (Carugo and Pongor, 2001):

$$RMSD = \sqrt{\frac{\sum_i d^2_i}{n}}$$

where  $d$  is the distance between each of the  $n$  pairs of equivalent atoms (excluding hydrogens). The lower the RMSD value, the more accurate is the binding model. The results are reported, along with the RMSD values, in figure 5.15.

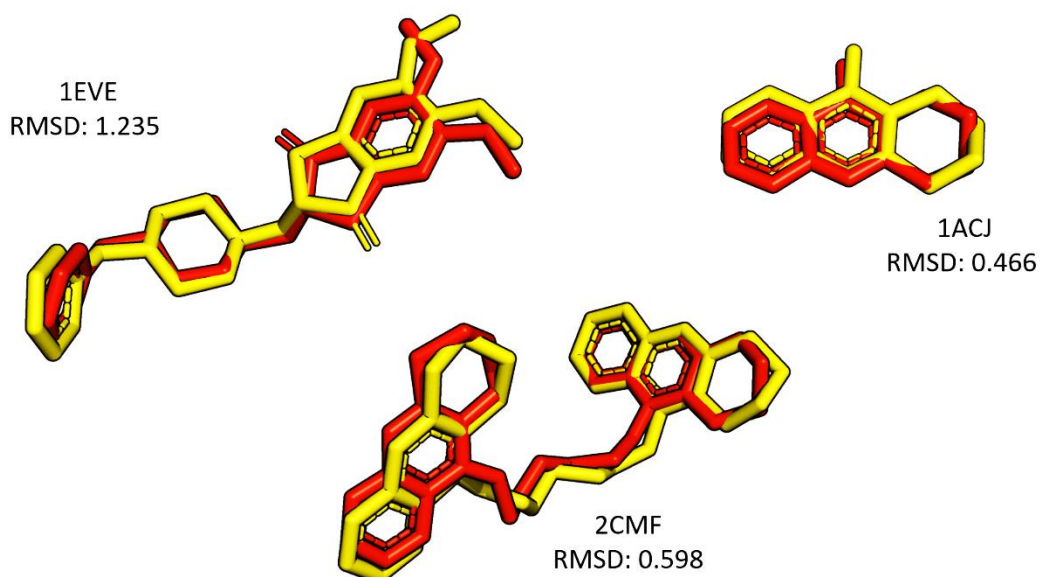


Figure 5.15. Superimposition of original (yellow) and redocked (red) ligands in their corresponding crystal structures and relative RMSD.

The structure bearing donepezil as ligand (1EVE) showed the lowest accuracy in the binding model, with a RMSD of 1.235. In particular, the oxygen in the indanone moiety of the re-docked ligand (showed as a C=O double bond in the figure above) is reversed compared to the original ligand. In contrast, both the tacrine dimer (2CMF) and tacrine (1ACJ) showed better accuracy with RMSD values of 0.598 and 0.466, respectively. It is worth noting that the RMSD calculated for structure pairs with different sizes cannot be directly compared since this value strongly depends on the number of atoms in the structure alignment (Carugo and Pongor, 2001). For this reason, although the 1ACJ model achieved a slight lower RMSD value, 2CMF model was chosen because of its more complex pattern. The two most efficient AChE inhibitors among the novel vanillin derivatives tested in the Ellman assay (**1d** and **1f**) were studied for their binding properties toward the 2CMF AChE crystal structure.

Again, the original ligand in the structure was removed before the docking process. The predicted binding model for both the compounds positioned the vanillin derivatives in the position of the original ligand as depicted in figure 5.16.

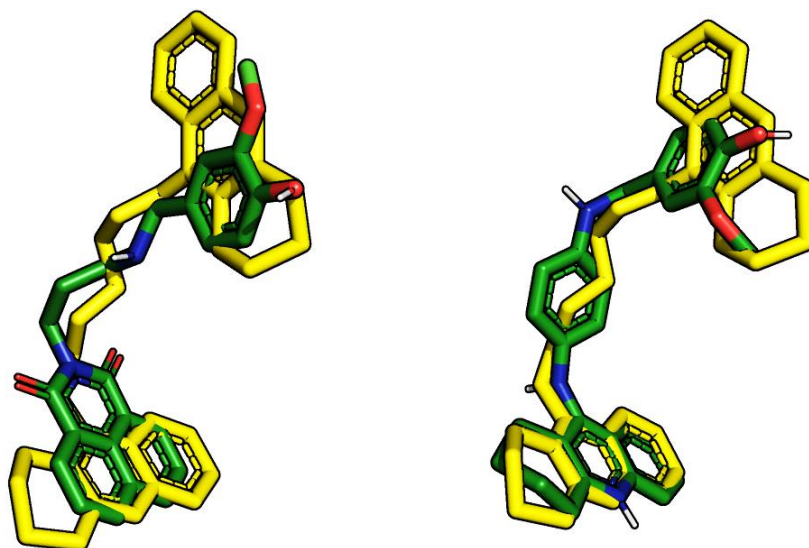


Figure 5.16. Superimposed structures of compound **1d** (left) and **1f** (right) with the original ligand (yellow) in 2CMF AChE structure.

It is interesting to note that the planar portions of compounds **1f** and **1d**, i.e. the tacrine and naphthalimido moieties, are located in the same position of the tacrine structure from original ligand in the crystal structure. The importance of these planar structures can be appreciated by looking at the binding studies of the vanillin derivatives in the 2CMF crystal structure (see figures 5.17-5.18 in the following page).

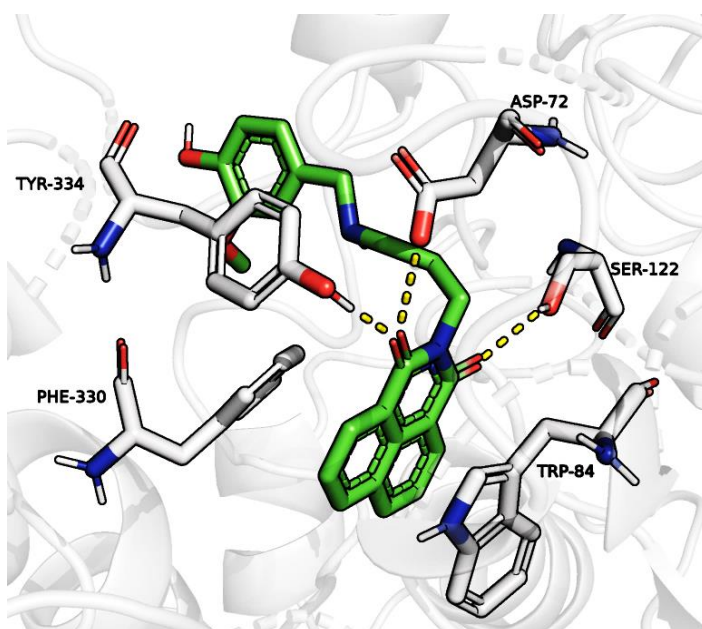


Figure 5.17. Predicted binding model of **1d** in the CAS of 2CMF AChE structure.

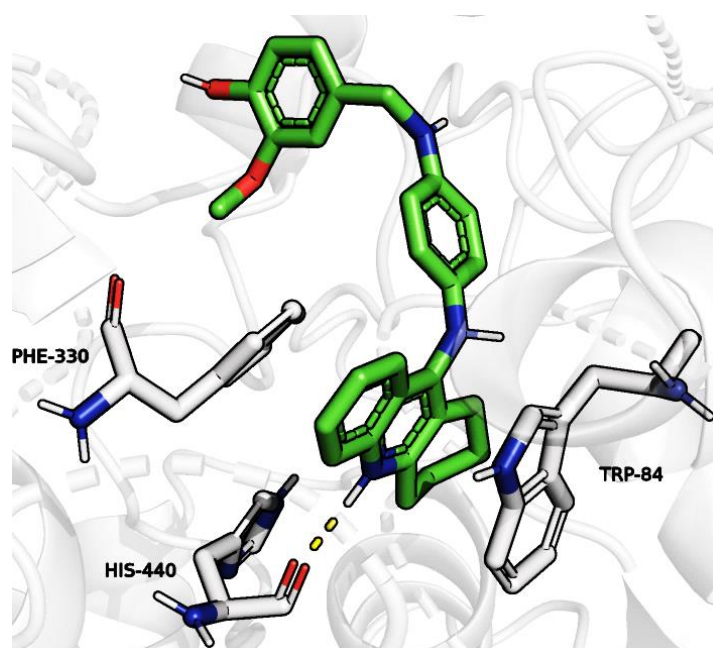


Figure 5.18. Predicted binding model of **1f** in the CAS of 2CMF AChE structure.

The latter planar moieties are stacked between the residues PHE-330 and TRP-84 ( $\pi$ - $\pi$  stacking) in the CAS. Although the stacking between these two residues is common for the tacrine moiety and already reported in several works, e.g. (Harel *et al.*, 1993; Luo *et al.*, 2011; Chand *et al.*, 2016), it has never been reported for the naphthalimido moiety.

In fact, molecular modelling studies performed on the ranitidine derivatives by Gao *et al.* reported  $\pi$ - $\pi$  stacking between the latter moiety and TRP-286 of mouse AChE (*mAChE*), which correspond to TRP-279 of *TcAChE* in the PAS (Colletier *et al.*, 2006; Gao *et al.*, 2016).

In addition, the carbonyl groups in compound **1d** are involved in hydrogen bonding with the residues ASP-72, TYR-334 and SER-122 (3.2, 1.9 and 2.5 Å, respectively) whereas the protonated nitrogen in the tacrine moiety of compound **1f** formed hydrogen bond with the oxygen in the carbonyl group of HIS-440 (2.0 Å).

Moreover, two hydrogen bonds are established between the phenolic group of the vanillin moiety of derivative **1d** and the carbonyl group of ILE-287 (2.7 Å) and between the nitrogen linked to the vanillin structure and the hydroxyl group of TYR-121 (2.1 Å) in the PAS, as depicted in figure 5.19.

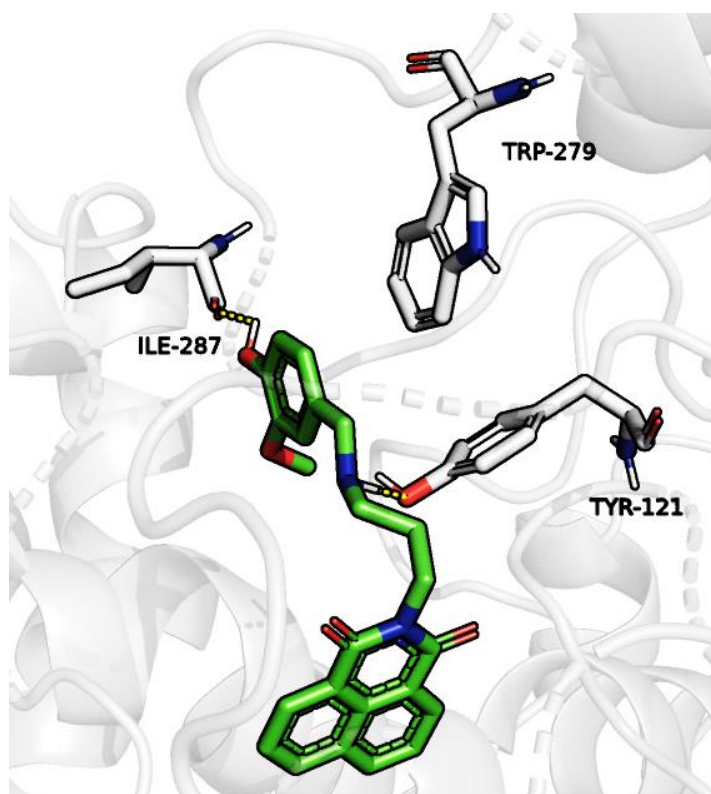


Figure 5.19. Predicted binding model of **1d** in the PAS of 2CMF AChE structure.

In addition, hydrophobic interactions between the vanillin moiety and TRP-279 occur.

Similarly, the phenolic group of the vanillin moiety in derivative **1f** establishes one hydrogen bond with the carbonyl group of ILE-287 (3.9 Å) in the PAS (see figure 5.20). However, the same phenolic moiety is involved in another hydrogen bond with TYR-334 (3.8 Å) due to a favoured position of the hydrogen compared to the same structure in derivative **1d**.

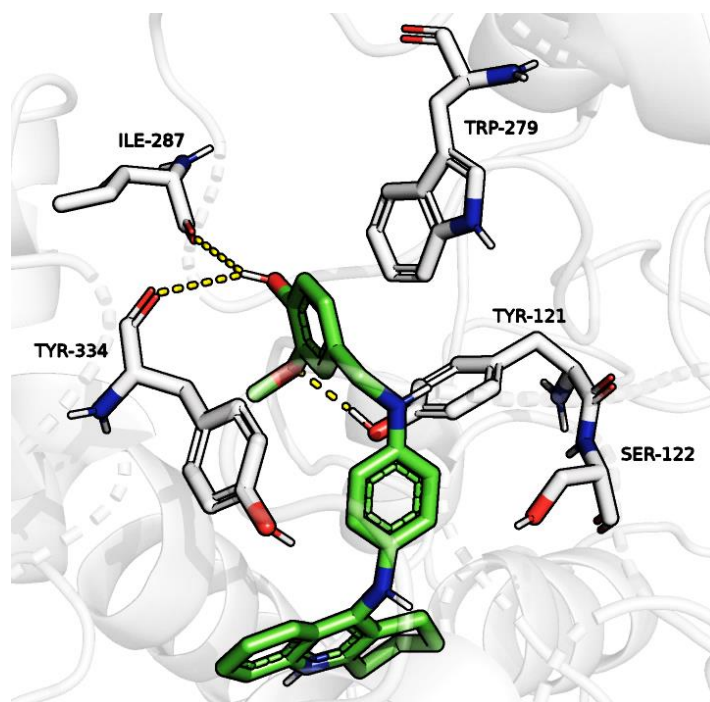


Figure 5.20. Predicted binding model of **1f** in the PAS of 2CMF AChE structure.

Furthermore, the oxygen in the methoxy group of the vanillin structure establishes an additional hydrogen bond with TYR-121 (2.2 Å). Two OH- $\pi$  interactions are established between the aromatic linker of compound **1f** and the hydroxy groups of SER-122 and TYR-334. Finally, hydrophobic interactions between the vanillin ring and TRP-279 also occur.

The molecular modelling results obtained for the two vanillin derivatives within the gorge of AChE (2CMF) can be appreciated in figure 5.21.

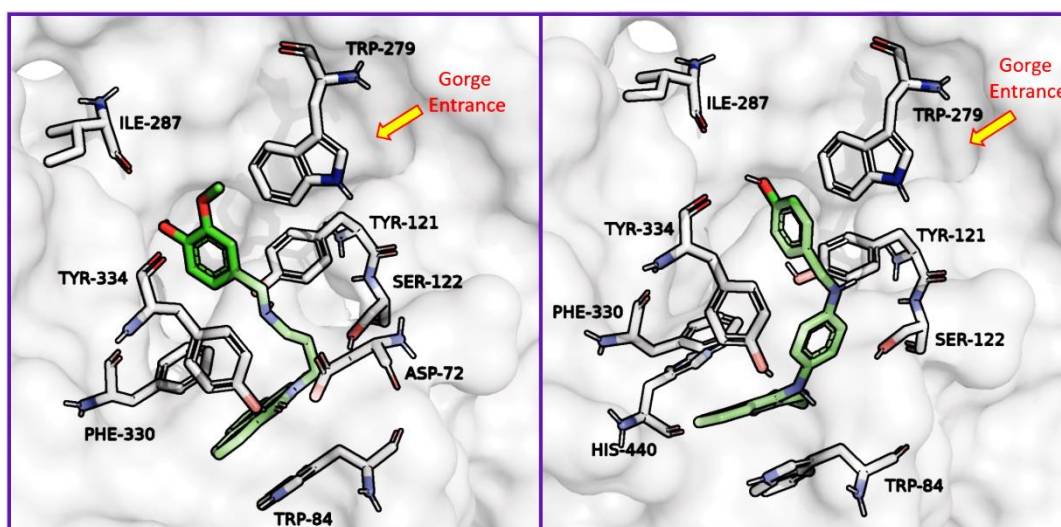


Figure 5.21. Predicted binding models for compounds **1d** and **1f** within the active site of *TcAChE*.

When considering the free binding energies, a good correlation was found between the calculated docking scores and the inhibitory activity determined by Ellman assay.

The original bis-tacrine ligand in the 2CMF structure gave the lowest score (-14.6 Kcal/mol), indicating a good affinity with the AChE structure (the more negative the docking score, the stronger the interaction).

On the other hand, the scores for the derivatives **1f** and **1d** were -13.3 and -12.0 Kcal/mol, respectively, showing lower affinity for the enzyme compared to the original ligand with the tacrine-vanillin hybrid displaying better affinity compared to the naphthalimido-vanillin derivative and thus confirming the results obtained in the Ellman assay.

#### 5.4.3 $A\beta_{(1-42)}$ Aggregation Inhibition Assay

A selection of five vanillin derivatives (**1b**, **1d**, **1e**, **1f** and **4c**, see figure 5.10), based on the inhibitory activity toward AChE, was tested, along with tacrine and curcumin, for their ability to inhibit the self-mediated aggregation of  $A\beta_{(1-42)}$  peptide.

ThT fluorescence assay was employed for the determination of the inhibitory activities of those selected compounds. The ThT fluorescence assay is a well-known method based on the enhanced fluorescence of the Thioflavin T upon binding to  $\beta$ -sheet rich proteins such as the amyloid protein. The concentrations used in this assay were 10  $\mu$ M for both the amyloid protein and the inhibitors. The results are reported in figure 5.22.

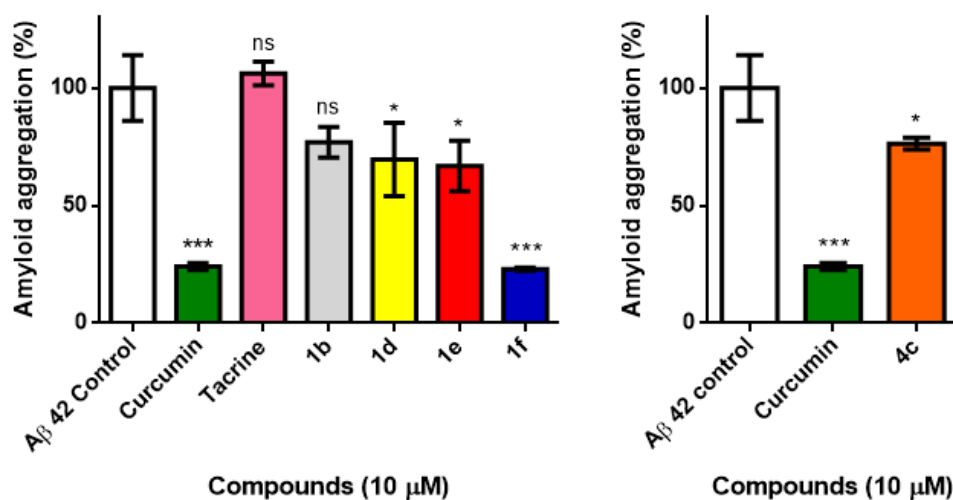


Figure 5.22. Self-mediated amyloid aggregation inhibitory effects of vanillin derivatives. All the compounds were tested at concentration of 10 μM. Values are expressed as the percentage of the control and represented as mean ± SD of three independent experiments in each group. \*\*\*p < 0.001, \*p < 0.05, ns = no significantly different compared to the control.

Imine **1b** and tacrine did not show significant inhibition toward self-mediated amyloid aggregation. On the other hand, all the remaining vanillin derivatives displayed significant activity in this assay.

The tetramer **4c** reduced the amyloid aggregation by 24% compared to control, whereas the vanillin derivative **1d** and the syringaldehyde derivative **1e** showed the same inhibitory activity toward amyloid aggregation, reducing the latter by 30.4 and 33.2%, respectively.

The tacrine derivative **1f** turned out to be the most efficient amyloid aggregation inhibitor, reducing the latter by 77.1% compared to the control, showing similar activity to the positive control curcumin (75.9%).

The inhibitory activities of these vanillin derivatives could be explained by the work of Reinke and Gestwicki, which suggested the importance of two aromatic end groups capable of taking part of hydrogen bonding (Reinke and Gestwicki, 2007).

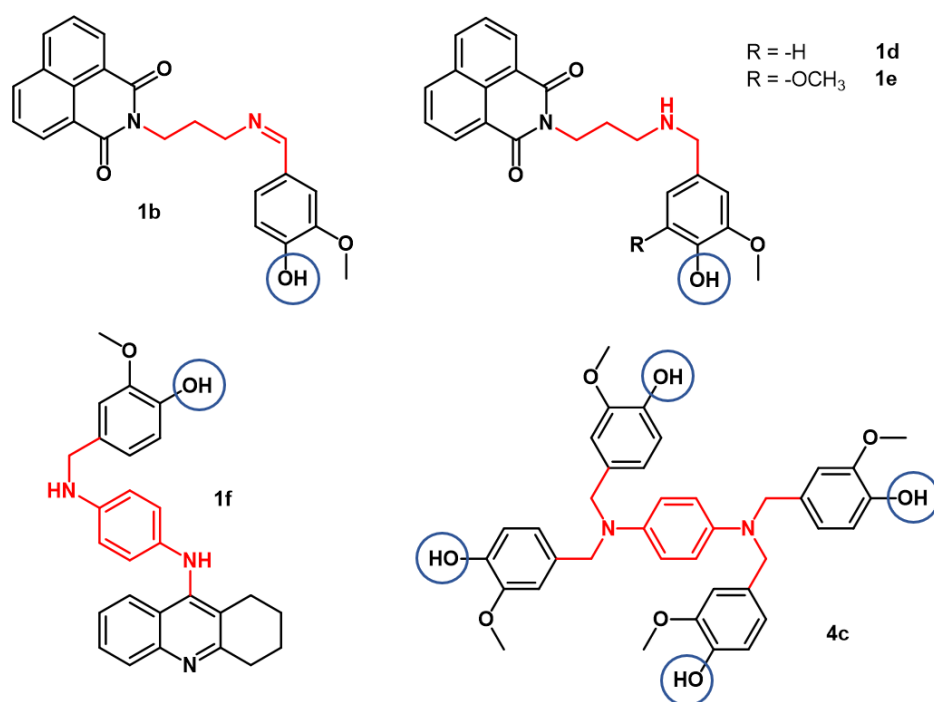


Figure 5.23. Vanillin derivatives tested in the amyloid aggregation inhibition assay. The aromatic moieties are coloured in black whereas the linker is rendered in red. Phenolic moieties are circled in blue.

In fact, each compound tested in this assay bears at least two aromatic structures (rendered in black, in figure 5.23), one of which is vanillin, able to establish hydrogen bonding due to the phenolic group (circled in blue).

The inability of compound **1b** to prevent amyloid aggregation could be explained by the length of the linker, which has been reported to play a critical role in amyloid aggregation inhibition. In fact, Reinke and Gestwicki reported an optimal length of the linker to range between 8 and 16 Å.

The length of the linker in compound **1b**, calculated using PyMOL software, is 6.9 Å compared to compounds **1d**, **1e**, **1f** and positive control curcumin (7.3, 7.3, 8.7, and 9.2 Å respectively).

The shorter length of the linker in compound **1b** is due to the presence of the imine bond, which is shorter compared to the corresponding amine bond in compounds **1d** and **1e**. On the other hand, the linker in compound **4c** cannot be directly measured since more than two aromatic moieties are present in the structure.

Finally, the remarkable activities of compound **1f** in inhibiting the amyloid aggregation could be explained by the presence of the aromatic linker, which confers low flexibility important for the aggregation inhibitory activity (Reinke and Gestwicki, 2007).

#### 5.4.4 Prediction of BBB Permeation

The ability of drugs to cross the BBB is of critical importance for the treatment of neurodegenerative diseases. In fact, satisfactory treatments for certain neurological disorders are lacking due to insufficient crossing of therapeutic moieties through BBB to the brain (Nagpal, Singh and Mishra, 2013).

For this reason, the same selection of vanillin derivatives (**1b**, **1d**, **1e**, **1f** and **4c**) was tested, along with tacrine, for its ability to cross the BBB using an online predictor for BBB permeation ([www.cbligand.org/BBB](http://www.cbligand.org/BBB)).

The latter method generates a score for each molecule in analysis and predicts if those compounds are able to cross (CNS+) or not (CNS-) the BBB (see the example in figure 5.24).

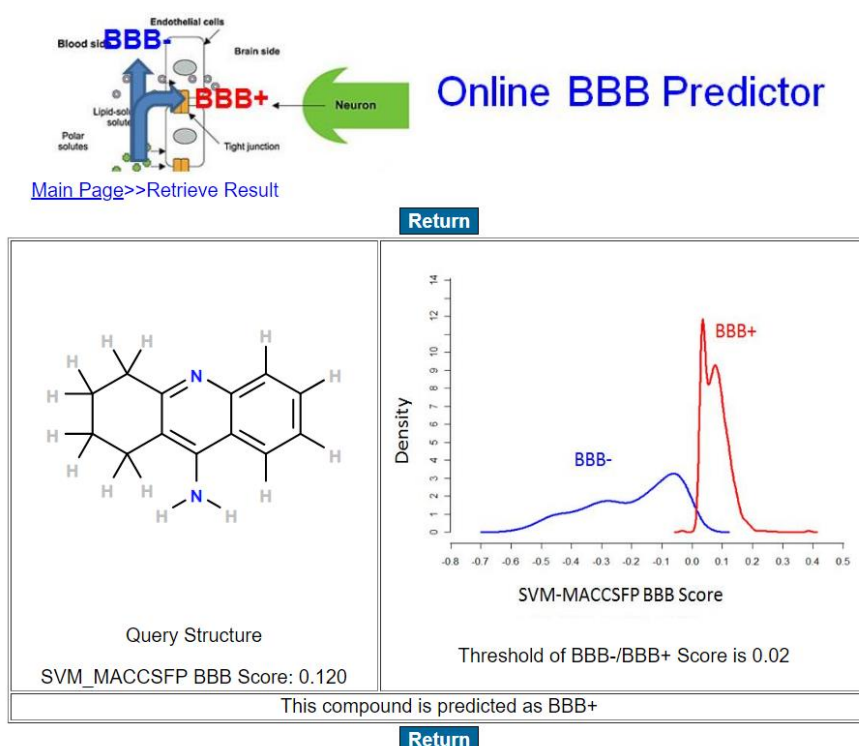


Figure 5.24. Prediction of BBB permeation for tacrine obtained through the online predictor [www.cbligand.org/BBB](http://www.cbligand.org/BBB).

The figure shows high predicted BBB permeation molecule's scores ranging approximately from 0.05-0.1, represented by the red curve in the graph. Low predicted BBB permeation scores ranges approximately below values of

0.01 and above 0.15, represented by the blue colour. The results are reported in table 5.2.

Table 5.2. BBB permeation prediction for selected vanillin derivatives

Compound	BBB Score	BBB Permeation ( $\pm$ )
1b	0.057	BBB +
1d	0.006	BBB -
1e	0.005	BBB -
1f	0.031	BBB +
4c	- 0.053	BBB -
Tacrine	0.120	BBB +

Tacrine displayed the highest predicted BBB permeation properties; with a score of 0.120, it lies on the top of the red curve where the density of molecule in the CNS is maximum. It is worth noting that tacrine is the first AChE inhibitor approved for AD treatment and its ability to cross the blood-brain-barrier is well recognised (Mehta, Adem and Sabbagh, 2012).

Among the vanillin derivatives, the imine **1b** and the tacrine derivative **1f** displayed high-predicted BBB permeation, with scores of 0.057 and 0.031, respectively, whereas the monomers **1d** and **1e** were predicted not to be able to cross the BBB, with scores of 0.006 and 0.005 respectively.

The high predicted BBB permeation of **1b** and **1f** could depend on the imine group of the first (which reduce the polarity of the molecule) and the tacrine moiety of the second, which confer lipophilic properties to these two molecules.

However, the tacrine derivative **1f** experienced a lower predicted ability to cross the blood-brain-barrier compared to the starting compound tacrine (0.031 and 0.120, respectively); this could be explained by the increased molecular weight and the increased hydrophilic properties of the latter due to the presence of the phenolic moiety and the secondary amino groups in the molecular structure.

On the other hand, the monomers **1d** and **1e** showed lower lipophilic properties compared to **1b** due to the presence of a tertiary amino group, which confers hydrophilic properties.

Finally, tetramer **4c** showed the lowest predicted ability to cross the BBB with a negative score (-0.053).

This could be due to the presence of two tertiary amino groups and four phenolic moieties in the molecule which increase the hydrophilic properties of this derivative.

## 5.5 Conclusions

A selection of vanillin derivatives, based on their chemical structures, was tested for their potential use in the multi-targeted-directed therapy of AD. The latter is a multi-factorial neurodegenerative disease characterized by neuronal death, oxidative stress, depleted cholinergic transmission and amyloid plaques. Thus, making multi-targeted-directed therapy approach amenable to AD.

In previous years, the design and synthesis of novel synthetic compounds able to hit the multiple targets involved in AD, usually by combining two or more pharmacophores known to target specific biological structures involved in the disease, has shown intense interest among the scientific community.

In this chapter, nine vanillin derivatives, selected by their chemical structures, were tested for their inhibitory activity toward the AChE enzyme, using Ellman assay. Only five compounds showed interesting activities; the derivatives bearing a naphthalimido moiety (**1b**, **1d** and **1e**) or the tacrine moiety (**1f**) showed  $IC_{50}$  ranging from 128.3-2.1  $\mu$ M whereas the tetramer **4c** (tested at maximum concentration of 15.5  $\mu$ M due to solubility issues) showed to inhibit the 26.9% of the enzyme.

In order to show further light on the molecular elements involved in the observed AChE inhibitory activities of compound **1d** ( $IC_{50}$ : 10.1  $\mu$ M) and **1f** ( $IC_{50}$ : 2.1  $\mu$ M), molecular modelling studies were performed on the latter derivatives. The results strongly demonstrated the ability of both compounds to bind at the catalytic and peripheral anionic sites of the enzyme.

The five vanillin derivatives which displayed AChE inhibitory properties (**1b**, **1d**, **1e**, **1f** and **4c**) were tested for their ability to inhibit amyloid peptide aggregation using ThT assay.

All the compounds displayed significant inhibitory activities except for imine **1b**, with the tacrine derivative **1f** the most active, inhibiting the aggregation

by 77.1% compared to the amyloid control, showing similar activity to positive control curcumin.

Finally, the same vanillin derivatives were tested for their ability to cross the BBB using an online predictor ([www.cbligand.org/BBB](http://www.cbligand.org/BBB)). Only imine **1b** and the tacrine derivative **1f** were predicted to cross the BBB, although they showed lower permeation properties compared to tacrine, due to the presence of polar moieties such as phenolic groups in the vanillin moieties or substituted amino groups.

Compound **1f** turned out to be the most efficient AChE and amyloid aggregation inhibitor. Furthermore, as described in chapter 3, it showed strong antioxidant properties, especially in the ORAC assay, where it was found to be 6.4-fold times more active than the synthetic agent Trolox. To our knowledge, only the ferulic acid-tacrine-melatonin hybrids reported by Benchekroun *et al.* achieved such high antioxidant activity in ORAC assay in the multi-targeted-directed approach to AD (Benchekroun *et al.*, 2016).

In addition, monomer **1f** was found to exert neuroprotective effects in hydrogen peroxide-based oxidative stress model, displaying significant protective effects in SH-SY5Y cells against hydrogen peroxide-induced death at concentration as low as 1  $\mu$ M (see chapter 4, page 162).

Taken together, these results support derivative to be the lead candidate compound for the development of novel multi-targeted-directed ligand for the treatment of AD.

# **Chapter 6: Conclusion and Future Work**

The link between oxidative stress and neurodegenerative diseases such as Parkinson's and Alzheimer's diseases has suggested the possible use of antioxidants in the prevention or treatment of the latter. However, contrasting results have been obtained in the evaluation of the potential use of natural and synthetic antioxidants in such diseases (Uttara *et al.*, 2009; Jomova *et al.*, 2010; Kelsey, Wilkins and Linseman, 2010; Firuzi *et al.*, 2011; Kim *et al.*, 2015).

The aim of this project was the synthesis of novel vanillin derivatives with enhanced antioxidant properties compared to the starting compound. The choice of using vanillin as starting compound was based on previous work reporting the protective effects of this natural compound in several oxidative stress models, both *in vitro* and *in vivo* (Kamat, Ghosh and Devasagayam, 2000; Makni *et al.*, 2012; Dhanalakshmi *et al.*, 2015; Lee *et al.*, 2016).

In this work the vanillin derivatives were prepared by exploiting the reductive amination reaction, which entails the conversion of the carbonyl group in vanillin into the corresponding amine *via* an imine intermediate (Baxter and Reitz, 2002). A selection of amines was employed to generate derivatives bearing only one vanillin moiety (monomers), two vanillin moieties (dimers) or four vanillin moieties (tetramers).

All the derivatives synthesised, were then evaluated for their antioxidant properties using different assays:

- DPPH Assay, for the evaluation of the free radical scavenging activity of vanillin derivatives toward the stable 2,2-diphenyl-1-picrylhydrazyl radical
- FRAP Assay, for the assessment of the reducing ability of vanillin derivatives toward the Fe<sup>3+</sup> ion.

- ORAC Assay, for the evaluation of the hydrogen transfer ability of the selected vanillin derivatives in the scavenging of the peroxy free radical generated by AAPH at physiological pH.
- DNA damage protection Assay, for the determination of the protective effects of selected vanillin derivatives against oxidative stress-mediated DNA strand breakage (in the presence of AAPH stressor) with supercoiled DNA plasmid.

Almost all the synthesized derivatives showed improved antioxidant activities compared to the starting compound vanillin.

In addition, a structure-activity relationship (SAR) on the antioxidant activity of vanillin derivatives have been hypothesised based on the results in the four antioxidant assays. The number of vanillin moieties, the nucleophilicity of the nitrogen atom(s), the delocalisation of nitrogen's electrons and the phenolic and methoxy moieties in the vanillin structures appear to strongly contribute to the antioxidant activity of these derivatives.

The tetramer **4c** turned out to be the most active compound in all the antioxidant assays, with an  $IC_{50}$  of 5.8  $\mu$ M in DPPH assay, 5.29 TE in FRAP assay, 20.4 TE in ORAC assay and an  $IC_{50}$  of 0.6  $\mu$ M in DNA protection assay.

Once the antioxidant properties of the vanillin derivatives were established, a selection of three compounds was chosen for further studies on cellular model. Neuroblastoma SH-SY5Y cell line was chosen for the *in vitro* studies and two different neurodegenerative models, based on hydrogen peroxide and rotenone/oligomycin A mixture as stressors, were employed.

Before the evaluation of the protective effects of selected vanillin derivatives (**1f**, **2b** and **4c**) in oxidative stress models, their toxicities toward the SH-SY5Y cell line were determined through the MTT assay, after compounds exposure for 24 hours. The dimer **2b** was found to be the safest compound with an  $LC_{50}$  higher than 1 mM, whereas monomer **1f** and tetramer **4c** showed higher toxicities with  $LC_{50}$ s of 43.7 and 45.1  $\mu$ M, respectively.

Toxicity test with hydrogen peroxide and the rotenone/oligomycin A mixture were carried out to determine their cytotoxic effects toward the same cell line and their IC<sub>50</sub> were calculated; 400 μM for hydrogen peroxide (after 24 hours incubation) and 3 and 1 μM for the rotenone/oligomycin A mixture (after 48 hours incubation). The latter conditions were chosen for the evaluation of the protective effects of the selected vanillin derivatives.

Compounds **1f**, **2b** and **4c** were finally tested for their protective effects toward SH-SY5Y against oxidative stress-induced cell death. The cells were then pre-treated with the selected vanillin derivatives for 24 hours before the addition of the stressors.

All the three vanillin derivatives showed protective effects against hydrogen peroxide-induced (400 μM) cell death. It is worth to note that vanillin did not show significant protection even at the highest concentration tested (800 μM). The monomer **1f** exhibited significant cellular protection at concentration as low as 1 μM and a maximum protection at 5 μM, with an increase of cell viability of 15 and 30%, respectively. The dimer **2b** displayed the weakest protective effects, with significant protection at concentration as low as 5 μM and a maximum effect at 200 μM, by increasing the cell viability by 6 and 20%, respectively. Tetramer **4c** showed significant protective effects at concentration as low as 0.1 μM and a maximum protection at 10 μM, by increasing the cell viability of 10 and 30%, respectively.

However, with rotenone/oligomycin A (3 and 1 μM, respectively) mixture as the stress model, only compound **4c** had the ability to protect the SH-SY5Y cell line from oxidative stress, displaying significant protective effects at concentration of 5 and 10 μM with increasing cell viability by 20 and 25%, respectively.

Furthermore, vanillin derivatives were studied for their ability to reduce ROS production in the same cell line, after treatment with hydrogen peroxide (1 mM) for 30 minutes. In this experiment, ROS were detected using the fluorescent probe 2',7'-dichlorodihydrofluorescein diacetate and measured through flow cytometry.

Compounds **2b** and **4c** were tested at their highest concentration employed in the previous assays (200  $\mu\text{M}$  and 10  $\mu\text{M}$ , respectively) whereas monomer **1f** was not tested due to instrumental issues. A significant reduction of ROS was found in pre-treated cells with tetramer **4c** (24 hours) exhibiting a 76% ROS reduction when compared to the peroxide control whereas the dimer **2b** showed a reduction in ROS by 40%.

Both **2b** and **4c** were then tested for their protective effects against hydrogen peroxide-induced DNA damage in SH-SY5Y cell line using the DNA comet method. The latter is a technique for the evaluation of DNA damage based on its single cell electrophoretic separation (Olive and Banáth, 2006). The cells were pre-treated for 24 hours with the usual concentrations of **2b** or **4c** before treatment with hydrogen peroxide (300  $\mu\text{M}$ ) for 30 minutes. However, both the compounds did not show significant protection against oxidative stress-induced DNA damage.

However, a direct antioxidant mechanism based on the free radical scavenging and reducing properties of the latter compounds can partially explain their protective effects. In fact, the increased cell viabilities achieved at concentrations as low as 0.1  $\mu\text{M}$  suggest a more complex mechanism.

In order to evaluate a possible mechanism behind the interesting protective effects of compound **4c**, the latter was evaluated for its ability to trigger the Antioxidant Responsive Element (ARE) pathway, which is known to be involved in the antioxidant response in eukaryotic cells. In particular, the ability of selected vanillin derivative to induce Nrf2 translocation into the nucleus, is a known phenomenon to be linked with antioxidant enzymes expression, was determined through western blotting methodology (Johnson *et al.*, 2008)(Nguyen, Nioi and Pickett, 2009)(Jin *et al.*, 2015). Although an increased concentration of a protein was picked up by the Nrf2 antibody in the nuclear cell extract after pre-treated with compound **4c** for 24 hours in our laboratory, the molecular weight of the latter protein suggested a non-specific binding of the antibody used.

In addition, similar experiments performed by Professor Galli and co-workers at University of Perugia confirmed the inability of the latter vanillin derivative **4c** to induce Nrf2 nuclear translocation.

Finally, a selection of vanillin derivatives was tested for their potential use in a multi-targeted-directed approach for Alzheimer disease. The latter approach is aimed to target different hallmarks of this neurodegenerative disease, such as oxidative stress, acetylcholine depletion and amyloid peptide aggregation (Cavalli *et al.*, 2008; Bolognesi, Cavalli and Melchiorre, 2009; Bolognesi *et al.*, 2011).

For these reasons, the ability of selected vanillin derivatives to inhibit acetylcholinesterase and A $\beta$ <sub>(1-42)</sub> peptide aggregation was evaluated through Ellman assay and ThT assay, respectively. In addition, *in silico* studies were performed for the evaluation of AChE inhibition and BBB permeation properties of selected vanillin derivatives.

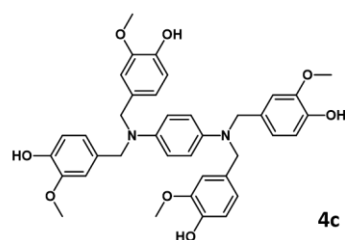
Monomers **1d** and **1f** turned out to be the most active AChE inhibitors, with IC<sub>50</sub> of 10.1 and 2.1  $\mu$ M, respectively with the latter two-fold less active than tacrine. In addition, molecular modelling studies highlighted their ability to bind both the CAS and the PAS of the AChE enzyme.

Furthermore, monomer **1f** turned out to be the most effective amyloid aggregation inhibitor in ThT assay, showing comparable activity to positive control curcumin.

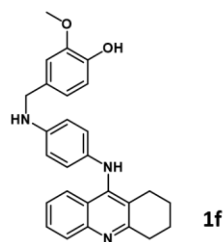
Finally, *in silico* studies predicted monomer **1f** to cross the blood-brain barrier, which is essential for targeting neurodegenerative diseases.

Overall, the novel vanillin derivatives showed promising potential for the treatment or the prevention of neurodegenerative diseases. In fact, the compounds described in this thesis showed interesting antioxidant properties, cellular protective effects in oxidative stress models and inhibitory activities toward acetylcholinesterase enzyme and amyloid aggregation. In particular, compounds **4c** and **1f** can be selected as lead

compounds for the development of novel vanillin derivatives with enhanced biological activities.



- **Strong Antioxidant Properties**
  - DPPH (IC<sub>50</sub>): **5.8 ± 0.1 μM**
  - FRAP: **5.29 ± 0.62 TE**
  - ORAC: **20.4 ± 1.3 TE**
  - DNA plasmid protection (IC<sub>50</sub>): **0.6 ± 0.1 μM**
- **Strong Protective effects in SH-SY5Y cells**
  - Significant protection against H<sub>2</sub>O<sub>2</sub>-induced (400 μM) cell death at **concentration of 0.1 μM**.
  - Significant protection against rotenone/oligomycin A-induced (3 and 1 μM, respectively) cell death at **concentration of 5 μM**.
  - Reduction of H<sub>2</sub>O<sub>2</sub>-induced (1 mM) ROS formation by 76% at **concentration of 10 μM**.



- **Good Antioxidant Properties**
  - DPPH (IC<sub>50</sub>): **20.5 ± 0.3 μM**
  - FRAP: **1.54 ± 0.15 TE**
  - ORAC: **6.4 ± 1.6 TE**
  - DNA plasmid protection : not tested.
- **Good Protective effects in SH-SY5Y cells**
  - Significant protection against H<sub>2</sub>O<sub>2</sub>-induced (400 μM) cell death at **concentration of 1 μM**.
- **Good activities in MTDL strategy to AD**
  - Good inhibitory activity toward AChE (IC<sub>50</sub> **2.1 ± 0.1 μM**).
  - Strong inhibitory activity toward amyloid aggregation (77.1% at concentration of **10 μM**).

Figure 6.1. Summary of the properties of most promising vanillin derivatives, monomer **1f** and tetramer **4c**.

### Future Work

The evaluation of vanillin derivatives' abilities to inhibit the NFκB activation and to activate AP-1 transcription factor could bring more information regarding their mechanism of action at the base of the protective effects in SH-SY5Y cells against oxidative stress models (see figure 6.2). Western blotting analysis could be employed for this purpose.

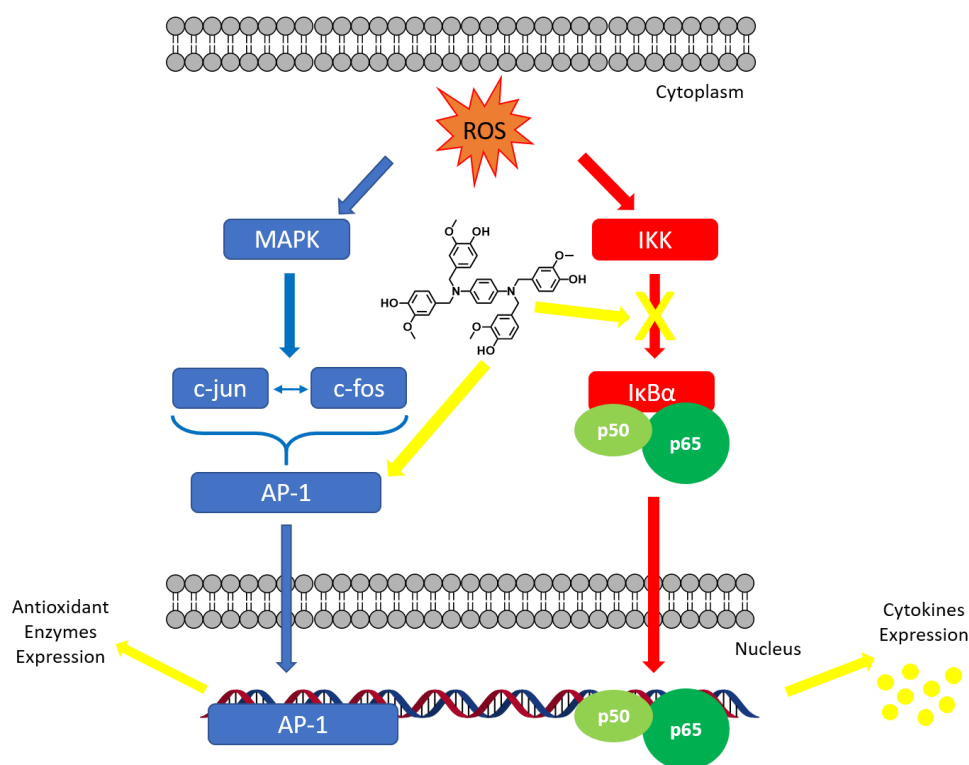


Figure 6.2. Possible mechanisms behind the protective effects of compound 4c in SH-SY5Y cell line. Adapted from (Mattson and Camandola, 2001; Palanki, 2002; Ye *et al.*, 2014; Lan *et al.*, 2017)

*In vivo* experiments (using mammalian models such as rats or mice) are necessary for the determination of the toxic effects of the vanillin derivatives and the evaluation of their protective effects in oxidative stress models.

Should these compounds show low toxicity and positive effects on such animal models, they could be further tested in clinical studies as neuroprotective agents. In addition, due to the solubility of compound **4c** in lipophilic solvents such as chloroform, it could be tested as preservative in food industry.

Regarding the multi-target-directed approach for AD, the evaluation of the inhibitory activity of vanillin derivatives toward the butyrylcholinesterase needs to be assessed since this enzyme plays a fundamental role in the progression of AD (Greig, Lahiri and Sambamurti, 2002; Panek *et al.*, 2017). Contrarily to AChE, the latter enzyme prevent amyloid A $\beta$  formation hence selectivity toward AChE inhibition is preferred (Saini and Saxena, 2018). The BChE inhibitory properties of selected vanillin derivatives could

be measured through Ellman assay, following the same protocol described in chapter 5.

Furthermore, the chelating properties of the compounds toward  $\text{Cu}^{2+}$  and  $\text{Zn}^{2+}$  should be determined, since the homeostasis of the latter ions is dysregulated in AD (Cuajungco *et al.*, 2006) and positive results could increase the number of targets involved in this neurodegenerative disease. A UV-Vis analysis could be carried out for this purpose.

The evaluation of the toxic effects of the tacrine-vanillin hybrid **1f** toward hepatic cells should be assessed, since the tacrine moiety is known to exert toxic effect in liver. For this purpose, a human hepatocellular carcinoma cell line (HepG2) could be employed (Dgachi *et al.*, 2017) and the toxicity could be measured through MTT assay, following the same protocol described in chapter 4.

Structural modification to the lead compound **1f** could be made (see figure 6.1); in particular, the aromatic linker can be replaced by an alkyl chain composed of 7 to 9 methylene moieties, which has shown to increase the affinity to AChE since it is known to fit in the narrow gorge of AChE (Luo *et al.*, 2011; Agatonovic-Kustrin, Kettle and Morton, 2018).

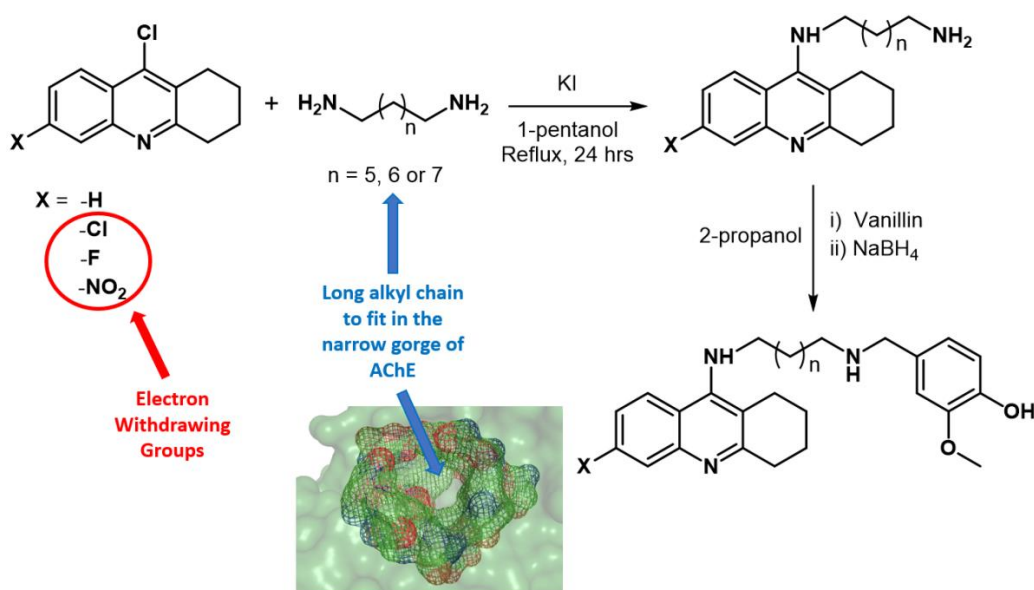


Figure 6.3. Synthetic strategy for novel vanillin-tacrine hybrids.

On the other hand, this will impact negatively on the antioxidant activity of the compound, since the delocalisation of nitrogen's electrons plays a critical role in scavenging and reducing activity of the vanillin derivatives. However, substitution in the tacrine moiety could be made in order to increase the affinity of compound **1f** to AChE enzyme; for example, it is known that an electron withdrawing group, such as -NO<sub>2</sub> and -Cl, in the position 6 of tacrine moiety is linked with an increased affinity to AChE enzyme thus improving the inhibitory activity (Recanatini *et al.*, 2000; Agatonovic-Kustrin, Kettle and Morton, 2018).

## References

Agatonovic-Kustrin, S., Kettle, C. and Morton, D. W. (2018) 'A molecular approach in drug development for Alzheimer's disease', *Biomedicine and Pharmacotherapy*. Elsevier, 106(June), pp. 553–565. doi: 10.1016/j.biopha.2018.06.147.

Agholme, L. *et al.* (2010) 'An In Vitro Model for Neuroscience: Differentiation of SH-SY5Y Cells into Cells with Morphological and Biochemical Characteristics of Mature Neurons', *Journal of Alzheimer's Disease*, 20(4), pp. 1069–1082. doi: 10.3233/JAD-2010-091363.

Ahmed, T. *et al.* (2015) 'Berberine and neurodegeneration: A review of literature', *Pharmacological Reports*. Institute of Pharmacology, Polish Academy of Sciences, 67(5), pp. 970–979. doi: 10.1016/j.pharep.2015.03.002.

Ainsworth, E. A. and Gillespie, K. M. (2007) 'Estimation of total phenolic content and other oxidation substrates in plant tissues using Folin-Ciocalteu reagent', *Nature Protocols*, 2(4), pp. 875–877. doi: 10.1038/nprot.2007.102.

Ajami, M. *et al.* (2017) 'Therapeutic role of sirtuins in neurodegenerative disease and their modulation by polyphenols', *Neuroscience and Biobehavioral Reviews*. Elsevier Ltd, 73, pp. 39–47. doi: 10.1016/j.neubiorev.2016.11.022.

Akaishi, T. and Abe, K. (2018) 'CNB-001, a synthetic pyrazole derivative of curcumin, suppresses lipopolysaccharide-induced nitric oxide production through the inhibition of NF- $\kappa$ B and p38 MAPK pathways in microglia', *European Journal of Pharmacology*. Elsevier B.V., 819(December 2017), pp. 190–197. doi: 10.1016/j.ejphar.2017.12.008.

Alarcón, E. *et al.* (2008) 'Antioxidant capacity of herbal infusions and tea extracts: A comparison of ORAC-fluorescein and ORAC-pyrogallol red methodologies', *Food Chemistry*, 107(3), pp. 1114–1119. doi:

10.1016/j.foodchem.2007.09.035.

Alegria-Schaffer, A., Lodge, A. and Vатtem, K. (2009) *Performing and Optimizing Western Blots with an Emphasis on Chemiluminescent Detection*. 1st edn, *Methods in Enzymology*. 1st edn. Elsevier Inc. doi: 10.1016/S0076-6879(09)63033-0.

Alfonso-Prieto, M. *et al.* (2009) 'The molecular mechanism of the catalase reaction', *Journal of the American Chemical Society*, 131(33), pp. 11751–11761. doi: 10.1021/ja9018572.

Ali-Hassan-Sayegh, S. *et al.* (2014) 'Antioxidant supplementations for prevention of atrial fibrillation after cardiac surgery: An updated comprehensive systematic review and meta-analysis of 23 randomized controlled trials', *Interactive Cardiovascular and Thoracic Surgery*, 18(5), pp. 646–654. doi: 10.1093/icvts/ivu020.

Arciello, M., Rotilio, G. and Rossi, L. (2005) 'Copper-dependent toxicity in SH-SY5Y neuroblastoma cells involves mitochondrial damage', *Biochemical and Biophysical Research Communications*, 327(2), pp. 454–459. doi: 10.1016/j.bbrc.2004.12.022.

Alzheimer Association. (2015) '2015 Alzheimer's disease facts and figures', *Alzheimer's and Dementia*. Elsevier Ltd, 11(3), pp. 332–384. doi: 10.1016/j.jalz.2015.02.003.

Atwood, C. S. *et al.* (2002) 'Senile plaque composition and posttranslational modification of amyloid- $\beta$  peptide and associated proteins', *Peptides*, pp. 1343–1350. doi: 10.1016/S0196-9781(02)00070-0.

Ayala, A., Muñoz, M. F. and Argüelles, S. (2014) 'Lipid peroxidation: Production, metabolism, and signaling mechanisms of malondialdehyde and 4-hydroxy-2-nonenal', *Oxidative Medicine and Cellular Longevity*, 2014, pp. 1–31. doi: 10.1155/2014/360438.

Bachurin, S. O., Bovina, E. V and Ustyugov, A. A. (2017) 'Drugs in Clinical

Trials for Alzheimer's Disease: The Major Trends', *Medicinal Research Reviews*, 37(5), pp. 1186–1125. doi: 10.1002/med.

Badawy, M. E. I. and El-Aswad, A. F. (2014) 'Bioactive paper sensor based on the acetylcholinesterase for the rapid detection of organophosphate and carbamate pesticides', *International Journal of Analytical Chemistry*. Hindawi Publishing Corporation, 2014, pp. 1–8. doi: 10.1155/2014/536823.

Bajda, M. *et al.* (2011) 'Multi-Target-Directed Ligands in Alzheimer's Disease Treatment', *Current Medicinal Chemistry*, 18(32), pp. 4949–4975. doi: 10.2174/092986711797535245.

Bajda, M. *et al.* (2013) 'Structure-based search for new inhibitors of cholinesterases', *International Journal of Molecular Sciences*, 14(3), pp. 5608–5632. doi: 10.3390/ijms14035608.

Balkwill, F. and Mantovani, A. (2001) 'Inflammation and cancer: Back to Virchow?', *Lancet*, 357(9255), pp. 539–545. doi: 10.1016/S0140-6736(00)04046-0.

Barron, G. A. *et al.* (2010) 'Synthesis, cytotoxicity and DNA-binding of novel bisnaphthalimidopropyl derivatives in breast cancer MDA-MB-231 cells', *European Journal of Medicinal Chemistry*. Elsevier Masson SAS, 45(4), pp. 1430–1437. doi: 10.1016/j.ejmech.2009.12.047.

Bass, T. M. *et al.* (2007) 'Effects of resveratrol on lifespan in *Drosophila melanogaster* and *Caenorhabditis elegans*', *Mechanisms of Ageing and Development*. Elsevier, 128(10), pp. 546–552. doi: 10.1016/J.MAD.2007.07.007.

Baur, J. A. and Sinclair, D. A. (2006) 'Therapeutic potential of resveratrol: The in vivo evidence', *Nature Reviews Drug Discovery*, 5(6), pp. 493–506. doi: 10.1038/nrd2060.

Baxter, E. W. and Reitz, A. B. (2002) 'Reductive Aminations of Carbonyl Compounds with Borohydride and Borane Reducing Agents', *Organic* 232

*Reactions*, (18), pp. 1–170. doi: 10.1002/0471264180.or059.01.

Beckman, J. S. and Crow, J. P. (1993) 'Pathological implications of nitric oxide, superoxide and peroxynitrite formation', *Biochemical Society Transactions*, 21(2), pp. 330–334. doi: 10.1042/bst0210330.

Benchekroun, M. *et al.* (2016) 'The Antioxidant Additive Approach for Alzheimer's Disease Therapy: New Ferulic (Lipoic) Acid Plus Melatonin Modified Tacrines as Cholinesterases Inhibitors, Direct Antioxidants, and Nuclear Factor (Erythroid-Derived 2)-Like 2 Activators', *Journal of Medicinal Chemistry*, 59(21), pp. 9967–9973. doi: 10.1021/acs.jmedchem.6b01178.

Benson, A. M. *et al.* (1978) 'Elevation of Hepatic Glutathione S-Transferase Activities and Protection against Mutagenic Metabolites of Benzo(a)pyrene by Dietary Antioxidants', *Cancer Res.*, 38(12), pp. 4486–4495. Available at: <http://cancerres.aacrjournals.org/content/38/12/4486.full.pdf>.

Benzie, I. F. F. and Strain, J. J. (1996) 'Ferric reducing (antioxidant) power as a measure of antioxidant capacity: the FRAP assay', *Analytical Biochemistry*, 239(1), pp. 70–76.

Bermejo-Bescós, P., Piñero-Estrada, E. and Villar del Fresno, Á. M. (2008) 'Neuroprotection by *Spirulina platensis* protean extract and phycocyanin against iron-induced toxicity in SH-SY5Y neuroblastoma cells', *Toxicology in Vitro*, 22(6), pp. 1496–1502. doi: 10.1016/j.tiv.2008.05.004.

Betarbet, R. *et al.* (2000) 'Chronic systemic pesticide exposure reproduces features of Parkinson's disease', *Nature Neuroscience*, 3(12), pp. 1301–1306. doi: 10.1038/81834.

Bhabak, K. P. and Govindasamy, M. (2010) 'Functional Mimics of Glutathione Peroxidase: Bioinspired Synthetic Antioxidants', *Acc. Chem. Res*, 43(11), pp. 1408–1419.

Blesa, J. *et al.* (2015) 'Oxidative stress and Parkinson's disease', *Frontiers in Neuroanatomy*, 9(July), pp. 1–9. doi: 10.3389/fnana.2015.00091.

Blois, M. S. (1958) 'Antioxidant determinations by the use of a stable free radical', *Nature*, 181, pp. 1199–1200. doi: 10.1038/1811199a0.

Bolognesi, M. L. *et al.* (2010) 'Bis(7)-tacrine derivatives as multitarget-directed ligands: Focus on anticholinesterase and anti-amyloid activities', *ChemMedChem*, 5(8), pp. 1215–1220. doi: 10.1002/cmdc.201000086.

Bolognesi, M. L. *et al.* (2011) 'Multitargeted drugs discovery: Balancing anti-amyloid and anticholinesterase capacity in a single chemical entity', *Bioorganic and Medicinal Chemistry Letters*. Elsevier Ltd, 21(9), pp. 2655–2658. doi: 10.1016/j.bmcl.2010.12.093.

Bolognesi, M. L., Cavalli, A. and Melchiorre, C. (2009) 'Memoquin: A Multi-Target-Directed Ligand as an Innovative Therapeutic Opportunity for Alzheimer's Disease', *Neurotherapeutics*, 6(1), pp. 152–162. doi: 10.1016/j.nurt.2008.10.042.

Borch, R. F., Bernstein, M. D. and Durst, H. D. (1971) 'The Cyanohydridoborate Anion as a Selective Reducing Agent', *Journal of the American Chemical Society*, 93(12), pp. 2897–2904. doi: 10.1021/ja00741a013.

Borra, R. C. *et al.* (2009) 'A simple method to measure cell viability in proliferation and cytotoxicity assays MSc, Graduate Student – Graduate Program in A simple method to measure cell viability in proliferation and cytotoxicity assays', *Braz Oral Res*, 23(3), pp. 255–262. doi: 10.1590/S1806-83242009000300006.

Bouayed, J. and Bohn, T. (2010) 'Exogenous antioxidants - Double-edged swords in cellular redox state: Health beneficial effects at physiologic doses versus deleterious effects at high doses', *Oxidative Medicine and Cellular Longevity*, 3(4), pp. 228–237. doi: 10.4161/oxim.3.4.12858.

Bradford, M. M. (1976) 'A rapid and sensitive method for the quantitation of microgram quantities of protein utilizing the principle of protein-dye binding', *Analytical Biochemistry*, 72, pp. 248–254. doi: 10.1016/0003-234

2697(76)90527-3.

Bramblett, G. T. *et al.* (1993) 'Abnormal tau phosphorylation at Ser396 in alzheimer's disease recapitulates development and contributes to reduced microtubule binding', *Neuron*, 10(6), pp. 1089–1099. doi: 10.1016/0896-6273(93)90057-X.

Brand-Williams, W., Cuvelier, M. E. and Berset, C. (1995) 'Use of a free radical method to evaluate antioxidant activity', *LWT - Food Science and Technology*, 28(1), pp. 25–30. doi: 10.1016/S0023-6438(95)80008-5.

Brown, R. C., Lockwood, A. H. and Sonawane, B. R. (2005) 'Neurodegenerative diseases: An overview of environmental risk factors', *Environmental Health Perspectives*, 113(9), pp. 1250–1256. doi: 10.1289/ehp.7567.

Bryan, H. K. *et al.* (2013) 'The Nrf2 cell defence pathway: Keap1-dependent and -independent mechanisms of regulation', *Biochemical Pharmacology*. Elsevier Inc., 85(6), pp. 705–717. doi: 10.1016/j.bcp.2012.11.016.

Buée, L. *et al.* (2000) 'Tau protein isoforms, phosphorylation and role in neurodegenerative disorders', *Brain Research Reviews*, 33(1), pp. 95–130. doi: 10.1016/S0165-0173(00)00019-9.

Buendia, I. *et al.* (2015) 'New melatonin–cinnamate hybrids as multi-target drugs for neurodegenerative diseases: Nrf2-induction, antioxidant effect and neuroprotection', *Future Medicinal Chemistry*, 7(15), pp. 1961–1969. doi: 10.1016/B978-0-12-544952-6.50001-0.

Buenger, J. *et al.* (2006) 'An interlaboratory comparison of methods used to assess antioxidant potentials', *International Journal of Cosmetic Science*, 28(2), pp. 135–146. doi: 10.1111/j.1467-2494.2006.00311.x.

Burnette, N. W. (1981) "Western Blotting": Electrophoretic transfer of proteins from sodium dodecyl sulfate-polyacrylamide gels to unmodified nitrocellulose and radiographic detection with antibody and radioiodinated

protein A', *Analytical Biochemistry*, 112, pp. 195–203. doi: doi.org/10.1016/0003-2697(81)90281-5.

Butterfield, D. A., Swomley, A. M. and Sultana, R. (2013) 'Amyloid  $\beta$  - Peptide (1–42)-Induced Oxidative Stress in Alzheimer Disease: Importance in Disease Pathogenesis and Progression', *Antioxidants & Redox Signaling*, 19(8), pp. 823–835. doi: 10.1089/ars.2012.5027.

Cabrera, M. *et al.* (2015) 'New hits as phase II enzymes inducers from a focused library with heteroatom – heteroatom and Michael-acceptor motives', *Future Science OA*, 1(3), pp. 1–15.

Cadenas, E. and Davies, K. J. a. (2000) 'Mitochondrial free radical generation, oxidative stress, and aging', *Free Radical Biology and Medicine*, 29(3–4), pp. 222–230. doi: 10.1016/S0891-5849(00)00317-8.

Canas, N. *et al.* (2007) 'Chondroitin sulfate protects SH-SY5Y cells from oxidative stress by inducing heme oxygenase-1 via phosphatidylinositol 3-Kinase/Akt', *Journal of Pharmacology and Experimental Therapeutics*, 323(3), pp. 946–953. doi: 10.1124/jpet.107.123505.

Cao, G., Alessio, H. M. and Cutler, R. G. (1993) 'Oxygen-radical absorbance capacity assay for antioxidants', *Free Radical Biology and Medicine*, 14(3), pp. 303–311. doi: 10.1016/0891-5849(93)90027-R.

Carocho, M. and Ferreira, I. C. F. R. (2013) 'A review on antioxidants, prooxidants and related controversy: Natural and synthetic compounds, screening and analysis methodologies and future perspectives', *Food and Chemical Toxicology*, 51(1), pp. 15–25. doi: 10.1016/j.fct.2012.09.021.

Carreiras, M. C. *et al.* (2013) 'The Multifactorial Nature of Alzheimer's Disease for Developing Potential Therapeutics', *Current Topics in Medicinal Chemistry*, 13(15), pp. 1745–1770. doi: 10.2174/15680266113139990135.

Carugo, O. and Pongor, S. (2001) 'A normalized root-mean-square distance for comparing protein three-dimensional structures', *Protein Science*, 10, 236

pp. 1470–1473. doi: 10.1110/ps.690101.of.

Caulfield, M. P. (1993) 'Muscarinic Receptors-Characterization, coupling and function', *Pharmacology and Therapeutics*, 58(3), pp. 319–379. doi: 10.1016/0163-7258(93)90027-B.

Cavalli, A. *et al.* (2008) 'Multi-target-directed ligands to combat neurodegenerative diseases', *Journal of Medicinal Chemistry*, 51(3), pp. 347–372. doi: 10.1021/jm7009364.

Chand, K. *et al.* (2016) 'Tacrine-(hydroxybenzoyl-pyridone) hybrids as potential multifunctional anti-Alzheimer's agents: AChE inhibition, antioxidant activity and metal chelating capacity', *Journal of Inorganic Biochemistry*. Elsevier Inc., 163, pp. 266–277. doi: 10.1016/j.jinorgbio.2016.05.005.

Chao, X. *et al.* (2012) 'Design, synthesis and pharmacological evaluation of novel tacrine-caffeic acid hybrids as multi-targeted compounds against Alzheimer's disease', *Bioorganic and Medicinal Chemistry Letters*. Elsevier Ltd, 22(20), pp. 6498–6502. doi: 10.1016/j.bmcl.2012.08.036.

Cheignon, C. *et al.* (2018) 'Oxidative stress and the amyloid beta peptide in Alzheimer's disease', *Redox Biology*. Elsevier B.V., 14, pp. 450–464. doi: 10.1016/j.redox.2017.10.014.

Chen, X. *et al.* (2014) 'Acetylcholinesterase inhibitors with photoswitchable inhibition of  $\beta$ -amyloid aggregation', *ACS Chemical Neuroscience*, 5(5), pp. 377–389. doi: 10.1021/cn500016p.

Chen, Y. *et al.* (2012) 'Tacrine-ferulic acid-nitric oxide (NO) donor trihybrids as potent, multifunctional acetyl- and butyrylcholinesterase inhibitors', *Journal of Medicinal Chemistry*, 55(9), pp. 4309–4321. doi: 10.1021/jm300106z.

Chen, Y. *et al.* (2013) 'NO-donating tacrine derivatives as potential butyrylcholinesterase inhibitors with vasorelaxation activity', *Bioorganic and*

*Medicinal Chemistry Letters*. Elsevier Ltd, 23(11), pp. 3162–3165. doi: 10.1016/j.bmcl.2013.04.008.

Cheung, Y. T. *et al.* (2009) 'Effects of all-trans-retinoic acid on human SH-SY5Y neuroblastoma as in vitro model in neurotoxicity research', *NeuroToxicology*, 30(1), pp. 127–135. doi: 10.1016/j.neuro.2008.11.001.

Chigurupati, S. *et al.* (2018) 'Synthesis of azomethines derived from cinnamaldehyde and vanillin: in vitro acetylcholinesterase inhibitory, antioxidant and insilico molecular docking studies', *Medicinal Chemistry Research*. Springer US, 27(3), pp. 807–816. doi: 10.1007/s00044-017-2104-6.

Chong, J., Poutaraud, A. and Hugueney, P. (2009) 'Metabolism and roles of stilbenes in plants', *Plant Science*, 177(3), pp. 143–155. doi: 10.1016/j.plantsci.2009.05.012.

Chow, V. W. *et al.* (2010) 'An Overview of APP Processing Enzymes and Products', *Neuromolecular Med*, 12(1), pp. 1–12. doi: 10.1007/s12017-009-8104-z.

Colletier, J. P. *et al.* (2006) 'Conformational flexibility in the peripheral site of *Torpedo californica* acetylcholinesterase revealed by the complex structure with a bifunctional inhibitor', *Journal of the American Chemical Society*, 128(14), pp. 4526–4527. doi: 10.1021/ja058683b.

Collins, A. R. (2004) 'The comet assay for DNA damage and repair', *Molecular Biotechnology*, 26, pp. 249–261. doi: 10.1385/MB:26:3:249.

Colovic, M. B. *et al.* (2013) 'Acetylcholinesterase Inhibitors: Pharmacology and Toxicology', *Current Neuropharmacology*, 11(3), pp. 315–335. doi: 10.2174/1570159X11311030006.

Conner, E. M. and Grisham, M. B. (1996) 'Inflammation, free radicals and antioxidants', *Nutrition*, 12(4), pp. 274–277. doi: 10.1016/S0899-9007(96)00000-8.

Coombes, J. S. *et al.* (2000) 'Effect of combined supplementation with vitamin E and alpha-lipoic acid on myocardial performance during in vivo ischaemia-reperfusion', *Acta Physiologica Scandinavica*, 169(4), pp. 261–269. doi: 10.1046/j.1365-201X.2000.00740.x.

Coussens, L. M. and Werb, Z. (2002) 'Inflammation and Cancer', *Nature*, 420, pp. 860–867. doi: 10.1007/978-1-59745-447-6.

Creagan, E. T. *et al.* (1979) 'Failure of High-Dose Vitamin C (Ascorbic Acid) Therapy to Benefit Patients with Advanced Cancer — A Controlled Trial', *N Engl J Med*, 301(13), pp. 687–690. doi: 10.1056/NEJM198603063141003.

Crismon, M. L. (1994) 'Tacrine: First drug approved for Alzheimer's disease', *The Annals of Pharmacotherapy*, 28(6), pp. 744–751.

Cuajungco, M. P. *et al.* (2006) 'Metal Chelation as a Potential Therapy for Alzheimer's Disease', *Annals of the New York Academy of Sciences*, 920(1), pp. 292–304. doi: 10.1111/j.1749-6632.2000.tb06938.x.

Cummings, J. *et al.* (2018) 'Alzheimer's disease drug development pipeline: 2018', *Alzheimer's and Dementia: Translational Research and Clinical Interventions*. Elsevier Inc., 4, pp. 195–214. doi: 10.1016/j.trci.2018.03.009.

Dahlgren, C. and Karlsson, A. (1999) 'Respiratory burst in human neutrophils', *Journal of Immunological Methods*, 232(1–2), pp. 3–14. doi: 10.1016/S0022-1759(99)00146-5.

Dai, J. and Mumper, R. J. (2010) 'Plant phenolics: Extraction, analysis and their antioxidant and anticancer properties', *Molecules*, 15(10), pp. 7313–7352. doi: 10.3390/molecules15107313.

Daneman, R. and Prat, A. (2015) 'The Blood – Brain Barrier', *Cold Spring Harb Perspect Biol*, 7, pp. 1–24. doi: 10.1101/cshperspect.a020412.

Dangar, V. R., Borkhataria, K. N. and Shah, V. R. (2014) 'Synthesis,

Characterization and antimicrobial activity of Schiff's base derivatives of vanillin analog', *Journal of current chemical & pharmaceutical sciences*, 4(2), pp. 76–81.

Day, B. J. (2009) 'Catalase and glutathione peroxidase mimics', *Biochemistry Pharmacology*, 77(3), pp. 285–296. doi: 10.1016/j.bcp.2008.09.029.Catalase.

DeLange, R. J. and Glazer, A. N. (1989) 'Phycoerythrin fluorescence-based assay for peroxy radicals: A screen for biologically relevant protective agents', *Analytical Biochemistry*, 177(2), pp. 300–306. doi: 10.1016/0003-2697(89)90056-0.

Delanty, N. and Dichter, M. A. (2000) 'Antioxidant Therapy in Neurologic Disease', *Archives of Neurology*, 57(9), pp. 1265–1270. doi: 10.1001/archneur.57.9.1265.

Dennis, E. A. and Norris, P. C. (2015) 'Eicosanoid Storm in Infection and Inflammation', *Nature Reviews Immunology*, 15(8), pp. 511–523. doi: 10.1038/nri3859.Eicosanoid.

Detsi, A. *et al.* (2007) 'Design and synthesis of novel quinolinone-3-aminoamides and their alpha-lipoic acid adducts as antioxidant and anti-inflammatory agents', *J Med Chem*, 50(10), pp. 2450–2458. doi: 10.1021/jm061173n.

Dexter, D. T. *et al.* (1989) 'Basal Lipid Peroxidation in Substantia Nigra Is Increased in Parkinson's Disease', *Journal of Neurochemistry*, 52(2), pp. 381–389. doi: 10.1111/j.1471-4159.1989.tb09133.x.

Dgachi, Y. *et al.* (2017) 'Tetrahydropyranodiquinolin-8-amines as new, non hepatotoxic, antioxidant, and acetylcholinesterase inhibitors for Alzheimer's disease therapy', *European Journal of Medicinal Chemistry*. Elsevier Ltd, 126, pp. 576–589. doi: 10.1016/j.ejmech.2016.11.050.

Dhanalakshmi, C. *et al.* (2015) 'Neurosupportive Role of Vanillin, a Natural

240

Phenolic Compound, on Rotenone Induced Neurotoxicity in SH-SY5Y Neuroblastoma Cells', *Evidence-based Complementary and Alternative Medicine*, 2015. doi: 10.1155/2015/626028.

Di, L. *et al.* (2003) 'High throughput artificial membrane permeability assay for blood-brain barrier', *European Journal of Medicinal Chemistry*, 38(3), pp. 223–232. doi: 10.1016/S0223-5234(03)00012-6.

Du, J., Cullen, J. J. and Buettner, G. R. (2012) 'Ascorbic acid: Chemistry, biology and the treatment of cancer', *Biochimica et Biophysica Acta - Reviews on Cancer*. Elsevier B.V., 1826(2), pp. 443–457. doi: 10.1016/j.bbcan.2012.06.003.

Dudonné, S. *et al.* (2009) 'Comparative Study of Antioxidant Properties and Total Phenolic Content of 30 Plant Extracts of Industrial Interest Comparative Study of Antioxidant Properties and Total Phenolic Content of 30 Plant Extracts of Industrial Interest Using DPPH , ABTS , FRAP', *Journal of agricultural and food chemistry*, 57, pp. 1768–1774. doi: 10.1021/jf803011r.

Duthie, S. J. *et al.* (2009) 'Folate Deficiency In Vitro Induces Uracil Misincorporation and DNA Hypomethylation and Inhibits DNA Excision Repair in Immortalized Normal Human Colon Epithelial Cells', *Nutrition and Cancer*, 37(2), pp. 245–251. doi: 10.1207/S15327914NC372.

Dvir, H. *et al.* (2010) 'Acetylcholinesterase: From 3D structure to function', *Chemico-Biological Interactions*. Elsevier Ireland Ltd, 187(1–3), pp. 10–22. doi: 10.1016/j.cbi.2010.01.042.

Ellman, G. L. *et al.* (1961) 'A new and rapid colorimetric determination of acetylcholinesterase activity', *Biochemical Pharmacology*, 7(2), pp. 88–95. doi: 10.1016/0006-2952(61)90145-9.

Eruslanov, E. and Kusmartsev, S. (2010) 'Identification of ROS using oxidized DCFDA and flow-cytometry', *Methods in molecular biology*, 594, pp. 57–72. doi: 10.1007/978-1-60761-411-1\_4.

Fahlbusch, K.-G. *et al.* (2012) 'Flavors and fragrances', *Ullmann's Encyclopedia of industrial Chemistry*, 15, pp. 74–198. doi: 10.1002/14356007.a11.

Fang, L. *et al.* (2014) 'Design, synthesis and anti-Alzheimer properties of dimethylaminomethyl- substituted curcumin derivatives', *Bioorganic and Medicinal Chemistry Letters*. Elsevier Ltd, 24(1), pp. 40–43. doi: 10.1016/j.bmcl.2013.12.011.

Fedorova, T. N. *et al.* (2016) 'The protective effect of (S)-trolox-carnosine on a human neuroblastoma SH-SY5Y cell culture under the impact of heavy metals', *Neurochemical Journal*, 33(1), pp. 63–69. doi: 10.1134/S1819712416010086.

Feng, F. *et al.* (2007) 'Continuous fluorometric assays for acetylcholinesterase activity and inhibition with conjugated polyelectrolytes', *Angewandte Chemie - International Edition*, 119, pp. 8028–8032. doi: 10.1002/anie.200701724.

Fernandez, M. T. *et al.* (2002) 'Iron and copper chelation by flavonoids: an electrospray mass spectrometry study', *Journal of Inorganic Biochemistry*, 92, pp. 105–111. doi: 10.1016/S0162-0134(02)00511-1.

Firuzi, O. *et al.* (2005) 'Evaluation of the antioxidant activity of flavonoids by "ferric reducing antioxidant power" assay and cyclic voltammetry', *Biochimica et Biophysica Acta - General Subjects*, 1721(1–3), pp. 174–184. doi: 10.1016/j.bbagen.2004.11.001.

Firuzi, O. *et al.* (2011) 'Antioxidant therapy: current status and future prospects.', *Current medicinal chemistry*, 18(25), pp. 3871–88. doi: 10.2174/092986711803414368.

Fitzgerald, D. J. *et al.* (2004) 'Mode of antimicrobial of vanillin against *Escherichia coli*, *Lactobacillus plantarum* and *Listeria innocua*', *Journal of Applied Microbiology*, 97(1), pp. 104–113. doi: 10.1111/j.1365-2672.2004.02275.x.

Floegel, A. *et al.* (2011) 'Comparison of ABTS/DPPH assays to measure antioxidant capacity in popular antioxidant-rich US foods', *Journal of Food Composition and Analysis*. Elsevier Inc., 24(7), pp. 1043–1048. doi: 10.1016/j.jfca.2011.01.008.

Folin, O. and Ciocalteu, V. (1927) 'On Tyrosine and Tryptophane in Proteins', *Journal of Biological Chemistry*, 73(2), pp. 627–648.

Foti, M. C., Daquino, C. and Geraci, C. (2004) 'Electron-Transfer Reaction of Cinnamic Acids and Their Methyl Esters with the DPPH Radical in Alcoholic Solutions', *Journal of Organic Chemistry*, 69(7), pp. 2309–2314. doi: 10.1021/jo035758q.

Fragoso, Y. D. *et al.* (2012) 'Systematic review of the literature on vitamin A and memory', *Dementia & Neuropsychologia*, 6(4), pp. 219–222. doi: 10.1590/S1980-57642012DN06040005.

Friling, R. S. *et al.* (1990) 'Xenobiotic-inducible expression of murine glutathione S-transferase Ya subunit gene is controlled by an electrophile-responsive element', *Proceedings of the National Academy of Sciences of the United States of America*, 87(16), pp. 6258–62. doi: 10.1073/PNAS.87.16.6258.

Gandhi, S. and Abramov, A. Y. (2012) 'Mechanism of oxidative stress in neurodegeneration', *Oxidative Medicine and Cellular Longevity*, 2012, pp. 1–11. doi: 10.1155/2012/428010.

Gao, J. *et al.* (2016) 'Synthesis and biological evaluation of ranitidine analogs as multiple-target-directed cognitive enhancers for the treatment of Alzheimer's disease', *Bioorganic and Medicinal Chemistry Letters*. Elsevier Ltd, 26(22), pp. 5573–5579. doi: 10.1016/j.bmcl.2016.09.072.

Gao, Z. *et al.* (1999) 'Free radical scavenging and antioxidant activities of flavonoids extracted from the radix of *Scutellaria baicalensis* Georgi', *Structure*, 1472, pp. 643–650.

Gaspar, A. *et al.* (2009) 'New insights into the antioxidant activity of hydroxycinnamic acids: Synthesis and physicochemical characterization of novel halogenated derivatives', *European Journal of Medicinal Chemistry*, 44(5), pp. 2092–2099. doi: 10.1016/j.ejmech.2008.10.027.

Gerenu, G. *et al.* (2015) 'Curcumin/Melatonin Hybrid 5-(4-Hydroxy-phenyl)-3-oxo-pentanoic Acid [2-(5-Methoxy-1H-indol-3-yl)-ethyl]-amide Ameliorates AD-Like Pathology in the APP/PS1 Mouse Model', *ACS Chemical Neuroscience*, 6(8), pp. 1393–1399. doi: 10.1021/acschemneuro.5b00082.

Ghani, M. A. *et al.* (2017) 'Measurement of antioxidant activity with the thiobarbituric acid reactive substances assay', *Food Chemistry*. Elsevier Ltd, 230, pp. 195–207. doi: 10.1016/j.foodchem.2017.02.127.

Gilgun-Sherki, Y. *et al.* (2002) 'Antioxidant therapy in acute central nervous system injury: current state', *Pharmacol. Rev.*, 54(2), pp. 271–284. doi: 10.1124/pr.54.2.271.

Gloire, G., Legrand-Poels, S. and Piette, J. (2006) 'NF- $\kappa$ B activation by reactive oxygen species: Fifteen years later', *Biochemical Pharmacology*, 72(11), pp. 1493–1505. doi: 10.1016/j.bcp.2006.04.011.

Gordon, J., Amini, S. and White, M. K. (2013) 'General overview of neuronal cell culture', *Methods Mol. Biol.*, 1078, pp. 1–8. doi: 10.1007/978-1-62703-640-5.

Goszcz, K. *et al.* (2015) 'Antioxidants in Cardiovascular Therapy: Panacea or False Hope?', *Frontiers in Cardiovascular Medicine*, 2(July), pp. 1–22. doi: 10.3389/fcvm.2015.00029.

Gotti, C. and Clementi, F. (2004) 'Neuronal nicotinic receptors: from structure to pathology.', *Progress in neurobiology*, 74(6), pp. 363–96. doi: 10.1016/j.pneurobio.2004.09.006.

Greig, N. H., Lahiri, D. K. and Sambamurti, K. (2002) 'Butyrylcholinesterase: An important new target in Alzheimer's disease  
244

therapy', *International Psychogeriatrics*, 14(SUPPL. 1), pp. 77–91. doi: 10.1017/S1041610203008676.

Gülçin, I. (2006) 'Antioxidant activity of caffeic acid (3,4-dihydroxycinnamic acid)', *Toxicology*, 217(2–3), pp. 213–220. doi: 10.1016/j.tox.2005.09.011.

Gülden, M. *et al.* (2010) 'Cytotoxic potency of H<sub>2</sub>O<sub>2</sub> in cell cultures: Impact of cell concentration and exposure time', *Free Radical Biology and Medicine*. Elsevier Inc., 49(8), pp. 1298–1305. doi: 10.1016/j.freeradbiomed.2010.07.015.

Gutteridge, J. M. C. (1994) 'Biological origin of free radicals, and mechanisms of antioxidant protection', *Chemico-Biological Interactions*, 91(2–3), pp. 133–140. doi: 10.1016/0009-2797(94)90033-7.

Gutteridge, J. M. C. and Wilkins, S. (1983) 'Copper salt-dependent hydroxyl radical formation. Damage to proteins acting as antioxidants', *Biochimica et Biophysica Acta*, 759(1–2), pp. 38–41. doi: 10.1016/0304-4165(83)90186-1.

Hager, K. *et al.* (2007) 'α-Lipoic acid as a new treatment option for Alzheimer's disease — a 48 months follow-up analysis', *Journal of Neural Transmission*, 72, pp. 189–193. doi: 10.1007/978-3-211-73574-9\_24.

Hagerman, A. E. *et al.* (1998) 'High Molecular Weight Plant Polyphenolics (Tannins) as Biological Antioxidants', *Journal of Agricultural and Food Chemistry*, 46(5), pp. 1887–1892. doi: 10.1021/jf970975b.

Halliwell, B. (1990) 'How To Characterize a Biological Antioxidant', *Free Rad. Res. Comms*, 9(I), pp. 1–32.

Halliwell, B. (2007) 'Biochemistry of oxidative stress', *Biochemical Society Transactions*, 35(5), pp. 1147–1150. doi: 10.1042/BST0351147.

Halliwell, B. and Gutteridge, J. M. C. (1990) 'Role of free radicals and catalytic metal ions in human disease: An overview', *Methods in*

*Enzymology*, 186(C), pp. 1–85. doi: 10.1016/0076-6879(90)86093-B.

Halliwell, B. and Gutteridge, J. M. C. (1995) 'THE DEFINITION AND MEASUREMENT OF ANTIOXIDANTS IN BIOLOGICAL SYSTEMS', *Free Radical Biology and Medicine*, 18(I), pp. 125–126.

Harel, M. *et al.* (1993) 'Quaternary ligand binding to aromatic residues in the active-site gorge of acetylcholinesterase', *Proc. Natl. Acad. Sci.*, 90(October), pp. 9031–9035. doi: 10.1073/pnas.90.19.9031.

Harikumar, K. B. and Aggarwal, B. B. (2008) 'Resveratrol: A multitargeted agent for age-associated chronic diseases', *Cell Cycle*, 7(8), pp. 1020–1037. doi: 10.4161/cc.7.8.5740.

Harini, S. T. *et al.* (2012) 'Synthesis, antioxidant and antimicrobial activity of novel vanillin derived piperidin-4-one oxime esters: Preponderant role of the phenyl ester substituents on the piperidin-4-one oxime core', *Bioorganic and Medicinal Chemistry Letters*. Elsevier Ltd, 22(24), pp. 7588–7592. doi: 10.1016/j.bmcl.2012.10.019.

Hasselmo, M. E. (2006) 'The role of acetylcholine in learning and memory', *Current Opinion in Neurobiology*, 16(6), pp. 710–715. doi: 10.1016/j.conb.2006.09.002.

He, Y. *et al.* (2012) 'Soluble oligomers and fibrillar species of amyloid  $\beta$ -peptide differentially affect cognitive functions and hippocampal inflammatory response', *Biochemical and Biophysical Research Communications*, pp. 125–130. doi: 10.1016/j.bbrc.2012.10.129.

Heleno, S. A. *et al.* (2015) 'Bioactivity of phenolic acids: Metabolites versus parent compounds: A review', *Food Chemistry*. Elsevier Ltd, 173, pp. 501–513. doi: 10.1016/j.foodchem.2014.10.057.

Heuser, V. D. *et al.* (2007) 'Evaluation of genetic damage in Brazilian footwear-workers: Biomarkers of exposure, effect, and susceptibility', *Toxicology*, 232(3), pp. 235–247. doi: 10.1016/j.tox.2007.01.011.

Hix, S. and Augusto, O. (1999) 'DNA methylation by tert-butyl hydroperoxide-iron (II). A role for the transition metal ion in the production of DNA base adducts', *Chemico-Biological Interactions*, 118(2), pp. 141–149. doi: 10.1016/S0009-2797(99)00079-4.

Hocman, G. (1988) 'Chemoprevention of cancer: Phenolic antioxidants (BHT, BHA)', *International Journal of Biochemistry*, 20(7), pp. 639–651. doi: 10.1016/0020-711X(88)90158-9.

Hodges, M. D. *et al.* (1999) 'Improving the thiobarbituric acid-reactive-substances assay for estimating lipid peroxidation in plant tissues containing anthocyanin and other interfering compounds', *Planta*, 207, pp. 604–611.

Hollman, P. and Katan, M. (1997) 'Absorption, metabolism and health effects of dietary flavonoids in man', *Biomedicine & Pharmacotherapy*, 51(8), pp. 305–310. doi: 10.1016/S0753-3322(97)88045-6.

Houghton, P. J., Ren, Y. and Howes, M.-J. (2006) 'Acetylcholinesterase inhibitors from plants', *Phytomedicine*, 23, pp. 181–199. doi: 10.1016/j.phymed.2007.02.002.

Hu, F. *et al.* (2015) 'The plasma level of retinol, vitamins A, C and  $\alpha$ -tocopherol could reduce breast cancer risk? A meta-analysis and meta-regression', *J Cancer Res Clin Oncol*, 141(4), pp. 601–614. doi: 10.1007/s00432-014-1852-7.

Huang, D. *et al.* (2002) 'High-throughput assay of oxygen radical absorbance capacity (ORAC) using a multichannel liquid handling system coupled with a microplate fluorescence reader in 96-well format', *Journal of Agricultural and Food Chemistry*, 50(16), pp. 4437–4444. doi: 10.1021/jf0201529.

Huang, D., Boxin, O. U. and Prior, R. L. (2005) 'The chemistry behind antioxidant capacity assays', *Journal of Agricultural and Food Chemistry*, 53(6), pp. 1841–1856. doi: 10.1021/jf030723c.

Huang, L. *et al.* (2012) 'Multitarget-directed benzylideneindanone derivatives: Anti- $\beta$ -amyloid ( $A\beta$ ) aggregation, antioxidant, metal chelation, and monoamine oxidase B (MAO-B) inhibition properties against Alzheimer's disease', *Journal of Medicinal Chemistry*, 55(19), pp. 8483–8492. doi: 10.1021/jm300978h.

Hurtado-Puerto, A. M., Russo, C. and Fregni, F. (2018) 'Alzheimer s disease', *Neuromethods*, 138, pp. 297–338. doi: 10.1007/978-1-4939-7880-9\_9.

Hussain, S. P., Hofseth, L. J. and Harris, C. C. (2003) 'Radical causes of cancer', *Nature Reviews Cancer*, 3(4), pp. 276–285. doi: 10.1038/nrc1046.

Iaccarino, L. *et al.* (2018) 'Local and distant relationships between amyloid, tau and neurodegeneration in Alzheimer's Disease', *NeuroImage: Clinical*. Elsevier, 17, pp. 452–464. doi: 10.1016/j.nicl.2017.09.016.

Iqbal, K. *et al.* (2005) 'Tau pathology in Alzheimer disease and other tauopathies', *Biochimica et Biophysica Acta - Molecular Basis of Disease*, 1739(2), pp. 198–210. doi: 10.1016/j.bbadis.2004.09.008.

Isa, N. M. *et al.* (2012) 'In vitro anti-inflammatory, cytotoxic and antioxidant activities of boesenbergin A, a chalcone isolated from *Boesenbergia rotunda* (L.) (fingerroot)', *Brazilian Journal of Medical and Biological Research*, 45(6), pp. 524–530. doi: 10.1590/S0100-879X2012007500022.

Itoh, K. *et al.* (1999) 'Keap1 represses nuclear activation of antioxidant responsive elements by Nrf2 through binding to the amino-terminal Neh2 domain', *Genes and Development*, 13(1), pp. 76–86. doi: 10.1101/gad.13.1.76.

Jaisin, Y. *et al.* (2011) 'Curcumin I protects the dopaminergic cell line SH-SY5Y from 6-hydroxydopamine-induced neurotoxicity through attenuation of p53-mediated apoptosis', *Neuroscience Letters*. Elsevier Ireland Ltd, 489(3), pp. 192–196. doi: 10.1016/j.neulet.2010.12.014.

Janero, D. R. (1990) 'Malondialdehyde and thiobarbituric acid-reactivity as diagnostic indices of lipid peroxidation and peroxidative tissue injury', *Free Radical Biology and Medicine*, 9(6), pp. 515–540. doi: 10.1016/0891-5849(90)90131-2.

Janssen, Y. M. *et al.* (1995) 'Asbestos induces nuclear factor cB (NF-KcB) DNA-binding activity and NF-kB-dependent gene expression in tracheal epithelial cells', *Proceedings of the National Academy of Sciences of the United States of America*, 92(August), pp. 8458–8462. doi: 10.1073/pnas.92.18.8458.

Jayaraj, R. L. *et al.* (2013) 'Neuroprotective effect of CNB-001, a novel pyrazole derivative of curcumin on biochemical and apoptotic markers against rotenone-induced SK-N-SH cellular model of Parkinson's disease', *Journal of Molecular Neuroscience*, 51(3), pp. 863–870. doi: 10.1007/s12031-013-0075-8.

Jayaraj, R. L. *et al.* (2014) 'CNB-001 a novel curcumin derivative, guards dopamine neurons in MPTP model of Parkinson's disease', *BioMed Research International*, 2014, pp. 1–11. doi: 10.1155/2014/236182.

Jenner, P. (2003) 'Oxidative Stress in Parkinson's Disease', *Ann Neurol.*, 53(Suppl 3), pp. S26–S38. doi: 10.1002/ana.10483.uitination.

Jeong, J. B. *et al.* (2009) 'Protective effect of the extracts from *Cnidium officinale* against oxidative damage induced by hydrogen peroxide via antioxidant effect', *Food and Chemical Toxicology*. Elsevier Ltd, 47(3), pp. 525–529. doi: 10.1016/j.fct.2008.11.039.

Jin, X. *et al.* (2015) 'Pinocembrin Attenuates 6-OHDA-induced Neuronal Cell Death Through Nrf2/ARE Pathway in SH-SY5Y Cells', *Cellular and Molecular Neurobiology*, 35(3), pp. 323–333. doi: 10.1007/s10571-014-0128-8.

Johnson, G. and Moore, S. W. (2006) 'The peripheral anionic site of acetylcholinesterase: structure, functions and potential role in rational drug design.', *Current pharmaceutical design*, 12(2), pp. 217–225. doi:

10.2174/138161206775193127.

Johnson, J. A. *et al.* (2008) 'The Nrf2-ARE Pathway: An Indicator and Modulator of Oxidative Stress in Neurodegeneration', *Ann N Y Acad Sci.*, 1147, pp. 61–69. doi: 10.1196/annals.1427.036.

Johnson, J., Maher, P. and Hanneken, A. (2009) 'The flavonoid, eriodictyol, induces long-term protection in arpe-19 cells through its effects on Nrf2 activation and phase 2 gene expression', *Investigative Ophthalmology and Visual Science*, 50(5), pp. 2398–2406. doi: 10.1167/iops.08-2088.

Johnson, P. H. and Grossman, L. I. (1977) 'Electrophoresis of DNA in Agarose Gels. Optimizing Separations of Conformational Isomers of Double- and Single-Stranded DNAs', *Biochemistry*, 16(19), pp. 4217–4225. doi: 10.1021/bi00638a014.

Jomova, K. *et al.* (2010) 'Metals, oxidative stress and neurodegenerative disorders', *Molecular and Cellular Biochemistry*, 345(1–2), pp. 91–104. doi: 10.1007/s11010-010-0563-x.

Jomova, K., Baros, S. and Valko, M. (2012) 'Redox active metal-induced oxidative stress in biological systems', *Transition Metal Chemistry*, 37(2), pp. 127–134. doi: 10.1007/s11243-012-9583-6.

Kagan, V. E. and Tyurina, Y. Y. (1998) 'Recycling and Redox Cycling of Phenolic Antioxidants', *Ann N Y Acad Sci*, 854, pp. 425–434. doi: 10.1111/j.1365-3040.2007.01761.x.

Kaidery, N. A. *et al.* (2013) 'Targeting Nrf2-Mediated Gene Transcription by Extremely Potent Synthetic Triterpenoids Attenuate Dopaminergic Neurotoxicity in the MPTP Mouse Model of Parkinson's Disease', *Antioxidants & Redox Signaling*, 18(2), pp. 139–157. doi: 10.1089/ars.2011.4491.

Kamat, J. P., Ghosh, A. and Devasagayam, T. P. A. (2000) 'Vanillin as an antioxidant in rat liver mitochondria: Inhibition of protein oxidation and lipid peroxidation induced by photosensitization', *Molecular and Cellular* 250

*Biochemistry*, 209(1-2), pp. 47-53. doi: 10.1023/a:1007048313556.

Kansy, M., Senner, F. and Gubernator, K. (1998) 'Physicochemical High Throughput Screening : Parallel Artificial Membrane Permeation Assay in the Description of Passive Absorption Processes Screening : Parallel Artificial Membrane Permeation Assay in the Description of', *Journal of Medicinal Chemistry*, 41(7), pp. 1007-1010. doi: 10.1021/jm970530e.

Kaplowitz, N. (1981) 'The importance and regulation of hepatic glutathione', *Yale Journal of Biology and Medicine*, 54(6), pp. 497-502. doi: 10.1055/s-2008-1040481.

Kapoor, S. (2013) 'Multiorgan Anticarcinogenic Effects of Vanillin', *Journal of Medicinal Food*, 16(9), p. 777. doi: 10.1089/jmf.2013.0017.

Kaur, J. and Bachhawat, A. K. (2009) 'A modified Western blot protocol for enhanced sensitivity in the detection of a membrane protein', *Analytical Biochemistry*. Elsevier Inc., 384(2), pp. 348-349. doi: 10.1016/j.ab.2008.10.005.

Kedare, S. B. and Singh, R. P. (2011) 'Genesis and development of DPPH method of antioxidant assay', *Journal of Food Science and Technology*, 48(4), pp. 412-422. doi: 10.1007/s13197-011-0251-1.

Kelsey, N. A., Wilkins, H. M. and Linseman, D. A. (2010) 'Nutraceutical antioxidants as novel neuroprotective agents', *Molecules*, 15(11), pp. 7792-7814. doi: 10.3390/molecules15117792.

Kennedy, D. O. *et al.* (2010) 'Effects of resveratrol on cerebral blood flow variables and cognitive performance in humans: a double-blind , placebo-controlled , crossover investigation', *American Journal of Clinical Nutrition*, 91(5), pp. 1590-1597. doi: 10.3945/ajcn.2009.28641.The.

Khaledi, H. *et al.* (2011) 'Antioxidant, cytotoxic activities, and structure-activity relationship of gallic acid-based indole derivatives', *Arch. Pharm. Chem. Life Sci.*, 344(11), pp. 703-709. doi: 10.1002/ardp.201000223.

Kim, B. seaok, Moon, S. S. and Hwang, B. K. (1999) 'Isolation, identification, and antifungal activity of a macrolide antibiotic, oligomycin A, produced by *Streptomyces libani*', *Canadian Journal of Botany*, 77(6), pp. 850–858. doi: 10.1139/b99-044.

Kim, G. H. *et al.* (2015) 'The Role of Oxidative Stress in Neurodegenerative Diseases', *Experimental Neurobiology*, 24(4), p. 325. doi: 10.5607/en.2015.24.4.325.

King, A. A. *et al.* (2007) 'Antimutagenicity of Cinnamaldehyde and Vanillin in Human Cells: Global Gene Expression and Possible Role of DNA Damage and Repair', *Mutat Res*, 616(1–2), pp. 60–69. doi: 10.1016/j.mrfmmm.2006.11.022.

Klaunig, J. E. *et al.* (1998) 'The role of oxidative stress in chemical carcinogenesis', *Environmental Health Perspectives*, 106(Suppl 1), pp. 289–295. doi: 10.1289/ehp.98106s1289.

Kobayashi, A. *et al.* (2004) 'Oxidative Stress Sensor Keap1 Functions as an Adaptor for Cul3-Based E3 Ligase To Regulate Proteasomal Degradation of Nrf2', *Molecular and Cellular Biology*, 24(16), pp. 7130–7139. doi: 10.1128/MCB.24.16.7130.

Kojo, S. (2004) 'Vitamin C: Basic Metabolism and Its Function as an Index of Oxidative Stress', *Current Medicinal Chemistry*, 11(8), pp. 1041–1064. doi: 10.2174/0929867043455567.

Koufaki, M. *et al.* (2001) 'Novel potent inhibitors of lipid peroxidation with protective effects against reperfusion arrhythmias', *Journal of Medicinal Chemistry*, 44(24), pp. 4300–4303. doi: 10.1021/jm010962w.

Kovalevich, J. and Langford, D. (2013) 'Considerations for the Use of SH-SY5Y Neuroblastoma Cells in Neurobiology', *Methods Mol Biol.* 2013, 1078, pp. 9–21. doi: 10.1007/978-1-62703-640-5.

Kroemer, G., Galluzzi, L. and Brenner, C. (2007) 'Mitochondrial Membrane  
252

Permeabilization in Cell Death', *Physiology Review*, 87, pp. 99–163. doi: 10.1152/physrev.00013.2006.

Kryger, G., Silman, I. and Sussman, J. L. (1999) 'Structure of acetylcholinesterase complexed with E2020 (Aricept): Implications for the design of new anti-Alzheimer drugs', *Structure*, 7(3), pp. 297–307. doi: 10.1016/S0969-2126(99)80040-9.

Kubrak, O. I. *et al.* (2011) 'Cobalt-induced oxidative stress in brain, liver and kidney of goldfish *Carassius auratus*', *Chemosphere*. Elsevier Ltd, 85(6), pp. 983–989. doi: 10.1016/j.chemosphere.2011.06.078.

Kumar, S. S., Priyadarsini, K. I. and Sainis, K. B. (2004) 'Inhibition of Peroxynitrite-Mediated Reactions by Vanillin', *Journal of Agricultural and Food Chemistry*, 52(1), pp. 139–145. doi: 10.1021/jf030319d.

Kurien, B. T. and Scofield, R. H. (2006) 'Western blotting', *Methods*, 38(4), pp. 283–293. doi: 10.1016/j.ymeth.2005.11.007.

Kwon, S. H. *et al.* (2011) 'Loganin protects against hydrogen peroxide-induced apoptosis by inhibiting phosphorylation of JNK, p38, and ERK 1/2 MAPKs in SH-SY5Y cells', *Neurochemistry International*. Elsevier Ltd, 58(4), pp. 533–541. doi: 10.1016/j.neuint.2011.01.012.

Lan, X. *et al.* (2017) '(–)-Epicatechin, a Natural Flavonoid Compound, Protects Astrocytes Against Hemoglobin Toxicity via Nrf2 and AP-1 Signaling Pathways', *Molecular Neurobiology*, 54(10), pp. 7898–7907. doi: 10.1007/s12035-016-0271-y.

Landis, G. N. and Tower, J. (2005) 'Superoxide dismutase evolution and life span regulation', *Mechanisms of Ageing and Development*, 126(3), pp. 365–379. doi: 10.1016/j.mad.2004.08.012.

Langston, J. *et al.* (1983) 'Chronic Parkinsonism in humans due to a product of meperidine-analog synthesis', *Science*, 219(4587), pp. 979–980. doi: 10.1126/science.6823561.

Lardy, H. A., Connelly, J. L. and Johnson, D. (1964) 'Antibiotics as Tools for Metabolic Studies. II. Inhibition of Phosphoryl Transfer in Mitochondria by Oligomycin and Aurovertin', *Biochemistry*, 3(12), pp. 1961–1968. doi: 10.1021/bi00900a030.

Lau, A. *et al.* (2013) 'The Predicted Molecular Weight of Nrf2: It Is What It Is Not', *Antioxidants & Redox Signaling*, 18(1), pp. 91–93. doi: 10.1089/ars.2012.4754.

Lee, C. Y. *et al.* (2009) 'Synthesis and antioxidant properties of dendritic polyphenols', *Bioorganic and Medicinal Chemistry Letters*. Elsevier Ltd, 19(22), pp. 6326–6330. doi: 10.1016/j.bmcl.2009.09.088.

Lee, C. Y. *et al.* (2015) 'Effect of electron donating groups on polyphenol-based antioxidant dendrimers', *Biochimie*. Elsevier Ltd, 111, pp. 125–134. doi: 10.1016/j.biochi.2015.02.001.

Lee, H. J. *et al.* (2004) 'Syntheses and radical scavenging activities of resveratrol derivatives', *Bioorganic and Medicinal Chemistry Letters*, 14(2), pp. 463–466. doi: 10.1016/j.bmcl.2003.10.038.

Lee, J.-C. *et al.* (2002) 'Antioxidant Property of an Ethanol Extract of the Stem of *Opuntia ficus-indica* var. *Saboten*', *Journal of Agricultural and Food Chemistry*, 50(22), pp. 6490–6496. doi: 10.1021/jf020388c.

Lee, S. Y. *et al.* (2016) 'Vanillin attenuates negative effects of ultraviolet A on the stemness of human adipose tissue-derived mesenchymal stem cells', *Food and Chemical Toxicology*. Elsevier Ltd, 96, pp. 62–69. doi: 10.1016/j.fct.2016.07.023.

Leon, R., Garcia, A. G. and Marco-Contelles, J. (2013) 'Recent Advances in the Multitarget-Directed Ligands Approach for the Treatment of Alzheimer's Disease', *Medicinal Research Reviews*, 33(1), pp. 139–189. doi: doi.org/10.1002/med.20248.

Lewis, J. G., Stewart, W. and Adams, D. O. (1988) 'Role of Oxygen Radicals  
254

in Induction of DNA Damage by Metabolites of Benzene', *Cancer Research*, 48(17), pp. 4762–4765.

Li, N. *et al.* (2003) 'Mitochondrial complex I inhibitor rotenone induces apoptosis through enhancing mitochondrial reactive oxygen species production', *Journal of Biological Chemistry*, 278(10), pp. 8516–8525. doi: 10.1074/jbc.M210432200.

Li, S. Y., Wang, X. B. and Kong, L. Y. (2014) 'Design, synthesis and biological evaluation of imine resveratrol derivatives as multi-targeted agents against Alzheimer's disease', *European Journal of Medicinal Chemistry*, 71, pp. 36–45. doi: 10.1016/j.ejmech.2013.10.068.

Li, Y. *et al.* (2014) 'Design, synthesis and evaluation of rivastigmine and curcumin hybrids as site-activated multitarget-directed ligands for Alzheimer's disease therapy', *Bioorganic and Medicinal Chemistry*. Elsevier Ltd, 22(17), pp. 4717–4725. doi: 10.1016/j.bmc.2014.07.009.

Lin, M. T. and Beal, M. F. (2006) 'Mitochondrial dysfunction and oxidative stress in neurodegenerative diseases', *Nature*, 443(7113), pp. 787–795. doi: 10.1038/nature05292.

Lirdprapamongkol, K. *et al.* (2009) 'Vanillin suppresses metastatic potential of human cancer cells through PI3K inhibition and decreases angiogenesis in Vivo', *Journal of Agricultural and Food Chemistry*, 57(8), pp. 3055–3063. doi: 10.1021/jf803366f.

Liu, H. *et al.* (2014) 'AlzPlatform: An Alzheimer's disease domain-specific chemogenomics knowledgebase for polypharmacology and target identification research', *Journal of Chemical Information and Modeling*, 54(4), pp. 1050–1060. doi: 10.1021/ci500004h.

Liu, Q. *et al.* (2015) 'Design, synthesis and evaluation of chromone-2-carboxamido-alkylbenzylamines as multifunctional agents for the treatment of Alzheimer's disease', *Bioorganic and Medicinal Chemistry*. Elsevier Ltd, 23(5), pp. 911–923. doi: 10.1016/j.bmc.2015.01.042.

Liu, Y. *et al.* (2008) 'A broadly neuroprotective derivative of curcumin', *Journal of Neurochemistry*, 105(4), pp. 1336–1345. doi: 10.1111/j.1471-4159.2008.05236.x.

Lopes, F. M. *et al.* (2010) 'Comparison between proliferative and neuron-like SH-SY5Y cells as an in vitro model for Parkinson disease studies', *Brain Research*. Elsevier B.V., 1337, pp. 85–94. doi: 10.1016/j.brainres.2010.03.102.

López-Alarcón, C. and Denicola, A. (2013) 'Evaluating the antioxidant capacity of natural products: A review on chemical and cellular-based assays', *Analytica Chimica Acta*. Elsevier B.V., 763(1), pp. 1–10. doi: 10.1016/j.aca.2012.11.051.

Lovell, M. A. *et al.* (1998) 'Copper, iron and zinc in Alzheimer's disease senile plaques M.A.', *Journal of the Neurological Sciences*, 158, pp. 47–52. doi: 10.1177/1066896907302118.

Lu, Z. *et al.* (2006) 'Structure-activity relationship analysis of antioxidant ability and neuroprotective effect of gallic acid derivatives', *Neurochemistry International*, 48(4), pp. 263–274. doi: 10.1016/j.neuint.2005.10.010.

Luo, W. *et al.* (2011) 'Design, synthesis and evaluation of novel tacrine-multialkoxybenzene hybrids as dual inhibitors for cholinesterases and amyloid beta aggregation', *Bioorganic and Medicinal Chemistry*. Elsevier Ltd, 19(2), pp. 763–770. doi: 10.1016/j.bmc.2010.12.022.

M., W. (1999) 'Selectivity of cholinesterase inhibition: Clinical implications for the treatment of Alzheimer's disease', *CNS Drugs*, 12(4), pp. 307–323. Available at: <http://www.embase.com/search/results?subaction=viewrecord&from=export&id=L29503416>.

Ma, K. *et al.* (2015) 'Neurotoxicity effects of atrazine-induced SH-SY5Y human dopaminergic neuroblastoma cells via microglial activation', *Mol. BioSyst.*, 11(11), pp. 2915–2924. doi: 10.1039/C5MB00432B.

Ma, Q. (2014) 'Advances in mechanisms of anti-oxidation', *Discovery Medicine*, 17(93), pp. 121–130. doi: 10.1177/0963721412473755.Surging.

MacDonald-Wicks, K. L., Wood, L. G. and Garg, M. L. (2006) 'Methodology for the determination of biological antioxidant capacity in vitro: a review', *J Sci Food Agric*, 86, pp. 2046–2056. doi: 10.1002/jsfa.

Madamanchi, N. R., Vendrov, A. and Runge, M. S. (2005) 'Oxidative stress and vascular disease', *Arteriosclerosis, Thrombosis, and Vascular Biology*, 25(1), pp. 29–38. doi: 10.1161/01.ATV.0000150649.39934.13.

Mahmood, T. and Yang, P. C. (2015) 'Western blot: Technique, theory, and trouble shooting', *North American Journal of Medical Sciences*, 4(9), pp. 429–434. doi: 10.4103/1947-2714.100998.

Makni, M. *et al.* (2011) 'Evaluation of the antioxidant, anti-inflammatory and hepatoprotective properties of vanillin in carbon tetrachloride-treated rats', *European Journal of Pharmacology*. Elsevier B.V., 668(1–2), pp. 133–139. doi: 10.1016/j.ejphar.2011.07.001.

Makni, M. *et al.* (2012) 'Protective effect of vanillin against carbon tetrachloride (CCI 4)-induced oxidative brain injury in rats', *Toxicology and Industrial Health*, 28(7), pp. 655–662. doi: 10.1177/0748233711420472.

Manach, C. *et al.* (2004) 'Polyphenols: food sources and bioavailability', *The American Journal of Clinical Nutrition*, 79(5), pp. 727–747. doi: 10.1038/nature05488.

Mantovani, A. (2005) 'Inflammation by remote control', *Nature*. Nature Publishing Group, 435, p. 752. Available at: <http://dx.doi.org/10.1038/435752a>.

Marnett, L. J. *et al.* (1999) 'Arachidonic Acid Oxygenation by COX-1 and COX-2: Mechanisms of Catalysis and Inhibition', *The Journal of Biological Chemistry*, 274(33), pp. 22903–22907.

Massoulié, J. *et al.* (1993) 'Molecular and cellular biology of cholinesterases', *Progress in Neurobiology*, 41(1), pp. 31–91. doi: 10.1016/0301-0082(93)90040-Y.

Matralis, A. N. and Kourounakis, A. P. (2014) 'Design of Novel Potent Antihyperlipidemic Agents with Antioxidant / Anti-inflammatory Properties: Exploiting Phenothiazine's Strong Antioxidant Activity', *Journal of Medicinal Chemistry*, 57, pp. 2568–2581. doi: doi.org/10.1021/jm401842e.

Mattson, M. P. and Camandola, S. (2001) 'NF- $\kappa$ B in neuronal plasticity and neurodegenerative disorders', *Journal of Clinical Investigation*, pp. 247–254. doi: 10.1172/JCI11916.

McCain, J. (2013) 'The MAPK (ERK) Pathway: Investigational Combinations for the Treatment Of BRAF-Mutated Metastatic Melanoma', *P & T*., 38(2), pp. 96–108. Available at: <http://www.pubmedcentral.nih.gov/articlerender.fcgi?artid=3628180&tool=pmcentrez&rendertype=abstract>.

McCarty, R. E. (1992) 'A plant biochemist's view of H<sup>+</sup>-ATPases and ATP synthases', *Journal of Experimental Biology*, 172, pp. 431–441.

Mecocci, P. and Polidori, M. C. (2012) 'Antioxidant clinical trials in mild cognitive impairment and Alzheimer's disease', *Biochimica et Biophysica Acta*. Elsevier B.V., 1822(5), pp. 631–638. doi: 10.1016/j.bbadis.2011.10.006.

Mehta, M., Adem, A. and Sabbagh, M. (2012) 'New acetylcholinesterase inhibitors for alzheimer's disease', *International Journal of Alzheimer's Disease*, 2012. doi: <http://dx.doi.org/10.1155/2012/728983>.

Mesulam, M. (2004) 'The Cholinergic Lesion of Alzheimer's Disease: Pivotal Factor or Side Show?', *Learning and Memory*, 11(1), pp. 43–49. doi: 10.1101/lm.69204.

Meyers, C. L. F. and Meyers, D. J. (2008) 'Thin-layer chromatography', *Current Protocols in Nucleic Acid Chemistry*, (SUPPL. 34), pp. 1–13. doi: 10.1002/0471142700.nca03ds34.

Miller, N. J. *et al.* (1993) 'A Novel Method for Measuring Antioxidant Capacity and its Application to Monitoring the Antioxidant Status in Premature Neonates', *Clinical Science*, 84(4), pp. 407–412. doi: 10.1042/cs0840407.

Mohamed, T. and Rao, P. P. N. (2017) '2,4-Disubstituted quinazolines as amyloid- $\beta$  aggregation inhibitors with dual cholinesterase inhibition and antioxidant properties: Development and structure-activity relationship ( SAR ) studies', *European Journal of Medicinal Chemistry*. Elsevier Masson SAS, 126, pp. 823–843. doi: 10.1016/j.ejmech.2016.12.005.

Mohan, N. and Meltz, M. L. (1994) 'Induction of nuclear factor kappa B after low-dose ionizing radiation involves a reactive oxygen intermediate signaling pathway.', *Radiation research*, 140(1), pp. 97–104. doi: 10.2307/3578574.

Molecular Probes Invitrogen detection technologies (2004) 'Amplex <sup>®</sup> Red Acetylcholine / Acetylcholinesterase Assay Kit (A12217)', *Molecular Probes manual*, pp. 1–4. Available at: <https://www.lifetechnologies.com/order/catalog/product/A12217?ICID=search-product%5Cnhttp://tools.lifetechnologies.com/content/sfs/manuals/mp12217.pdf>.

Moncada, S. and Higgs, E. A. (1991) 'Endogenous nitric oxide: physiology, pathology and clinical relevance', *European Journal of Clinical Investigation*, 21, pp. 361–374.

Monji, A. *et al.* (2001) 'The relationship between the aggregational state of the amyloid- $\beta$  peptides and free radical generation by the peptides', *Journal of Neurochemistry*, 77(6), pp. 1425–1432. doi: 10.1046/j.1471-

4159.2001.00392.x.

Moon, J. and Shibamoto, T. (2009) 'Antioxidant Assays for Plant and Food Components', *J. Agr. Food Chem*, 57, pp. 1655–1666. doi: 10.1021/jf803537k.

Morris, G. A. (1986) 'Modern Techniques for Structure Elucidation', *Mag. Res. Chem.*, 24(December), pp. 371–403.

Moulin, C. *et al.* (1998) 'Synthesis and anti-inflammatory activity of N-(aza)arylcarboxamides derived from Trolox', *European Journal of Medicinal Chemistry*, 33(4), pp. 321–329. doi: 10.1016/S0223-5234(98)80065-2.

Mufson, E. J. *et al.* (2009) 'Cholinergic system during the progression of Alzheimer's disease: therapeutic implications', *Expert Review of Neurotherapeutics*, 8(11), pp. 1703–1718. doi: 10.1586/14737175.8.11.1703.Cholinergic.

Munoz, D. G. and Feldman, H. (2000) 'Causes of Alzheimer's disease', *Cmaj*, 162(1), pp. 65–72. doi: 10.1108/09526860010336984.

Mytilineou, C. and Cohen, G. (1985) 'Deprenyl Protects Dopamine Neurons from the Neurotoxic Effect of 1-Methyl-4-Phenylpyridinium Ion', *Journal of Neurochemistry*, 45(6), pp. 1951–1953. doi: 10.1111/j.1471-4159.1985.tb10556.x.

Nagpal, K., Singh, S. K. and Mishra, D. N. (2013) 'Drug targeting to brain: a systematic approach to study the factors, parameters and approaches for prediction of permeability of drugs across BBB', *Expert Opinion on Drug Delivery*, 10(7), pp. 927–955. doi: 10.1517/17425247.2013.762354.

Nakata, R., Takahashi, S. and Inoue, H. (2012) 'Recent Advances in the Study on Resveratrol', *Biol. Pharm. Bull*, 353(March), pp. 273–279. doi: JST.JSTAGE/bpb/35.273 [pii].

Nalivaeva, N. N. and Turner, A. J. (2013) 'The amyloid precursor protein: A  
260

biochemical enigma in brain development, function and disease', *FEBS Letters*. Federation of European Biochemical Societies, 587(13), pp. 2046–2054. doi: 10.1016/j.febslet.2013.05.010.

Newhouse, K. *et al.* (2004) 'Rotenone-induced apoptosis is mediated by p38 and JNK MAP kinases in human dopaminergic SH-SY5Y cells', *Toxicological Sciences*, 79(1), pp. 137–146. doi: 10.1093/toxsci/kfh089.

Newton, K. and Dixit, V. M. (2012) 'Signaling in innate immunity and inflammation', *Cold Spring Harbor Perspectives in Biology*, 4(3), pp. 1–19. doi: 10.1101/cshperspect.a006049.

Nguyen, T., Nioi, P. and Pickett, C. B. (2009) 'The Nrf2-Antioxidant Response Element Signaling Pathway and Its Activation by Oxidative Stress', *The Journal of Biological Chemistry*, 284(20), pp. 13291–13295. doi: 10.1146/annurev-pharmtox-011112-14032.

Niki, E. (1987) 'Antioxidants in relation to lipid peroxidation', *Chemistry and Physics of Lipids*, 44(2–4), pp. 227–253. doi: 10.1016/0009-3084(87)90052-1.

Nimse, S. B. and Pal, D. (2015) 'Free radicals, natural antioxidants, and their reaction mechanisms', *RSC Advances*. Royal Society of Chemistry, 5(35), pp. 27986–28006. doi: 10.1039/c4ra13315c.

Noro, J. *et al.* (2015) 'Evaluation of New Naphthalimides as Potential Anticancer Agents against Breast Cancer MCF-7, Pancreatic Cancer BxPC-3 and Colon Cancer HCT- 15 Cell Lines', *Organic Chemistry: Current Research*, 4(3), pp. 1–11. doi: 10.4172/2161-0401.1000144.

Ogita, H. and Liao, J. K. (2004) 'Endothelial Function and Oxidative Stress', *Endothelium*, 11(2), pp. 123–132. doi: 10.1080/10623320490482664.

Ojha, S. *et al.* (2015) 'Neuroprotective potential of ferulic acid in the rotenone model of Parkinson's disease', *Drug Design, Development and Therapy*, 9, pp. 5499–5510. doi: 10.2147/DDDT.S90616.

Olanow, C. W. *et al.* (1995) 'The effect of Deprenyl and Levodopa on the progression of Parkinson's disease', *Ann Neurol*, 38, pp. 771–777.

Olive, P. L. and Banáth, J. P. (2006) 'The comet assay: A method to measure DNA damage in individual cells', *Nature Protocols*, 1(1), pp. 23–29. doi: 10.1038/nprot.2006.5.

Olivieri, G. *et al.* (2001) 'Melatonin protects SHSY5Y neuroblastoma cells from cobalt-induced oxidative stress, neurotoxicity and increased  $\beta$ -amyloid secretion', *Journal of Pineal Research*, 31(4), pp. 320–325. doi: 10.1034/j.1600-079X.2001.310406.x.

Ostling, O. and Johanson, K. J. (1984) 'Microelectrophoretic study of radiation-induced DNA damages in individual mammalian cells', *Biochemical and Biophysical Research Communications*, 123(1), pp. 291–298. doi: doi.org/10.1016/0006-291X(84)90411-X.

Othman, S. Ben and Yabe, T. (2015) 'Use of Hydrogen Peroxide and Peroxyl Radicals To Induce Oxidative Stress in Neuronal Cells', *Reviews in Agricultural Science*, 3(0), pp. 40–45. doi: 10.7831/RAS.3.40-45.

Ou, B., Hampsch-Woodill, M. and Prior, R. L. (2001) 'Development and validation of an improved oxygen radical absorbance capacity assay using fluorescein as the fluorescent probe', *Journal of Agricultural and Food Chemistry*, 49(10), pp. 4619–4626. doi: 10.1021/jf010586o.

Packer, L., Witt, E. H. and Tritschler, H. J. (1995) 'Alpha-lipoic acid as biological antioxidant', *Free Radic Biol Med*, 19(2), pp. 227–250. doi: 10.1016/0891-5849(95)00017-R.

Palanki, M. S. S. (2002) 'Inhibitors of AP-1 and NF- $\kappa$ B Mediated Transcriptional Activation. Therapeutic Potential in Autoimmune Diseases and Structural Diversity', *Current Medicinal Chemistry*, 9, pp. 219–227. doi: doi.org/10.2174/0929867023371265.

Pandey, P. K., Sharma, A. K. and Gupta, U. (2016) 'Blood brain barrier: An  
262

overview on strategies in drug delivery, realistic in vitro modeling and in vivo live tracking', *Tissue Barriers*, 4(1), pp. 1–14. doi: 10.1080/21688370.2015.1129476.

Panek, D. *et al.* (2017) 'Advances toward multifunctional cholinesterase and  $\beta$ -amyloid aggregation inhibitors', *Future Medicinal Chemistry*, 9(15), pp. 1835–1854. doi: 10.4155/fmc-2017-0094.

Panek, D. *et al.* (2018) 'Design, Synthesis, and Biological Evaluation of 1-Benzylamino-2-hydroxyalkyl Derivatives as New Potential Disease-Modifying Multifunctional Anti-Alzheimer's Agents', *ACS Chemical Neuroscience*, 9(5), pp. 1074–1094. doi: 10.1021/acschemneuro.7b00461.

Pardridge, W. M. (2003) 'Blood-Brain Barrier Drug Targeting: the Future of Brain Drug Development', *Molecular Interventions*, 3(2), pp. 90–105. doi: 10.1124/mi.3.2.90.

Parent, M. J. *et al.* (2013) 'Cholinergic Depletion in Alzheimer's Disease Shown by [  $^{18}\text{F}$  ] FEOBV Autoradiography', *International Journal of Molecular Imaging*, 2013, pp. 1–6.

Payet, B., Sing, A. S. C. and Smadja, J. (2005) 'Assessment of antioxidant activity of cane brown sugars by ABTS and DPPH radical scavenging assays: Determination of their polyphenolic and volatile constituents', *Journal of Agricultural and Food Chemistry*, 53(26), pp. 10074–10079. doi: 10.1021/jf0517703.

Pearse, A. G. E. (1957) 'Intracellular localisation of dehydrogenase systems using monotetrazolium salts and metal chelation of their formazans', *Journal of Histochemistry & Cytochemistry*, 5(5), pp. 515–527.

Pearson, G. *et al.* (2001) 'Mitogen-Activated Protein (MAP) Kinase Pathways: Regulation and Physiological Functions', *Endocrine Reviews*, 22(2), pp. 153–183. doi: 10.1210/edrv.22.2.0428.

Pease, L. F. *et al.* (2008) 'Determination of Protein Aggregation With

Differential Mobility Analysis: Application to IgG Antibody', *Biotechnology and Bioengineering*, 101(6), pp. 1214–1222. doi: 10.1002/bit.22017.

Pérez-Cruz, K. *et al.* (2018) 'Synthesis and antioxidant study of new polyphenolic hybrid-coumarins', *Arabian Journal of Chemistry*, 11(4), pp. 525–537. doi: 10.1016/j.arabjc.2017.05.007.

Perron, N. R. and Brumaghim, J. L. (2009) 'A review of the antioxidant mechanisms of polyphenol compounds related to iron binding', *Cell Biochemistry and Biophysics*, 53(2), pp. 75–100. doi: 10.1007/s12013-009-9043-x.

Perry, E. K. *et al.* (1978) 'Correlation of cholinergic abnormalities with senile plaques and mental test scores in senile dementia', *British Medical Journal*, 2, pp. 1457–1459.

Picciano, A. L. and Vaden, T. D. (2013) 'Complexation between Cu(II) and curcumin in the presence of two different segments of amyloid  $\beta$ ', *Biophysical Chemistry*. Elsevier B.V., 184, pp. 62–67. doi: 10.1016/j.bpc.2013.09.004.

Pignatello, J. J., Oliveros, E. and MacKay, A. (2006) 'Advanced oxidation processes for organic contaminant destruction based on the fenton reaction and related chemistry', *Critical Reviews in Environmental Science and Technology*, 36(1), pp. 1–84. doi: 10.1080/10643380500326564.

Pinnen, F. *et al.* (2009) 'Codrugs Linking L -Dopa and Sulfur-Containing Antioxidants: New Pharmacological Tools against Parkinson ' s Disease', *J. Med. Chem.*, 52(2), pp. 559–563. doi: 10.1021/jm801266x.

Pisoschi, A. M. and Pop, A. (2015) 'The role of antioxidants in the chemistry of oxidative stress: A review', *European Journal of Medicinal Chemistry*. Elsevier Masson SAS, 97, pp. 55–74. doi: 10.1016/j.ejmech.2015.04.040.

Pohl, F. *et al.* (2018) 'Revalorisation of rapeseed pomace extracts: An in vitro study into its anti-oxidant and DNA protective properties', *Food*

*Chemistry*. Elsevier Ltd, 239, pp. 323–332. doi: 10.1016/j.foodchem.2017.06.129.

Pohl, F. (2019) 'The Potential Application of Rapeseed Pomace Extracts in the prevention and Treatment of Neurodegenerative Disease', Doctoral Dissertation.

Poljsak, B. and Milisav, I. (2012) 'The neglected significance of "antioxidative stress"', *Oxidative Medicine and Cellular Longevity*, 2012, pp. 1–12. doi: 10.1155/2012/480895.

Poljsak, B., Šuput, D. and Milisav, I. (2013a) 'Achieving the balance between ROS and antioxidants: When to use the synthetic antioxidants.', *Oxidative medicine and cellular longevity*, 2013, pp. 1–11. doi: 10.1155/2013/956792.

Poljsak, B., Šuput, D. and Milisav, I. (2013b) 'Achieving the balance between ROS and antioxidants: When to use the synthetic antioxidants', *Oxidative Medicine and Cellular Longevity*, 2013, pp. 1–12. doi: 10.1155/2013/956792.

van Poppel, G. and van den Berg, H. (1997) 'Vitamins and cancer', *Cancer Letters*, 114, pp. 195–202. doi: doi.org/10.1016/S0304-3835(97)04662-4.

Prince, M. *et al.* (2014) *Dementia UK: Second edition*. Available at: [http://eprints.lse.ac.uk/59437/1/Dementia\\_UK\\_Second\\_edition\\_-\\_Overview.pdf](http://eprints.lse.ac.uk/59437/1/Dementia_UK_Second_edition_-_Overview.pdf) [http://www.alzheimers.org.uk/site/scripts/download\\_info.php?fileID=2323](http://www.alzheimers.org.uk/site/scripts/download_info.php?fileID=2323).

Pu, X., Wang, Z. and Klaunig, J. E. (2015) 'Alkaline comet assay for assessing DNA damage in individual cells', *Current Protocols in Toxicology*, 2015(August), p. 3.12.1-3.12.11. doi: 10.1002/0471140856.tx0312s65.

Pulido, R., Bravo, L. and Saura-Calixto, F. (2000) 'Antioxidant activity of dietary polyphenols as determined by a modified ferric reducing/antioxidant power assay', *Journal of Agricultural and Food Chemistry*, 48(8), pp. 3396–3402. doi: 10.1021/jf9913458.

Radomski, M. W., Palmer, R. M. and Moncada, S. (1990) 'An L-arginine/nitric oxide pathway present in human platelets regulates aggregation.', *Proc. Natl. Acad. Sci.*, 87, pp. 5193–5197. doi: 10.1073/pnas.87.13.5193.

Rahman, K. (2007) 'Studies on free radicals, antioxidants, and co-factors.', *Clinical interventions in aging*, 2(2), pp. 219–236. doi: <http://dx.doi.org/>.

Ramassamy, C. (2006) 'Emerging role of polyphenolic compounds in the treatment of neurodegenerative diseases: A review of their intracellular targets', *European Journal of Pharmacology*, 545(1), pp. 51–64. doi: 10.1016/j.ejphar.2006.06.025.

Rangaswamy, J. *et al.* (2012) 'Synthesis of benzofuran based 1,3,5-substituted pyrazole derivatives: As a new class of potent antioxidants and antimicrobials-A novel accost to amend biocompatibility', *Bioorganic and Medicinal Chemistry Letters*. Elsevier Ltd, 22(14), pp. 4773–4777. doi: 10.1016/j.bmcl.2012.05.061.

El Razik, H. A. *et al.* (2017) 'Benzodioxole–pyrazole hybrids as anti-inflammatory and analgesic agents with COX-1,2/5-LOX inhibition and antioxidant potential', *Arch. Pharm. Chem. Life Sci.*, 350, pp. 1–19. doi: 10.1002/ardp.201700026.

Recanatini, M. *et al.* (2000) 'SAR of 9-Amino-1,2,3,4-tetrahydroacridine-Based Acetylcholinesterase Inhibitors: Synthesis, Enzyme Inhibitory Activity, QSAR, and Structure-Based CoMFA of Tacrine Analogues', *Journal of Medicinal Chemistry*, pp. 2007–2018. doi: 10.1021/jm990971t.

Reinke, A. A. and Gestwicki, J. E. (2007) 'Structure-activity relationships of amyloid beta-aggregation inhibitors based on curcumin: Influence of linker length and flexibility', *Chemical Biology and Drug Design*, 70(3), pp. 206–215. doi: 10.1111/j.1747-0285.2007.00557.x.

Reuter, S. *et al.* (2010) 'Oxidative stress, inflammation, and cancer: How  
266

are they linked?', *Free Radical Biology and Medicine*. Elsevier Inc., 49(11), pp. 1603–1616. doi: 10.1016/j.freeradbiomed.2010.09.006.

Rodríguez-Franco, M. I. *et al.* (2006) 'Novel tacrine-melatonin hybrids as dual-acting drugs for alzheimer disease, with improved acetylcholinesterase inhibitory and antioxidant properties', *Journal of Medicinal Chemistry*, 49(2), pp. 459–462. doi: 10.1021/jm050746d.

Rodriguez-Pallares, J. *et al.* (2007) 'Mechanism of 6-hydroxydopamine neurotoxicity: The role of NADPH oxidase and microglial activation in 6-hydroxydopamine-induced degeneration of dopaminergic neurons', *Journal of Neurochemistry*, 103(1), pp. 145–156. doi: 10.1111/j.1471-4159.2007.04699.x.

Rodriguez-Rodriguez, C. *et al.* (2010) 'Crystal structure of thioflavin-T and its binding to amyloid fibrils: insights at the molecular level', *ChemComm*, 46, pp. 1156–1158. doi: 10.1039/b912396b.

Rosini, M. *et al.* (2005) 'Rational approach to discover multipotent anti-Alzheimer drugs', *Journal of Medicinal Chemistry*, 48(2), pp. 360–363. doi: 10.1021/jm049112h.

Rosini, M. *et al.* (2008) 'Inhibition of acetylcholinesterase,  $\beta$ -amyloid aggregation, and NMDA receptors in Alzheimer's disease: A promising direction for the multi-target-directed ligands gold rush', *Journal of Medicinal Chemistry*, 51(15), pp. 4381–4384. doi: 10.1021/jm800577j.

Rosini, M. *et al.* (2013) 'Oxidative Stress in Alzheimer ' s Disease : Are We Connecting the Dots?', *Journal of Medicinal Chemistry*, 57, pp. 2821–2831.

Rothman, S. M. and Olney, J. W. (1987) 'Excitotoxicity and the NMDA receptor', *Trends in Neurosciences*, 10(7), pp. 299–302. doi: 10.1016/0166-2236(87)90177-9.

Rothstein, J. D. (2017) 'Edaravone: A new drug approved for ALS', *Cell*. Elsevier, 171(4), p. 725. doi: 10.1016/j.cell.2017.10.011.

Rothwell, N. J. (1992) 'Eicosanoids, thermogenesis and thermoregulation', *Prostaglandins, Leukotrienes and Essential Fatty Acids*, 46(1), pp. 1–7. doi: 10.1016/0952-3278(92)90051-J.

Roy, M. K. *et al.* (2010) 'ORAC and DPPH assay comparison to assess antioxidant capacity of tea infusions: Relationship between total polyphenol and individual catechin content', *International Journal of Food Sciences and Nutrition*, 61(2), pp. 109–124. doi: 10.3109/09637480903292601.

Ruffels, J., Griffin, M. and Dickenson, J. M. (2004) 'Activation of ERK1/2, JNK and PKB by hydrogen peroxide in human SH-SY5Y neuroblastoma cells: Role of ERK1/2 in H<sub>2</sub>O<sub>2</sub>-induced cell death', *European Journal of Pharmacology*, 483(2–3), pp. 163–173. doi: 10.1016/j.ejphar.2003.10.032.

Rydberg, E. H. *et al.* (2006) 'Complexes of Alkylene-linked tacrine dimers with *Torpedo californica* acetylcholinesterase: Binding of bis(5)-tacrine produces a dramatic rearrangement in the active-site gorge', *Journal of Medicinal Chemistry*, 49(18), pp. 5491–5500. doi: 10.1021/jm060164b.

Saini, R. and Saxena, A. K. (2018) 'The Structural Hybrids of Acetylcholinesterase Inhibitors in the Treatment of Alzheimer's Disease: A Review', *HSOA Journal of Alzheimer's and Neurodegenerative Diseases*, 4(1), pp. 1–25. doi: 10.24966/AND-9608/100015.

Sameem, B. *et al.* (2017) 'A review on tacrine-based scaffolds as multi-target drugs (MTDLs) for Alzheimer's disease', *European Journal of Medicinal Chemistry*, 128, pp. 332–345. doi: 10.1016/j.ejmech.2016.10.060.

Sano, M. *et al.* (1997) 'A Controlled Trial of Selegiline, Alpha-Tocopherol, or Both as Treatment for Alzheimer's Disease', *New England Journal of Medicine*, 336(17), pp. 1216–1222. doi: 10.1056/NEJM199704243361704.

Savaskan, E. *et al.* (2003) 'Red wine ingredient resveratrol protects from  $\beta$ -amyloid neurotoxicity', *Gerontology*, 49(6), pp. 380–383. doi: 10.1159/000073766.

Sawa, T., Akaike, T. and Maeda, H. (2000) 'Tyrosine nitration by peroxynitrite formed from nitric oxide and superoxide generated by xanthine oxidase', *Journal of Biological Chemistry*, 275(42), pp. 32467–32474. doi: 10.1074/jbc.M910169199.

Schneider, L. *et al.* (2011) 'Differentiation of SH-SY5Y cells to a neuronal phenotype changes cellular bioenergetics and the response to oxidative stress', *Free Radic Biol Med*, 51(11), pp. 2007–2017. doi: 10.1016/j.freeradbiomed.2011.08.030.Differentiation.

Scott, J. W. *et al.* (1974) '6-Hydroxychroman-2-carboxylic acids: Novel antioxidants', *Journal of the American Oil Chemists' Society*, 51(5), pp. 200–203. doi: 10.1007/BF02632894.

Sesso, H. D. *et al.* (2013) 'Multivitamins in the Prevention of Cardiovascular Disease in Men: The Physicians' Health Study II Randomized Controlled Trial', *Journal of the American Medical Association*, 308(17), pp. 1751–1760. doi: 10.1001/jama.2012.14805.Multivitamins.

Shinkai, H. (2012) 'Cholesteryl ester transfer-protein modulator and inhibitors and their potential for the treatment of cardiovascular diseases', *Vasc. Health Risk Manag.*, 8, pp. 323–331.

Shiple, M. M., Mangold, C. A. and Szpara, M. L. (2016) 'Differentiation of the SH-SY5Y Human Neuroblastoma Cell Line', *Journal of Visualized Experiments*, (108), pp. 1–11. doi: 10.3791/53193.

Sies, H. (1991) 'Oxidative stress: From basic research to clinical application', *The American Journal of Medicine*, 91(3 SUPPL. 3), pp. 31–38. doi: 10.1016/0002-9343(91)90281-2.

Sies, H. (2015) 'Oxidative stress: A concept in redox biology and medicine', *Redox Biology*. Elsevier, 4, pp. 180–183. doi: 10.1016/j.redox.2015.01.002.

Singh, M. *et al.* (2016) 'Hybrids: a new paradigm to treat Alzheimer's disease', *Molecular Diversity*. Springer International Publishing, 20(1), pp. 271–297. doi: 10.1007/s11030-015-9628-9.

Singleton, V. L., Orthofer, R. and Lamuela-Raventós, R. M. (1999) 'Analysis of total phenols and other oxidation substrates and antioxidants by means of folin-ciocalteu reagent', *Methods in Enzymology*, 299(1974), pp. 152–178. doi: 10.1016/S0076-6879(99)99017-1.

Siuzdak, G. (1996) *Ion sources and sample introduction, Mass Spectrometry for Biotechnology*. Academic Press CA, USA.

Skovronsky, D. M., Lee, V. M.-Y. and Trojanowski, J. Q. (2006) 'NEURODEGENERATIVE DISEASES: New Concepts of Pathogenesis and Their Therapeutic Implications', *Annual Review of Pathology: Mechanisms of Disease*, 1(1), pp. 151–170. doi: 10.1146/annurev.pathol.1.110304.100113.

Smith, M. A. *et al.* (2000) 'Oxidative stress in Alzheimer's disease', *Biochimica et Biophysica Acta*, 1502, pp. 139–144.

Smith, W. W. *et al.* (2005) 'α-Synuclein Phosphorylation Enhances Eosinophilic Cytoplasmic Inclusion Formation in SH-SY5Y Cells', *Journal of Neuroscience*, 25(23), pp. 5544–5552. doi: 10.1523/JNEUROSCI.0482-05.2005.

Soares, D. G., Andrezza, A. C. and Salvador, M. (2003) 'Sequestering ability of butylated hydroxytoluene, propyl gallate, resveratrol, and vitamins C and E against ABTS, DPPH, and hydroxyl free radicals in chemical and biological systems', *Journal of Agricultural and Food Chemistry*, 51(4), pp. 1077–1080. doi: 10.1021/jf020864z.

Soto-Otero, R. *et al.* (2000) 'Autoxidation and neurotoxicity of 6-hydroxydopamine in the presence of some antioxidants: Potential implication in relation to the pathogenesis of Parkinson's disease', *Journal of Neurochemistry*, 74(4), pp. 1605–1612. doi: 10.1046/j.1471-4159.2000.0741605.x.

Spencer, B. J. and Verma, I. M. (2007) 'Targeted delivery of proteins across  
270

the blood-brain barrier', *Proceedings of the National Academy of Sciences*, 104(18), pp. 7594–7599. doi: 10.1073/pnas.0702170104.

Spencer, J. P. E. (2008) 'Flavonoids: Modulators of brain function?', *British Journal of Nutrition*, 99(E-SUPPL. 1), pp. 60–77. doi: 10.1017/S0007114508965776.

Stahl, W. and Sies, H. (2003) 'Antioxidant activity of carotenoids', *Molecular Aspects of Medicine*, 24(6), pp. 345–351. doi: 10.1016/S0098-2997(03)00030-X.

Suematsu, N., Hosoda, M. and Fujimori, K. (2011) 'Protective effects of quercetin against hydrogen peroxide-induced apoptosis in human neuronal SH-SY5Y cells', *Neuroscience Letters*. Elsevier Ireland Ltd, 504(3), pp. 223–227. doi: 10.1016/j.neulet.2011.09.028.

Sung, C.-C. *et al.* (2013) 'Oxidative Stress and Nucleic Acid Oxidation in Patients with Chronic Kidney Disease', *Oxidative Medicine and Cellular Longevity*, 2013, pp. 1–15. doi: 10.1155/2013/301982.

Szymański, P., Zurek, E. and Mikiciuk-Olasik, E. (2006) 'New tacrine-hydrazinonicotinamide hybrids as acetylcholinesterase inhibitors of potential interest for the early diagnostics of Alzheimer's disease', *Pharmazie*, 61(4), pp. 269–273. doi: 10.1002/chin.200629134.

Tai, A. *et al.* (2011) 'Evaluation of antioxidant activity of vanillin by using multiple antioxidant assays', *Biochimica et Biophysica Acta*. Elsevier B.V., 1810(2), pp. 170–177. doi: 10.1016/j.bbagen.2010.11.004.

Tai, A., Sawano, T. and Yazama, F. (2011) 'Antioxidant Properties of Ethyl Vanillin in Vitro and in Vivo', *Bioscience, Biotechnology, and Biochemistry*, 75(12), pp. 2346–2350. doi: 10.1271/bbb.110524.

Tamai, I. and Tsuji, A. (2000) 'Transporter-Mediated Permeation of Drugs Across the Blood–Brain Barrier', *Journal of Pharmaceutical Sciences*, 89(11), pp. 1371–1388. doi: 10.1002/1520-6017(200011)89:11<1371::aid-

jps1>3.0.co;2-d.

Tang, X. *et al.* (2014) 'Mitochondria, endothelial cell function, and vascular diseases', *Frontiers in Physiology*, 5 MAY(May), pp. 1–17. doi: 10.3389/fphys.2014.00175.

Tanumihardjo, S. A. (2011) 'Vitamin A: Biomarkers of nutrition for development', *American Journal of Clinical Nutrition*, 94(2), pp. 658–665. doi: 10.3945/ajcn.110.005777.

Tennant, J. R. (1964) 'Evaluation of the Trypan Blue Technique for Determination of Cell Viability.', *Transplantation*, 2(6), pp. 685–94. doi: 10.1097/00007890-196411000-00001.

Teppola, H. *et al.* (2016) 'Morphological Differentiation Towards Neuronal Phenotype of SH-SY5Y Neuroblastoma Cells by Estradiol, Retinoic Acid and Cholesterol', *Neurochemical Research*. Springer US, 41(4), pp. 731–747. doi: 10.1007/s11064-015-1743-6.

Terpinc, P. *et al.* (2011) 'Antioxidant properties of 4-vinyl derivatives of hydroxycinnamic acids', *Food Chemistry*, 128(1), pp. 62–69. doi: 10.1016/j.foodchem.2011.02.077.

Thapa, A., Jett, S. D. and Chi, E. Y. (2016) 'Curcumin Attenuates Amyloid- $\beta$  Aggregate Toxicity and Modulates Amyloid- $\beta$  Aggregation Pathway', *ACS Chemical Neuroscience*, 7(1), pp. 56–68. doi: 10.1021/acschemneuro.5b00214.

Tinkel, J., Hassanain, H. and Khouri, S. J. (2012) 'Cardiovascular antioxidant therapy: A review of supplements, pharmacotherapies, and mechanisms', *Cardiology in Review*, 20(2), pp. 77–83. doi: 10.1097/CRD.0b013e31823dbbad.

Tonelli, C., Chio, I. I. C. and Tuveson, D. A. (2017) 'Transcriptional Regulation by Nrf2', *Antioxidants & Redox Signaling*, 29(17), pp. 1727–1745. doi: 10.1089/ars.2017.7342.

Towbin, H., Staehelint, T. and Gordon, J. (1979) 'Electrophoretic transfer of proteins from polyacrylamide gels to nitrocellulose sheets: Procedure and some applications', *Proc. Natl. Acad. Sci.*, 76(9), pp. 4350–4354. doi: 10.1073/pnas.76.9.4350.

Tramutola, A. *et al.* (2017) 'Oxidative Stress, Protein Modification and Alzheimer Disease', *Brain Research Bulletin*. Elsevier Inc., 133(1–3), pp. 88–96. doi: doi.org/10.1016/j.brainresbull.2016.06.005.

Trott, O. and Olson, A. (2010) 'AutoDock Vina: improving the speed and accuracy of docking with a new scoring function, efficient optimization and multithreading', *Journal of Computational Chemistry*, 31(2), pp. 455–461. doi: 10.1002/jcc.21334.

Uttara, B. *et al.* (2009) 'Oxidative Stress and Neurodegenerative Diseases: A Review of Upstream and Downstream Antioxidant Therapeutic Options', *Current Neuropharmacology*, 7(1), pp. 65–74. doi: 10.2174/157015909787602823.

Valko, M. *et al.* (2004) 'Role of oxygen radicals in DNA damage and cancer incidence', *Molecular and Cellular Biochemistry*, 266(1–2), pp. 37–56. doi: 10.1023/b:mcbi.0000049134.69131.89.

Valko, M. *et al.* (2007) 'Free radicals and antioxidants in normal physiological functions and human disease', *International Journal of Biochemistry and Cell Biology*, 39(1), pp. 44–84. doi: 10.1016/j.biocel.2006.07.001.

Valko, M., Morris, H. and Cronin, M. (2005) 'Metals, Toxicity and Oxidative Stress', *Current Medicinal Chemistry*, 12(10), pp. 1161–1208. doi: 10.2174/0929867053764635.

Veitch, N. C. (2004) 'Horseradish peroxidase: A modern view of a classic enzyme', *Phytochemistry*, 65(3), pp. 249–259. doi: 10.1016/j.phytochem.2003.10.022.

Verma, M., Vats, A. and Taneja, V. (2015) 'Toxic species in amyloid disorders: Oligomers or mature fibrils', *Annals of Indian Academy of Neurology*, 18, pp. 138–145. doi: 10.4103/0972-2327.144284.

Villaño, D. *et al.* (2007) 'Radical scavenging ability of polyphenolic compounds towards DPPH free radical', *Talanta*, 71(1), pp. 230–235. doi: 10.1016/j.talanta.2006.03.050.

Wang, C. *et al.* (2012) 'Nanoscale Observation of molecular inhibition and binding structures of amyloid peptides', *Nanoscale*, 4, pp. 1895–1909. doi: 10.1039/c2nr11508e.

Wang, D. and DuBois, R. N. (2010) 'Eicosanoids and cancer', *Nature Reviews Cancer*, 10(3), pp. 181–193. doi: 10.1038/nrc2809.

Wang, J. *et al.* (2017) 'Novel cinnamamide-dibenzylamine hybrids: Potent neurogenic agents with antioxidant, cholinergic, and neuroprotective properties as innovative drugs for Alzheimer's disease', *European Journal of Medicinal Chemistry*. Elsevier Masson SAS, 139, pp. 68–83. doi: 10.1016/j.ejmech.2017.07.077.

Wang, M. *et al.* (2009) 'Convenient and continuous fluorometric assay method for acetylcholinesterase and inhibitor screening based on the aggregation-induced emission', *Analytical Chemistry*, 81(11), pp. 4444–4449. doi: 10.1021/ac9002722.

Wang, M., Jin, Y. and Ho, C. T. (1999) 'Evaluation of resveratrol derivatives as potential antioxidants and identification of a reaction product of resveratrol and 2,2-diphenyl-1-picrylhydrazyl radical', *Journal of Agricultural and Food Chemistry*, 47(10), pp. 3974–3977. doi: 10.1021/jf990382w.

Watanabe, T., Tahara, M. and Todo, S. (2008) 'The novel antioxidant edaravone: From bench to bedside', *Cardiovascular Therapeutics*, 26(2), pp. 101–114. doi: 10.1111/j.1527-3466.2008.00041.x.

Watkins, P. B. *et al.* (1994) 'Hepatotoxic Effects of Tacrine Administration in Patients With Alzheimer's Disease', *JAMA: The Journal of the American Medical Association*, 271(13), pp. 992–998. doi: 10.1001/jama.1994.03510370044030.

Wei, Q. Y. *et al.* (2006) 'Synergistic effect of green tea polyphenols with trolox on free radical-induced oxidative DNA damage', *Food Chemistry*, 96(1), pp. 90–95. doi: 10.1016/j.foodchem.2005.01.053.

Whittemore, E. R. *et al.* (1995) 'A detailed analysis of hydrogen peroxide-induced cell death in primary neuronal culture', *Neuroscience*, 67(4), pp. 921–932. doi: 10.1002/jnr.10190.

Wiesner, J. *et al.* (2007) 'Acetylcholinesterases – the structural similarities and differences Acetylcholinesterases – the structural similarities and differences', *Journal of Enzyme Inhibition and Medicinal Chemistry*, 22(4), pp. 417–424. doi: 10.1080/14756360701421294.

Williams, D. R. (2006) 'Tauopathies: Classification and clinical update on neurodegenerative diseases associated with microtubule-associated protein tau', *Internal Medicine Journal*, pp. 652–660. doi: 10.1111/j.1445-5994.2006.01153.x.

Witt, A., Macdonald, N. and Kirkpatrick, P. (2004) 'Memantine hydrochloride', *Nature Reviews Drug Discovery*, 3, pp. 109–110. doi: 10.1038/nrd1311.

Wojtala, A. *et al.* (2014) *Methods to monitor ROS production by fluorescence microscopy and fluorometry*. 1st edn, *Methods in Enzymology*. 1st edn. Elsevier Inc. doi: 10.1016/B978-0-12-416618-9.00013-3.

Wolfe, L. S. *et al.* (2010) 'Protein-induced photophysical changes to the amyloid indicator dye thioflavin T', *Proceedings of the National Academy of Sciences*, 107(39), pp. 16863–16868. doi: 10.1073/pnas.1002867107.

Worek, F., Eyer, P. and Thiermann, H. (2012) 'Determination of acetylcholinesterase activity by the Ellman assay: A versatile tool for in vitro research on medical countermeasures against organophosphate poisoning', *Drug Testing and Analysis*, 4(3–4), pp. 282–291. doi: 10.1002/dta.337.

Xia, Z. *et al.* (1995) 'Opposing Effects of ERK and JNK-p38 MAP Kinases on Apoptosis', *Science*, 270(5240), pp. 1326–1331. doi: 10.1126/science.270.5240.1326.

Xicoy, H., Wieringa, B. and Martens, G. J. M. (2017) 'The SH-SY5Y cell line in Parkinson's disease research: a systematic review', *Molecular Neurodegeneration*. *Molecular Neurodegeneration*, 12(1), pp. 1–11. doi: 10.1186/s13024-017-0149-0.

Xu, X.-L., Shang, Y. and Jiang, J.-G. (2016) 'Plant species forbidden in health food and their toxic constituents, toxicology and detoxification', *Food & Function*. Royal Society of Chemistry, 7(2), pp. 643–664. doi: 10.1039/C5FO00995B.

Xu, Y. *et al.* (2008) 'Flexibility of aromatic residues in the active-site gorge of acetylcholinesterase: X-ray versus molecular dynamics', *Biophysical Journal*, 95(5), pp. 2500–2511. doi: 10.1529/biophysj.108.129601.

Yang, X. *et al.* (2017) 'Pyridoxine-resveratrol hybrids Mannich base derivatives as novel dual inhibitors of AChE and MAO-B with antioxidant and metal-chelating properties for the treatment of Alzheimer's disease', *Bioorganic Chemistry*. Elsevier Inc., 71, pp. 305–314. doi: 10.1016/j.bioorg.2017.02.016.

Ye, N. *et al.* (2014) 'Small Molecule Inhibitors Targeting Activator Protein 1 (AP-1)', *Journal of Medicinal Chemistry*, 57(16), pp. 6930–6948. doi: 10.1021/jm5004733.

Yiannopoulou, K. G. and Papageorgiou, S. G. (2013) 'Current and future treatments for Alzheimer's disease', *Therapeutic Advances in Neurological Disorders*, 6(1), pp. 19–33. doi: 10.1177/1756285612461679.

Yoshida, H. *et al.* (2006) 'Neuroprotective effects of edaravone: A novel free radical scavenger in cerebrovascular injury', *CNS Drug Reviews*, 12(1), pp. 9–20. doi: 10.1111/j.1527-3458.2006.00009.x.

Yu, M. J. *et al.* (1992) 'Phenothiazines as Lipid Peroxidation Inhibitors and Cytoprotective Agents', *Journal of Medicinal Chemistry*, 35(4), pp. 716–724. doi: 10.1021/jm00082a012.

Zangar, R. C., Davydov, D. R. and Verma, S. (2004) 'Mechanisms that regulate production of reactive oxygen species by cytochrome P450', *Toxicology and Applied Pharmacology*, 199(3), pp. 316–331. doi: 10.1016/j.taap.2004.01.018.

Zha, X. *et al.* (2016) 'Novel Tacrine-Benzofuran Hybrids as Potent Multitarget-Directed Ligands for the Treatment of Alzheimers Disease: Design, Synthesis, Biological Evaluation, and X-ray Crystallography', *Journal of Medicinal Chemistry*, 59(1), pp. 114–131. doi: 10.1021/acs.jmedchem.5b01119.

Zhai, X. *et al.* (2013) 'Dietary flavonoid genistein induces Nrf2 and phase II detoxification gene expression via ERKs and PKC pathways and protects against oxidative stress in Caco-2 cells', *Molecular Nutrition and Food Research*, 57(2), pp. 249–259. doi: 10.1002/mnfr.201200536.

Zhang, L. *et al.* (2007) 'Protective effects of salidroside on hydrogen peroxide-induced apoptosis in SH-SY5Y human neuroblastoma cells', *European Journal of Pharmacology*, 564(1–3), pp. 18–25. doi: 10.1016/j.ejphar.2007.01.089.

Zhang, L. *et al.* (2010) 'Neuroprotective effects of salidroside against beta-amyloid-induced oxidative stress in SH-SY5Y human neuroblastoma cells', *Neurochemistry International*, pp. 547–555. doi: 10.1016/j.neuint.2010.06.021.

Zhang, P. and Omaye, S. T. (2001) 'DNA strand breakage and oxygen

tension: Effects of  $\beta$ -carotene,  $\alpha$ -tocopherol and ascorbic acid', *Food and Chemical Toxicology*, 39(3), pp. 239–246. doi: 10.1016/S0278-6915(00)00131-9.

Zhao, K. *et al.* (2005) 'Mitochondria-targeted peptide prevents mitochondrial depolarization and apoptosis induced by tert-butyl hydroperoxide in neuronal cell lines', *Biochemical Pharmacology*, 70(12), pp. 1796–1806. doi: 10.1016/j.bcp.2005.08.022.

Zhou, R. *et al.* (2011) 'A role for mitochondria in NLRP3 inflammasome activation', *Nature*, 469(7329), pp. 221–226. doi: 10.1038/nature09663.

## ***Appendix***

### *Spectral Data*

**I-1**

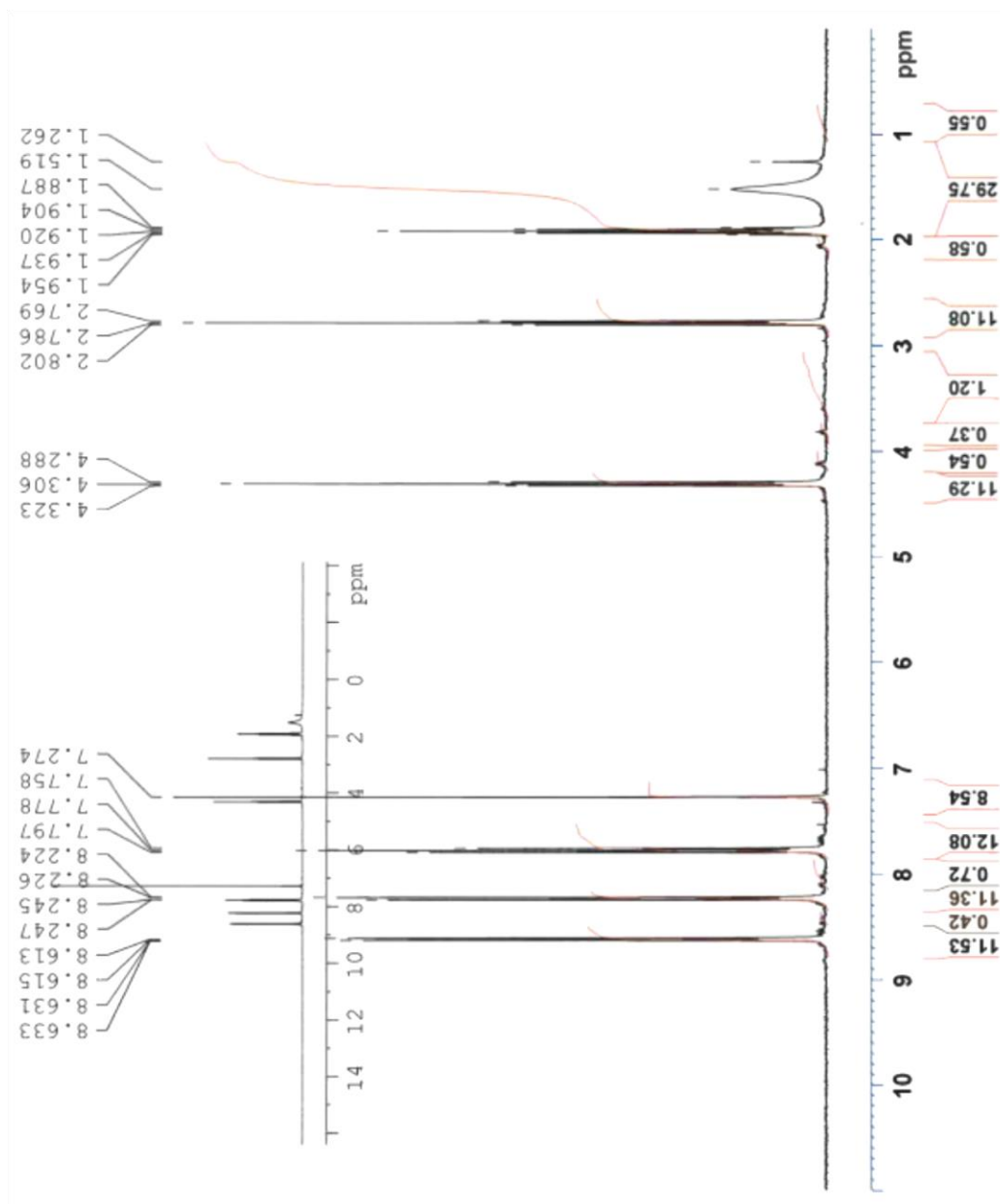
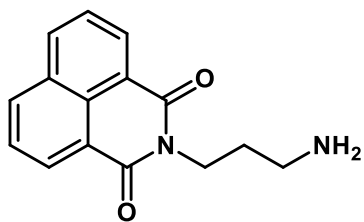


Figure A1. <sup>1</sup>H NMR spectrum of intermediate I-1.

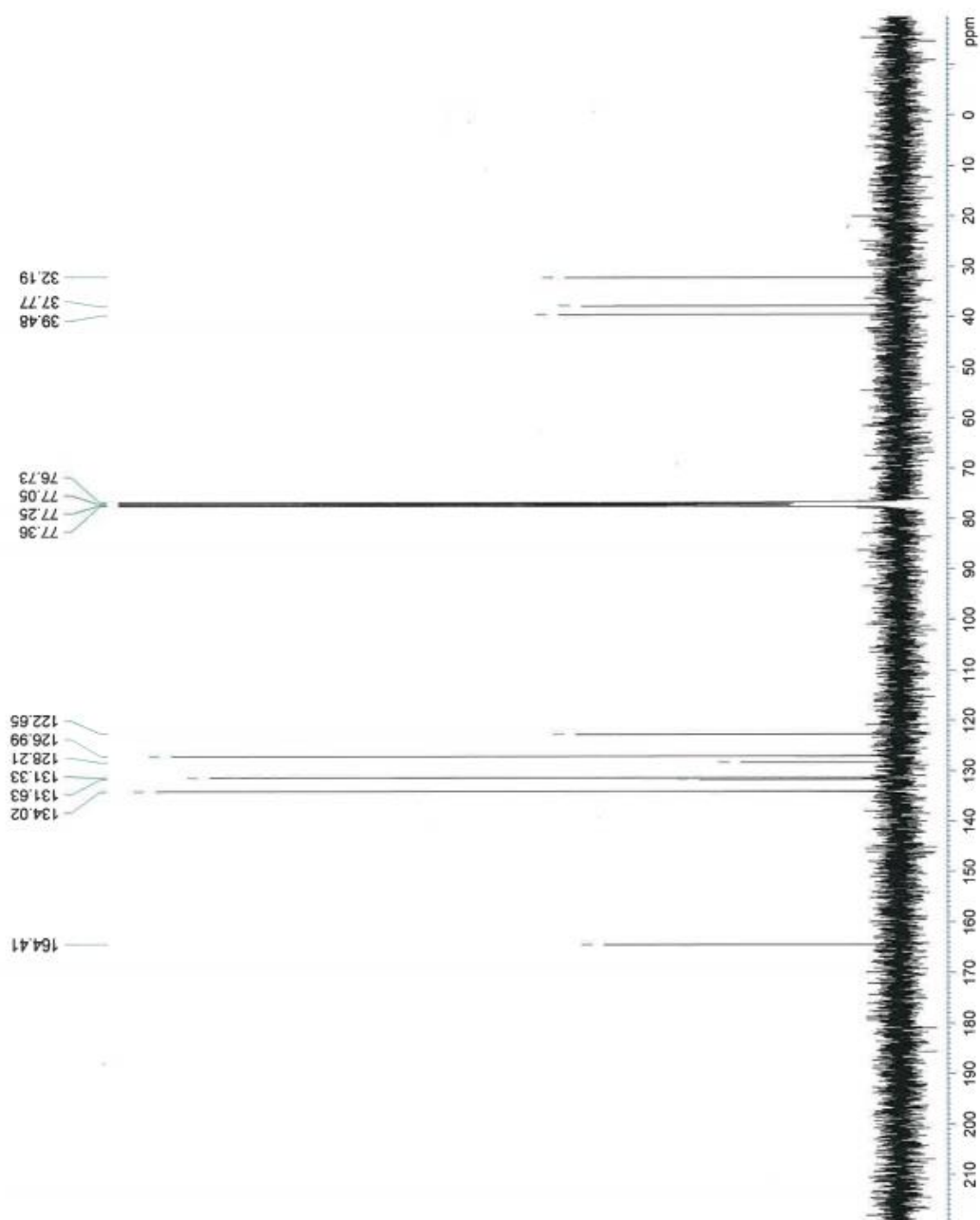


Figure A2.  $^{13}\text{C}$  NMR spectrum of intermediate **I-1**.

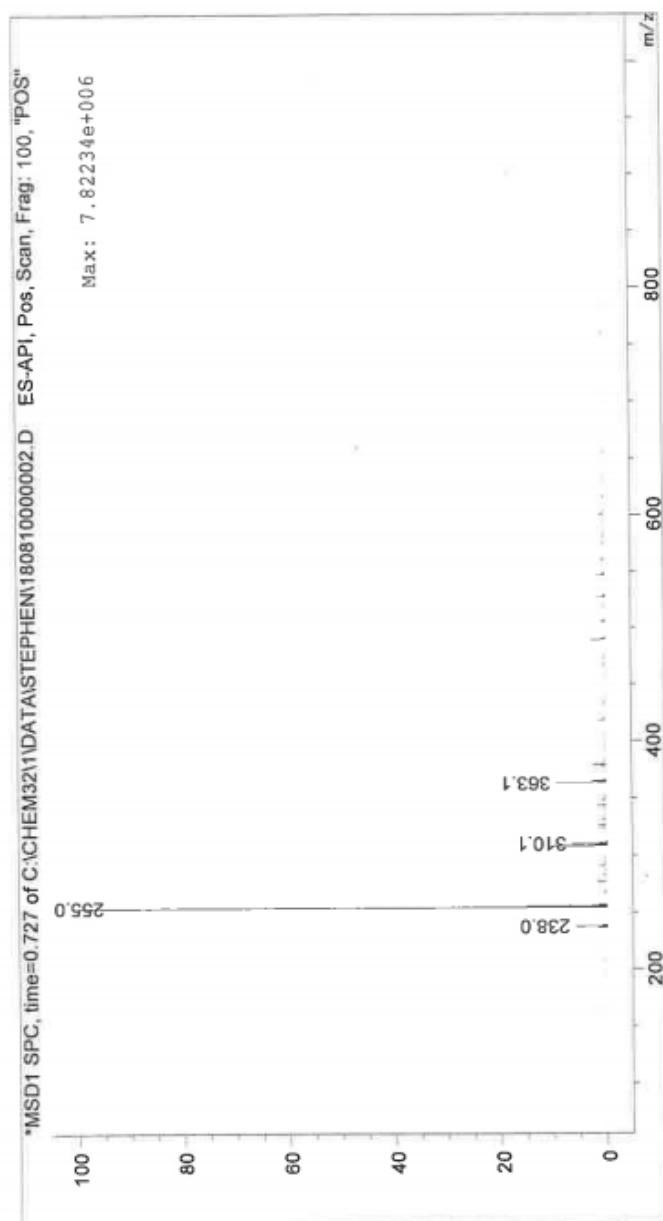


Figure A3. LRMS spectrum of intermediate **I-1**.

**I-2**

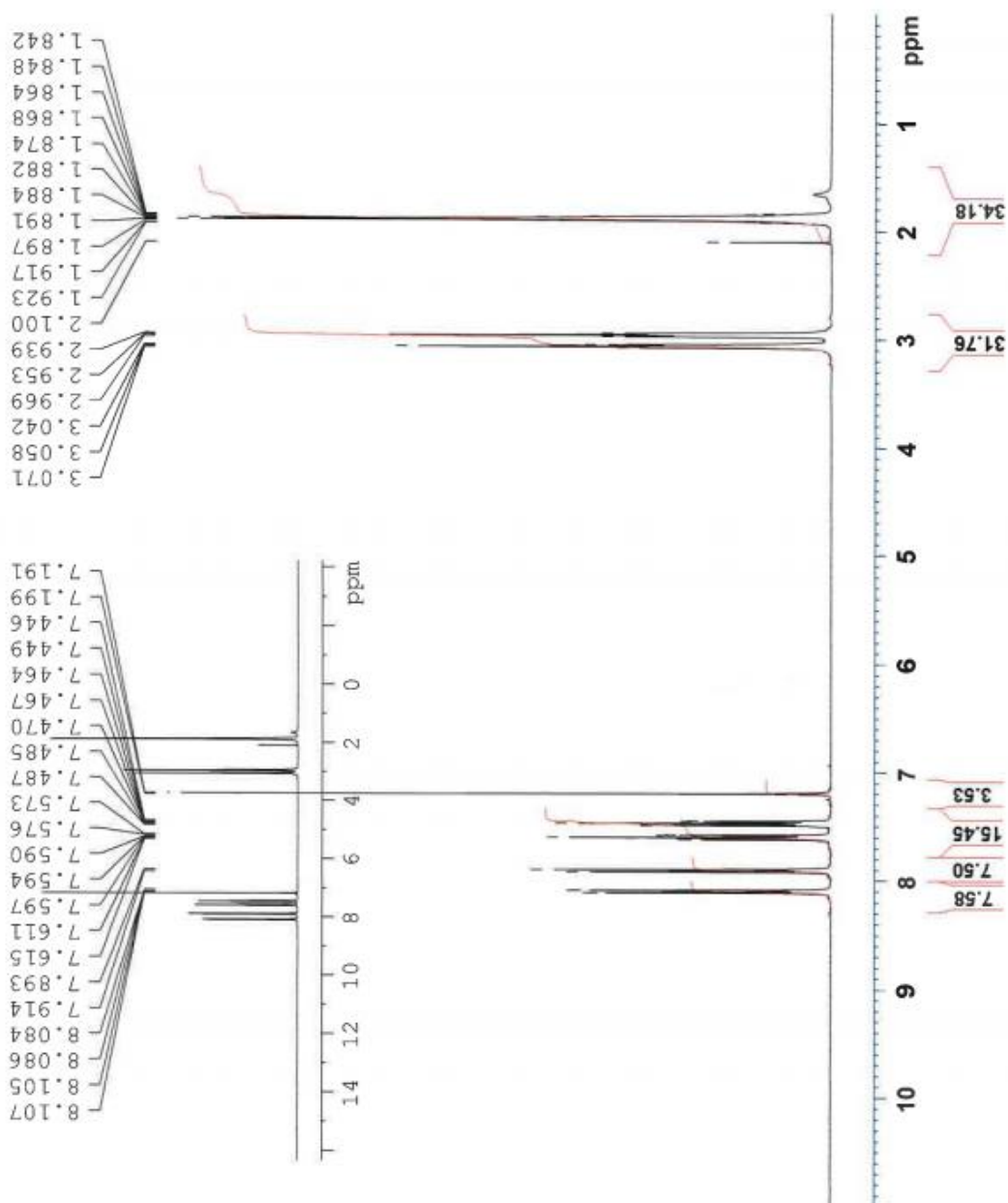
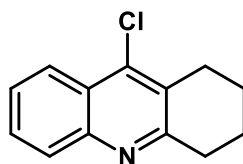


Figure A4. <sup>1</sup>H NMR spectrum of intermediate I-2.

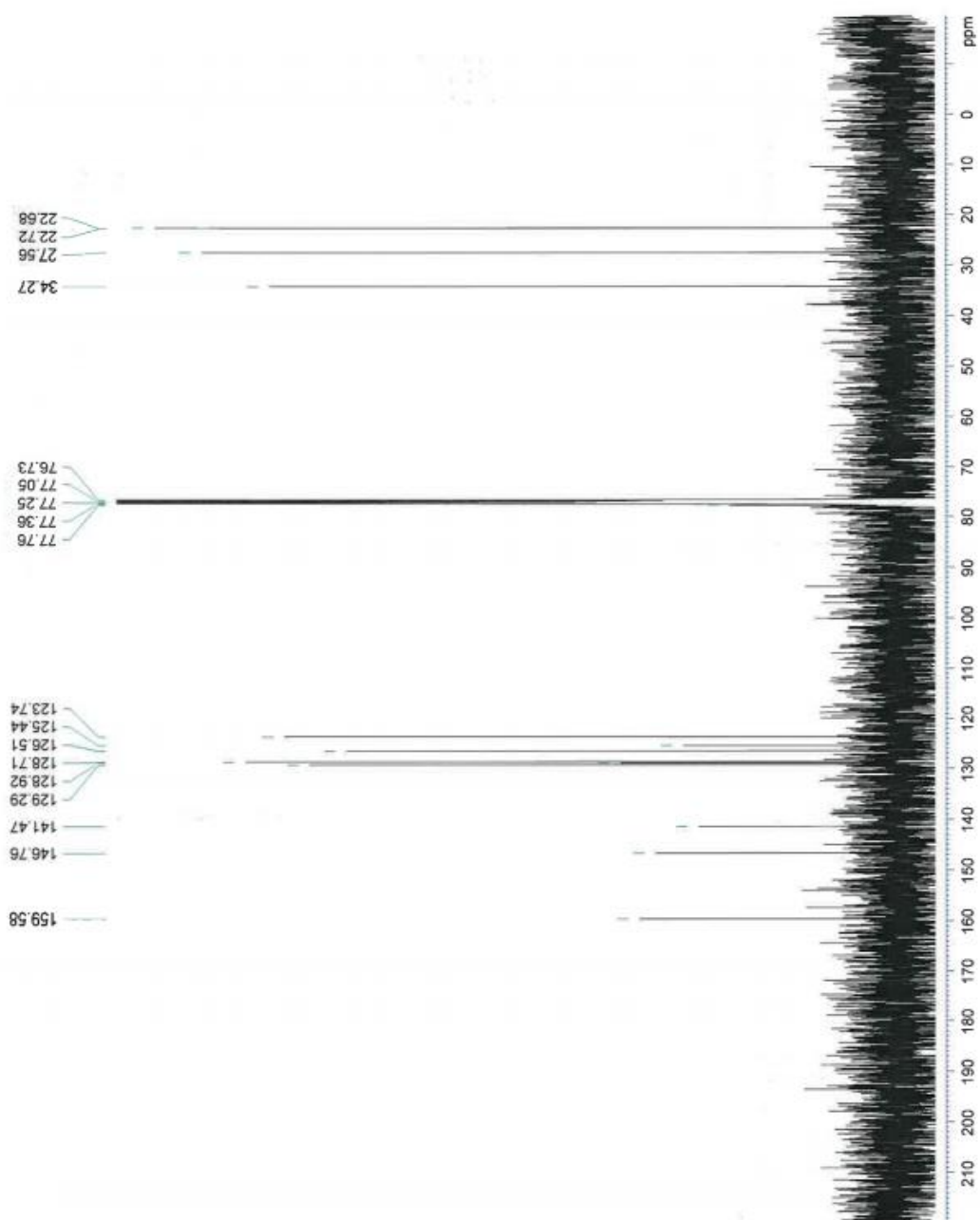


Figure A5.  $^{13}\text{C}$  NMR spectrum of intermediate **I-2**.

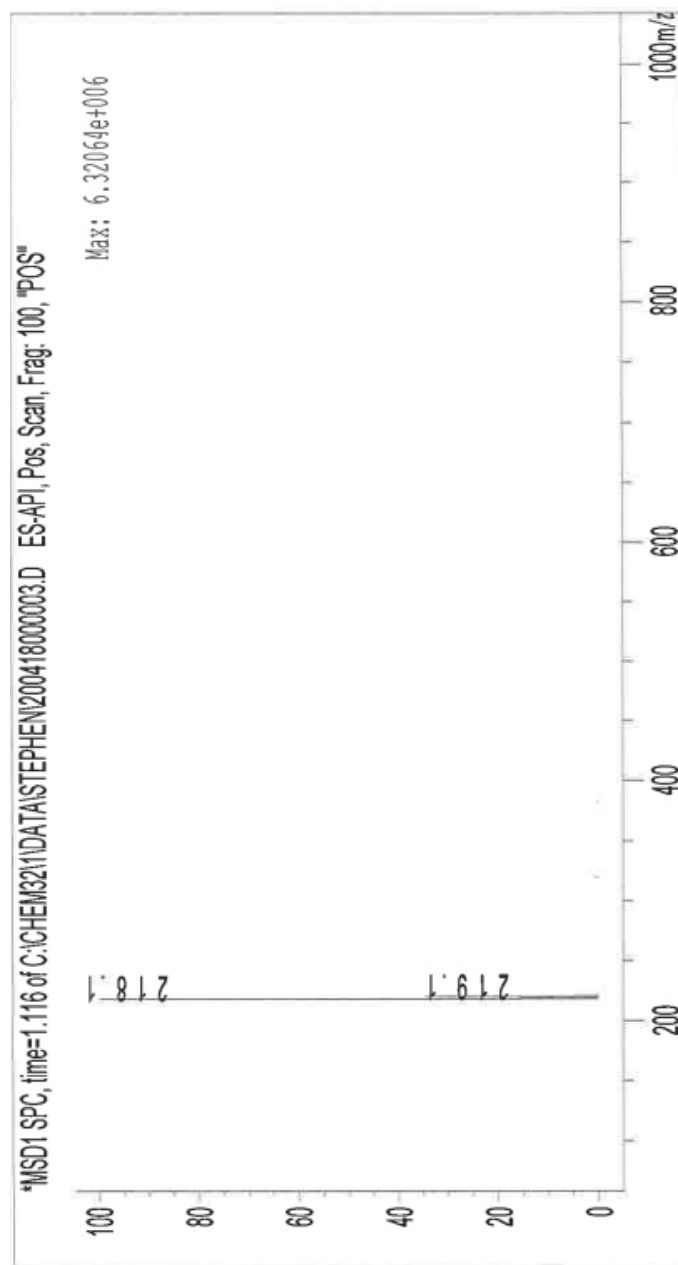


Figure A6. LRMS spectrum of intermediate **I-2**.

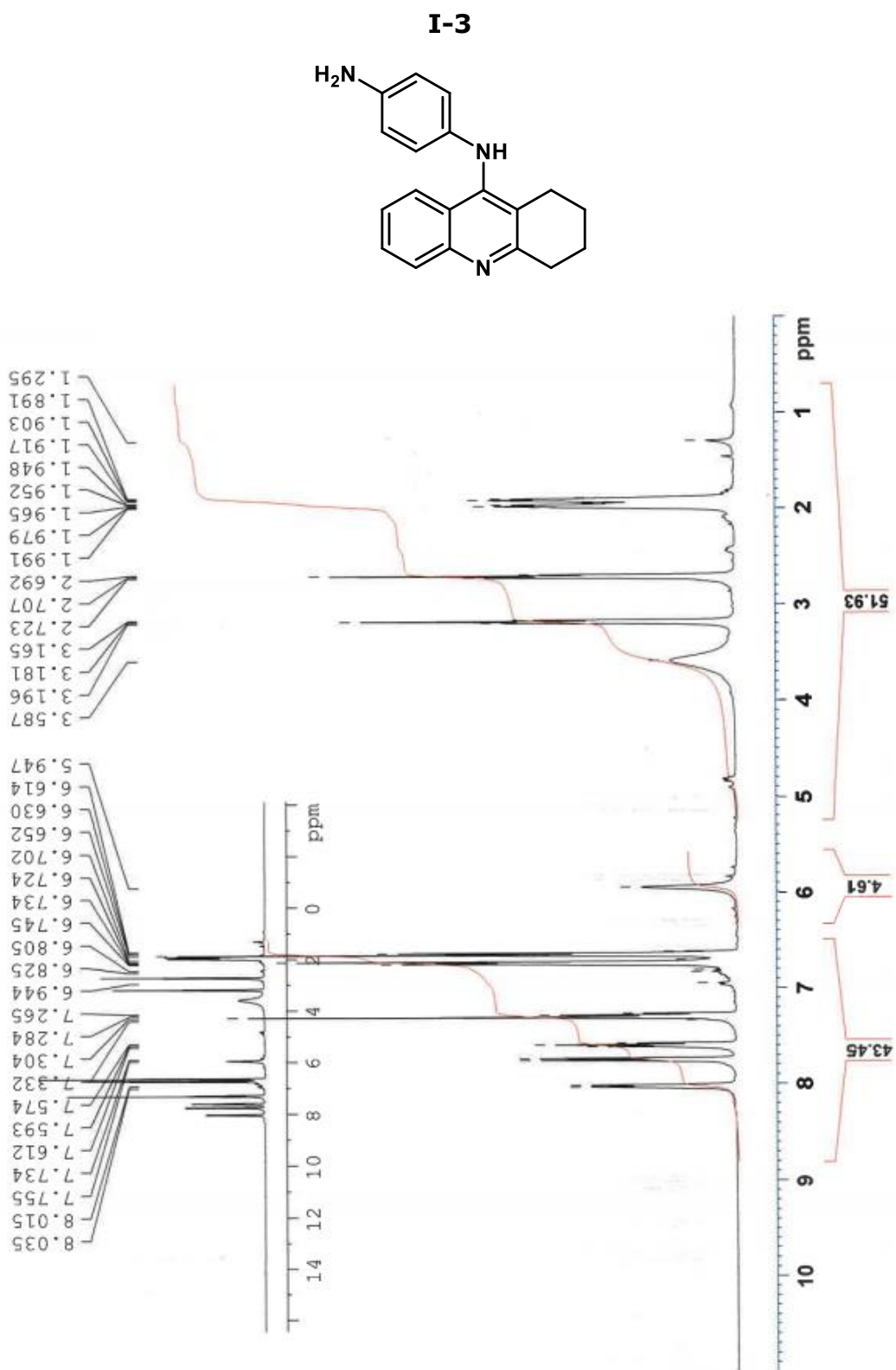


Figure A7.  $^1\text{H}$  NMR spectrum of intermediate **I-3**.

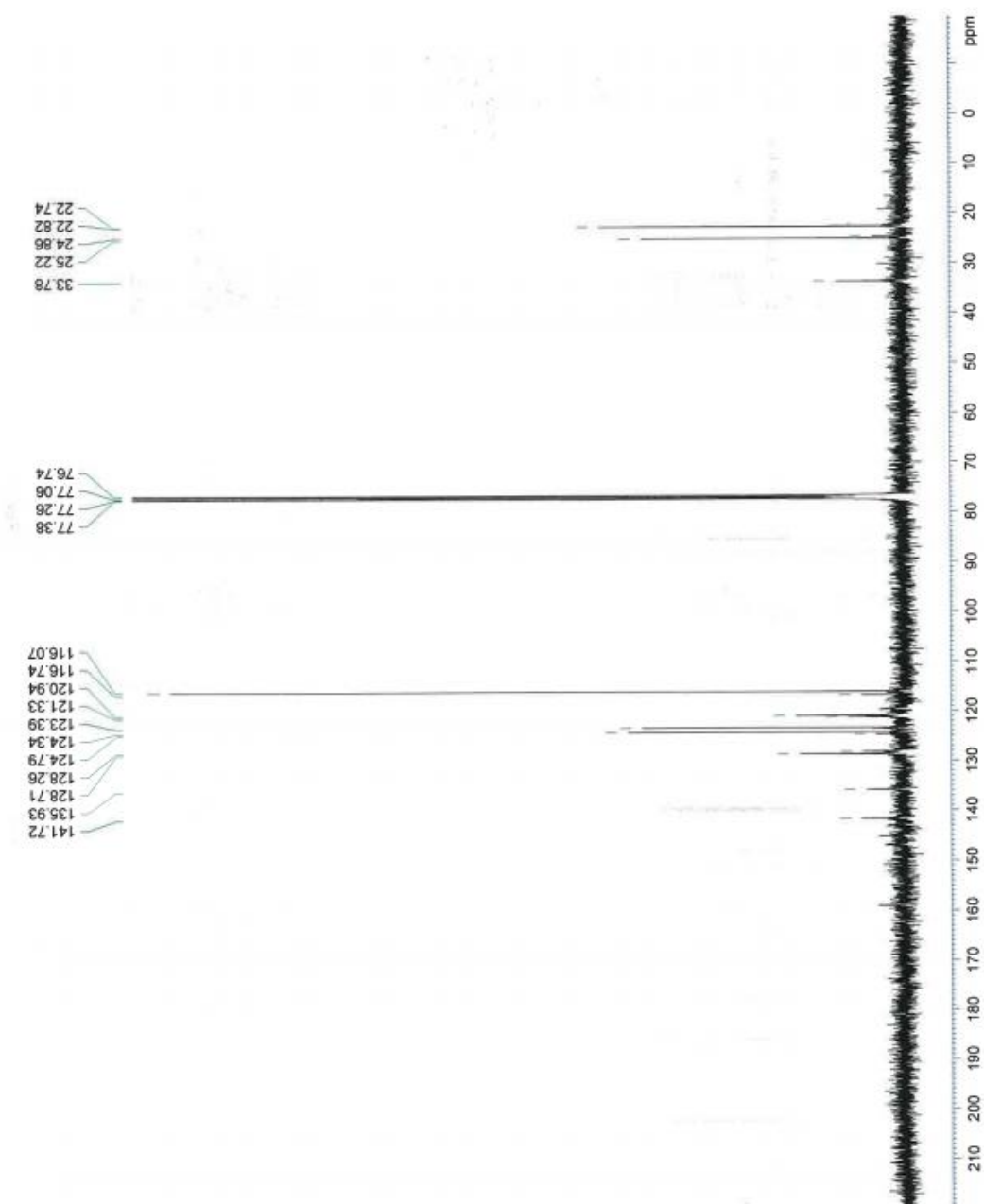


Figure A8.  $^{13}\text{C}$  NMR spectrum of intermediate I-3.

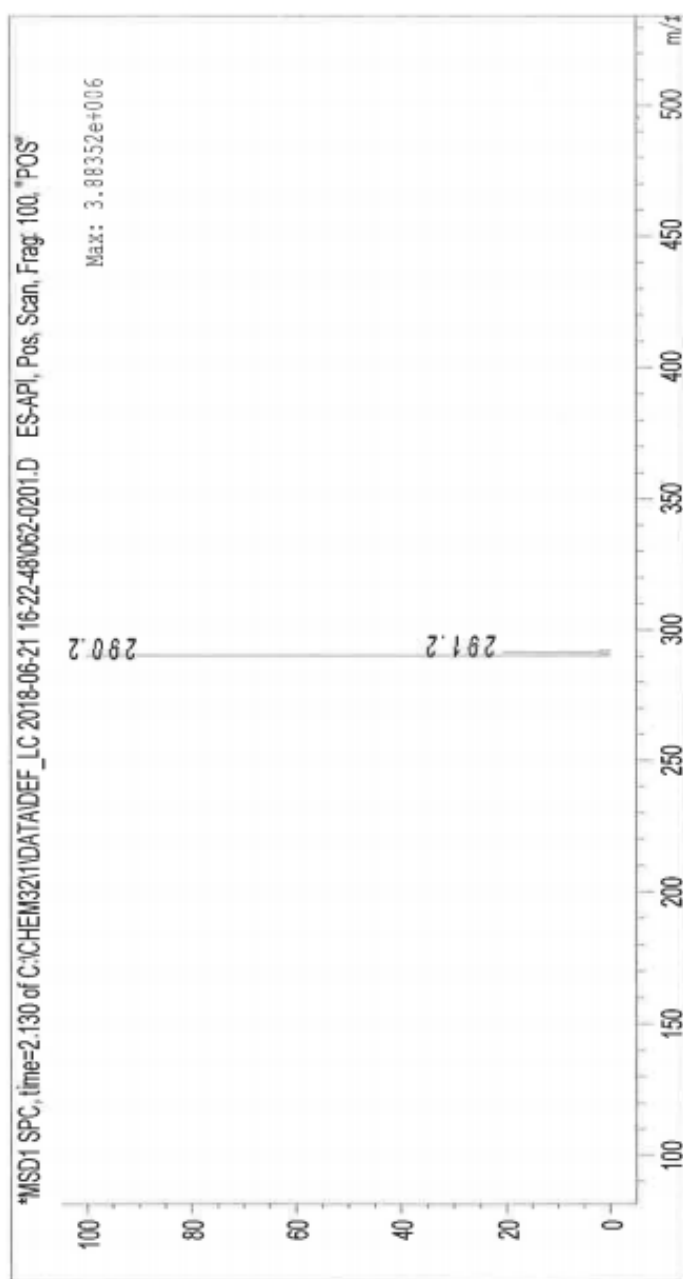


Figure A9. LRMS spectrum of intermediate **I-3**.

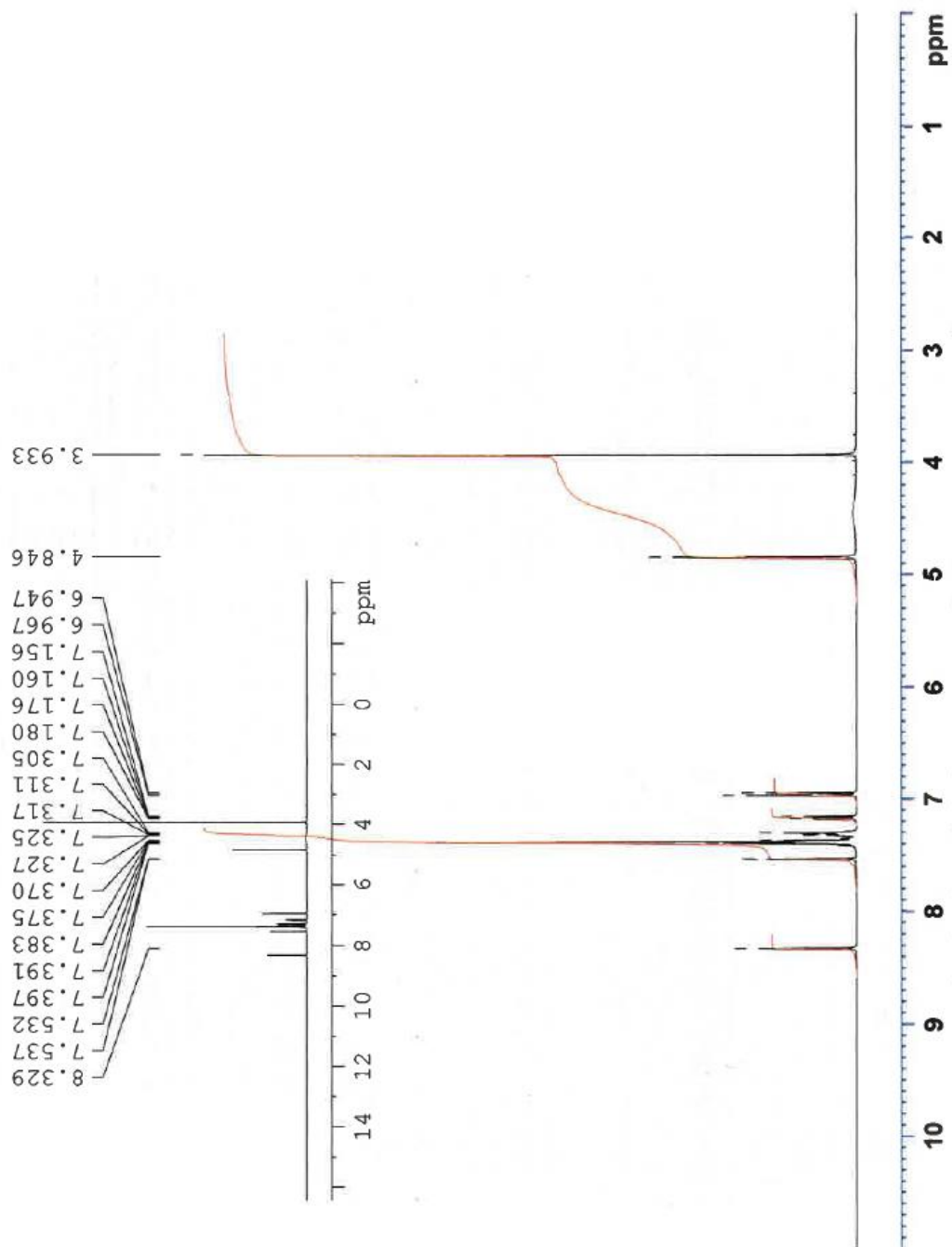
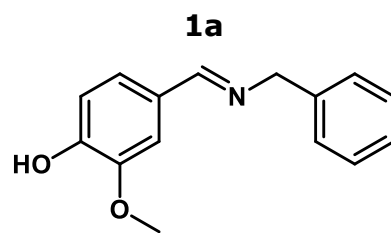


Figure A10. <sup>1</sup>H NMR spectrum of compound **1a**.

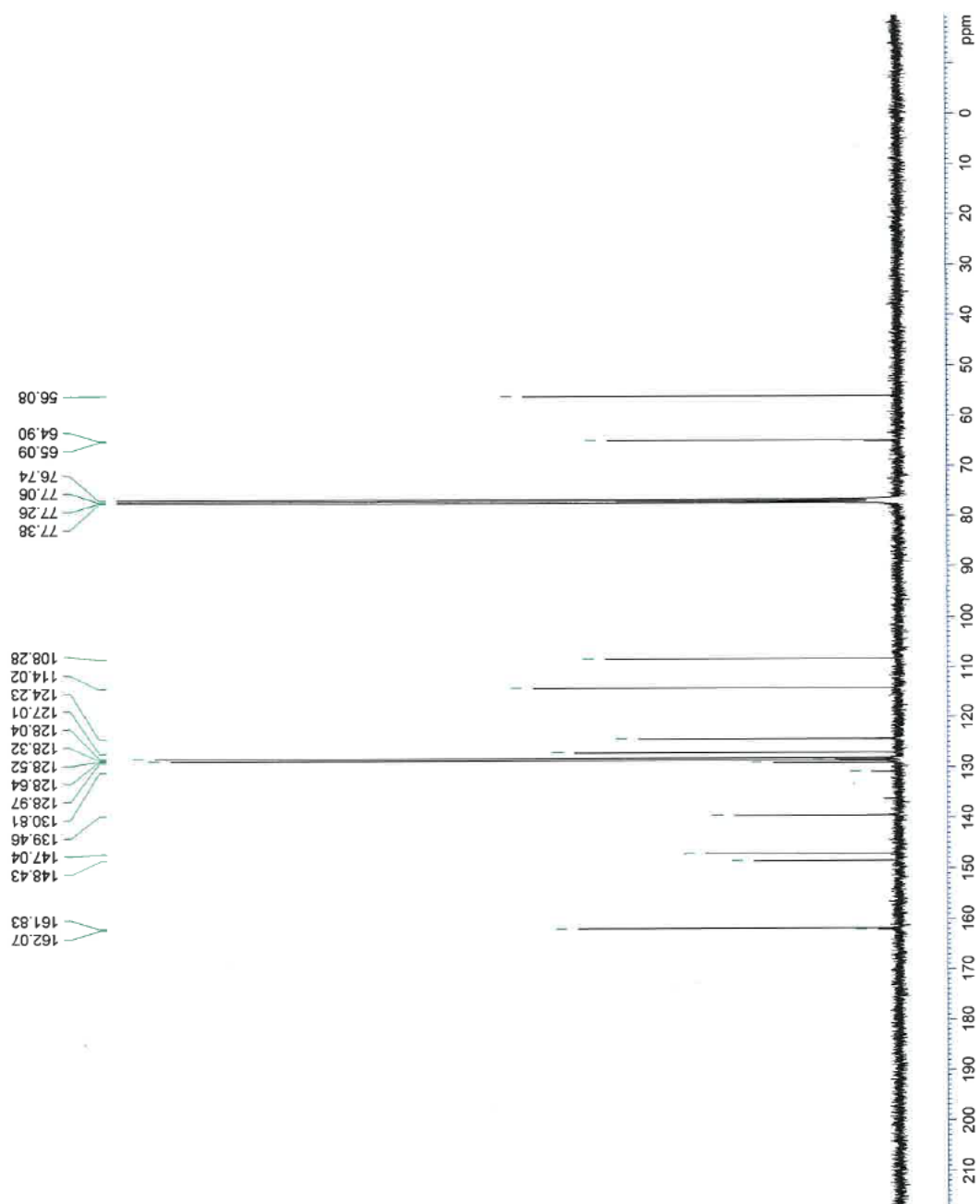


Figure A11.  $^{13}\text{C}$  NMR spectrum of compound **1a**.

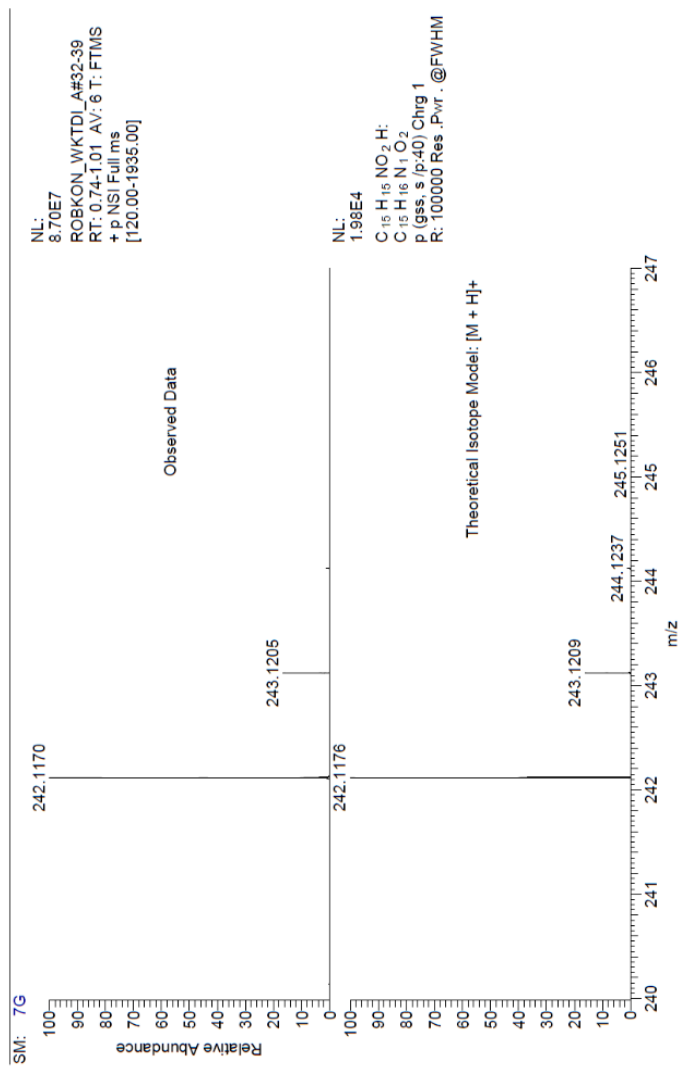


Figure A12. HRMS spectrum of compound **1a**.

**1b**

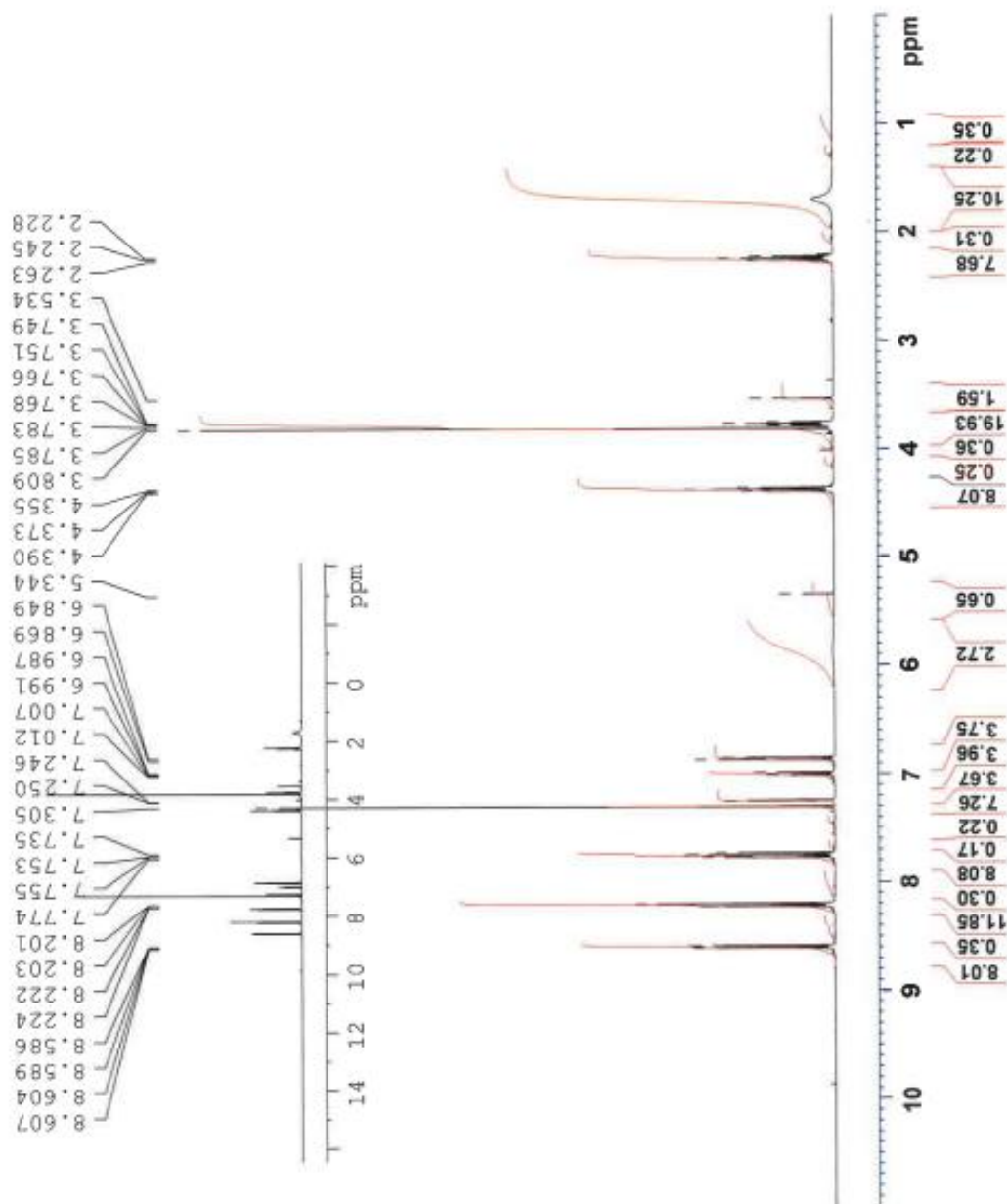
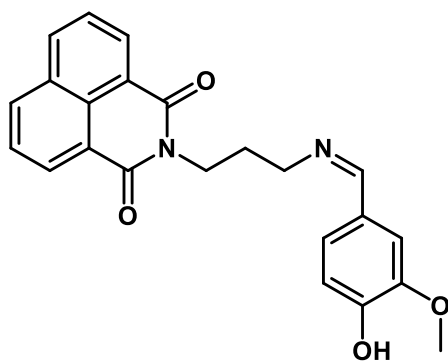


Figure A13. <sup>1</sup>H NMR spectrum of compound **1b**.

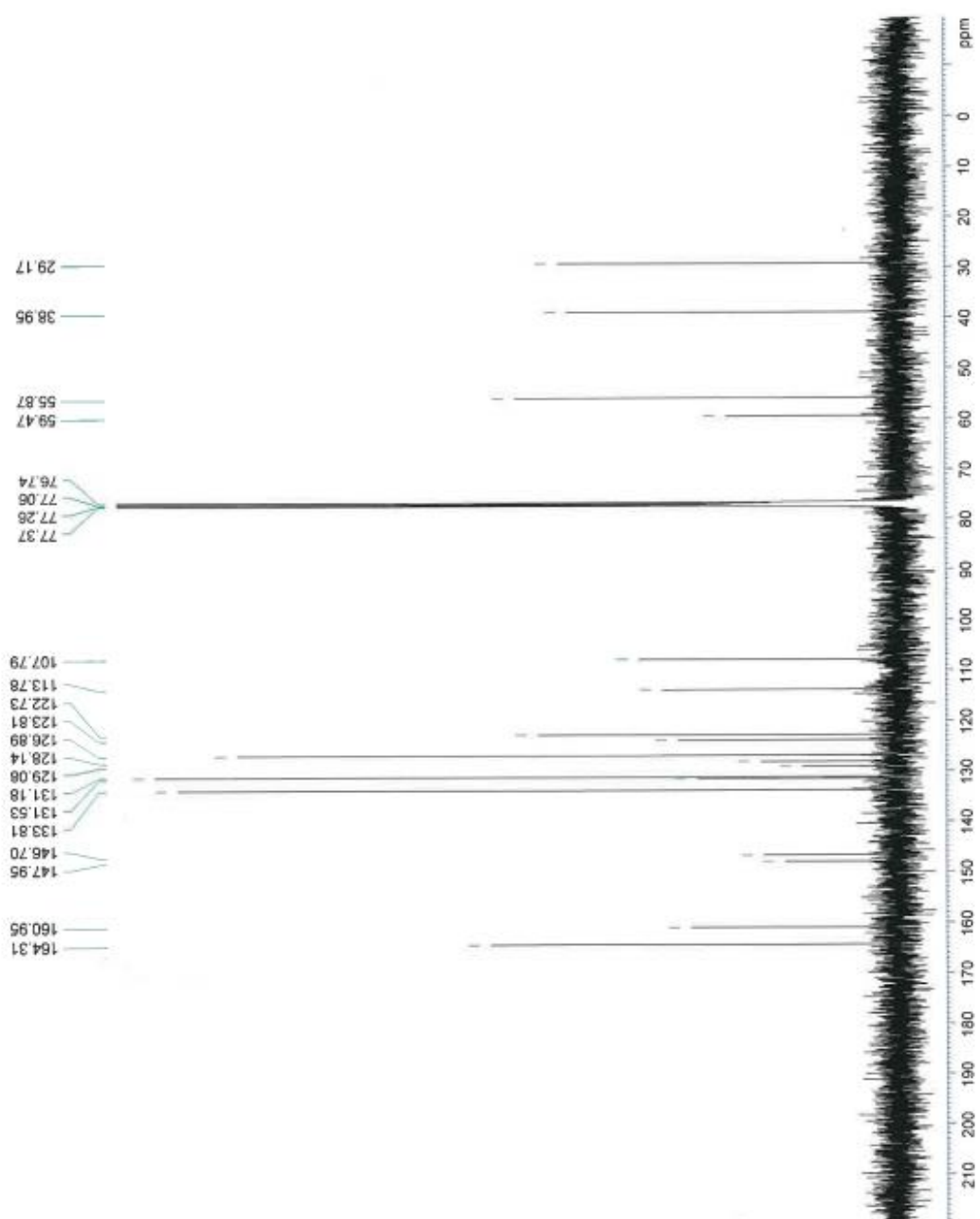


Figure A14.  $^{13}\text{C}$  NMR spectrum of compound **1b**.

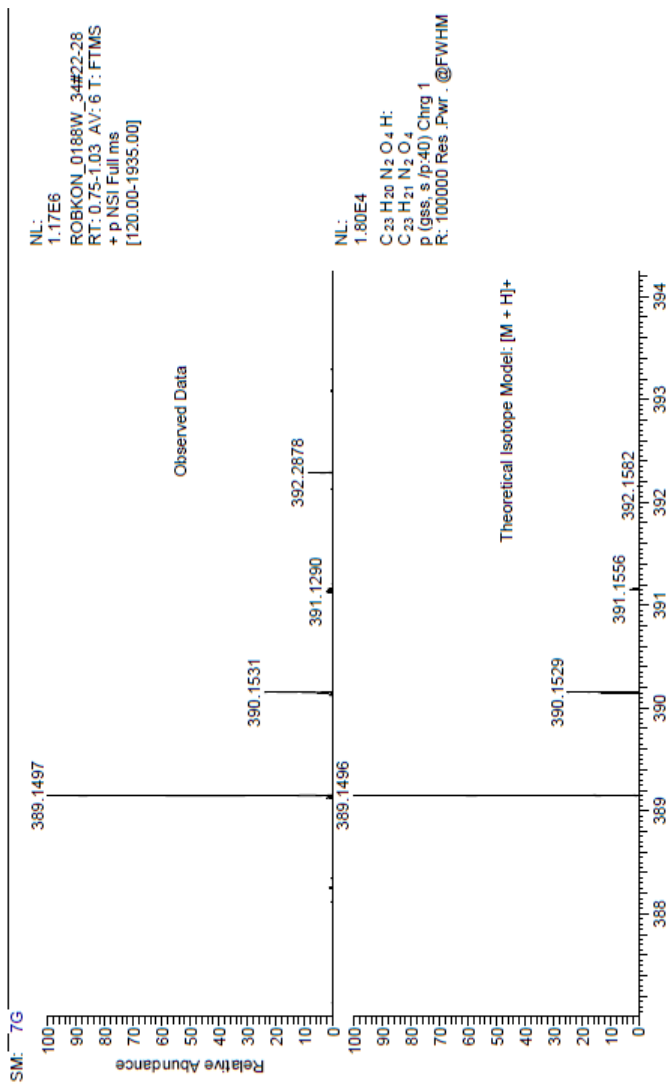


Figure A15. HRMS spectrum of compound **1b**.

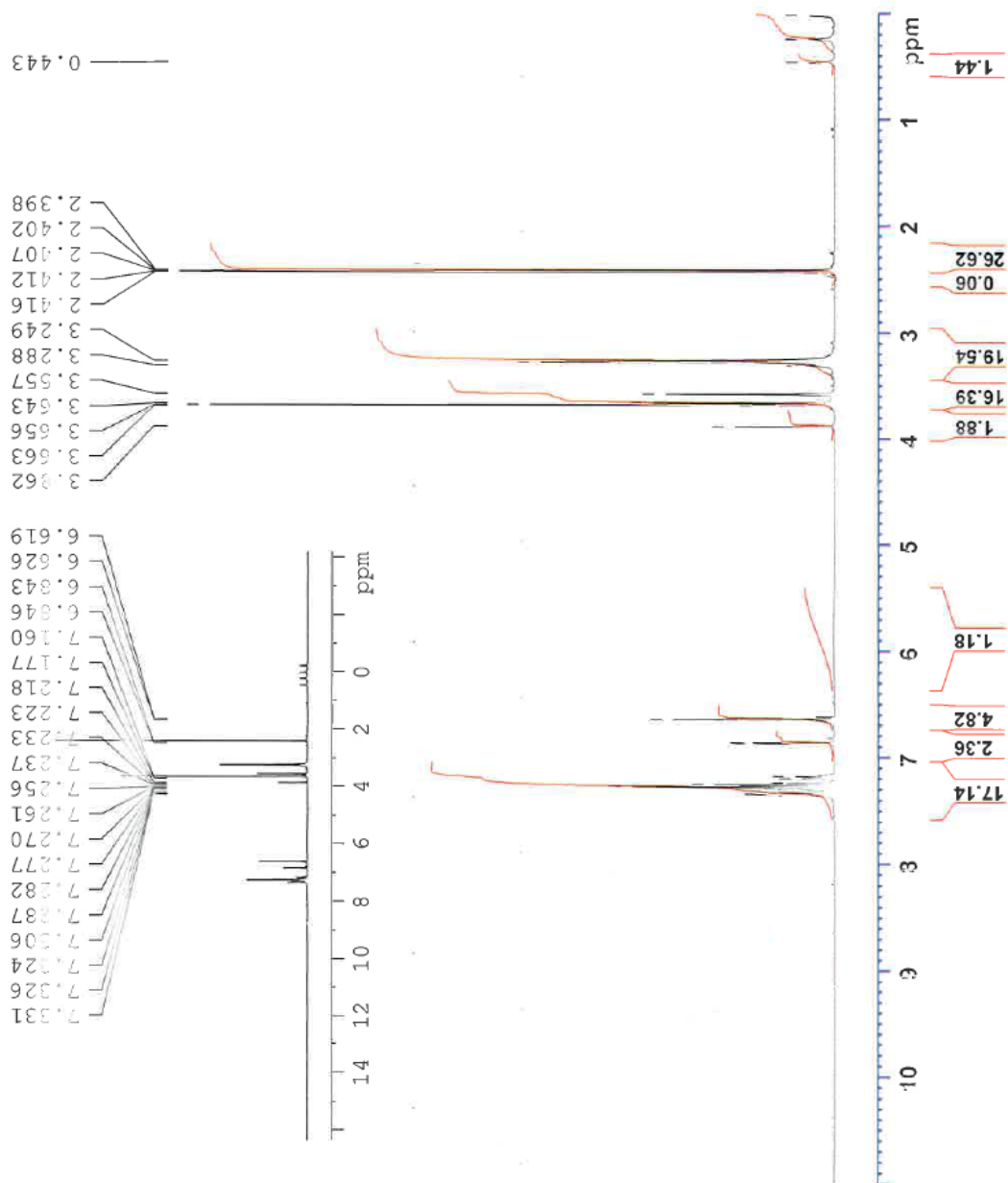
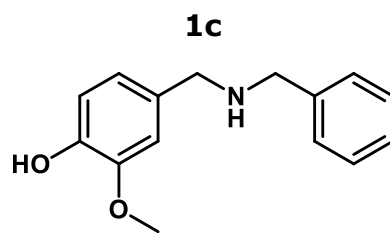


Figure A16.  $^1\text{H}$  NMR spectrum of compound **1c**.

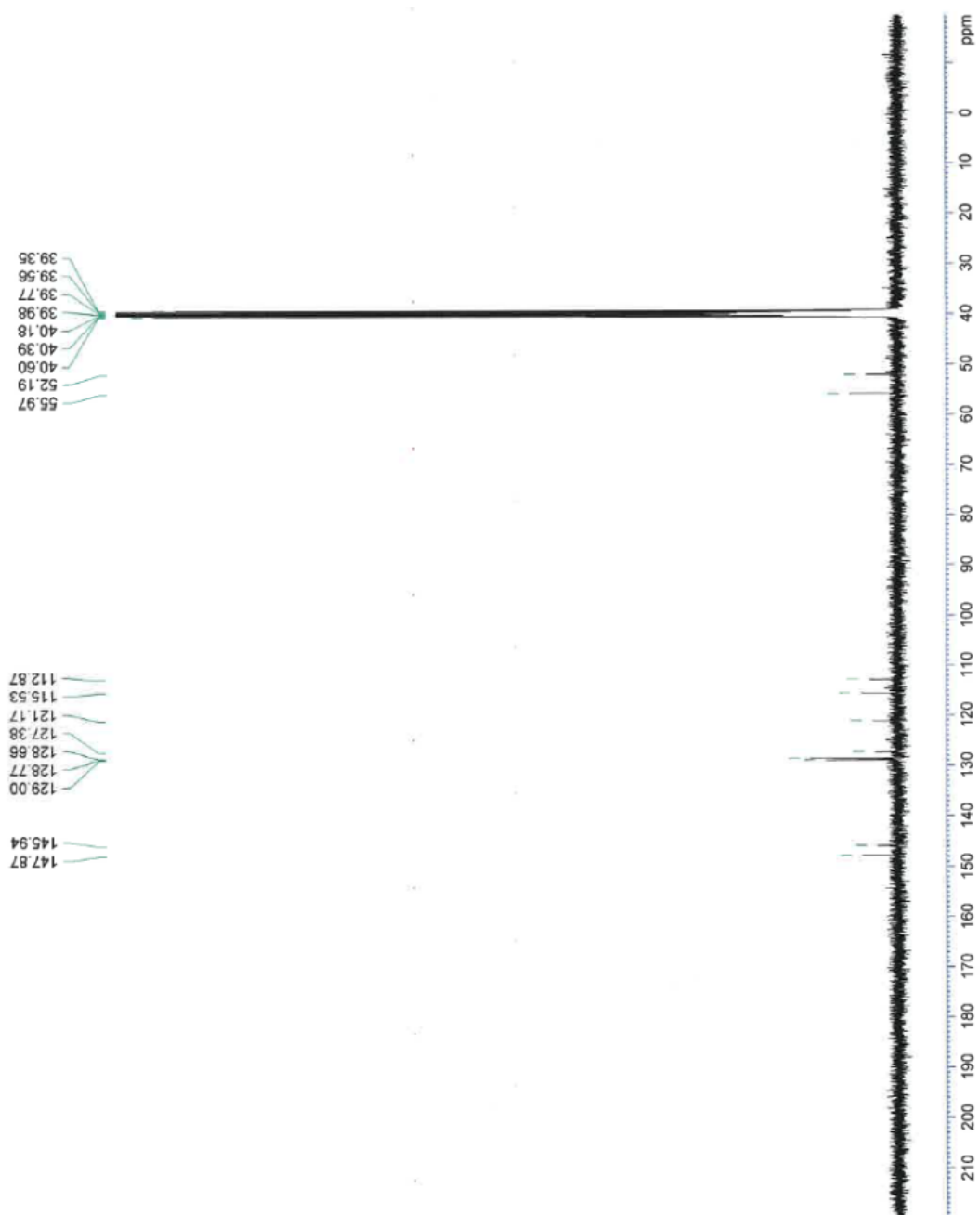


Figure A17.  $^{13}\text{C}$  NMR spectrum of compound **1c**.

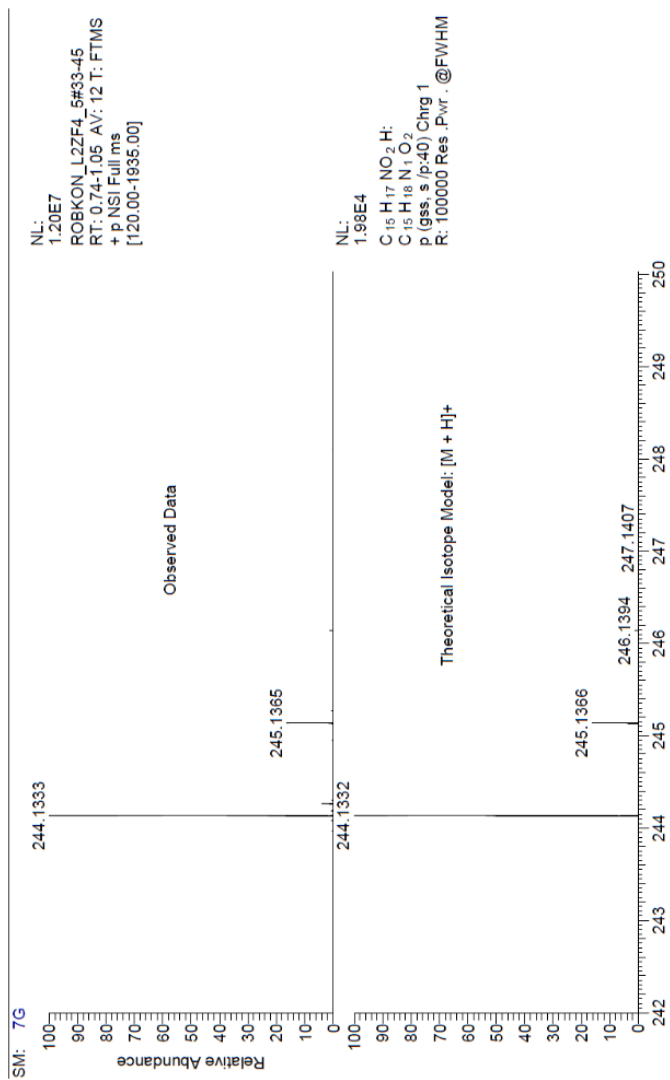


Figure A18. HRMS spectrum of compound **1c**.

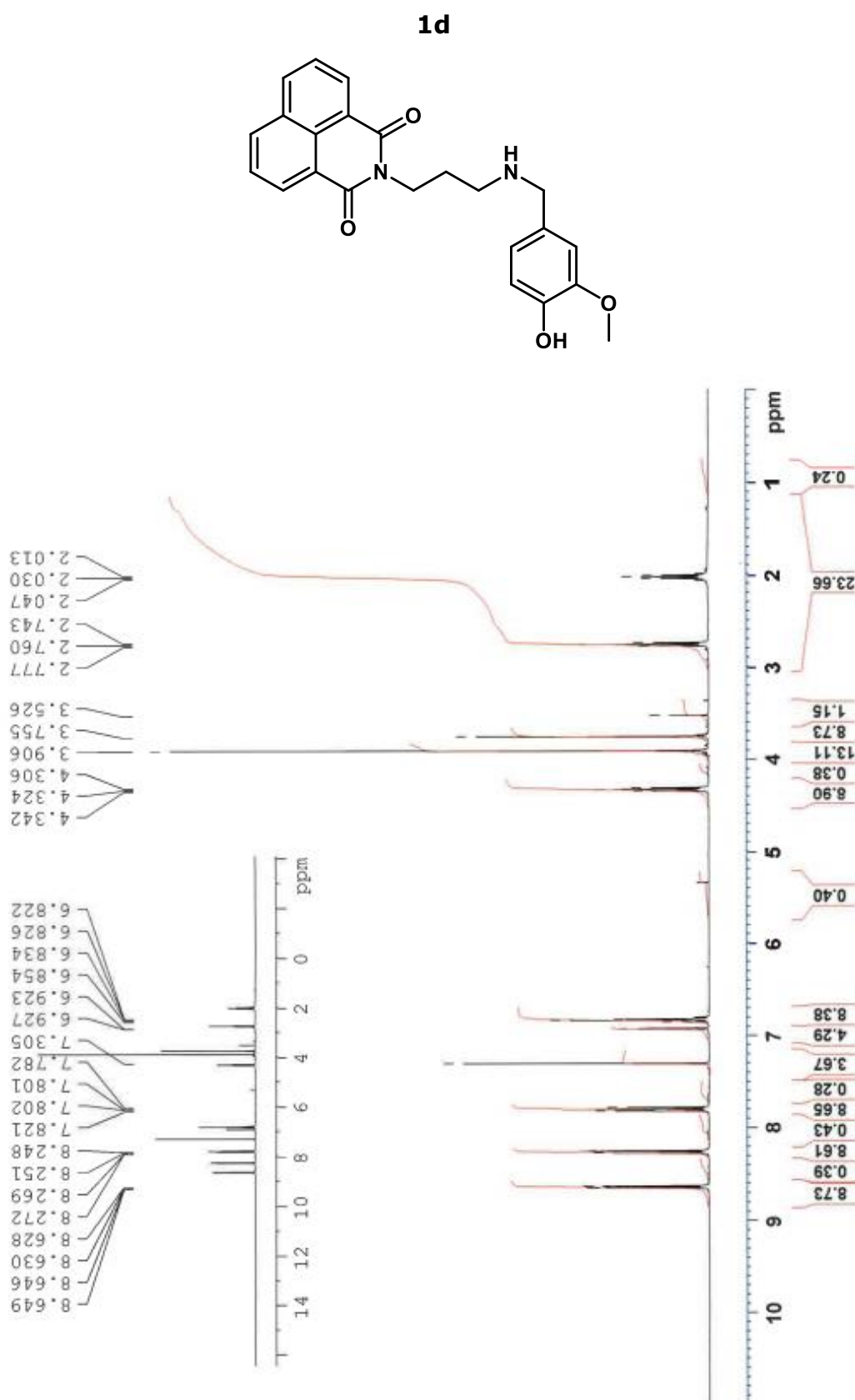


Figure A19. <sup>1</sup>H NMR spectrum of compound **1d**.

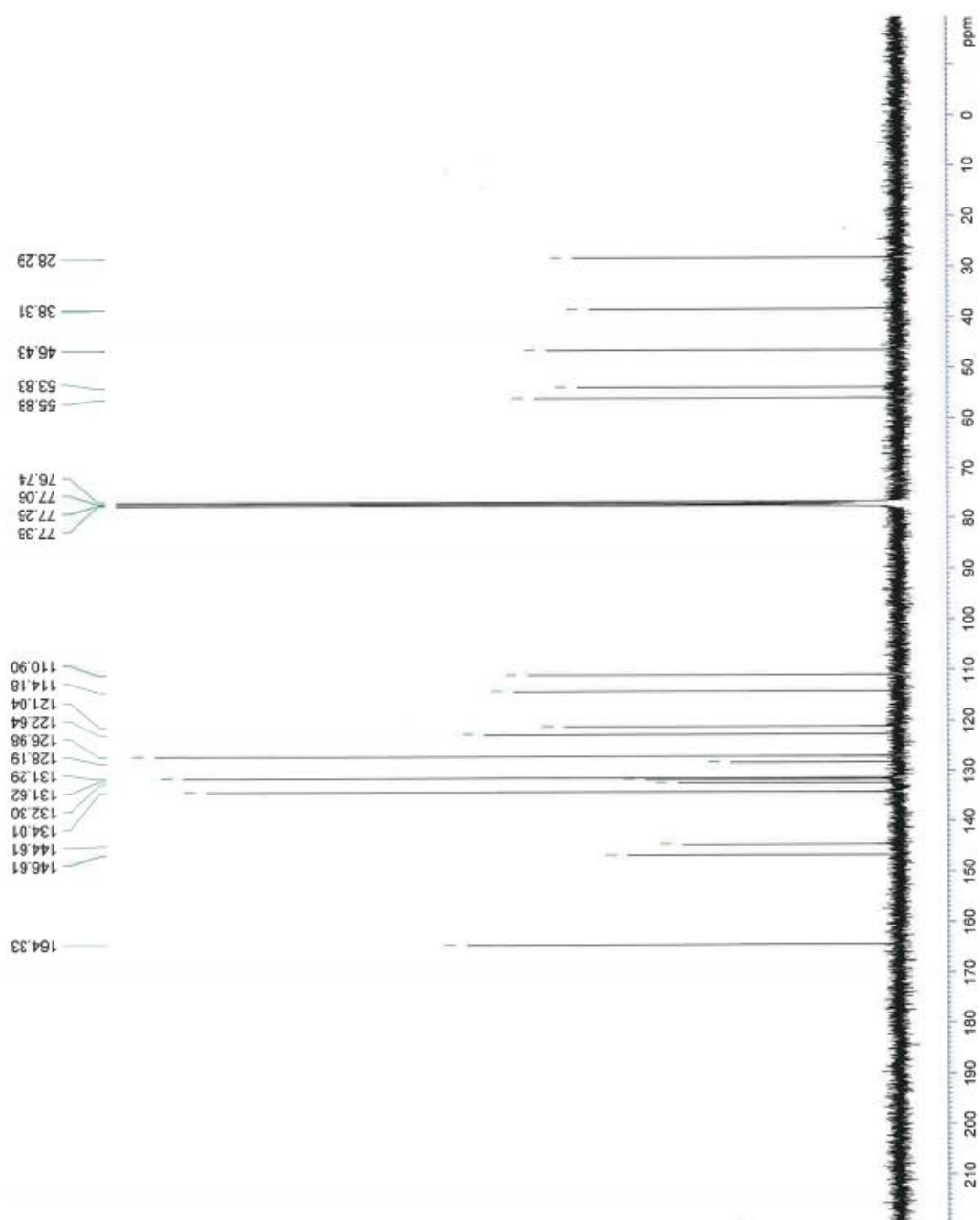


Figure A20.  $^{13}\text{C}$  NMR spectrum of compound **1d**.

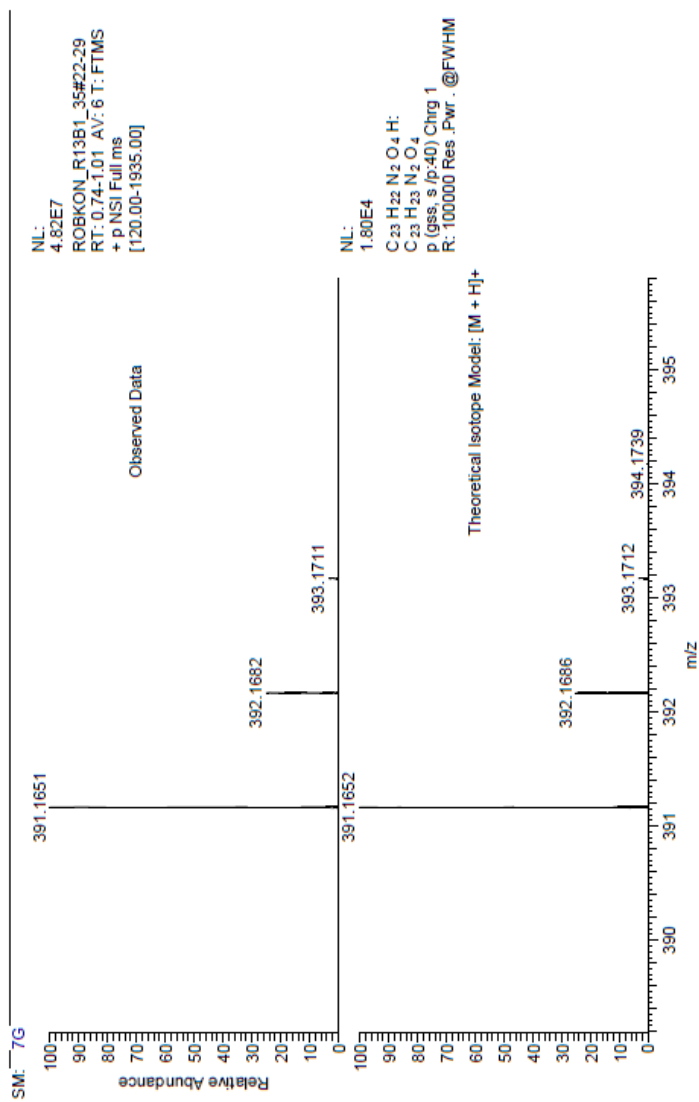


Figure A21. HRMS spectrum of compound **1d**.

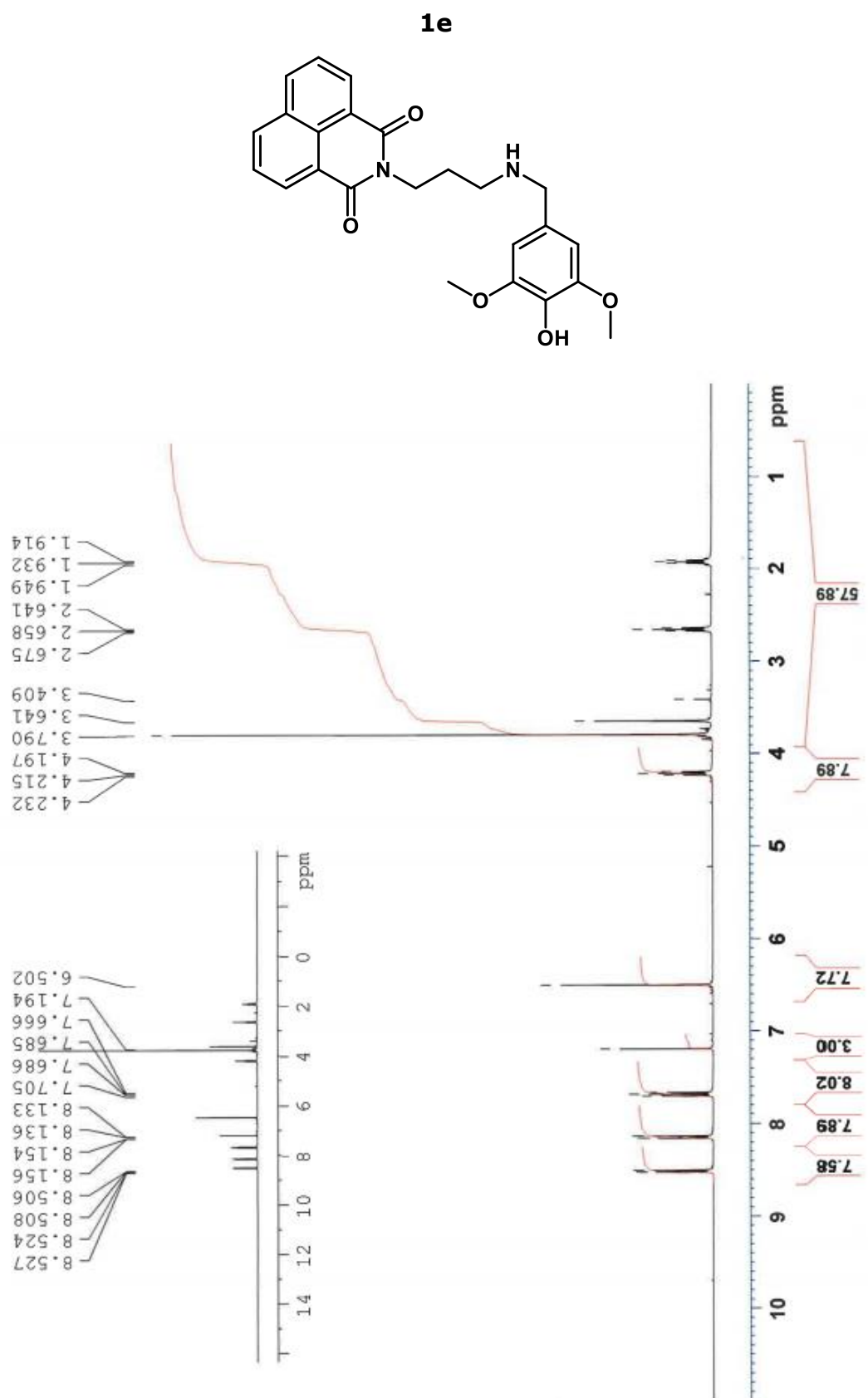


Figure A22.  $^1\text{H}$  NMR spectrum of compound **1e**.

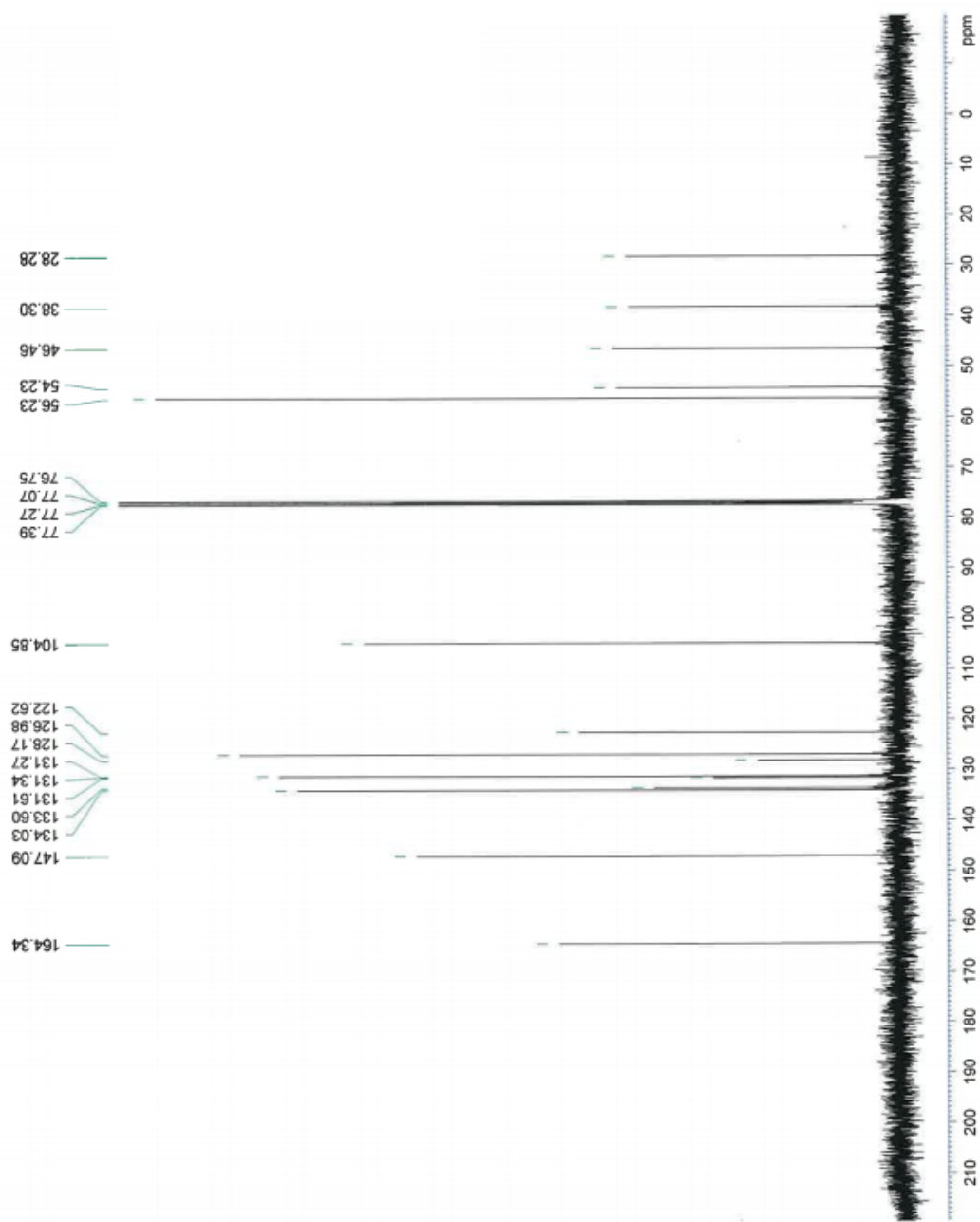


Figure A23. <sup>13</sup>C NMR spectrum of compound **1e**.

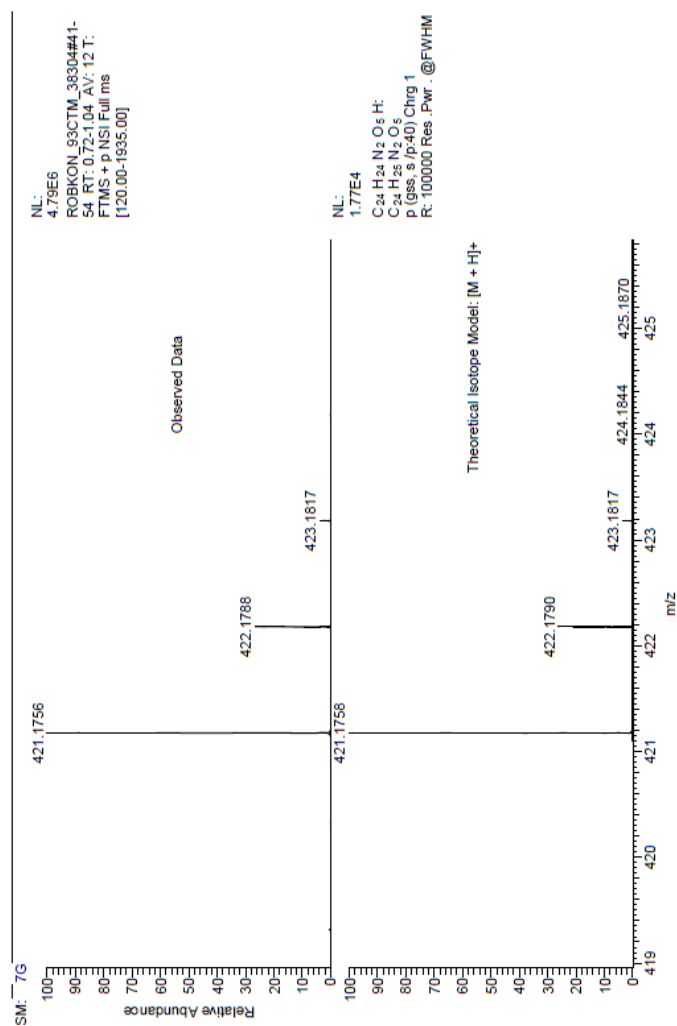


Figure A24. HRMS spectrum of compound **1e**.



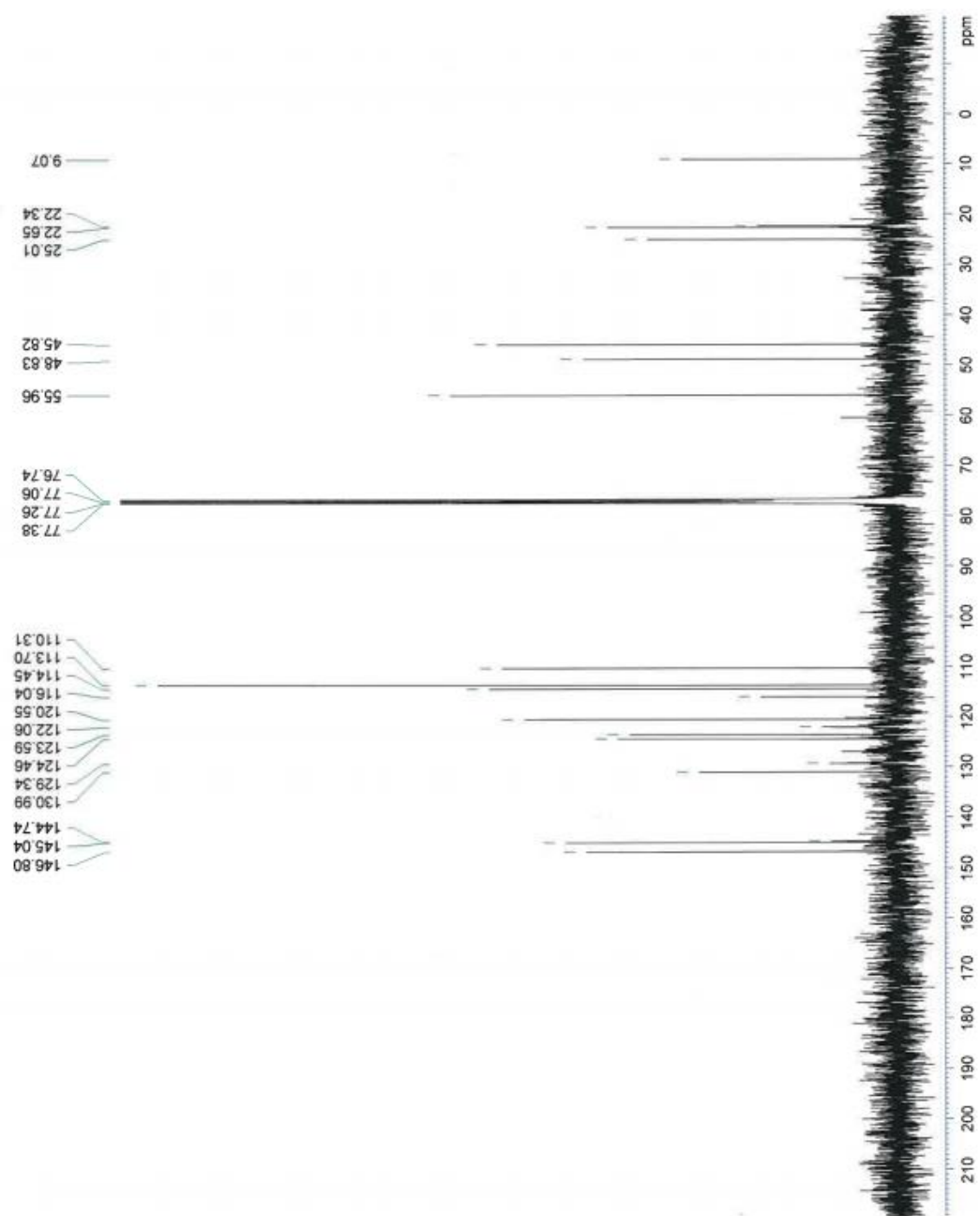


Figure A26.  $^{13}\text{C}$  NMR spectrum of compound **1f**.

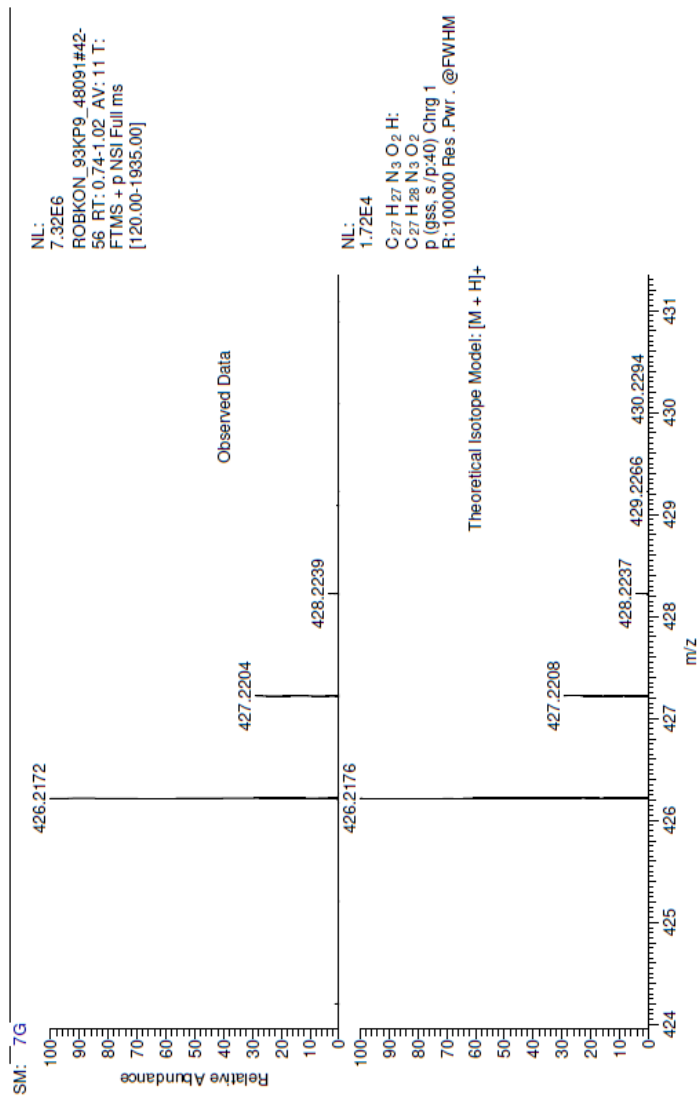


Figure A27. HRMS spectrum of compound **1f**.

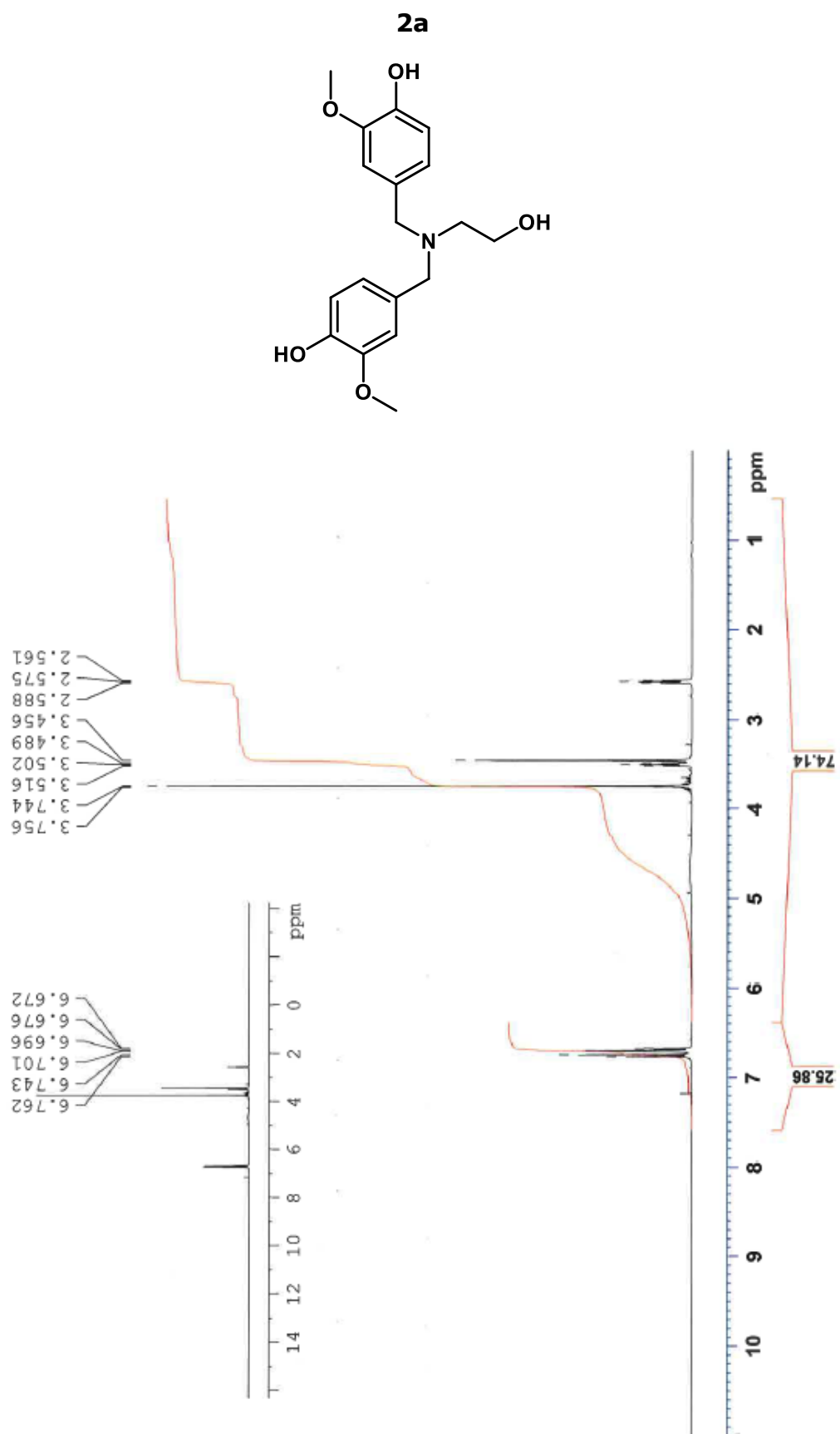


Figure A28. <sup>1</sup>H NMR spectrum of compound 2a.

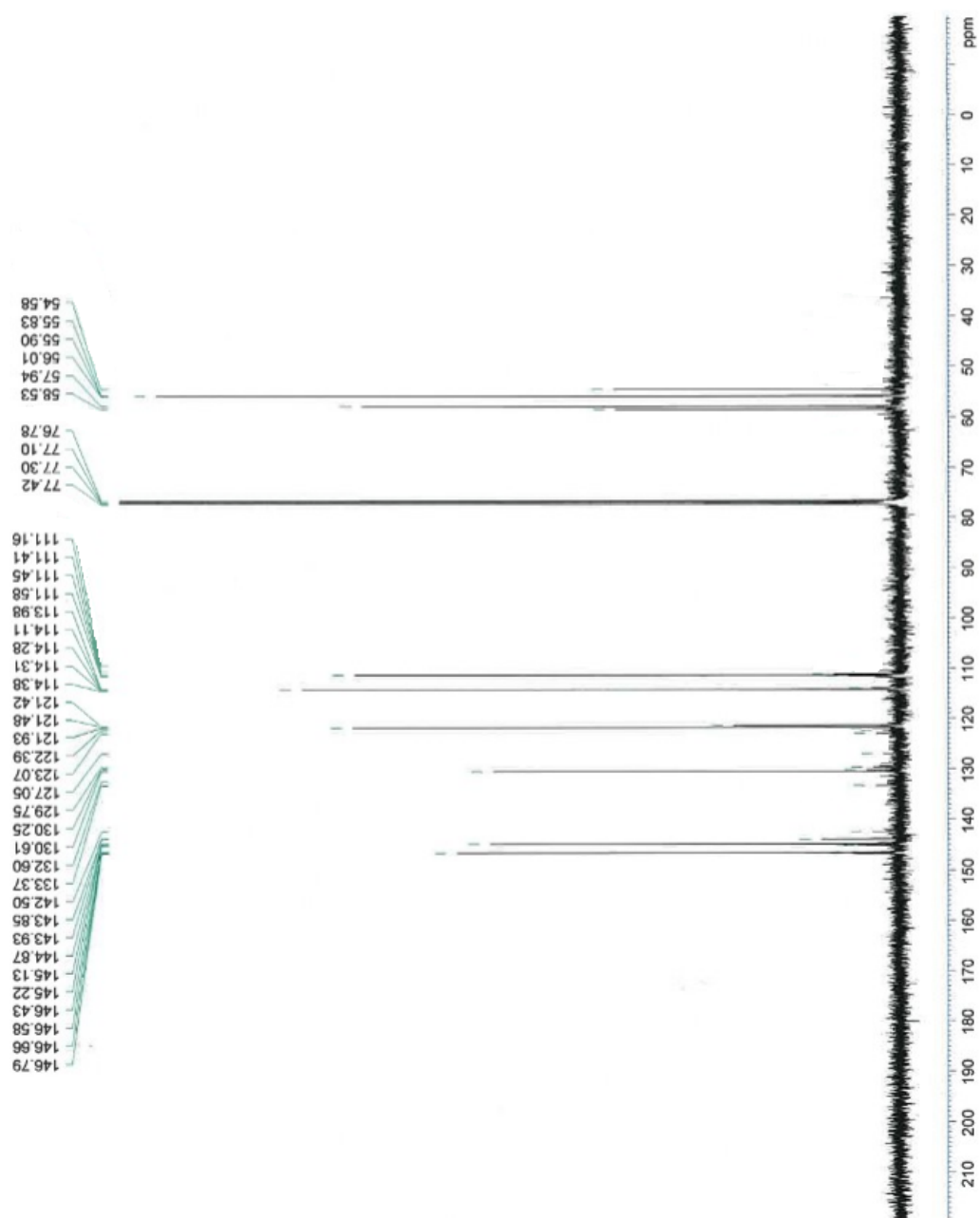


Figure A29.  $^{13}\text{C}$  NMR spectrum of compound **2a**.

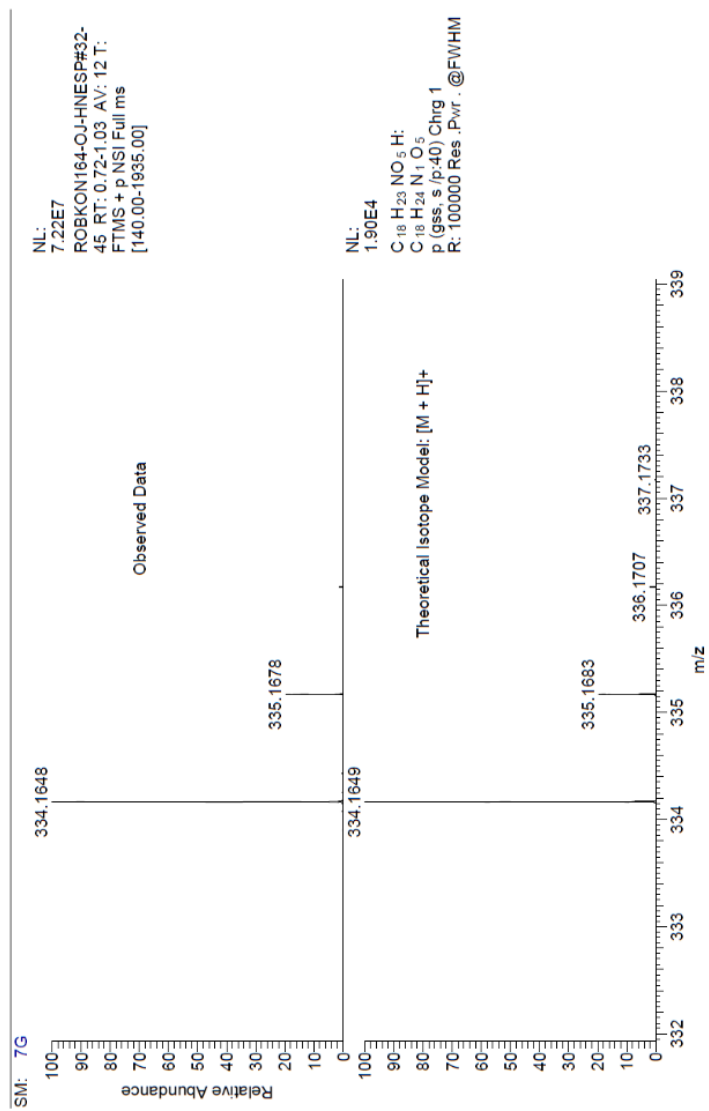


Figure A30. HRMS spectrum of compound **2a**.

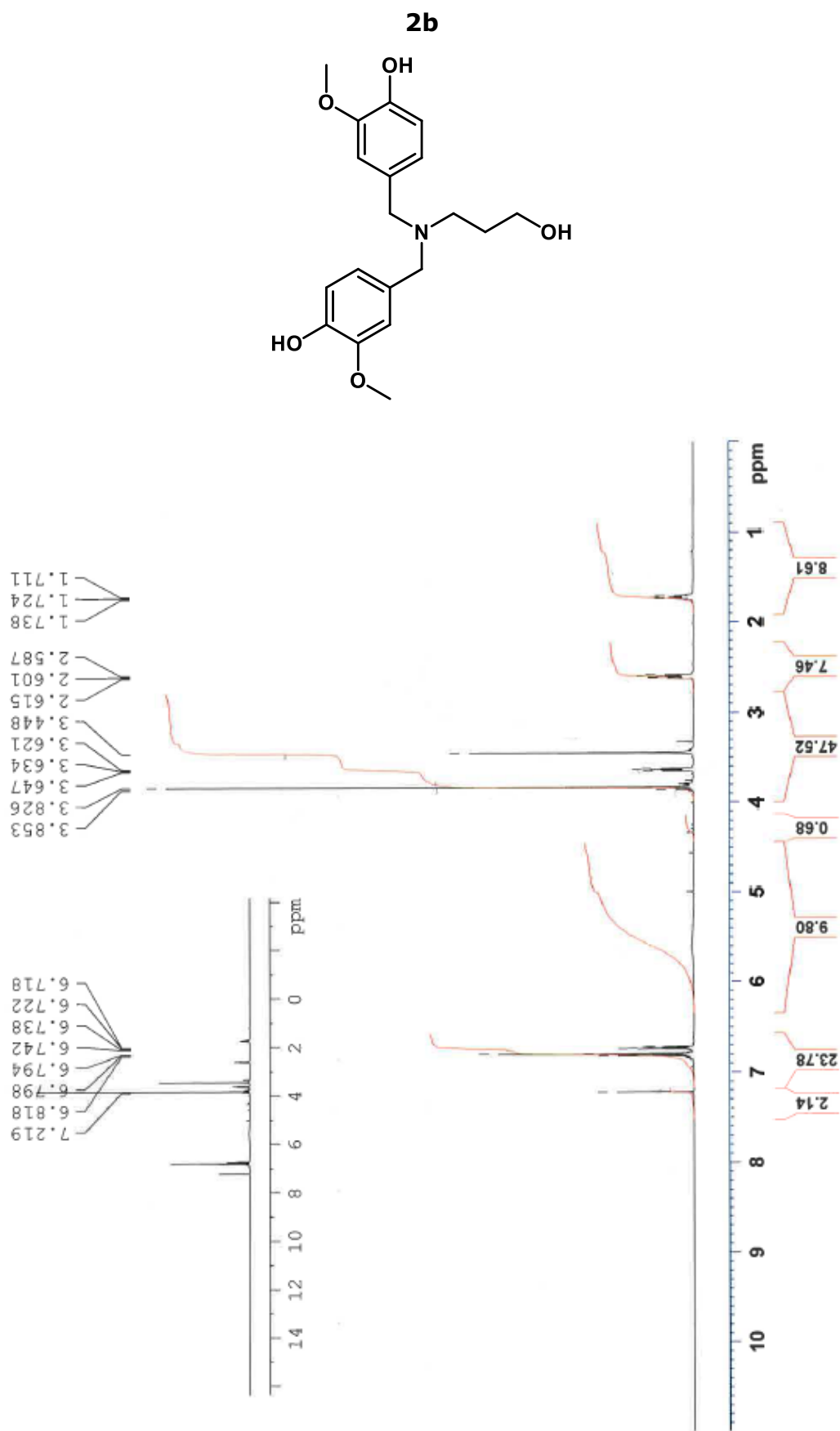


Figure A31.  $^1\text{H}$  NMR spectrum of compound **2b**.

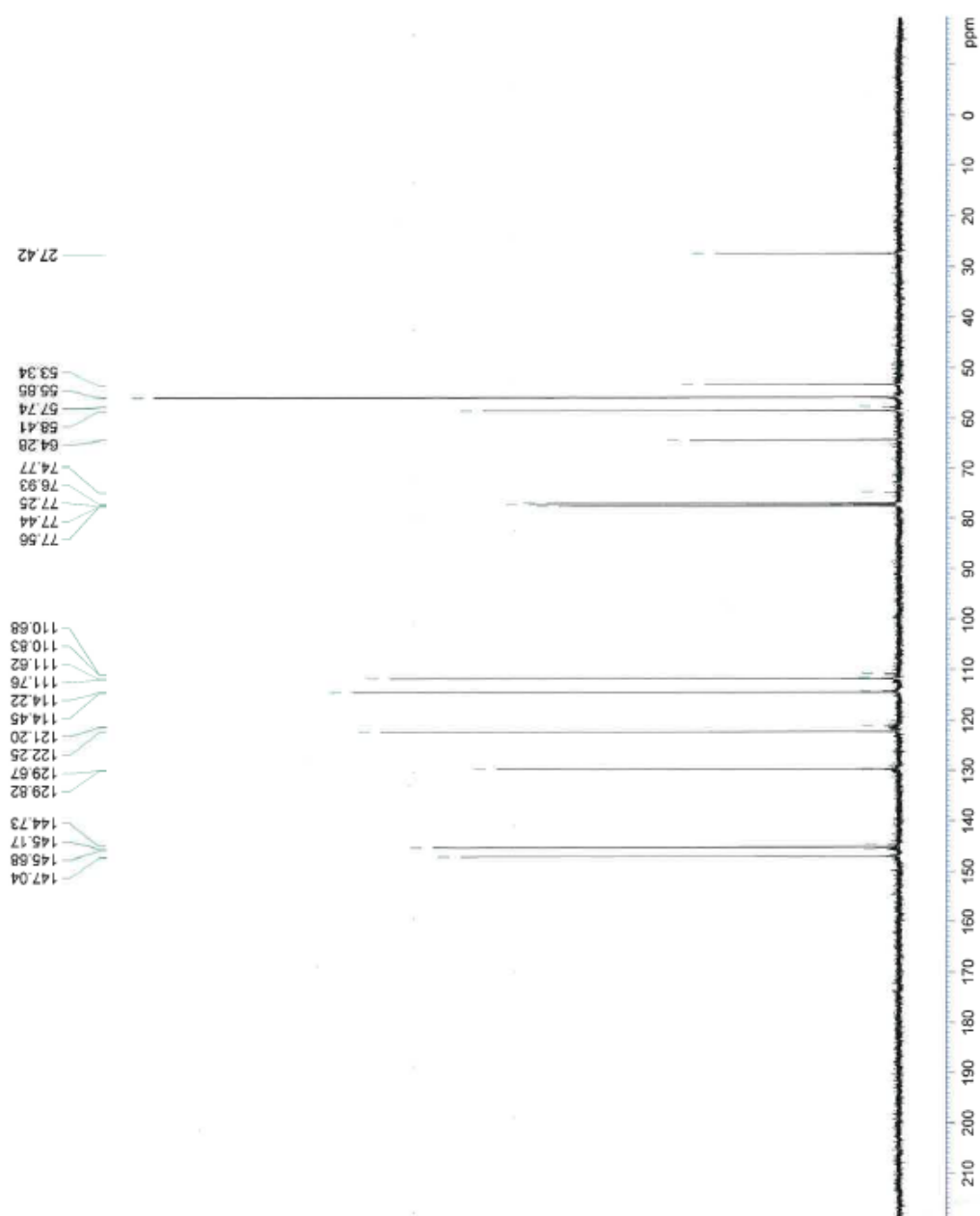


Figure A32.  $^{13}\text{C}$  NMR spectrum of compound **2b**.

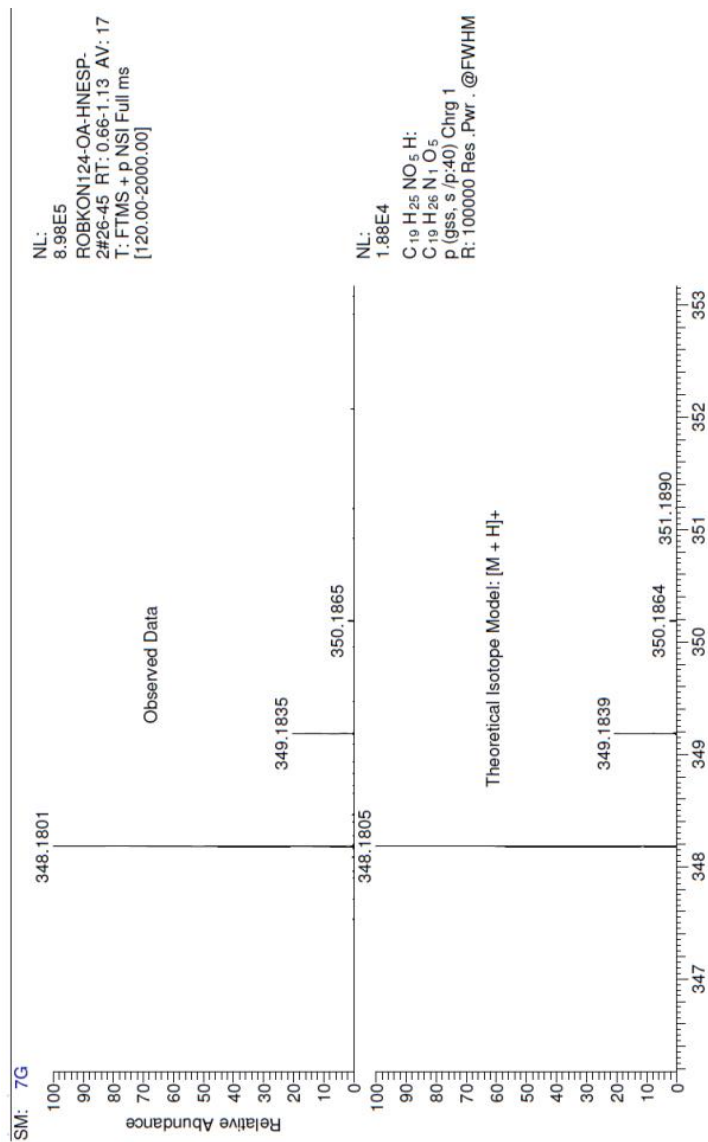


Figure A33. HRMS spectrum of compound **2b**.

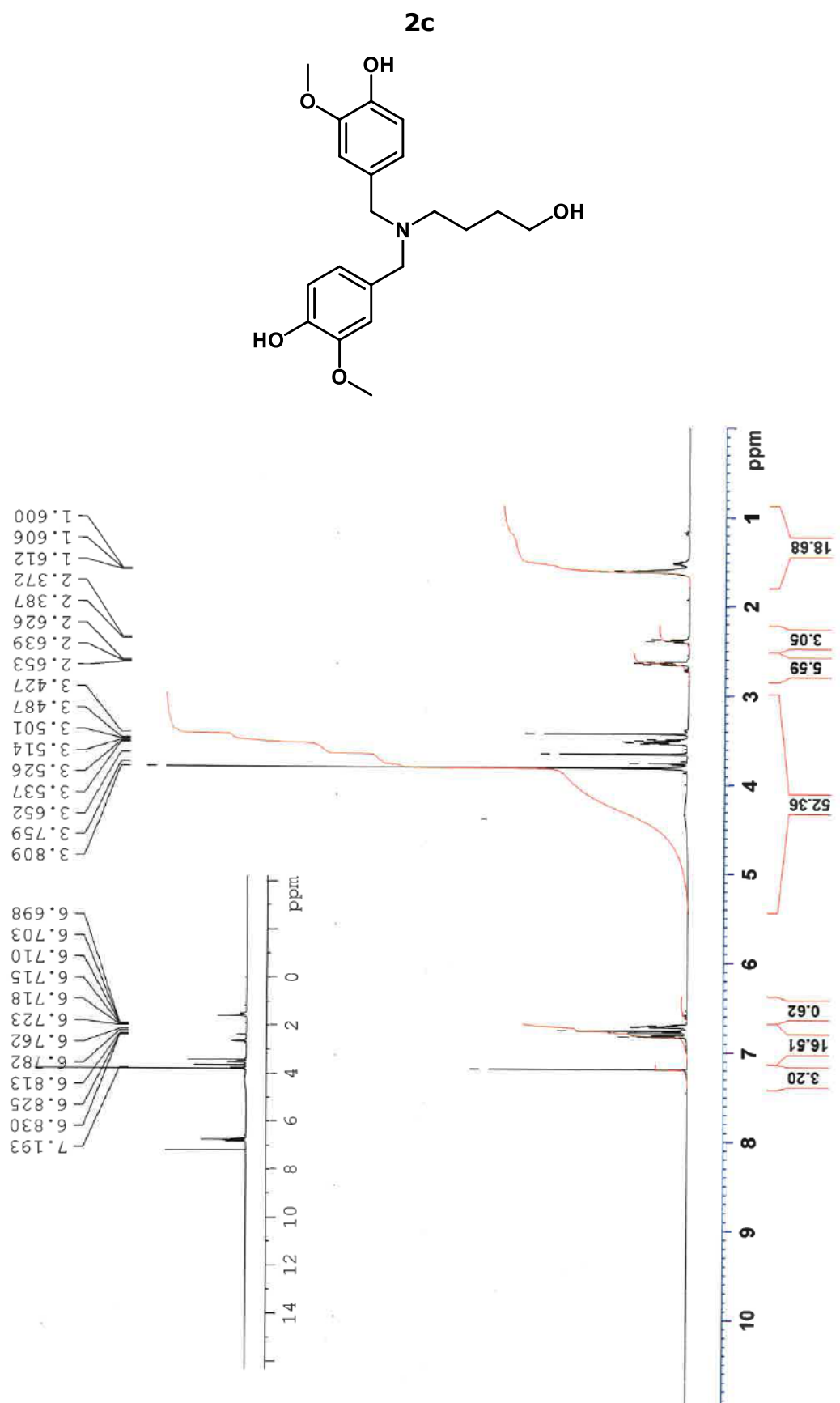


Figure A34. <sup>1</sup>H NMR spectrum of compound 2c.

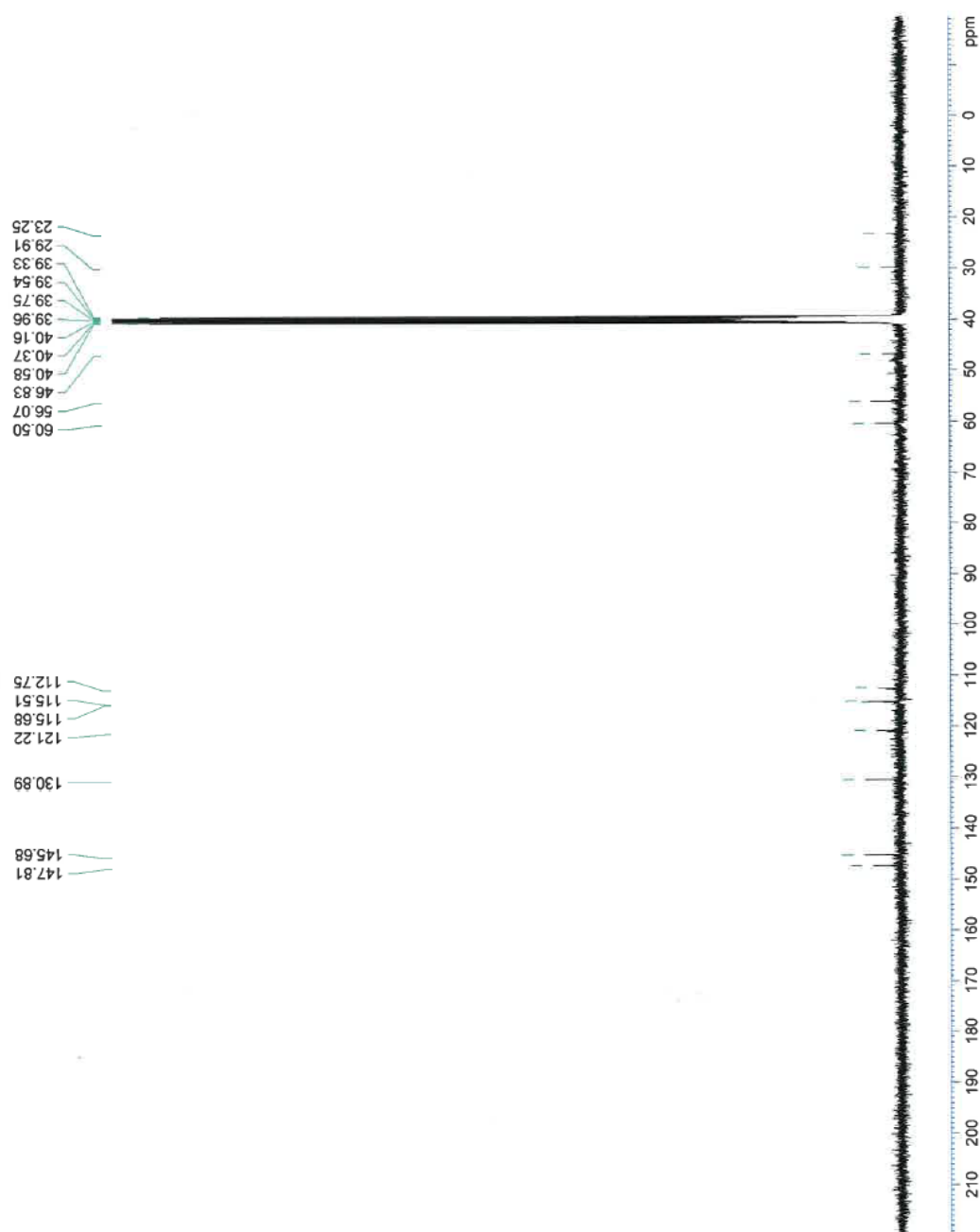


Figure A35. <sup>13</sup>C NMR spectrum of compound **2c**.

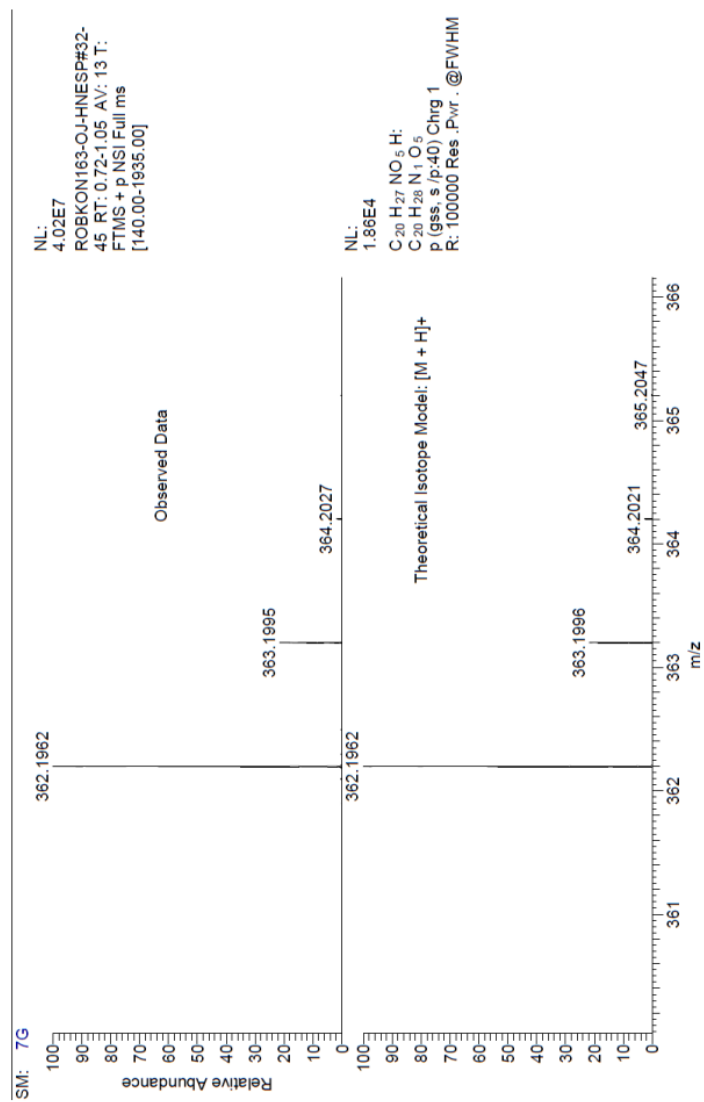


Figure A36. HRMS spectrum of compound **2c**.

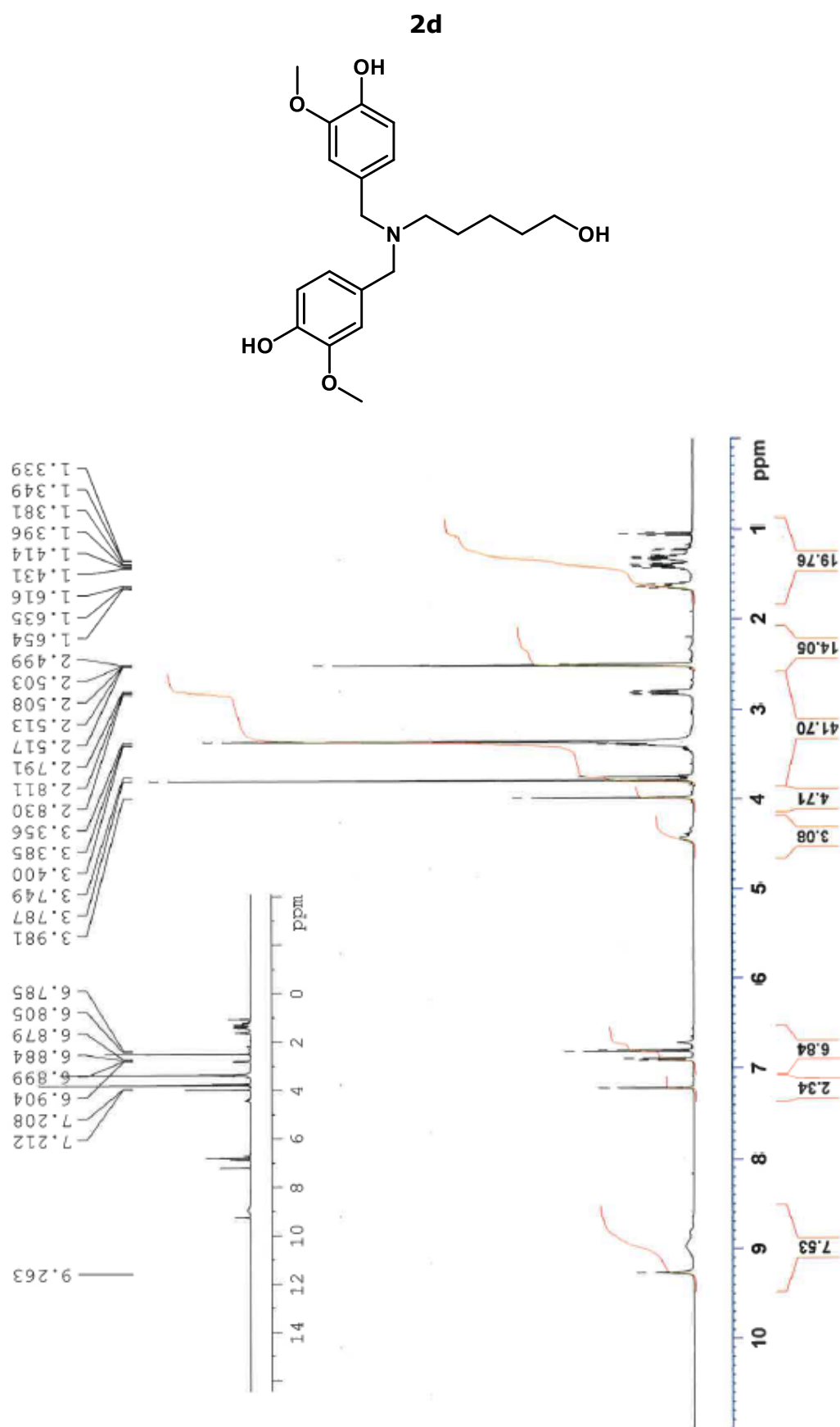


Figure A37.  $^1\text{H}$  NMR spectrum of compound **2d**.

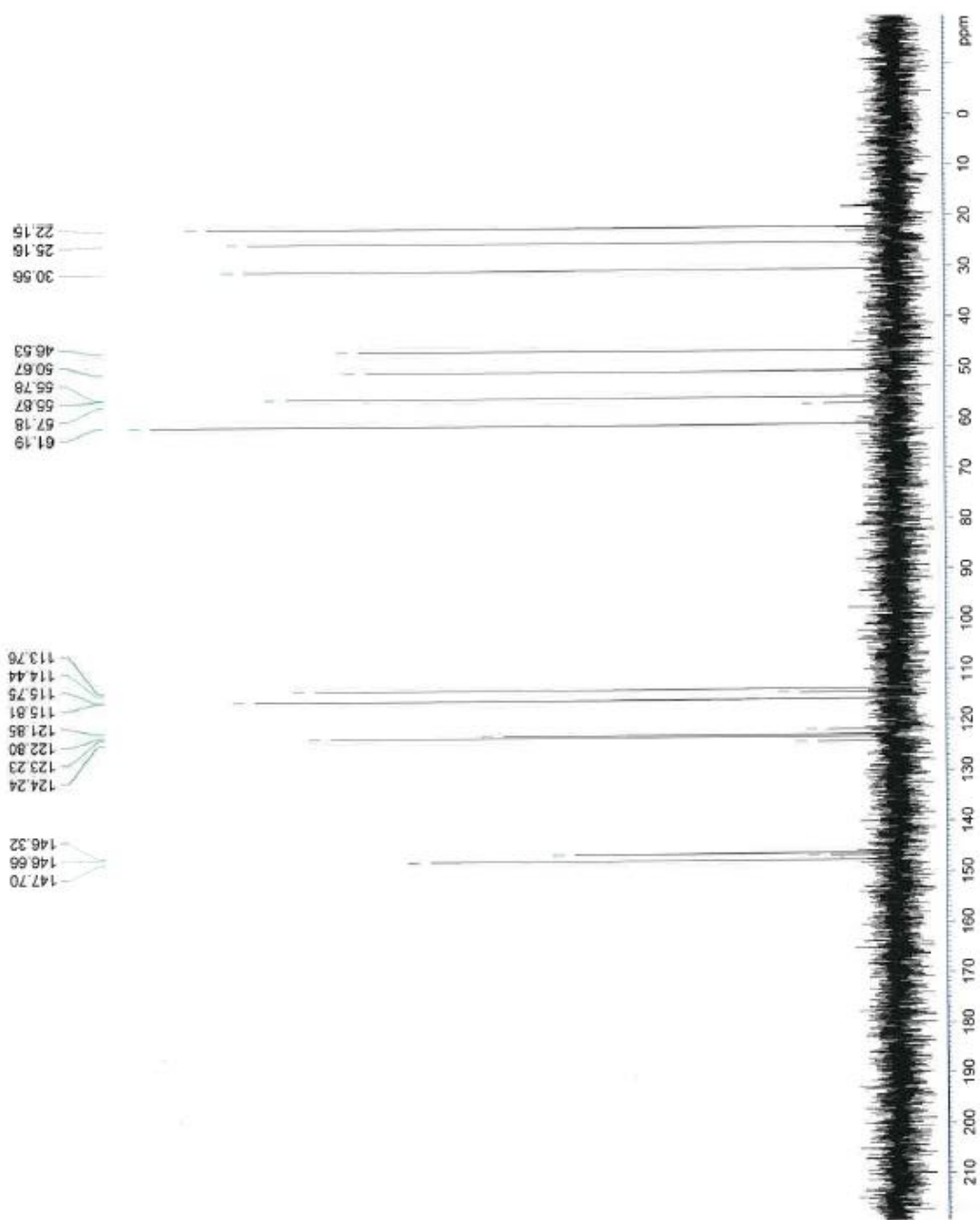


Figure A38.  $^{13}\text{C}$  NMR spectrum of compound 2d.

NL:  
2.34E7  
ROBKON\_VN69E\_9#27-44  
RT: 0.65-1.04 AV: 16 T: FTMS  
+ p.NSI Full ms  
[120.00-1935.00]

NL:  
1.84E4  
C<sub>21</sub>H<sub>29</sub>NO<sub>5</sub>H:  
C<sub>21</sub>H<sub>30</sub>N<sub>1</sub>O<sub>5</sub>  
p (gss, s/p;40) Chrg 1  
R: 100000 Res.Pwr. @FWHM

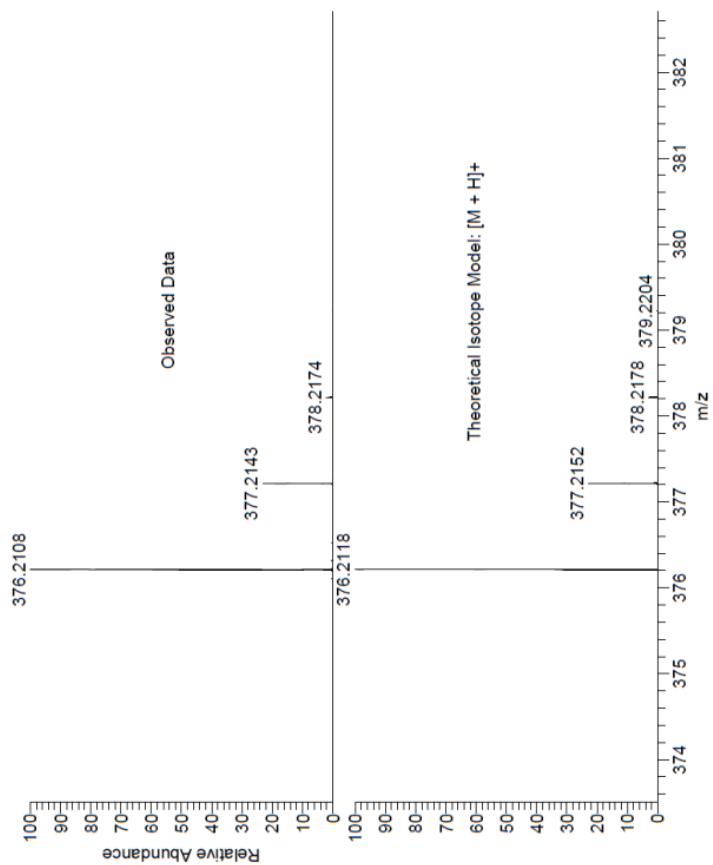


Figure A39. HRMS spectrum of compound **2d**.

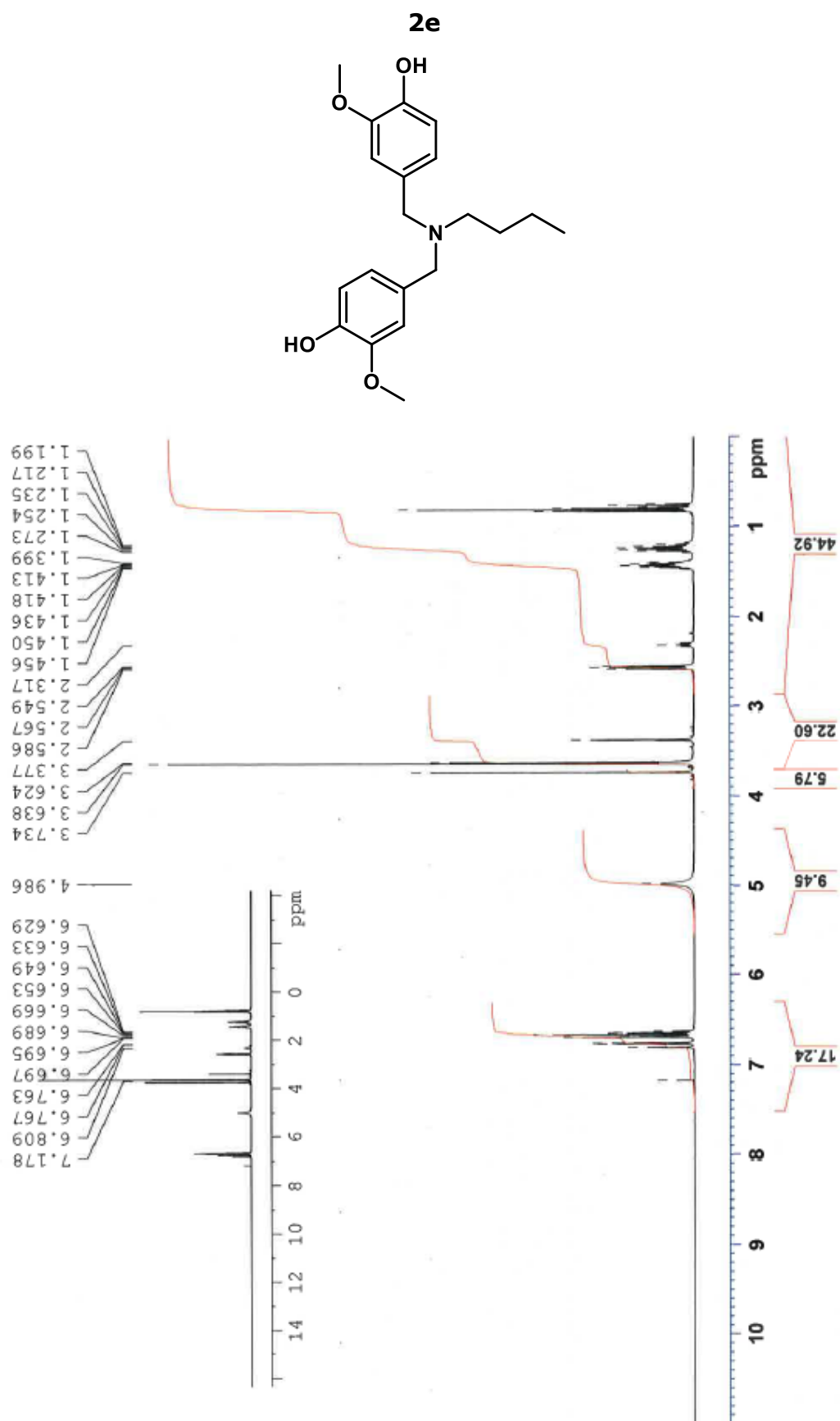


Figure A40. <sup>1</sup>H NMR spectrum of compound **2e**.

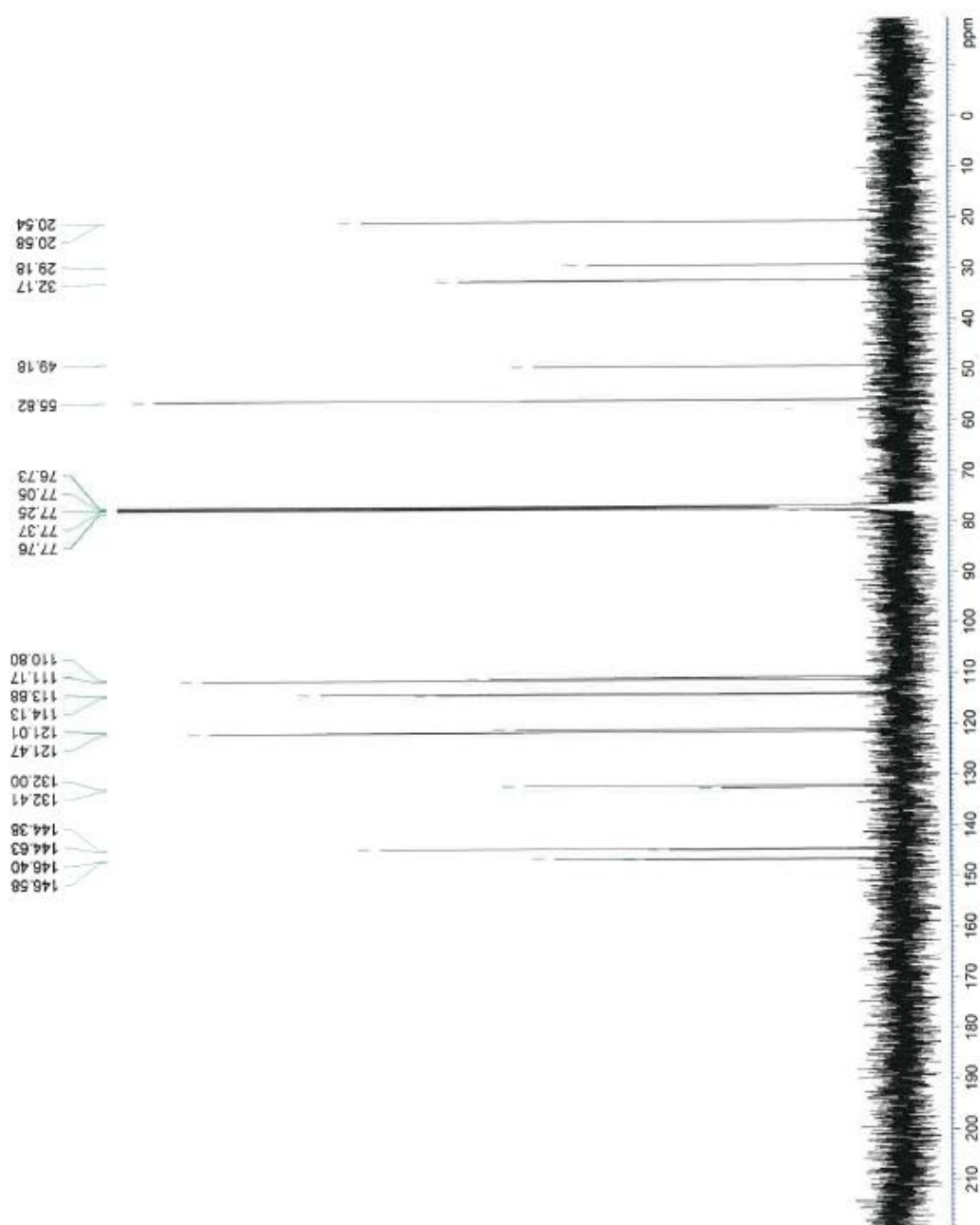


Figure A41.  $^{13}\text{C}$  NMR spectrum of compound **2e**.

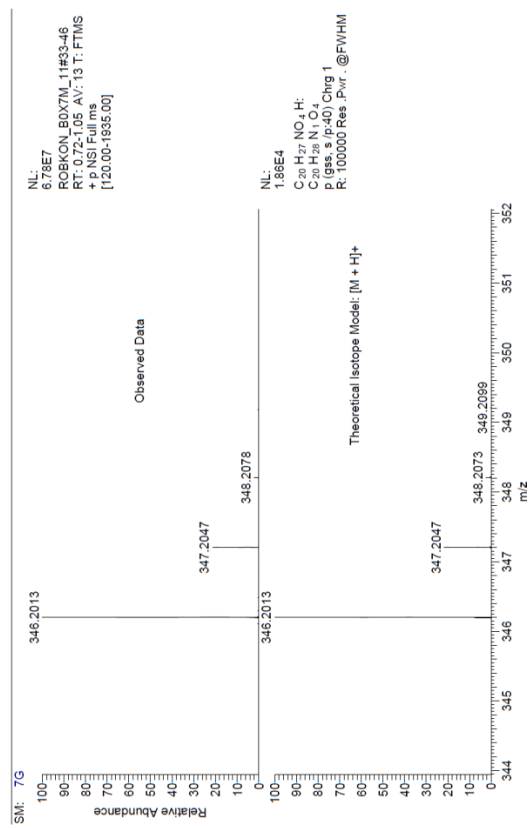


Figure A42. HRMS spectrum of compound **2e**.

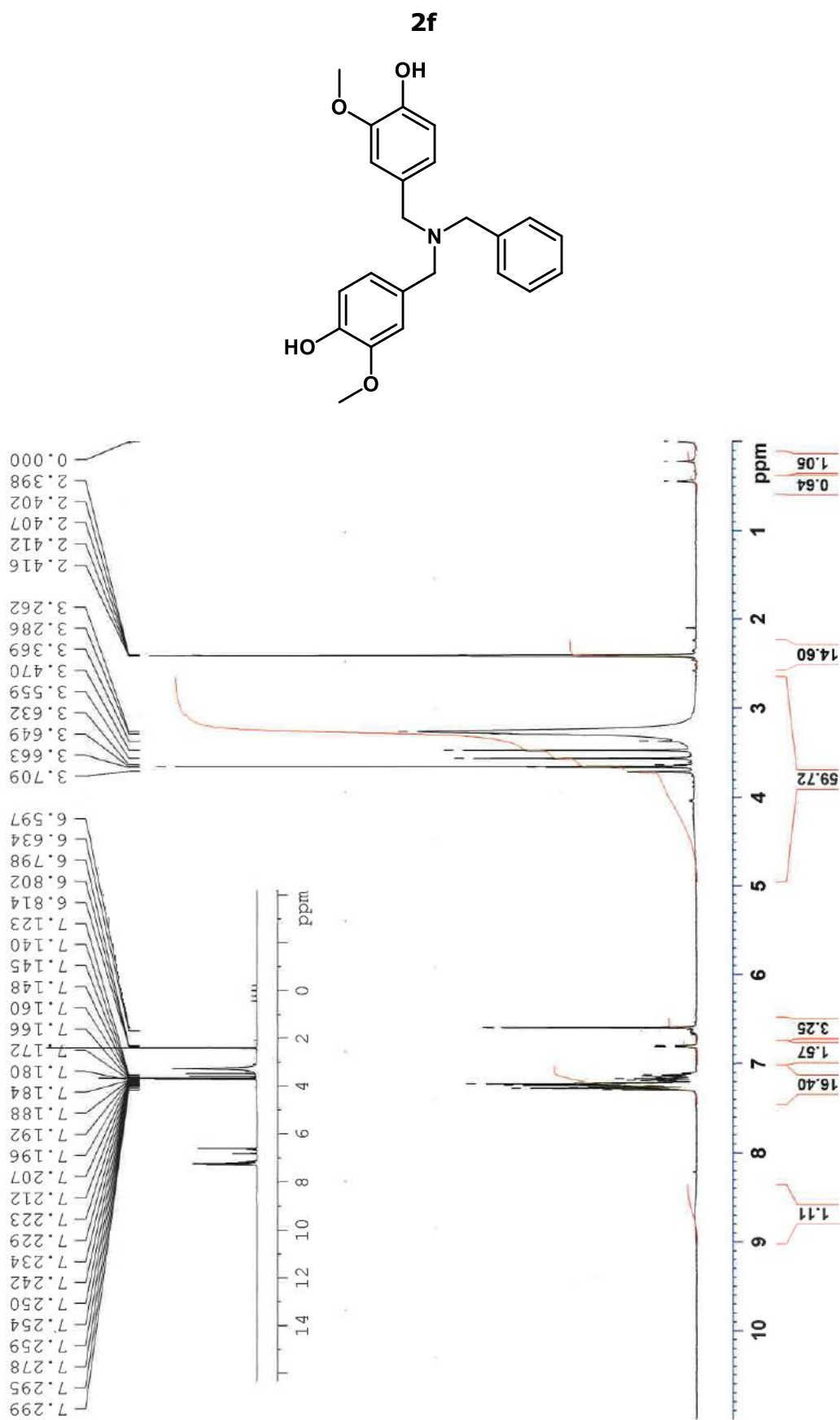


Figure A43. <sup>1</sup>H NMR spectrum of compound **2f**.

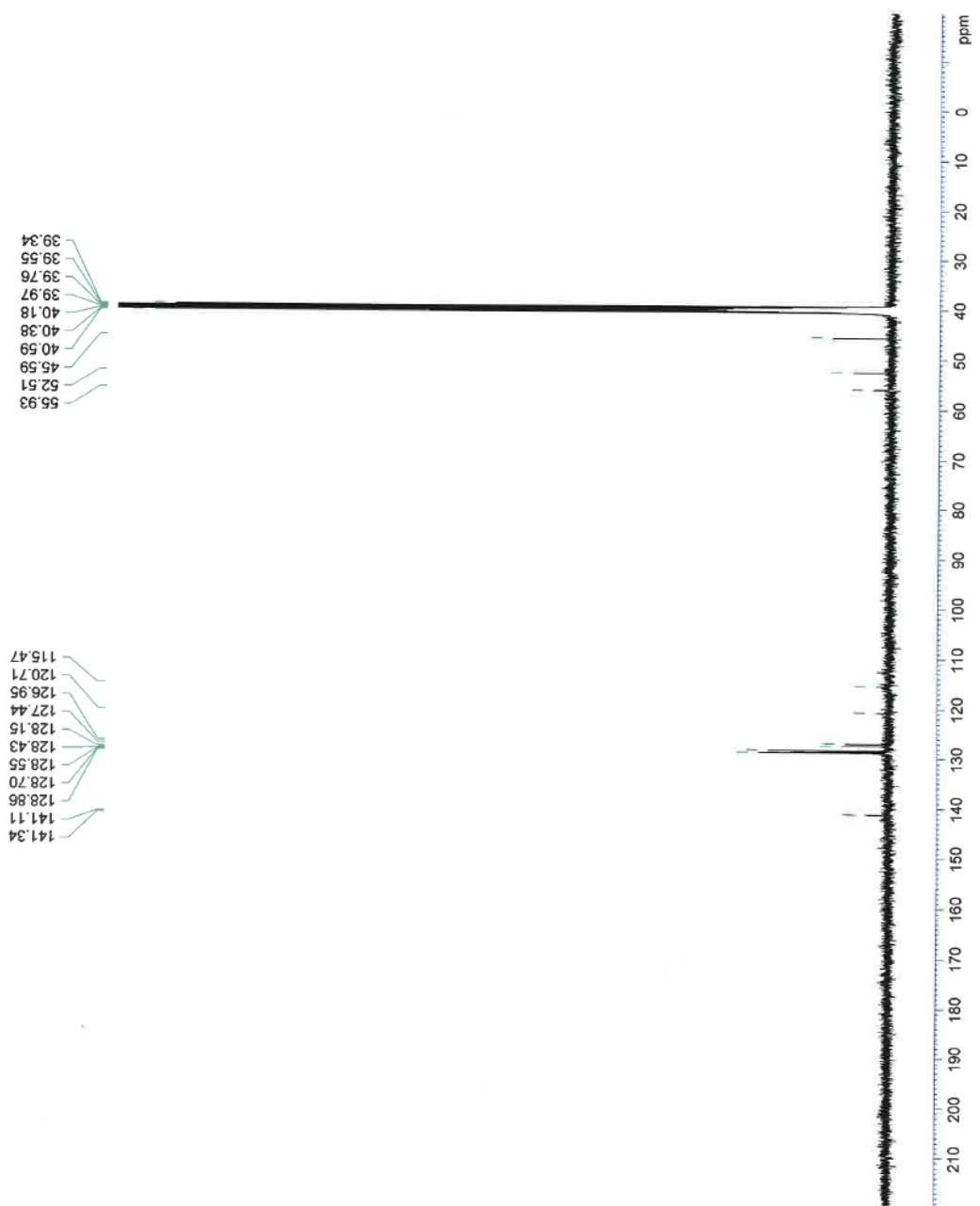
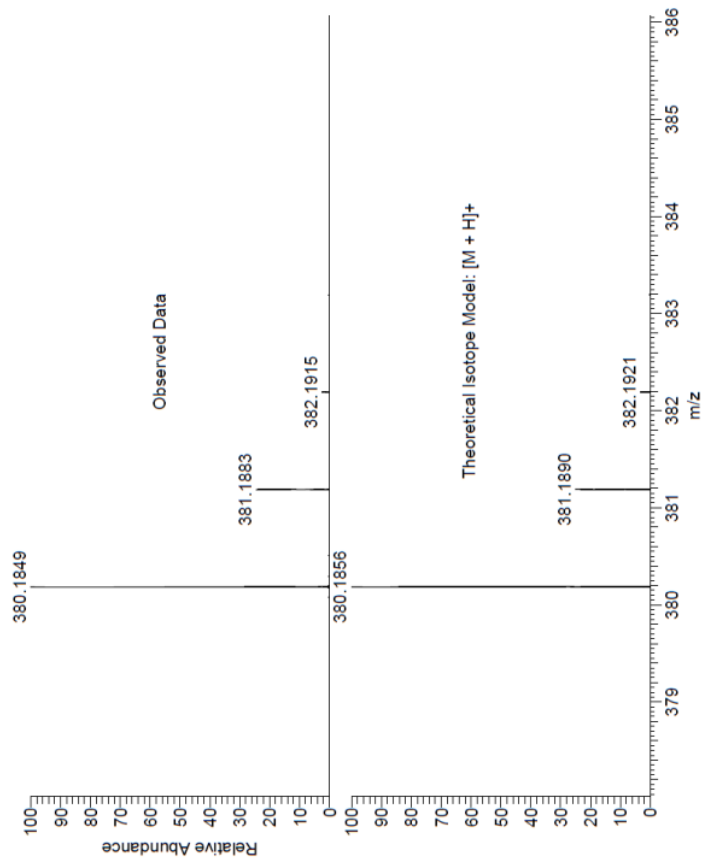


Figure A44.  $^{13}\text{C}$  NMR spectrum of compound 2f.

NL:  
3.69E7  
ROBKON\_9Y1IF\_10#28-45  
RT: 0.66-1.04 AV: 16 T: FTMS  
+ P NSI Full ms  
[120.00-1935.00]



NL:  
1.80E4  
C<sub>23</sub>H<sub>25</sub>NO<sub>4</sub>H:  
C<sub>23</sub>H<sub>26</sub>N<sub>1</sub>O<sub>4</sub>  
P (gss, s (p=40) Chrg 1  
R: 100000 Res .P.wr. @FWHM

Figure A45. HRMS spectrum of compound **2f**.

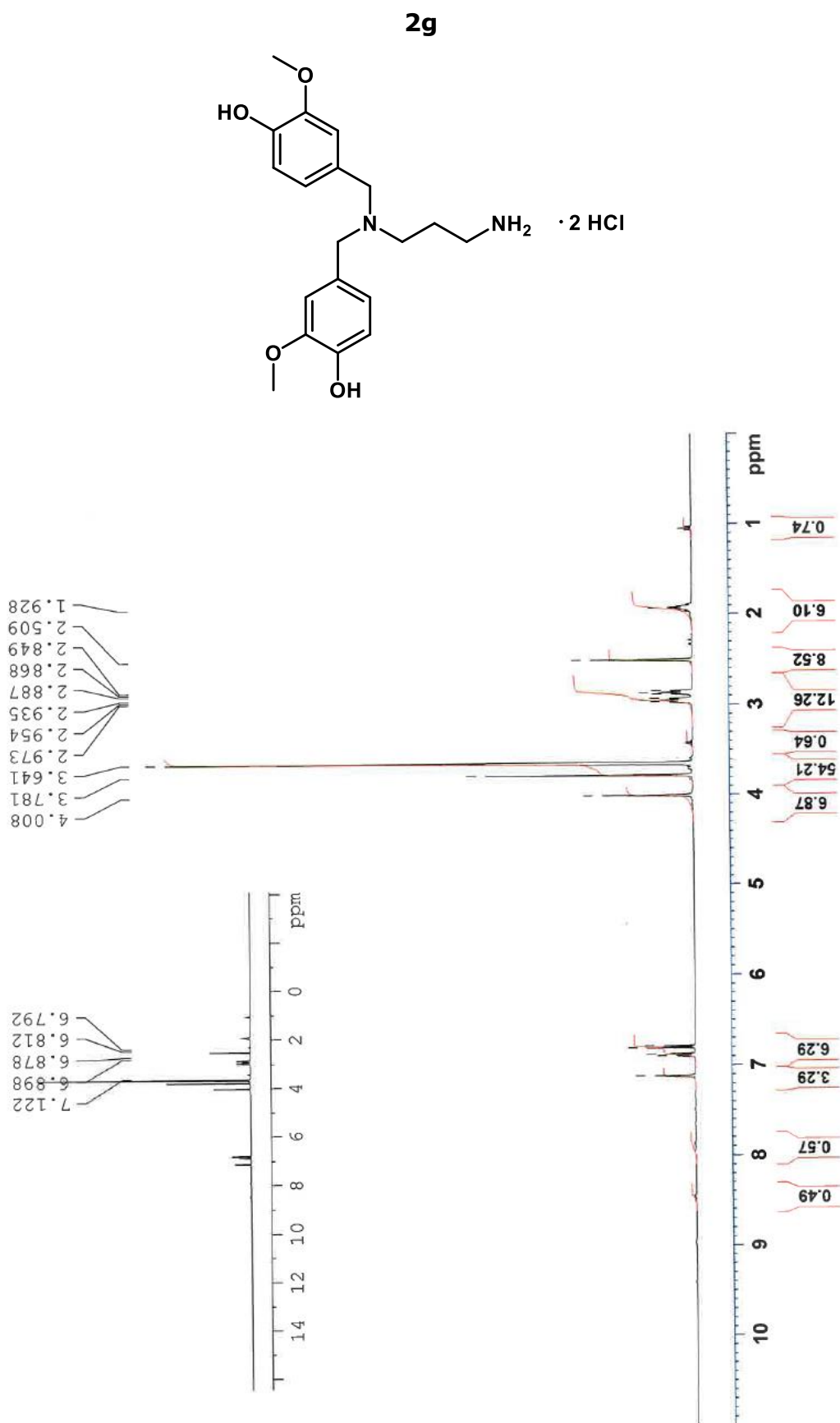


Figure A46.  $^1\text{H}$  NMR spectrum of compound **2g**.

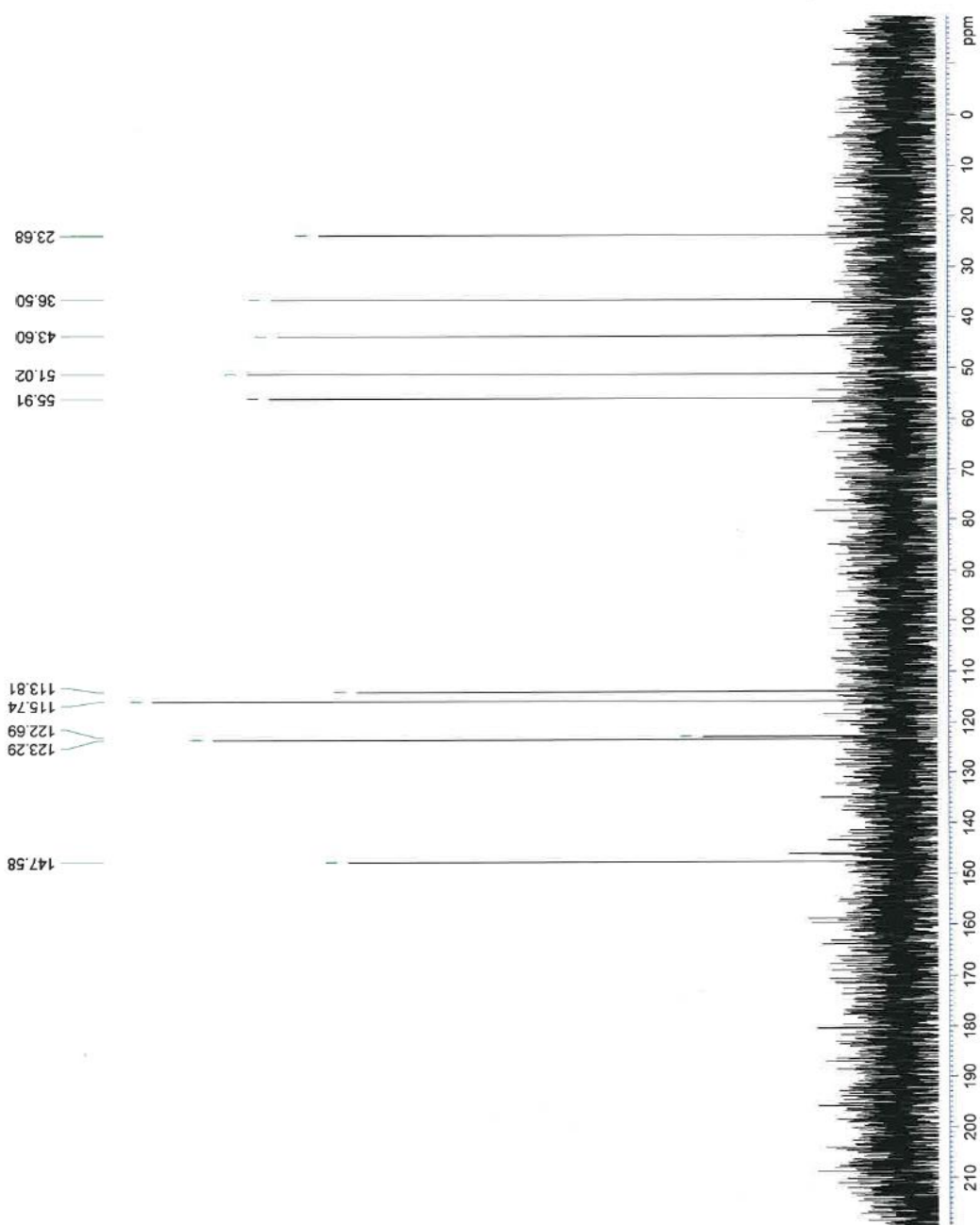


Figure A47. <sup>13</sup>C NMR spectrum of compound **2g**.

NL:  
8.23E6  
ROBKON\_S77NK\_16#33-46  
RT: 0.74-1.04 AV: 12 T: FTMS  
+ p.NSI Full ms  
[120.00-1935.00]

NL:  
1.87E4  
C<sub>19</sub>H<sub>27</sub>N<sub>2</sub>O<sub>4</sub>  
C<sub>19</sub>H<sub>27</sub>N<sub>2</sub>O<sub>4</sub>  
p (gss, s /p:40) Chrg 1  
R: 100000 Res .Pwr. @FWHM

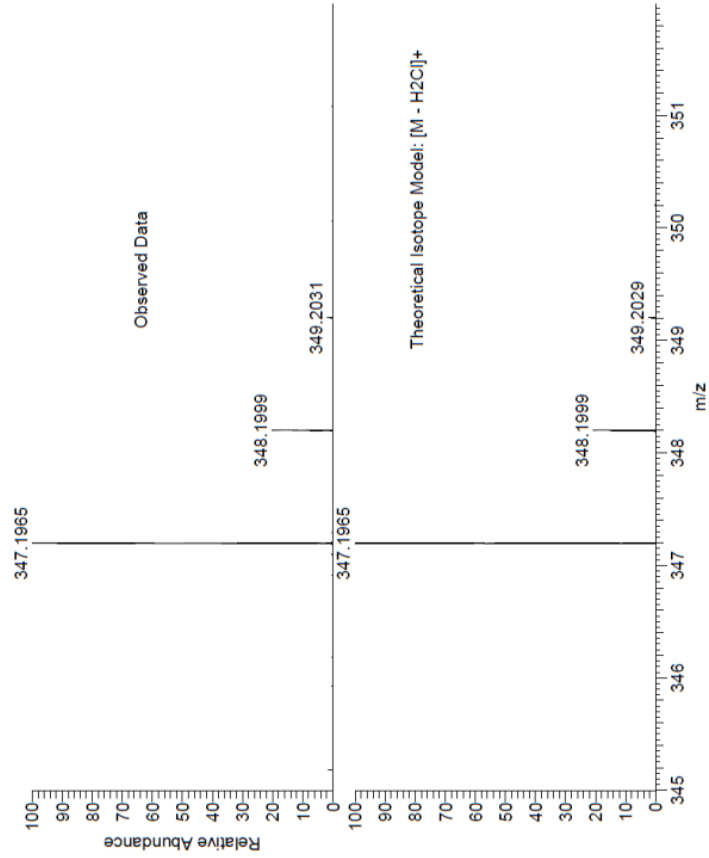


Figure A48. HRMS spectrum of compound **2g**.

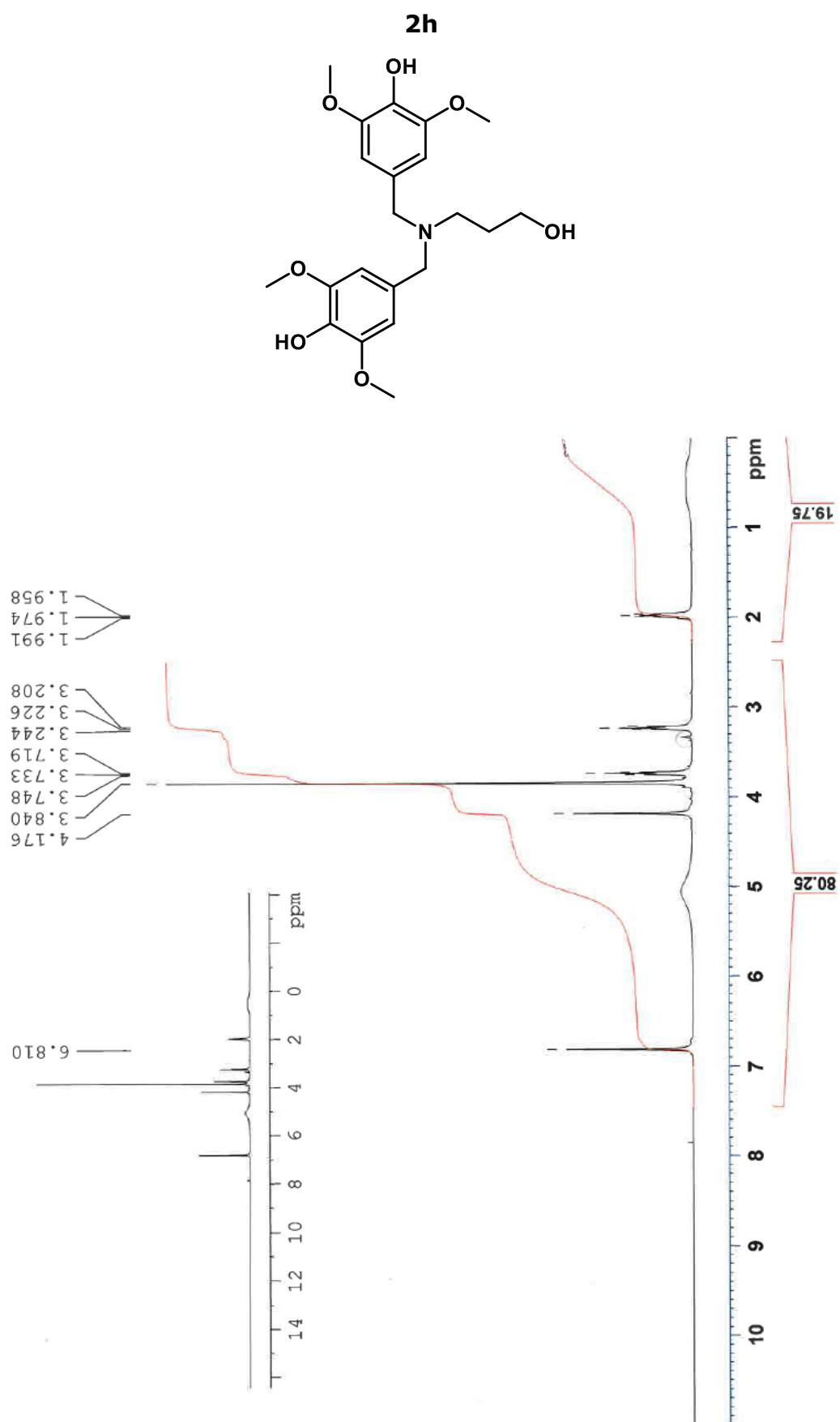


Figure A49. <sup>1</sup>H NMR spectrum of compound **2h**.

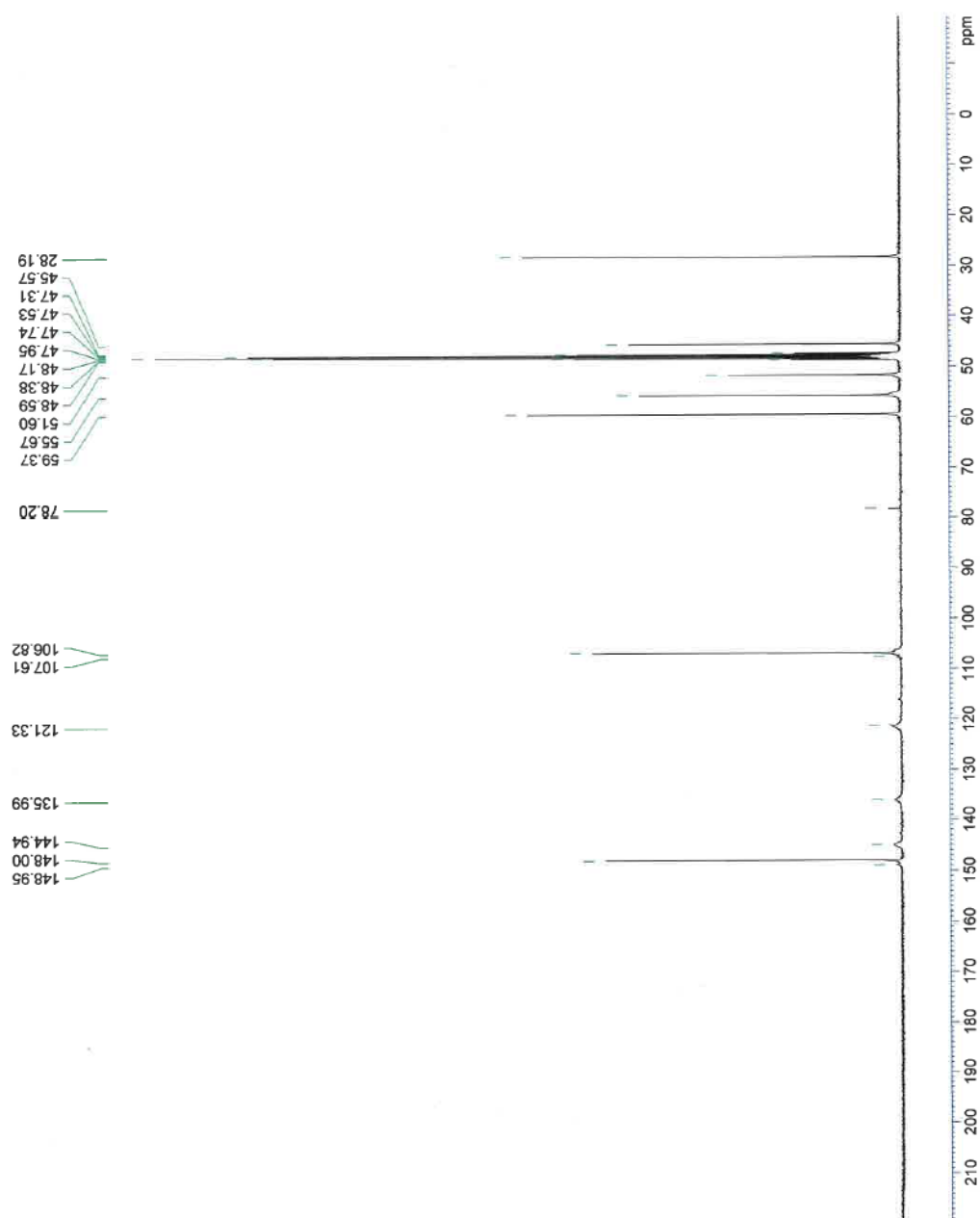


Figure A50. <sup>13</sup>C NMR spectrum of compound **2h**.

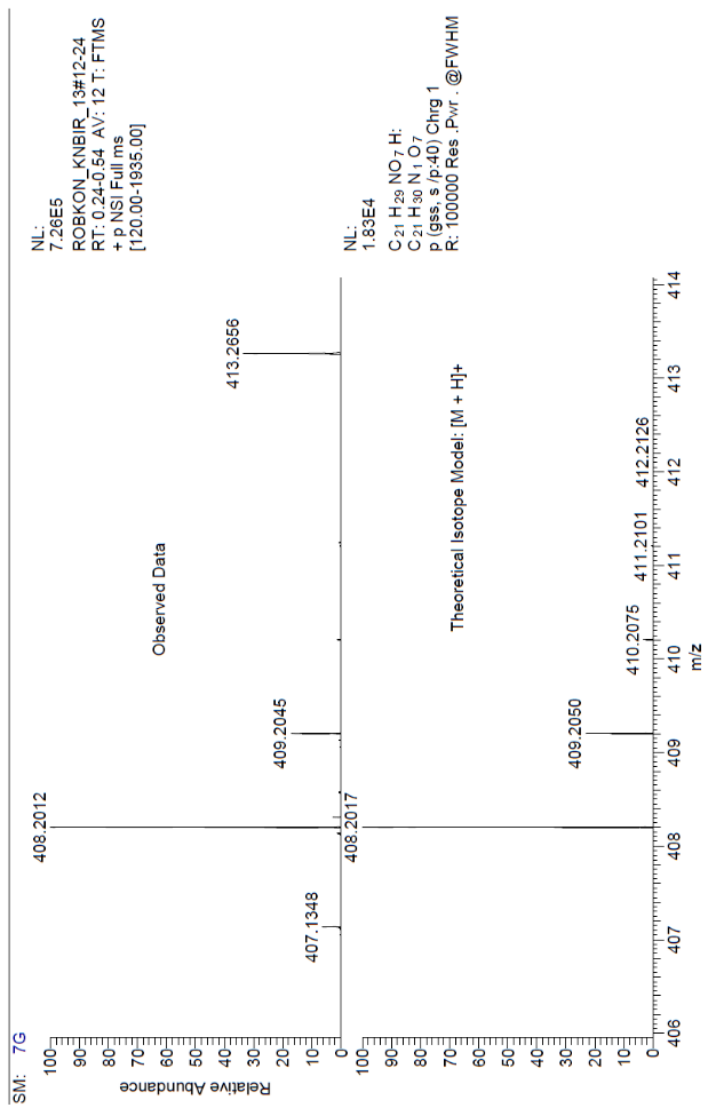


Figure A51. HRMS spectrum of compound **2h**.

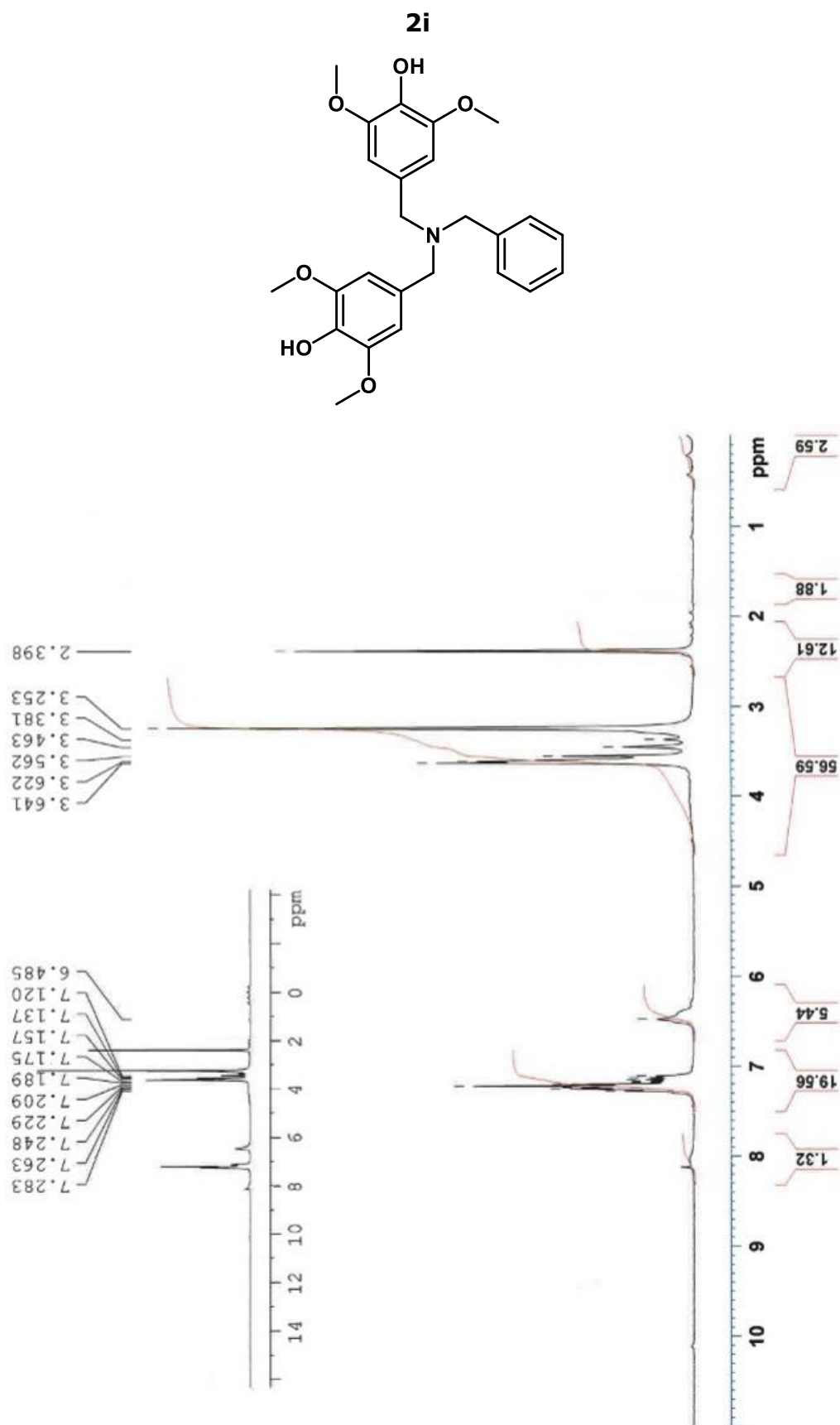


Figure A52. <sup>1</sup>H NMR spectrum of compound **2i**.

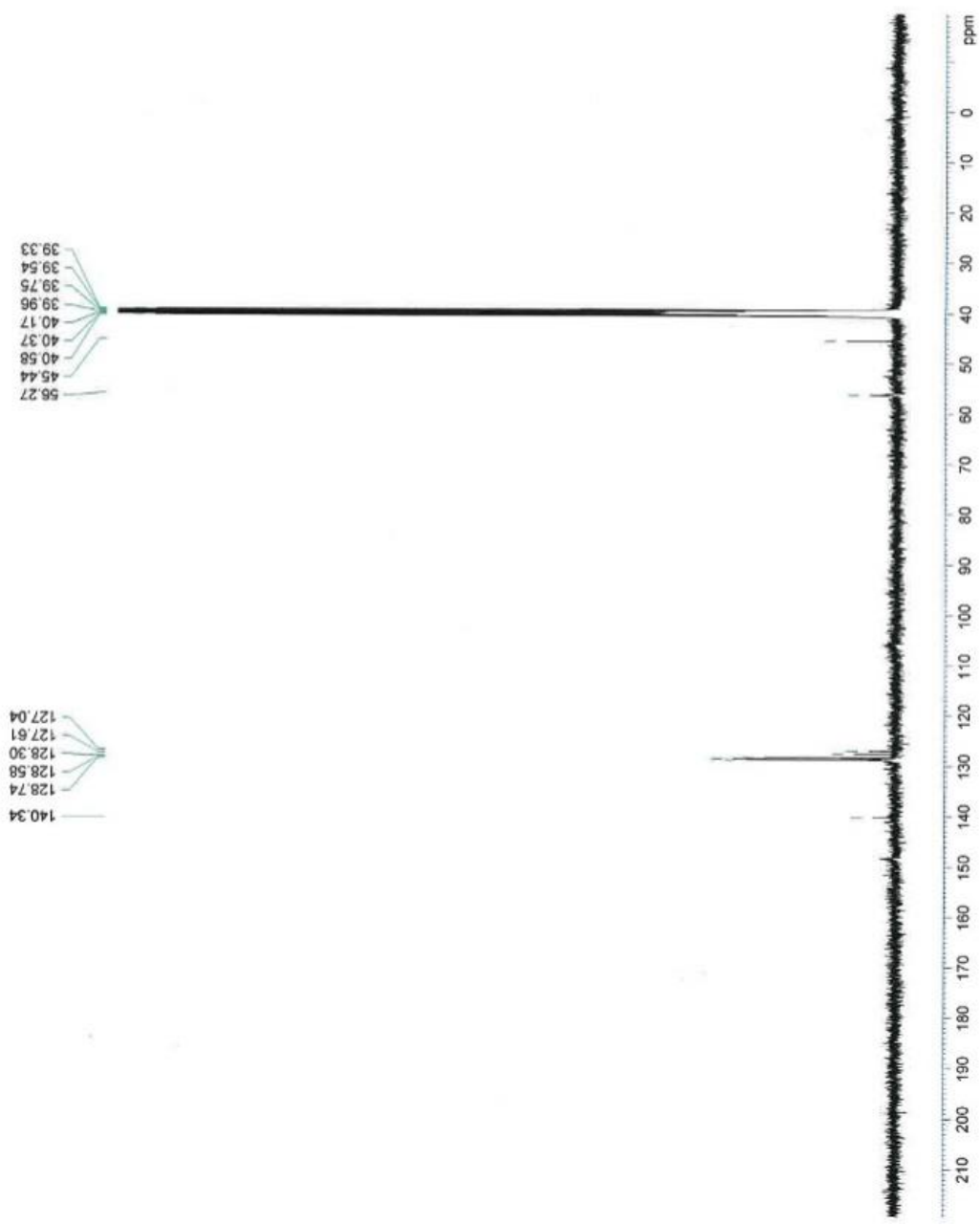


Figure A53.  $^{13}\text{C}$  NMR spectrum of compound **2i**.

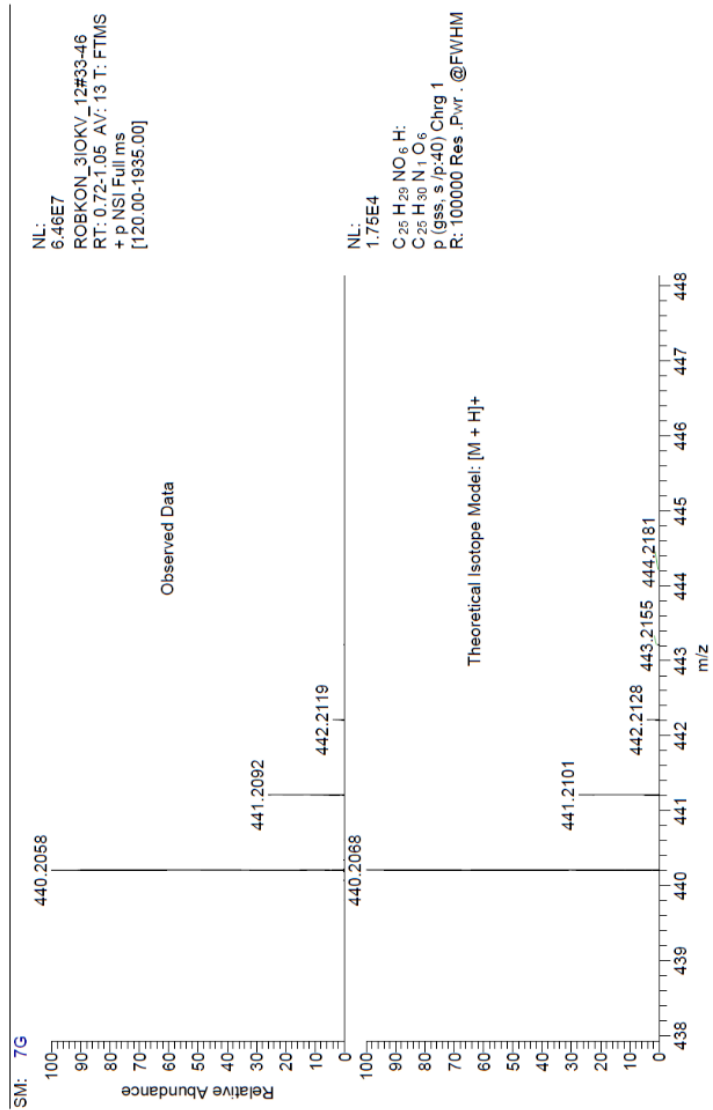


Figure A54. HRMS spectrum of compound **2i**.

**4a**

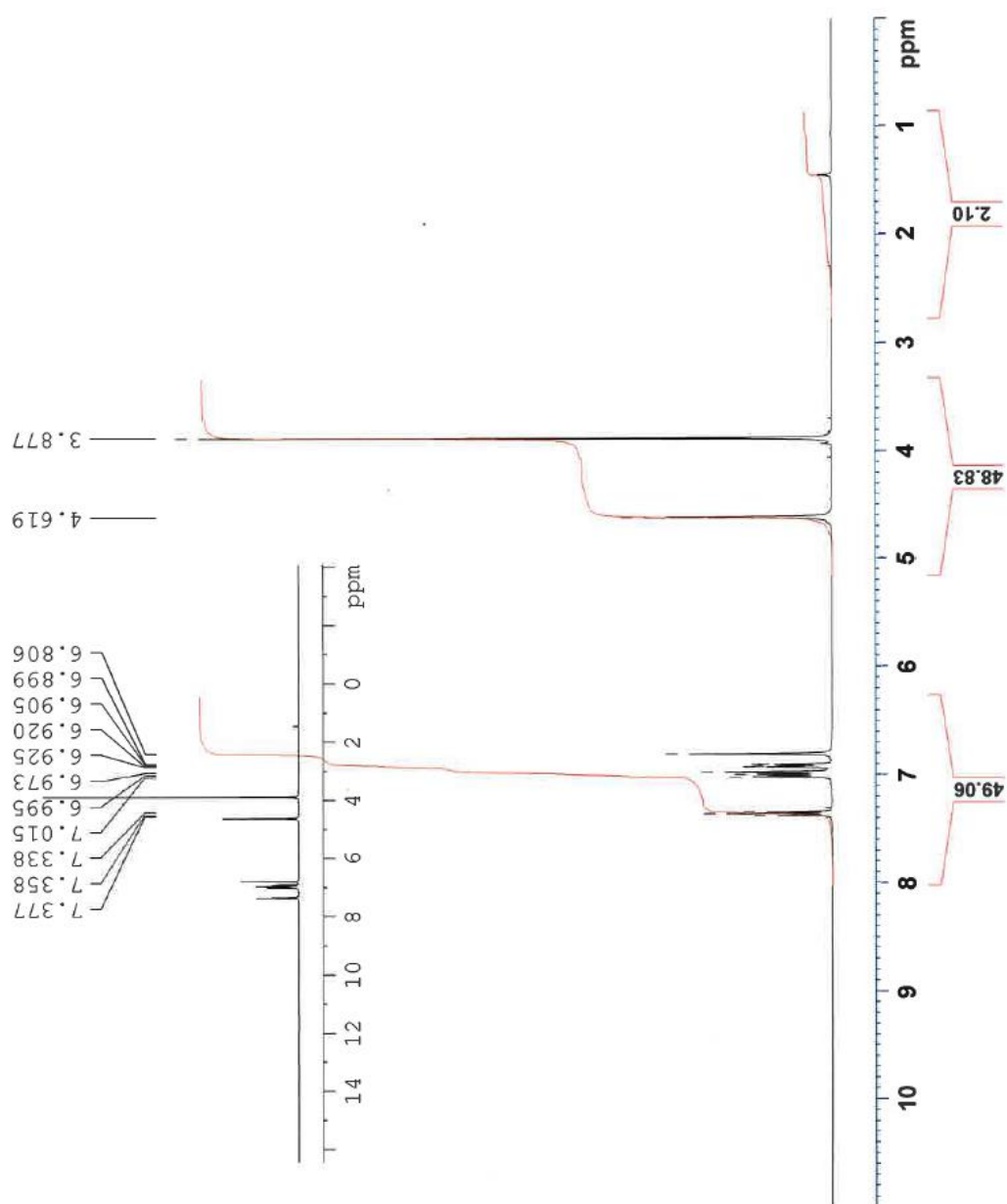
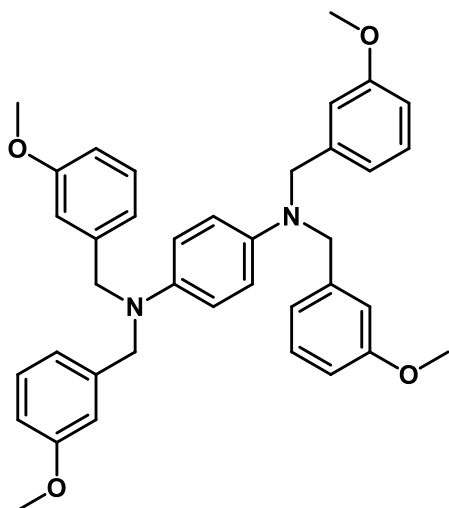


Figure A55. <sup>1</sup>H NMR spectrum of compound 4a.

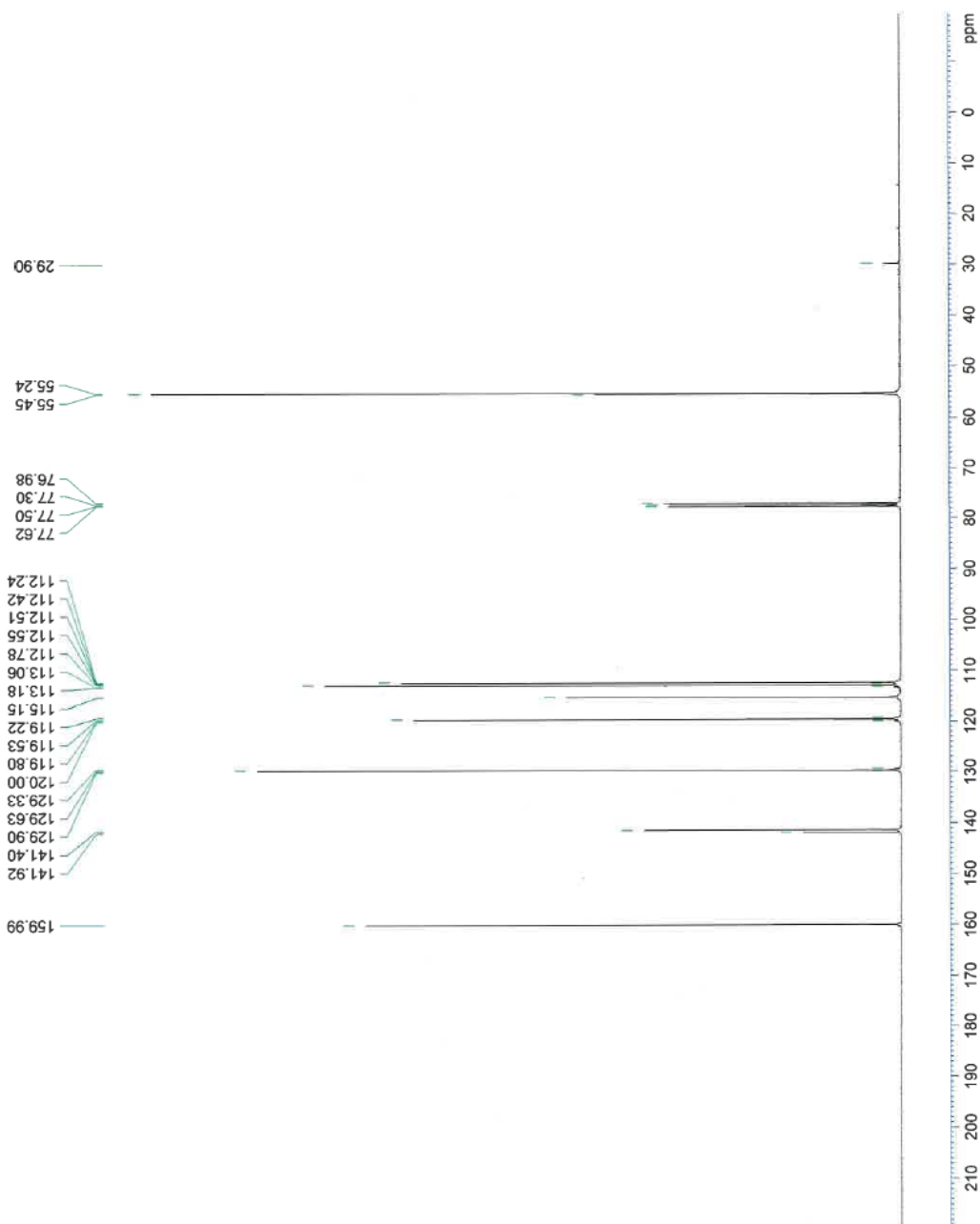


Figure A56. <sup>13</sup>C NMR spectrum of compound 4a.

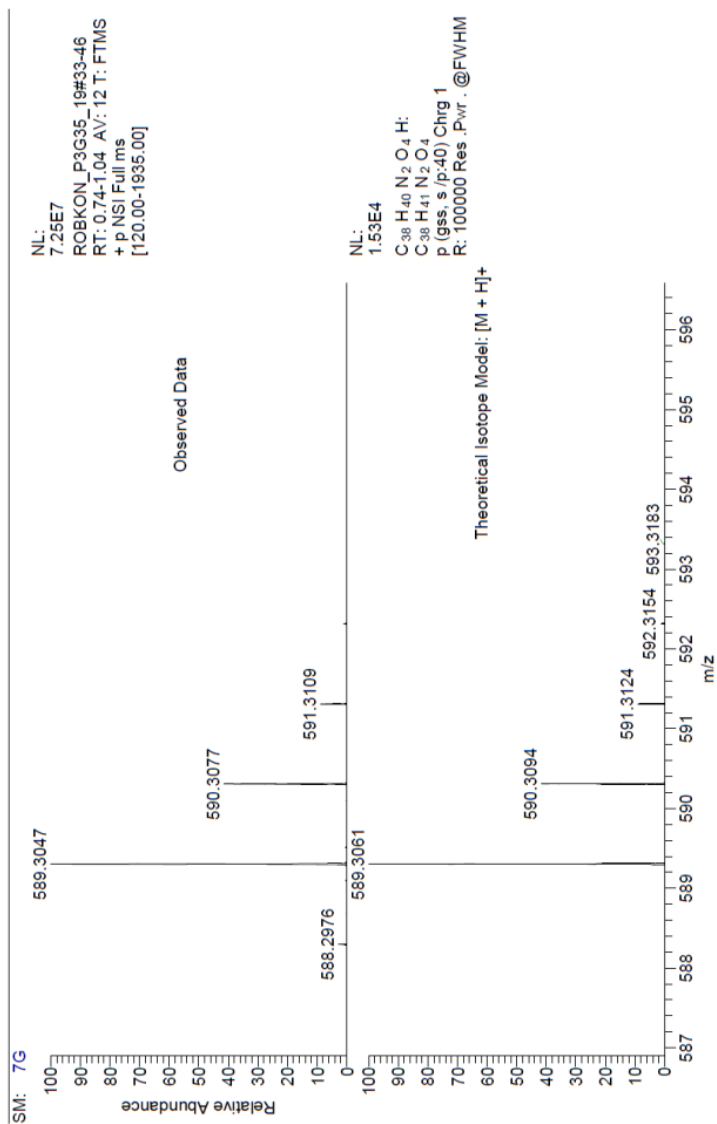


Figure A57. HRMS spectrum of compound **4a**.

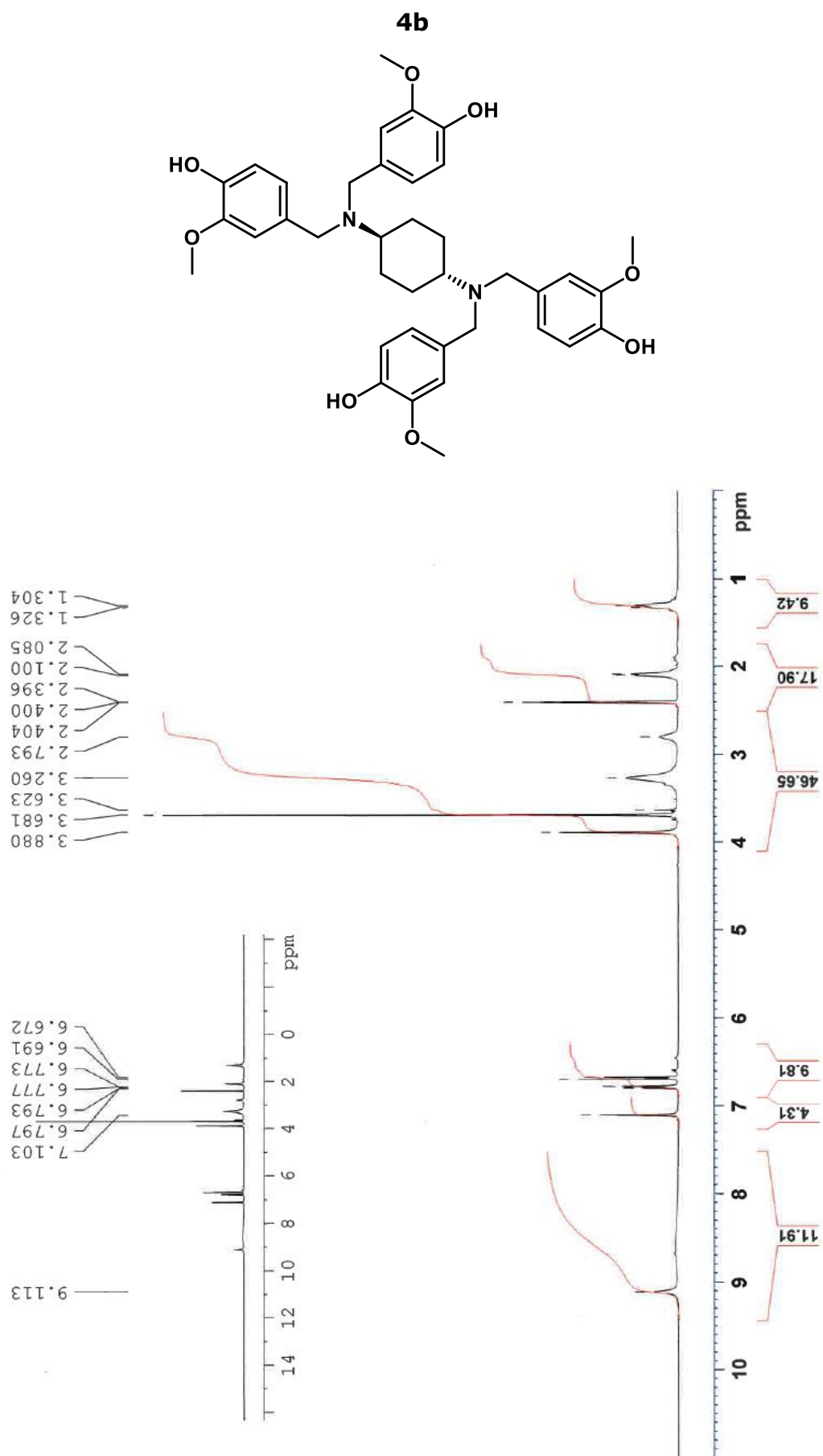


Figure A58. <sup>1</sup>H NMR spectrum of compound **4b**.

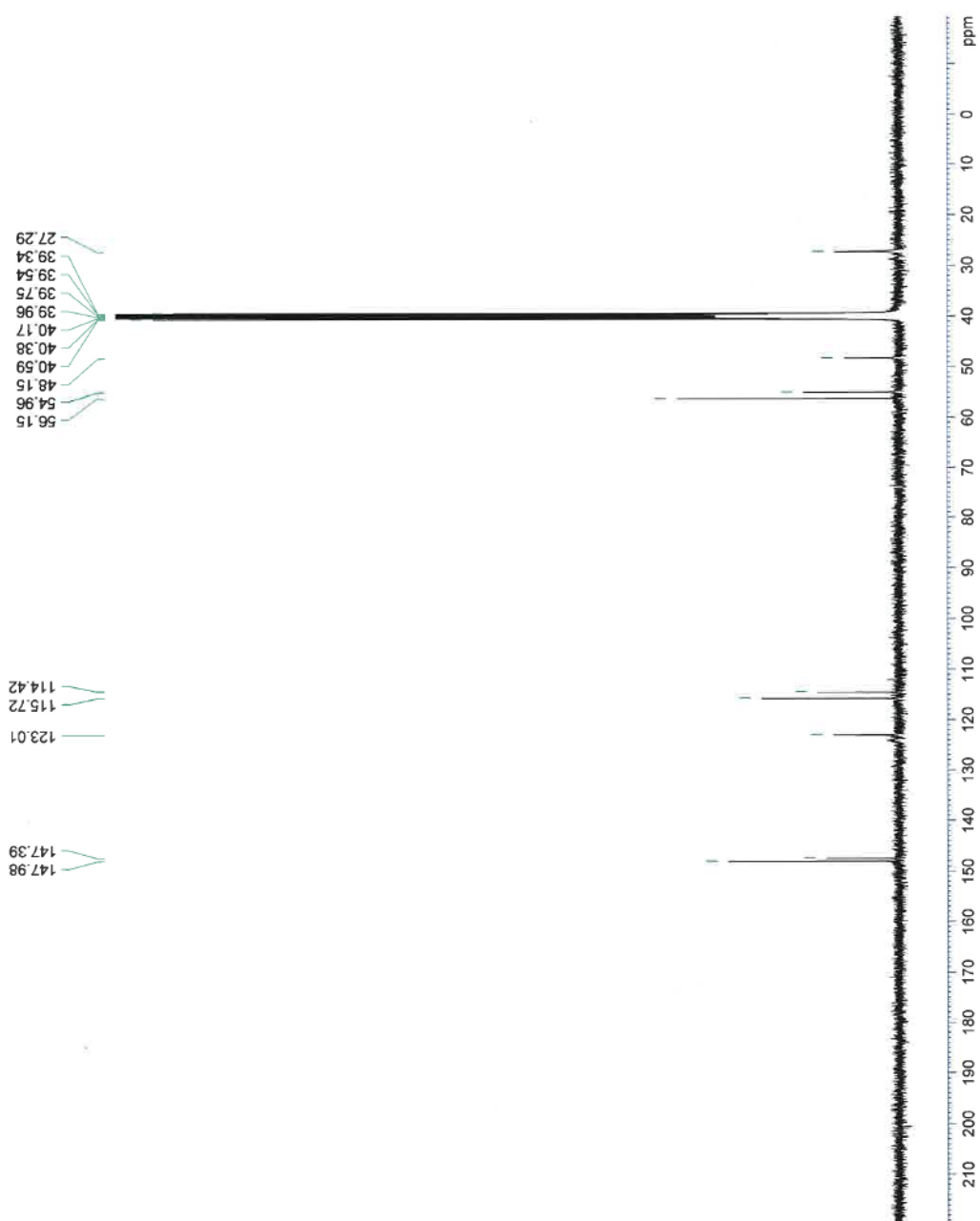


Figure A59. <sup>13</sup>C NMR spectrum of compound **4b**.

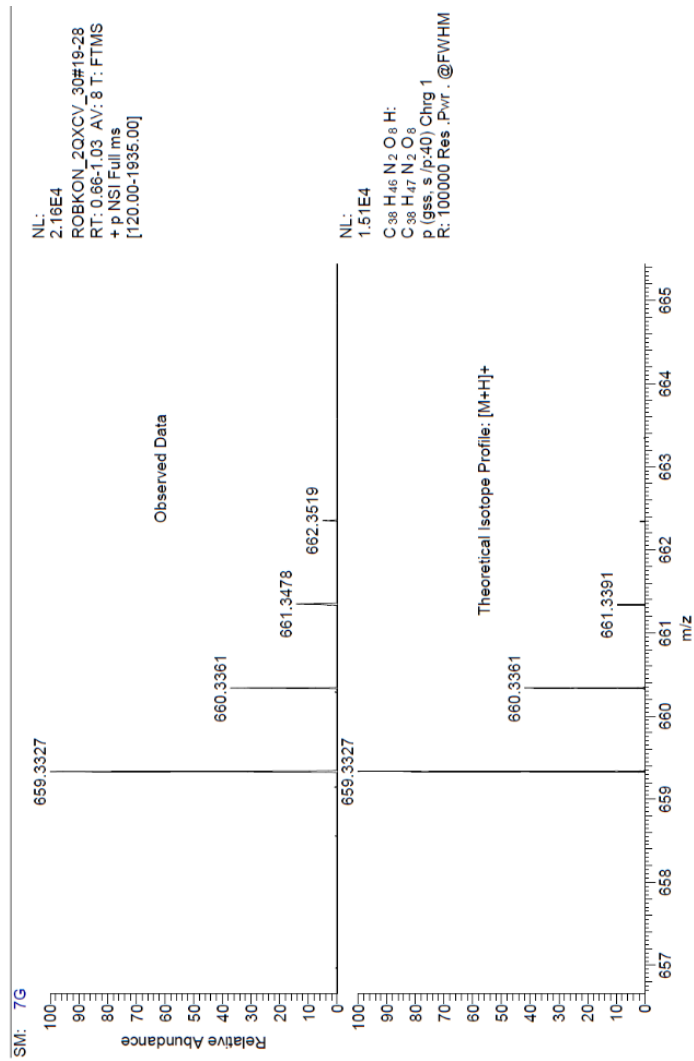


Figure A60. HRMS spectrum of compound **4b**.

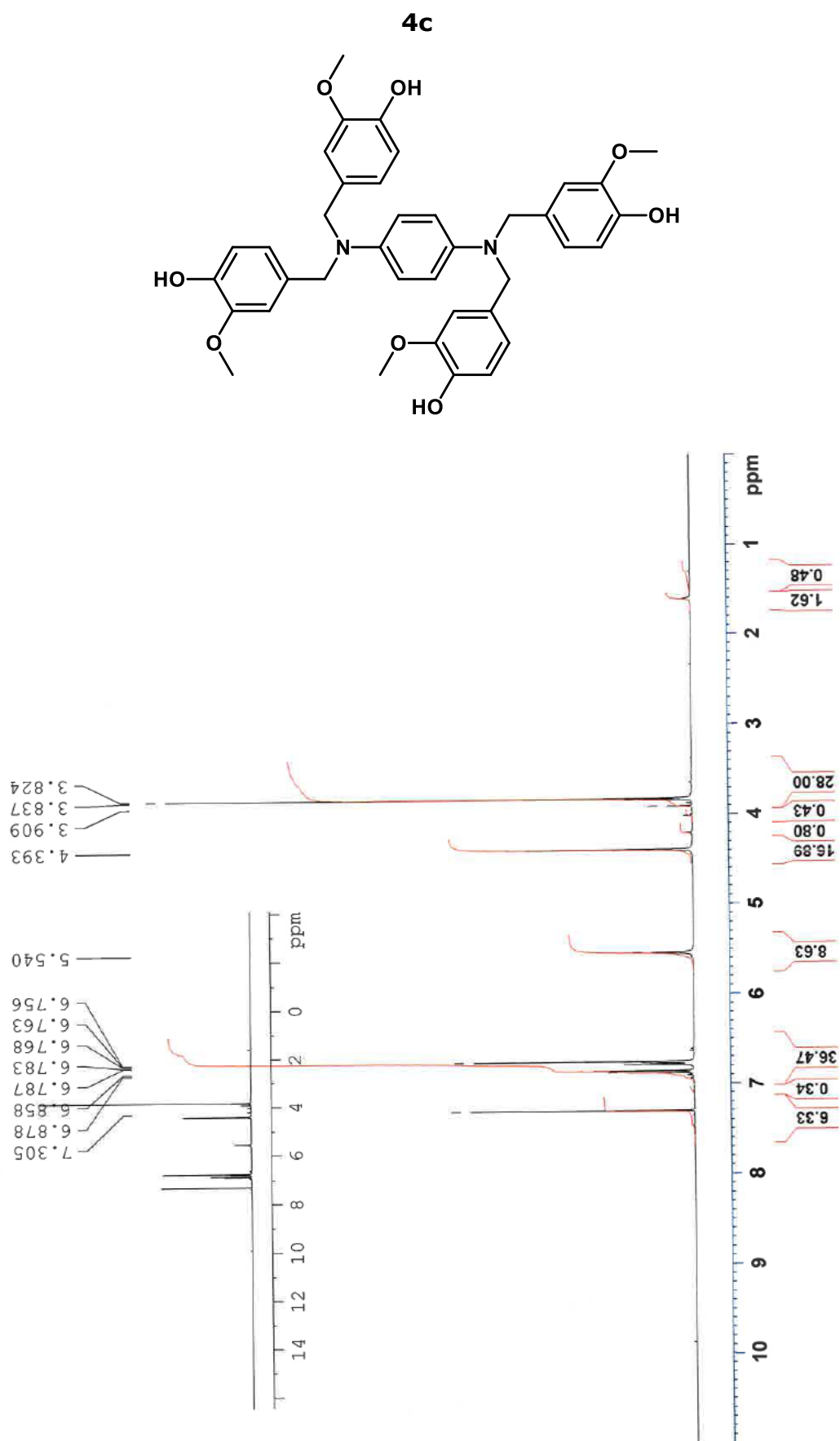


Figure A61. <sup>1</sup>H NMR spectrum of compound **4c**.

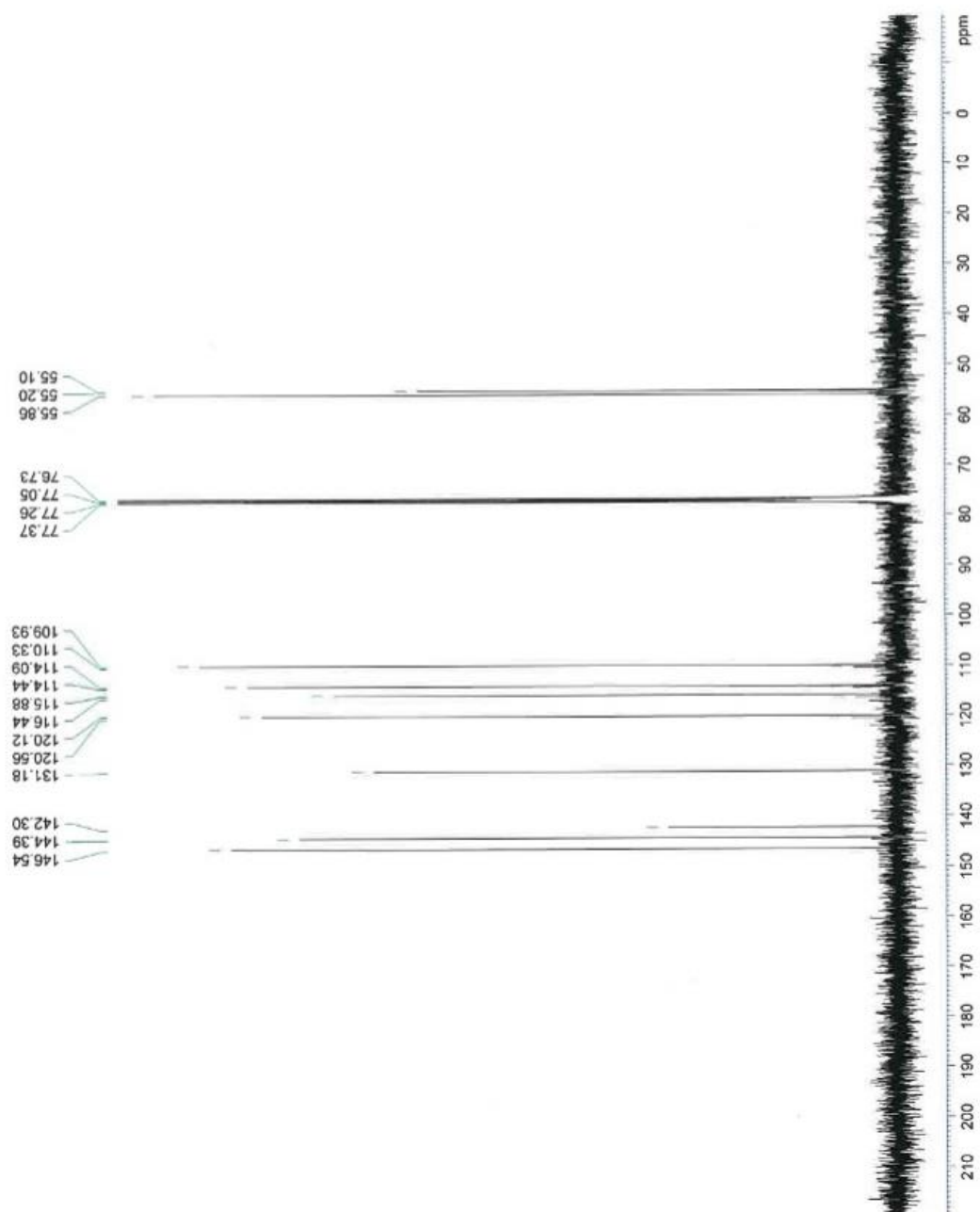


Figure A62. <sup>13</sup>C NMR spectrum of compound 4c.

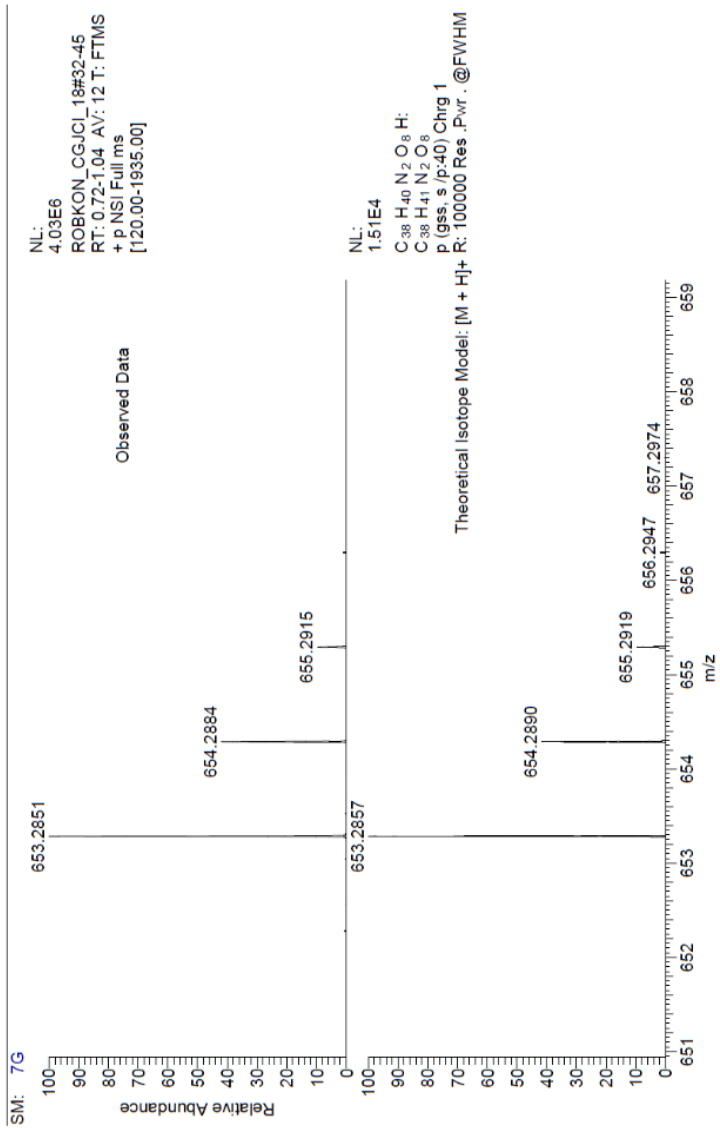


Figure A63. HRMS spectrum of compound 4c.

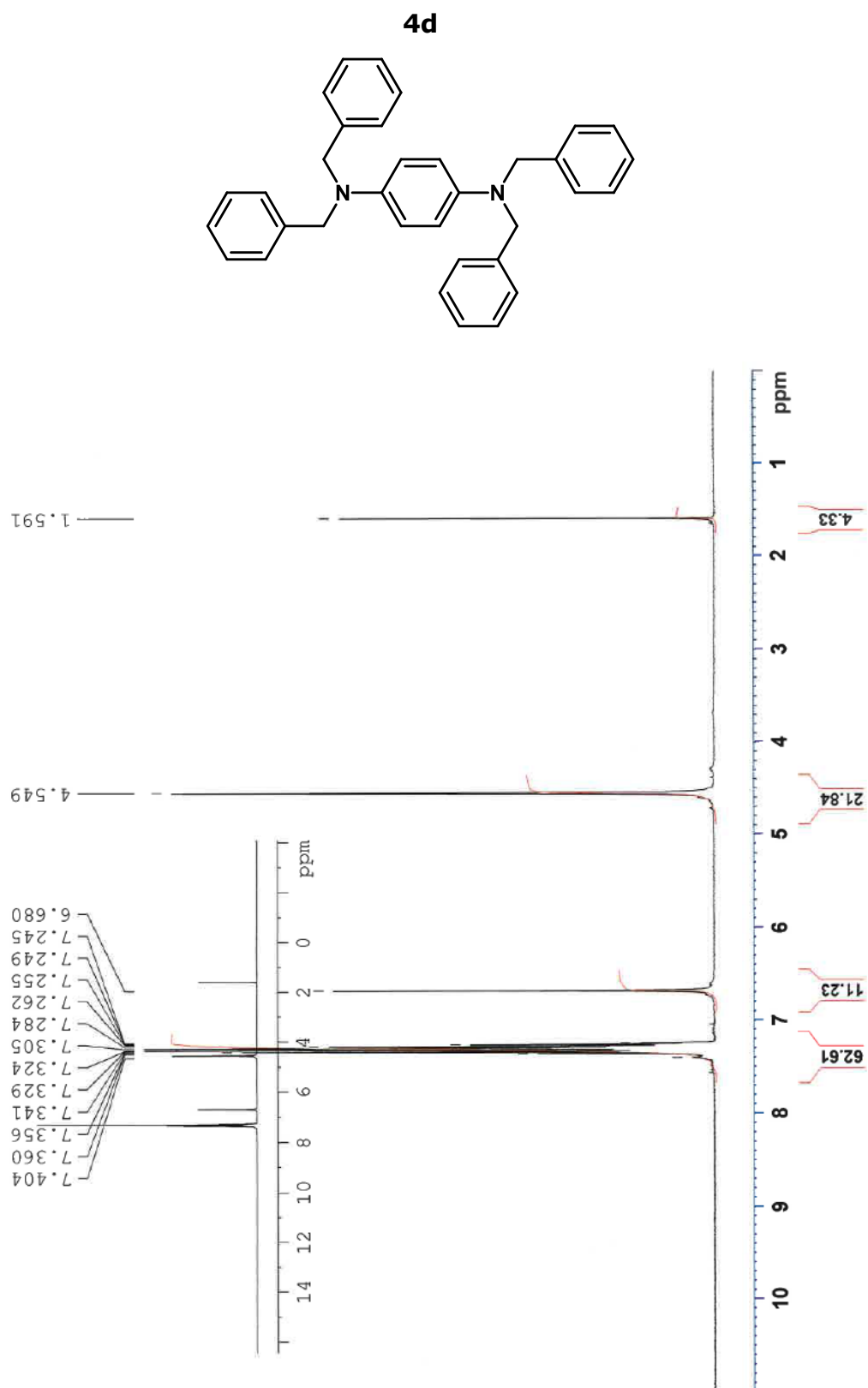


Figure A64.  $^1\text{H}$  NMR spectrum of compound **4d**.

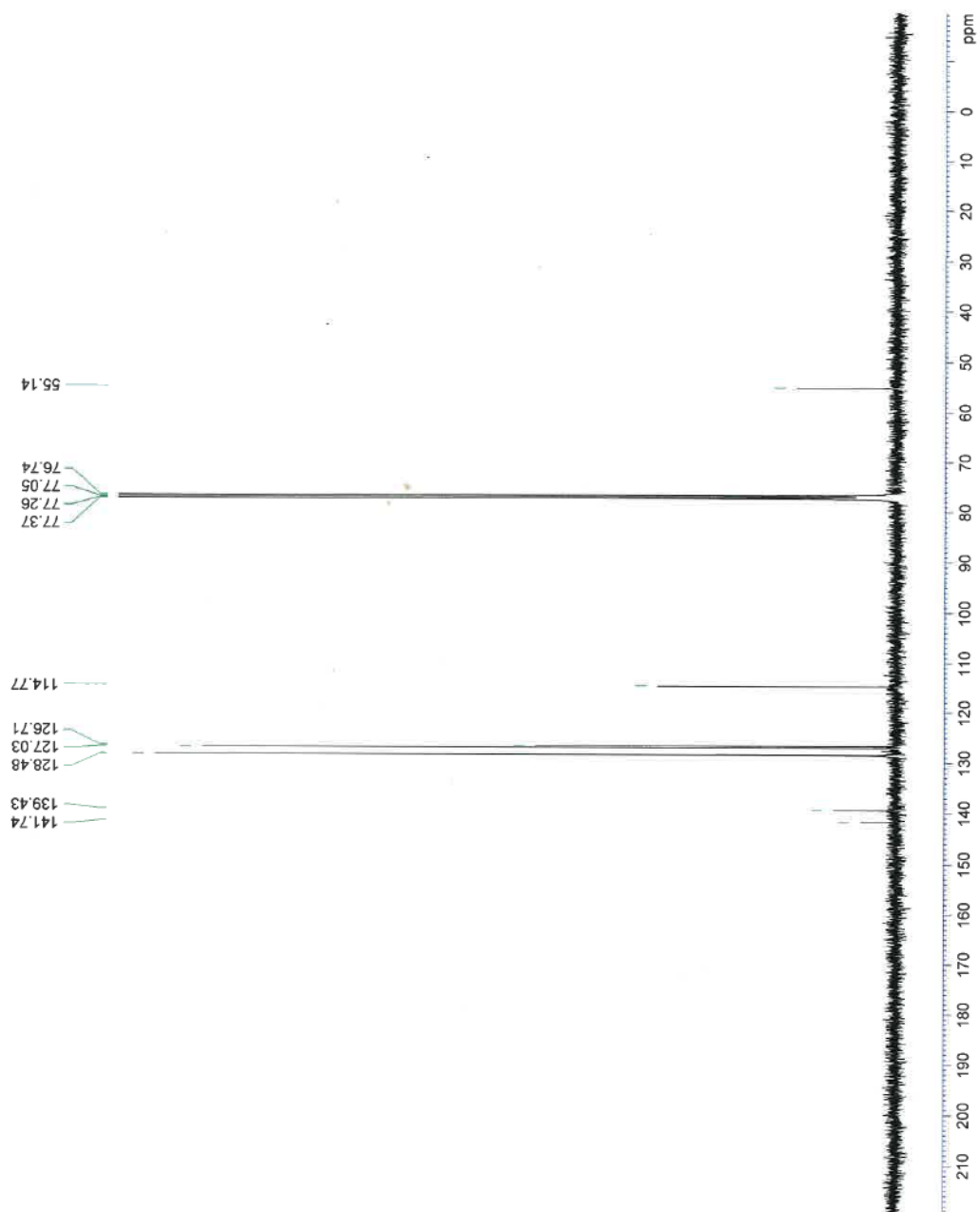


Figure A65.  $^{13}\text{C}$  NMR spectrum of compound **4d**.

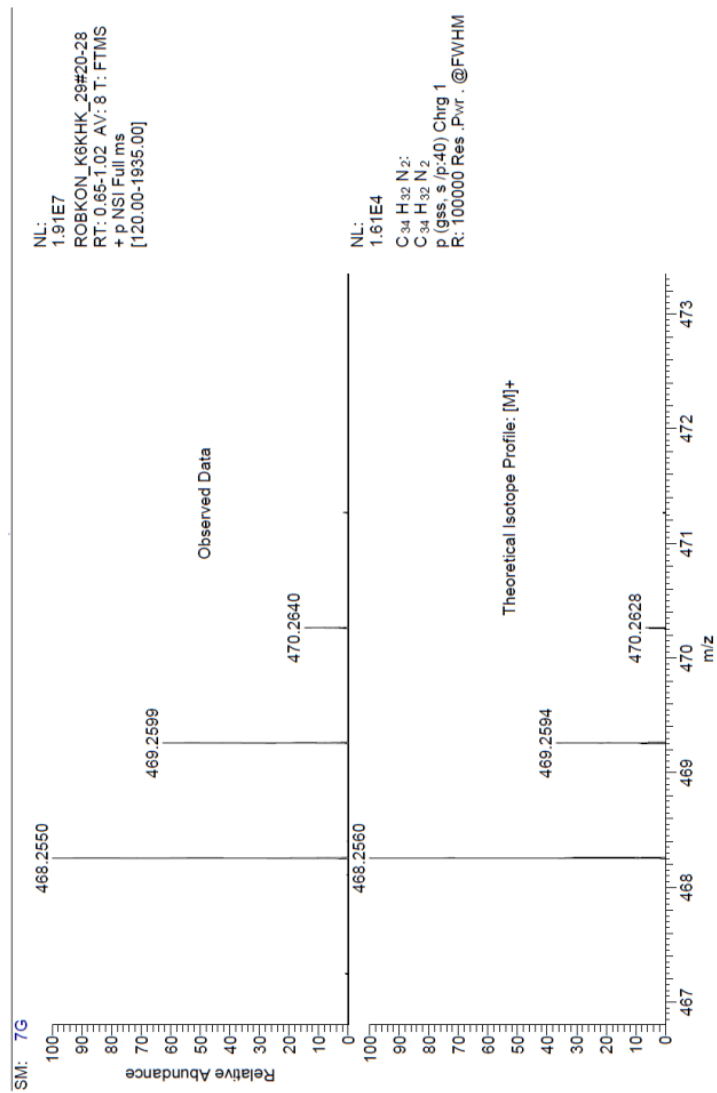


Figure A66. HRMS spectrum of compound **4d**.



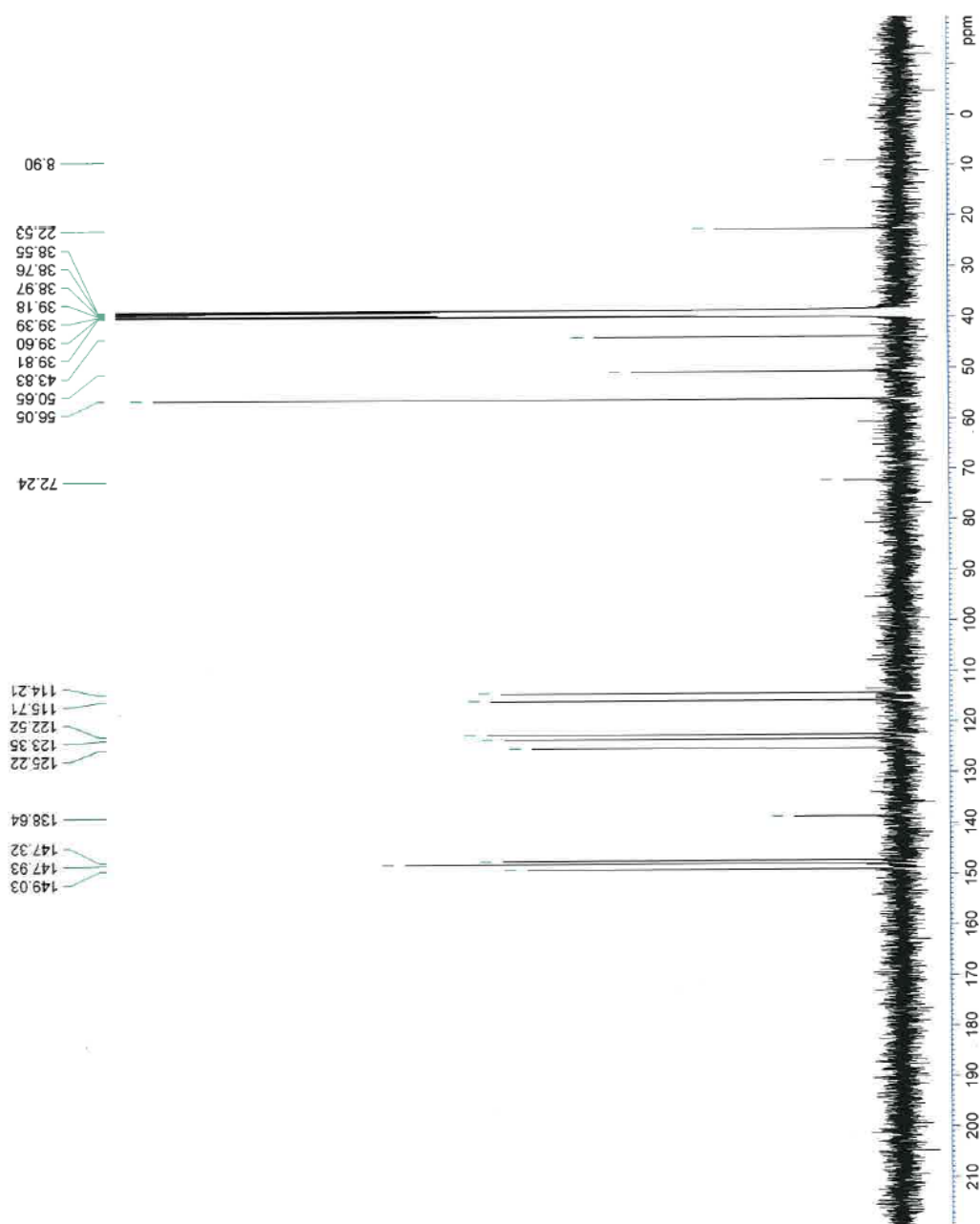


Figure A68.  $^{13}\text{C}$  NMR spectrum of compound 4e.

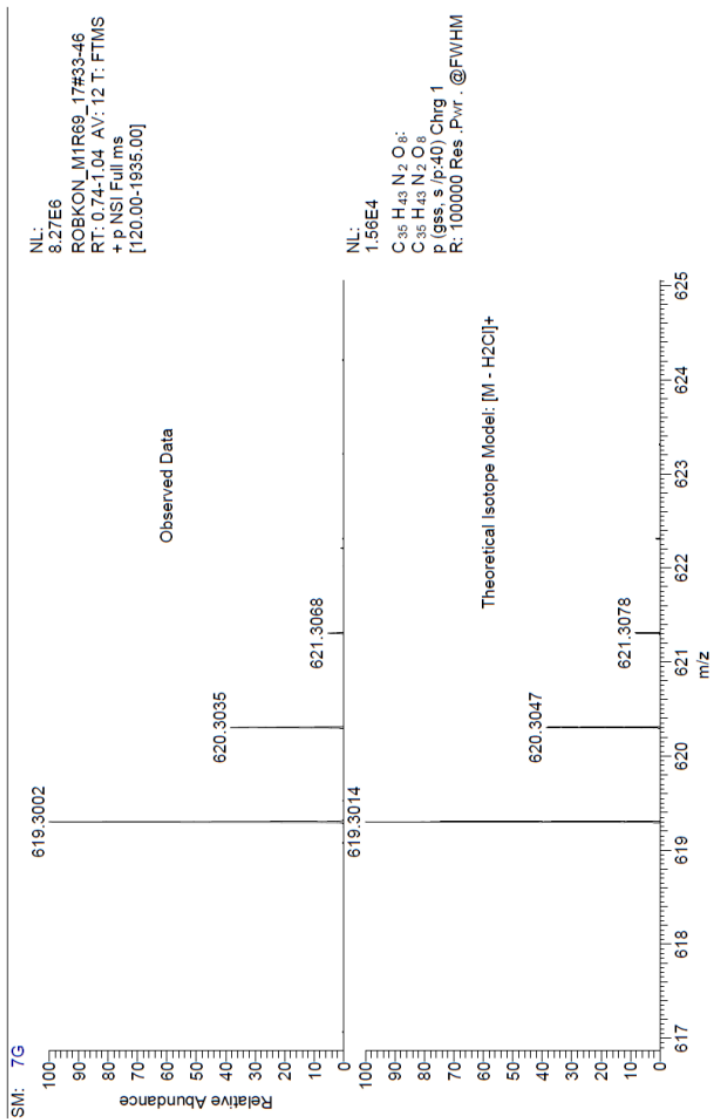


Figure A69. HRMS spectrum of compound **4e**.

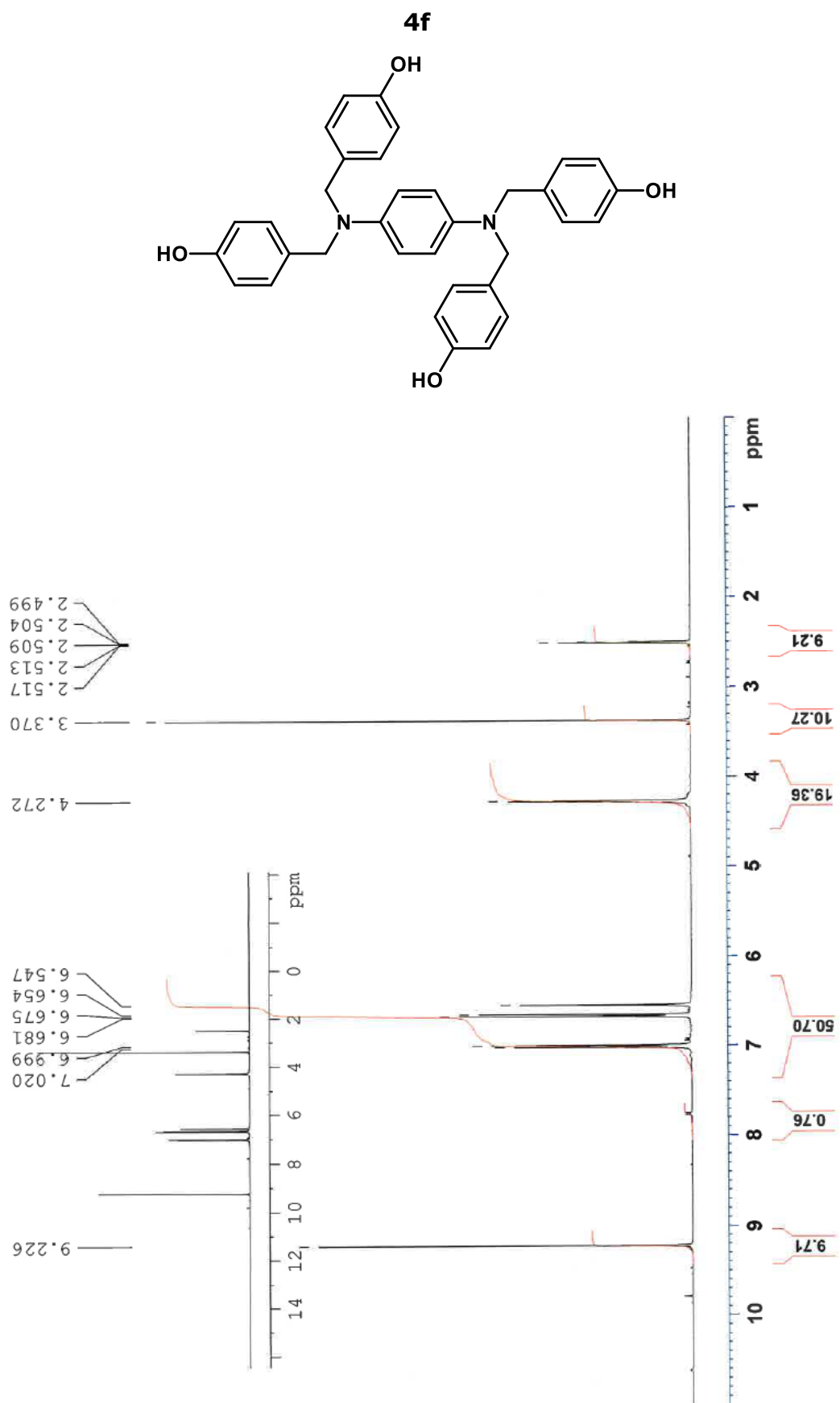


Figure A70.  $^1\text{H}$  NMR spectrum of compound **4f**.

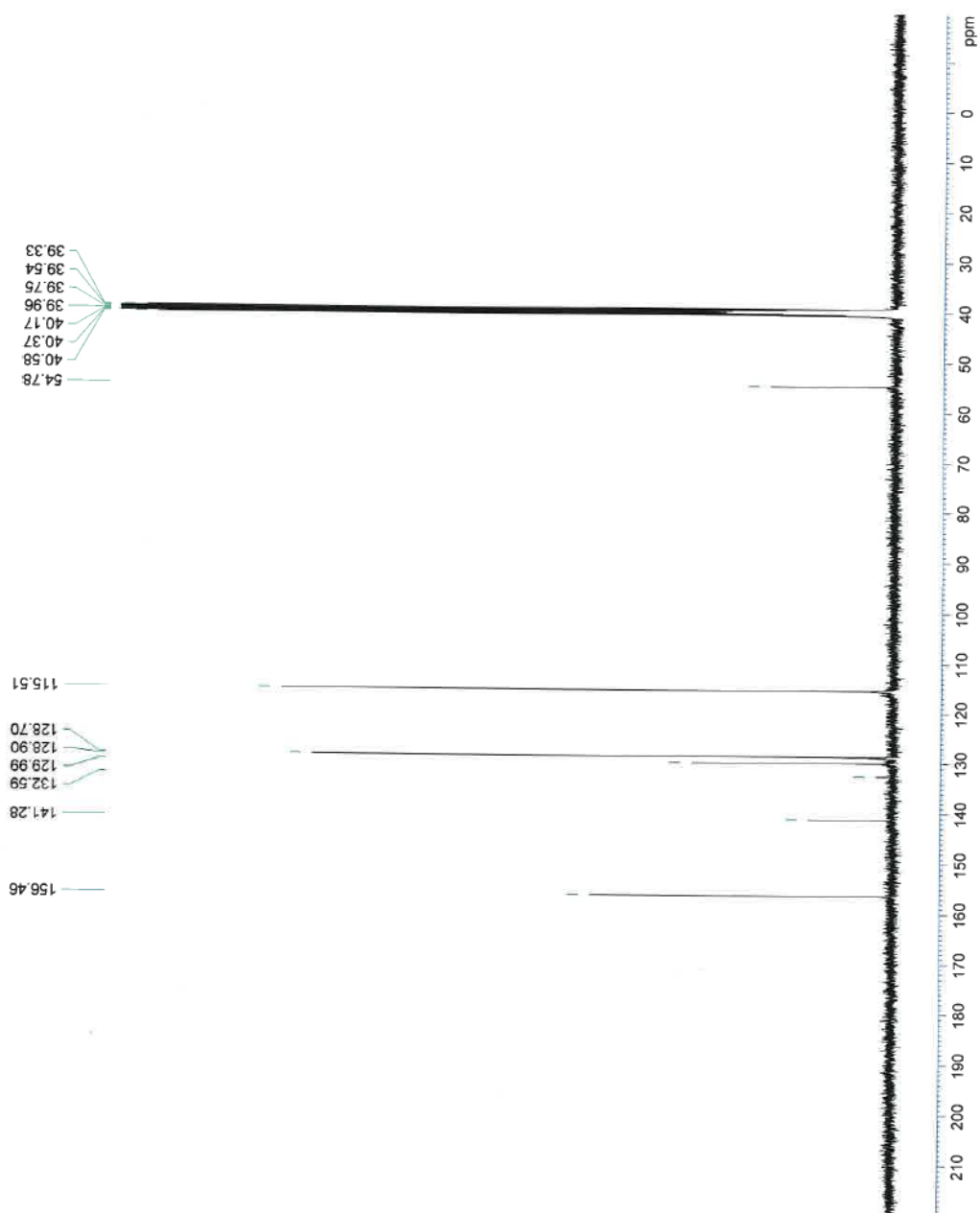


Figure A71.  $^{13}\text{C}$  NMR spectrum of compound 4f.

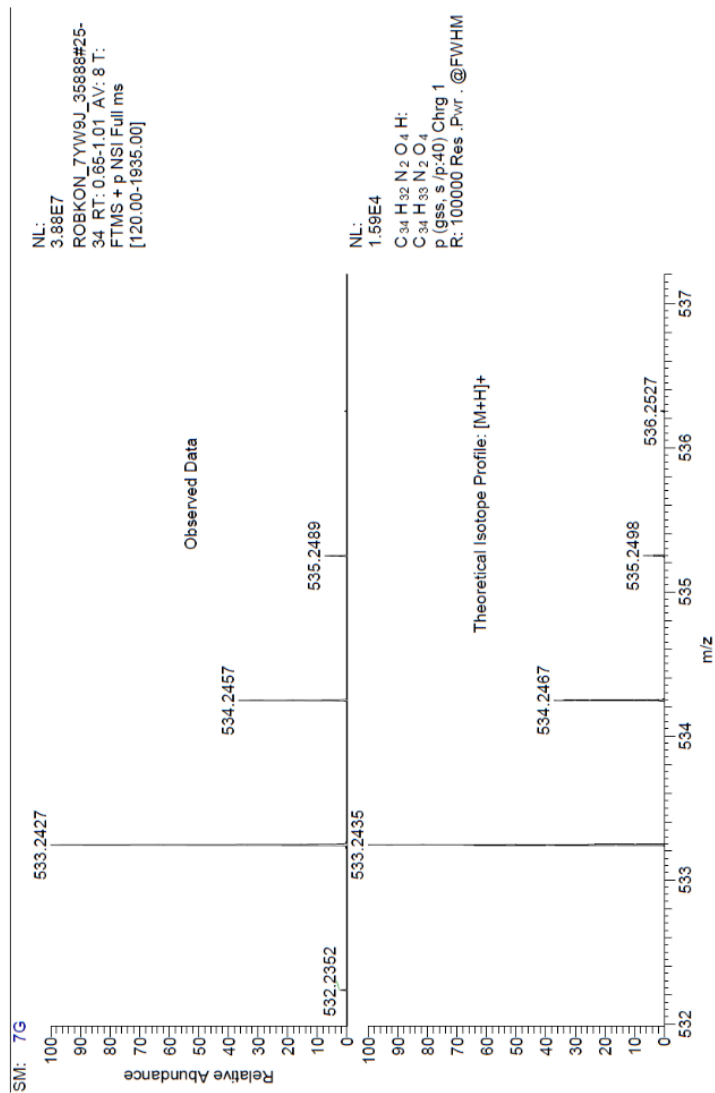


Figure A71. HRMS spectrum of compound **4f**.